ACTA TECHNICA

ACADEMIAE SCIENTIARUM HUNGARICAE

REDIGIT: M. MAJOR

TOMUS 91
FASCICULI 1—2

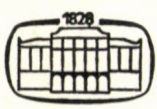

AKADÉMIAI KIADÓ, BUDAPEST 1980

ACTA TECHNICA

Az *Acta Technica* angol, francia, német és orosz nyelven közöl értekezéseket a műszaki tudományok köréből.

Az *Acta Technica* változó terjedelmű füzetekben jelenik meg, több füzet alkot egy kötetet.

A közlésre szánt kéziratok a következő címre küldendők:

Acta Technica
1051 Budapest, Münnich Ferenc u. 7.

Ugyanerre a címre küldendő minden szerkesztőségi és kiadóhivatali levelezés.

Megrendelhető a belföld számára az „Akadémiai Kiadó"-nál (1363 Budapest Pf. 24. Bankszámla 215-11448), a külföld számára pedig a „Kultura" Külkereskedelmi Vállalatnál (1389 Budapest 62, P.O.B. 149 Bankszámla: 218-10990) vagy annak külföldi képviseleteinél és bizományosainál.

Die *Acta Technica* veröffentlichen Abhandlungen aus dem Bereiche der technischen Wissenschaften in deutscher, englischer, französischer und russischer Sprache.

Die *Acta Technica* erscheinen in Heften wechselnden Umfanges. Vier Hefte bilden einen Band.

Die zur Veröffentlichung bestimmten Manuskripte sind an folgende Adresse zu senden:

Acta Technica
H-1051 Budapest
Münnich Ferenc u. 7.
Ungarn

An die gleiche Anschrift ist auch jede für die Schriftleitung und den Verlag bestimmte Korrespondenz zu richten.

Bestellbar bei »Kultura« Außenhandelsunternehmen (H-1389 Budapest 62, P.O.B. 149, Bankkonto Nr. 218-10990) oder seinen Auslandsvertretungen.

ACTA TECHNICA

ACADEMIAE SCIENTIARUM HUNGARICAE

REDIGIT: M. MAJOR

TOMUS 91

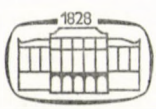

AKADÉMIAI KIADÓ, BUDAPEST 1980

ACTA TECHNICA

TOMUS 91 FASC. 1—4

INDEX

ACTA TECHNICA

ACADEMIAE SCIENTIARUM HUNGARICAE

REDIGIT: M. MAJOR

TOMUS 91

FASCICULI 1–2

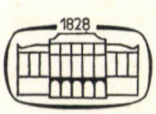

AKADÉMIAI KIADÓ, BUDAPEST 1980

Acta Technica Academiae Scientiarum Hungaricae, Tomus 91 (1—2), pp. 3—18 (1980)

HUNTINGS IN 3-PHASE MACHINES

SOME SPECIAL FEATURES

K. P. KOVÁCS,[1] W. GEYSEN,[2] G. PFAFF[3]

[Manuscript received 16 October, 1979]

In last decade or so the problem of self-excited huntings in synchronous and induction machines became the subject of new investigations. A newly observed phenomenon (the electromagnetically self-excited oscillations in synchronous machines supplying a passive inductive network) gave things a new aspect. This article is dealing with a new simple method of determining of damping factor in synchronous and induction 3-phase machines. We do calculate the damping factor in two steps: at first one calculates this factor with stator resistances neglected (m_d^s; $R_s = 0$), at second we are making the same process with supposingly negligible rotor resistances (m_d^r; $R_r = 0$). The real damping factor of machine will be given as the algebraic sum of both component damping factors ($m_d^s + m_d^r = m_d$). We are showing that this simple method makes a good approximation at supplying frequencies close to the rated frequency only. By using this superposition method we are determining stability limiting curves in some special cases. In last part we are dealing with oscillations of a synchronous machine supplying a passive (inductive) network.

Introduction

In the last decade or so many authors were dealing with hunting problems of electric machines; a great number of studies were published in books and papers f.i. [1] to [4]. These informations are so numerous that even to count the published results is almost impossible. So we are making our investigations consciously so as not to attempt any completeness, but only to call the attention to some interesting view-points of the subject.

We know that since the digital computer age the solution of most sophisticated problems is easily available, but on the other hand, as a consequence, the background of the occurrences are unfortunately often over-shadowed.

We will try to enlighten the physical background of the phenomena during our investigations.

We are describing first a general, but simple method to determine the damping factor in synchronous and induction machines connected to an infinite bus. The sign of the damping factor is characteristic for the stable

[1] Prof. K. P. KOVÁCS, Member of the Hung. Acad. of Sciences; scientifical adviser of the chair "Elektrotechnika" of the Technical University Budapest; H-1011 Budapest, Vám u. 2., Hungary.

[2] Prof. Dr.-Ing. W. GEYSEN Catholic Univ. of Leuven. Inst. El. Engng., Belgium.

[3] Prof. Dr.-Ing. G. PFAFF Univ. Erlangen, Inst. El. Antriebe BRD.

(sign+) or unstable (sign—) working of machines regarding torsional hunting phenomena. Rased on this general method we will examine the damping factor by using a simple superposition principle [5]. It can be shown that this simplification leads to a good approximation if the supply frequency is not less than 0.6 (in p.u. system). To demonstrate this we will investigate the influence of frequency speedcontrol on the damping factor, using the general method. We will compare the results of both methods. In the last part of the paper, using our general method, we will investigate the stability of synchronous machines supplying a passive network.

Introductory remarks

To obtain the most simple conditions, without influencing the generality of our discussion, we are using the following assumptions:

1) The synchronous machine has a round rotor (the air-gap is uniform over the circumference).

2) The rotor is equipped with a two-phase symmetrical winding system. One of these windings is the exciter-winding, which is short-circuited over the exciter machine. The impedance of exciter machine is negligible compared to the rotor impedance. If the excitation current is zero, the machine goes over into induction machine operation.

3) We suggest that the magnetic field distribution over the pole-pitch is sinusoidal.

4) We are using a coordinate system fixed to the rotor where the real axis (d direction) is coaxial to the exciter winding and the imaginary axis (q direction) is in quadrature to the d axis i.e. displaced by 90° in a positive direction (counter clockwise).

5) We are using the p.u. system and dimensionless form of equations.

6) We shall linearize our equations by confining to small changes only; i.e. that we assume that during oscillations the average speed of machine is constant or only slowly changing. Due to the linearization one can go over to the Laplace-domain.

Line of thoughts on calculating method

a) We assume that the steady-state running of machine is disturbed by a small ΔT unit torque-step.

b) We have calculated the response function $\Delta\omega = \Delta\omega(p)$; i.e. the variation of speed caused by the torque-step ΔT. p is the Laplace variable; one must imagine that the symbol s, generally used as a Laplace variable, in electric machine theory, is used to denote the slip of machine.

c) We define the operator impedance of huntings as:

$$Z_h(p) = \frac{-\Delta T}{p\Delta\omega} . \tag{1}$$

d) To obtain the damping factor we have first to define the response function of a periodically changing torque disturbance. That is:

$$\overline{\Delta T} = \Delta T e^{j\Omega\tau}. \tag{2}$$

If such a torque is acting on the shaft a harmonically changing steady-state oscillation of rotor is attained. This response function may be derived from operator impedance — Eq. (1) — by setting:

$$p = j\Omega$$

The complex hunting impedance — in case of sinusoidally changing torque disturbance at steady-state oscillations — is:

$$\bar{Z}_h(j\Omega) = -\frac{\overline{\Delta T}}{\overline{\Delta\omega}}, \tag{3}$$

and

$$\overline{\Delta\omega} = -\frac{\overline{\Delta T}}{\bar{Z}_h(j\Omega)}. \tag{4}$$

e) The real part of hunting impedance is the damping factor:

$$d = \mathrm{Re}[\bar{Z}_h(j\Omega)] = -\mathrm{Re}\left[\frac{\overline{\Delta T}}{\overline{\Delta\omega}}\right]. \tag{5}$$

f) The imaginary part of the complex hunting impedance is proportional to the synchronizing torque caused by rotor oscillations. That is:

$$T_s = j\Omega\mathrm{Im}[\bar{Z}_h(j\Omega)] = -j\Omega\mathrm{Im}\left[\frac{\overline{\Delta T}}{\overline{\Delta\omega}}\right]. \tag{6}$$

g) If the damping factor is positive, any disturbances will be damped, and even in case of periodically changing forced torque oscillations only constant small hunting amplitudes remain. Stochastically distributed small torque disturbances which may be approximated by periodically changing small orque deviations, are in the case of positive damping factor so far damp ed hat the smooth running of machine is not influenced at all.

h) If the damping factor is negative the amplitudes of the torsional oscillations are increasing until a steady-state hunting of machine-system takes place whose amplitudes are due to electromechanical nonlinearities and due to mechanical friction limited only. In some special cases a pull-out of synchronism may occur.

In case when the damping factor has a negative value, even the smallest stochastically distributed torque disturbances may cause increasing hunting amplitudes and a steady-state hunting of large amplitude will take place. In these latter cases the frequency of oscillations is the natural frequency (fundamentally defined by the rotating system's mass moment of inertia and of the synchronizing torques). No forced periodically changing torque disturbances are necessary to uphold the unstable conditions.

Equations for small changes

We shall set down the equations in the Laplace-domain for small changes directly, resolved into real and imaginary parts (d and q directions). For the sake of simplicity, without influencing the general validity, we assume that the stator and rotor leakage reactances are mutually equal. That is: $X_{sl} = X_{rl}$ and therefore $X_d = X_r$; $X'_d = \mathbf{X}'_r$ and $X_m/X_d = K_s = X_m/X_r = K_r = K$.

Suggesting that the machine was running with synchronous rated speed before the torque disturbance ΔT acted: is $\omega = 1$. In the voltage equations below we shall use the following symbols: $s_a = R_s/X'_d$ and $s_p = R_r/X'_r = R_r/X'_d$.

Stator voltage equations:

$$\begin{aligned} \Delta U_d &= U_s \cos\delta\Delta\delta = (p + s_a)\Delta\psi_d - \Delta\psi_q - \psi_q\Delta\omega - Ks_a\Delta\psi_{rd}, \\ \Delta U_q &= -U_s \sin\delta\Delta\delta = \Delta\psi_d + (p + s_a)\Delta\psi_q + \psi_d\Delta\omega - Ks_a\Delta\psi_{rq}. \end{aligned} \tag{7}$$

Rotor voltage equations:

$$\begin{aligned} 0 &= (p + s_p)\Delta\psi_{rd} - Ks_p\Delta\psi_d, \\ 0 &= (p + s_p)\Delta\psi_{rq} - Ks_p\Delta\psi_q. \end{aligned} \tag{8}$$

Torque equation:

$$\begin{aligned} hp\Delta\omega + \frac{\Delta T}{p} &= \mathrm{Im}(\bar{\psi}_s^*\Delta\bar{i}_s + \overline{\Delta\psi}_s^*\bar{i}_s) = \\ &= -K/X'_d(\psi_d\Delta\psi_{rq} - \psi_q\Delta\psi_{rd} + \psi_{rq}\Delta\psi_d - \psi_{rd}\Delta\psi_q). \end{aligned} \tag{9}$$

In Eqs (7), (8) and (9) the symbols δ, ψ_d, ψ_q, ψ_{rd} and ψ_{rq} (the load angle and flux linkages, respectively) are steady-state values of the machine before the disturbance caused by the unit torque step ΔT occurred; h is the p.u. value of moment of inertia: $h = J\omega_1^3/P_R$ where J = moment of inertia (Wsec^3); P_R = rated power (W).

Superposition method

To determine the damping properties of three-phase machines a superposition principle may be used based on the suggestion that the overall damping factor of the machine may be resolved into two separated components. The first component can be obtained if the stator resistance is neglected ($R_s=0$; $s_a = 0$) and the rotor resistance has a certain value ($R_r \neq 0$; $s_p \neq 0$). We will denote this component of damping factor as d_r. The other component can be calculated if we suggest that the rotor resistance equals zero ($R_r = 0$; $s_p = 0$) and the stator resistance has a certain value ($R_s \neq 0$; $s_a \neq 0$). This component damping factor may be denoted by d_s. Under well definable conditions the real damping factor of machine can be given by a linear superposition:

$$d = d_r + d_s. \tag{10}$$

The permissible use of this simple method has certain limits and we will show further on under which conditions this intelligible method leads to a fairly close approximation.

First damping factor component

$R_s = 0$; $R_r \neq 0$. For the sake of further simplification we start from the no load point of machine, i.e. $\delta = 0 (s = 0)$.

In this case is $\overline{U_s} = j\overline{\psi_s}$ or $U_d = -\psi_q$ and $U_q = \psi_d$. On the other hand are:

$$\Delta\psi_d = \Delta U_q = -U_s \sin \delta \Delta\delta = 0 \quad \text{and} \quad \Delta\psi_q = -\Delta U_d = -U_s \cos \delta \Delta\delta = -U_s \Delta\delta.$$

By using Eqs (8) and (9) and with respect to Eqs (3) and (5) we obtain:

$$j\Omega h\overline{\Delta\omega} + \overline{\Delta T} = 2T_p \frac{1}{s_p + j\Omega}\overline{\Delta\omega} + \frac{U_s U_p}{j\Omega X_d}\overline{\Delta\omega}, \tag{11}$$

and the first damping factor component may be calculated as:

$$d_r = \mathrm{Re}\left[\frac{2T_p}{s_p + j\Omega}\right] = \frac{2T_p s_p}{s_p^2 + \Omega^2}. \tag{12}$$

In Eq. (12) T_p is the induction machine pull-out torque:

$$T_p = K^2 U_s^2 / 2X_d'.$$

From Eq. (12) one can see that this damping factor component is independent of the excitation of the synchronous machine and, therefore, this damping factor component is valid for the induction machine operation, too ($U_p = 0$).

Second damping factor component

$R_s \neq 0$; $R_r = 0$. In this case is $\Delta\psi_{rd} = \Delta\psi_{rq} = 0$. By using Eqs (3), (5), (8) and (9) for this damping factor component we obtain:

$$d_s = -s_a \frac{1 - s_a^2 - \Omega^2}{(1 + s_a^2 - \Omega^2)^2 + 4s_a^2\Omega^2}\left[2T_p + \frac{U_s U_p}{X_d}\right]. \tag{13}$$

From Eq. (13) two physically important conclusions about the role of the stator resistance on the damping factor of machine are to be obtained:

a) This component damping factor is, in practical cases, always negative. The value of s_a is, namely, in the range of 0,08 to 0,15 ($s_a^2 = 6{,}4 \cdot 10^{-3} - 0{,}0225$) and the natural frequency of torsional oscillations is in the range of $\Omega = 0{,}03$ to 0,3 ($\Omega^2 = 9 \cdot 10^{-4} - 0{,}09$) and, therefore, $1 \gg s_a^2 + \Omega^2$. The lower figure is valid for big sized turbo-alternators and the upper limit stands for machines of about 1—2 kW output. If the electric machine is mechanically coupled with a prime-mover or a mechanical load, these values of natural frequencies are lower.

b) This component depends on the excitation of the synchronous machine. If the excitation U_p is increasing, the second damping factor component becomes more negative which means that the stability of machine is becoming worse. The negative value of this component has a minimum if the excitation equals zero, i.e. the machine is going over into induction machine operation.

Overall damping factor

By using Eqs (10), (12) and (13) we obtain the damping factor of the machine as

$$d = d_r + d_s = \frac{2T_p s_p}{s_p^2 + \Omega^2} - \left(2T_p + \frac{U_p U_s}{X_d}\right) s_a \frac{1 - s_a^2 - \Omega^2}{(1 + s_a^2 - \Omega^2)^2 + 4\Omega^2 s_a^2}. \tag{14}$$

In Eqs (13) and (14) is $U_s U_p / X_d = T_{\max}$ the maximum output of the synchronous machine at constant excitation current ($U_p = i_r \cdot X_m$). By introducing the symbol $m = T_{\max}/2T_p$, for the damping factor we obtain:

$$d = 2T_p\left[\frac{s_p}{s_p^2 + \Omega^2} - (1 + m)s_a \frac{1 - s_a^2 - \Omega^2}{(1 + s_a^2 - \Omega^2)^2 + 4\Omega^2 s_a^2}\right]. \tag{15}$$

The limit between stable conditions ($d > 0$) and unstable conditions ($d < 0$) is represented by the equation:

$$d = 0 = \frac{s_p}{s_p^2 + \Omega^2} - (1 + m)\frac{1 - s_a^2 - \Omega^2}{(1 + s_a^2 - \Omega^2)^2 + 4s_a^2\Omega^2} s_a. \tag{16}$$

In case of a fully symmetrical machine ($s_p = s_a$) we obtain for the limit conditions at no load:

$$\Omega^4 - \left(\frac{3+m}{2+m} - 2s_a^2\right)\Omega^2 + \frac{(1-m)s_a^2+1}{2+m} + s_a^4 = 0. \tag{17}$$

In case of a squirrel-cage or wound-rotor induction machine is $m = T_{max}/2T_p = 0$ and assuming that $s_p = s_a = 0{,}15$, for the frequency of a possible self-excited oscillation we obtain an equation of the fourth grade in Ω:

$$\Omega^4 - 1{,}46\,\Omega^2 + 0{,}512 = 0$$

which has two positive roots $\Omega_1 = 0{,}935$ and $\Omega_2 = 0{,}765$. That means that although self-excited huntings are not excluded in principle, but between the limits $\Omega_1 \to \Omega_2$ only are possible ($f_1 = 0{,}935 \cdot 50 = 47$ Hz and $f_2 = 0{,}765 \cdot 50 = 38$ Hz); these frequencies are lying greatly over the expectable natural frequencies of the rotating system, and therefore this instability has no influence on the smooth running of the machine discussed. In harmony with experience, it may be stated that if a synchronous machine has a good and symmetrical damperwinding (in our case the two-phase winding-system on the rotor) or in case of normally designed induction machines, self excited oscillations are practically impossible.

Controlled supply frequency

Until now we were dealing with cases in which the machine was connectep to an infinite main of rated frequency. Now we will discuss the behaviour of a frequency controlled machine, with respect to the damping factor. Our starting point is the equation system given by Eqs (7), (8) and (9), but extended to variable input frequencies. The voltage equations are at no load ($\delta = 0$) and at the supply frequency ω: for the stator:

$$\begin{aligned} \Delta U_d &= (p + s_a)\Delta\psi_d - \omega\Delta\psi_q - \psi_q\Delta\omega - Ks_a\Delta\psi_{rd}, \\ \Delta U_q &= \omega\Delta\psi_d + (\psi_q p + s_a)\Delta + \psi_d\Delta\omega - Ks_q\Delta\psi_{ra}, \end{aligned} \tag{18}$$

for the rotor:

$$\begin{aligned} 0 &= (p + s_p)\Delta\psi_{rd} - Ks_p\Delta\psi_d, \\ 0 &= (p + s_p)\Delta\psi_{rq} - Ks_p\Delta\psi_q. \end{aligned} \tag{19}$$

The torque equation is:

$$hp\Delta\omega + \frac{\Delta T}{p} = -\frac{K}{X_{d'}}(\psi_d\Delta\psi_{rq} - \psi_q\Delta\psi_{rd} + \psi_{rq}\Delta\psi_d - \psi_{rd}\Delta\psi_q). \tag{20}$$

To determine of steady-state quantities, before the disturbing torque ΔT has acted, the stator resistance may be neglected, i.e. $\bar{U}_s = j\omega\bar{\psi}_s$; $U_d = -\omega\psi_q$ and $U_q = \omega\psi_d$. At no load is $U_s = U_q = \omega\psi_d$; $U_d = -\omega\psi_q = 0$. The small voltage changes may be calculated as:

$$\Delta U_d = \omega\psi_d \Delta\delta \quad \text{and} \quad \Delta U_q = 0.$$

It may be seen that we suggested that the supply voltage is proportionally varied to the actual supply frequency. From Eqs (18), (19) and (20), by neglecting the third order quantity $s_p \cdot s_a \cdot (1 - k^2)$, for the damping factor we obtain to a very close approximation:

$$d = -\mathrm{Re}\left[\frac{\overline{\Delta T}}{\overline{\Delta\omega}}\right] =$$

$$= 2T_p \frac{s_p(s_p^2 + \Omega^2)\left(\omega^2 - \Omega^2 \dfrac{s_p + s_a}{s_p}\right)\left(\omega^2 - \Omega^2 \dfrac{(s_p + s_a)^2 + \Omega^2}{s_p^2 + \Omega^2}\right)}{4\Omega^2 s_p^2 \left(\omega^2 - \Omega^2 \dfrac{s_p + s_a}{s_p}\right)^2 + (s_p^2 - \Omega^2)^2 \left(\omega^2 - \Omega^2 \dfrac{(s_p + s_a)^2 - \Omega^2}{s_p^2 - \Omega^2}\right)^2} \quad (21)$$

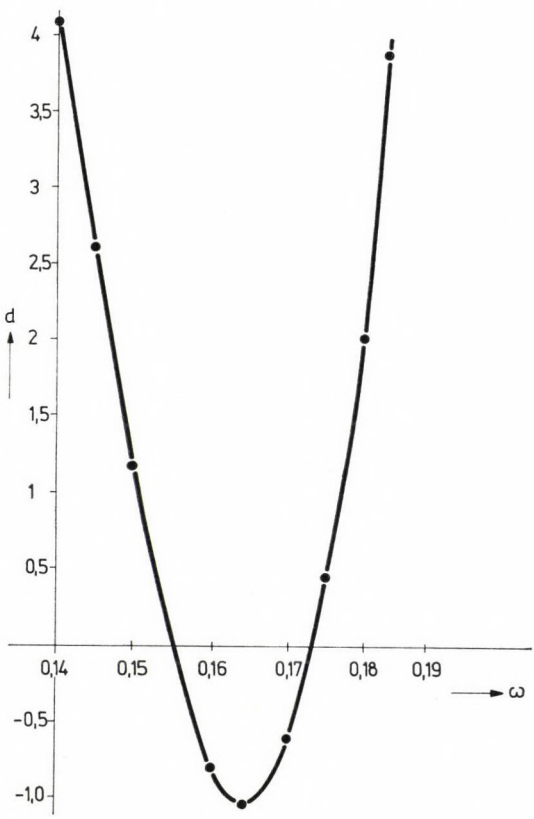

Fig. 1

The denominator of Eq. (21) is always positive (every term is the square of a number). The numerator is a function of the fourth grade, given in a form where the roots are directly available. The zeros are:

$$\omega_1 = \Omega \sqrt{\frac{s_p + s_a}{s_p}},$$
$$\omega_2 = \Omega \sqrt{\frac{(s_p + s_a)^2 + \Omega^2}{s_p^2 + \Omega^2}}. \tag{22}$$

Only positive values of ω are to be taken into account. Taking as a practical example: $s_p = 0{,}15$; $s_a = 0{,}1$ and $\Omega = 0{,}12$, we obtain

$$\omega_1 = 0{,}12 \sqrt{\frac{0{,}25}{0{,}15}} = 0{,}155 \quad \text{and} \quad \omega_2 = 0{,}12 \sqrt{\frac{0{,}25^2 + 0{,}12^2}{0{,}15^2 + 0{,}12^2}} = 0{,}173.$$

The damping factor has in the interval $\omega_1 = 0{,}155$ to $\omega_2 = 0{,}173$ negative values. Under $\omega_1 = 0{,}155$ and over $\omega_2 = 0{,}173$ the damping factor is positive. (See Fig. 1.) This property of frequency control leading to induction machines is since a long time well known [1] and means that the machine is tendenced to perform self-excited oscillations at certain low supply frequencies. Under and over this unstable domain the damping is markedly positive.

Validity limits of superposition method

From Eq. (21), by setting $s_a = 0$ we obtain the damping factor in case of a frequency speed controlled induction machine and stator resistances neglected. That is

$$d_s = 2T_p \frac{s_p}{s_p^2 + \Omega^2}. \tag{23}$$

If the stator resistance is neglected the damping factor is independent of supply frequency.

In case of $R_r = 0$ (rotor resistance neglected), by putting $s_p = 0$ into Eq. (21), we obtain the second component of damping factor in case of supply frequency control. That is:

$$d_r = -2T_p s_a \frac{\omega^2 - s_a^2 - \Omega^2}{(\omega^2 + s_a^2 - \Omega^2)^2 + 4\Omega^2 s_a^2}. \tag{24}$$

Eq. (24) shows that the negative component of the overall damping factor is, in case of frequency speed control, supply frequency dependent. We obtain

by using Eqs (23) and (24) the resultant damping factor as

$$d = d_s + d_r = 2T_p \left(\frac{s_p}{s_p^2 + \Omega^2} - s_a \frac{\omega^2 - s_a^2 - \Omega^2}{(\omega^2 + s_a^2 - \Omega^2)^2 + 4s_a^2\Omega^2} \right) . \qquad (25)$$

Now we are able to compare the results of Eq. (21) and Eq. (25). Both equations are related to induction machines at no-load. In table I are given the

Table I

ω	d Eq. (21)	d Eq. (25)	$\Delta\%$
1	20,3	20,2	−0,5
0,8	20,3	20,2	−0,5
0,6	20,25	20,0	−1,2
0,5	20,2	19,8	−2
0,3	19,4	17,9	−8

values by using Eq. (21) compared with values available from Eq. (25) calculated with machine constants: $s_a = 0{,}1$; $s_p = 0{,}15$; $2T_p = 5$ and $\Omega = 0{,}12$.

From Table I it can be concluded that for the chosen machine constants the superposition method is a fairly good approximation only if the supply frequency is not less than 0,6.

We can summarize that the superposition method, due to its simple calculating demand, is very useful for the fast and fairly precise first inspect of machines from the view-point of self-excited oscillations. This method seems to be advantageous if one should like to evade the use of digital computer in the first instant, and the supply frequency is not less than 0,6.

For higher values of s_a the approximation limit is approaching the supply frequency 0.8.

Self-excited huntings of synchronous machines supplying a passive network

Until now we have discussed oscillation phenomena of synchronous machines connected to an infinite network (the network had a constant 3-phase voltage at constant frequency and of constant phase). It was the general scientific opinion that a synchronous machine supplying a passive (inductive) network is not able to perform oscillations having electromagnetic origin.

In the last years it was discovered that a salient-pole machine of smaller size (on board a ship) driven by a combustion motor as prime mover, without any damper winding, performed self-excited huntings [2] to [4]. This non-desirable hunting of the machine group was fully eliminated by subsequent mounting of a good symmetrical damper on the rotor.

Now we intend to discuss such an operation of a synchronous machine using our general method. In Figure 2 we have plotted the schematic of the electric circuit, while a generator supplies the passive network with the

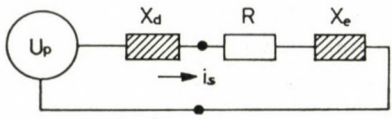

Fig. 2

lumped elements (external reactance: X_e and the load resistance, R which latter includes the internal resistance of the synchronous machine). The voltage equation of this machine at steady-state operation and a suggested three-phase symmetrical load is:

$$\bar{U}_p + \bar{i}_s(R + jX) = 0. \tag{26}$$

In Eq. (26) is $\bar{U}_p = ji_{rd}X_m$, the excitation voltage; and $\bar{i}_s = i_d + ji_q$, the stator current, the reactance $X = X_e + X_d$ is the total reactance of stator circuit.

By separating the real and imaginary parts in Eq. (26) one obtains:

$$\begin{aligned} i_d &= -U_p \frac{X}{R^2 + X^2} = -U_p \frac{X}{Z^2}, \\ i_q &= -U_p \frac{R}{R^2 + X^2} = -U_p \frac{R}{Z^2}. \end{aligned} \tag{27}$$

The linked stator-circuit fluxes at a steady-state operation are:

$$\begin{aligned} \psi_d &= i_d X + i_{rd} X_m = i_d X + U_p \\ \psi_q &= i_q X. \end{aligned} \tag{28}$$

From Eqs (27) and (28) we obtain:

$$\begin{aligned} \psi_d &= U_p \frac{R^2}{Z^2}, \\ \psi_q &= -U_p \frac{RX}{Z^2}. \end{aligned} \tag{29}$$

At a steady-state operation the mechanical shaft power equals the electric output. That is

$$T_m = T_e = \mathrm{Im}(\bar{\psi}_s^* \bar{i}_s) = \mathrm{Im}[(\bar{i}_s^* X + U_p)\, \bar{i}_s] = U_p i_q$$

and using Eq. (27) we obtain

$$T_m = T_e = -\frac{U_p^2}{Z^2} R = -i_s^2 R. \tag{30}$$

One most only take care that, due to our convention, the mechanical driving torque input is negative, and a mechanical loading torque (the machine is operating as a synchronous motor) is positive.

Until the machine runs at a constant speed, no synchronizing torque exists, as the infinite bus has, in the case discussed, no voltage (the voltage of the neutral point of the passive network). But if the machine is beginning to hunt, for any reason, an oscillation-dependent synchronising (and damping) torque may be expected. Namely, at the very instant of a sudden change, the flux linked with the rotor is keeping its position relative to the rotor and its value unchanged. That means, that at the instant of the sudden change the rotor and stator flux linkages are becoming independent and a synchronizing effect between both quantities is developing; for the same reason a damping effect will occur. To check mathematically this phenomenon we will calculate the synchronizing and damping torque in the case of a round rotor machine with a symmetrical rotor winding system supplying a passive network. The general voltage and torque equations in the rotor coordinates are:

$$\begin{aligned} 0 &= \frac{\bar{\psi}_s - K_r \bar{\psi}_r}{X'} R + \frac{d\bar{\psi}_s}{d\tau} + j\omega \bar{\psi}_s, \\ 0 &= \frac{\bar{\psi}_r - K_s \bar{\psi}_s}{X_r'} R_r + \frac{d\bar{\psi}_r}{d\tau}, \\ h \frac{d\omega}{d\tau} &+ T_m = -\frac{K_r}{X'} \mathrm{Im}(\bar{\psi}_s^* \bar{\psi}_r). \end{aligned} \tag{31}$$

In Eq. (31) are the symbols: $X' = X_e + X_d'$; $k_r = X_m/X_r = X_m/(X_m + X_{r1})$; $k_s = X_m/X = X_m/(X_d + X_e) = X_m/(X_m + X_{s1} + X_e)$. We shall introduce the following symbols: $s_a = R/X'$ and $s_p = R_r/X_r'$. For the sake of simplicity we shall assume that the stator and rotor leakage reactances are mutually equal and therefore $X_d = X_r$ and $X_d' = X_r'$. Using the same method, in principle, with which was calculated the speed-response function caused by a small single unit torque impulse, we shall linearize our equations. We will draw the attention that our investigations are equally valid if a small electric power

change occurs in the passive electric circuit, for instance due to a small change in the resistance of the network. Nevertheless we shall assume for the sake of conformity with former investigations that the torque input of the shaft of the synchronous machine suddenly changes by a small torque value ΔT. The only thing we have to consider is that the sign of this small torque change does not influence the overall flow-direction of energy, as the machine is driven by the prime-mover and can supply electrical energy into the passive network only. As in our former calculations we assumed that due to the sudden small torque change, all electric and magnetic quantities are changing by small Δ's, and that the products of these Δ's (of second order) are negligible. Using these premises, from Eq. (31) one obtains in the Laplace-domain:
for the stator voltage equations

$$\begin{aligned} \psi_q \Delta\omega &= (p + s_a)\Delta\psi_d - \omega\Delta\psi_q - s_a K_r \Delta\psi_{rd}, \\ -\psi_d \Delta\omega &= \omega\Delta\psi_d + (p + s_a)\Delta\psi_q - s_a K_r \Delta\psi_{rq}, \end{aligned} \tag{32}$$

and for the rotor voltage equations

$$\begin{aligned} 0 &= (p + s_p)\Delta\psi_{rd} - s_p K_s \Delta\psi_d, \\ 0 &= (p + s_p)\Delta\psi_{rq} - s_p K_s \Delta\psi_q. \end{aligned} \tag{33}$$

In Eqs (32) and (33) the values ψ_d, ψ_q and ω are related to the steady-state operation of a machine, before the sudden torque change occurred. Assuming that the synchronous machine is turning with synchronous speed (rated speed), at a steady-state operation, we can put $\omega = 1$. With these assumptions from Eqs (32) and (33) we may derive the following equations:

$$\begin{aligned} \psi_q \Delta\omega &= f(p)\Delta\psi_d - \Delta\psi_q, \\ -\psi_d \Delta\omega &= \Delta\psi_d + f(p)\Delta\psi_q. \end{aligned} \tag{34}$$

In Eq. (34) is

$$f(p) = p + s_a - \frac{s_a s_p K_r K_s}{p + s_p}.$$

The torque equation is:

$$hp\Delta\omega + \frac{\Delta T}{p} = -\mathrm{Im}(\bar{\psi}_s^* \Delta\bar{i}_s + \Delta\bar{\psi}_s^* \bar{i}_s). \tag{35}$$

The minus sign on the right hand side of Eq. (35) refers to the circumstance that in a machine connected to a passive network, a positive (motoric) torque-change is lowering the speed and at the same time the electric output on the stator side is decreasing too.

Eq. (35) may be written in a real form as:

$$hp\Delta\omega + \frac{\Delta T}{p} = \frac{K_r}{X'}(\psi_d \Delta\psi_{rq} - \psi_q \Delta\psi_{rd} + \psi_{rq}\Delta\psi_d - \psi_{rd}\Delta\psi_q). \tag{35'}$$

By using Eqs (34) and (35') we obtained:

$$hp\Delta\omega + \frac{\Delta T}{p} = \frac{K_r}{X'} \frac{\Delta\omega}{f^2(p)+1} [f(p)(\psi_d\psi_{rd} + \psi_q\psi_{rq}) - (\psi_d\psi_{rq} - \psi_q\psi_{rd}) - a(p)\, f(p)\, \psi_s^2]. \tag{36}$$

In Eq. (36) is:

$$a(p) = \frac{s_p K_s}{p + s_p}.$$

For our further calculations we have taken into account that

a) $-\frac{K_r}{X'}(\psi_d\psi_{rq} - \psi_q\psi_{rd}) = -i_s^2 R = T_0$ (steady-state torque);

b) by using Eq. (29) is: $\psi_s^2 = \psi_d^2 + \psi_q^2 = i_s^2 R^2$ and $\psi_d(K_r\psi_{rd}) + \psi_q(K_r\psi_{rq}) = i_s^2 R^2$.

At last we obtain the hunting impedance — as the response function — of a single torque step. That is:

$$Z_h(p) = \frac{-\Delta T}{p\Delta\omega} = hp + \frac{i_s^2 R}{f^2(p)+1} + \frac{a(p)f(p)K_r}{X'[f^2(p)+1]} i_s^2 R^2 - \frac{f(p)}{X'[f^2(p)+1]} i_s^2 R^2. \tag{37}$$

And in the case of periodically changing torque variation of small amplitude we obtain (for steady-state oscillations):

$$\bar{Z}_h(j\Omega) = \frac{-\overline{\Delta T}}{\overline{\Delta\omega}} = j\Omega h + \frac{i_s^2 R}{f^2(j\Omega)+1} + \frac{a(j\Omega)f(j\Omega)K_r}{X'[f^2(j\Omega)+1]} i_s^2 R^2 - \frac{f(j\Omega)}{X'[f^2(j\Omega)+1]} i_s^2 R^2. \tag{38}$$

Performing further necessary calculations, we obtain

$$\bar{Z}_h(j\Omega) = \frac{-\overline{\Delta T}}{\overline{\Delta\omega}} = \frac{(as_a)^2 - b(b-1)\Omega^2 - 1 + j\Omega(as_a)(2b-1)}{1 + (as_a)^2 - (b\Omega)^2 + j2(as_a)(b\Omega)}. \tag{39}$$

The meaning of symbols a and b are explained further on. Now we can separate the real and imaginary parts in Eq. (39), while the real part is the damping factor and the imaginary part is proportional to the synchronizing torque.

That is

$$\mathrm{Re}[\bar{Z}_h(j\Omega)] = d = i_s^2 R \frac{b^3(b-1)\Omega^4 + b[(as_a)^2(2b-1)+1]\Omega^2 + (as_a)^4 - 1}{[1+(as_a)^2 - (b\Omega)^2]^2 + 4(as_a)^2\,(b\Omega)^2} \tag{40}$$

In Eqs (39) and (40) are

$$a = 1 - K_r K_s \frac{s_p^2}{s_p^2 + \Omega^2},$$
$$b = 1 + K_r K_s \frac{s_p s_a}{s_p^a + \Omega^2}. \tag{41}$$

We have calculated values of damping factor d versus $s_p = R_r/X_r'$. s_p is the characteristic quantity which shows the quality of the damper winding; low values of s_p stand for well designed dampers; high values of s_p interpret poor dampers with high resistance. In Fig. 3 we plotted d vers. s_p using Eqs (40) and (41) at $\cos\varphi = 1 (X_e = 0)$, and therefore $s_a = R/X_d' = 1/0,\ 1/0{,}5 = 6,7$; $K_s = K_r = X_m/X_d = 2{,}2/2{,}27 = 0{,}97$. The curve is plotted for rated output

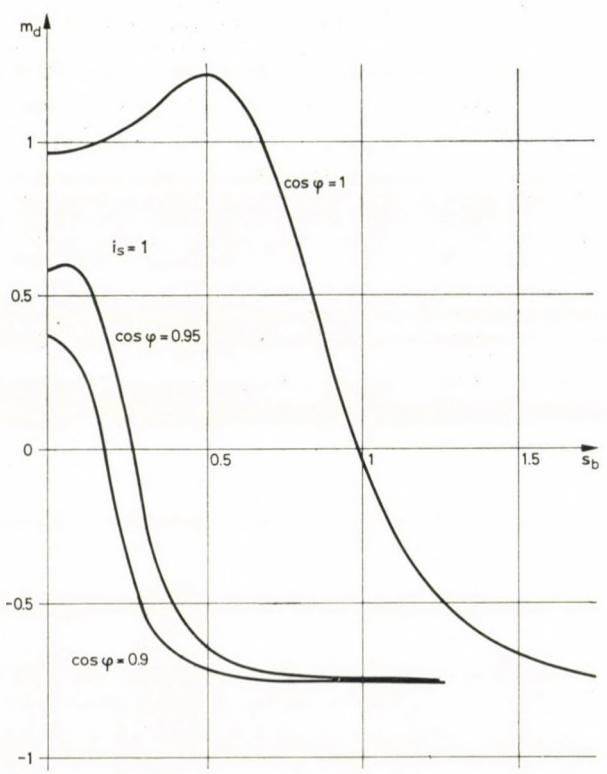

Fig. 3

($i_s^2 R = 1$, at $\cos\varphi = 1$).[1] From Fig. 3 it may be seen that at high values of s_p (the damper is poor), negative values of damping factor may occur the result of which is in harmony with practical experience [2]. It may be stated that even in synchronous generators supplying a passive network, self-excited hunting states are possible. It is worth mentioning that the same calculations may be carried out for other power factors; the only consideration may be that the output at rated current equals the power factor and that $X_e/R = \tan\varphi$; at the same time is $K_s = X_m/(X_e + X_d)$ and $K_r = X_m/X_d$. In Fig. 3 the natural hunting frequency was selected to $\Omega = 0{,}12$ (6 Hz).

REFERENCES

1. G. PFAFF: Regelung Elektrischer Antriebe I. Oldenbourg Verlag München—Wien 1971
2. GEYSEN, W.—JORDAN, H.—KOVÁCS, K. P.—SOÓS, K. V.—VANDENPUT, A.: Anfachung von Drehschwingungen bei Drehstrommaschinen, Wiss. Ber. AEG **51** (1978), 2/3, 139
3. CUPSA, A.—GEYSEN, W.—JORDAN, H.—SOÓS, K. V.—VANDENPUT, A.—WALCARIUS, H.: Stability Analysis of Oscillating Induction Machines, *Acta Techn.* CSAV, No. 5. 1978, 521
4. GEYSEN, W.—JORDAN, H.—VANDENPUT, A.—WALCARIUS, H.: Self-excited and Free Oscillations of an Idealized Synchronous Machine, ICEM 1978 Brussels. *Proceedings* S 1/3—1
5. KOVÁCS, K. P.—JORDAN, H.: Simple Calculating Method of Self-Excited Huntings in Three-Phase Machines. ICEM 1978 Brussels. *Proceedings* S 3/1—1

These References build up only a small part of the related literature.

Pendelungen dreiphasiger Maschinen. Im letzten Jahrzehnt wurde das Problem von selbsterregte Pendelungen synchroner und asynchroner Maschinen der Gegenstand neuer Untersuchungen. Eine neubeobachtete Erscheinung, nämlich die selbsterregte Pendelungen von Synchronmaschinen welche an ein passives Netzwerk angeschlossen sind, gaben neue Aspekte. Dieser Aufsatz befaßt sich mit einer neuen und einfachen Methode für die Berechnung des Dämpfungsfaktors von synchrone und asynchrone dreiphasige Maschinen. Der Dämpfungsfaktor wird in zwei Schritten berechnet: zunächst wird dieser Faktor bei Vernachlässigung des Ständerwiderstandes berechnet; dann berechnen wir den Dämpfungsfaktor vorausgesetzt, daß der Rotorwiderstand null gesetzt werden darf. Der Gesamtdämpfungs faktor wird als die algebraische Summe beider Komponenten berechnet. Wir zeigen, daß diese einfache Methode nur im Bereich von Nennfrequenz eine gute Näherung darstellt. Diese Überlagerungsmethode wird für die Bestimmung Stabilitätsgrenzkurven benützt. Im letzten Teil befassen wir uns mit Pendelungen synchroner Maschinen, die an ein passives Netzwerk angeschlossen sind.

[1] These results are in harmony with the results in paper [2], calculated by another method.

Acta Technica Academiae Scientiarum Hungaricae, Tomus 91 (1—2), pp. 19—55 (1980)

ANALYSE DES VERHÄLTNISSES ZWISCHEN MEMBRAN- UND BIEGESCHNITTKRÄFTEN IN SATTELFÖRMIGEN, FLACHEN, NORMALKRAFTFREI GELAGERTEN HP-SCHALEN UNTER GLEICHMÄßIG VERTEILTER BELASTUNG

L. JANKÓ*

[Eingegangen am 28. Dezember, 1978]

Diese Abhandlung bildet den ersten Teil einer dreiteiligen Artikel-Serie. Der zweite bzw. der dritte Artikel behandeln die Stabilitätserscheinungen der sattelförmigen HP-Schalen, die entlang der Hauptkrümmungslinien durch Randbogen abgestützt sind, die in der horizontalen Richtung vernachlässigbare Biege- bzw. Drillsteifigkeiten besitzen. In der vorliegenden Abhandlung — vor der Stabilitätsuntersuchungen — werden folgende Themen behandelt: das Problem der Existenz und der Eindeutigkeit der *Membranlösung*, die Schwierigkeiten, die sich aus der *kinematischen Unbestimmtheit* der Fläche ergeben, und die Frage, bei welchen geometrischen Parametern (mit guter Annäherung) diese Schalen als *Membranschalen* zu betrachten sind.

Bezeichnungen

$C_{ij} = \cos\frac{i\pi}{2a}x \cdot \cos\frac{j\pi}{2b}y$;

$C_{mn} = \cos\frac{m\pi}{2a}x \cdot \cos\frac{n\pi}{2b}y$;

$D = \frac{Eh}{1-\mu^2}$ spezifische Dehnungssteifigkeit;

E Elastizitätsmodul;
F Spannungsfunktion der Mittelflächenkräfte ($F'' = N_x$, $F' = -N_{xy}$, $F' = N_y$);

$B = \frac{Eh^3}{12(1-\mu^2)}$ spezifische Biegesteifigkeit;

M_x, M_y bzw. $M_{xy} = M_{yx}$ Biege- bzw. Drillmomente;
N_x, N_{xy}, N_y Mittelflächenkräfte;
N_{xb}, N_{xyb}, N_{yb} Mittelflächenkräfte nach der Biegetheorie;
N_{xm}, N_{xym}, N_{ym} Membrankräfte;

$S_{ij} = \sin\frac{i\pi}{2a}x \cdot \sin\frac{j\pi}{2b}y$;

$S_{mn} = \sin\frac{m\pi}{2a}x \cdot \sin\frac{n\pi}{2b}y$;

$2a$, $2b$ Spannweiten der Randbogen in den x- bzw. y-Richtungen;
f_a, f_b Pfeilhöhen der in den x- bzw. y-Richtungen liegenden Randbogen;
h Schalendicke;
i, j Halbwellenzahlen in den x- bzw. y-Richtungen (der Index n weist auf dehnungslose Verformung hin);

* Dr.-Ing. L. JANKÓ, Lajos u. 142. H-1036 Budapest, Ungarn

p Intensität der gleichmäßig verteilten, in Richtung der Achse z wirkenden, symmetrischen Belastung (bezogen auf die Flächeneinheit der Grundrißprojektion);
u, v Verschiebungen in Richtungen der Flächentangenten parallel zur x—z- bzw. y—z-Ebene;
$z(x, y)$; $\bar{z}(\bar{x}, \bar{y})$ Ordinaten der Schalenmittelfläche;
w Verschiebung eines Mittelflächenpunktes in Richtung der Flächennormale ($w = w_0 + \bar{w}$);
$\alpha = f_a/f_b$ Pfeilhöhenverhältnis;
$\beta = a/h$ Schalenparameter;
$\gamma = a/b$ Seitenverhältnis;
η Koordinate in Richtung einer der beiden geraden Erzeugenden vom Punkt $x = a$, $y = b$ (η verläuft parallel zur zweiten Leitebene);
μ Querdehnungszahl (in den Berechnungen: $\mu = 0.2$);
ξ Koordinate in Richtung einer der beiden geraden Erzeugenden vom Punkt $x = a$, $y = b$ (ξ verläuft parallel zur ersten Leitebene);
$\varrho = f_b/b$ Schalenparameter;
ω Hälfte des Winkels zwischen den Leitebenen;
$\Delta\Delta(\ ) = (\ )^{IV} + (\ )^{,,} + (\ )^{::}$ der biharmonische Differentialoperator;
$L_p(f_1, f_2) = f_1'' f_2'' - 2f_1' f_2' + f_1'' f_2''$ der Puchersche-Differentialoperator.

1. Einleitung. Zweckbestimmung

Wegen ihrer gefälligen Form und den günstigen Ausführungsmöglichkeiten, die die geraden Erzeugenden bieten, werden immer häufiger Schalenkonstruktionen in Form des hyperbolischen Paraboloids (im weiteren HP-Schalen) gebaut.

Die HP-Schalen sind im allgemeinen entlang ihren Flächenerzeugenden oder den Hauptkrümmungslinien auf Randträgern gelagert.

Die statischen Probleme der längs der Erzeugenden abgestützten HP-Schalen wurden sowohl nach der Theorie I. Ordnung als auch nach der Theorie II. Ordnung ausführlich erörtert.

Im Falle der sattelförmigen HP-Schalen (Bild 1) jedoch, die entlang der Hauptkrümmungslinien durch Randbogen abgestützt sind, die in der horizontalen Richtung vernachlässigbare Biege- bzw. Drillsteifigkeiten besitzen (im weiteren »normalkraftfreie« oder »halbsteife« Randträger), liegen die Dinge anders. Die Ausarbeitung des (linearen und nichtlinearen) Stabilitätstragverhaltens der erwähnten HP-Schalen steht jedoch aus.

Vor der Stabilitätsuntersuchungen muß man sich beschäftigen jedoch

— mit dem Problem der *Existenz und der Eindeutigkeit der Membranlösung* und
— mit den Schwierigkeiten, die sich aus der *kinematischen Unbestimmtheit* der Fläche ergeben, sowie
— mit der Frage, bei welchen geometrischen Parametern diese Schalen mit guter Annäherung als *Membranschalen* zu betrachten sind.

Bekanntlich wurde das Membrankräftespiel der sattelförmigen, an ihren Rändern normalkraftfreien HP-Schalen durch Erschaffung der sog. »geomet-

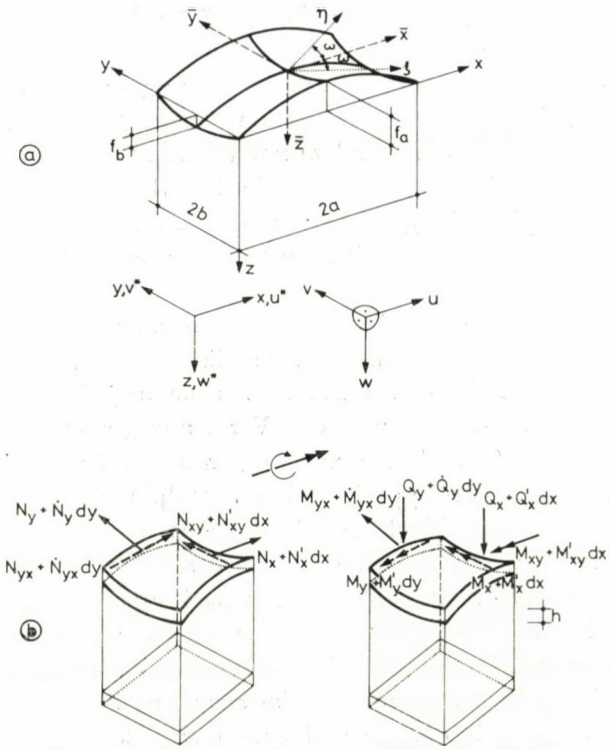

Bild 1. Geometrische Angaben der sattelförmigen HP-Schale. Vorzeichenregel der inneren Kräften und der Verschiebungen

rischen« Theorie von AIMOND untersucht. Nach dieser Theorie, die unstätigen Lösungen bietet, sind die Membrankräfte der HP-Schalen mit bestimmten geometrischen Verhältnissen hinreichend genau zu bestimmen.

Im Hinblick darauf, daß eine eindeutige Membranlösung nur für die HP-Schalen mit bestimmten speziellen Verhältnissen f_a/f_b existiert, und daß auch Störungsmomente längs der Ränder immer auftreten, mußten die Beanspruchungen der erwähnten HP-Schalen auch *nach der Biegetheorie* untersucht werden. Für die flachen Schalen gab HRUBAN [11] die grundlegenden Zusammenhänge zur Bestimmung der inneren Kräfte und der Verformungen nach der Biegetheorie an.

Er bestimmte nicht das ganze Biegekräftespiel, sondern nur die Randstörungseffekte. HRUBAN nahm an, daß der Verformungszustand in den Schnitten parallel zu den Rändern unverändert ist. Er schlug vor, daß die Randstörungen von flachen Schalen über Rechteckgrundriß an einem »Schmiegezylinder« gleicher Querkrümmung und drehsymmetrischer Störung berechnet werden sollen. In der drehsymmetrischen belasteten Ersatz-Kreiszylinderschale treten in Ringrichtung konstante Ringkräfte auf. Deswegen wird in jedem

Fall Seitendruck auf die senkrecht zu den gestörten Rändern liegenden Ränder abgetragen.

Dieser Wiederspruch wurde durch die Lösung von TARNAI [22] beseitigt. In dieser Lösung ist der erwähnte Verformungszustand längs des gestörten Randes veränderlich. Aus den von TARNAI veröffentlichten Ergebnissen folgt, daß die Hrubansche Näherung auch bei flachen Schalen mit anderen Grundrissen für praktische Zwecke gut angewendet werden kann, vorausgesetzt, daß die Hauptkrümmungslinien parallel und quer zum gestörten (im Grundriß geraden) Rand verlaufen.

Von BELEŞ und SOARE [1] stammen die Funktionen der inneren Kräfte der sattelförmigen, an ihren Rändern normalkraftfreien, gleichmäßig belasteten HP-Schalen. Mit Hilfe dieser Funktionen ist in jedem Punkt der Schale sowohl der Spannungs-, als auch der Verformungszustand zu bestimmen.

Tatsache ist, daß im Zusammenhang mit der Stabilität der an ihren Rändern normalkraftfreien hyperbolischen Sattelparaboloidschalen nur einige Ergebnisse zu finden sind. Nach Ansicht des Verfassers erklärt sich dies einerseits aus dem Problem der *Existenz und der Eindeutigkeit der Membranlösung*, und anderseits aus den Schwierigkeiten, die sich aus der *kinematischen Unbestimmtheit* der Fläche ergeben. Aus den erwähnten Gründen werden vor den Stabilitätsuntersuchungen zuerst *die Schalenparametersbereiche ermittelt*, in welchen der Effekt der *Biege- und Drillmomente* im Vergleich zum Effekt der Mittelflächenkräfte nach der Biegetheorie *vernachlässigbar* klein ist. Unter solchen geometrischen Verhältnissen genügt es die HP-Schalen bloß nach der Membrantheorie zu bemessen. Im gegebenen Fall muß man sich mit den Biegeeffekten nur in den Randbereichen beschäftigen.

In solchen Fällen ist es richtig auch den Verlauf des Stabilitätsverlustes nach der »linearen« Stabilitätstheorie zu untersuchen unter dem Titel: *Verzweigung*. Das ist das Thema des folgenden Artikels vom Verfasser [12], das sich auf die vorliegende Arbeit stützen wird.

Die Schalen, von welchen es sich in dieser Abhandlung herausstellt, daß sie den überwiegenden Teil ihrer Belastungen durch Biegeschnittkräfte tragen, werden in einer späteren Veröffentlichung *nach der Theorie von großen Verformungen* untersucht [13].

Zur Erleichterung der praktischen Anwendung sind die zur Bemessung gut geeigneten Resultate in Formeln und Schaubilder sowie Tabellen dargestellt.

2. Die geometrischen Verhältnisse der Fläche

Werden als die drei Koordinatenachsen die durch den Schalenmittelpunkt ($\bar{x} = 0, \bar{y} = 0$) durchgehenden zwei Erzeugenden (ξ, η) und die $\bar{z}$-Achse (die Schnittlinie der Leitebenen) gewählt, so ist es möglich, die Gleichung der

Fläche in diesem »birektangularen« Koordinatensystem [3] wie folgt aufzuschreiben:

$$\bar{z} = k\xi\eta. \tag{2.1}$$

Die Konstante k (Einheitsverwölbung), welche die spezifische Steilheit der Schale kennzeichnet, ist aus dem Zusammenhang

$$k = \frac{4f_a}{a^2}\cos^2\omega \tag{2.2}$$

zu bestimmen. Der Winkel 2ω *zwischen den Leitebenen* ($\xi, \bar{z}$ bzw. $\eta, \bar{z}$) wird durch die Formel

$$\tan^2\omega = \frac{b^2}{a^2}\frac{f_a}{f_b} \tag{2.3}$$

berechnet.

Das hyperbolische Paraboloid enthält zwei *gerade Systeme der Erzeugenden* (die sog. Asymptotenlinien, deren Projektionen die durch die Gleichung $\bar{y} = \pm \tan\omega\,\bar{x} + c$ definierten Charakteristiken sind). Jeder von ihnen ist parallel zu einer der Leitebenen.

Die beiden *Leitebenen* können miteinander beliebige Winkel 2ω bilden.

Die winkelhalbierenden Ebenen der Leitebenen (die Ebenen $\bar{x} = 0$, bzw. $\bar{y} = 0$) schneiden Parabeln aus der Fläche aus. Diese Hauptparabeln wölben sich teils nach oben, teils nach unten, d. h. die Fläche ist umgekehrt zweimal gekrümmt (»antiklastisch«). Jeder der übrigen ebenen Schnitten und deren Projektionen auf die Ebene $\bar{z} = 0$ sind Hyperbeln. Die zu der Achse $-\bar{z}$ parallelen Schnitte sind Parabeln, bzw. wenn sie auch zu den Leitebenen parallel sind, arten sie in ein gerades Erzeugendenpaar aus.

In jedem Punkt negativer Gaußscher Krümmung ($1/R_1R_2 < 0$) gibt es zwei reelle und verschiedene Asymptotenrichtungen.

Auf Grund des Besagten kann die Schale, als Translationsfläche, durch Bewegung der zur Ebene $\bar{x} = 0$ parallelen Hauptparabel auf der zur Ebene $\bar{y} = 0$ parallelen inversen Hauptparabel, wie folgt, abgeleitet werden:

$$\bar{z} = \frac{f_a}{a^2}\bar{x}^2 - \frac{f_b}{b^2}\bar{y}^2. \tag{2.4}$$

Diese Abhandlung verwendet die auf flache Schalen bezügliche Schalentheorie.

Wie bekannt, bedeutet geometrisch *die Annahme der Flachheit*, daß die Metrik der Fläche mit der euklidischen (ebenen) Metrik identisch angenommen werden kann, und daß die geodetischen Krümmungen der Fläche infolge ihrer Kleinheit vernachlässigt werden können.

Die Flachheit kann geometrisch mit Hilfe der Richtungstangenten der Fläche, wie folgt, definiert werden:

$$z'^2 \ll 1, \quad z^{\cdot 2} \ll 1, \quad z'z^{\cdot} \approx 0. \tag{2.5ac}$$

3. Die dehnungslose Verformung

Eine besondere Beachtung verdient die dehnungslose Formänderung, die ohne Dehnung und Winkelverzerrung der Schalenfläche in beiden Richtungen (x, y) zustandekommen kann, der gegenüber also die Schale außerordentlich »weich« ist. An dieser Stelle muß auf diese spezifische Eigenheit der hyperbolischen Schalen eingegangen werden, weil dies deren *Stabilität* in gewissen Fällen beeinflussen kann. Die dehnungslose Verformung beschränkt sich auf eine Verkrümmung und Verwindung, und so kommt nur die Biege-, nicht aber die Membransteifigkeit der Schale zur Geltung.

Wenn die Biegesteifigkeit der Schale vernachlässigt wird, ist es bei gewissen geometrischen Verhältnissen und Randbedingungen möglich, daß die Schale ohne Widerstand zur Verformung fähig ist.

Wlassow [25], [26] ermittelte *die statischen Kriterien* der Entstehung der labilen Mechanismen bezogen auf die membranen Rotationsschalen. Durch diese bestimmt er jene Umstände, unter welchen unendlich große innere Kräfte in gewissen Konstruktionen mit bestimmten Geometrie- und Lagerungsverhältnissen infolge beliebiger kleiner endlicher Belastung entstehen.

Geyling [6] stellte die Differentialgleichung der dehnungslosen Verformung dadurch auf, daß er in den allgemeinen Formänderungsgleichungen der Membranschale [2], [6] die inneren Kräfte gleich Null setzte:

$$L_p(w, z) = 0. \tag{3.1}$$

Der Zusammenhang (3.1) stammt aus einer Verträglichkeitgleichung und daher kann daraus das *kinematische Kriterium* der dehnungslosen Verformung abgeleitet werden. Die Gleichung (3.1) bestimmt also unter welchen Bedingungen sich die Schale auch ohne innere Kräfte verformen kann.

Kollár [15] setzte die Biegesteifigkeit und die Spannungsfunktion der Schale in den auf die flachen Schalen bezogenen homogenen Gleichungen gleich Null. Als Endergebnis erhielt er die Differentialgleichung der behandelten Erscheinung.

Haas [10] leitete die Gleichung $L_p(w, z) = 0$ unmittelbar aus den Ausdrücken der Verformungselemente (Verzerrungen) der Mittelfläche ab.

Somit kann die Differentialgleichung der dehnungslosen Verformung bezogen auf die sattelförmigen, an ihren Rändern normalkraftfreien HP-

Schalen mit den entsprechenden Randbedingungen wie folgt, aufgeschrieben werden:

$$\frac{2f_a}{a^2} w^{\cdot\cdot} - \frac{2f_b}{b^2} w'' = 0, \tag{3.2}$$

$$w = 0, \quad \Big|_{\substack{x=0 \\ x=2a}} \tag{3.3a–b}$$

$$w = 0. \quad \Big|_{\substack{y=0 \\ y=2b}} \tag{3.3c–d}$$

Im Hinblick darauf, daß in den Gleichungen (3.1), bzw. (3.2) die Biegesteifigkeit der Schale vernachlässigt wurde, wird der Wert der Verdrehung an den Rändern entlang nicht festgelegt, denn die vollkommen elastische Membran kann jeder am Rand entstehenden Verdrehung ohne Widerstand folgen. Daraus folgt, daß die Randbedingungen bezogen auf $w^{||}$ und $w^{\cdot\cdot}$ entfallen.

Um die erwähnten Schalen gründlich untersuchen zu können, müssen wir vor allem die Frage stellen: bei welchen Randbedingungen und Schalengleichungen es eine eindeutige Lösung der partiellen Differentialgleichung hyperbolischen Typs (3.1) im Inneren des untersuchten Bereiches gibt. Die Antwort darauf gab TARNAI [21].

Er bewies anhand der Theorie der partiellen Differentialgleichungen [7], [14], [19], [24], daß *an drei Randstrecken* des Rechteckbereiches im Bild 1a *insgesamt vier* Randbedingungen angegeben werden müssen, damit eine eindeutige Lösung der Gleichung (3.2) existieren kann. Im allgemeinen Fall kann die partielle Differentialgleichung hyperbolischen Typs (3.2) nur bei auf *offenen* Randkurven vorgeschriebenen Randwerten eine eindeutige Lösung haben. Falls z. B. an den Rändern $x = 0$ und $x = 2a$ die Bedingung $w = 0$, weiterhin am Rand $y = 0$ die Bedingungen $w = 0$ und $\dot{w} = 0$ vorgeschrieben werden, so hat die Gleichung (3.2) die Lösung $w = 0$ [8], [10], [15], [21]. Die Aufgabe ist unter solchen Umständen *mathematisch korrekt* (die Lösung existiert, nur eine Lösung existiert und diese hängt stetig von den Randbedingungen ab). Aus dem Besagten folgt, daß man beim Vorschreiben von Randbedingungen (3.3 a—d) damit rechnen muß, daß wenn es auch eine Lösung existiert, die *nicht eindeutig* ist.

Die Charakteristiken der Gleichung (3.2) sind die Geradenscharen der Gleichung

$$y = \pm \tan \omega x + C_0 \tag{3.4}$$

die mit den Charakteristiken der Differentialgleichung des hyperbolischen Paraboloids zusammenfallen.

Man soll die Lösung der Eigenwertprobleme (3.2)—(3.3) mit Hilfe der Fourierschen Methode suchen [7], [19], [24].

Setzt man den Produktenansatz

$$W(x, y) = X(x)\ Y(y) \tag{3.5}$$

in die Gleichung (3.2) ein, so erhält man die gewöhnlichen Differentialgleichungen

$$Y'' + \frac{d^2}{\tan^2 \omega} Y = 0,$$

$$X'' + d^2 X = 0.$$

Hier ist d der gesuchte Eigenwert.

Ihre allgemeine Lösungen stellten die trigonometrischen Funktionen

$$Y = C_1 \sin \frac{d}{\tan \omega} y + C_2 \cos \frac{d}{\tan \omega} y, \tag{3.6a—b}$$

$$X = C_3 \sin dx \qquad + C_4 \cos dx$$

dar. Unter Beachtung der Randbedingungen (3.3a) und (3.3c) ergeben sich

$$C_4 = 0,$$
$$C_2 = 0. \tag{3.7a—b}$$

Drücken wir den Eigenwert d sowohl aus der Gleichung (3.3b) als auch aus der Gleichung (3.3d), so erhalten wir

$$d^2 = \frac{i_n^2 \pi^2}{4a^2} = \frac{j_n^2 \pi^2}{4b^2} \tan^2 \omega. \tag{3.8}$$

In diesen Ausdrücken sind $i_n = 1, 2, 3, \ldots$, bzw. $j_n = 1, 2, 3, \ldots$, die Anzahl der Halbwellen der Durchbiegungsfunktion w in den Richtungen x bzw. y.

Setzt man den Zusammenhang (2.3) in die Gleichung (3.8) ein, so läßt sich *das kinematische Kriterium der* dehnungslosen Verformungsmöglichkeit der an ihren Rändern normalkraftfreien Schale in Form eines hyperbolischen Sattelparaboloids in folgender Form aufschreiben:

$$i_n^2 = \frac{f_a}{f_b} j_n^2. \tag{3.9}$$

Daraus ist klar ersichtlich, daß der Charakter der dehnungslosen Verformung durch das Verhältnis f_a/f_b bestimmt wird. Mit Rücksicht darauf, daß die

Größen i_n und j_n nur ganze Zahlen sein können, kann die dehnungslose Verformung nur dann zustande kommen, wenn das Verhältnis f_a/f_b *dem Quadrat einer rationellen Zahl gleich ist.* Es soll bemerkt werden, daß sich die rationellen Zahlen i_n, j_n unter den reellen Zahlen »häufig« befinden (eine Menge von zählbaren unendlichen Elementengruppen) und so existiert eine dehnungslose Verformung praktisch in der Nähe jedes Verhältnisses f_a/f_b.

Die Wellenzahlen sind aber in den meisten Fällen sehr groß, darum zeigt sich die Schale in diesen Fällen mit großen Wellenzahlen als starr (vgl. noch mit dem Fall, wenn $B \neq 0$ ist.)

Das Kriterium (3.9) bedeutet auch, daß wenn die Schale an allen vier Rändern durch normalkraftfreie (»halbstarre«) Randträger versteift ist, dann kann sie sich bei den Krümmungsverhältnissen

$$\frac{R_y}{R_x} = -\frac{i_n^2}{j_n^2}\frac{b^2}{a^2} \tag{3.10}$$

dehnungslos verformen.

Letzten Endes erhalten wir für die Durchbiegungsfunktion w den Ausdruck

$$w = \sum_{i_n}\sum_{j_n} w_{i_n j_n} S_{i_n j_n}. \tag{3.11a}$$

Hier ist:

$$S_{i_n j_n} = \sin\frac{i_n \pi}{2a}x \cdot \sin\frac{j_n \pi}{2b}y. \tag{3.11b}$$

Wie es zu erwarten war, ist die Lösung *nicht eindeutig*, da die Koeffizienten $w_{i_n j_n}$ unbestimmte Größen sind. Die hier soeben erörterte dehnungslose Verformung erfordert an den Rändern der im Bild 1 dargestellten sattelförmigen HP-Schale *waagerechte Verschiebungen* (u, v), die die »Halbstarren« Endscheiben bzw. Randbogen auch zulassen.

Auch auf Grund der Analyse der Gleichungen (2.3) und (3.9) läßt sich folgendes einsehen: wenn man für alle Ränder die Bedingung $w = 0$ vorschreibt (d. h. die Randträger *nur in ihrer eigenen Ebene* gegen Biegung unendlich steif sind), dann kommt es in den Fällen zu dehnungslosen Verformungen, in denen man von einem Randpunkt ausgehend, längs eines geschlossenen Streckenzuges der Erzeugenden mit einer endlichen Zahl von »Reflexionen« an den Rändern zum Ausgangspunkt zurückkehren kann. Diese Feststellung ist mit dem Namen von GEYLING [6] verbunden.

Wie wohl bekannt, lautet die Bedingung der Anwendbarkeit der *Aimondschen geometrischen Theorie* (bezogen auf die Bestimmung des Membrankräftespieles) genauso.

Die Verbindung zwischen der Existenz der Membranlösung und der Möglichkeit der dehnungslosen Verformungen wird ausführlich im Abschnitt 4. erörtert.

Dort wird auch darauf verwiesen, daß wenn die geometrischen Verhältnisse der Konstruktion (f_a/f_b) die Bildung irgendeiner sinusförmigen Durchbiegungsfläche ermöglichen, dann läßt sich die *gleichförmige* Belastungskomponente allein durch Membrankräfte nicht in Gleichgewicht halten.

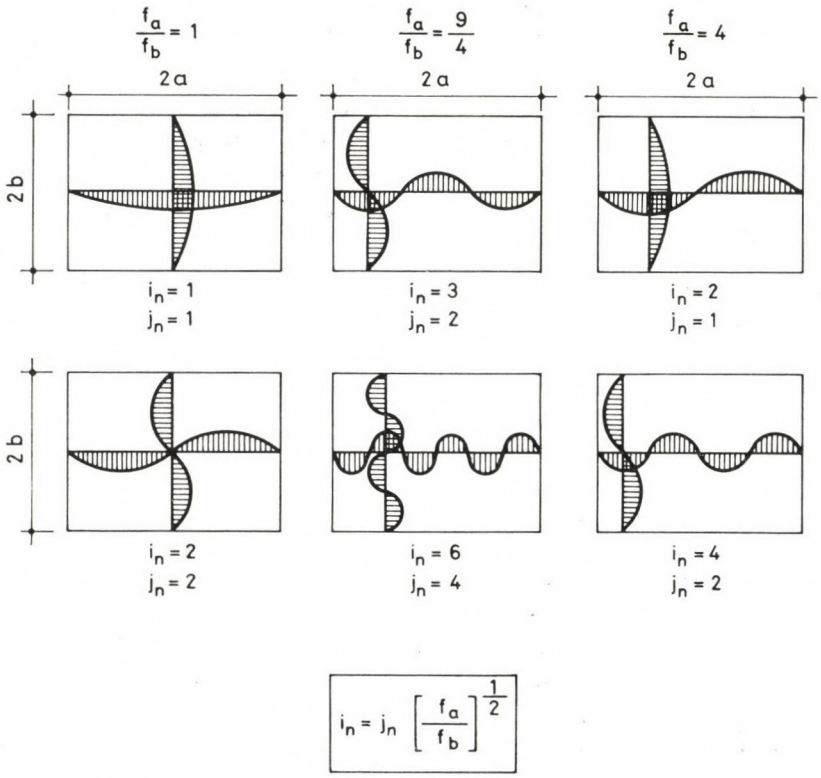

Bild 2. Charakteristische dehnungslose Verformungen

Die Tafel I und das Bild 2 bieten ein anschauliches Bild über den Charakter der dehnungslosen Verformungsfunktionen der an Rändern normalkraftfreien, sattelförmigen HP-Schalen mit verschiedenen f_a/f_b-Verhältnissen.

Beachtenswert ist, daß die dehnungslose Verformung der entlang der Charakteristiken abgestützten HP-Schalen durch die für zwei anschließende Ränder vorgeschriebene Bedingung $w = 0$ völlig verhindert wird [15], [21] (Goursatsches Problem).

Tafel I

$\frac{f_a}{f_b}$	$\left(\frac{f_a}{f_b}\right)^{\frac{1}{2}}$	j_n	i_n
1	1	1, 2, 3, . . .	1, 2, 3, . . .
$\frac{121}{100} = 1{,}21$	$\frac{11}{10}$	10, 20, 30, . . .	11, 22, 33, . . .
$\frac{25}{16} = 1{,}5625$	$\frac{5}{4}$	4, 8, 12, . . .	5, 10, 15, . . .
$\frac{16}{9} = 1{,}77\ldots$	$\frac{4}{3}$	3, 6, 9, . . .	4, 8, 12, . . .
$\frac{49}{25} = 1{,}96$	$\frac{7}{5}$	5, 10, 15, . . .	7, 14, 21, . . .
$\frac{9}{4} = 2{,}25$	$\frac{3}{2}$	2, 4, 6, . . .	3, 6, 9, . . .
$\frac{25}{9} = 2{,}77\ldots$	$\frac{5}{3}$	3, 6, 9, . . .	5, 10, 15, . . .
$\frac{49}{16} = 3{,}0625$	$\frac{7}{4}$	4, 8, 12, . . .	7, 14, 21, . . .
$\frac{81}{25} = 3{,}24$	$\frac{9}{5}$	5, 10, 15, . . .	9, 18, 27, . . .
4	2	1, 2, 3, . . .	2, 4, 6, . . .

4. Existenz und Eindeutigkeit der Membranlösung

Mit Rücksicht darauf, daß in der Fachliteratur ein entsprechendes Wissensgut zur Bestimmung der Membrankräften zur Verfügung steht, wollen wir uns in diesem Abschnitt in erster Reihe mit den *Existenz- und Eindeutigkeitsbedingungen* befassen. Überdies wird auf die Verbindung zwischen der Existenz der eindeutigen Membranlösung und der *dehnungslosen Verformungsmöglichkeit* verwiesen.

Zu den weiteren Erörterungen schreiben wir die Puchersche Differentialgleichung — vorausgesetzt, daß auf die Schale nur vertikale Lasten $p(x, y)$ einwirken — in kartesischen Grundrißkoordinaten auf:

$$L_p(F, z) = -p(x, y). \tag{4.1}$$

Mit der Existenz und Eindeutigkeit der Lösung der Differentialgleichung (4.1) ist dieselbe Schwierigkeit verbunden, die bei der Erörterung der Gleichung (3.2) schon erwähnt wurde. Wir können also die Frage stellen, ob und unter

welchen Bedingungen bei einer normalkraftfreien Lagerung (wo die Randbogen bloß Membranschubkräfte aufnehmen können) ein Membranzustand möglich ist.

Auf den drei Randabschnitten des Rechteckbereiches (dargestellt im Bild 1) muß man insgesamt vier Bedingungen angeben (z. B. sei der Rand $x = 0$ volkommen frei und die Ränder $y = 0$ und $y = 2b$ seien normalkraftfrei), damit eine eindeutige Lösung der Differentialgleichung (4.1) — auch bei beliebigen Werten der Parametern in Gl. (4.1) — existieren kann (TARNAI [21]).

Die Randbedingungen

$$F'' = 0, \quad \Big|_{\substack{x=0 \\ x=2a}} \qquad F^{\text{II}} = 0 \quad \Big|_{\substack{y=0 \\ y=2b}} \tag{4.2a–d}$$

des Problems schreiben für jeden der vier Ränder je eine Normalkraft vor. Darum *läßt sich nicht* bei allen geometrischen Verhältnissen eine *eindeutige Membranlösung erwarten.*

Falls die auf die Ebenen $\bar{x} = 0$ und $\bar{y} = 0$ symmetrische Last $p(x, y) = p = \text{konst.}$ in eine doppelte Fouriersche Reihe entwickelt wird (s. (5.5)), so kann eine die Randbedingungen (4.2a–d) erfüllende analytische Lösung der Gleichung (4.1) mit der unendlichen Reihe

$$F = -\frac{32}{\pi^4} p \frac{a^2 b^2}{f_b} \sum_m \sum_n \frac{1}{mn} \frac{1}{m^2 - \alpha n^2} S_{mn} \tag{4.3}$$

$$m = 1, 3, 5, \ldots, M$$

$$n = 1, 3, 5, \ldots, N$$

angegeben werden.

In diesem Ausdruck besitzt die Funktion S_{mn} den gleichen Aufbau wie die Funktion S_{ij} (vgl. (3.11b) mit (5.10a)). Der Parameter $\alpha = f_a/f_b$ bedeutet das Verhältnis der Pfeilhöhen.

Anhand der Gleichung (4.3) stellt sich heraus, daß die Membranlösung im allgemeinen nicht möglich ist, weil der zu den bestimmten Zahlpaaren m, n gehörige, endliche symmetrische Lastanteil in den Fällen

$$\alpha = \frac{f_a}{f_b} = \frac{m^2}{n^2} \tag{4.4}$$

$$m = 1, 3, 5, \ldots, M$$

$$n = 1, 3, 5, \ldots, N$$

bloß durch unendlich große Membrankräfte in Gleichgewicht gehalten werden könnte [1], [5], [16], [17], [20].

Diese Feststellung steht mit den Ergebnissen der Aimondschen »geometrischen« Theorie in Einklang. Laut dieser Theorie läßt sich nur bei bestimmten f_a/f_b-Verhältnissen eine Lösung finden, aber das Spannungsbild wird in der Schale unstetig (diskontinuierlich) sein.

Die »geometrische« Theorie nützt die spezielle Eigenschaft der HP-Schalen aus, daß der Wert der Spannungsfunktion bei vertikaler Belastung für je einen Punkt auf jeder Charakteristik beliebig vorgeschrieben werden kann.

Dies bedeutet statisch, daß Normalkräfte entlang dieser Erzeugenden (asymptotischen Linien) unverändert vom einen Rand zum anderen weitergeführt werden können. Die Existenz des Membrankräftespieles hängt nach der »geometrischen« Theorie davon ab, auf welche Art die auf den Rand $x = 0$ wirkende Kraft $N_x \cdot dy$ mit Hilfe der Erzeugenden, durch »Reflexionen«, zu den anderen Rändern hinübergelangen kann (Bild 3).

Ist das Verhältnis der beiden Pfeilhöhen f_a und f_b dem Quadrat einer geraden Zahl gleich (Tafel II, Zeile 2):

$$\frac{f_a}{f_b} = 2^2, 4^2, 6^2, \ldots$$

so *treffen sich* am Rand $x = 2a$ *zwei Zugdiagonalen* [5], [16]. Es entstehen also an diesem Rand nur Schubkräfte. Die ausgleichende Kraft dieser Zugdiagonalkräfte ist die Gegenkraft zu $N_x \cdot dy$.

Daraus folgt, daß wenn man den inneren Kräften des Grundträgers (s. Bild 3. oben) — der die Flächenlast allein durch reine Bogenwirkung trägt — die inneren Kräfte, die aus den Gegenkräften der entlang den Rändern $x = 0$ und $x = 2a$ auftretenden Reaktionen entstehen, überlagert, dann wird jeder Randträger die Lasten bloß durch Schubkräfte tragen. Bei der »normalen« HP-Schale (»voile normal«, $f_a/f_b = 4$) sind diese Schubkräfte an den Rändern $x = 0$ und $x = 2a$ gleich Null.

Wenn

$$\frac{f_a}{f_b} = 1^2, 3^2, 5^2, \ldots; \left(\frac{5}{3}\right)^2, \quad \left(\frac{7}{5}\right)^2, \ldots$$

beträgt, *so sind die* erwähnten *Erzeugenden gedrückt.* In diesem Fall ist es also nicht möglich, die Randnormalkräfte auf Kosten der Randschubkräfte zu beheben.

Unter solchen Umständen kann die an den Rändern normalkraftfreie Schale bloß die Last durch Membrankräfte tragen, die *antimetrisch* auf die Ebene $\bar{x} = 0$ oder $\bar{y} = 0$ ($m = 2, 4, 6, \ldots$ oder $n = 2, 4, 6, \ldots$) ist. (Tafel II, Zeile 1)

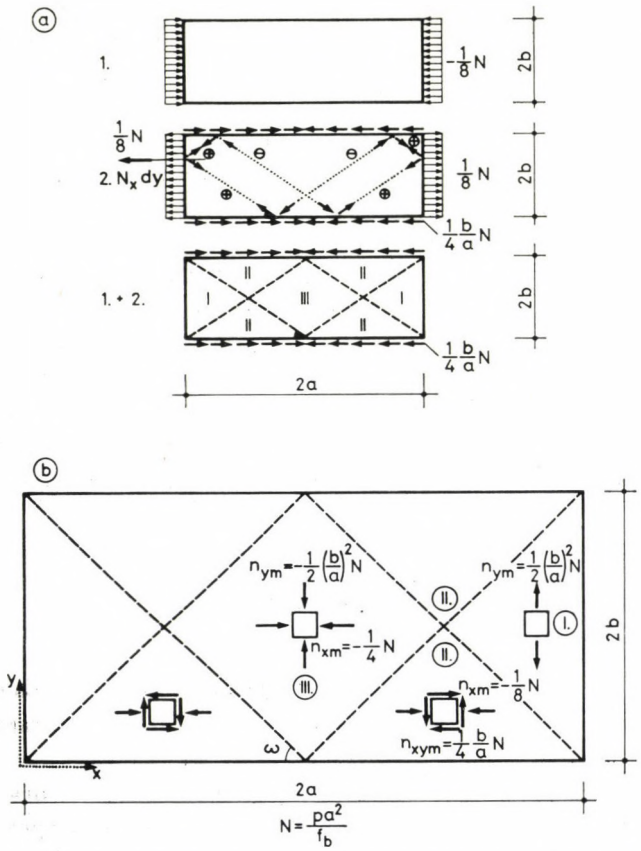

Bild 3. Membrankräfte der »normalen« HP-Schale (»voile normale«)

Falls das Verhältnis f_a/f_b von den Quadraten der rationellen Zahlen abweicht (Tafel II, Zeile 3), so trifft sich am Rand $x = 2a$ jede ***Zugdiagonale*** mit je einer ***Druckdiagonale:*** es entstehen also auch an diesem Rand nur Schubkräfte.

Somit können diese Schalen bei Schubkraftstützung der Ränder für alle Lastfälle im Membrangleichgewicht bleiben (die Last kann sowohl symmetrisch als auch antimetrisch auf die Ebene $\bar{x} = 0$ bzw. $\bar{y} = 0$ wirken).

Wie wohl bekannt, sind die vorangehenden Lösungen unstetig aber eindeutig.

Es sei bemerkt, daß der in der Zeile 3 der Tafel II dargestellte Fall nicht aus der »geometrischen« Theorie, sondern aus der Gleichung (4.4) folgt. Der Grund hiefür liegt darin, daß »Reflexionen« mit einer endlichen Zahl nur dann möglich sind, wenn das Verhältnis f_a/f_b dem Quadrat der rationellen Zahlen gleich ist (vgl. mit (2.3)). Auf Grund des Zusammenhanges (4.4) ist eine

Tafel II

	$\frac{f_a}{f_b}$	Membranlösung existiert: + nicht existiert: −			Dehnungslose Verformung existiert: + nicht existiert: −
		p: symmetrisch $m = 1, 3, 5, \ldots$ $n = 1, 3, 5, \ldots$	p: antimetrisch $m = 2, 4, 6, \ldots$ $n = 1, 3, 5, \ldots$	p: antimetrisch $m = 1, 3, 5, \ldots$ $n = 2, 4, 6, \ldots$	
1.	$1^2, 3^2, 5^2, \ldots$ $\left(\frac{5}{3}\right)^2, \left(\frac{7}{5}\right)^2, \ldots$	−	+	+	+ $i_n = 1, 3, 5, \ldots$ $j_n = 1, 3, 5, \ldots$
2.	$2^2, 4^2, 6^2, \ldots$	+	−	+	+ $i_n = 2, 4, 6, \ldots$ $j_n = 1, 2, 3, \ldots$
3.	$2, 3, 5, 6, \ldots$ $\frac{3}{2}, \frac{5}{3}, \ldots$	+	+	+	−
4.	$\left(\frac{4}{3}\right)^2, \left(\frac{6}{5}\right)^2, \ldots$	+	−	+	+ $i_n = 4, 6, \ldots$ $j_n = 3, 5, \ldots$
5.	$\left(\frac{3}{2}\right)^2, \left(\frac{5}{2}\right)^2, \ldots$	+	+	−	+ $i_n = 3, 5, \ldots$ $j_n = 2, 4, \ldots$

Membranlösung auch dann möglich, wenn das Verhältnis f_a/f_b einer irrationellen Zahl gleich ist.

Anhand der Bedingung (3.9) ist in der Tafel II auch dargestellt, bei welchen Verhältnissen f_a/f_b die Schale zur dehnungslosen Verformungen fähig ist.

Die Ergebnisse in Tafel II stehen mit unserer Anschauung in Einklang: wenn irgendeine Lastkomponente $p_{mn}(x, y)$ durch Membrankräfte mit endlichen Größen nicht in Gleichgewicht gehalten werden kann, dann *ist* die Schale *zu einer dehnungslosen Verformung* $w_{i_m i_n}(x, y)$ in Form des erwähnten Lastgliedes $p_{mn}(x, y)$ *fähig*.

Die Grundlage der besagten Behauptung ist der *Sturm—Liouvill*sche Satz [7] (oder im Bereich der Integralgleichungen der *Fredholm*sche Alternative-Satz [7]).

Dies besagt, bezogen auf die Differentialgleichungen mit homogenen Randbedingungen (s. die Gln. (3.2)—(3.3) bzw. (4.1)—(4.2)): wenn die *homogene* Differentialgleichung (s. (3.2)) bei einem bestimmten Parameter (in unserem Fall: Eigenwert) eine eindeutige Lösung hat, dann hat die entsprechende *inhomogene* Differentialgleichung (s. (4.1)) — bei *demselben* Parameter — keine Lösung.

5. Die inneren Kräfte nach der Biegetheorie

5.1 *Grundgleichungen*

Eine dünnwandige ($h/R \ll 1$) Schalenkonstruktion ist als flach zu betrachten, wenn folgende geometrische und statische Bedingungen erfüllt werden [1], [5], [18], [26]:

- Die geometrischen Bedingungen (2.5a—c).
- Die Größen t/R können gegenüber Eins vernachlässigt werden ($t/R \ll 1$), wobei t eine der Tangentialverschiebungen u, v und R der Radius der Normalkrümmung oder Verwindung der Fläche sind.
- Der Einfluß der Querkräfte Q_x und Q_y in den Projektionsgleichungen ist in Richtung der Tangentialebene vernachlässigbar.

Anhand der aufgezählten Bedingungen ist die Gleichgewichts- und Verträglichkeitsgleichung der flachen Schalen mit verteilter Last in der Richtung $\bar{z}$ durch Anwendung der allgemeinen Methoden der Schalenstatik, wie folgt, aufzuschreiben [1], [11], [26]:

$$L_p(F, z) - B\Delta\Delta w + p(x, y) = 0, \tag{5.1}$$

$$\Delta\Delta F + D(1 - \mu^2)L_p(w, z) = 0. \tag{5.2}$$

Falls die Last $\tilde{p}(x, y)$ in Richtung der Flächennormale liegt (wie die Verschiebung w), so gelangt man ebenfalls zu Gleichungen der vorangehenden Formen [5].

Der Grund hierfür liegt darin, daß aus den Flachheits-Bedingungen (2.5 a—c) auch das folgt, daß die Flächennormalen der flachen Schalen beinahe parallel zur Achse z angesehen werden können.

Daraus folgt auch die Richtigkeit der Gleichungen in Veröffentlichungen [17], [18], [20]. Diese Gleichungen haben gleiche Formen wie die Zusammenhänge (5.1) und (5.2), obwohl die Verschiebung w^* und die Last $p(x, y)$ in ihrem Koordinatensystem in Richtung zu $\bar{z}$ liegen.

Die Randbogen werden *in ihrer Ebene als starr* (senkrecht zu ihrer Ebene dagegen als vollkommen nachgiebig) angenommen. Mit anderen Worten: die Randträger werden gegen seitliche Biegung und Drillung als weich, jedoch gegen Biegung in ihrer eigenen Ebene und gegen Dehnungen als vollkommen steif betrachtet (sog. »halbsteife« Randträger):

$$\left.\begin{aligned} N_{xb} = 0, \quad & M_x = 0, \\ w = 0 \quad & \varepsilon_y = 0, \end{aligned}\right\}_{\substack{x=0 \\ x=2a}} \tag{5.3a—d}$$

$$\left.\begin{aligned} N_{yb} = 0, \quad & M_y = 0, \\ w = 0, \quad & \varepsilon_y = 0. \end{aligned}\right\}_{\substack{y=0 \\ y=2b}} \tag{5.4a—d}$$

Wenn man die gleichmäßig verteilte, auf die Flächeneinheit der Grundrißprojektion bezogene Last $p(x, y) = p = \text{konst.}$ in eine doppelte Fouriersche Reihe entwickelt

$$p(x, y) = \frac{16}{\pi^2} p \sum\sum \frac{1}{mn} \sin \frac{m\pi}{2a} x \sin \frac{n\pi}{2b} y, \tag{5.5}$$

$$m = 1, 3, 5, \ldots, M$$

$$n = 1, 3, 5, \ldots, N,$$

dann können die Gleichungen (5.1)—(5.2), die die Randbedingungen (5.3)—(5.4) erfüllen, mit Hilfe der Hilfsveränderlichen

$$\alpha = \frac{f_a}{f_b}, \quad \beta = \frac{a}{h},$$

$$\gamma = \frac{a}{b}, \quad \varrho = \frac{f_b}{b} \tag{5.6a—d}$$

wie folgt, aufgeschrieben werden:

$$A_{mn} = \frac{768(1 - \mu^2)}{\pi^4} (\varrho\beta\gamma)^2 \cdot (m^2 - \alpha n^2), \tag{5.7}$$

$$B_{mn} = (m^2 + \gamma^2 n^2)^2, \tag{5.8}$$

$$N_{mn} = - \frac{A_{mn}}{A_{mn}(m^2 - \alpha n^2) + B_{mn}^2} \tag{5.9}$$

$$S_{mn} = \sin \frac{m\pi}{2a} x \cdot \sin \frac{n\pi}{2b} y,$$

$$C_{mn} = \cos \frac{m\pi}{2a} x \cdot \cos \frac{n\pi}{2b} y, \tag{5.10a—b}$$

$$n_x^\circ = - \frac{8}{\pi^2} \sum_m \sum_n \frac{n}{m} N_{mn} S_{mn},$$

$$n_{xy}^\circ = - \frac{8}{\pi^2 \gamma} \sum_m \sum_n N_{mn} C_{mn}, \tag{5.11a—c}$$

$$n_y^\circ = - \frac{8}{\pi^2 \gamma^2} \sum_m \sum_n \frac{m}{n} N_{mn} S_{mn},$$

$$m = 1, 3, 5, \ldots, M$$

$$n = 1, 3, 5, \ldots, N$$

$$m_x^\circ = -\frac{64}{\pi^4}\sum_m\sum_n \frac{m}{n}\frac{B_{mn}}{A_{mn}} N_{mn} S_{mn},$$

$$m_{xy}^\circ = -\frac{64(1-\mu)}{\pi^4}\gamma\sum_m\sum_n \frac{B_{mn}}{A_{mn}} N_{mn} C_{mn},$$

$$m_y^\circ = -\frac{64}{\pi^4}\gamma^2\sum_m\sum_n \frac{n}{m}\frac{B_{mn}}{A_{mn}} N_{mn} S_{mn}, \qquad (5.12a-d)$$

$$w^\circ = -\frac{3072(1-\mu^2)}{\pi^6}\beta^4\sum_m\sum_n \frac{1}{mn}\frac{B_{mn}}{A_{mn}} N_{mn} S_{mn},$$

$$m = 1, 3, 5, \ldots, M$$

$$n = 1, 3, 5, \ldots, N$$

$$N_{xb} = n_x^\circ \frac{pa^2}{f_b},$$

$$N_{xyb} = n_{xy}^\circ \frac{pa^2}{f_b}, \qquad (5.13a-c)$$

$$N_{yb} = n_y^\circ \frac{pa^2}{f_b},$$

$$M_x = (m_x^\circ + \mu m_y^\circ)pa^2,$$

$$M_{xy} = m_{xy}^\circ pa^2, \qquad (5.14a-d)$$

$$M_y = (m_y^\circ + \mu m_x^\circ)pa^2,$$

$$w = \frac{ph}{E} w^\circ.$$

Die angegebenen Zusammenhänge entsprechen der Lösung von [1].

Auf Grund der Gl. (5.1) bestimmten wir auch die Formel des durch Mittelflächenkräfte bzw. Biegeschnittkräfte getragenen Lastanteils p^m bzw. $p^b (B = 0$, bzw. $z = 0)$:

$$\frac{p^m}{p} = -\frac{16}{\pi^2}\sum_m\sum_n \frac{m^2 - \alpha n^2}{mn} N_{mn} S_{mn}, \qquad (5.15)$$

$$m = 1, 3, 5, \ldots, M$$

$$n = 1, 3, 5, \ldots, N$$

$$\frac{p^b}{p} = -\frac{16}{\pi^2}\sum_m\sum_n \frac{1}{mn}\frac{B_{mn}^2}{A_{mn}} N_{mn} S_{mn}. \qquad (5.16)$$

$$m = 1, 3, 5, \ldots, M$$

$$n = 1, 3, 5, \ldots, N$$

5.2 *Numerische Untersuchungen*

Im Laufe der Berechnungen wurde der Parameter f_a/f_b zwischen den Werten 1 und 4 geändert.

Vor allem geben wir über den Charakter der Verteilung der inneren Kräfte im Bereich x, y ein übersichtliches Bild (Bilder $4a-4f$).

Beachtenswert ist, daß sich die Momente *der »halbnormalen« Schale* (»voile seminormal«, $f_a/f_b = 1$, Bild 4a—b) gleich den Momenten der ebenen Platte verteilen. Das Tragverhalten dieser Schale weicht jedoch vom Tragverhalten der ebenen Platte ab, denn in ihr treten wegen der Kompatibilität auch Mittelflächenkräfte auf. Ihre Momente sind etwas größer als die Plattenmomente. Auf Grund der Zeile 1. in Tabelle II ist leicht einzusehen, daß Mittelflächenkräfte in der Schale durch diejenigen (symmetrischen) Lastkomponenten entstehen, deren Formen die Ungleichung $m \neq n$ erfüllen. Durch andere Lastkomponenten werden *wegen der dehnungslosen Verformung* keine Mittelflächenkräfte hervorgerufen. Im Schalenmittelpunkt ($x = a$, $y = b$) ist die Normal-

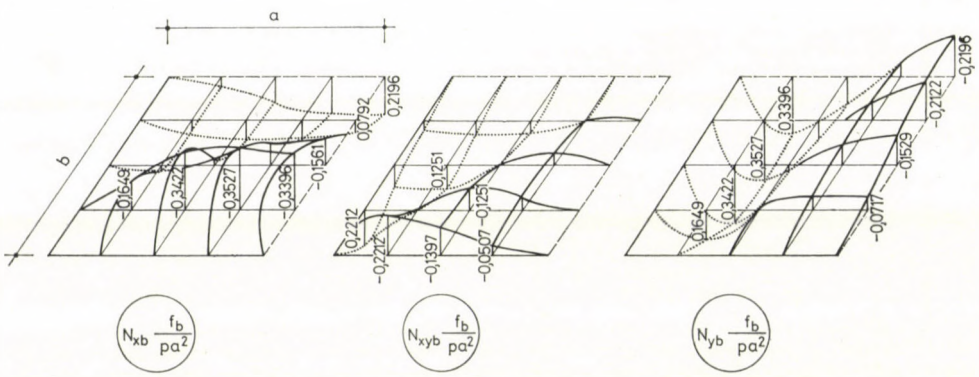

Bild 4a. **Mittelflächenkräfte der »halbnormalen« HP-Schale (»voile seminormal«) im ersten Viertel des Koordinatensystems x, y ($x = 0 \div a$, $y = 0 \div b$; $f_a/f_b = 1$, $a/b = 1$, $a/h = 200$, $f_b/b = 0{,}3$)**

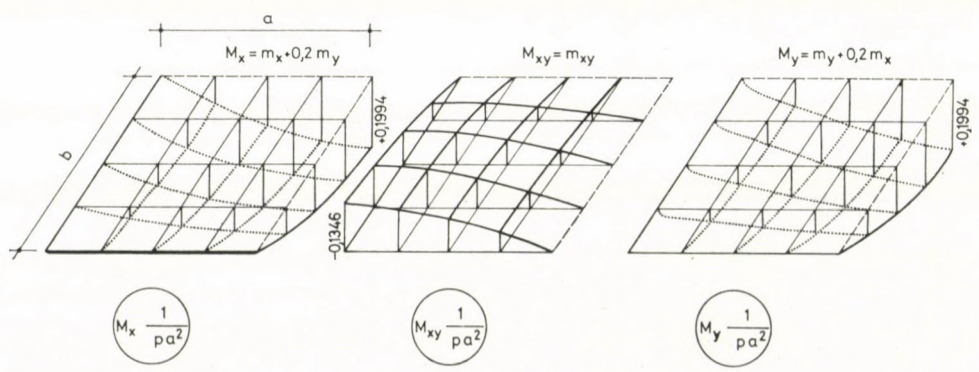

Bild 4b. **Biege- und Drillmomente der »halbnormalen« HP-Schale (»voile seminormal) im ersten Viertel des Koordinatensystems x, y ($x = 0 \div a$, $y = 0 \div b$; $f_a/f_b = 1$, $a/b = 1$, $a/h = 200$, $f_b/b = 0{,}3$)**

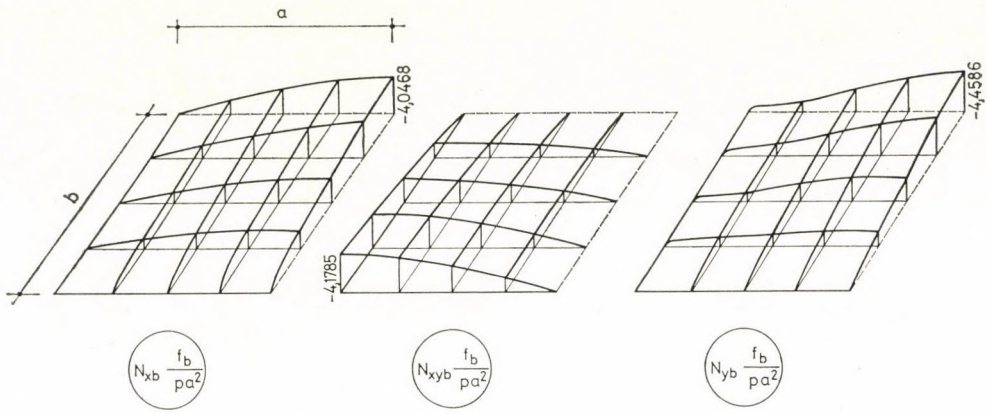

Bild 4c. Die im Falle $f_a/f_b = 1{,}2$ entstehenden Mittelflächenkräfte der HP-Schale im ersten Viertel des Koordinatensystems x, y ($x = 0 \div a$, $y = 0 \div b$; $a/b = 1$, $a/h = 200$, $f_b/b = 0{,}3$)

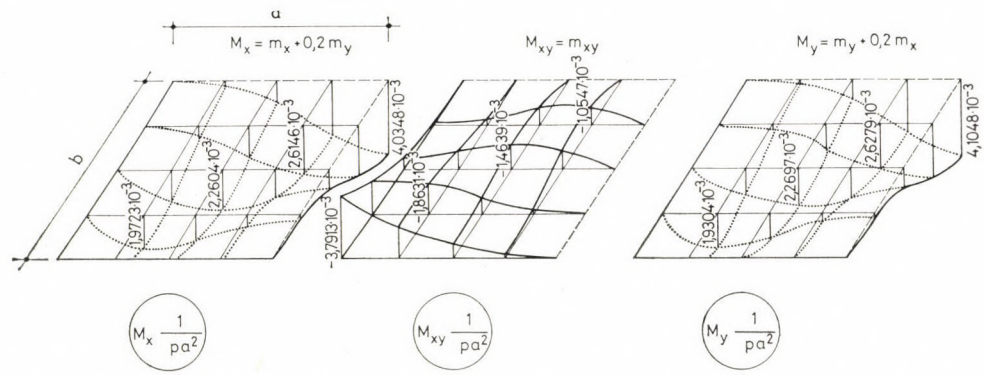

Bild 4d. Die im Falle $f_a/f_b = 1.2$ entstehenden Biege- und Drillmomente der HP-Schale im ersten Viertel des Koordinatensystems x, y ($x = 0 \div a$, $y = 0 \div b$; $a/b = 1$, $a/h = 200$, $f_b/b = 0{,}3$)

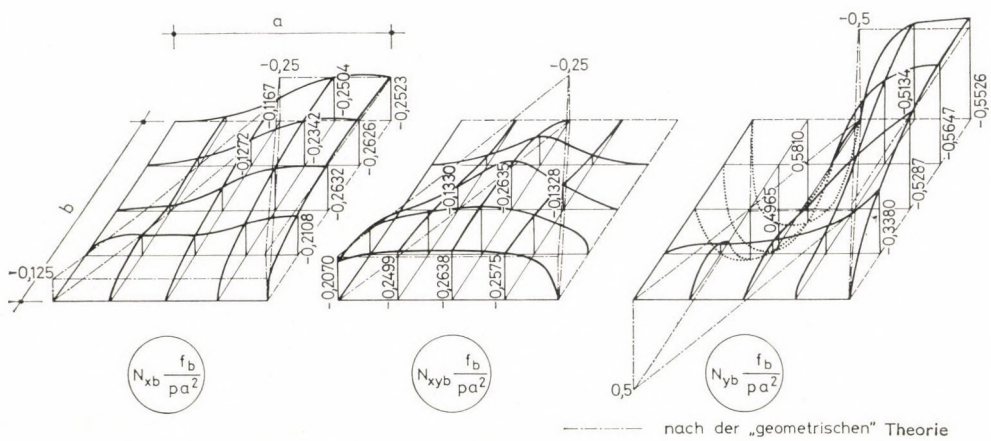

Bild 4e. Mittelflächenkräfte der »normalen« HP-Schale (»voile normal«) im ersten Viertel des Koordinatensystems x, y ($x = 0 \div a$, $y = 0 \div b$; $f_a/f_b = 4$, $a/b = 1$, $a/h = 200$, $f_b/b = 0{,}3$)

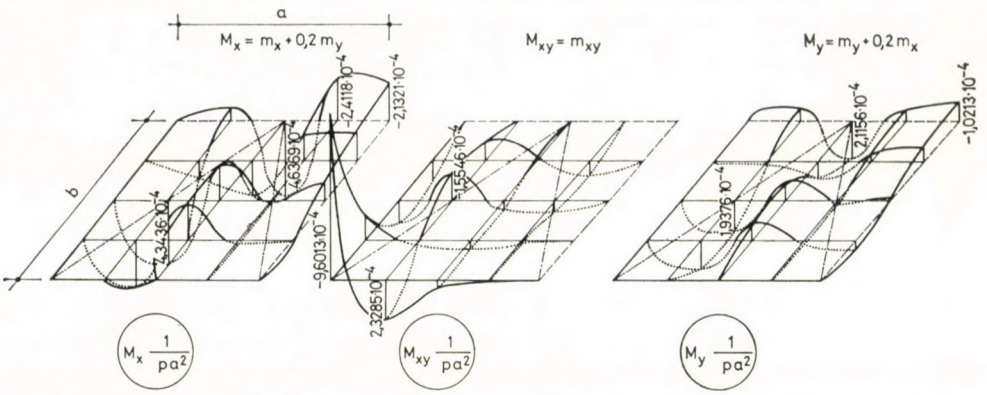

Bild 4f. Biege- und Drillmomente der »normalen« HP-Schale (»voile normal«) im ersten Viertel des Koordinatensystems x, y ($x = 0 \div a$, $y = 0 \div b$; $f_a/f_b = 4$, $a/b = 1$, $a/h = 200$, $f_b/b = 0{,}3$)

kraft eine Zugkraft. Infolgedessen ist der durch Mittelflächenkräfte getragene Lastanteil *negativ* (Bild 6). Daraus folgt selbstverständlich, daß die Momente der »halbnormalen« Schale größer sind als diejenige der entsprechenden ebenen Platte. Die Biegemomente der ebenen Platte mit Abmessungsverhältnissen $a/b = 1$, $a/h = 200$ im Punkt $x = a$, $y = b$ sind nach [23]: $M_x^{\text{Pl.}} = M_y^{\text{Pl.}} = 0{,}1767\,pa^2$. (Es wurde eine Transformation von $\mu = 0{,}3$ zu $\mu = 0{,}2$ durchgeführt). Wie aus Bild 4b. ersichtlich ist, gehören zur behandelten Schale Momente mit den Größen $M_x = M_y = 0{,}1994\,pa^2 \simeq 1{,}13\,M_x^{\text{Pl.}}$.

Der durch die Biegeschnittkräfte getragene Lastanteil wird selbstverständlich durch die Krümmungen der Funktionen der Biege- und Drillmomente bestimmt. Wie Bild 6 deutlich erkennen läßt, wuchsen die Krümmungen der Momentefunktionen gegenüber den entsprechenden Krümmungen der ebenen Platte stärker als die Absolutbeträge der Momente an.

Die von den Mittelflächenkräfte der »halbnormalen« HP-Schale stammende Durchbiegung (bzw. Krümmung[en]) *ist* zu der durch die Biegeschnittkräfte hervorgerufenen Durchbiegung (bzw. Krümmung[en]) *entgegengesetzt gerichtet.* Hieraus erklärt sich also, daß die Größe der Durchbiegung der HP-Schale im Schalenmittelpunkt ($x = a$, $y = b$) $w = 1{,}229 \times 10^9\,p/E$ beinahe völlig mit der Durchbiegung der entsprechenden ebenen Platte ($\mu = 0{,}2$) übereinstimmt [23].

Von der »halbnormalen« HP-Schale ist also festzustellen, daß sie hinsichtlich des Tragverhaltens *ungünstiger ist als die entsprechende ebene Platte.* Infolgedessen ist die Anwendung dieser Konstruktion nur bei den geometrischen Verhältnissen zweckmäßig, die die ebenen Platten kennzeichnen ($a/h = 15 \div 20$).

Interessant ist in den Bildern 4c. und 4d. zu beobachten, daß die Mittelflächenkräfte der Schalen mit Verhältnissen f_a/f_b, die von dem Verhältnis f_a/f_b der »halbnormalen« Schale nur wenig abweichen (z. B. $f_a/f_b = 1, 2$), entge-

gen der Mittelflächenkräfte der »halbnormalen« HP-Schale sehr stark anwuchsen.

Gleichzeitig verminderten sich selbstverständlich die Biege- und Drillmomente um eine Größenordnung.

Bezüglich der normalen Schale ($f_a/f_b = 4$, Bilder 4e, 4f) sieht das Bild der inneren Kräfte ganz anders aus, als das für den Fall der »halbnormalen« Schale dargelegt wurde. Die Abbildung der Mittelflächenkräfte nach der Biegetheorie liegt den unstetigen Abbildungen nach der Aimondschen »geometrischen« Theorie nahe. Dementsprechend *kommt den Biegeeffekten eine sehr kleine Bedeutung zu.* Wie ersichtlich, verteilen sich die Biegemomente der »normalen« Schale in der Grundrißprojektion nicht so, wie die der elastischen Platte — die in der Nähe des Plattenmittelpunktes am größten sind —, sondern die Maximalwerte der Schalenmomente liegen in den Bereichen längs der Rändern. Von den Rändern nach innen nehmen diese Momente abnehmende positive und negative Werte auf, ähnlich wie die nach der Mitte zu abklingenden Schwingungen. Diese Feststellung steht mit den Ergebnissen von HRUBAN [11] und TARNAI [22] in Einklang.

Sie bestimmten die Biegewirkungen nach der Lösung des Randstörungsproblems.

Zur Bemessung der »normalen« Schale mit Hilfe der Theorie I. Ordnung sind ihre Lösungen gut anzuwenden. (Die Behandlung der in dem vorliegenden Aufsatz gestellten Aufgabe war natürlich nur durch eine Untersuchung möglich, die sich auf den ganzen Grundrißbereich erstreckte.) Auf Grund der Bilder 5a—5b wird das bisher Gesagte noch anschaulicher. Wenn die Pfeilhöhenverhältnisse der behandelten HP-Schale mit den Parametern $f_b/b = 0{,}3$, $a/h = 200$ von dem Wert $f_a/f_b = 4$ (»normale« Schale) etwa bis zu dem Wert $f_a/f_b = 2 \div 1{,}5$ verändert werden, dann wachsen die Biegewirkungen nur sehr wenig an und weisen sehr kleine Absolutbeträge auf.

In diesem Bereich können also die behandelten sattelförmigen HP-Schalen mit guter Näherung *als Membranschalen betrachtet werden.*

Für diese Pfeilhöhenverhältnisse ist an Hand der Tafel II. festzustellen, daß die dehnungslosen Verformungen mit wenigsten symmetrischen Wellenzahlen zu den Schalen mit den Parametern $(f_a/f_b)^{1/2} = 7/5,\ 5/3,\ 9/5$ gehören.

Das Gewicht der Lastglieder p_{mn}, bestimmt nach den Zsammenhängen (4.4) und (5.5), ist unbedeutend. Daher *spielt die dehnungslose Verformung keine wichtige Rolle.* Eine weitere Vermindung des Pfeilhöhenverhältnisses — also eine Annäherung an die, den überwiegenden Anteil ihrer Lasten »plattenartig« tragende, »halbnormale« Schale ($f_a/f_b = 1$) — führt zur rapiden Vergrößerung der Momente. Da es sich um eine Schale handelt, würde die Konstruktion infolge ihrer verhältnismäßig großen Dehnungsteifigkeit die Lasten durch Mittelflächenkräfte tragen. So werden wegen der Kompatibilität mit der raschen Zunahme der Momente auch die der Mittelflächenkräfte größer.

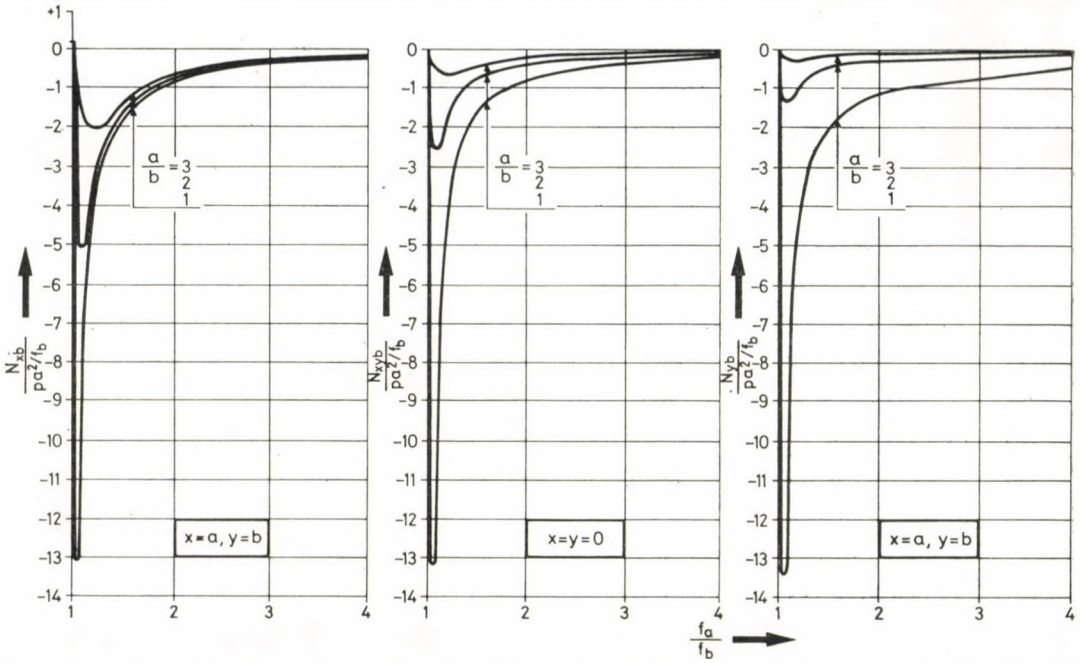

Bild 5a. Die nach der Biegetheorie bestimmten Mittelflächenkräfte im Schalenmittelpunkt ($f_b/b=0{,}3$, $a/h=200$)

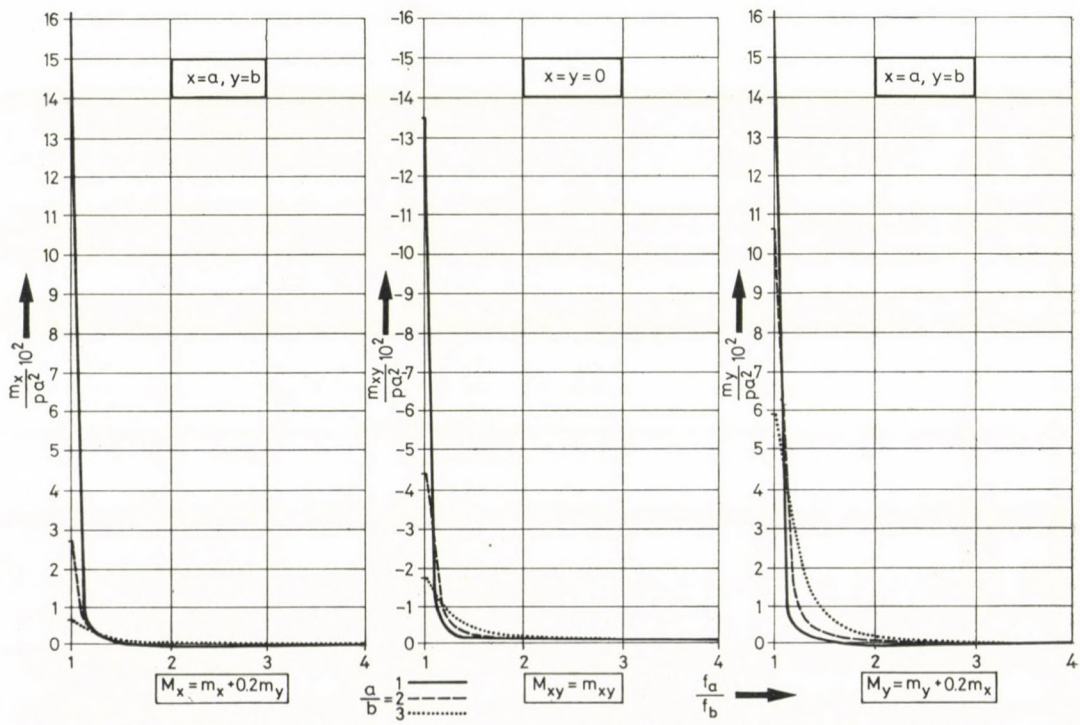

Bild 5b. Biege- und Drillmomente im Schalenmittelpunkt ($f_b/b=0{,}3$, $a/h=200$)

Hätte die Schale keine Biegesteifigkeit, so würden die Mittelflächenkräfte nach unendlich großen Werten streben. Im Hinblick darauf, daß die Schale endliche Biegesteifigkeit hat, übernehmen die Biegeschnittkräfte den entschei-

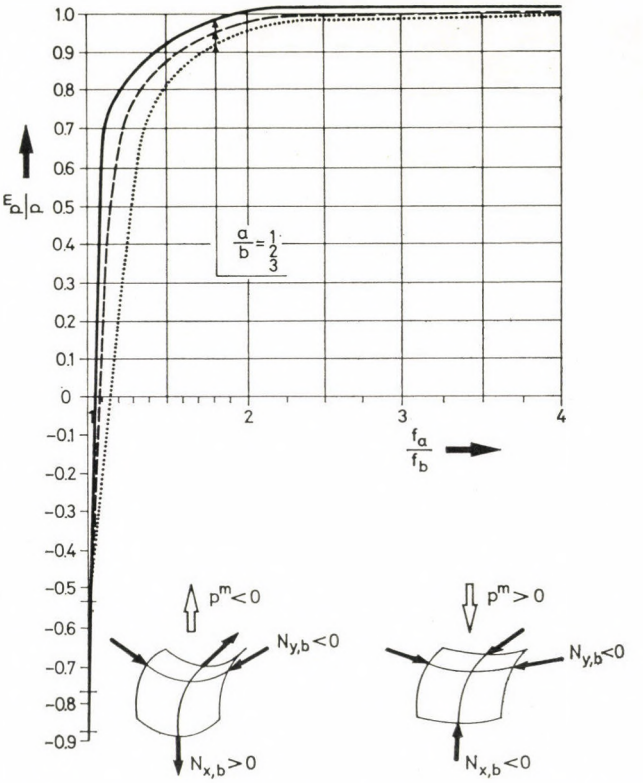

Bild 6. Die durch Mittelflächenkräfte getragegen Lastanteile im Schalenmittelpunkt ($a/h = 200$, $f_b/b = 0{,}3$)

denden Anteil der Belastung. Folglich nehmen für den Fall der »halbnormalen« Schale die Mittelflächenkräfte wieder kleine Werte an.

Wie schon erwähnt, *spielt die dehnungslose Verformung* bei der »halbnormalen« Schale eine *entscheidende Rolle*: nur aus den nicht dominanten Lastkomponenten, die durch die Ungleichung $m \neq n$ gekennzeichnet werden können, entstehen Mittelflächenkräfte.

Das Fehlen der den übrigen Lastkomponenten entsprechenden Normal- und Schubkräfte muß durch die Biegewirkungen ersetzt werden.

Im Bild 6 sind die durch Mittelflächenkräfte getragenen Lastanteile der Schale mit den bereits behandelten geometrischen Angaben dargestellt.

All diese Resultate lassen wieder erkennen, daß die Schale die Lasten etwa im Bereich $f_a/f_b = (1{,}5-2) \div 4$ *überwiegend durch Mittelflächenkräfte trägt.*

Tafel III/1

$\frac{f_b}{b}$	$\frac{a}{h}$	$\frac{a}{b}$	$\frac{f_a}{f_b}$	$\frac{N_{xb}}{pa^2/f_b}$	$\frac{N_{xyb}}{pa^2/f_b}$	$\frac{N_{yb}}{pa^2/f_b}$
			1	0,1682	0	−0,1682
			1,2	−2,5237	−2,6533	−2,8367
		1	1,6	−1,2027	−1,2794	−1,4896
			2,25	−0,6105	−0,6356	−0,8780
			4	−0,2781	−0,2284	−0,5343
			1	−0,00014	0,0606	−0,0455
			1,2	−0,6550	−0,2692	−0,2112
0,1	100	2	1,6	−0,8519	−0,3716	−0,2647
			2,25	−0,5651	−0,2293	−0,1977
			4	−0,2685	−0,0701	−0,1462
			1	−0,0207	0,0420	−0,0182
			1,2	−0,1282	0,0057	−0,0305
		3	1,6	−0,2866	−0,0466	−0,0495
			2,25	−0,3548	−0,0684	−0,0584
			4	−0,2531	−0,0314	−0,0497

Die vorangehenden ausführlichen Untersuchungen wurden auch für die Parameter a/h, f_b/b und a/b (Tafeln III—IV.), die die geometrischen Verhältnissen der meisten Stahlbetonschalen gut kennzeichnen, durchgeführt. Wir gelangten zu der Feststellung, daß *die HP-Schalen auch in diesen Fällen als Membranschalen zu betrachten sind*, wenn man den Bereich $f_a/f_b = (1{,}5-2) \div 4$ nicht verläßt.

Aus den in den Tafeln angegebenen Werten können mit Hilfe der Pucherschen Gleichgewichtsgleichung die durch Mittelflächenkräfte getragenen Lastanteile schnell bestimmt werden (Bild 6). Auch daraus ist auf das Maß der Membranwirkung zu folgern.

In Tafel III sind die Werte der Schubkräfte im Punkt $x = 0$, $y = 0$, weiterhin die Werte der Normalkräfte im Punkt $x = a$, $y = b$, bezogen auf die geometrischen Verhältnisse $a/b = 1, 2, 3$, $a/h = 100, 150, 200$, $f_b/b = 0{,}1,\ 0{,}2\ 0{,}3$, $f_a/f_b = 1,\ 1{,}2,\ 1{,}6,\ 2{,}25,\ 4$ zusammengefaßt.

In Tafel IV. sind die Werte der Drillmomente im Punkt $x = 0$, $y = 0$ und die Werte der Biegemomente und der Durchbiegungen im Punkt $x = a$, $y = b$ (bezogen auf die vorangehenden geometrischen Verhältnisse) enthalten. In Verbindung mit der Verwendung der Tafeln sie bemerkt, daß zu gleichen

Tafel III/2

$\frac{f_b}{b}$	$\frac{a}{h}$	$\frac{a}{b}$	$\frac{f_a}{f_b}$	$\frac{N_{xb}}{pa^2/f_b}$	$\frac{N_{xyb}}{pa^2/f_b}$	$\frac{N_{yb}}{pa^2/f_b}$
			1	0,1776	0	−0,1776
			1,2	−3,1614	−3,2921	−3,4910
		1	1,6	−1,2659	−1,3344	−1,5670
			2,25	−0,6302	−0,6437	−0,9186
			4	−0,2866	−0,2070	−0,5793
			1	0,0235	0,0664	−0,0495
			1,2	−1,2038	−0,5508	−0,3587
0,1	150	2	1,6	−1,0492	−0,4764	−0,3238
			2,25	−0,5931	−0,2453	−0,2140
			4	−0,2762	−0,0619	−0,1461
			1	−0,0204	0,0485	−0,0216
			1,2	−0,2541	−0,0292	−0,0481
		3	1,6	−0,4997	−0,1106	−0,0766
			2,25	−0,4764	−0,1015	−0,0762
			4	−0,2741	−0,0264	−0,0593

Tafel III/3

$\frac{f_b}{b}$	$\frac{a}{h}$	$\frac{a}{b}$	$\frac{f_a}{f_b}$	$\frac{N_{xb}}{pa^2/f_b}$	$\frac{N_{xyb}}{pa^2/f_b}$	$\frac{N_{yb}}{pa^2/f_b}$
			1	0,1867	0	−0,1867
			1,2	−3,4685	−3,6031	−3,8160
		1	1,6	−1,2976	−1,3628	−1,6162
			2,25	−0,6414	−0,6439	−0,9406
			4	−0,2879	−0,1978	−0,5922
			1	0,0497	0,0686	−0,0512
			1,2	−1,7197	−0,8192	−0,4958
0,1	200	2	1,6	−1,1394	−0,5289	−0,3533
			2,25	−0,6046	−0,2534	−0,2219
			4	−0,2805	−0,0593	−0,1515
			1	−0,0174	0,0523	−0,0229
			1,2	−0,4147	−0,0803	−0,0678
		3	1,6	−0,6839	−0,1700	−0,0992
			2,25	−0,5391	−0,1209	−0,0857
			4	−0,2798	−0,0238	−0,0641

Tafel III/4

$\frac{f_b}{b}$	$\frac{a}{h}$	$\frac{a}{b}$	$\frac{f_a}{f_b}$	$\frac{N_{xb}}{pa^2/f_b}$	$\frac{N_{xyb}}{pa^2/f_b}$	$\frac{N_{yb}}{pa^2/f_b}$
			1	0,1867	0	−0,1867
			1,2	−3,4685	−3,6031	−3,8160
		1	1,6	−1,2976	−1,3628	−1,6162
			2,25	−0,6414	−0,6439	−0,9406
			4	−0,2879	−0,1978	−0,5922
			1	0,0497	0,0686	−0,0512
			1,2	−1,7197	−0,8192	−0,4958
0,2	100	2	1,6	−1,1394	−0,5289	−0,3533
			2,25	−0,6064	−0,2534	−0,2219
			4	−0,2805	−0,0593	−0,1515
			1	−0,0174	0,0523	−0,0229
			1,2	−0,4147	−0,0803	−0,0678
		3	1,6	−0,6839	−0,1700	−0,0992
			2,25	−0,5391	−0,1209	−0,0857
			4	−0,2798	−0,0238	−0,0641

Tafel III/5

$\frac{f_b}{b}$	$\frac{a}{h}$	$\frac{a}{b}$	$\frac{f_a}{f_b}$	$\frac{N_{xb}}{pa^2/f_b}$	$\frac{N_{xyb}}{pa^2/f_b}$	$\frac{N_{yb}}{pa^2/f_b}$
			1	0,1984	0	−0,1984
			1,2	−3,7513	−3,8869	−4,1210
		1	1,6	−1,3415	−1,3938	−1,6805
			2,25	−0,6551	−0,6407	−0,9698
			4	−0,2835	−0,1931	−0,5874
			1	0,0955	0,0691	−0,0536
			1,2	−2,4939	−1,2236	−0,7012
0,2	150	2	1,6	−1,2189	−0,5765	−0,3815
			2,25	−0,6214	−0,2623	−0,2306
			4	−0,2826	−0,0593	−0,1540
			1	−0,0072	0,0564	−0,0242
			1,2	−0,8032	−0,2100	−0,1136
		3	1,6	−0,9320	−0,2544	−0,1298
			2,25	−0,5892	−0,1400	−0,0946
			4	−0,2814	−0,0227	−0,0687

Tafel III/6

$\frac{f_b}{b}$	$\frac{a}{h}$	$\frac{a}{b}$	$\frac{f_a}{f_b}$	$\frac{N_{xb}}{pa^2/f_b}$	$\frac{N_{xyb}}{pa^2/f_b}$	$\frac{N_{yb}}{pa^2/f_b}$
			1	0,2073	0	−0,2073
			1,2	−3,8893	−4,0240	−4,2757
		1	1,6	−1,3692	−1,4080	−1,7247
			2,25	−0,6651	−0,6319	−0,9932
			4	−0,2769	−0,1929	−0,5721
			1	0,1262	0,0683	−0,0554
			1,2	−2,9697	−1,4708	−0,8275
0,2	200	2	1,6	−1,2605	−0,5983	−0,3963
			2,25	−0,6350	−0,2669	−0,2363
			4	−0,2803	−0,0611	−0,1525
			1	0,0063	0,0585	−0,0248
			1,2	−1,2215	−0,3863	−0,1623
		3	1,6	−1,0657	−0,3028	−0,1469
			2,25	−0,6050	−0,1489	−0,0983
			4	−0,2813	−0,0232	−0,0698

Tafel III/7

$\frac{f_b}{b}$	$\frac{a}{h}$	$\frac{a}{b}$	$\frac{f_a}{f_b}$	$\frac{N_{xb}}{pa^2/f_b}$	$\frac{N_{xyb}}{pa^2/f_b}$	$\frac{N_{yb}}{pa^2/f_b}$
			1	0,1984	0	−0,1984
			1,2	−3,7513	−3,8869	−4,1210
		1	1,6	−1,3415	−1,3938	−1,6806
			2,25	−0,6551	−0,6407	−0,9698
			4	−0,2835	−0,1931	−0,5874
			1	0,0955	0,0691	−0,0536
			1,2	−2,4939	−1,2236	−0,7012
0,3	100	2	1,6	−1,2189	−0,5765	−0,3815
			2,25	−0,6214	−0,2623	−0,2306
			4	−0,2826	−0,0593	−0,1540
			1	−0,0072	0,0564	−0,0242
			1,2	−0,8032	−0,2100	−0,1136
		3	1,6	−0,9320	−0,2544	−0,1298
			2,25	−0,5892	−0,1400	−0,0946
			4	−0,2814	−0,0227	−0,0687

Tafel III/8

$\frac{f_b}{h}$	$\frac{a}{h}$	$\frac{a}{b}$	$\frac{f_a}{f_b}$	$\frac{N_{xb}}{pa^2/f_b}$	$\frac{N_{xyb}}{pa^2/f_b}$	$\frac{N_{yb}}{pa^2/f_b}$
0,3	150	1	1	0,2110	0	−0,2110
			1,2	−3,9381	−4,0721	−4,3312
			1,6	−1,3797	−1,4121	−1,7419
			2,25	−0,6695	−0,6265	−1,0042
			4	−0,2737	−0,1927	−0,5641
		2	1	0,1366	0,0677	−0,0562
			1,2	−3,1336	−1,5554	−0,8709
			1,6	−1,2763	−0,6056	−0,4019
			2,25	−0,6408	−0,2683	−0,2386
			4	−0,2786	−0,0620	−0,1511
		3	1	0,0137	0,0592	−0,0250
			1,2	−1,4248	−0,4225	−0,1860
			1,6	−1,1076	−0,3189	−0,1526
			2,25	−0,6089	−0,1518	−0,0995
			4	−0,2811	−0,0237	−0,0701

Tafel III/9

$\frac{f_b}{b}$	$\frac{a}{h}$	$\frac{a}{b}$	$\frac{f_a}{f_b}$	$\frac{N_{xb}}{pa^2/f_b}$	$\frac{N_{xyb}}{pa^2/f_b}$	$\frac{N_{yb}}{pa^2/f_b}$
0,3	200	1	1	0,2196	0	−0,2196
			1,2	−4,0468	−4,1786	−4,4558
			1,6	−1,4032	−1,4191	−1,7813
			2,25	−0,6861	−0,6094	−1,0245
			4	−0,2628	−0,2070	−0,5406
		2	1	0,1554	0,0658	−0,0579
			1,2	−3,4551	−1,7205	−0,9559
			1,6	−1,3137	−0,6213	−0,4147
			2,25	−0,6548	−0,2702	−0,2447
			4	−0,2710	−0,0723	−0,1456
		3	1	0,0371	0,0603	−0,0255
			1,2	−1,9698	−0,6109	−0,2496
			1,6	−1,1832	−0,3496	−0,1636
			2,25	−0,6236	−0,1577	−0,1018
			4	−0,2825	−0,0298	−0,0700

Tafel IV/1

$\frac{f_b}{b}$	$\frac{a}{h}$	$\frac{a}{b}$	$\frac{f_a}{f_b}$	$\frac{w/h_{10^{-5}}}{p/E}$	$\frac{m_x 10^5}{pa^2}$	$\frac{-m_{xy} 10^5}{pa^2}$	$\frac{m_y 10^5}{pa^2}$
0,1	100	1	1	764,901	16 340,02	13 820,10	16 340,02
			1,2	263,601	5 582,01	5 181,02	5 652,10
			1,6	41,065	764,81	1 302,01	916,32
			2,25	8,435	−22,96	719,70	212,11
			4	−1,376	−486,81	519,71	−33,73
		2	1	122,560	2 529,01	4 584,02	10 110,02
			1,2	101,650	2 097,03	3 903,03	8 421,20
			1,6	43,569	841,31	1 914,02	3 488,04
			2,25	13,127	177,22	907,74	947,90
			4	1,129	−181,60	541,31	26,21
		3	1	30,044	567,91	7 628,10	5 637,01
			1,2	29,207	546,31	2 372,02	5 477,02
			1,6	23,929	425,12	1 542,11	4 462,31
			2,25	14,058	208,51	323,53	2 565,70
			4	3,124	−88,50	609,50	477,81

Tafel IV/2

$\frac{f_b}{b}$	$\frac{a}{h}$	$\frac{a}{b}$	$\frac{f_a}{f_b}$	$\frac{w/h_{10^{-5}}}{p/E}$	$\frac{m_x 10^5}{pa^2}$	$\frac{-m_{xy} 10^5}{pa^2}$	$\frac{m_y 10^5}{pa^2}$
0,1	150	1	1	3 880,202	16 470,02	13 670,11	16 470,02
			1,2	736,901	3 152,03	2 996,03	3 188,03
			1,6	96,422	378,21	757,23	460,42
			2,25	18,809	−135,82	470,12	102,83
			4	−4,895	−286,20	354,45	−32,12
		2	1	612,570	2 579,31	4 502,91	10 191,12
			1,2	447,843	1 779,02	9 020,83	7 035,33
			1,6	122,881	476,32	1 142,34	1 914,42
			2,25	31,337	83,60	543,12	437,21
			4	1,976	−103,71	349,73	4,37
		3	1	153,421	609,52	1 759,72	5 690,04
			1,2	144,392	569,21	1 671,13	5 348,44
			1,6	98,011	368,20	1 206,72	3 587,63
			2,25	43,419	136,05	692,92	1 521,12
			4	6,988	−60,07	373,64	168,03

Tafel IV/3

$\frac{f_b}{b}$	$\frac{a}{h}$	$\frac{a}{b}$	$\frac{f_a}{f_p}$	$\frac{w/h_{10^{-5}}}{p/E}$	$\frac{m_x 10^5}{pa^2}$	$\frac{-m_{xy} 10^5}{pa^2}$	$\frac{m_y 10^5}{pa^2}$
			1	12 273,10	16 520, 04	13 590,10	16 520,04
			1,2	1 434,82	1 990,20	1 951,03	2 015,53
		1	1,6	175,21	223,93	523,81	283,31
			2,25	32,80	—42,08	353,92	51,01
			4	—10,57	—189,51	269,42	—27,66
			1	1 954,82	2 601,23	4 459,04	10 260,12
			1,2	1 098,41	1 452,42	2 617,73	5 716,80
0,1	200	2	1,6	239,74	296,50	764,91	1 182,11
			2,25	56,99	47,06	386,81	259,02
			4	2,98	—67,02	265,21	—2,26
			1	486,64	627,71	1 723,12	5 714,81
			1,2	438,31	561,73	1 569,62	5 136,31
		3	1,6	243,30	297,62	946,61	2 796,02
			2,25	88,48	90,22	482,03	948,21
			4	12,11	—40,17	264,61	71,68

Tafel IV/4

$\frac{f_b}{b}$	$\frac{a}{h}$	$\frac{a}{b}$	$\frac{f_a}{f_b}$	$\frac{w/h_{10^{-5}}}{p/E}$	$\frac{m_x 10^5}{pa^2}$	$\frac{-m_{xy} 10^5}{pa^2}$	$\frac{m_y 10^5}{pa^2}$
			1	767,04	16 552,04	13 590,10	16 552,04
			1,2	89,68	1 990,20	1 951,03	2 015,51
		1	1,6	10,95	223,93	523,81	283,31
			2,25	2,05	—42,08	353,92	51,01
			4	—0,66	—189,51	269,42	—27,66
			1	122,18	2 601,23	4 459,04	10 260,12
			1,2	68,65	1 452,42	2 617,73	5 716,80
0,2	100	2	1,6	14,98	296,50	764,91	1 182,11
			2,25	3,56	47,06	386,81	259,02
			4	0,186	—67,02	265,21	—2,26
			1	30,41	627,71	1 723,12	5 714,81
			1,2	27,39	561,73	1 569,62	5 136,31
		3	1,6	15,21	297,62	946,61	2 796,02
			2,25	5,53	90,22	482,03	948,21
			4	0,757	—40,17	264,61	71,68

Tafel IV/5

$\frac{f_b}{b}$	$\frac{a}{h}$	$\frac{a}{b}$	$\frac{f_a}{f_b}$	$\frac{w/h_{10^{-5}}}{p/E}$	$\frac{m_x 10^5}{pa^2}$	$\frac{-m_{xy} 10^5}{pa^2}$	$\frac{m_y 10^5}{pa^2}$
0,2	150	1	1	3 885,61	16 578,02	13 554,03	16 578,02
			1,2	217,85	1 026,30	1 099,12	1 042,41
			1,6	25,22	109,51	359,78	147,93
			2,25	4,31	—54,33	244,74	11,39
			4	—1,78	—99,90	184,25	—19,81
		2	1	619,71	2 628,12	4 436,74	10 378,03
			1,2	225,24	956,78	1 757,23	3 745,51
			1,6	36,37	150,03	461,87	592,16
			2,25	8,18	16,60	250,84	125,28
			4	0,33	—35,93	176,01	—9,28
		3	1	154,43	646,12	1 713,62	5 743,41
			1,2	123,85	516,03	1 403,52	4 586,52
			1,6	47,57	191,62	629,25	1 698,04
			2,25	13,83	45,42	286,44	438,47
			4	1,64	—21,02	168,32	20,55

Tafel IV/6

$\frac{f_b}{b}$	$\frac{a}{h}$	$\frac{a}{b}$	$\frac{f_a}{f_b}$	$\frac{w/h_{10^{-5}}}{p/E}$	$\frac{m_x 10^5}{pa^2}$	$\frac{-m_{xy} 10^5}{pa^2}$	$\frac{m_y 10^5}{pa^2}$
0,2	200	1	1	12 283,12	16 602,12	13 506,04	16 602,12
			1,2	401,22	643,84	729,36	655,57
			1,6	45,29	59,99	261,09	89,11
			2,25	6,82	—59,27	191,76	—4,17
			4	—3,44	—57,99	140,97	—13,75
		2	1	1 960,81	2 637,31	4 404,03	10 459,02
			1,2	477,26	648,57	1 217,12	2 548,22
			1,6	66,80	89,10	320,08	365,95
			2,25	14,56	3,09	189,38	69,10
			4	0,44	—22,64	136,19	—10,90
		3	1	488,70	650,96	1 695,12	5 763,93
			1,2	339,77	451,04	1 216,22	3 980,91
			1,6	97,81	125,77	437,32	1 087,62
			2,25	25,49	26,23	201,81	244,48
			4	2,85	—13,16	125,85	8,90

Tafel IV/7

$\frac{f_b}{b}$	$\frac{a}{h}$	$\frac{a}{b}$	$\frac{f_a}{f_b}$	$\frac{w/h_{10^{-5}}}{p/E}$	$\frac{m_x 10^5}{pa^2}$	$\frac{-m_{xy} 10^5}{pa^2}$	$\frac{m_y 10^5}{pa^2}$
			1	761,51	16 578,2	13 554,03	16 578,2
			1,2	43,03	1 026,3	1 099,12	1 042,41
		1	1,6	4,98	109,51	359,78	147,93
			2,25	0,85	−54,33	244,74	11,39
			4	−0,35	−99,90	184,25	−19,81
			1	122,41	2 628,12	4 436,74	10 378,03
			1,2	44,49	956,78	1 757,23	3 745,51
0,3	100	2	1,6	7,18	150,03	461,87	592,16
			2,25	1,62	16,60	250,84	125,28
			4	0,064	−35,93	176,01	−9,28
			1	30,51	646,12	1 713,62	5 743,41
			1,2	24,46	516,03	1 403,52	4 586,52
		3	1,6	9,40	191,62	629,25	1 698,04
			2,25	2,73	45,42	286,44	438,47
			4	0,32	−21,02	168,32	20,55

Tafel IV/8

$\frac{f_b}{b}$	$\frac{a}{h}$	$\frac{a}{b}$	$\frac{f_a}{f_b}$	$\frac{w/h_{10^{-5}}}{p/E}$	$\frac{m_x 10^5}{pa^2}$	$\frac{-m_{xy} 10^5}{pa^2}$	$\frac{m_y 10^5}{pa^2}$
			1	3 886,80	16 610,03	13 490,12	16 610,03
			1,2	101,53	533,90	619,55	544,21
		1	1,6	11,35	46,02	229,23	71,93
			2,25	1,59	−60,05	173,93	−8,39
			4	−0,88	−44,65	126,23	−11,36
			1	620,68	2 640,51	4 391,81	10 488,12
			1,2	125,88	544,19	1 033,30	2 142,63
0,3	150	2	1,6	16,88	71,84	276,90	301,41
			2,25	3,62	−1,11	169,58	51,70
			4	0,095	−18,44	122,84	−10,66
			1	154,69	652,41	1 688,52	5 773,72
			1,2	99,51	418,39	1 127,42	3 685,41
		3	1,6	25,52	104,01	373,95	891,99
			2,25	6,43	20,57	176,08	192,45
			4	0,71	−10,90	112,46	6,16

Tafel IV/9

$\frac{f_b}{b}$	$\frac{a}{h}$	$\frac{a}{b}$	$\frac{f_a}{f_b}$	$\frac{w/h_{10^{-5}}}{p/E}$	$\frac{m_x 10^5}{pa^2}$	$\frac{-m_{xy} 10^5}{pa^2}$	$\frac{m_y 10^5}{pa^2}$
			1	12 286,10	16 625,04	13 455,12	16 625,04
			1,2	185,35	335,34	379,13	342,80
		1	1,6	20,26	22,38	167,31	41,72
			2,25	2,13	−58,47	137,08	−14,58
			4	−1,57	−20,08	96,01	−6,20
			1	1 963,21	2 647,03	4 365,61	10 547,11
			1,2	246,51	345,32	679,47	1 367,13
0,3	200	2	1,6	30,70	42,32	196,20	187,99
			2,25	6,27	−8,65	130,57	20,05
			4	0,11	−10,31	95,28	−8,51
			1	489,36	655,22	1 673,72	5 802,31
			1,2	246,49	329,52	891,89	2 893,22
		3	1,6	48,90	63,41	253,53	537,98
			2,25	11,60	10,47	128,36	108,28
			4	1,22	−6,89	86,48	1,44

Parametern $a/h \times f_b/b$ gleiche innere Kräfte gehören, falls das Seitenverhältnis a/b und das Pfeilhöhenverhältnis f_a/f_b festgesetzt ist. (Vgl. mit Gln. (5.7)—(5.14).)

Schließlich soll über die Konvergenz der den Berechnungen zugrunde liegenden Fourierschen Reihen geschrieben werden. Die Konvergenzuntersuchungen wurden in den Punkten $x = 0$, $y = 0$ und $x = 2a$, $y = 2b$ durchgeführt.

Es wurde festgestellt, daß man, wenn die Mittelflächenkräfte *der »halbnormalen« HP-Schale* mit Hilfe von Fourierschen Reihen mit 49 Gliedern ($M = N = 13$) errechnet werden, um etwa 4% kleinere Werte als die Summen der Reihen mit 256 Gliedern ($M = N = 31$) erhält. Nimmt man zwei Glieder ($M = 3$, $N = 1$) in Betracht, so beträgt die Abweichung etwa minus 13%.

Bei der Berechnung der Durchbiegungen und Momente der *»halbnormalen«* Schalen wäre es genügend gewesen, bloß das erste Glied der entsprechenden Fourierschen Reihen ($M = N = 1$) zu berücksichtigen. (Die maximale Abweichung beträgt etwa minus 2%). Dies entspricht der Lösung von [23] bezogen auf die ebene Platte.

Bestimmt man die Mittelflächenkräfte der »*normalen*« *HP-Schale* ($f_a/f_b = 4$) mit Hilfe von Fourierschen Reihen mit 36 bzw. 49 Gliedern ($M = N = 11$, bzw. $M = N = 13$), so ergeben sich um etwa 3 bzw. 2% kleinere (N_{xb}) bzw. größere (N_{yb}) Werte als die Summen der Reihen mit 256 Gliedern. Berücksichtigt man zwei Glieder ($M = 3$, $N = 1$), so beträgt die Abweichung bei N_{xb} etwa plus 3%, bei N_{yb} etwa 20%. Die Funktionen der sehr geringen Momente der »normalen« HP-Schale konvergierten am langsamsten, d. h. zum Erreichen der für die Praxis genügenden Genauigkeit waren Fouriersche Reihen mit mindestens 256 Gliedern ($M = N = 31$) notwendig.

6. Zusammenfassung

In dieser Abhandlung wurde das Verhältnis zwischen Membran- und Biegekräftespiel der sattelförmigen, flachen, an den Rändern normalkraftfreien HP-Schalen mit in der Grundprojektion gleichmäßig verteilter Belastung untersucht. Im Laufe der Behandlung wurde großes Gewicht auf die Untersuchung *der Existenz und Eindeutigkeit der Membranlösung* und der *Möglichkeit der dehnungslosen Verformung* gelegt. Es stellte sich heraus, daß der Charakter des Kräftespieles der behandelten HP-Schalen grundlegend durch *das Pfeilhöhenverhältnis* bestimmt wird. Es wurde festgestellt, daß wenn irgendeine (sinusförmige) Lastkomponente durch endliche Membrankräfte nicht in Gleichgewicht gehalten werden kann, dann ist die Schale zu einer dehnungslosen Verformung von Form der erwähnten Lastkomponente fähig. Es wurden die zu den Schalen mit verschiedenen Pfeilhöhenverhältnissen gehörenden charakteristischen dehnungslosen Verformungsfunktionen zusammengefaßt.

Für die die Mehrheit der Stahlbetonschalen gut charakterisierenden geometrischen Verhältnisse wurden die charakteristischen Werte der inneren Kräfte nach der Biegetheorie bestimmt und für einige wichtige Fälle wurden auch die Verteilungen der inneren Kräfte über den Grundrißbereich dargestellt.

Es wurde ermittelt, auf welche Weise sich der durch Mittelflächenkräfte getragene Lastanteil ändert.

An Hand der Untersuchungen kann festgestellt werden, daß sich *die »halbnormale« HP-Schale* ungünstiger als die entsprechende ebene Platte verhält, weil in ihr außer der Momente, die um etwas größer als jene einer ebenen Platte sind, auch Normal- und Schubkräfte auftreten, die den Biegeschnittkräften entgegenwirken. Das Kräftespiel der »halbnormalen« Schale wird grundlegend durch *die dehnungslose Verformung* bestimmt.

Bezüglich der «*normalen*« *HP-Schale* ändert sich grundlegend das plattenartige Bild der inneren Kräfte, das bei der »halbnormalen« HP-Schale

behandelt wurde. Die nach der Biegetheorie ermittelten Mittelflächenkräfte der »normalen« HP-Schale werden durch die Membrankräfte nach der »geometrischen« Theorie von AIMOND entsprechend angenähert. Es wurde *der Pfeilhöhenverhältnisbereich* bestimmt, in dem die Wirkung der Momente ähnlich wie bei der »normalen« HP-Schale verschwindend gering ist. In diesem Bereich ist es gerechtfertigt, die Stabilitätsuntersuchung der sattelförmigen, an den Rändern normalkraftfreien HP-Schalen nach der linearen Theorie vorzunehmen. Das werden wir in unserem folgenden Artikel [12] darlegen.

SCHRIFTTUM

1. BELEŞ, A.—SOARE, M.: Das elliptische und hyperbolische Paraboloid im Bauwesen. VEB Verlag für Bauwesen, Berlin—Akademie-Verlag, Bukarest 1970
2. BÖLCSKEI, E.: Déformation des voiles minces. *Acta Techn. Hung.* **5** (1952), 489—506
3. CANDELA, F.: General Formulas for Membrane Stresses in Hyperbolic Paraboloidical Shells. *ACI Journal* (1960) September, 353—371
4. FLÜGGE, W.: Statik und Dynamik der Schalen. 3. Aufl. Springer-Verlag, Berlin—Göttingen—Heidelberg 1962
5. FLÜGGE, W.: Stresses in Shells. 2. Ed. Springer Verlag, Berlin—Heidelberg—New York 1973
6. FLÜGGE, W.—GEYLING, F. T.: General Theory of Deformations of Membrane Shells. *International Association for Bridge and Structural Engineering* **17** (1957) 23—46.
7. FRANK, PH.—MISES, R. v.: Die Differential- und Integralgleichungen der Mechanik und Physik. Bd. I. 2. Aufl. Vieweg u. Sohn, Braunschweig 1930
8. FRANZ, G.: Konstruktionslehre des Stahlbetons. 1—2. Band. Springer-Verlag, Berlin—Heidelberg—New York 1969
9. GOL'DENVEISER, A. L.: The Theory of Thin Elastic Shells. Pergamon, New York 1961
10. HAAS, A. M.: Entwurf und Konstruktion dünner Betonschalen. Werner-Verlag, Düsseldorf 1969
11. HRUBAN, K.: Die Biegetheorie der Translationsflächen und ihre Anwendung im Hallenbau. *Acta Techn. Hung.* **7** (1953), 425—464.
12. JANKÓ, L.: Untersuchung der Stabilität sattelförmiger, flacher, normalkraftfrei gelagerter HP-Schalen unter gleichmäßig verteilter Belastung. *Acta Techn. Hung.* **91** (1980)
13. JANKÓ, L.: Untersuchung der Gleichgewichtszustände sattelförmiger, flacher, normalkraftfrei gelagerter HP-Schalen unter gleichmäßig verteilter Belastung, mit besonderer Berücksichtigung des Durchschlagens und der Abzweigung. *Acta Techn. Hung.* **91** (1980)
14. KANTOROVICS, L. V.—KRÜLOV, V. I.: A felsőbb analízis közelítő módszerei. Akadémiai Kiadó, Budapest 1953. (auf ungarisch) (Näherungsmethoden der höheren Analysis)
15. KOLLÁR, L.: Héjak nyúlásmentes alakváltozásai. *Építés- és Építészettudomány*, **3** (1971), 19—38. (auf ungarisch) (Dehnungslose Verformungen der Schalen)
16. KOLLÁR, L.: Schalenkonstruktionen. Sonderdruck aus dem *Beton-Kalender* 1974. Verlag von Wilhelm Ernst und Sohn, Berlin—München—Düsseldorf 1974
17. MENYHÁRD, I.: Héjszerkezetek. Műszaki Könyvkiadó, Budapest, 1966. (auf ungarisch) (Schalenkonstruktionen)
18. REISSNER, E.: On Some Aspects of the Theory of Thin Elastic Shells. Boston Society of Civil Engineers 1955, pp. 100—133
19. SOMMERFELD, A.: Vorlesungen über theoretische Physik. Bd. VI. Partielle Differentialgleichungen der Physik. Akademische Verlagsgesellschaft Geest u. Portig, Leipzig 1954
20. SZMODITS, K.: Statik der Schalenkonstruktionen. B. G. Teubner V., Leipzig — Akadémiai Kiadó, Budapest 1966
21. TARNAI, T.: Existence and Uniqueness Criteria of the Membrane State Shells. I. Hyperbolic Shells. *Acta Techn. Hung.* (im Druck)
22. TARNAI, T.: Edge Disturbancies of Second-order Shallow Translational Shells on a Rectangular Base. *Acta Techn. Hung.* **74** (1973)
23. TIMOSHENKO, S.—WOINOWSKY-KRIEGER, S.: Theory of Plates and Shells. Second Edition. McGraw-Hill Book Company, New York—Toronto—London 1959

24. TIKHONOV, A. N.—SAMARSKII, A. A.: Partial Differential Equations in Mathematical Physics, Holden-Day, San Francisco 1964
25. VLASZOV, V. Z. (WLASSOW, W. S.)—GARAI, T.: Nyomatékmentes forgáshéjak kinematikai határozatlanságának feltétele. *MTA VI. Műsz. Oszt. Közl.* **19** (1956), 211—223. (auf ungarisch) (Bedingung der kinematischen Unbestimmtheit von membranen Drehschalen)
26. WLASSOW, V. S.: Allgemeine Schalentheorie und ihre Anwendung in der Technik. Akademie-Verlag, Berlin 1958

Comparison of the Membrane and Bending Theory of Shallow Saddle-shaped Hypar Shells, Supported by Shear Diaphragms, under Uniform Load. — The paper is the first part of a series consisting of three parts. The 2nd and 3rd chapters deal with the phenomena of the stability of the saddle-shaped hypar shells which are supported along the lines of the principal curvature by edge arches possessing flexural and torsional rigidity being negligible in the horizontal plane. In the paper at hand, prior to the investigations of the stability, the following problems will be discussed: the problem of existence and uniqueness of the *membrane solution;* the difficulties emerging from the *kinematic uncertainty* of the shell and the problem what are the geometric parameters on the basis of which these shells, with a close approximation, as *membrane shells* could be considered.

Acta Technica Academiae Scientiarum Hungaricae, Tomus 91 (1—2), pp. 57—80 (1980)

THE FIELD EQUATIONS AND BOUNDARY CONDITIONS WITH FORCE STRESSES AND COUPLE STRESSES IN THE LINEARIZED THEORY OF MICROPOLAR ELASTOSTATICS

I. KOZÁK* and GY. SZEIDL**

[Manuscript received March 5, 1979]

Authors determined in two different ways the independent, necessary and sufficient conditions of the compatibility of the strain fields i.e., the six field equations of compatibility to be selected in various ways as well as the boundary conditions of compatibility; first based on the conditions of the single-valued displacements and rotations on the boundary surface, second, on the basis of the principle of minimum complementary energy. The field equations and boundary conditions written to the stress fields of the linearized theory of the micropolar elastostatics are summed up, then, on the basis of the uniqueness of the solutions the necessity and sufficiency of the field equations and boundary conditions justified.

1. Introduction

The change in the geometric state of the micropolar elastic solid under external effects may be described with the aid of two vector fields, by the displacements and by the rotations. The system of internal forces is determined by two vector fields, by the force stress field and the couple stress field. The strain state of the solid is also determined by two tensor fields, by the asymmetric strain field and by the curvature twist tensor field.

In the arbitrary system of curvilinear coordinates x^1, x^2, x^3 let us use the following notation:

$\mathbf{u} = u_k \mathbf{g}^k$ — displacements;
$\boldsymbol{\omega} = \omega^a \mathbf{g}_a$ — rotations;
$\mathbf{T} = t^{kl} \mathbf{g}_k \mathbf{g}_l$ — force stress field;
$\mathbf{M} = \mu^{ab} \mathbf{g}_a \mathbf{g}_b$ — couple stress field (t^{kl} and μ^{ab} together mean stress fields);
$\mathbf{A} = a_{kl} \mathbf{g}^k \mathbf{g}^l$ — assymmetric strain field;
$\mathbf{K} = \varkappa_{ab} \mathbf{g}^a \mathbf{g}^b$ — curvature twist tensor field (a_{kl} and $\varkappa_{ab}$ together mean strain fields);
x — all of the coordinates;
g_{kl} — covariant metric tensor;
ε_{klm} — covariant permutation tensor.

The indices behind the comma designate the partial differentiation and those, following the semicolon, the covariant differentiation. Let us here use

* I. Kozák, Candidate of the Techn. Sci., Dózsa György út 14, H-3525, Miskolc, Hungary
** Gy. Szeidl, Rácz Ádám u. 2, H-3532 Miskolc, Hungary

the conventional summation. In the case of the symbolic way of notation, the point put between the tensors (vectors) is the sign of the scalar, and the cross, that of the vectorial product.

Be the solid bounded by a single, simply connected closed surface. It is assumed that the material of the solid is homogeneous, centrosymmetrical and the solid is loaded by the system of body forces $\mathbf{B} = b^i \mathbf{g}_i$ and by the system of body couples $\mathbf{C} = c_b \mathbf{g}^b$ (b^i and c_b together mean body force systems). Let us denote the region of the space occupied by the solid with V, its boundary with S and the normal vector directed outwards from the body with $\mathbf{n} = n_k \mathbf{g}^k$.

The field equations of the boundary-value problem of the linearized micropolar elastostatics formulated to the fields $u_k(x)$ and $\omega^a(x)$ are as follows [1]:

the equilibrium equations:

$$t^{kl}_{..;k} + b^l = 0, \tag{1.1}_1$$

$$\mu^a_{.b\,;a} + \varepsilon_{bpq} t^{pq} + c_b = 0; \tag{1.1}_2$$

the form of Hooke's law to the centrosymmetric solid reads as follows:

$$a_{kl} = c_{klpq} t^{pq}, \tag{1.2}_1$$

$$\varkappa_{ab} = \lambda_{abpq} \mu^{pq}; \tag{1.2}_2$$

the kinematic equations are:

$$a_{kl} = u_{l;k} + \varepsilon_{lks} \omega^s, \tag{1.3}_1$$

$$\varkappa^{\ b}_{a} = \omega^b_{\ ;a}. \tag{1.3}_2$$

In the paper, the following, rather general boundary conditions are assumed: of dynamic nature

$$n_k t^{kl} = \tilde{t}^l \quad \text{and} \quad n_a \mu^a_{\ .b} = \tilde{\mu}_b \quad x \in S_t, \tag{1.4}_1$$

of kinematic nature

$$u_k = \tilde{u}_k \quad \text{and} \quad \omega^a = \tilde{\omega}^a \quad x \in S_u. \tag{1.4}_2$$

In the formulae $\tilde{t}^l$ and $\tilde{\mu}_b$ are prescribed loads at the S_t section of the boundary, and $\tilde{u}_k$ and $\tilde{\omega}^a$ prescribed displacement and rotation, respectively, at the section S_u of the boundary.

$$S_t \cup S_u = S, \quad S_t \cap S_u = 0.$$

The strain energy per unit volume may be calculated from the equation

$$u = \frac{1}{2} t^{kl} a_{kl} + \frac{1}{2} \mu^a_{\ .b} \varkappa^{\ b}_{a}. \tag{1.5}$$

It is proved [1] that the boundary-value problem (1.1) to (1.4) of the linearized theory of the micropolar elastostatics gives unique solutions to the fields $u_k(x)$ and $\omega^a(x)$ outside the rigid-body like motion forms of the solid, and thus, also to the fields $a_{kl}(x)$, $\varkappa_{ab}(x)$, $t^{kl}(x)$, $\mu^{ab}(x)$ and $u(x)$.

The constitutive equations (1.2) give mutual and unambiguous interconnection between the fields $a_{kl}(x)$ and $t^{pq}(x)$, respectively, between the fields $\varkappa_{ab}(x)$ and $\mu^{pq}(x)$. Therefore, it is sufficient to investigate two fields, either those $a_{kl}(x)$ and $\varkappa_{ab}(x)$ or $t^{kl}(x)$ and $\mu^{ab}(x)$.

In the following, assuming the constitutive equations to be valid, the fields $t^{kl}(x)$ and $\mu^{ab}(x)$ will always be considered as those being investigated.

The purpose of the paper is to formulate the boundary-value problems of the linearized micropolar elastostatics to the force stress field and couple stress field, i.e., the establishment of field equations and boundary conditions wherein only force-stress and couple-stress coordinates enter and which are necessary and sufficient for the unique solutions of the boundary-value problem both in the case of the fields $t^{kl}(x)$, $\mu^{ab}(x)$ and to the fields $u_k(x)$, $\omega^a(x)$, (leaving out of consideration the rigid-body like forms of motion with respect to the displacements).

An analogous problem relating to the classic case (in which no couple stresses occur) of the linearized elastostatics has been investigated by two papers of I. KOZÁK [3], [4] as a completion of the study of K. WASHIZU published in 1957 [2]. The same result was obtained in two different ways, partly by making use of the conditions of the single-valued displacements on the boundary surface and Bianchi's identity, partly with the aid of the principle of minimum complementary energy, i.e. three suitably selected scalar compatibility equations as field equations, should be attached to the equilibrium equations, and the usual boundary conditions should be completed with the so-called boundary conditions of compatibility.

In this paper, paragraph 2 presents on the basis of [6] and [1: pp. 42—45] the conditions of the single-valued displacements and rotations to be calculated from the stress fields in the volume region, then determines the conditions of single-valuedness in relation with the surface region.

In paragraph 3 the independent, necessary and sufficient conditions of the compatibility of the strain fields are presented: i.e., the compatibility field equations to be selected in several ways and the boundary conditions of compatibility.

In paragraph 4 the field equations and boundary conditions of the linearized theory of the micropolar elastostatics which are written by force stresses and couple stresses are summed up, and based on the investigation of the unique solutions the necessity and, at the same time, the sufficiency of the presented field equations and boundary conditions are pointed out.

In paragraph 5, with the aid of the stress functions, by formal trans-

formations it is proved that the independent, necessary and sufficient compatibility conditions of the strain fields are derived from the principle of minimum complementary energy: the equations of compatibility and the boundary conditions of compatibility. At the same time also the conditions prescribed for the stress fields, following from the kinematic boundary conditions, are obtained.

Paragraph 6 summarizes the results obtained.

2. Conditions of the single-valued rotations and displacements to be calculated from the stress fields

2.1. Let us consider the force stress field $t^{kl}(x)$ and the couple stress field $\mu^{ab}(x)$ as well as the strain fields $a_{kl}(x)$ and $\varkappa_a^{\cdot b}(x)$ to be calculated by the constitutive equations (1.2) as given quantities.

Let the curve h determined by the equation $x^k = x^k(s)$ (s being a parameter measured along the curve) connect the points O and P to be chosen arbitrarily on the solid (Fig. 1). Along the curve where

$$\mathbf{t} = t^k \mathbf{g}_k = \frac{d\mathbf{r}}{ds}, \qquad t^k = \frac{dx^k}{ds}$$

s the tangent vector ($\mathbf{r}$ being the position vector) and $d\mathbf{r} = \mathbf{t}ds$, the differential of the rotations may, according to Eq. $(1.3)_2$, be written as follows

$$d\boldsymbol{\omega} = \mathbf{g}_b \omega^b_{\cdot;a} dx^a = \mathbf{t} \cdot (\varkappa_a^{\cdot b}\, \mathbf{g}^a \mathbf{g}_b) ds = \mathbf{t} \cdot \mathbf{K} ds, \tag{2.1}_1$$

and the differential of the displacements, according to Eq. $(1.3)_1$ reads as follows

$$d\mathbf{u} = \mathbf{g}^l\, u_{l;k}\, dx^k = \mathbf{t} \cdot (a_{kl} + \varepsilon_{kls}\, \omega^s)\, \mathbf{g}^k\, \mathbf{g}^l\, ds = \mathbf{t} \cdot \mathbf{B} ds. \tag{2.1}_2$$

The integrals of Eq. (2.1) along the curve h from point 0 to point P yield in point P the displacement $\mathbf{u}_P$ and the rotation ω_P:

$$\boldsymbol{\omega}_P = \boldsymbol{\omega}_0 + \int_h \mathbf{t} \cdot \mathbf{K}\, ds, \tag{2.2}_1$$

$$\mathbf{u}_P = \mathbf{u}_0 + \int_h \mathbf{t} \cdot \mathbf{B}\, ds. \tag{2.2}_2$$

Considering that in formulae (2.2) P may be any of the points of the solid, with the aid of the formulaes (2.2) all the displacements and rotations of the whole solid may be produced in the case where the strain fields $a_{kl}(x)$ and

$\varkappa_a^b(x)$, and at a point, for example, point 0, the displacement $\mathbf{u}_0$ and rotation $\boldsymbol{\omega}_0$ are given.

The formulae (2.2) correspond to the Cesaro's formula of the classical linearized elastostatics. The identity may readily be revealed by introducing

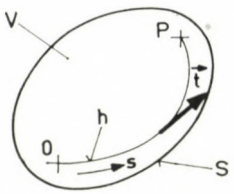

Fig. 1

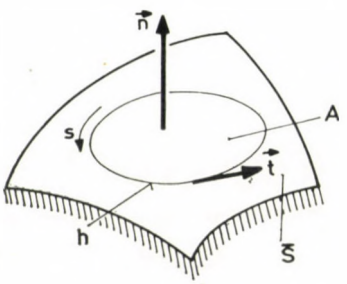

Fig. 2

the antisymmetrical rotation tensor ψ interpreted by the formula

$$-\varepsilon_{kls}\omega^s \mathbf{g}^k \mathbf{g}^l = \psi_{kl}\mathbf{g}^k\mathbf{g}^l = \psi$$

and, consequently, by carrying out in Eq. $(2.1)_2$ the following substitution:

$$\mathbf{t} \cdot (\varepsilon_{kls}\,\omega^s\,\mathbf{g}^k\,\mathbf{g}^l)\,ds = \psi \cdot \frac{d\mathbf{r}}{ds}\,ds = -\frac{d}{ds}\,[\psi \cdot (\mathbf{r}_P - \mathbf{r})] + \frac{d\psi}{ds} \cdot (\mathbf{r}_P - \mathbf{r}).$$

Taking hereupon the integral of Eq. $(2.1)_2$ from point O to point P along the curve h indeed yields the familiar shape of Cesaro's formula [3], [5]:

$$\mathbf{u}_P = \mathbf{u}_0 + \psi_0 \cdot (\mathbf{r}_P - \mathbf{r}_0) + \int_h \left[\mathbf{t} \cdot \mathbf{A} + \frac{d\psi}{ds} \cdot (\mathbf{r}_P - \mathbf{r})\right] ds. \qquad (2.3)$$

From Eq. (2.2) it is also to be read that infinitely many displacements and rotations are associated with the same fields $a_{kl}(x)$ and $\varkappa_a^b(x)$ which, however, may not differ from each other except rigid-body like motions of

the solid determined by the vectors $\mathbf{u}_0$ and $\boldsymbol{\omega}_0$:

$$\mathbf{u}_0 + \boldsymbol{\psi}_0 \cdot (\mathbf{r}_P - \mathbf{r}_0) = \mathbf{u}_0 + \boldsymbol{\omega}_0 \times (\mathbf{r}_P - \mathbf{r}). \tag{2.4}$$

2.2. With a knowledge of the strain fields $a_{kl}(x)$ and $\varkappa_a^{\cdot b}(x)$ as well as of $\mathbf{u}_0$ and $\boldsymbol{\omega}_0$, the formulae (2.2) yield the displacement and rotation in point P independently of the choice of the curve h between the points 0 and P, in the case, when in the regions of the curves h which may come into question, the following equations will be satisfied with respect to the integrands of the integrals along the curve:

$$\nabla \times \mathbf{K} = \varepsilon^{mpa}\, \varkappa_{a.;p}^{\cdot b} \mathbf{g}_m \mathbf{g}_b = \mathbf{0}, \tag{2.5}_1$$

$$\nabla \times \mathbf{B} = \varepsilon^{mpk}(a_{kl;p} + \varepsilon_{kls}\omega^s_{\cdot;p})\, \mathbf{g}_m\, \mathbf{g}^l = \mathbf{0}. \tag{2.5}_2$$

Introduction of the incompatibility tensors

$$e^{mb} = \varepsilon^{mpa}\, \varkappa_{a.;p}^{\cdot b} \tag{2.6}_1$$

and

$$d^m_{\cdot l} = \varepsilon^{mpk}(a_{kl;p} + \varepsilon_{kls}\, \varkappa_p^{\cdot s}) \tag{2.6}_2$$

consideration of Eqs (2.5) and $(1.3)_2$ permit to state that the fulfilment of the equations

$$e^{mb}(x) = \varepsilon^{mpa} \varkappa_{a.;p}^{\cdot b} = 0 \quad x \in V \tag{2.7}_1$$

and

$$d^m_{\cdot l}(x) = \varepsilon^{mpk}(a_{kl;p} + \varepsilon_{kls} \varkappa_p^{\cdot s}) = 0 \quad x \in V \tag{2.7}_2$$

is the necessary and sufficient condition of the requirement that in the case of given $\mathbf{u}_0$, $\boldsymbol{\omega}_0$ and with the knowledge of $a_{kl}(x)$ and $\varkappa_a^{\cdot b}(x)$ the displacements $u_k(x)$ and rotations $\omega^a(x)$ in the region V should be single-valued, i.e., the strain fields should be compatible. The Eqs (2.7) are the compatibility (integrability) equations whose number is 18.

Considering Eqs (1.3) it can readily be understood that with a knowledge of the displacements and rotations, the compatibility equations (2.7) will identically be satisfied. Otherwise (without the knowledge of the displacements and rotations) Eqs (2.7) constitute the conditions of compatibility of the strain fields.

2.3. The equations of compatibility (2.7) are not independent of each other, because, as is to be understood from the interpretation (2.6) of the incompatibility tensors, the equations

$$e^{mb}_{\cdot\cdot\,;m} = 0 \tag{2.8}_1$$

and

$$d^m_{\cdot l;m} + \varepsilon_{lpq}\, e^{pq} = 0 \tag{2.8}_2$$

will identically be satisfied.

The conclusions to be drawn from the identities (2.8) are dealt with in paragraph 3.

2.4. Consider first the conditions of the single-valued displacements and rotations to be calculated from the strain fields on a surface by making use of formulae (2.2). Be the considered surface $\bar{S}$ wholly within the region of the solid V or, wholly or partially at its boundary S.

The formulae (2.2) give single-valued displacements and rotations at the surface $\bar{S}$ if with respect to any closed curve h to be selected on this surface (Fig. 2) the following are true

$$\oint_h \mathbf{t} \cdot \mathbf{K}\, ds = \mathbf{0} \quad \text{and} \quad \oint_h \mathbf{t} \cdot \mathbf{B}\, ds = \mathbf{0}.$$

From the above, by denoting the part of area confined by the curve h with A, according to Stokes's theorem the equations

$$\oint_h \mathbf{t} \cdot \mathbf{K}\, ds = \int_A (\mathbf{n} \times \nabla) \cdot \mathbf{K}\, dA = \mathbf{0}$$

and

$$\oint_h \mathbf{t} \cdot \mathbf{B}\, ds = \int_A (\mathbf{n} \times \nabla) \cdot \mathbf{B}\, dS = \mathbf{0}$$

are obtained which, in the case of arbitrary h and A may only be valid if the conditions

$$(\mathbf{n} \times \nabla) \cdot \mathbf{K} = \mathbf{n} \cdot (\nabla \times \mathbf{K}) = \mathbf{0} \quad x \in \bar{S}$$

and

$$(\mathbf{n} \times \nabla) \cdot \mathbf{B} = \mathbf{n} \cdot (\nabla \times \mathbf{B}) = \mathbf{0} \quad x \in \bar{S}.$$

are satisfied.

Considering Eqs (2.5) and (2.6) may be stated that the displacements and rotations to be determined at the surface $\bar{S}$ from the strain fields are single valued in the case, when the conditions

$$n_m e^{mb} = 0 \qquad x \in \bar{S} \tag{2.9}_1$$

and

$$n_m d^m_{\cdot l} = 0 \qquad x \in \bar{S} \tag{2.9}_2$$

are fulfilled

The conditions (2.9) remain valid also when related to the whole boundary S of the solid.

3. Independent conditions of the compatibility of the strain fields

3.1. According to the identities (2.8), the compatibility conditions of the strain fields, i.e., the equations of compatibility are not independent of each other. Let us examine this problem in a more detailed way.

Let us form for this purpose, by changing the indices, the following scalar products of the arbitrary, differentiable vector fields $v_b(x)$, $w^l(x)$ and of the identities (2.8):

$$v_b \, e^{ab}_{..;a} = 0; \quad w^l \, d^k_{.l;k} + w^l \, \varepsilon_{lpq} \, e^{pq} = 0,$$

and then integrate the expressions obtained, in the region V. The partial integration yields:

$$\int_V v_b \, e^{ab}_{..;a} \, dV = \int_S n_a \, e^{ab} \, v_b dS - \int_V v_{b;a} \, e^{ab} \, dV = 0,$$

and

$$\int_V w^l \, d^k_{.l;k} \, dV = \int_S n_k \, d^k_{.l} \, w^l dS - \int_V w^l_{.;k} \, d^k_{.l} \, dV = -\int_V w^l \, \varepsilon_{lpq} \, e^{pq} \, dV.$$

Hereafter, by describing the conditions of single-valued displacements and rotations at the whole boundary S the following equations are obtained:

$$\int_V v_{b;a} \, e^{ab} \, dV = 0 \tag{3.1}_1$$

and

$$\int_V w^l_{.;k} \, d^k_{.l} \, dV = \int_V w^l \, \varepsilon_{lpq} \, e^{pq} dV. \tag{3.1}_2$$

Now, let us analyse Eq. $(3.1)_1$. Taking into account that all of the nine scalar coordinates of the gradient $v_{b;a}$ cannot be chosen arbitrarily, from $(3.1)_1$ it does not follow that e^{ab} disappears at every point of region V. However, three such pairs of indices may be chosen in various ways which permit a solution to the equation

$$v_{B;A} = \alpha_{BA}(x) \tag{3.2}_1$$

with respect to $v_b(x)$, even in the case of three fully arbitrarily chosen functions $\alpha_{BA}(x)$. The three pairs of indices are denoted by the connected letters AB. By using the vector field $v_b(x)$ chosen in the way mentioned above instead of Eq. $(3.1)_1$ the following may be written:

$$\int_V \left[\sum_{(AB)} \alpha_{BA} \, e^{AB} + \sum_{(XY)} v_{Y;X} \, e^{XY} \right] dV = 0. \tag{3.3}_1$$

In the equation the coordinates designated by the indices AB and XY yield all of the coordinates of e^{ab}; (AB) and (XY) under the summation sign mean that the summation should be carried out according to the pairs of indices (and not according to the convention of summation!)

From Eq. $(3.3)_1$ it follows that in case of the validity of the equations

$$e^{XY} = 0, \qquad x \in V$$

due to the functions $\alpha_{BA}(x)$ arbitrarily chosen, also the equations

$$e^{AB} = 0, \quad x \in V$$

are true.

Going on, in the case of fulfilment of $e^{pq} = 0$; $x \in V$, the right-hand side of Eq. $(3.1)_2$ becomes zero, which means that the same chain of ideas can be repeated was shown in connection with Eq. $(3.1)_1$. Thus, instead of Eq. $(3.1)_2$

$$\int_V \left[\sum_{(KL)} w^L_{.K}\, d^K_{.L} + \sum_{(ST)} w^T_{.S}\, d^S_{.T} \right] dV = 0, \qquad (3.3)_2$$

may be written, in which the connected letters KL designate three pairs of indices, to be selected in several ways, of the gradient $w^l_{.;k}$ with which the equation

$$w^L_{.;K} = \beta^L_{.K}(x) \qquad (3.2)_2$$

has a solution to $w^l(x)$ even in the case of three wholly arbitrarily selected functions $\beta^L_{.K}(x)$, and the coordinates of the pairs of indices KL and ST yield all of the coordinates of $d^k_{.l}$.

Hereafter, from Eq. $(3.3)_2$ it follows that in case of the validity of the equations

$$d^S_{.T} = 0 \quad x \in V,$$

due to the functions $\beta^L_{.K}(x)$ arbitrarily chosen, also the equations

$$d^K_{.L} = 0, \qquad x \in V$$

are valid.

3.2. For summing up, the following statement may be made: In case of the fulfilment of the equations

$$e^{XY} = 0; \qquad d^S_{.T} = 0, \qquad x \in V, \qquad (3.4)$$

and

$$n_a\, e^{ab} = 0; \qquad n_k\, d^k_{.l} = 0, \qquad x \in S \qquad (3.5)$$

also the equations

$$e^{AB} = 0; \qquad d^K_{.L} = 0, \qquad x \in V \qquad (3.6)$$

are valid.

In the above equations XY and ST designate six pairs of indices each; AB and KL designate three pairs of indices each, in which from the values

1, 2, 3 otherwise admissible only certain of them may be possible. In fact, the pairs of indices XY and AB as well as ST and KL should yield all the possible pairs of indices and meanwhile, the three pairs of indices AB and KL should be chosen with the view of obtaining a solution for the equations

$$v_{B;A} = \alpha_{BA}(x)$$

and

$$w^L_{\cdot;K} = \beta^L_{\cdot K}(x)$$

with respect to the vector fields $v_b(x)$ and $w^l(x)$ even in the case of the fully arbitrarily selected functions $\alpha_{BA}(x)$ and $\beta^L_{\cdot K}(x)$.

In conformity with that said above, the equations of compatibility (3.4) and boundary conditions of compatibility (3.5) are equivalent with the equations of compatibility (integrability) (2.7), i.e., they mean the independent, and at the same time, necessary and sufficient conditions of the compatibility of strain fields.

4. Field equations and boundary conditions written with force stresses and couple stresses. Uniqueness of the solutions

4.1. According to the results obtained, to the boundary value-problems of the micropolar elastostatics formulated to the force stresses and couple stresses the following field equations and boundary conditions are coordinated. Field equations:

$$t^{kl}_{\cdot\cdot;k} + b^l = 0, \tag{4.1}_1$$

$$\mu^a_{\cdot b;a} + \varepsilon_{bpq} t^{pq} + c_b = 0, \tag{4.1}_2$$

$$a_{kl} = c_{klpq}\, t^{pq}, \tag{4.2}_1$$

$$\varkappa_{ab} = \lambda_{abpq} \mu^{pq}, \tag{4.2}_2$$

$$e^{XY} = \varepsilon^{Xpa}\, \varkappa^{\cdot Y}_{a\cdot;p} = 0, \tag{4.3}_1$$

$$d^S_{\cdot T} = \varepsilon^{Spk}(a_{kT;p} + \varepsilon_{kTq}\, \varkappa^{\cdot q}_{\cdot p}) = 0. \tag{4.3}_2$$

Boundary conditions:

$$n_k t^{kl} = \tilde{t}^l \quad \text{and} \quad n_a \mu^a_{\cdot b} = \tilde{\mu}_b, \quad x \in S_t, \tag{4.4}$$

$$u_k = \tilde{u}_k \quad \text{and} \quad \omega^a = \tilde{\omega}^a, \quad x \in S_u, \tag{4.5}$$

$$n_a e^{ab} = 0 \quad \text{and} \quad n_k d^k_{\cdot l} = 0, \quad x \in S. \tag{4.6}$$

The strain energy per unit volume $u(x)$ may be formulated, as a scalar field, according to (1.5).

The pairs of indices of the six compatibility equations (4.3) should be chosen according to paragraph 3.2. The boundary conditions replacing the kinematic boundary conditions (4.5) and containing the force stress field and couple stress field are established in paragraph 5.12. The Eq. (4.6) are the boundary conditions of compatibility.

4.2. The solution to the boundary-value problems (4.1) to (4.6) is single-valued with respect to the force stress field $t^{kl}(x)$ and to the couple stress field $\mu^a_{.b}(x)$, further, leaving the rigid-body motions out of consideration, to the displacements $u^k(x)$ and rotations $\omega^a(x)$.

To prove this statement let us start out from the assumption that two associated force stress fields and couple stress fields

$$\underset{1}{t}^{kl}(x) \neq \underset{2}{t}^{kl}(x), \qquad \text{or} \qquad \underset{1}{\mu}^a_{.b}(x) \neq \underset{2}{\mu}^a_{.b}(x)$$

exist which, in pairs, satisfy all the field equations and boundary conditions (4.1) to (4.3) and (4.4) to (4.6), respectively.

Let us first provide the scalar product of the equilibrium equations (4.1) and the arbitrary, differentiable fields $\underset{1}{w}_k(x)$ and $\underset{1}{\psi}^a(x)$

$$\underset{i}{t}^{kl}_{..;k}\, \underset{1}{w}_l + b^l_{\blacksquare}\, \underset{1}{w}_l = 0; \qquad i = 1, 2$$

$$\underset{i}{\mu}^a_{.b;a}\, \underset{1}{\psi}^b + \varepsilon_{klb}\, \underset{i}{t}^{kl}\, \underset{1}{\psi}^b + c_b\, \underset{1}{\psi}^b = 0; \quad i = 1, 2,$$

hereafter, let us integrate the expressions obtained in region V. Partial integration yields

$$\int_V (\underset{i}{t}^{kl}\, \underset{1}{w}_{l;k} + b^l\, \underset{1}{w}_l)\, dV = \int_S n_k\, \underset{i}{t}^{kl}\, \underset{1}{w}_l\, dS, \qquad i = 1, 2$$

and

$$\int_V (\underset{i}{\mu}^a_{.b}\, \underset{1}{\psi}^b_{.;a} + \underset{i}{t}^{kl}\, \varepsilon_{lkb}\, \underset{1}{\psi}^b + c_b\, \underset{1}{\psi}^b) dV = \int_S n_a\, \underset{i}{\mu}^a_{.b}\, \underset{1}{\psi}^b\, dS; \qquad i = 1, 2. \quad (4.7)$$

Subtracting now the equations containing quantities denoted by $i = 1$ from the equations of the very same character containing quantities denoted by $i = 2$, and adding the resulting equations by taking the dynamic boundary conditions (4.4) into account. The same sequence of ideas may be followed in making use of the arbitrary, derivable vector fields $\underset{2}{w}_k(x) \neq \underset{1}{w}_k(x)$ and $\underset{2}{\psi}^a(x) \neq$ $\neq \underset{1}{\psi}^a(x)$. Finally one obtains:

$$\int_V \{(\underset{2}{\mu}^a_{.b} - \underset{1}{\mu}^a_{.b})\, (\underset{2}{\psi}^b_{.;a} - \underset{1}{\psi}^b_{.;a}) + (\underset{2}{t}^{kl} - \underset{1}{t}^{kl})\, [(\underset{2}{w}_{l;k} + \varepsilon_{lks}\, \underset{2}{\psi}^s) - (\underset{1}{w}_{l;k} + \varepsilon_{lks}\, \underset{1}{\psi}^s)]\}\, dV =$$

$$= \int_{S_u} [n_a(\underset{2}{\mu}^a_{.b} - \underset{1}{\mu}^a_{.b})\, (\underset{2}{\psi}^b - \underset{1}{\psi}^b) + n_k(\underset{2}{t}^{kl} - \underset{1}{t}^{kl})\, (\underset{2}{w}_l - \underset{1}{w}_l)]\, dS. \quad (4.8)$$

Eqs (4.7) and (4.8) are also valid for the so-called statically admissible force stress fields and couple stress fields satisfying the dynamic boundary conditions (4.4) and the equilibrium equations (4.1), as well as for arbitrary vector fields $w_l(x)$ and $\psi^b(x)$.

Assuming further that by making use of the statically admissible stress fields $\underset{i}{t}^{kl}(x)$, $\underset{i}{\mu}^a_{.b}(x)$; $i = 1, 2$ and the strain fields determined by them with the constitutive equations (4.2), i.e. the fields

$$\underset{i}{a}_{kl} = c_{klpq} \underset{i}{t}^{pq}, \quad i = 1, 2$$

$$\underset{i}{\varkappa}_{ab} = \lambda_{abpq} \underset{i}{\mu}^{pq}, \quad i = 1, 2$$

satisfying the equations of compatibility (4.3) and the boundary conditions of compatibility (4.6), that is to say they are compatible; hence, it follows that the displacements and rotations $\underset{i}{u}_l(x)$ and $\underset{i}{\omega}^b(x)$; $i = 1, 2$ calculated according to paragraph 2.1 from the stress fields $\underset{i}{t}^{kl}(x)$ and $\underset{i}{\mu}^b(x)$; $i = 1, 2$ being, in conformity with the basic assumption, different from each other, are single-valued (assuming the same rigid-body motion of the solid), and also different.

Prescription of the identities

$$\underset{i}{w}_l(x) = \underset{i}{u}_l(x) \qquad \text{and} \qquad \underset{i}{\psi}^b(x) = \underset{i}{\omega}^b(x), \qquad i = 1, 2$$

for the otherwise arbitrary vector fields and the requirement of fulfilment of the kinematic boundary conditions (4.5) in connection with the fields $u_l(x)$ and $\underset{i}{\omega}^b(x)$; $i = 1, 2$, replacement into Eq. (4.8) yield

$$\int_V \left[(\underset{2}{\mu}^a_{.b} - \underset{1}{\mu}^a_{.b}) (\underset{2}{\varkappa}^{.b}_a - \underset{1}{\varkappa}^{.b}_a) + (\underset{2}{t}^{kl} - \underset{1}{t}^{kl}) (\underset{2}{a}_{kl} - \underset{1}{a}_{kl}) \right] dV = 0. \tag{4.9}$$

Considering on the basis of (1.5) that the integrand of Eq. (4.9) is twice as large as the strain energy per unit volume associated with the stress fields

$$\underset{2}{\mu}^a_{.b} - \underset{1}{\mu}^a_{.b} \qquad \text{and} \qquad \underset{2}{t}^{kl} - \underset{1}{t}^{kl}$$

as well as that the strain energy is never negative, contrary to the basic assumption, from Eq. (4.9) if follows

$$\underset{2}{\mu}^a_{.b} = \underset{1}{\mu}^a_{.b} \qquad \text{and} \qquad \underset{2}{t}^{kl} = \underset{1}{t}^{kl}, \tag{4.9b}$$

or, taking (1.2) into account

$$\underset{2}{\varkappa}{}^{a}_{.b} = \underset{1}{\varkappa}{}^{a}_{.b} \qquad \text{and} \qquad \underset{2}{a}_{kl} = \underset{1}{a}_{kl} \tag{4.9c}$$

which, in other words means that the solution to the boundary-value problem (4.1) to (4.6) is unique with respect to the stress fields $\mu^{a}_{.b}(x)$ and $t^{kl}(x)$, further to the strain fields $a_{kl}(x)$, $\varkappa^{.b}_{a}(x)$, as well as to the rotations $\omega^{b}(x)$ and displacements $u_k(x)$ (assuming the same rigid-body motion of the solid).

Considering that all the Eqs (4.1) to (4.6) have been used for the justification of the uniqueness of the solution, it follows that the field Eqs (4.1) to (4.3) and the boundary conditions (4.4) to (4.6) constitute, in the linearized theory of the micropolar elastostatics, the necessary and sufficient field equations and boundary conditions formulated to the force stresses and couple stresses.

5. Derivation of the boundary conditions of compatibility with the aid of the principle of minimum complementary energy

5.1. According to the principle of minimum of the complementary energy among all the statically admissible stress fields $\mu^{a}_{.b}(x)$ and $t^{kl}(x)$, which satisfy the equilibrium equations (4.1) and the dynamic boundary conditions (4.4), by the actual stress fields, by which the conditions of the compatibility of strain fields and the kinematic boundary conditions are satisfied have the total complementary energy absolute minimum value.

There from it follows that in the case of actual fields of stresses, the complementary energy is stationary, and as a variation principle the equation

$$\delta K = \int_V (\varkappa^{.b}_{a}\, \delta\mu^{a}_{.b} + a_{kl}\, \delta t^{kl})\, dV - \int_{S_u} (n_a\, \delta\mu^{a}_{.b}\, \tilde{\omega}^{b} + n_k\, \delta t^{kl}\, \tilde{u}_l)\, dS = 0 \tag{5.1}_1$$

is valid wherein

$$\varkappa_{ab} = \lambda_{abpq}\, \mu^{pq} \quad \text{and} \quad a_{kl} = c_{klpq}\, t^{pq}, \tag{5.1}_2$$

further, the variations $\delta\mu^{a}_{.b}(x)$ and $\delta t^{kl}(x)$ of the statically admissible stress fields $\mu^{pq}(x)$ and $t^{pq}(x)$ satisfy the following conditions:

$$\delta\mu^{a}_{.b;a} = 0 \qquad x \in V, \tag{5.2}_1$$

$$n_a \delta\mu^{a}_{.b} = 0 \qquad x \in S_t \tag{5.2}_2$$

and

$$\delta t^{kl}_{..;k} = 0 \qquad x \in V, \tag{5.3}_1$$

$$n_k \delta t^{kl} = 0 \qquad x \in S_t. \tag{5.3}_2$$

It is concluded from the principle of minimum complementary energy that from all the statically admissible stress fields of a boundary-value problem those which satisfy the principle of minimum complementary energy are, at the same time, also compatible, and satisfy the kinematic boundary conditions.

Thus, from the principle of minimum complementary energy follow the independent, necessary and sufficient conditions of the compatibility of the strain fields, i.e., the field equations of compatibility (4.3) and the boundary conditions of compatibility (4.6), furthermore the boundary conditions which are equivalent to (4.5) to be prescribed at the boundary section S_u. In the following, the above statements will be proved.

Taking into amount that in the sense of the conditions (5.2) and (5.3) the stress fields cannot arbitrarily be varied, it will be convenient to carry out the investigations with the aid of stress functions.

5.2. W. GÜNTHER suggested in his paper [7] a solution which, in the case of zero body-force and body-couple systems, identically satisfies the equilibrium equations (4.1) of the micropolar elastostatics. The solution suggested by W. GÜNTHER is not complete: it cannot be applied in cases where the solid is bounded by several closed surfaces and the force and couple system applied on them are not self-equilibrated, or when the solid is also loaded by body-force system. D. E. CARLSON and H. SCHAEFER [9] independently reported a complete solutions by complementing the Günther's solution. In this paper, the solution developed by SCHAEFER will be used as a basis. Accordingly, any of the solutions to the equilibrium equations (4.1) may be deduced from the stress functions $h^{\cdot}_{yl}(x)$, $f_{yb}(x)$ which may be differentiable as many times as needed, otherwise being arbitrarily chosen and from the vector fields $p^l(x)$, $q_b(x)$ satisfying the conditions $(5.4)_3$:

$$t^{kl} = \varepsilon^{kmy} h^{\cdot\, l}_{y\cdot;m} + p^l_{\cdot;m}\, g^{mk}, \tag{5.4}_1$$

$$\mu^a_{\cdot b} = \varepsilon^{apy}(f_{yb;\,p} + \varepsilon_{bps} h^{\cdot s}_{y}) + g^{am}\varepsilon_{mby}\, p^y + q_{b;m}\, g^{ma}, \tag{5.4}_2$$

$$g^{mn}\, p^l_{\cdot;mn} = -b^l_{\cdot}, \quad g^{mn}\, q_{b;mn} = -c_b \qquad x \in V. \tag{5.4}_3$$

It may readily be understood that the above formulas of the stress fields $t^{kl}(x)$, $\mu^a_{\cdot b}(x)$ really satisfy the equilibrium equations (4.1).

Likewise, the conditions $(5.2)_1$ and $(5.3)_1$ will identically be fulfilled provided the variation of the stress fields is carried out by the variation of the stress functions

$$\delta t^{kl} = \varepsilon^{kmy}\, \delta h^{\cdot\, l}_{y\cdot;m}, \tag{5.5}_1$$

$$\mu^a_{\cdot b} = \varepsilon^{apy}(\delta f_{yb;p} + \varepsilon_{bps}\, \delta h^{\cdot s}_{y}). \tag{5.5}_2$$

5.3. The stress fields determined according to formulae (5.4) do not vary if instead of f_{yb} and $h^{\cdot\, l}_{y}$ the stress functions

$$f_{yb} + \overset{*}{f}_{yb} = \bar{f}_{yb}, \tag{5.6}_1$$

and

$$h_y^{\cdot l} + \overset{*}{h}{}_y^{\cdot l} = \bar{h}_y^{\cdot l}, \tag{5.6}_2$$

respectively, will be replaced wherein $\overset{*}{f}_{yb}$ and $\overset{*}{h}{}_y^{\cdot l}$ will be deduced from the arbitrary vector fields $w_b(x)$ and $r^l(x)$ differentiable as many times as is needed, in the following way:

$$\overset{*}{f}_{yb} = w_{b;y} + \varepsilon_{bys}\, r^s, \tag{5.7}_1$$

$$\overset{*}{h}{}_y^{\cdot l} = r^l_{\cdot;y}. \tag{5.7}_2$$

In accordance with formulae (5.6) each of the coordinates of f_{AB} and h^L_K, which are separately three and designated with the pairs of indices AB and KL, respectively, of the tensors of the stress functions may be taken as equal to zero for which the equations

$$r^L_{\cdot;K} = \beta^L_{\cdot K}(x), \tag{5.8}_1$$

or

$$w_{B;A} + \varepsilon_{BAs}\, r^s = \alpha_{BA}(x) \tag{5.8}_2$$

have solutions to $r^l(x)$ and $w_b(x)$ even in the case of arbitrary functions $\beta^L_{\cdot K}(x)$ and $\alpha_{BA}(x)$.

In this way, instead of the stress functions $h_y^{\cdot l}$ nine in number and f_{yb}, also equally nine, it is sufficient to calculate with the six functions $h_S^{\cdot T}$ and with the six functions f_{XY}, the pairs of indices of which ST and XY, together with those KL and AB yield all the possible values of the pairs of indices yl (tensor $h_y^{\cdot l}$) and yb (tensor f_{yb}), respectively.

5.4. By replacing (5.4) and (5.5) into (5.1), the variation of the total complementary energy may be obtained with the aid of the variation of the stress functions. After carrying out the substitution, Eq. (5.1) may be brought, by partial integration and by suitable changing the indices, to the following form:

$$\delta K = \delta K_V + \delta \bar{K}_{S_t} + \delta \bar{K}_{S_u} = 0, \tag{5.9}_1$$

in which

$$\delta K_V = \int_V \left[-\varepsilon^{apy}{}_{\cdot}\, \varkappa^{\cdot b}_{a\cdot;p}\, \delta f_{yb} - \varepsilon^{kmy}(a_{kl;m} + \varepsilon_{kls}\, \varkappa^{\cdot s}_{m})\, \delta h_y^{\cdot l} \right] dV, \tag{5.9}_2$$

$$\delta \bar{K}_{St} = \int_{S_t} \left[n_p\, \varepsilon^{apy}\, \varkappa^{\cdot b}_{a}\, \delta f_{yb} + n_m\, \varepsilon^{kmy}\, a_{kl}\, \delta h_y^{\cdot l} \right] dS, \tag{5.9}_3$$

$$\delta \bar{K}_{Su} = \int_{S_u} \left[n_p\, \varepsilon^{apy}\, \varkappa^{\cdot b}_{a}\, \delta f_{yb} + n_m\, \varepsilon^{kmy}\, a_{kl}\, \delta h_y^{\cdot l} - \right.$$

$$\left. - n_a\, \varepsilon^{apy}\, \tilde{\omega}_b(\delta f_{yb;p} + \varepsilon_{bps}\, \delta h_y^{\cdot s}) - n_k\, \varepsilon^{kmy}\, \tilde{u}_l\, \delta h_{y\cdot;m}^{\cdot l} \right] dS. \tag{5.9}_4$$

Considering that from among the conditions (5.2)—(5.3) prescribed for the variation of the stress fields the conditions $(5.2)_1$ and $(5.3)_1$ are identically fulfilled in the case where the stress field (and its variation) is (are) deduced from the stress functions (and from their variations), it follows that δf_{yb} and $\delta h_y^{\cdot l}$ may be arbitrary in the region V.

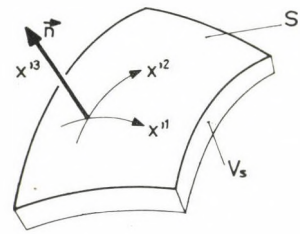

Fig. 3

At the boundary section S_u, the variation $n_k \delta t^{kl}$ of the force stresses, similarly the variation $n_a \delta \mu^a_{\cdot b}$ of the couple stresses may be arbitrary, consequently, also the expressions.

$$n_k \delta t^{kl} = n_k \varepsilon^{kmy} \delta h^{\cdot l}_{y\cdot;m}, \quad x \in S_u, \tag{5.10}_1$$

$$n_a \, \delta \mu^a_{\cdot b} = n_a \varepsilon^{apy} (\delta f_{yb;p} + \varepsilon_{bps} \, \delta h^{\cdot s}_{y}); \quad x \in S_u \tag{5.10}_2$$

may be arbitrary. At the same time the conditions following from equations $(5.2)_2$ and $(5.3)_2$ should be satisfied by the variations of the stress functions on the boundary section S_t:

$$n_k \varepsilon^{kmy} \, \delta h^{\cdot l}_{y\cdot;m} = 0, \quad x \in S_t, \tag{5.10}_3$$

$$n_a \, \varepsilon^{apy} (\delta f_{yb;p} + \varepsilon_{bps} \, \delta h^{\cdot s}_{y}) = 0 \qquad x \in S_t. \tag{5.10}_4$$

5.5. With the view of further transformation of the surface integrals as well as for a better understanding, let us introduce at the boundary defined by the equation $x^k = x^k(x'^1, x'^2)$ (x'^1, x'^2 being the parameters of the boundary as a surface), also in the region V_S extending to its immediate surroundings the system of coordinates designated with primes, x'^1, x'^2, x'^3, nominated as connected to the surface. x'^3 is measured along the normal unit vector **n** directed outwards from the solid (Fig. 3). The formulae of transformation between the system of coordinates x^1, x^2, x^3 and of coordinates x'^1, x'^2, x'^3 connected to the surface are as follows:

$$c'^{k}_{\cdot\, l} = c^p_{\cdot q} \, \sigma^{\cdot k}_{p} \, \tau^{q}_{l}, \tag{5.11}_1$$

$$c^p_{\cdot q} = c'^{k}_{\cdot\, l} \, \tau^{p}_{k} \, \sigma^{\cdot l}_{q}. \tag{5.11}_2$$

Let us further apply the rule that the indices in Greek minuscules can only take at the values *1* and *2*.

Transforming the tensors entering the surface integrals into the system of coordinates x'^1, x'^2, x'^3, and bearing in mind that $n'_3 = 1$ and $n'_\alpha = 0$, the surface integrals $(5.9)_{3,4}$ also carrying out the change of the indices, will be as follows:

$$\delta\overline{K}_{St} = \int_{S_t} [-\varepsilon'^{3\alpha\eta}\, \varkappa'^{.b}_{\alpha}\, \delta f'_{\eta b} - \varepsilon'^{3\alpha\eta}\, a'_{\alpha l}\, \delta h'^{.l}_{\eta}]\, dS, \tag{5.12}_1$$

$$\delta\overline{K}_{Su} = \int_{S_u} [-\varepsilon'^{3\alpha\eta}\, \varkappa'^{.b}_{\alpha}\, \delta f'_{\eta b} - \varepsilon'^{3\alpha\eta}\, a'_{\alpha l}\, \delta h'^{.l}_{\eta} - \varepsilon'^{3\alpha\eta}\, \omega'^{b}(\delta f'_{\eta b;\alpha} + \varepsilon'_{b\alpha s}\, \delta h'^{.s}_{\eta}) -$$

$$- \varepsilon'^{3\alpha\eta}\, \tilde{u}'_l\, \delta h'^{.l}_{\eta.;\alpha}]\, dS. \tag{5.12}_2$$

5.6. The surface integrals obtained require different transformations at the boundary section S_t and S_u, because at the section S_u the expressions

$$\varepsilon'^{3\alpha\eta}(\delta f'_{\eta b;\alpha} + \varepsilon'_{b\alpha s}\, \delta h'^{.s}_{\eta}), \tag{5.12}_2\text{a}$$
$$\varepsilon'^{3\alpha\eta}\, \delta h'^{.l}_{\eta.;\alpha}$$

corresponding to $(5.10)_{1,2}$ and hereby also those

$$\varepsilon'^{3\alpha\eta}\delta h'^{.l}_{\eta} \quad \text{and} \quad \varepsilon'^{3\alpha\eta}\, \delta f'_{\eta b}, \quad x' \in S_u$$

formulated by the variations of the stress functions, i.e., the variations themselves $\delta h'^{.l}_{\eta}$ and $\delta f'_{\eta b}$ may be arbitrary; but at the section S_t the conditions $(5.10)_{3,4}$ must be fulfilled:

$$\varepsilon'^{3\alpha\eta}(\delta f'_{\eta b;\alpha} + \varepsilon'_{b\alpha s}\, \delta h'^{.s}_{\eta}) = 0; \quad x' \in S_t, \tag{5.13}_1$$

$$\varepsilon'^{3\alpha\eta}\, \delta h'^{.l}_{\eta.;\alpha} = 0 \qquad x' \in S_t. \tag{5.13}_2$$

The conditions (5.13) are identically fulfilled if the stress functions are deduced from the arbitrary, differentiable functions $\delta\varphi'_b(x'^1, x'^2)$ and $\delta\chi'^{l}(x'^1, x'^2)$ interpreted at the boundary section S_t as follows:

$$\delta f'_{\eta b} = \delta\varphi'_{b;\eta} + \varepsilon'_{b\eta s}\delta\chi'^{s}, \qquad x' \in S_t, \tag{5.14}_1$$

$$\delta h'^{.l}_{\eta} = \delta\chi'^{l}_{.;\eta} \qquad x' \in S_t. \tag{5.14}_2$$

5.7. To the transformation of the surface integrals also the Stoke's theorem is needed.

According to Fig. 4, let us denote the common boundary curve of the boundary surfaces S_t and S_u with h, and be s the length of arch measured in

the direction indicated on the curve h and with t'^{α} the associated tangent unit vector. According to the Stoke's theorem, to the arbitrary vector field $c'_{\alpha}(x'^1, x'^2)$ interpreted at the surface S_t or S_u or at both of them, the following equa-

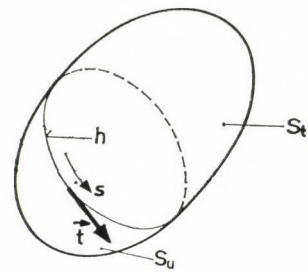

Fig. 4

tions are valid:

$$\int_S \varepsilon'^{3\alpha\eta}\, c'_{\alpha;\eta} dS = -\oint_h t'^{\alpha}\, c'_{\alpha} ds, \tag{5.15}_1$$

and

$$\int_{S_u} \varepsilon'^{3\alpha\eta}\, c'_{\alpha;\eta}\, dS = \oint_h t'^{\alpha}\, c'_{\alpha}\, ds. \tag{5.15}_2$$

5.8. Now the planned transformations of the surface integrals (5.12) may be carried out. Let us consider first the integral $\delta\overline{K}_{St}$ $(5.12)_1$ and replace the expressions (5.14) into the integrand. Making use of the rule of differentiation of products, then carrying out the arrangement and the application of the form $(5.15)_1$ of Stoke's theorem, results in:

$$\delta\overline{K}_{St} = \delta K_{St} + \delta K^h_{St}, \tag{5.16}_1$$

in which

$$\delta K_{St} = \int_{St} [\varepsilon'^{3\alpha\eta}\, \varkappa'^{.b}_{\alpha.;\eta}\, \delta\varphi'_b + \varepsilon'^{3\alpha\eta}(a'_{\alpha l;\eta} + \varepsilon'_{\alpha lb}\, \varkappa'^{.b}_{\eta})\delta\chi'^{l}]\, dS \tag{5.16}_2$$

is the integral carried out at the surface S_t, and

$$\delta K^h_{St} = \oint_h (t'^{\alpha}\, \varkappa'^{.b}_{\alpha}\, \delta\varphi'_b + t'^{\alpha}\, a'_{\alpha l}\, \delta\chi'^{l})\, ds \tag{5.16}_3$$

the integral taken on the curve h.

In transforming the integral $\delta\overline{K}_{Su}$ according to $(5.12)_2$ beside the application of the rule of differentiation of products also the form $(5.15)_2$ of Stoke's theorem and the appropriate change of the common indices will be applied.

Thus, one obtains:

$$\delta \overline{K}_{Su} = \delta K_{Su} + \delta K^h_{Su}, \tag{5.17}_1$$

in which

$$\delta K_{Su} = \int_{Su} \{ -\varepsilon'^{3\alpha\eta}(\varkappa'^{,b}_{\alpha} - \tilde{\omega}'^{b}_{\cdot;\alpha})\, \delta f'_{\eta b} - \varepsilon'^{3\alpha\eta}[a'_{\alpha l} - (\tilde{u}'_{l;\alpha} + \varepsilon'_{l\alpha s}\tilde{\omega}^{s})]\, \delta h'^{,l}_{\eta} \}\, dS \tag{5.17}_2$$

is the integral made at the surface S_u, and

$$\delta K^h_{Su} = \oint_h (t'^{\alpha}\, \tilde{\omega}'^{b}\, \delta f'_{\alpha b} + t'^{\alpha}\, \tilde{u}'_{l}\, \delta h^{,l}_{\alpha})\, ds \tag{5.17}_3$$

the integral taken along the curve h.

5.9. Let us take together the line-integrals $(5.16)_3$ and $(5.17)_3$ into one single integral. Assuming with this view, by designating the values taken along the curve h of the quantities interpreted at the boundary section S_t by one underline and of those interpreted at the section S_u by two underlines, that along the h, taking also into account the equations (5.14), we have

$$\underline{\underline{\delta f'_{\alpha b}}} = \underline{\delta f'_{\alpha b}} = \delta \varphi'_{b;\alpha} + \varepsilon'_{b\alpha s}\, \delta \underline{\chi}'^{s} \quad x \in h \tag{5.18}_1$$

and

$$\underline{\underline{\delta h_{\alpha}^{,l}}} = \underline{\delta h'^{,l}_{\alpha}} = \delta \chi'^{l}_{\cdot;\alpha}, \qquad x' \in h. \tag{5.18}_2$$

Replacement of the expressions (5.18) into $(5.17)_3$, application of the rule of integration of products and rearrangement, results in the following line integral:

$$\delta K^h = \delta K^h_{St} + \delta K^h_{Su} = \oint_h \{ t'^{\alpha}(\underline{\varkappa}'^{,b}_{\alpha} - \underline{\underline{\tilde{\omega}}}'^{b}_{\cdot;\alpha})\, \delta \varphi'_b + $$
$$+ t'^{\alpha}[\underline{a}'_{\alpha l} - (\underline{\underline{\tilde{u}}}'_{l;\alpha} + \varepsilon'_{l\alpha s}\, \underline{\underline{\tilde{\omega}}}'^{s})]\, \delta \chi'^{l} \}\, ds. \tag{5.19}$$

5.10. As a result of the transformation one obtains the equation

$$\delta K = \delta K_V + \delta K_{St} + \delta K_{Su} + \delta K^h = 0 \tag{5.20}$$

which is the condition of fulfilment of $\delta K = 0$, i.e., the principle of minimum complementary energy, where each of the quantities are interpreted in respective succession the formulae $(5.9)_2$, $(5.16)_2$, $(5.17)_2$ and (5.19).

5.11. In respect to the following, on the basis of those mentioned in paragraph 5.3, from among the coordinates of the tensors of the stress functions let us consider that in the system of coordinates x^1, x^2, x^3:

$$f_{AB} = 0 \qquad \text{and} \qquad h^L_K = 0, \qquad x \in V, \tag{5.21}_1$$

and

$$f_{XY} \text{ is arbitrary, and } h_S^T \text{ is arbitrary,} \quad x \in V. \tag{5.21}_2$$

Accordingly at the boundary S and in its immediate surroundings V_S in the system of coordinates x'^1, x'^2, x'^3 connected to the surface, according to the formula of transformation $(5.11)_1$ and according to $(5.21)_2$, the tensors of the stress functions are

$$f'_{yb} = f_{XY}\, \tau_{\cdot y}^{X}\, \tau_{\cdot b}^{Y}, \tag{5.22}_1$$

and

$$h'^{\cdot l}_{y} = h_S^T\, \tau_{\cdot y}^{S}\, \sigma_{T}^{\cdot l}. \tag{5.22}_2$$

According to the general rule treated in paragraph 5.3, three coordinates having pairs of indices f'_{AB} and $h'^{\cdot L}_{K}$ of the tensor f'_{yb} and $h'^{\cdot l}_{y}$ may also be set equal to zero with the aid of the arbitrary and differentiable vector fields $\psi'_b(x')$ and $\vartheta'^l(x')$, with respect to the pairs of indices of which the equations

$$\vartheta'^{L}_{\cdot;K} = \beta'^{L}_{\cdot K}(x') \tag{5.23}_1$$

and

$$\psi'_{B;A} + \varepsilon'_{BAs}\vartheta'^{s} = \alpha'_{BA}(x') \tag{5.23}_2$$

have solutions to $\vartheta'^l(x')$ and $\psi'_b(x')$ even in case of the arbitrary functions $\beta'^{L}_{\cdot K}(x')$ and $\alpha'_{AB}(x')$.

Let us choose the possible case with which the coordinates $f'_{\eta b}$ of the tensor f'_{yb} and the $h'^{\cdot l}_{\eta}$ coordinates of the tensor $h'^{\cdot l}_{y}$ are not of zero value (but $f'_{3b} = 0$ and $h'^{\cdot l}_{3} = 0$). Indeed, in this case, the equations which can be written on the basis of Eqs (5.6) and (5.23)

$$\vartheta'^{l}_{\cdot;3} = \overset{*}{h}{}'^{\cdot l}_{3} = -h'^{\cdot l}_{3} = \beta'^{l}_{\cdot 3},$$

or

$$\psi'_{b;3} + \varepsilon'_{b3s}\vartheta'^{s} = \overset{*}{f}{}'_{3b} = -f'_{3b} = \alpha'_{3b} \tag{5.23}_{2a}$$

have solutions, even in case of the arbitrary functions $h'^{\cdot l}_{3}(x')$ and $f'_{3b}(x')$, to $\vartheta'^l(x')$ and to $\psi'_b(x')$, respectively.

The formulae of transformation (5.22), by making use of the chosen stress functions, may be written in the following forms

$$\bar{f}'_{\eta b} = f_{XY}\, \tau_{\eta}^{\cdot X}\, \tau_{b}^{\cdot Y} + \overset{*}{f}{}'_{\eta b}, \tag{5.24}_1$$

and

$$\bar{h}'^{\cdot l}_{\eta} = h_S^T\, \tau_{\eta}^{\cdot S}\, \sigma_{T}^{\cdot l} + \overset{*}{h}{}'^{\cdot l}_{\eta}, \tag{5.24}_2$$

respectively.

The equations $(5.24)_1$ and $(5.24)_2$ represent relationships at the boundary S between six stress functions f_{XY} and h_S^T for each in the system of coordinates

x^1, x^2, x^3 as well as six stress functions $\bar{f}'_{\eta b}$ and $\bar{h}'^{.l}_{\eta}$ for each in the system of coordinates x'^1, x'^2, x'^3.

Transformation formulae of the same shapes can be written between the variations of the stress functions:

$$\delta\bar{f}'_{\eta b} = \delta f_{XY}\tau^{.X}_{\eta}\sigma^{.Y}_{b} + \delta f'_{\eta b}, \tag{5.25}_1$$

$$\delta\bar{h}'^{.l}_{\eta} = \delta h^{.T}_{S}\tau^{.S}_{\eta}\sigma^{.l}_{T} + \delta h'^{.l}_{\eta}. \tag{5.25}_2$$

(Hereafter, the distinctive overline will be omitted).

5.12. Eq. (5.20) may be fulfilled only in the case, where the integrals involved are separately equal to zero. And, considering that the integrands consist of the sum of products wherein one of the factors may, according to the paragraphs 5.4 and 5.6, arbitrarily be variated, examining each of the integrals in succession, and taking into account that mentioned in paragraph 5.11, the following statements should be fulfilled:

— in the system of coordinates x^1, x^2, x^3 from the equation $\delta K_V = 0$ to be written on the basis of the formula $(5.9)_2$ follows (because δf_{XY} and $\delta h^{.T}_{S}$ in the region V may be arbitrary):

$$e^{XY} = \varepsilon^{Xpa}\varkappa^{.Y}_{a.;p} = 0, \qquad x \in V, \tag{5.26}_1$$

$$d^{S}_{.T} = \varepsilon^{Smk}(a_{kT;m} + \varepsilon_{kTq}\varkappa^{.q}_{m}) = 0, \qquad x \in V; \tag{5.26}_2$$

— in the system of coordinates x'^1, x'^2, x'^3 connected to the surface from the equations $\delta K_{St} = 0$ to be written on the basis of the formulae $(5.16)_2$ follows (because, according to the paragraphs 5.6 and 5.11 $\delta\varphi'_b$ and $\delta\chi'^l$ on the surface S_t may be arbitrary):

$$e'^{3b} = \varepsilon'^{3\eta\alpha}\varkappa'^{b}_{\alpha.;\eta} = 0, \qquad x' \in S_t, \tag{5.27}_1$$

$$d'^{3}_{.l} = \varepsilon'^{3\eta\alpha}(a'_{\alpha l;\eta} + \varepsilon'_{\alpha ls}\varkappa'^{.s}_{\eta}) = 0, \qquad x' \in S_t; \tag{5.27}_2$$

similarly in the system of coordinates x^1, x^2, x^3:

$$n_a e^{ab} = n_a\,\varepsilon^{apq}\varkappa^{.b}_{q.;p} = 0, \qquad x \in S_t, \tag{5.27}_3$$

$$n_k d^{k}_{.l} = n_k\varepsilon^{kpq}(a_{ql;p} + \varepsilon_{qls}\varkappa^{.s}_{p}) = 0, \quad x \in S_t; \tag{5.27}_4$$

— in the system of coordinates x'^1, x'^2, x'^3 connected to the surface from the equation $\delta K_{Su} = 0$ to be written on the basis of the formula $(5.17)_2$ follows (because, according to the paragraphs 5.11 and 5.6 $\delta f'_{\eta b}$ and $\delta h'^{.l}_{\eta}$ on the surface S_u may be arbitrary):

$$\varkappa'^{.b}_{\alpha} - \tilde{\omega}'^{b}_{.;\alpha} = 0, \qquad x' \in S_u, \tag{5.28}_1$$

$$a'_{\alpha l} - (\tilde{u}'_{l;\alpha} + \varepsilon'_{l\alpha s}\tilde{\omega}^{s}) = 0, \qquad x' \in S_u; \tag{5.28}_2$$

— in the system of coordinates x'^1, x'^2, x'^3 connected to the surface from the equation $\delta K^h = 0$ to be written on the basis of formula (5.19) follows (because $\delta\varphi'_b$ and $\delta\chi'^l$ at the curve h according to the paragraphs 5.6, 5.9 and 5.11 may be arbitrary), if for convenience, a single underline means values taken at the boundary section S_t and on the curve h, and a double underline means values taken at the boundary section S_u and on the curve h:

$$t'^{\alpha}(\underline{\varkappa}'^{\cdot b}_{\alpha} - \underline{\underline{\tilde{\omega}}}'^{b}_{\cdot;\alpha}) = 0, \qquad x' \in h, \tag{5.29}_1$$

$$t'^{\alpha}[\underline{a}'_{\alpha l} - (\underline{\underline{\tilde{u}}}'_{l;\alpha} + \varepsilon'_{l\alpha s}\,\underline{\underline{\tilde{\omega}}}'^{s})] = 0, \qquad x' \in h. \tag{5.29}_2$$

5.13. The results summarized in paragraph 5.12 indeed justify the statement formulated in paragraph 5.1, because

— eqs (5.26) are the same as the equations of compatibility,

— the pairs of indices of the equations of compatibility are the same as those of the non-zero stress functions,

— the boundary conditions (5.27) are the same as the boundary conditions of compatibility at the boundary section S_t,

— fulfilment of the boundary conditions (5.28) partly means that at the boundary section S_u the equations

$$e'^{3b} = \varepsilon'^{3\eta\alpha}\varkappa'^{\cdot b}_{\alpha\cdot;\eta} = 0, \qquad x' \in S_u,$$

$$d'^{3}_{\cdot l} = \varepsilon'^{3\eta\alpha}(a'_{\alpha l;\eta} + \varepsilon'_{\alpha ls}\varkappa'^{s}_{\eta}) = 0 \qquad x' \in S_u$$

which are the same as the boundary conditions of compatibility (4.6), will identically be fulfilled, partly, the conditions, together with the constitutive equations, mean boundary conditions which are equivalent to the kinematic boundary conditions (4.5) stipulated in respect to the stress fields at the boundary section S_u.

The conditions (5.29) obtained to the curve h, together with the conditions (5.28), mean that along the curve h at the transition from one boundary section to the other, the strain fields $\varkappa'^{\cdot b}_{\alpha}(x'^1, x'^2)$ and $\alpha'_{\alpha l}(x'^1, x'^2)$ should be continuous. In solving the problems, one should take also care of the fulfilment of these obvious conditions.

6. Summary of the results

The boundary value problems of the linearized theory of the micropolai elastostatics formulated with the force stresses and couple stresses are investrgated in an arbitrary system of curvilinear coordinates in connection with the independence and the necessity and sufficiency of the field equations and boundary conditions further, in connection with the single-valuedness of the solutions, for the case of a solid bounded by a simply connected surface.

6.1. Based on the conditions of independence of the line integrals along chosen curves producing the rotations and displacements, the necessary and sufficient conditions of the single-valuedness of rotations and displacements on the surface region are presented.

6.2. The independent, necessary and sufficient conditions of the compatibility of the strain fields, i.e. the field equations and boundary conditions of compatibility are determined in two different ways. This is done partly, based on the conditions of the single-valuedness of the rotations and displacements to be calculated at the boundary, partly based on the principle of the minimum complementary energy by using the stress functions, with the aid of formal transformations.

6.3. It is proved that the equations of compatibility may be chosen in various ways, i.e., the pairs of indices XY and ST may be selected in as many ways and in the same manner as the non-zero coordinates of the tensors of the stress functions.

6.4. It is pointed out that in the case of the linearized theory of the micropolar elastostatics the necessary and sufficient equations and boundary conditions of the boundary-value problems formulated with force stresses and couple stresses may be obtained in the way that to the equilibrium equations and constitutive equations one adds six, in conformity with paragraph 6.3 possible equations of compatibility to each, and one complements the usual dynamic and kinematic boundary conditions with the boundary conditions of compatibility.

6.5. The conditions prescribed to the stress fields are given at the boundary section S_u where also the rotations and displacements are prescribed as kinematic boundary condition.

6.6. Finally it should be noted:

a) Elimination of the unnecessary compatibility conditions might be of significance in the approximate calculations having the aim to immediate determine the stress fields.

b) All of the approximate calculations, with the view of producing the stress field which, beside satisfying the conditions prescribed to the statically admissible stress fields, prescribe the fulfilment of the uniqueness of the rotations and displacements at certain places (at points, sections of curves and of surfaces), mean in fact the approximate satisfaction of the principle of minimum complementary energy.

REFERENCES

1. Nowacki, W.: Theory of Micropolar Elasticity, Springer-Verlag, Wien, New York, Udine (1970)
2. Washizu, K.: A Note on the Condition of Compatibility. *Journal of Mathematics and Physics*, **36**, (1957), 306—312

3. KOZÁK, I.: Notes on the Field Equations with Stresses and on the Boundary Conditions on the Linearized Theory of Elastostatics. *Acta Techn. Hung.*, **90** (3—4) (1980), 221—245
4. KOZÁK, I.: Determination of Compatibility Boundary Conditions in Linear Elastostatics with the Aid of the Principle of Minimum Complementary Energy. *Publ. Techn. Univ. Heavy Industry*, Ser. D. Natural Sciences, Vol. **34** (1980), 83—98
5. CESARO, E.: Sulle formole del Volterra, fondamentali nella teoria delle distorsioni elastiche. *Rend. Accad. Napoli*, **12** (1906), 311—321
6. KESSEL, S.: Die Spannungsfunktionen des Cosserat-Kontinuums, *ZAMM* **47** (1967), 329—321
7. GÜNTHER, W.: Zur Statik und Kinematik des Cosseratschen Kontinuums, *Abh. Braunschweig Wiss. Ges.*, **10** (1958), 195—213
8. CARLSON, D. E.: On Günther's stress Functions for Couple Stresses, *Quart. Appl. Math.*, **25** (1967), 139—146
9. SCHAEFER, H.: Die Spannungsfunktionen eines Kontinuums mit Momentenspannungen I. und II. *Bulletin de l'Académie Polonaise des Sciences*, Série des Siences Techniques, **15** (1967), 63—73

Feldgleichungen und Randbedingungen mit Kraft- und Momentenspannungen der linearen Theorie der mikropolaren Elastostatik. Die voneinander unabhängigen, notwendigen und hinreichenden Bedingungen der Kompatibilität der Verzerrungsfelder werden auf zwei verschiedenen Wegen ermittelt, einerseits aufgrund der Einwertigkeitsbedingungen der auf dem Rand herstellbaren Verschiebungs- und Rotationsfelder, anderseits aufgrund des Prinzips des Minimums der Komplementärenergie. Es werden die auf verschiedenen Wegen auswählbaren sechs Feldgleichungen der Kompatibilität und die Kompatibilitätsrandbedingungen festgelegt. Die Abhandlung faßt die auf die Spannungsfelder gestellten Feldgleichungen und Randbedingungen der linearen Theorie der mikropolaren Elastostatik zusammen, danach beweist aufgrund der Untersuchungen der Einwertigkeit der Lösungen, daß die ermittelten Feldgleichungen und Randbedingungen notwendig und zugleich hinreichend sind.

Acta Technica Academiae Scientiarum Hungaricae, Tomus 91 (1—2), pp. 81—110 (1980)

EXISTENCE AND UNIQUENESS CRITERIA OF THE MEMBRANE STATE OF SHELLS

I. HYPERBOLIC SHELLS

T. TARNAI*

[Manuscript received June 1, 1977]

In this paper the problem is dealt with, what sort of boundary conditions are to be prescribed on the edge of a shell that is to be in a statically determinate membrane state. Existence and uniqueness criteria of the solution of the membrane-shell equation are investigated, on the basis of the partial differential equations' theory, for various boundary conditions. This part of the paper implies the results obtained for hyperbolic shells.

1. Introduction

As is well known [11], the stresses and strains in membrane shells can be generally expressed by 3 statical, 3 geometrical, and 3 physical equations. At every boundary two conditions can be described. These can be:

a) both geometrical,
b) one geometrical, one statical,
c) both statical conditions.

For statically determinate membrane shells the statical equations and the statical boundary conditions are sufficient to determine the stresses in the shell. In this case, the geometrical and physical equations, and the geometrical boundary conditions can be disregarded.

Thus, at statically determinate membrane shells, for each boundary section can be given zero, one, or two boundary conditions. The question is, how these boundary conditions are to be prescribed, what kind of conditions must be fulfilled by the boundary curves, the middle surface of the shell, and external loadings on the shell, being in a unique membrane state.

This question is investigated in the present paper. We have made use of the partial differential equation theory for answering this question. We do not strive to reach completeness when dealing with different questions, all the less, since a good number of problems concerning the partial differential equations has not yet been cleared up.

* Dr. T. TARNAI, Kolostor u. 17. H-1037 Budapest, Hungary

For the sake of descriptiveness we shall use Puchers' differential equation for our investigations. Although, there are a few cases when system of the statical differential equations of the shell expressed by curvi-linear coordinates offers some advantages ([11] p. 106 (2.1), [21] p. 22 (1.23)), but the transformations and the treatment of complex functions required in this case would destroy the direct descriptiveness. It should be noted, that those were W. HAACK, G. HELLWIG and I. N. VEKUA whose names are mainly connected with the development of the mathematical background of the investigation using system of equations (see References of [14] and [20]). A short survey on the system of differential equations of shells concerning our problem was given by KAYA SAYAR [14].

In our investigations, we shall deal only with those shells which are loaded by vertical forces and for which the Gaussian curvature of the middle surface is of the same sign at every point of the shell.

2. Pucher's differential equation

Pucher's differential equation describing the equilibrium of membrane shells loaded by vertical forces is given by using the mutually rectangular coordinate axes xyz as follows:

$$\mathfrak{L}F = \frac{\partial^2 z}{\partial y^2}\frac{\partial^2 F}{\partial x^2} - 2\frac{\partial^2 z}{\partial x \partial y}\frac{\partial^2 F}{\partial x \partial y} + \frac{\partial^2 z}{\partial x^2}\frac{\partial^2 F}{\partial y^2} = -g \tag{1}$$

where $z = z(x, y)$ is the equation of the middle surface of the shell,

$$\mathfrak{L} = \frac{\partial^2 z}{\partial y^2}\frac{\partial^2}{\partial x^2} - 2\frac{\partial^2 z}{\partial x \partial y}\frac{\partial^2}{\partial x \partial y} + \frac{\partial^2 z}{\partial x^2}\frac{\partial^2}{\partial y^2}$$

is the Pucher operator, $g = g(x, y)$ is the function of the vertical load intensity (parallel with axis z) and $F(x, y)$ is the unknown stress-function, from which the membrane stresses can be derived as follows:

$$n_x = \frac{\partial^2 F}{\partial y^2}, \qquad n_{xy} = n_{yx} = -\frac{\partial^2 F}{\partial x \partial y}, \qquad n_y = \frac{\partial^2 F}{\partial x^2}.$$

If there are vertical tangential planes of the middle surface of the shell, then the solution of the Pucher differential equation and the real membrane stresses in the points of contact cannot be derived directly, but only as limits at a point (x, y), the character of the membrane equation (1) is determined by

the sign of the discriminant of the equation evaluated at the point (x, y):

$$D = \frac{\partial^2 z}{\partial x^2}\frac{\partial^2 z}{\partial y^2} - \left(\frac{\partial^2 z}{\partial x \partial y}\right)^2.$$

Depending on the sign of the discriminant D equation (1) can be grouped into one of the three types listed below:

1) $D < 0$ hyperbolic,
2) $D = 0$ parabolic,
3) $D > 0$ elliptic.

Since we have stipulated that the sign of the Gaussian curvature of the middle surface is unchanged all over the shell surface, therefore, the sign of the discriminant of Eq. (1), and thus the character of Eq. (1) is the same oll over the shell.

The characteristic curves of Eq. (1) are given by the solutions of the ordinary differential equation:

$$\frac{\partial^2 z}{\partial y^2} dy^2 + 2\frac{\partial^2 z}{\partial x \partial y} dxdy + \frac{\partial^2 z}{\partial x^2} dx^2 = 0.$$

For hyperbolic equations two real valued set of characteristic curves exist, for parabolic equations one real valued set of characteristic curves exists, and for elliptic equations there are not real valued characteristic curves.

Those lines of the middle surface whose projections on plan xy are characteristic curves, are denoted asymptotic lines.

If derivatives $\partial^2 z/\partial y^2$, $\partial^2 z/(\partial x \partial y)$, $\partial^2 z/\partial x^2$ are twice continuously differentiable, that is, if *function* $z(x, y)$ *is four times continuously differentiable* and the second derivatives of $z(x, y)$ are not simultaneously equal to zero then operator $\mathfrak{L}$ and Eq. (1), respectively, can be transformed to canonical form in some neighbourhood of a point (x_0, y_0) by new variables ξ, η ([17] p. 64). It should be noted that the twice continuously differentiable transforming functions $\xi(x, y)$, $\eta(x, y)$ are in close connection with the characteristic curves (curves $\xi = const.$ and $\eta = const.$ are characteristic curves themselves). In the following shells will be investigated for which there exists such a canonical transformation in the whole domain in ground plan of the shell and it is invertable.

The normal and tangential vectors belonging to a point P on the groundplan projection of the shell boundary will be denoted by n and t, respectively (Fig. 1). After prescribing the normal force in the direction $n(n_n = \partial^2 F/\partial t^2)$ or the tangential force in the direction $t\left(n_{nt} = -\partial^2 F/(\partial n \partial t)\right)$ or a combination or both of these, for some sections of the boundary, we look for the solution of Eq. (1) being a unique one apart from constants and linear terms, and being twice continuously differentiable.

The basic problem of the Pucher equation (1) is that, the boundary conditions given for the internal forces refer to the second derivatives of the unknown function. There are two aspects of this problem. One of these is that the investigation of partial differential equations with boundary conditions

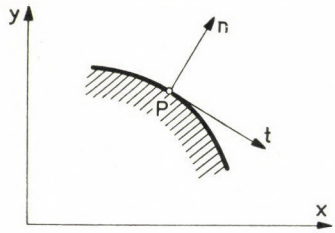

Fig. 1. Normal and tangential unit vectors fitting to a point of the boundary curve

given in its second derivatives is a rather unfinished field in mathematics. A few references concerning elliptic equations of this type are to be found in [16] (p. 235), for example. The boundary conditions given in second derivatives can only be reduced to derivatives of the order one or zero, in those simple cases, for which the theory of partial differential equations is elaborated.

The other aspect of the problem implies in many cases, that there cannot be found the statical meaning of the boundary conditions given in zeroth or first order derivatives, for which the existence and uniqueness of the solution of the shell equation have been proved.

Let us look over a few simple boundary conditions that can be reduced from derivatives of second order to derivatives of lower order. Further on, when using the word boundary, we mean the ground-plan (xy) projection of the shell boundary. The real boundary line will be denoted by $\bar{S}$, while its projection by S.

2.1. *The edge beam is only supported vertically*

In this case, the boundary line is the funicular curve of the boundary forces acting on the edge beam. The stress function on the boundary takes the shape $F = ax + b \cdot y(x) + c$, where a, b *and* c *are constants* and $y = y(x)$ is the equation of the boundary curve; that is the values of the stress function taken on the boundary line specify a plane-curve. As the stress function is to be modified in constant and linear terms without changing the stresses in the shell, in some cases, $F = 0$ can be stated instead of $F = ax + by(x) + c$ [4]. We note here that, in general, the vertical support of the edge beam ensures the equilibrium of the shell and the edge beam when the boundary line is a closed funicular curve, that is, when the values of the stress function taken

on the boundary give a closed plane-curve. If this funicular-feature condition is only fulfilled in parts of the boundary (the boundary curve is an opened funicular curve), then the equilibrium of that section of the edge beam needs the acting of concentrated forces on its ends being of tangential direction to the boundary curve.

2.2. *Value of normal force given along a straight boundary-section*

In this case,

$$n_n = \frac{\partial^2 F}{\partial t^2} = \varphi(s) \tag{2}$$

where $\varphi(s)$ is a given function and s is the arc-length parameter of the boundary.

Let us integrate expression (2), twice along the boundary, with respect to s. Thus, we get the following expression for the values of the stress function on the boundary:

$$F = \int (\int \varphi ds) ds + as + b$$

where a and b are *constants*. If the straight boundary is free of lateral pressure, that is, $n_n = \varphi(s) = 0$, then $F = as + b$ is obtained, that is, the stress function varies linearly along the boundary. If the edge beam is only supported vertically, then the boundary condition $F = as + b$ can be substituted by that from Sec. 2.1: $F = 0$. If there are more than three lateral-pressure-free straight boundaries of the shell jointing to each other, and the edge beams are supported not only vertically but also in their plane (e.g. in the joints of the boundary sections, concentrated forces appear), then the condition $F = 0$ cannot be prescribed for every boundary section [6]. Following from the foregoing, the funicular behaviour of the boundary is not equivalent with its exemption of lateral pressure, when the shell is built above a poligon having more than three sides. The first one is a special case of the second one.

2.3. *Value of the shearing force given on a straight boundary*

In this case,

$$n_{nt} = -\frac{\partial^2 F}{\partial n \partial t} = \psi(s) \tag{3}$$

where $\psi(s)$ is a given function and s is the arc-length parameter of the boundary. Let us integrate expression (3), along the boundary, with respect to s. Thus we get:

$$\frac{\partial F}{\partial n} = -\int \psi ds + a$$

where a is a constant. If there are no shearing forces on the straight boundary section, that is $n_{nt} = \psi(s) = 0$, then $\partial F/\partial n = a$ is obtained, there. If there are more than two straight boundary sections with no shearing forces, on the shell, the fulfilment of the condition $\partial F/\partial n = 0$ can only be reached, in general, only at two boundary sections by adding linear terms.

2.4. *Shearing forces given at a circular boundary line*

Reduced value of the shearing force can be expressed by using the cylindrical coordinates r, ϑ, z, as follows ([1] p. 113):

$$n_{r\vartheta} = \frac{1}{r^2}\frac{\partial F}{\partial \vartheta} - \frac{1}{r}\frac{\partial^2 F}{\partial r \partial \vartheta}.$$

The radius of the arc is $r = R$, and the centre of the arc lies on the axis z. If, hence, the shearing force at the circular boundary is of the value

$$n_{r\vartheta} = \chi(s) \tag{4}$$

where s denotes the arc length parameter, then by integrating Eq. (4), along the boundary, with respect to $s = R\vartheta$, we get the expression:

$$\frac{1}{R} F - \frac{\partial F}{\partial n} = \int \chi R d\vartheta + a$$

where a is a constant. If there are no shearing forces on the circular boundary, then it can be expressed as follows:

$$\frac{1}{R} F - \frac{\partial F}{\partial n} = a$$

where a is a constant.

2.5. *Given both inner forces at a straight boundary section*

Let us denote them by $n_n = \varphi(s)$ and $n_{nt} = \psi(s)$. By an integration, along the boundary, according to Secs 2.2 and 2.3, we get:

$$F = \int \left(\int \varphi ds\right) ds + as + b,$$

$$\frac{\partial F}{\partial n} = -\int \psi \, ds + c$$

where a, b, and c are constants. By adding constant and linear terms, a, b, and c can be set to zero. If the straight boundary section is free, the boundary

conditions $F = as + b$, $\partial F/\partial n = c$, or instead, sometimes, $F = 0$, $\partial F/\partial n = 0$ can be prescribed. In this case, the sress surface has a tangential plane such that the points of the stress surface above the boundary curve lie in it which can also be the coordinate plane xy.

2.6. *Free boundary*

The last statement of Sec. 2.5 can be generalized for smooth curved boundary, too [5]. Then the boundary conditions are:

$$n_n = \frac{\partial^2 F}{\partial t^2} = 0, \quad n_{nt} = -\frac{\partial^2 F}{\partial n \partial t} = 0$$

from which it follows that:

$$\frac{\partial F}{\partial x} = a, \quad \frac{\partial F}{\partial y} = b$$

where a and b are constants.

Instead of the above-mentioned boundary conditions $F = 0$ and $\partial F/\partial n = 0$ are to be produced by adding constant and linear terms to the stress function.

The question is, how can we determine the constants of integration appearing in the boundary conditions 2.1—2.6., and when can we set them to zero? When expressing the constants of integration we must use boundary conditions containing constant terms, as well. Thus, we have the possibility of fitting the condition functions prescribed at the joining boundary sections. (If, for instance, we prescribe the value of the stress function F at the joining boundary sections S_1 and S_2, then the ordinates of the condition functions given for the boundaries S_1 and S_2 must be equal, in the joint, as is required to fulfil the continuity of the stress function. Or, if we prescribe F at the boundary S_1 and not only F but also its derivative $\partial F/\partial i (i \neq t)$ on the boundary S_2, then in the joint of S_1 and S_2, the ordinates must be equal following from the continuity of F and the derivative of the function prescribed at S_1 must be equal with that computed from the functions prescribed at S_2 in the direction of the end tangent of S_1 following from the smoothness of F. If, in the latter example, we prescribe a derivative of F in any direction instead of the function F, at the boundary section S_1, then its value in the joint is determined by the functions given for S_2). Then, we may add an arbitrary linear expression $ax + by + c$ to the stress function. By choosing suitable constants for a, b and c a number (perhaps all) of the constants in the boundary conditions can be set to zero. (We note that, the effect of such an additive linear expression must be considered simultaneously for the whole boundary of the shell. It is not

permitted to choose different linear expressions, independently, for each boundary section that makes the constants vanish on the boundary examined and thus allows the setting of all the constants along the boundary to zero, because the completing of the stress function by adding a new linear expression can result in non-zero constants on such boundaries, where those had already been set to zero.) At some boundary-value problems of elliptic equations, the connection of the constants of integration is controlled by a so-called compatibility condition. It can occur that not all of the constants of integration are to be determined from the conditions and data given, not even by adding linear expressions. Furthermore, these constants must be considered free parameters.

At different statical problems of membrane shells, we look for such solutions of Eq. (1) which satisfy certain boundary conditions for the reduced internal forces n_x, n_y, n_{xy} taking the shape, in general:

$$f_1\left(\frac{\partial^2 F}{\partial x^2}, \frac{\partial^2 F}{\partial x \partial y}, \frac{\partial^2 F}{\partial y^2}\right) = \varphi_1 \tag{5}$$

where f_1 and φ_1 are given functions.

By integrating the functions of boundary condition, Eq. (5) takes the general shape below:

$$f_2\left(F, \frac{\partial F}{\partial x}, \frac{\partial F}{\partial y}\right) = \varphi_2\,(a_1, a_2, \ldots, a_m) \tag{6}$$

where $a_1, a_2, \ldots, a_m$ are the constants of integration. If Eq. (1) with boundary conditions (6) has obtained a solution for every considerable fixed values of $a_1, \ldots, a_m$, it means that Eq. (1) can be solved for the boundary conditions (5), and the shell is in a membrane state. If Eq. (1) with boundary conditions (6) has no solution for any considerable set of the constants $a_1, \ldots, a_m$, it means that Eq. (1) cannot be solved for the boundary conditions (5), and the shell is not in a membrane state.

If Eq. (1) with boundary conditions (6) has one and only one solution for every considerable set of constants $a_1, \ldots, a_m$, and the values of all of these constants can be determined or set to zero by satisfying the compatibility conditions above, and by adding the linear expression $ax + by + c$, then the shell is in a unique membrane state, that is, the internal forces of the shell are uniquely determined by the boundary conditions (5). Then, the shell is statically determinate. If we can only determine k ($k < m$) constants from those of $a_1, \ldots, a_m$, then there remain $k - m$ free parameters in (6). In this case, if Eq. (1) with boundary conditions (6) has a solution for every consider-

able set of constants $a_1, \ldots, a_m$, the shell is in membrane state but uniqueness is not valid, that is the internal forces of the shell are not uniquely determined by the boundary conditions (5). Then the shell is statically indeterminate.

In this paper, we are investigating when an only solution of Eq. (1) with boundary conditions (6) exists for a fixed set of constants $a_1, \ldots, a_m$, and when we can determine all of these constants, that is, when the shell is in a unique membrane state.

Now, then, let us survey the most important problems. As these problems are essentially different, depending on the character of Eq. (1), it is useful to arrange those according to whether Eq. (1) is elliptic, parabolic, or hyperbolic.

We investigate when the problems concerning Eq. (1) are properly posed. A problem is properly posed if ([2] p. 176):

(1) its solution does exist,

(2) uniqueness of the solution does hold,

(3) solution continuously depends on data.

First we will look over the problems concerning hyperbolic shells. Before starting with the detailed investigation, we note the followings:

The canonical form of Eq. (1), in a hyperbolic case, is written:

$$\frac{\partial^2 F}{\partial x \partial y} = -g(x, y). \tag{7}$$

General solution of this equation is obtained by integrations with respect to x and y:

$$F(x, y) = \varphi_1(x) + \varphi_2(y) - \iint g(x, y)\, dxdy.$$

In order that the stress function F be twice continuously differentiable, that is, the internal forces n_x, n_{xy}, n_y be continuous functions, it is necessary that the load function $g(x, y)$ is continuously differentiable, furthermore, the unknown functions φ_1 and φ_2 being determined from the boundary conditions are twice continuously differentiable. If we only look for a continuously differentiable (twice continuously differentiable on each boundary section) solution of Eq. (7), then the continuity of $g(x, y)$ and the continuous differentiable feature of φ_1, and φ_2 are only required. In the following part, we will look over such problems concerning Eq. (1), for which the solution is *once continuously differentiable*. (If we look for a *twice continuously differentiable* solution of the problem in question, then the load function must be continuously differentiable, and the functions in the boundary conditions must be twice continuously differentiable. The boundary curve itself must also be twice continuously differentiable. These are necessary conditions.)

3. Initial-value problem in a hyperbolic case (Cauchy problem)

For the distinction of the two sets of characteristics we will use the notations I. and II. Besides, let S denote an edge section of the shell bordered by the points A and B and projected onto the ground-plane, and let a unit vector i be given at every point of the edge S. On the edge S, let the stress function F take a value determined by a given function φ, and let the derivative of the function F with respect to the direction i take a value determined by another given function ψ. Then the solution of the Cauchy problem

$$\mathfrak{L}F = -g, \tag{8a}$$

$$F|_S = \varphi, \quad \left.\frac{\partial F}{\partial i}\right|_S = \psi \tag{8b}$$

exists and it is uniquely determined in the "square" ADBC bordered by the characteristics I and II that go through the points A and B (Fig. 2a), provided the following conditions are satisfied:

a) The edge S lies in the domain of definition of Eq. (8a),

b) both characteristics I and II intersect the edge S in not more than one point, and none of these are tangential to S,

c) S is twice continuously differentiable,

d) the direction i changes in a continuously differentiable manner along S,

e) the direction i is not parallel with the tangent of S, in any point of the edge S,

f) $g(x, y)$ is continuous,

g) φ and ψ are twice and once differentiable, respectively,

h) $z(x, y)$ is four times continuously differentiable.

On the basis of condition *h)*, Eq. (8a) can be transformed to canonical form while Eqs (8b) are also transformed, but the conditions *a)*—*g)* still hold. The proof of the above proposition, for canonical form, can be seen in [3] p. 165. We note that giving of the values $\partial F/\partial x$ and $\partial F/\partial y$ at the edge S and the value of F in one point of the edge, is equivalent with the condition (8b). The Cauchy problem is discussed with such conditions, for example, in [12] p. 114, [10] p. 801, and [2] p. 313.

In the latter one, S is only required to be continuously differentiable, while the partial derivatives $\partial F/\partial x$ and $\partial F/\partial y$ are required to be continuous. We note, that the uniqueness of the solution also holds when the edge S is only piecewise differentiable, that is, knee points of arbitrary but finit number are allowed, on the edge of the shell ([3] p. 162).

It follows from the foregoing, that, in the case of satisfying the above conditions *a)*—*h)*, the shell can only be in a unique membrane state if the

edge sections of the shell not belonging to S are fully in the "triangle" ABC or ADB (Fig. 2a), or are on its border. These edge sections, however, may not be regarded as mathematical boundaries.

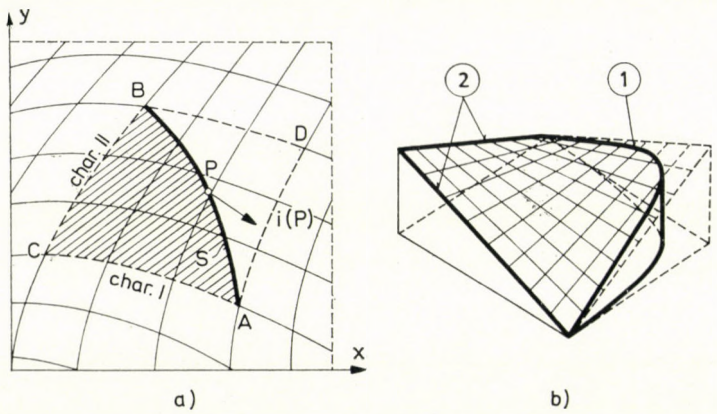

Fig. 2. a) Domain of solution of the initial-value problem; *b)* Hyperbolic paraboloid shell with a free edge section. ① free edge section ② fully supported edge section

Thus, in the present case, two conditions can be given at one edge section, while none for the others.

With the two boundary conditions allowed, S can for example be described to be a free edge section. Namely, if $\varphi \equiv \psi \equiv 0$, and $i \equiv n$, then the conditions (8b) become:

$$F|_S = 0, \quad \left.\frac{\partial F}{\partial n}\right|_S = 0.$$

Otherwise we note that the stipulation $i \equiv n$ is not necessary in this case, as

$$\left.\frac{\partial F}{\partial n}\right|_S = 0$$

follows from the conditions

$$F|_S = 0, \quad \text{and} \quad \left.\frac{\partial F}{\partial i}\right|_S = 0$$

and from the stipulations concerning the edge S and the direction i. Such a hypar shell of free edge is shown in Fig. 2b.

If S is a straight edge section, then the values of the reduced internal forces n_n, and n_{nt} can also be prescribed there. According to Section 2.5, this condition can be formed with the use of F, and $\partial F/\partial n$. With the boundary conditions above the internal forces of the shell are uniquely determined.

4. Boundary-value problems in a hyperbolic case (Goursat-problems)

Let S_1, and S_2 denote two edge sections in a ground-plan projection, joining together and being bordered by the points A and B, and A and C, respectively. Let S denote the boundary consisting of S_1, and S_2 ($S = S_1 \cup S_2$). Let the value of the stress function F be given by a function φ, along the boundary S. If the conditions below are valid:

a) the boundary S lies in the domain of definition of differential equation (9a),

b) S_1 and S_2 are continuously differentiable curves,

c) $g(x, y)$ is continuous,

d) φ is continuous and is continuously differentiable on S_1 and on S_2 (not necessary in point A),

e) $z(x, y)$ is four times continuously differentiable, then the boundary-value problem

$$\mathfrak{L}F = -g, \tag{9a}$$

$$F|_S = \varphi \tag{9b}$$

has got a unique solution in the following three cases ([17] p. 147):

4.1. The boundary section S_1 is identical with the section $\overset{\frown}{AB}$ of a characteristic curve belonging to set I, and the boundary section S_2 is identical with the section $\overset{\frown}{AC}$ of a characteristic curve of set II passing through point A. In this case the unique solution of the problem (9a, b) exists, in the "quadrangle" $ABDC$ bordered by the boundary sections S_1, and S_2 and by the characteristic curve of set II fitting to point B and the characteristic curve of set I fitting to point C (Fig. 3a).

4.2. The boundary section S_1 is identical with the section $\overset{\frown}{AB}$ of a characteristic curve of set I, while the boundary section S_2 starting from point A is intersected by any characteristic curve of set I not more than once, and S_2 is not separated from S_1 by any characteristic curve of set II, furthermore, the characteristic curve of set II fitting to the end point C of S_2 intersects the boundary section S_1 (Fig. 4a). In this case, the unique solution of the problem (9a, b) exists, in the "quadrangle" $ABDE$ bordered by the characteristics fitting to the end points of S_1 and S_2 (Fig. 4a).

4.3. The boundary sections S_1 and S_2 starting from the point A are not separated by any characteristic curve. The curve S_1 is intersected by the characteristics II and the curve S_2 is intersected by the characteristics I, respectively, in not more than one point; the characteristic curve of set I fitting to the end point B of S_1 intersects the curve S_2, and the characteristic curve of set II fitting to the end point C of S_2 intersects the curve S_1. In this case,

the unique solution of the problem (9a, b) exists, in the "quadrangle" AE^DF bordered by the characteristics fitting to the end points of S_1 and S_2 (Fig. 5a).

We note, that PETROVSKIJ mentions these three boundary-value problems when equation (9a) is of the canonical form. The condition *e)* however, ensures that Eq. (9a) could be transformed to the canonical form. As the features given in the conditions *a)—d)* do not get lost in the canonical transformation, the statement of [17] (p. 147) are also valid in the more general form given here. A more detailed investigation of the boundary-value problems above is to be found in [12] (pp. 119—123).

In all the three cases, the shell can only be in a unique membrane state if its edges over S lie inside (or on the border of) the domain $ABDC$. These

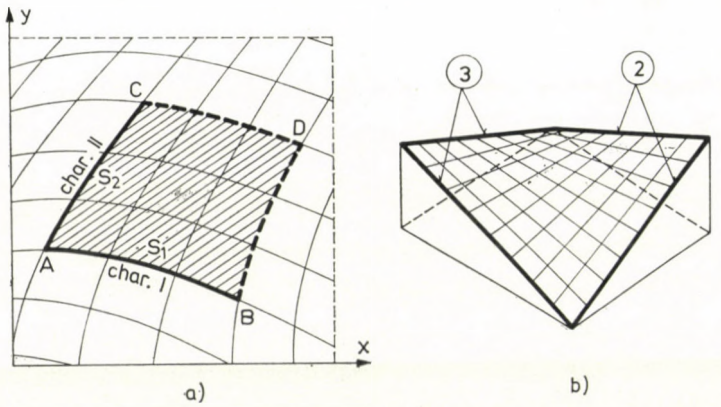

Fig. 3. a) Domain of solution of the boundary-value problem, when the boundary values are prescribed along the characteristics; *b)* Hyperbolic paraboloid shell of distorted quadrangle form; ② fully supported edge section, ③ vertically supported edge beam

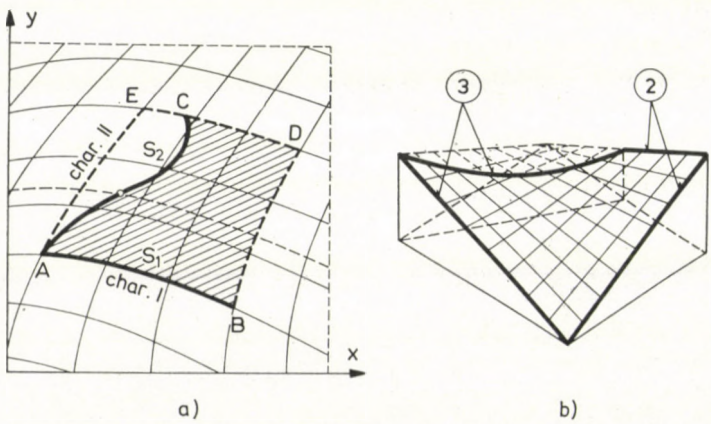

Fig. 4. a) Domain of solution of the boundary-value problem, when the bonudary values are prescribed along a characteristic line and a curve; *b)* Hyperbolic paraboloid shell, ② fully supported edge section, ③ vertically supported edge beam

boundary sections are not boundaries in the mathematical sense (just as in the case of the Cauchy-problem) for no boundary conditions can be given here. Physically it means that internal forces on these edges must be fully balanced by the supports.

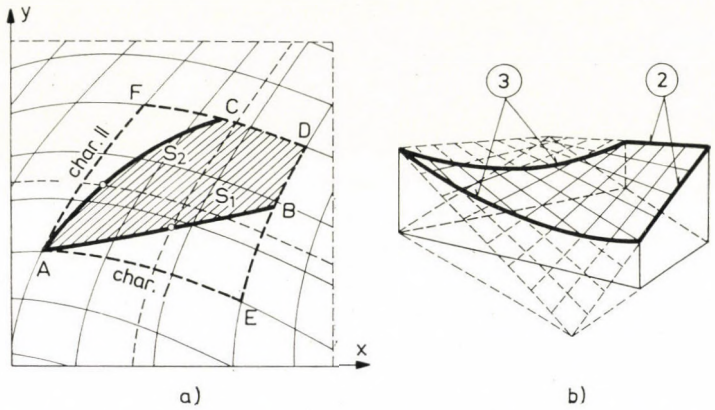

Fig. 5. a) Domain of solution of the boundary-value problem, when the boundary values are prescribed along two curves; *b)* Hyperbolic paraboloid shell, ② fully supported edge section, ③ vertically supported edge beam

On boundary S, that is on the boundary sections S_1 and S_2, we can prescribe the value of the stress function F. Thus, for example, we can stipulate that $F|_S$ let a single plan curve be. As is known, it means that the edge beam of the shell is vertically supported and in such a case, the boundary curve becomes a funicular curve of the forces acting on the edge beam.

For the demonstration of this kind of support mentioned above, we will show a hypar shell on a quadrilateral base (Figs 3b, 4b, 5b). If the edge sections are straight lines, then according to Sec. 2.2, the reduced normal force n_n can be prescribed. For these boundary conditions, the shell is in a unique membrane state and the internal forces of the shell are uniquely determined by the boundary conditions.

In connection with the problem of 4.2, it is mentioned in [15], that a problem for which F is given on S_1 and the linear combination

$$\alpha \frac{\partial F}{\partial n} + \beta F, \quad (\alpha^2 + \beta^2 \neq 0)$$

is given on S_2, is also properly posed. If $\alpha \neq 0$, it is also required that the curve S_2 should not be tangential to any characteristic curve. By reason of this, we can prescribe that the edge S_1 be supported only vertically (Sec. 2.1), while on the edge S_2 we can prescribe the value of the shearing force, provided that

S_2 is of straight or circular shape (Secs 2.3, 2.4). If the edge S_1 is a straight section, then the value of the normal force can be prescribed there as well (Sec. 2.2). Thus, if both S_1 and S_2 are straight sections, the edge S_1 can be free of lateral pressure, while the edge S_2 can be free of shearing force.

When matching the boundary conditions in the point of meet of S_1 and S_2 it becomes evident that because of the mixed boundary conditions above, the shell can only be in a unique membrane state when the boundary sections S_1 and S_2 are perpendicular to each other. There is an exception, namely, when both S_1 and S_2 are straight sections. In this case the perpendicularity of S_1 and S_2 is not required for the uniqueness of membrane state.

5. Initial- and boundary-value problems in a hyperbolic case

5.1. *Boundary consisting of two sections*

If the boundary sections S_1 and S_2 are separated by a characteristic curve, then the conditions given in Sec. 4.3 are not sufficient to ensure the uniqueness of membrane state. An initial value must be given to one of the boundary sections ([12] p. 121, [17] p. 148).

Let S_1 and S_2 be curved sections starting from one common point, and let us use the notation $S = S_1 \cup S_2$. Besides, let a unit vector i be ordered to every point of S_2. Let the value of the stress function F be given by a function φ at the edge S, and let the derivative of F with respect to i be given by a function ψ on the edge S_2. A unique solution of the initial- and boundary-value problem

$$\mathfrak{L}F = -g, \tag{10a}$$

$$F|_S = \varphi, \qquad \left.\frac{\partial F}{\partial i}\right|_{S_2} = \psi \tag{10b}$$

exists in the "quadrangle" $CDEF$ bordered by the characteristics fitting to the end points of S_1 and S_2 (Fig. 6a), if there are fulfilled the conditions relating to the boundary-value problem, on the boundary S, and moreover those relating to the initial-value problem, too, on the boundary section S_2. These conditions are as follows:

a) The boundary S lies inside the domain of definition of Eq. (10a),

b) the boundary sections S_1 and S_2 are separated by a characteristic curve of set II,

c) the characteristics of set II intersect the boundary sections S_1 and S_2 in not more than one point, furthermore, characteristics of set I intersect S_2 in not more than one point, and the characteristic curve of set I fitting to the end B of S_1 intersects the edge S_2, and besides, any characteristic curve is not tangential to S_2;

d) S_1 is continuously differentiable, S_2 is twice continuously differentiable;

e) direction i varies along S_2 in a continuously differentiable way;

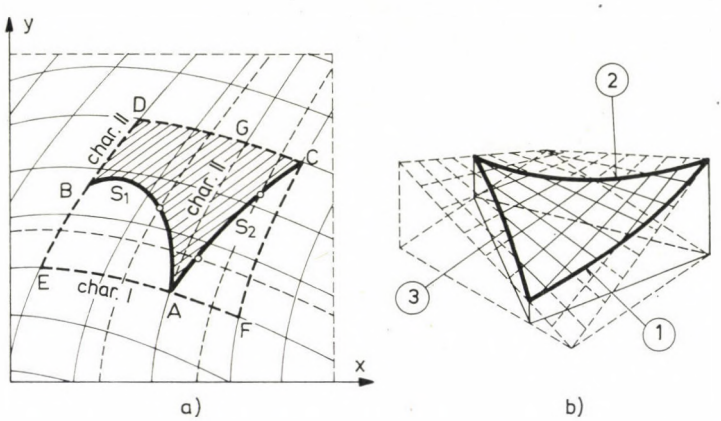

Fig. 6. a) Domain of solution in the case, when initial and boundary values are prescribed on two curves, respectively; *b)* Hyperbolic paraboloid shell on a triangle base, ① free edge section, ② fully supported edge section, ③ vertically supported edge beam

f) the direction i is not parallel with the tangent of the boundary curve S_2, in any point of S_2;

g) $g(x, y)$ is continuous;

h) φ is continuous on S, moreover it is continuously differentiable on S_1 and twice continuously differentiable on S_2; ψ is continuously differentiable on S_2;

i) $z(x, y)$ is four times continuously differentiable.

5.2. *Boundary consisting of three sections*

If an additional boundary section S_3 is fitted to the end point C of S_2 (Fig. 6), and S_2 and S_3 are separated by a characteristic curve of set I fitting to the point C, then the initial- and boundary-value problem (10a, b) can possibly have a unique solution also with the new boundary $S = S_1 \cup S_2 \cup S_3$. S_3 must be of the same features as S_1 with the exception of the one listed at *c)* in the Section 5.1. Instead, we require that the characteristics of set I should intersect the edge S_3 in not more than one point and the characteristic curve of set II fitting to the end point D of S_3 should intersect S_2 or S_1. It is also permissible at the curve S_1 that the characteristic curve of set I fitting to the point B may intersect S_3 instead of S_2. Thus, if we prescribe continuously differentiable boundary values for F, on S_1 and S_3, and twice and once continuously differentiable initial values, respectively, on the boundary S_2, then

a unique solution of the problem (10a, b) exists, in the "quadrangle" *EFGH* bordered by the characteristics fitting to the end points of the three edge sections (Fig. 7a) ([12] p. 125).

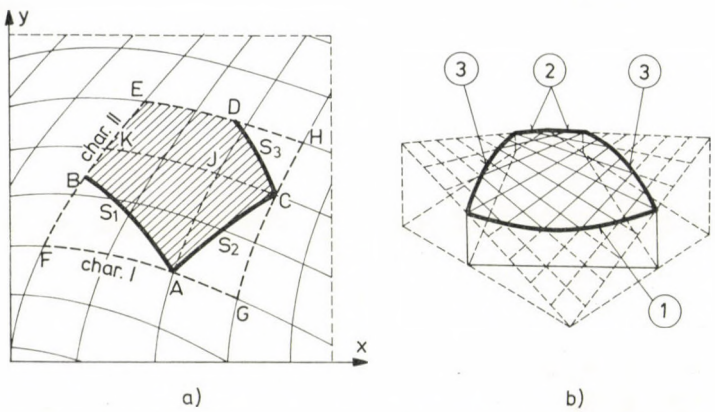

Fig. 7. a) Domain of solution in the case, when initial and boundary values are prescribed on three curves, respectively; *b)* Hyperbolic paraboloid shell on a pentagon base, ① free edge section, ② fully supported edge section, ③ vertically supported edge beam

The shell can only be in a unique membrane state if its boundary, not belonging to S, lies in the "quadrangle" *ACDB* (Fig. 6a — Sec. 5.1), or in the "pentagon" *ACDEB* (Fig. 7a — Sec. 5.2), respectively. On these boundaries no condition can be prescribed.

On the edges $S = S_1 \cup S_2$ and $S = S_1 \cup S_2 \cup S_3$, respectively, we can prescribe that the boundary S_2 be free, furthermore the boundaries S_1, and S_1 and S_3, respectively, be simply supported sections, that is, the edge beam should be the funicular curve of the forces acting on the edge beam. (A shell on such support can be seen in Figs 6b, and 7b.) The above conditions of a statical kind referring to a boundary consisting of three sections are equivalent with the mathematical conditions:

$$F|_{S_2} = 0, \quad \left.\frac{\partial F}{\partial n}\right|_{S_2} = 0, \quad F|_{S_1} = a_1 + b_1 x + c_1 y_1(x), \quad F|_{S_3} = a_3 + b_3 x + c_3 y_3(x)$$

where $a_1, b_1, c_1, a_3, b_3, c_3$ are constant, moreover, $y = y_1(x)$ and $y = y_3(x)$ are the equations of the boundaries S_1, and S_3, respectively.

At the end points A and C of the boundary sections S_1 and S_3, the values of the stress function F, just as its derivatives in direction of the end tangents of S_1 and S_3 are not to be prescribed arbitrarily, because of the conditions

$$F|_{S_3} = 0, \quad \left.\frac{\partial F}{\partial n}\right|_{S_3} = 0.$$

These conditions specify two of the constants a_1, b_1, c_1, and two of the constants a_3, b_3, c_3. If S_1 and S_3 are curved boundary sections than one constant remains undetermined in the condition for S_1 and also in the condition for S_3; this results in that the shell, however, is in a membrane state, but the internal forces are not uniquely determined by the boundary conditions.

On the contrary, if S_1 and S_3 are straight boundary sections, then $a_1 = b_1 = c_1 = a_3 = b_3 = c_3 = 0$ follows from the conditions

$$F|_{S_2} = 0, \left.\frac{\partial F}{\partial n}\right|_{S_2} = 0,$$

and the shell is in a unique membrane state. The situation is similar in the case shown in Fig. 6a.

The problem investigated in Sec. 5.2 (Fig. 7a) can be regarded as a generalization of the following problem: Let Eq. (1) be an equation of canonical form. Let the edge sections S_1, S_2, and S_3 be straight lines determined by the points as follows: S_1:$(x = 0,\ y = b)$, $(x = a,\ y = b)$; S_2: $(x = 0,\ y = 0)$, $(x = 0,\ y = b)$; and S_3: $(x = 0,\ y = 0)$, $(x = a,\ y = 0)$. (Such can be, for example, a saddle-shaped hyperbolic paraboloid — see in Fig. 8.) In this case, prescribing conditions $F|_{S_2} = 0$, $\left.\frac{\partial F}{\partial x}\right|_{S_2} = 0$ on S_2, $F|_{S_1} = 0$, on S_1, and $F|_{S_3} = 0$ on S_3, we can achieve that edges S_1 and S_3 of the shell be free

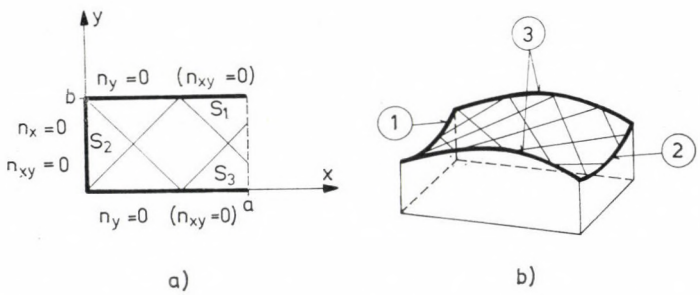

Fig. 8. Saddle-shaped hyperbolic paraboloid shell. *a)* Ground-plane projection of the shell; *b)* shell surface. ① free edge section, ② fully supported edge section, ③ vertically supported edge beam

of lateral pressure and S_2 be a free edge. On the edge section opposite to S_2, no boundary condition can be prescribed. Here, the edge beam is to bear all the loads given by the shell. In this case, we prescribed the value of the stress function F, on the boundaries S_1 and S_3, that is, we gave the first boundary-values.

Along the edge sections S_1 and S_3 (Fig. 8a), second boundary-values $\partial F/\partial n = \partial F/\partial y$ or third boundary values

$$\alpha \frac{\partial F}{\partial n} + \beta F, \quad (\alpha^2 + \beta^2 \neq 0)$$

can also be given, instead of F ([17] p. 145, [18] p. 95). If we prescribe the value of $\partial F/\partial y$, on the edges S_1 and S_3: $\left.\frac{\partial F}{\partial y}\right|_{S_1} = c_1$, $\left.\frac{\partial F}{\partial y}\right|_{S_3} = c_3$ ($c_1 = c_3 = 0$, from the condition $F|_{S_2} = 0$), we can achieve that S_2 be a free edge, and also that S_1 and S_3 be free of shearing force. Mixed boundary conditions can also be given ([19] p. 40). For example, we can prescribe the value of F, on S_1, and the value of $\partial F/\partial y$, on S_3. Let $F|_{S_1} = a_1 x$ and $\left.\frac{\partial F}{\partial y}\right|_{S_3} = c_3$ ($a_1 = c_3 = 0$ following from the conditions $F|_{S_2} = 0$, $\left.\frac{\partial F}{\partial x}\right|_{S_2} = 0$). So, the edge S_2 is free, the edge S_1 is free of lateral pressure, and the edge S_3 is free of shearing force. More complicated boundary conditions can also be prescribed ([19] p. 42, [2] p. 182). The hyperbolic shell shown in Fig. 8a, is in unique membrane state for all of the cases detailed above.

It is to be noted, that the problem discussed in the Section 5.1 is a combination of an initial-value problem (Fig. 2a) discussed in Sec. 3 (the solution of which was defined in the "quadrangle" $AFCG$ — Fig. 6a) and a boundary-value problem (Fig. 4a) discussed in Sec. 4.2 (the solution of which was defined in the "quadrangle" $AGDE$ — Fig. 6a).

Similarly, the problem discussed in Sec. 5.2 (Fig. 7a) is a combination of an initial-value problem (Fig. 2a) discussed in Sec. 4.2 (domain of solution: $AGCJ$) and two boundary-value problems (Fig. 4a) discussed in Sec. 4.2 (domain of solution is the union of $AJKF$ and $CHEK$). If the position of S_1 and S_3 is such that the characteristics fitting to their end points B, and D, do not intersect the boundary S_2, then the problem can be divided into parts, among which the boundary-value problem of Sec. 4.1 (Fig. 3a) can also be found.

It is to be noted, that the second, third, and mixed boundary-value problems specified for rectangular domain (Fig. 8a) can also be extended for the domain seen in Fig. 7a [15]. In that case (Fig. 7a), the boundary-values for F and $\partial F/\partial n$ are to be prescribed on S_2, while

$$\alpha_1 \frac{\partial F}{\partial n} + \beta_1 F, \quad (\alpha_1^2 + \beta_1^2 \neq 0) \quad \text{on} \quad S_1,$$

and

$$\alpha_3 \frac{\partial F}{\partial n} + \beta_3 F, \quad (\alpha_3^2 + \beta_3^2 \neq 0) \quad \text{on} \quad S_3.$$

With certain coefficients α_1, β_1, a_3, β_3, these conditions include the first, second, third, and mixed boundary values as well. If $\alpha_1 \neq 0$, $\alpha_3 \neq 0$, then the boundary curves S_1 and S_3 must not be tangential to any characteristic curve. Consequently, S_2 can be a free edge, or, if it is straight, the value of the reduced internal forces n_n, and n_{nt} can be prescribed there. Simultaneously, the boundary sections S_1 and S_3 cannot only be supported vertically, but, if those are straight lines, the values of the reduced internal forces n_n, and n_{nt} can be prescribed there, instead. The value of the reduced shearing force n_{nt} can also be given in the case when S_1 and S_3 are circular arcs. In the case of mixed boundary-value problems, for example, a vertically supported edge beam could appear at S_1, while S_3 (if it is a straight or a circular boundary) could be free of shearing force. If, in the problems above mentioned, the vertically supported edge is not straight, the uniqueness of membrane state cannot hold.

By combining the initial-value, boundary-value, and mixed problems, further variations can be created. In such combined cases the solution F is continuous, while there may appear discontinuities in the internal forces.

6. Problem of the closed boundary curve

On the three edge sections of the rectangular domain, in Fig. 8a, altogether four boundary conditions were necessary to get a unique solution of Pucher's equation.

As a natural question it arises whether one of the two conditions given on S_2, could be transferred onto the boundary opposite to S_2, and so, to look for the solution of Pucher's equation with one condition prescribed on each boundary. Unfortunately, *in general, the solution of a hyperbolic equation with boundary conditions prescribed on a closed boundary does not exist*, as it is stated in [10] p. 869, and [13] pp. 466—471. Let us discuss this problem in a few cases.

6.1. *Initial-value problem with closed boundary*

If the boundary curve, in the initial-value problem discussed in Sec. 3, satisfies the conditions *a)*, *b)*, *c)* given there, then the boundary is allowed to be a closed curve, as well. This fact can be demonstrated on the example below. Let us consider a simple hyperboloid of one sheet the equation of which is given by

$$\frac{x^2}{a^2} + \frac{y^2}{b^2} - \frac{z^2}{c^2} = 1.$$

For the sake of simplicity, let it be a hyperboloid of revolution ($a = b$). Let the boundary S be (in ground-plane projection) a twice continuously differenti-

able closed curve not intersecting itself. Let the domain bordered by S contain a circular domain T of radius a, which does not belong to the domain of definition of the membrane-shell-equation (and of the hyperboloid of revolution, respectively) (Fig. 9). Let the boundary S be intersected by any characteristic curve, in not more than one point. If the problem is considered, on the whole

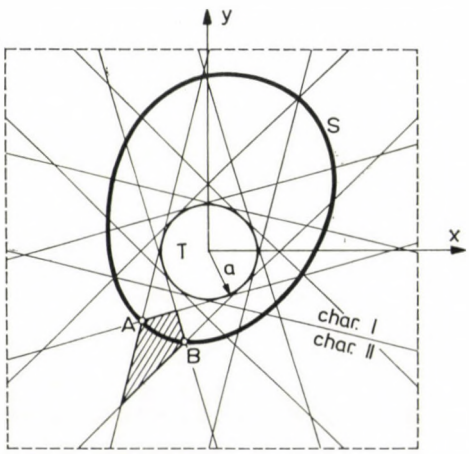

Fig. 9. Data of the initial-value problem concerning a hyperboloid of revolution

surface of the hyperboloid the characteristics I and II are in coincidence in the ground-plane projection, because the function of the hyperboloid is double-valued. Therefore, the characteristics appear to have two points of intersection with the boundary S (Fig. 9). Actually, however, there is only one. It can be seen, if we regard the surface equivalents of the characteristics and of the boundary S, that is to say, the asymptotic lines and the actual edge $\bar{S}$ of the shell. The asymptotic lines (straight generatrices of the hyperboloid) intersect the edge $\bar{S}$ only in one point (Fig. 10a). We stipulate that the asymptotic lines must not be tangential to the edge $\bar{S}$.

Let us prescribe the initial-value conditions of Sec. 3, on the whole boundary. When solving this initial-value problem, let us start from an arbitrary point A of S and let us move along S until a point B. Then, the unique solution of the problem exists in the quadrangle bordered by the characteristics fitting to point A and B (Figs 9, 10a). Moving further on, along S, the quadrangle domain of solution degenerates more and more and covers the plane xy more and more.

Arriving back at the point A, the "quadrangle domain" of solution is the whole plane that must be regarded as double-sheeted, with the exception of the domain T, where the surface is not defined, and the double angle domain bordered by the characteristics fitting to A. The interior of the angle domain

must be regarded if we move from the contact point on T to the direction of A, and its exterior if we move in opposite direction. For the sake of descriptivness, we figured the domain not belonging to the solution in axonometry, on the middle surface itself, in Fig 10b. In the figure, the parts CAD and EAF of the sheet belong to this domain which is to be considered as an infinite

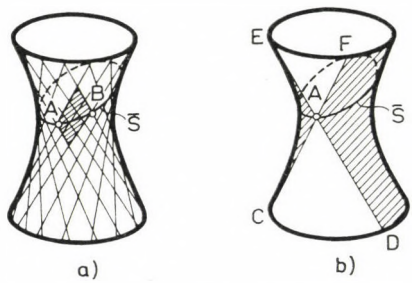

Fig. 10. Domain of solution of the initial-value problem concerning a hyperboloid of revolution: *a)* opened boundary curve; *b)* closed boundary curve

one. As, then the solution is uniquely determined also on the two characteristic curves fitting to A, if follows (applying the problem of Sec. 4.1) that the solution exists and its uniqueness holds, in the whole domain of definition (and on the whole superficies of hyperboloid, respectively). We note that the domain of definition is double-sheeted, as the hyperboloid of revolution is double-valued function. We note, in addition, that the solution obtained satisfies the differential equation $\mathfrak{L}F = -g$, along the border of T, only in limit, because of the vertical tangents of the surface. Therefore the actual value of the internal forces along this inner circle can only be computed as limit.

In the example discussed, we pointed out the uniqueness of the solution for two cases. One concerns the shell above $\bar{S}$, while the other concerns the shell under the edge $\bar{S}$. In the practice, only one half of the shell is dealt with.

When prescribing the initial-value conditions

$$F|_S = 0, \quad \left.\frac{\partial F}{\partial n}\right|_S = 0$$

we can realize that the whole boundary S be free. The membrane state of the shell requires another closed boundary that is to lie in the domain of definition of the problem (and that must contain the domain T), but no condition can be prescribed on this boundary. This boundary must be fully supported, that is, this edge must bear all the membrane forces given by the shell.

If we take such a closed boundary curve S, which does not contain the domain T, not belonging to the domain of definition, then the characteristics,

that is, the asymptotic lines intersect the boundary curve S (that is, the edge $\bar{S}$) in two points. For this reason, the problem is overdeterminated and insoluble. That is why hyperbolic shells having holes of free edge on its superficies cannot be in a membrane state. This will be discussed in the following section, that not even holes with an edge-ring are allowed, if the edge-ring gives only axial stiffening.

6.2. *Boundary-value problem with a closed boundary curve*

Let us consider the boundary-value problem discussed in Sec. 4.3. A unique solution of this problem always exists, if the end points B and C of the boundary sections S_1 and S_2, respectively, are not in coincidence (Fig. 5a). The points B and C can be arbitrarily close to each other, but not in coincidence ([13] p. 466). If B and C are in coincidence, the problem becomes overdeterminate. It can be explained as follows: Let $B \equiv C$ be, and let us divide the problem in parts by the characteristic curves fitting to an arbitrary point L inside the domain that is bordered by S_1 and S_2. In the first part we only consider section $\overset{\frown}{AH_1}$ of S_1 and section AG_1 of S_2, respectively, while in the second part, section $\overset{\frown}{CJ_1}$ of S_1 and rection $\overset{\frown}{CK_1}$ of S_2 (Fig. 11). Thus, the solution of the problem *4.3* is uniquely determined in the "quadrangles" $AHLG$ and $CKLJ$, respectively. If the two solutions in point L are identical, then this solution is to be continued, as the value of the function is known on the sections $\overset{\frown}{GL}$, $\overset{\frown}{KL}$, and $\overset{\frown}{HL}$, $\overset{\frown}{JL}$ of characteristics, respectively. Thus we have arrived at problems like those in Sec. *4.1*, which have a unique solution in the "quadrangles" $GLKF$ and $EJLH$, respectively. For this, the solution is determined on the section $\overset{\frown}{H_1J_1}$ of S_1 and on the section $\overset{\frown}{G_1K_1}$ of S_2, as well. Consequently, the value of the function F is not to be prescribed on these sections, else, the problem becomes overdeterminate. If the two solutions in the point L are different, then there is a discontinuity of the stress function, which is propagated along the characteristics. So in this case, there is no continuously differentiable solution in the domain considered, that is, a solution does not exist.

And now, let us study the problem mentioned in connection with Fig. 8, at the beginning of Sec. *6*. At present, however, the basis of the shell will be considered to be not a quadrangle but a smooth curve. At the initial- and boundary-value problems of hyperbolic equations, the edge section for which initial values are prescribed and the edge section for which boundary values are prescribed may join tangentially and may have a common tangential line with one of the characteristic curves fitting to the joint ([10] p. 809, [13] p. 467). (Naturally, in this case the initial-values and the boundary-values cannot be prescribed arbitrarily.) So, the problem discussed in Sec. 5.2 (Fig. 7a) may

have a unique solution even if all the edge sections are tangential to the characteristic curves fitting to the end points of the edge sections (Fig. 12). Let the edge S_4 join the end points of S_1 and S_3 tangentially (Fig. 12). As is known, prescribing boundary values on S_1 and S_3, and initial values on S_2, the stress function is uniquely determined on S_4. If one of the conditions

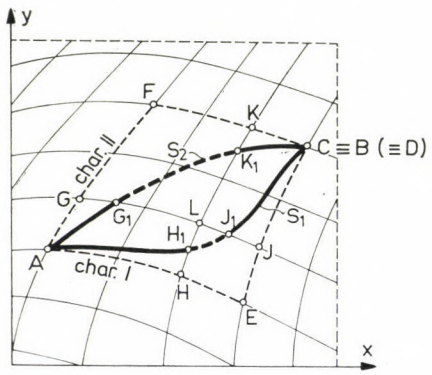

Fig. 11. Boundary-value problem — division in parts

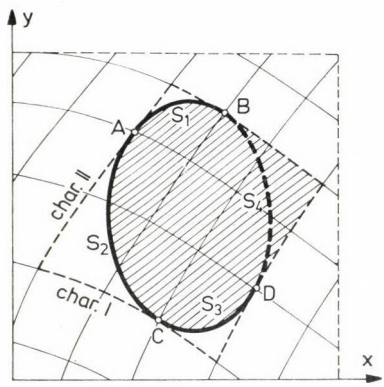

Fig. 12. Domain of solution of the initial- and boundary-value problem with a smooth boundary curve

prescribed earlier on S_2 is given up and a condition on S_4 is prescribed instead, in general, we arrive at an ill-posed problem ([13] p. 467).

However, there is one kind of shell which is in membrane state when prescribing $F|_S = 0$ on its closed boundary, and being subjected to a vertical load of polynomial distribution. This shell is the hyperbolic paraboloid on an ellipse base, and supported vertically along its edge [8, 9] (Fig. 13). A solution only exists if $f_a = K_i f_b$, where K_i denotes certain fixed constants, and f_a and f_b are the rises of the arch (Fig. 13).

It has not been cleared up so far why can a solution only be found for this special problem, and not in general. Probably, the special form of the boundary (analitic curve), the relation of the boundary curve to the characteristics, the special polynomial form of loading (analytical function), and the symmetry are in this respect, the most important.

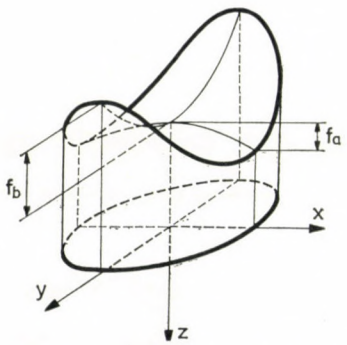

Fig. 13. Hyperbolic paraboloid surface on an ellipse base

We note here, that HADAMARD ([13] p. 469) showed an example for an ellipse domain where the equation $\partial^2 F/(\partial x \partial y) = 0$ had no solution, when the value of F was prescribed along the ellipse line.

There is another problem that is very similar to the above-mentioned one, namely the hyperbolic paraboloid (saddle-shaped) shell over a rhombus base, subjected to uniformly distributed load, and supported vertically along its full edge, which is always in a membrane state, if the two rises of arch in direction of principal curvatures are not equal [7]. By this problem, the stress function F must be prescribed to vary linearly on each side of the rhombus.

Similar, but in more special cases are the saddle-shaped shells of normal type, subjected to uniformly distributed load [1, 8], which can be in a membrane state while only shearing forces arise along the whole edge. At distorted and saddle-shaped shells of normal type, the condition $F = as + b$ is satisfied at each boundary section.

We also note, that such a boundary-value problem concerning hyperbolic shells, at which we prescribe conditions on two separated edges of the shell, is ill-posed. Therefore the hyperboloid shown in Fig. 10 cannot be in a unique membrane state, if there are stiffening rings at its lower and upper edges, and both are supported vertically (that is, the values of the stress function give plane curves at both edges).

This problem of the one-sheeted hyperboloid shell (similarly to that of the saddle-shaped shell being free of lateral pressure) is ill-posed for there is

an infinite number of "eigenshapes" at which the shell cannot bear external loads. The eigenshapes are placed among the possible shapes of the hyperboloid so dense as the rational numbers among the real numbers ([11a] p. 265). It means that, if there is a shape of shell at which a membrane state exists, another shape is always found there (arbitrarily close to the previous one) at which membrane state cannot exist.

7. A few comments on the construction of hyperbolic membrane shells with a free edge

7.1. The composite sectorial shell formed of a hyperbolic surface, is a shape greatly liked for its aesthetic appearance (Fig. 14). For each a sector, the edges between the neighbouring sectors are fully supported, while the third edge is absolutely free (Fig. 15). The shape of this free edge must be chosen according to the statements of Sec. 3. If, for example, the middle surface

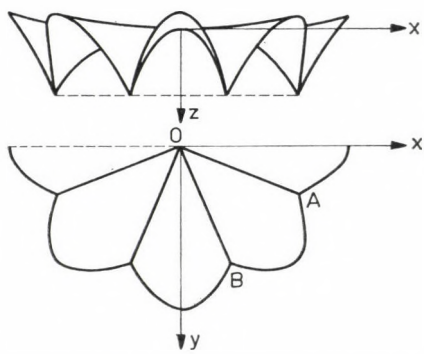

Fig. 14. Composite sectorial shell

of the shell is formed as hyperbolic paraboloid, then the free edge section $\widehat{AB}$ of the sector should be smooth enough and have such a form that every characteristic line should intersect it only at one point. That is, the curve of the free edge is to lie inside the angle domain ACB bordered by the characteristic lines fitting to the end points A and B, like the curve ① in Fig. 15. If there are points of the free edge that lie outside of the angle domain ACB (such as curve ⑪ in Fig. 15), then there are characteristics, which intersect the boundary curve at two points. This fact results in the over determination of the problem, that is a shell whose free edge has such a shape, cannot be in a membrane state.

7.2. By initial-value problems and at initial- and boundary-value problems, Cauchy's initial conditions can be so given on S_2, that the shell does

have a free edge in one or more sections of S_2. If only one section of S_2 is free, then the conditions $F = 0$ and $\partial F/\partial n = 0$ can be prescribed there. If there are two or more free edge sections on S_2 (not separated by free edge sections), then the conditions $F = 0$ and $\partial F/\partial n = 0$ can only be prescribed on one section, and not on the others. Such a case is, for example, when the curve S_2

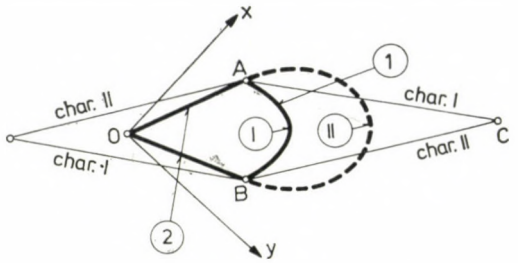

Fig. 15. Ground-plane projection of one sector of the shell. ① free edge section, ② fully supported edge section

has an inner straight section. On it, we prescribe the boundary forces n_n, n_{nt}, while the curved boundary sections joining to the straight section is required to be free. The forces n_n and n_{nt} are required to be continuous and to have zero value at the end points of the straight section. Then, on one of the free edge sections, the conditions $F = 0$ and $\partial F/\partial n = 0$ can be prescribed. If we prescribe $n_n = n_{nt} = 0$ on the straight line, that is the inner section is also free, then the whole boundary S_2 can be regarded as one edge section, where the conditions $F = 0$ and $\partial F/\partial n = 0$ can be prescribed.

If there are two or more free edge sections of a hyperbolic shell, and these do not fit to a curve that is intersected by every characteristic line, in not more than one point, then the shell cannot be in a membrane state, or, if there exists a membrane state, its uniqueness does not hold. If there is a curve mentioned before, but we prescribe boundary values instead of initial values between the free edge sections, then the solution of the shell equation will not be unique. This statement follows from those stated in Secs 3 and 5.

The saddle-shaped shell on a quadrangle base, being supported at its two opposite edges, is only in a membrane state when the load intensity is constant in the parallel direction to the free edges.

According to Sec. 3, an initial-value problem can surely obtain a solution if the boundary curve is twice continuously differentiable. However, it does not follow from this that if the boundary curve is not twice continuously differentiable, then the solution does not exist.

If there are two free edge sections on a shell joining each other in a knee, and the edge sections are twice continuously differentiable in themselves, and the curve consisting of these two sections is intersected by an every characteristic

line at not more than one point, then a continuous solution exists and is also unique in the "quadrangle" bordered by the characteristics fitting to the end points of the united boundary curve. In this case, the solution is not necessary to be continuously differentiable along the characteristics fitting to the joint,

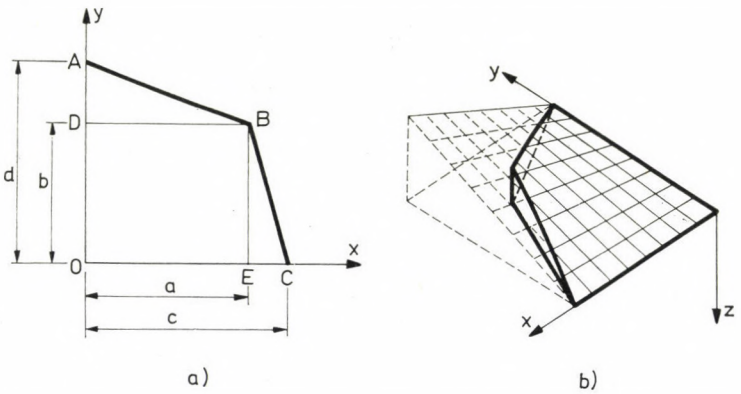

Fig. 16. a) Ground-plane projection of hyperbolic paraboloid shell with a free edge. The point B is a knee point on the free boundary line ABC. *b)* The shell surface

even then, if the load function $g(x, y)$ is continuous. Similarly, the solution obtained is not sure to be twice continuously differentiable, even then, if the load function $g(x, y)$ is continuously differentiable, that is, the internal forces in the shell may be discontinuous.

An example will be shown to illustrate it.

Let us look at a hyperbolic paraboloid shell subjected to a uniformly distributed load $g =$ constant. Let the equation of the middle surface be $2z = -xy$. In the ground-plane projection the shell is bordered by straight lines (Fig. 16). Let the boundary sections AO and OC be fully supported, while the sections AB and BC be free. There is a knee point B on the free boundary ABC. Then Pucher's differential equation for this problem is as follows:

$$\frac{\partial^2 F}{\partial x \partial y} = -g. \tag{11}$$

We consider the following boundary conditions: The value of the stress function F at point A be equal to zero, and the partial derivatives $\partial F/\partial x$ and $\partial F/\partial y$ along the boundary ABC be of zero value:

$$F(0, d) = 0, \left.\frac{\partial F}{\partial x}\right|_{ABC} = 0, \quad \left.\frac{\partial F}{\partial y}\right|_{ABC} = 0. \tag{12}$$

The solution of the problem consists of three parts: The solution F_1, F_2, and F_3 are valid in the triangles ABD, BCE, and in the quadrangle $ODBE$, respectively. The stress functions obtained are as follows:

$$F_1 = g\left(-\frac{ad^2}{2(d-b)} + dx + \frac{da}{d-b}y - \frac{d-b}{2a}x^2 - \frac{a}{2(d-b)}y^2 - xy\right),$$

$$F_2 = g\left(-\frac{bc^2}{2(c-a)} + \frac{cb}{c-a}x + cy - \frac{b}{2(c-a)}x^2 - \frac{c-a}{2b}y^2 - xy\right),$$

$$F_3 = g\left(-\frac{ad+bc}{2} + dx + cy - \frac{d-b}{2a}x^2 - \frac{c-a}{2b}y^2 - xy\right).$$

The reduced internal forces in the triangle ABD:

$$n_x^{(1)} = -\frac{a}{d-b}g,\ n_y^{(1)} = -\frac{d-b}{a}g,\ n_{xy}^{(1)} = g,$$

in the triangle BCE:

$$n_x^{(2)} = -\frac{c-a}{b}g,\quad n_y^{(2)} = -\frac{b}{c-a}g,\quad n_{xy}^{(2)} = g,$$

and in the quadrangle $ODBE$:

$$n_x^{(3)} = -\frac{c-a}{b}g,\ n_y^{(3)} = -\frac{d-b}{a}g,\quad n_{xy}^{(3)} = g.$$

The functions F_1, F_2, and F_3 are many times continuously differentiable, inside their domain of definition. Along and perpendicularly to the characteristics BE and DB, however, they are only once continuously differentiable. From this it follows that if we consider the functions F_1, F_2, and F_3 as only one function, it satisfies Eq. (11) and conditions (12), it is not twice continuously differentiable in the quadrangle $ABCO$. For this, there is discontinuity in the internal forces being parallel to the characteristics BD and BE, along these characteristics, respectively. Thus, for example $n_x^{(1)} \neq n_x^{(3)}$ along the characteristic BD and $n_y^{(2)} \neq n_y^{(3)}$ along the characteristic BE, respectively.

If the free boundary curve of the shell is twice continuously differentiable and the load function is smooth enough, as it is in general, then there is no discontinuity in the function of the internal forces. That is why knee points on the free edges of hyperbolic shells are to be rounded off, in practice.

REFERENCES

1. Bölcskei, E.—Orosz, Á.: Reinforced Concrete Structures. Shells. (In Hungarian), Tankönyvkiadó, Budapest 1973
2. Courant, R.—Hilbert, D.: Methoden der mathematischen Physik. 2. Band. Springer Verlag, Berlin 1937

3. CZÁCH, L.—SIMON, L.: Partial Differential Equations 1. (In Hungarian) (ELTE lecture note) Tankönyvkiadó, Budapest 1969
4. CSONKA, P.: On the Annular Edge Beam of Membrane Shells. *Acta Techn. Hung.* **33** (1961), 413—430
5. CSONKA P.: Membrane Shells with Perfectly Free Edges. *Acta Techn. Hung.* **40** (1962), 151—167
6. CSONKA, P.: The Boundary Line of the Stress Surface of Calotte Shells. *Acta Techn. Hung.* **48** (1964), 203—209
7. CSONKA, P.: Shell Curved in Two Directions Constructed over a Rhombus Plan-form. *Acta Techn. Hung.* **48** (1964), 401—409
8. CSONKA, P.: Membranschalen. Bauingenieur-Praxis, Heft 16. W. Ernst u. Sohn, Berlin—München 1966
9. DULÁCSKA, E.: Schalentragwerke über elliptischem Grundriß. *Acta Techn. Hung.* **27** (1959), 273—279
10. FRANK, PH.—MISES, R. v.: Die Differential- und Integralgleichungen der Mechanik und Physik. Bd. I. 2. Aufl., Vieweg u. Sohn, Braunschweig 1930
11. ГОЛЬДЕНВЕЙЗЕР, А. Л.: Теория упругих тонких оболочек. Гос. Изд. Технико-Теорет. Лит., Москва, 1953. (In English translation: GOL'DENVEISER, A. L.: The Theory of Thin Elastic Shells. Pergamon, New York 1961)
11a. ГОЛЬДЕНВЕЙЗЕР, А. Л.: Теория упругих тонких оболочек. Изд. второе. Изд. Наука, Москва 1976
12. GOURSAT, É.: Cours d'Analyse Mathématique. Tom. III. 4. éd. Gauthiers-Villars, Paris 1927
13. HADAMARD, J.: Le problème de Cauchy et les équations aux dérivées partielles linéaires hyperboliques. Ed. Hermann, Paris 1932
14. KAYA SAYAR, F.: Untersuchung des Membranspannungszustandes der verallgemeinerten Rohrschalen mit besonderer Berücksichtigung der negativen Flächenkrümmung. Dissertation. Technische Hochschule Hannover, 1961
15. KORN, G. A.—KORN, T. M.: Mathematical Handbook for Scientists and Engineers. McGraw-Hill Book Comp. Inc. New York—Toronto—London 1961
16. MIRANDA, C.: Partial Differential Equations of Elliptic Type. Springer-Verlag, Berlin—Heidelberg—New York 1970
17. ПЕТРОВСКИЙ, И. Г.: Лекции об уравнениях с частными производными. Гос. Изд. Физико-Мат. Лит., Москва 1961 (In English translation: PETROVSKII, I. G.: Lectures on Partial Differential Equations. Interscience, New York 1955)
18. СМИРНОВ, М. М.: Дифференциальные уравнения в частных производных второго порядка. Изд. БГУ., Минск 1974
19. ТИХОНОВ, А. Н. — САМАРСКИЙ, А. А.: Уравнения математической физики. Изд. Наука, Москва 1972. (In English translation: TIKHONOV, A. N.—SAMARSKII, A. A.: Partial Differential Equations in Mathematical Physics. Holden-Day, San Francisco 1964)
20. VEKUA, I. N.: Systeme von Differentialgleichungen erster Ordnung vom elliptischen Typus und Randwertaufgaben mit einer Anwendung in der Theorie der Schalen. VEB Deutscher Verlag der Wissenschaften, Berlin 1956
21. ВЛАСОВ, В. З.: Общая теория оболочек и ее приложения в технике. Гос. Изд. Технико-Теорет. Лит., Москва — Ленинград 1949 (In German translation: WLASSOW, W. S.: Allgemeine Schalentheorie und ihre Anwendung in der Technik. Akademie-Verlag, Berlin 1958)

Die Existenz- und Eindeutigkeitsbedingungen des Membranzustandes von Schalenkonstruktionen — I. Hyperbolische Schalen. Behandelt wird das Problem, ob welcherart Randbedingungen festgelegt werden sollten am Rand einer Schale um einen statisch bestimmten Zustand desselben hervorzurufen. Die Existenz- und Eindeutigkeitsbedingungen der Lösung der Membranschalengleichung werden untersucht aufgrund der Theorie der partiellen Differentialgleichungen, für verschiedene Randbedingungen. Dieser Teil der Abhandlung enthält die für die Hyperbelschalen erhaltenen Ergebnisse.

Acta Technica Academiae Scientiarum Hungaricae, Tomus 91 (1—2), pp. 111—119 (1980)

GESETZMÄSSIGKEITEN DER SCHOLLENZERKLEINERUNG BEI DER SAATBETTVORBEREITUNG

GY. SITKEI* und J. FEHÉR**

[Eingegangen am 15 Mai 1979]

Aufgrund von in einer Bodenrinne durchgeführten Versuchen wurde ein Zusammenhang zwischen der Schollengröße, der kritischen Werkzeuggeschwindigkeit und dem Feuchtigkeitsgehalt des Bodens ermittelt. Anhand einer vereinfachten Theorie wurde der vom Feuchtigkeitsgehalt abhängige spezifische Energiebedarf für die Schollenzerkleinerung bestimmt. Auch der Einfluß des Innenporenanteils auf den Energiebedarf der Zerkleinerung wurde untersucht. Aufgrund der Versuche konnte man feststellen, daß die Erhöhung der Werkzeuggeschwindigkeit über etwa 11 bis 12 km/h nicht zweckmäßig zu sein scheint, da dies in diesem Bereich nur zu einer minderwertigen weiteren Schollenzerkleinerung führt.

1. Einleitung

Die geeignete Saatbettvorbereitung ist eine grundlegende Vorbedingung für einen hohen Ernteertrag. Um eine schnelle Keimung und ein schnelles Aufgehen der Saat zu sichern, sollte man im allgemeinen eine feinkrümelige Bodenstruktur schaffen, die beim Anbau, zur Verhinderung der Austrocknung der Bodenfläche gewissermaßen verdichtet werden soll.

In der herbstlichen Jahreszeit ist der Feuchtigkeitsgehalt des Bodens häufig geringer als das Optimum und deswegen erfordert die Vorbereitung eines Saatbetts einen bedeutenden Aufwand an Arbeit und Energie. Bei der Ackerbestellung eines trockenen Bodens entstehen verhältnismäßig große und harte Schollen, die in kleinere Bodenteile eingebettet sind. Dei Aufgabe der Saatbettvorbereitung besteht in einer derartigen Zerkleinerung dieser im Boden eingebetteten Schollen, daß die Fraktion der Schollen den Anforderungen der gegebenen Pflanze entspricht.

Das grundlegende Gerät für die Saatbettvorbereitung ist heutzutage der Kombinator, dessen Hauptteile die Federzinken sind. Die sich im Boden bewegenden Federzinken stoßen gegen die Schollen, die entweder zerkleinert werden, oder dem Werkzeug ausweichen. Dieser letztere Fall tritt dann ein, wenn die Stoßenergie zu einer weiteren Zerkleinerung nicht ausreicht.

Auch kann beobachtet werden, daß im Fall der Verschiebung der Schollen dieselben immer mehr an die Bodenoberfläche gelangen. Da die an die

* Gy. Sitkei, Széher u. 19, H-1021 Budapest, Ungarn
** J. Fehér, Révai u. 18, H-9700, Szombathely, Ungarn

Oberfläche des Bodens gelangenen Schollen über keine Stütze verfügen, verschlechtern sich die Bedingungen für eine weitere Zerkleinerung mit einem passiven Werkzeug. Deswegen werden immer verschiedene Nachläufer angewandt, die die auf der Oberfläche befindlichen kleineren und mittelgroßen Schollen weiter zerkleinern.

2. Mechanik der Schollenzerkleinerung

Die Lage der im Boden eingebetteten Schollen und die auf diese wirkenden Kräfte sind im Bild 1 dargestellt. Das sich mit einer Geschwindigkeit v bewegende Werkzeug stoßt gegen die Scholle, wobei sich die Stoßkraft sich aus der Trägheitskraft und der Stützkraft zusammensetzt:

$$P = \frac{G}{g} \cdot a + pF, \tag{1}$$

wo
G das Gewicht der Scholle,
a die Beschleunigung und
F den Projektionsquerschnitt der Scholle
bedeuten.

Der bei der horizontalen Verschiebung der Scholle auftretende Druck kann mit Hilfe der Gleichung in der Form

$$p = k\left(\frac{z}{d}\right)^n$$

angenähert werden, wo z die horizontale Verschiebung und d den Durchmesser der Bodenscholle bedeuten. Der Koeffizient k ist eine Funktion der Körnung und des Feuchtigkeitsgehalts des Materials; sein Wert ändert sich von 1,0 bis 2,0 daN/cm² [1].

Unter Berücksichtigung des Besagten kann die Gleichung (1) auch, wie folgt, geschrieben werden:

$$P = \frac{G}{g} \cdot \frac{dv}{dt} + k\frac{d^2\pi}{4}\left(\frac{z}{d}\right)^n. \tag{1a}$$

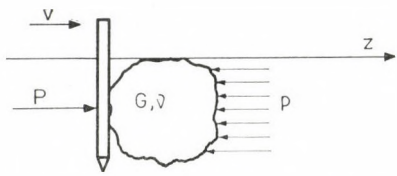

Bild 1. Die auf die im Boden eingebetteten Schollen wirkende Kräfte

Während des Anstoßes befindet sich die Verschiebung der Scholle, im allgemeinen, zwischen 1,0 und 1,4 cm (manchmal auch darunter), infolgedessen ergibt sich als Quotient z/d für den größeren Schollen ein Wert von etwa 0,1. Der Anfangsabschnitt der Kurve $p - z/d$ kann mit einer geraden Linie gut angenähert werden, folglich können wir den Wert $n = 1{,}0$ benutzen (in solchen Fällen bezieht sich der Wert von k auf den Anfangsabschnitt der Kurve).

Das Werkzeug beschleunigt die Scholle im Grenzfall auf die eigene Geschwindigkeit v, d. h., in der Gleichung (1a) kann der Wert von dv durch $v - o = v$ substituiert, und infolgedessen die Gleichung (1a) in folgender Form aufgeschrieben werden:

$$P = \frac{G}{g}\frac{v}{\Delta t} + k\frac{d^2\pi}{4}\left(\frac{z}{d}\right), \tag{1b}$$

wo Δt die Zeit des Anstoßes bedeutet.

Zur weiteren Lösung der Aufgabe sollte man die Bruchbedingung der Scholle, d. h., die Änderung der kritischen Bruchkraft in Abhängigkeit von den Stoffkennwerten und der Schollendimension untersuchen.

Die Untersuchung des Anstoßzerkleinerungsvorgangs [2] für Getreidekörner zeigte, daß die zur Zerkleinerung angewandte Leistung zur hergestellten neuen Fläche proportional ist:

$$N = v'\frac{dF}{dt}, \tag{2}$$

wo v' den spezifischen Energiebedarf (cmdaN/cm^2) bedeutet. Für einen mit Bruch geendeten Anstoßvorgang kann — unter Berücksichtigung, daß die hergestellte neue Fläche proportional zu d^2 ist — die Gleichung (2) wie folgt, aufgeschrieben werden:

$$\frac{\int Pdz}{\Delta t} = v'\frac{k_1 d^2}{\Delta t},$$

oder

$$\int Pdz = v'k_1 d^2, \tag{2a}$$

wo z die Verformung der Scholle bedeutet und die Integration bis zum Bruch durchgeführt werden muß. Zwecks einer weiteren Vereinfachung wird angenommen, daß die Kraft P sich linear ändert, und die zum Bruch gehörende Verformung z proportional zum Durchmesser d ist. Demgemäß wird der Wert der kritischen Bruchkraft aus der Gleichung (2a) bestimmt

$$P_{kr} = v'\frac{k_1 d^2}{k_2 d} = vd, \tag{3}$$

wo der Koeffizient v die Proportionalitätsfaktoren v', k_1 und k_2 enthält.

Der Bruch der Scholle kommt nur dann zustande, wenn die durch die Gleichung (1b) bestimmte Kraft gleich oder größer, als die nach der Gleichung (3) erforderliche ist, d. h.,

$$vd = \frac{G}{g}\frac{v}{\Delta t} + k\frac{d^2\pi}{4}\left(\frac{z}{d}\right),$$

woraus

$$G = \frac{g\Delta t d}{v}\left[v - k\frac{z\pi}{4}\right]. \tag{4}$$

Gleichung (4) stellt einen theoretischen Zusammenhang zwischen dem Schollengewicht, den Materialkennwerten und der zum Bruch erforderlichen Werkzeuggeschwindigkeit fest. Zur Berechnung müssen die Bodenkennwerte v und k, sowie die Stoßzeitdauer Δt bekannt sein.

Die Stoßzeit Δt kann auch aufgrund von verschiedenen theoretischen Erwägungen ermittelt werden. Aus der Elastizitätslehre ist bekannt, daß die Stoßzeit aus der nachstehenden einfachen Beziehung berechnet werden kann [3]:

$$\Delta t = 2{,}94\frac{z_0}{v},$$

wo z_0 die Verformung und v die Anstoßgeschwindigkeit bedeuten.

Unter der Annahme, daß die Scholle gegen eine starre ebene Fläche anstößt, kann der Ausdruck der Stoßzeit, wie folgt, aufgeschrieben werden:

$$\Delta t = 0{,}1577d\frac{\left(\gamma\dfrac{1-\nu_1^2}{E}\right)^{0{,}4}}{v^{0{,}2}} \tag{5}$$

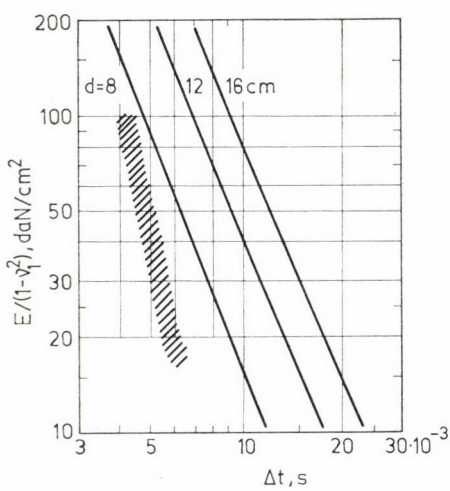

Bild 2. Beziehung zwischen Anstoßdauer und Elastizitätsmodul für verschiedene Schollendurchmesser

Gleichung (5) ist im Bild 2 graphisch dargestellt. Wie ersichtlich, ist die Gesamtstoßzeit für die Werte $E/(1 - \nu_1^2) \geq 80$ kleiner, als 10^{-2} sec.

Die effektive Stoßzeit kann jedoch durch Berechnung nicht mit genügender Genauigkeit bestimmt werden. Teils kann das Werkzeug nicht als eine ebene Fläche betrachtet werden (es ist vielmehr ein zylindrischer Körper), teils kann der Bruch vor dem Erreichen der ganzen Anstoßzeit eintreten. Demgemäß ist es zweckmäßig die effektive Anstoßzeit mittels Versuchen zu ermitteln oder mit Hilfe der Gleichungen (3) und (4) zu berechnen.

Durch Anwendung der Methode der Dimensionsanalyse kann man zur folgenden Ähnlichkeitsgleichung zur Beschreibung des Zerkleinerungsvorgangs gelangen:

$$\frac{G}{vd} = C \left(\frac{g \Delta t}{v}\right)^a \cdot \left(\frac{kd}{v}\right)^b . \tag{6}$$

Da die Abstützung und dadurch der Keoffizient k einen kleineren Einfluß auf den Vorgang ausübt, kann die einfachere Ähnlichkeitsgleichung

$$\frac{G}{vd} = C \left(\frac{g \Delta t}{v}\right)^a \tag{6a}$$

mit guter Annäherung angewandt werden.

3. Die Methode der Versuchsuntersuchungen

Zum Zweck der Ermittlung des Zusammenhanges zwischen Schollengröße und Werkzeuggeschwindigkeit wurden Untersuchungen in einer Bodenrinne durchgeführt. Die Bodenrinne war mit feinkrümeligen Boden in natürlichem Zustand gefüllt und die Bodenschollen wurden darin eingebettet. Die Oberfläche der Scholle lag immer an der Bodenoberfläche. Die Bodenschollen wurden ebenfalls im natürlichen Zustand vom gepflügten Ackerfeld eingebracht. Die originalen Formen der Schollen wurden nur dann abgeändert, wenn sie von der Kugelform stark abweichen.

Der Feuchtigkeitsgehalt der Schollen änderte sich von 4 bis 18 Prozent; die trockeneren Zustände wurden durch Trocknung erzielt. Die Innenporosität der Schollen änderte sich zwischen 38 und 48 Prozent. Es handelte sich um mittelbindigen Lehmboden.

Das Werkzeug wurde auf dem Wagen der Bodenrinne starr befestigt. Als Werkzeuge dienten zugespitzte Eggenzinken mit Durchmessern von 25 und 30 mm. Die auf die Eggenzinken wirkenden Kräfte wurden mit Dehnungsmeßstreifen gemessen.

Für die Untersuchungen sollte die Werkzeuggeschwindigkeit so gewählt werden, daß der Bruch der Scholle gerade noch eintritt. Um diese Bedingung

mit genügender Genauigkeit zu sichern, mußten viele Messungen durchgeführt werden. Die Annäherung an den kritischen Wert fand immer von beiden Seiten statt.

4. Die Versuchsergebnisse

Den durch die Messungen festgestellten Zusammenhang zwischen dem Schollengewicht und der kritischen Werkzeugfahrgeschwindigkeit stellt Bild 3 dar. Die Kurven gelten für Schollen mit einer Innenporosität von 42% und unterschiedlichem Feuchtigkeitsgehalt. Die Kurven sind nach Gleichung (4) verzerrte Hyperbeln, deren Exponent in der Richtung der kleineren Feuchtigkeitsgehalte zunimmt.

Aus dem Bild kann eine wichtige Folgerung gezogen werden. Bei Erhöhung der Fahrgeschwindigkeit nimmt das noch zerkleinbare Schollengewicht zunächst rasch ab, was bedeutet, daß die Erhöhung der Arbeitsgeschwindigkeit die Intensität der Schollenzerkleinerung im gegebenen Bereich wirksam vergrößert. Jedoch nimmt das noch zerkleinbare Schollengewicht im Geschwindigkeitsbereich über 11 bis 12 km/h nur in kleinerem Maße ab, d. h.

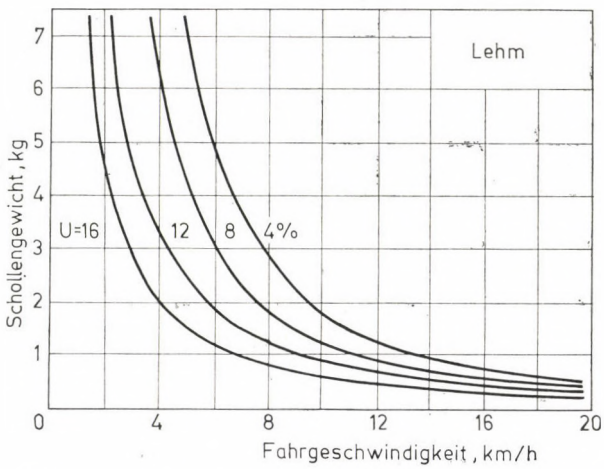

Bild 3. Beziehung zwischen dem Schollengewicht und der kritischen Werkzeuggeschwindigkeit für verschiedene Feuchtigkeitsgehalte

vom Standpunkt der Zerkleinerung aus betrachtet wird die Energieausnutzung schlechter. Deshalb ist es nicht zweckmäßig die Fahrgeschwindigkeit der Kombinatoren über $v = 12$ km/h zu erhöhen.

Im Bild 4 ist die Änderung der Bruchkraft in Abhängigkeit von der kritischen Werkzeuggeschwindigkeit bei verschiedenen Feuchtigkeitsgehalten

ersichtlich. Im Diagramm sind auch die Linien der konstanten Schollengewichte dargestellt.

Mit der Verminderung des Feuchtigkeitsgehalts nimmt die Bruchkraft wesentlich zu.

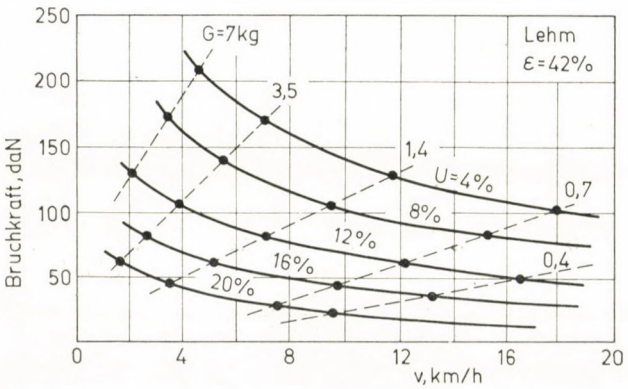

Bild 4. Änderung der Bruchkraft in Abhängigkeit von der kritischen Werkzeuggeschwindigkeit

Wenn das Werkzeug gegen die Scholle mit einer höheren Geschwindigkeit, als die kritische, anstoßt, dann nimmt die Bruchkraft zu, und infolge des Energieüberschusses zerfällt die Scholle in mehrere Teile und dementsprechend ensteht eine neue, größere Bruchfläche. Im Bild 5 ist die Änderung der Bruchkraft ersichtlich bei überkritischen Fahrgeschwindigkeiten für verschiedene Schollengewichte. Die Angaben des Diagramms gelten für Schollen mit einem Feuchtigkeitsgehalt von 16 Prozent.

Mit Hilfe der Versuchsergebnisse und der Gleichungen (3) und (4) konnten die spezifische Bruchenergie v und die effektive Zeitdauer des Stoßes Δt ermittelt werden.

Die Änderung der spezifischen Bruchenergie v in Abhängigkeit von dem Feuchtigkeitsgehalt ist im Bild 6 dargestellt. Wie sichtlich, vermindert sich die spezifische Bruchenergie stark mit der Zunahme des Feuchtigkeitsgehaltes. Die Streuung der Meßpunkte bleibt innerhalb des im Diagramm eingezeichneten Streifens.

Die aufgrund der gemessenen Bruchkraftwerte berechnete Anstoßdauer änderte sich von 4,0 bis 6,0 · 10^{-3} sec. Die größeren Werte ergaben sich für die Schollen mit höherem Feuchtigkeitsgehalt und größeren Abmessungen. Im Bild 2 wurde der Streifen eingezeichnet, der die berechneten Werte enthält. Im Verlauf dieser Untersuchungen konnten weder genauere Δt-Werte ermittelt, noch die Auswirkungen der verschiedenen Veränderlichen genauer analysiert werden.

Der Einfluß des Innenporenanteils auf die spezifische Bruchenergie ist bei den trockeneren Bodenzuständen bedeutend groß. Im Bild 7 ist der Zusammenhang zwischen der spezifischen Bruchenergie und dem Innenporenanteil

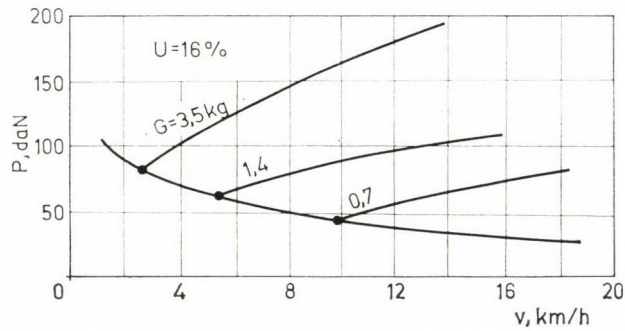

Bild 5. Änderung der Bruchkraft bei überkritischen Werkzeuggeschwindigkeiten und einem Feuchtigkeitsgehalt des Bodens von 16%

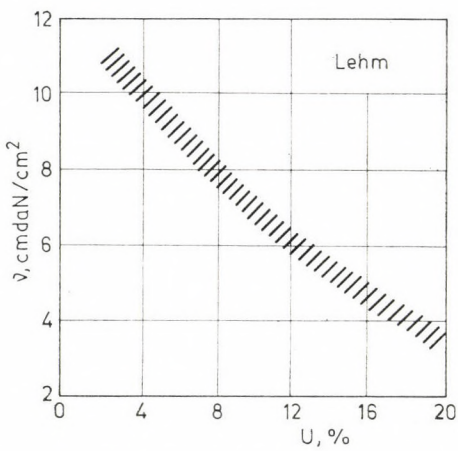

Bild 6. Die feuchtigkeitsabhängige Änderung der spezifischen Bruchenergie

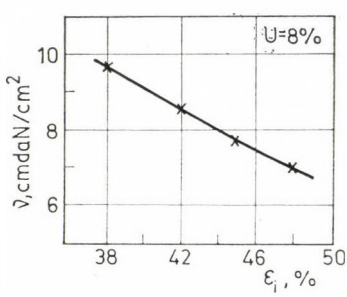

Bild 7. Auswirkung des Innenporenanteils auf die spezifische Bruchenergie

für einen Boden mit einem Feuchtigkeitsgehalt von 8 Prozent veranschaulicht. Bei Erhöhung des Feuchtigkeitsgehaltes vermindert sich der Einfluß des Innenporenanteils.

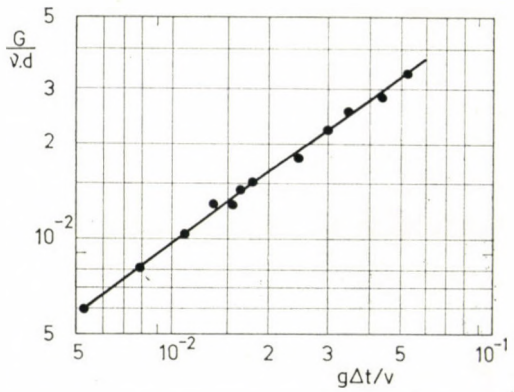

Bild 8. Die Ähnlichkeitsbeziehung des Schollenbruches

Die Versuchsergebnisse wurden auch aufgrund der Ähnlichkeitsgleichung (6a) bearbeitet. Im Bild 8 ist jener Zusammenhang dargestellt, der für den gegebenen Bodentyp mit einem Feuchtigkeitsgehalt von 4 bis 20% bei beliebigen Verhältnissen gültig wird. Zwischen den Ähnlichkeitszahlen ergab sich ein enger Zusammenhang mit kleinem Streubereich.

SCHRIFTTUM

1. Sitkei, Gy.: Bemessungsmethoden für die landwirtschaftlichen Fahrwerke. Akadémiai Kiadó, Budapest 1972
2. Bölöni, I. und Mitarbeiter: Einige betriebliche und theoretische Beziehungen der Hammermühlen. Akadémiai Kiadó, Budapest 1973
3. Timoshenko, S.—Goodier, J.: Theory of Elasticity. New York 1951

Regularities of the Clod Comminution at the Preparation of Seed Beds. On the basis of the experiments performed with a soil bin a relationship has been established between the clod size, critical value of the tool velocity and the moisture content of the soil. By making use of a simplified theory, the specific power demand for the clod comminution has been determined. Also the effect of the internal porosity on the power demand has been investigated On the basis of the experiments could be pointed out that by increasing the tool velocity over about 11 or 12 km/h does not seem to be convenient, because it leads, in this region, only to a further clod comminution of inferior value.

Acta Technica Academiae Scientiarum Hungaricae, Tomus 91 (1—2), pp. 121—135 (1980)

OPTIMUM DESIGN OF BEAMS AND FRAMES OF WELDED I-SECTIONS BY MEANS OF BACKTRACK PROGRAMMING

J. FARKAS*
DOCTOR OF TECHN. SCI.

L. SZABÓ**

[Manuscript received September 24, 1979]

A brief description of backtrack programming method is given. This combinatorial discrete programming method can be successfully applied to optimization problems with nonlinear objective function and constraints if the number of unknowns is not too large. This method is advantageous in the case of welded beams, mainly because the thicknesses of the plates should be rounded. The paper presents the application of the backtrack method for the following optimization problems. 1) Suboptimization of welded I-sections subjected to bending and compression. The application of these suboptimized I-sections to the elastic minimum weight design of frames is demonstrated by a numerical example of a single-bay pitched-roof portal frame. 2) Minimum cost design of welded homogeneous and hybrid I-beams, simply supported and loaded with an uniformly distributed normal load. In the objective function the cost of materials, welding and painting are taken into account. The constraints of bending and shear stresses as well as those of local buckling of web and flange are considered. The lowering of flange thickness with a welded splice is also taken into consideration.

Symbols

A	cross-sectional area
$A_f = sv$; $A_g = hv_g$	area of flange and web, respectively
a	distance between stiffeners, Fig. 4
C	cost
C_m, C_w, C_p	cost of material, welding and painting, resp.
c_f, c_g	material cost parameters for flanges and web, resp.
c_w, c_{w_1}	welding cost parameters
c_p	painting cost parameter
E	modulus of elasticity
h	depth of web
I	moment of inertia
K_x	section modulus
k_M, k_N, k_T	factors of local buckling of the web plate loaded in bending, compression and shear, resp.
L	span length, Fig. 4
L_1	distance of flange splice, Fig. 4
M	bending moment
$m = 100\ M/(\sigma_H h_0^3)$	dimensionless bending moment parameter
N	compressive axial force
$n = Nh_0/(2M)$	dimensionless compressive force parameter
N_s, N_{s_1}	numbers of vertical stiffeners, Fig. 4
p	intensity of uniformly distributed normal load
s, s_1	flange widths, Fig. 4
T	shear force

* Prof. Dr. J. FARKAS, Technical University Miskolc, H-3515 Miskolc-Egyetemváros, Hungary

** Dr. L. SZABÓ, H-3529 Miskolc, Csabai kapu 1. Hungary

v, v_1	flange thicknesses, Fig. 4
v_g	web thickness, Fig. 4
β^g	web slenderness parameter, Eq. (8)
δ	flange slenderness parameter, Eq. (10)
λ_p	plate slenderness, Eq. (5)
μ, μ_M, μ_N	parameters, Eq. (12)
ν	Poisson's ratio
ϱ	density
$\xi = \sigma_{Fg}/\sigma_{Hf}$	stress ratio of a hybrid I-section
σ_M, σ_N	stresses caused by bending and compression, resp. Eqs (2), (3), (4)
σ_H	limit stress
σ_{Hf}	limit stress of flange material
σ_F	yield stress
σ_{Fg}	yield stress of web material
τ	shear stress
τ_{Hg}	limit shear stress of web material
$\omega = I_2/I_1$	ratio of moments of inertia

1. Introduction

The mathematical programming methods used in optimum design of structures may be divided into two main groups: 1) methods operating with continuous functions (gradient methods, e.g. SUMT-method treated in [4], etc.); 2) discrete programming methods. In the design of metal structures, the designer can easily prescribe the list of discrete values for the sizes, taking into account the points of view of fabrication (thickness and width of plate elements), therefore discrete programming methods may be effectively used for the solution of these optimization problems.

The rod structures (trusses, frames, continuous beams) are constructed of parts of a constant (mainly I- or box) cross section. For these parts a series of cross sections suboptimized for various loads can be used. In these suboptimization procedures the number of unknowns is relatively small ($n < 10$), therefore, the backtrack programming method can successfully be used.

The aim of this paper is to show the application of the backtrack method for the following optimization problems: 1) suboptimization of homogeneous I-sections loaded in bending and compression; optimum design of a simple frame constructed from two suboptimized I-sections; 2) optimum design of simply supported, homogeneous and hybrid I-beams loaded in bending and shear.

2. The backtrack programming method

The general exposition of backtrack was given by WALKER [12], later by GOLOMB and BAUMERT [7] as well as by BITNER and REINGOLD [2]. This combinatorial method was applied to welded girder designs by LEWIS [10] and ANNAMALAI [1]. SZABÓ [11] has used this method for the minimum cost

design of hybrid I-beams. An estimation procedure of efficiency of backtrack programming was treated by KNUTH [8].

The backtrack method solves the constrained function minimization problems by a systematical search procedure. A partial search is carried out for each variable and, if the possibilities are exhausted, then a backtrack and a new partial search is performed. In the optimum design of welded beams a substantial search reduction may be achieved by utilizing the fact that the cost function becomes maximum if the variables take their maximum values. Thus, the optimum solution can be found by decreasing the variables.

We should search for a vector of variables $\mathbf{x}(x_1, x_2, \ldots, x_n)$ for which the cost function will be minimal: $C(\mathbf{x}) \rightarrow \min$ and which satisfies the design constraints: $g_j(\mathbf{x}) \geq 0$ $(j = 1, \ldots, p)$. The series of discrete values of variables are determined by $x_{i\min}$, $x_{i\max}$ and by the constant steps Δx_i between them. The flow diagram of backtrack for three variables is given in Fig. 1. The main phases of the calculation are described as follows.

1) With constant values of $x_{2\max}$ and $x_{3\max}$ the minimum x_{1m} value is searched for, which still satisfies the design constraints. For the sake of simplic-

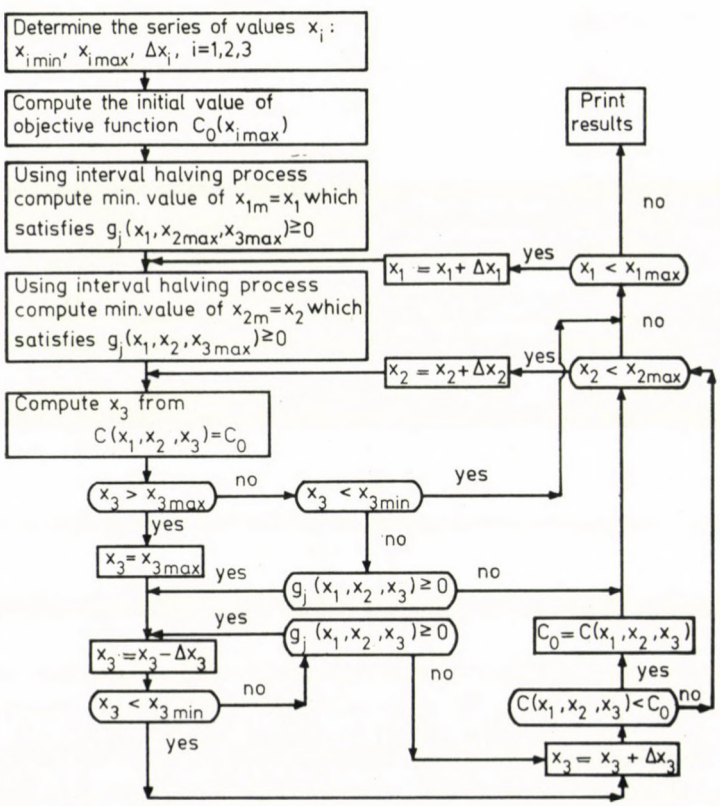

Fig. 1. Flow diagram of the backtrack programming method

ity, we use further on the notation $x_{1m} = x_1$. The search may be more efficient by using the interval halving procedure. The flow diagram of this method for x_1 can be seen in Fig. 2. First, $x_{1\min}$ value is proved. If $x_{1\min}$ dissatisfies the

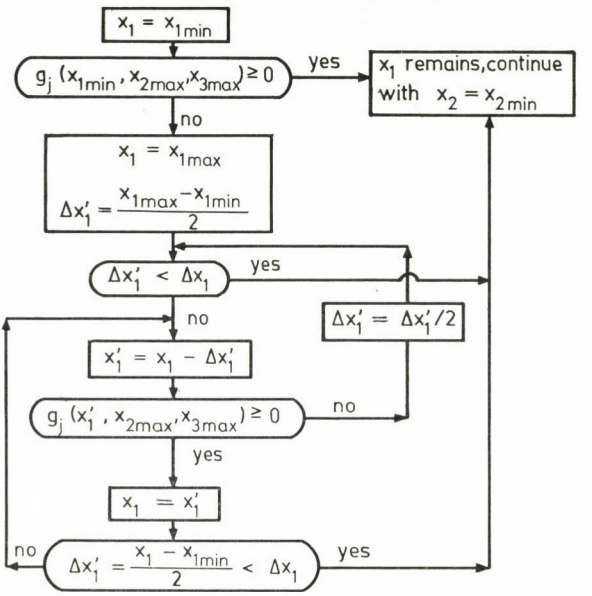

Fig. 2. Flow diagram of interval halving method

requirements, the interval $x_{1\max} - x_{1\min}$ is halved. For the halving method it should be $x_{i\max} - x_{i\min} = \Delta x_i \cdot 2^q$ where q is an integer. Note that it is possible to determine x_{1m} only if the $x_{2\max}$ and $x_{3\max}$ values satisfy the design constraints with an x_{1m} value.

2) Similarly to the first phase, the minimum $x_2 = x_{2m}$ value is determined by means of a halving process, which satisfies the design criteria.

3) In order to obtain the next x_3-value, we do not use the interval halving method. In general, x_3 may easily be expressed from the equation $C(x_1, x_2, x_3) = C_0$, so this will be the next x_3-value. Thus, for the series of x_3-values it is not necessary to prescribe the condition $x_{3\max} - x_{3\min} = \Delta x_3 \cdot 2^q$. Regarding the next x_3-value, three cases may occur.

3a) If $x_3 < x_{3\max}$, we take $x_3 = x_{3\max}$ and decrease it step-by-step till x_{3m} which satisfies the constraints or till $x_{3\min}$. Then the first partial search region is explored and we must backtrack to x_2. If $x_2 < x_{2\max}$, we continue the calculation with $x_2 + \Delta x_2$; if $x_2 = x_{2\max}$, we backtrack to x_1.

3b) If $x_3 < x_{3\min}$, we must backtrack.

3c) If $x_{3\min} < x_3 < x_{3\max}$ and x_3 dissatisfies the constraints, we backtrack to x_2. If the constraints are satisfied, we continue the calculation according to 3a.

An illustrating numerical example is given in Section 3.1.

3. Minimum weight design of a portal frame constructed of parts of suboptimized welded I-section

3.1. *Suboptimization by means of backtrack method: minimization of the cross section area of welded I-rods subjected to bending and compression*

The objective function is (Fig. 3)

$$A = hv_g + 2A_f \tag{1}$$

The constraint of max stress is

$$\sigma_M + \sigma_N \leq \sigma_H \tag{2}$$

where

$$\sigma_M = M/K_x;\ K_x = h(A_f + hv_g/6) \tag{3}$$

and

$$\sigma_N = N/A \tag{4}$$

The constraint of web buckling may be similarly expressed as in [3] or [4]:

$$\lambda_p^2 = \frac{12(1-\nu^2)}{k_{\text{red}}}\left(\frac{h}{v_g}\right)^2 \leq \lambda_{p0}^2 = \frac{\pi^2 E}{\sigma_H} \tag{5}$$

where

$$k_{\text{red}} = \frac{\sigma_M + \sigma_N}{\sqrt{(\sigma_M/k_M)^2 + (\sigma_N/k_N)^2}}. \tag{6}$$

From (5) we obtain

$$\frac{h}{v_g} \leq \sqrt{k_{\text{red}}}\sqrt{\frac{\pi^2 E}{12(1-\nu^2)\sigma_H}}. \tag{7}$$

For 370-steels of yield stress $\sigma_F = 240$ MPa and limit stress $\sigma_H = 200$ MPa, $E = 210$ GPa, $\nu = 0{,}3$ the limit web slenderness is given by

$$\frac{1}{\beta} = \frac{h}{v_g} = 30{,}81997\sqrt{k_{\text{red}}}. \tag{8}$$

For bending and compression we take the values of $1/\beta$ 145 and 40, respectively, then from (8) we obtain $k_M = 22{,}13$ and $k_N = 1{,}684$. With these values

(7) can be written as

$$\frac{h}{v_g} \leq 145 \sqrt[4]{\frac{(1 + \sigma_N/\sigma_M)^2}{1 + 173\,(\sigma_N/\sigma_M)^2}} \,. \tag{9}$$

The buckling constraint of the compressed flange may be given as

$$\frac{v}{s} \geq \delta = \frac{1}{30} \sqrt{\frac{\sigma_{Hf}}{\sigma_{H370}}} \,. \tag{10}$$

For homogeneous beams made of 370-steel it is

$$\frac{v}{s} \geq \delta = \frac{1}{30} \,. \tag{11}$$

In the following *numerical example* we take $M = 320$ kNm, $N = 128$ kN; $\sigma_H = 200$ MPa; the lists of discrete values are as follows: $h = 66$; 68; 70; 72; 74 cm; $v_g = 0{,}5$; 0,6; 0,7; 0,8; 0,9; $A_{f\min} = 14$; $A_{f\max} = 22$ cm^2; $\Delta A_f = 1$ cm^2. Thus, the total number of variations is $5 \cdot 5 \cdot 9 = 225$.

The steps of the calculations are shown in Table 1. It can be seen that the backtrack method requires only 37 tests to obtain the optimum values, which are as follows: $h = 70$ cm; $v_g = 0{,}6$ cm; $A_f = 18$ cm^2. The sizes of flanges can be obtained using (11): $v = \sqrt{A_f/30} = 0{,}78$ cm, rounded $v = 0{,}8$ cm; $s = 18/0{,}8 = 22{,}5$ cm.

Table 2 gives some results of calculations carried out with a FORTRAN program of backtrack method on the computer ODRA 1304 at Techn. Univ. Miskolc. The optimal sizes are given for a series of dimensionless parameters $m = 100\ M/(\sigma_H h_0^3)$ and $n = Nh_0/(2M)$. For $\sigma_H = 200$ MPa and $h_0 = 100$ cm it is $m = 5 \cdot 10^{-4}\,M$ [kNm] and $n = 0{,}5\ N$ [kN]/M [kNm] or M [kNm] = = 2000 m and N[kN] = 4000 mn.

Note that a similar table of optimal sections was published in [9] using the design rules of DIN 4114.

A significant search reduction in backtrack method can be achieved by using first a coarse scale of discrete values (larger Δx_i) and then continuing with smaller Δx_i values in a smaller region near the optimum found in the first procedure. For example, in the suboptimization procedure described above Δx_i-values were in the first phase (in cm): $\Delta h = 32$; $\Delta s = 16$; $\Delta v_g = 0{,}4$; $\Delta v = 0{,}8$ and in second phase $\Delta h = 2$; $\Delta s = 2$; $\Delta v_g = 0{,}1$; $\Delta v = 0{,}2$.

For M and N values which differ from the tabulated ones the following calculation can be proposed. The h and v_g values can be taken according to the nearest m- and n-values; knowing the area of web $A_g = hv_g$, the area of a flange $A_f = sv$ may be calculated from Eqs (1), (2), (3) and (4) in the follow-

Table 1

Numerical example illustrating the steps of backtrack method in the case of three unknowns. Notation: + satisfies, — dissatisfies

$x_1 = h$ [cm]	$x_2 = v_g$ [cm]	$x_3 = A_f$ [cm²]	$C = A$ [cm²]	g_1 Eq. (2)	g_2 Eq. (9)	Comments
74	0,9	22	110,6	+	+	$C_0 = 110{,}6$ cm²
66	0,9	22	103,4	+	+	$x_{1\min}$ satisfies, it is not necessary to use
66	0,5	22	77,0	+	—	the halving process for x_1, only for x_2
66	0,7	22	90,2	+	+	
66	0,6	22	83,6	+	+	
66	0,6	22	83,6	+	+	$x_3 = (110{,}6 - 66 \cdot 0{,}6)/2 = 35{,}5 > x_{3\max}$
66	0,6	21	81,6	+	+	$C_0 = 79{,}6$
66	0,6	20	79,6	+	+	backtrack with x_2
66	0,6	19	77,6	—	+	
66	0,7	16	78,2	—	+	$x_3 = (79{,}6 - 66 \cdot 0{,}6)/2 = 16{,}7$
66	0,8	13				$x_3 < x_{3\min}$, backtrack with x_1
68	0,9	22	105,2	+	+	halving process for x_2
68	0,5	22	78,0	+	—	
68	0,7	22	91,6	+	+	
68	0,6	22	84,8	+	+	
68	0,6	19	78,8	+	+	$x_3 = (79{,}6 - 68 \cdot 0{,}6)/2 = 19{,}4$
68	0,6	18	76,8	—	+	$C_0 = = 78{,}8$, backtrack with x_2
68	0,7	15	77,6	—	+	$x_3 = (78{,}8 - 68 \cdot 0{,}7)/2 = 15{,}6$
68	0,8	12				$x_3 < x_{3\min}$, backtrack with x_1
70	0,9	22	107,0	+	+	halving process for x_2
70	0,5	22	79,0	+	—	
70	0,7	22	93,0	+	+	
70	0,6	22	86,0	+	+	
70	0,6	18	78,0	+	+	$x_3 = (78{,}8 - 70 \cdot 0{,}6)/2 = 18{,}4$
70	0,6	17	76,0	—	+	$C_0 = 78{,}0$, backtrack with x_2
70	0,7	14	77,0	—	+	$x_3 = (78{,}0 - 70 \cdot 0{,}7)/2 = 14{,}5$
70	0,8	11				$x_3 < x_{3\min}$, backtrack with x_1
72	0,9	22	108,8	+	+	halving process for x_2
72	0,5	22	80,0	+	—	
72	0,7	22	94,4	+	+	
72	0,6	22	87,2	+	—	
72	0,7	13				$x_3 = (78{,}0 - 72 \cdot 0{,}7)/2 = 13{,}8 < x_{3\min}$, backtrack with x_1
74	0,9	22	110,6	+	+	halving process for x_2
74	0,5	22	81,0	+	—	
74	0,7	22	95,8	+	+	
74	0,6	22	88,4	+	—	
74	0,7	13				$x_3 = (78{,}0 - 74 \cdot 0{,}7)/2 = 13{,}1 < x_{3\min}$; $x_1 = x_{1\max}$; results: $C_{0\min} = 78{,}0$; $x_2 = 70$; $x_2 = 0{,}6$; $x_3 = 18$

Table 2

Optimal sizes of welded I-sections subjected to bending and compression for various values of the dimensionless parameters

$m = 100\ M/(\sigma_H h_0^3) = 5 \cdot 10^{-4}\ M$ [kNm] and $n = Nh_0/(2M) = 0{,}5\ N$ [kN]/M [kNm]

m	n	h cm	v_g cm	$A_f = sv$ cm²	m	n	h cm	v_g cm	$A_f = sv$ cm²
	0,00	56	0,4	7,2		0,00	70	0,5	14,4
	0,05	52	0,4	8,4		0,05	68	0,5	16,0
	0,10	54	0,4	8,0		0,10	64	0,5	18,0
	0,15	50	0,4	9,6		0,15	62	0,5	19,2
0,06	0,20	46	0,4	11,2	0,14	0,20	58	0,5	21,6
	0,25	46	0,4	11,2		0,25	64	0,6	18,0
	0,30	54	0,5	8,0		0,30	72	0,7	14,0
	0,35	48	0,5	10,0		0,35	68	0,7	16,0
	0,40	50	0,5	9,6		0,40	68	0,7	16,8
	0,00	56	0,4	10,8		0,00	72	0,5	16,8
	0,05	56	0,4	11,2		0,05	70	0,5	18,0
	0,10	52	0,4	12,8		0,10	78	0,6	14,0
	0,15	64	0,5	8,0		0,15	74	0,6	16,0
0,08	0,20	60	0,5	9,6	0,16	0,20	68	0,6	19,2
	0,25	46	0,4	16,0		0,25	74	0,7	16,0
	0,30	52	0,5	12,8		0,30	70	0,7	18,0
	0,35	50	0,5	14,0		0,35	68	0,7	19,6
	0,40	50	0,5	14,4		0,40	64	0,7	22,0
	0,00	56	0,4	14,4		0,00	72	0,5	19,2
	0,05	68	0,5	9,6		0,05	68	0,5	22,0
	0,10	54	0,4	16,0		0,10	80	0,6	16,0
	0,15	60	0,5	12,8		0,15	74	0,6	19,2
0,10	0,20	58	0,5	14,0	0,18	0,20	70	0,6	21,6
	0,25	58	0,5	14,4		0,25	74	0,7	19,2
	0,30	54	0,5	16,8		0,30	70	0,7	21,6
	0,35	52	0,5	18,0		0,35	68	0,7	24,0
	0,40	50	0,5	19,2		0,40	66	0,7	25,2
	0,00	72	0,5	11,2		0,00	72	0,5	22,0
	0,05	70	0,5	12,0		0,05	70	0,5	24,0
	0,10	64	0,5	14,4		0,10	88	0,7	14,0
	0,15	62	0,5	16,0		0,15	88	0,7	14,4
0,12	0,20	58	0,5	18,0	0,20	0,20	78	0,7	19,2
	0,25	56	0,5	19,2		0,25	74	0,7	22,0
	0,30	74	0,7	9,6		0,30	72	0,7	24,0
	0,35	64	0,7	14,0		0,35	70	0,7	25,6
	0,40	70	0,7	12,0		0,40	66	0,7	28,8

ing form:

$$\mu = \frac{A_f}{A_g} = \mu_M + \mu_N - \frac{1}{3} + \sqrt{\left(\mu_M + \mu_N - \frac{1}{3}\right)^2 + \mu_M + \frac{\mu_N}{3} - \frac{1}{12}} \tag{12}$$

where

$$\mu_M = \frac{M}{2\sigma_H A_g h} \quad \text{and} \quad \mu_N = \frac{N}{4\sigma_H A_g}.$$

The utilization of the series of suboptimized sections in the optimum design of frames is shown by the following numerical example.

3.2. *Elastic minimum weight design of a single-bay pitched-roof portal frame constructed of two different welded I-sections (Fig. 3)*

With the notation $\omega = I_2/I_1$ (moments of inertia for columns and rafters are I_1 and I_2, respectively), using formulae of GLUSHKOV [6] we obtain for the maximum bending moments and axial forces [3] (it was proved that it is not necessary to consider the wind loads too) for columns

$$M_1 = |M_A| \text{ [kNm]} = \frac{3266{,}8895\ \omega + 989{,}5919}{1{,}0175\ \omega^2 + 13{,}86245\ \omega + 0{,}73031}, \tag{13}$$

$$N_1 = N_A = 116{,}6 \text{ kN}, \tag{14}$$

and for rafters at point F

$$M_2 = |M_F| = 8{,}174696\ H_A - |M_A| - 206{,}2564, \tag{15}$$

$$N_2 = |N_F| = 28{,}373 + 0{,}957826\ H_A, \tag{16}$$

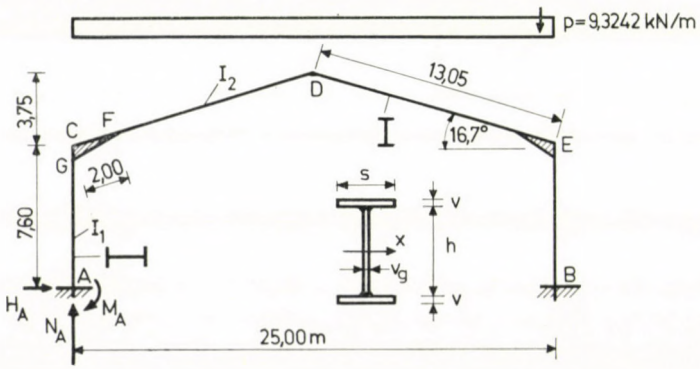

Fig. 3. Numerical example of a single-bay pitched-roof portal frame constructed of two suboptimized welded I-sections

Table 3

Iteration cycles of fully stressed elastic design of the portal frame shown in Fig. 3

$\omega = I_2/I_1$	Section	M [kNm]	N [kN]	Rounded		h [cm]	v_g [cm]	A_f [cm²] rounded	I [cm⁴]
				m	n				
1	1	273	117	0,14	0,20	58	0,5	21,6	44 461
	2	163	104	0,08	0,35	50	0,5	14,0	22 708
0.5107	1	329	117	0,16	0,20	68	0,6	19,8	61 499
	2	168	111	0,08	0,35	50	0,5	16,0	25 208
0.4099	1	354	117	0,18	0,15	74	0,6	19,2	72 831
	2	167	114	0,08	0,35	50	0,5	16,0	25 208
0.3461	1	375	117	0,18	0,15	74	0,6	21,6	79 402
	2	166	116	0,08	0,35	50	0,5	16,0	25 208
0.3175	1	387	117	0,18	0,15	74	0,6	21,6	79 402
	2	165	117	0,08	0,35	50	0,5	14,4	23 208
0.2923	1	399	117	0,18	0,15	74	0,6	21,6	79 402
	2	164	119	0,08	0,35	50	0,5	14,4	23 208

where

$$H_A = \frac{|M_A| + M_C}{7{,}6} \quad \text{and} \quad M_C = \frac{4963{,}8363\,\omega + 88{,}6588}{1{,}0175\,\omega^2 + 13{,}86245\,\omega + 0{,}73031}$$

The optimal sections of the fully stressed design (without deflection and global buckling constraints) may be obtained by an iterative procedure, taking first $\omega = 1$. The steps of the calculation are shown in Table 3. It can be seen that in the sixth iteration the ω-value did not change more. The final sizes of flanges may be obtained using (11): for the section 1: $s = 24$ cm, $v = 0{,}9$ cm; section 2: $s = 18$ cm, $v = 0{,}8$ cm. The half volume of the frame $V/2 = 760\,A_1 + 1305\,A_2 = 136{,}785$ cm³.

It is worth noting that we have solved this optimal design problem by backtrack method taking as unknowns the *eight* sizes of the two I-sections of the portal frame. The lists of the discrete values were as follows (in cm):

$$h_{1\min} = 60;\ h_{1\max} = 76;\ h_{2\min} = 44;\ h_{2\max} = 60;$$

$$v_{gi.\min} = 0{,}4;\ v_{gi.\max} = 0{,}8;\ s_{i.\min} = 14;\ s_{i.\max} = 30;$$

$$v_{i.\min} = 0{,}6;\ v_{i.\max} = 1{,}0;\ \Delta h_i = \Delta s_i = 2;\ \Delta v_{gi} = \Delta v_i = 0{,}1 \quad (i = 1, 2).$$

The total number of the possible variations was $9^4 \cdot 5^4 = 4\,100\,625$, the number of variations investigated by the program was only 49 144. The optimal sizes are as follows (in cm): $h_1 = 64$; $h_2 = 58$; $v_{g1} = v_{g2} = 0{,}6$; $s_1 = 22$; $s_2 = 18$; $v_1 = 1$; $v_2 = 0{,}6$. The half volume is $V/2 = 136\,226$ cm^3.

4. Minimum cost design of homogeneous and hybrid I-beams (Fig. 4)

The approximate analytical optimization of hybrid I-beams was treated in [5]. If a more intricate objective function is defined and the dead weight should also be taken into account, it is impossible to derive simple formulae for the optimal sections. Thus, the backtrack method may be used. In the following the results obtained by this method for three numerical examples will be given. The main sizes of a simply supported, uniformly loaded welded I-section beam are shown in Fig. 4. The lists of discrete values used in the calculations are given in Table 4. The total number of possible variations without L_1 is $9^2 \cdot 17^2 = 23\,409$. The backtrack method reduces this number to $800 \div 1000$.

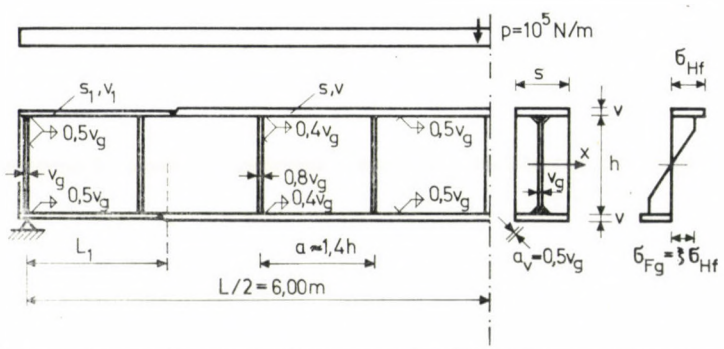

Fig. 4. Numerical example of a simply supported welded I-beam with one flange splice

Table 4

Series of discrete values used in calculations
(sizes in cm)

	min	max	Δ	Number of elements
h	80	120	5	9
s	10	42	2	17
v_g	0,4	2,0	0,1	17
v	0,8	2,4	0,2	9
L_1	0,1 L	0,3 L	0,025 L	9

The distance of the vertical stiffeners is $N_s = L/a - 1$, $a = 1{,}4$ h. N_s is an integer rounded down, and denotes the number of intermediate stiffeners. The thicknesses of the intermediate and end stiffeners are 0,8 v_g and v_g, respectively. The intermediate and end stiffeners are attached to the web and flanges with double fillet welds of size 0,4 v_g and 0,5 v_g, respectively. The material of the stiffeners is the same as that of the web. The case of a symmetrical welded splice of flanges is also considered. Then $N_{s1} = L_1/a$ is an integer rounded down.

The objective function expresses the costs of material, welding and painting:

$$C = C_m + C_w + C_p \tag{17}$$

where

$$\begin{aligned} C_m &= c_g \varrho h v_g L + 4 c_f \varrho s_1 v_1 L_1 + 2 c_f \varrho s v (L - 2L_1) + 2 c_g \varrho h v_g s_1 + \\ &+ 1{,}6 c_g N_{s1} \varrho h v_g s_1 + 0{,}8 c_g \varrho (N_s - 2N_{s1}) h v_g s \\ C_w &= 2 c_w v_g L + 4 c_w v_g (h + s_1) + 3{,}2 c_w N_{s1} v_g (h + s_1) + \\ &+ 1{,}6 c_w (N_s - 2N_{s1}) v_g (h + s) + 4 c_{w1} s_1 v_1 \\ C_p &= c_p (2h + 4s)(L - 2L_1) + 2 c_p (2h + 4s_1) L_1 + \\ &+ 2(N_s - 2N_{s1}) c_p h s + 4(1 + N_{s1}) c_p h s_1. \end{aligned}$$

The specific prices are as follows: *welding*: $c_w = 0{,}17$ Forints/cm² (fillet welds), $c_{w1} = 0{,}11$ Fts/cm² (butt welds in splices); *painting*: $c_p = 0{,}0027$ Fts/cm². Three steel types are considered: Hungarian steels 37B and 52C as well as Soviet steel C85 [13] with data given in Table 5. The density is $\varrho = 7850$ kg/m³.

In beams without splices in Eq. (17) it is $L_1 = N_{s1} = c_{w1} = 0$ and $s_1 = s$.

The following design constraints are taken into account.

1) *Constraint of max. bending stress*

$$\sigma_{\max} = M_{\max}/K_x \leq \sigma_{Hf} \tag{18}$$

Table 5

Limit and yield stresses as well as material cost parameter of steels considered in the calculations (stresses in MPa)

Material	σ_H	σ_F	c_g, c_f [Ft/kg]
37B	200	240	6,85
52C	280	400	7,60
C85	550	750	11,10

$M_{\max}$ is determined also considering the dead weight of the beam, but neglecting the dead weight of stiffeners. K_x is calculated on the basis of stress distribution shown in Fig. 4 (see also [5]):

$$K_x = I_x/(h/2 + v); \quad I_x = \frac{v_g h^3}{24}(3\xi - \xi^3) + \frac{sv}{2}(h + v)^2 \tag{19}$$

$$\xi = \sigma_{Fg}/\sigma_{Hf}$$

2) *Constraint of max. shear stress*

$$\tau_{\max} = T_{\max}/(hv_g) \leq \tau_{Hg} = 0{,}45\ \sigma_{Fg}. \tag{20}$$

$T_{\max}$ is the max. shear force at the supports.

3) *Web buckling constraints* relating to bending and shear, respectively:

$$h/v_g \leq 140\sqrt{200/\sigma_g}\,. \tag{21}$$

σ_g is the max. stress in web [MPa]. If $\sigma_g > \sigma_{Hg}$, $\sigma_g = 200$ MPa.

$$\frac{h}{v_g} \leq 90\sqrt{\frac{k_T\,\tau_{Hg}}{5{,}34\tau_{\max}}}, \tag{22}$$

$$k_T = 5{,}34 + 4/(a/h)^2.$$

4) *Flange buckling constraint*

$$s/v \leq 30\sqrt{200/\sigma_f}\,. \tag{23}$$

σ_f is the max. stress in flange [MPa].

The constraints of lateral buckling and that of deflection are not considered. The design of vertical stiffeners is not treated.

The calculations are carried out first for beams without splices. The results are summarized in Table 6. Thus, hybrid beams result in 17÷30% savings in total cost. This result agrees with that obtained by analytical optimization [5].

Note that the homogeneous beams made of steel 52C or C85 are less economical than the hybrid ones. For example, the homogeneous beam made of steel 52C gives only 10% savings in total cost.

In Table 7 the data of beams only optimized on the basis of material cost are summarized. It can be seen that the consideration of a more real cost function can result in savings of about 4%.

Table 6

Data of optimal beams without splices optimized on the basis of total cost
(sizes in cm)

Materials	h	v_g	s	v	Total cost [1000 Fts]	Savings %
37B homogeneous	120	0,9	30	2,0	17,8	0
52C/37B hybrid	120	0,9	16	2,4	14,8	17
C85/37B hybrid	120	0,9	12	1,4	12,5	30

Table 7

Data of optimal beams without splices optimized on the basis of material cost
(sizes in cm)

Materials	h	v_g	s	v	Total cost [1000 Fts]	Total cost from Table 6	Savings %
37B homogeneous	120	0,9	42	1,4	18,6	17,8	4,3
52C/37B hybrid	120	0,9	24	1,6	15,4	14,8	3,9

Table 8

Data of optimal beams with a flange splice optimized on the basis of total cost
(sizes in cm)

Materials	h	v_g	s	v	s_1	v_1	L_1	Total cost [1000 Fts]	Total cost from Table 6	Savings %
37B homogeneous	120	0,9	30	2,0	12	1,8	180	15,8	17,8	11,2
52/37 hybrid	120	0,9	16	2,4	10	1,4	210	13,3	14,8	10,1
85/37 hybrid	120	0,9	12	1,4	10	0,8	240	11,7	12,5	6,4

The optimization of beams with splices is carried out in the following manner. Starting with data of optimal beam without splices, we take the distance of splice L_1 (see Table 4), then calculate the bending moment in this cross section. Knowing h, v_g and $M_{\max}$, we search s_1 and v_1 by means of backtrack method taking into account the total cost function. The calculation should be carried out for all L_1-values. The optimal L_1-value will be the one for which the total cost is minimal.

Data for beams with splices are summarized in Table 8. It may be seen that the application of splices can result in savings of about $6 \div 11\%$.

REFERENCES

1. ANNAMALAI, N.—LEWIS, A. D. M. GOLDBERG, J. E.: Cost Optimization of Welded Plate Girders. — *J. Struct. Div. Proc. ASCE* **98** (1972), No. ST10, 2235—2246
2. BITNER, J. R.—REINGOLD, E. M.: Backtrack Programming Techniques. — *Communications of ACM* **18** (1975), 651—656
3. FARKAS, J.: Elastic and Plastic Minimum Weight Design of the Welded I-Sections of a Single-Bay Pitched-Roof Portal Frame (in Hungarian). — *Magyar Építőipar* **27** (1978), 490—497
4. FARKAS, J.: Minimization of the Cross Section Area of Welded Unstiffened Plate and Box Girders Subjected to Bending and Shear. — *Acta Techn. Hung.* **87** (1978), 295—306
5. FARKAS, J.: Optimum Design for Bending and Ultimate Shear Strength of Hybrid I-Beams- — *Acta Techn. Hung.* **90** (1980), 259—273
6. GLUSHKOV, G. et al.: Formulas for Designing Frames. Moscow, Mir, 1975
7. GOLOMB, S. W.—BAUMERT, L. D.: Backtrack Programming. — *J. Assoc. Computing Machinery* **12** (1965), 516—524
8. KNUTH, D. E.: Estimating the Efficiency of Backtrack Programs. — *Mathematics of Computation* **29** (1975), 121—136
9. LAWO, M.—THIERAUF, G.: Geschweißte gewichtsoptimierte I- und Kasten-Profile aus St 37. Merkblatt Nr. 449. Düsseldorf, 1978. Beratungsstelle für Stahlverwendung
10. LEWIS, A. D. M.: Backtrack Programming in Welded Girder Design. — *Proc. 5th Annual SHARE-ACM-IEEE Design Automation Workshop*, Washington, (1968), 28/1—28/9
11. SZABÓ, L.: Optimum Design of Hybrid I-Beams. — Ph.D. Dissertation. Techn. Univ. Miskolc, 1978 (in Hungarian)
12. WALKER, R. J.: An Enumerative Technique for a Class of Combinatorical Problems. — *Proc. of Symposia in Applied Mathematics. Amer. Math. Soc. Providence, R. I.* **10** (1960), 91—94
13. Строительные Нормы и Правила. Стальные конструкции. СНиП II-B. 3.72. Стройиз. дат, Москва, 1974.

Optimalbemessung von Balken und Rahmen geschweißten I-Querschnitts mittels der Backtrack-Programmierungsmethode. Der Artikel gibt eine kurze Beschreibung der Backtrack-Programmierungsmethode. Diese kombinatorische diskrete Methode ist auf die Optimierungsprobleme mit nichtlinearen Zielfunktion und Nebenbedingungen gut anwendbar, wenn die Anzahl der Unbekannten nicht sehr groß ist. Diese Methode ist vorteilhaft für geschweißte Träger, denn haupsächlich die Plattendicken sollen abgerundet werden. Es wird die Anwendung der Backtrack-Methode auf die folgenden Optimierungsprobleme behandelt. 1) Die Suboptimierung der auf Biegung und Druck beanspruchten geschweißten I-Querschnitte. Die Anwendung dieser suboptimierten I-Profile auf die elastische Gewichtsminimierung von Rahmen wurde am numerischen Beispiel eines einschiffigen Portalrahmens gezeigt. 2) Die Kostenminimierung von geschweißten, homogenen und hybriden einfeldrigen, gleichmäßig belasteten I-Trägern. In der Zielfunktion wurden die Material-, Schweiß- und Anstrichkosten berücksichtigt. Es wurde mit der Bedingung der maximalen Normal- und Schubspannung, ferner mit der Beulbedingung des Stegs und des gedrückten Gurtblechs gerechnet. Eine mit geschweißtem Stumpfstoß durchgeführte Gurtblechminderung wurde auch berücksichtigt.

Acta Technica Academiae Scientiarum Hungaricae, Tomus 91 (1—2), pp. 137—202 (1980)

GEOMETRY AND MECHANICS OF REGULAR STRANDED CONSTRUCTIONS

P. HOFFMANN*

[Manuscript received March 20, 1978]

The mechanical stresses are investigated which are generated during the manufacturing of regular strands which are built up from simple and double stranded elements and by the tensile and flexural loading of the ready-made strands. In order to introduce the mechanical stresses, the equations and geometric parameters of the simple and double stranded helicoidal lines as well as the space requirement and surface area of the simple stranded elements of circular cross section are determined by making use of the methods of the vector algebra. With the known value of the space requirement of the stranded element, the relationships between the number of the elements in each layer, the height of thread and size relation of the regular strand are determined in the case of the penetration-free contact of the layers and elements.

Introduction

The resulting mechanical characteristics of stranded elements or constructions containing such elements as — helical springs, cables, stranded ropes — (and also the resulting electrical characteristics of stranded electrical conductors) are functions of the geometrical arrangement of the construction. For characterizing geometrically the construction the relations between the so-called stranding parameters (D, d, n, α) must be known.

In the technical literature numerous attempts have been made to determine the relationship between the stranding parameters and between them and the resulting physical parameters [1—20]. But the published results are mostly valid only within narrowly defined ranges (either for small or for large pitch angles) and for their approximate character it is just the space requirement of the stranded element and the periodicity appearing in its places, subject to concentrated stress, which are not enhanced.

The present paper shows that the geometrical characteristics of the concentrically stranded element are complied for any pitch angle in the range $0 \leq \alpha \leq \pi/2$ and for any number of elements $n \geq 1$. It will also be shown that the torsional and bending stresses acting on section $dV = A_0 \cdot dS$ of the stranded element of diameter $d > 0$ can be separated, therefore, to a surface element dA of the section can be ordered tensile/compression and

* P. HOFFMANN, KG INFORMATIK, Arany J. u. 24. H-1051 Budapest, Hungary.

shear stresses, and afterwards their variation can also be determined for the case of bending or tensile stresses acting upon the stranded construction.

Finally knowing the space requirements of the stranded element of diameter $d > 0$ we are informed of the geometrical conditions of the constructions built up from $n \geq 1$ number of elements, as well as of the relation between the space requirements of the elements and the flexibility of the constructions, the standards and the technical literature attempting only empirical answers to this latter question so far.

Symbols

Scalar quantities

c	geometrical torsion
d	element diameter
g	geometrical curvature
h	length of lay
i	arc length
n	number of elements
t	time
v	haul-off speed
x, y, z	coordinates
A_0	cross section of the element
A	area of plane section
D	diameter
E	modulus of elasticity
G	modulus of shear
I_b, I_n	equatorial second-order moments of the cross section of the element
I_p	polar second-order moment of the cross section of the element
L	work
M	mass
N	index number of the layer
R	radius in the XY plane
R'	radius in the plane normal to the centroid S
S, S'	arc length
T, T'	period time
U	intrinsic energy
V	volume
α	pitch angle
β	stranding angle
γ	density
η	angle of direction change of the unit vector **t**
ϑ	angle of direction change of the unit vector **b**
$\varkappa$	filling factor
λ	strain
$\mu = T/T'$	ratio of period times
$\nu = 1/T$	r.p.m.
$\pi =$	3,14159
ϱ	radius varying in the range $0 \leq \varrho \leq R'$
σ	tensile/compression stress
τ	shear stress
$\varphi = \omega \cdot t$	angular movement in the XY plane ($0 \leq \varphi \leq \infty$)
$\chi = 2\pi/n$	central angle
$\psi = \omega \cdot t$	angular displacement in the plane normal to the centroid S or angular displacement in the range $0 \leq \psi \leq 2\pi$ independent of time
$\omega = 2\pi/T = 2\pi \cdot \nu$	angular velocity

Vector quantities:

$\mathbf{b}$	binormal unit vector
$\mathbf{i}$	unit vector in the X axis direction
$\mathbf{j}$	unit vector in the Y axis direction
$\mathbf{k}$	unit vector in the Z axis direction
$\mathbf{n}$	normal unit vector
$\mathbf{r}$	position vector
$\dot{\mathbf{r}}$	velocity vector
$\ddot{\mathbf{r}}$	acceleration vector
$\mathbf{t}$	tangent unit vector
$\mathbf{M}$	moment
$\mathbf{M}_t$	moment forcing the element to twist
$\mathbf{M}_r$	moment forcing the element to untwist
$\mathbf{P}$	force
$\mathbf{P}_t$	force, forcing the element to twist
$\mathbf{P}_r$	force, forcing the element to untwist
$\xi = \mathbf{r} + \rho$	resulting vector
ρ	position vector in the normal plane ($\lvert\rho\rvert = R'$)

1. Structure of the regular stranded constructions

Regular stranded constructions are called those stranded constructions, where the *core* located in the axis is surrounded by a *layer* consisting of one or more *elements* stranded in a determined direction of lay and with a determined pitch angle.

The lay of the layers covering each other in a regular cable may be the same or different from layer to layer.

Stranding a new layer on the cable consisting of the core and its covering layer, for this new layer the core + first layer together form a *core of composite construction*. For each N-th layer the regular stranded construction built up from $N-1$ layers form a core of composite construction.

The element of the regular stranded construction is called a *simple* one if along its whole length it is a solid thread having a constant cross section A_0. The element is of *composite construction*, if in itself, it is also a regular stranded construction.

The centroid of the layer element (elements) of the once stranded regular construction is a *helical* space curve.

The elements of the twice stranded regular construction (core and layer elements) are composite, i.e. once stranded regular constructions which by repeated stranding are united into a *stranded-cable*. The centroid of most simple elements of the stranded cable built up from a composite core and layer elements are *double twisted helical space curves*, which will be called DTH curves.

The direction of lay of the simple elements of so-called *bunched constructions* are equal, but the relative positions of the elements varies irregularly (maybe intentionally so) along the length of the construction. Because of the

irregular placing of the elements the geometrical description of the bunch is impossible, so far as can be foreseen.

For the univocal description of the once twisted regular cable the following characteristics are used:

- layer index, N (for the core $N = 0$, for the first, second, etc. layers $N = 1, 2, \ldots, N$),
- the lay of the N-th layer (right or left thread),
- the number n_N of the elements built into the N-th layer (numerical value for the core $n_0 = 1$, for the first, second, etc. layer $n_1 \geq 1$, $n_2 \geq 1, \ldots, n_N \geq 1$, positive integer),
- the cross section A_{0N} of the elements of the layer. For each element of the N-th layer $A_{0N} = \text{const.}$,
- the pitch angle α_N of the elements of the N-th layer. For every element of the N-th layer $\alpha_N = \text{const.}$ (for the core $\alpha_0 = \pi/2$, for every layer of index $N \geq 1$, $0 \leq \alpha \leq \pi/2$),
- the diameter D_N of the enveloping circle of the N-th layer section (for the composite core supporting the N-th layer: D_{N-1}).

For the definition of stranded cables all enumerated characteristics must also be written for the arrangement of the composite elements. In that case the characteristics with superscripts (N', D', ... etc.) refer to the construction of the composite structure, those without indices refer to the regular constructions built up from composite elements.

2. The geometry of the simple helix

The helix which can be traced on the mantle of a cylinder originates from the movement of a point moving at angular velocity $\omega = \text{const.}$ on the circumference of the base circle of radius R, while the plane of the circle is rising at velocity $v = \text{const.}$ along the axis normal to the plane of the circle and passing through its centre.

In order to establish the equation of the helix let us place the cylinder of radius R in the right-angled co-ordinate system XYZ so that its axis coincides with the axis of coordinates Z and let us prescribe that the point at the time $t = 0$ starts from the position $x = R$, $y = z = o$.

The point moving on the circumference of the circle of radius R during the time t covers an arc $i = \varphi R$. To the arc i belongs an angular displacement

$$\varphi = \omega t = 2\pi \frac{t}{T} = 2\pi v t. \tag{1}$$

During that same time t the base circle of radius R rises to the height

$$z = z(t) = vt. \tag{2}$$

According to Fig. 1 a right-hand or a left-hand helix can be generated according to the chosen direction of the angular displacement. In Eq. (1) the time t may change within the interval $0 \leq t \leq \infty$, therefore, its sign can

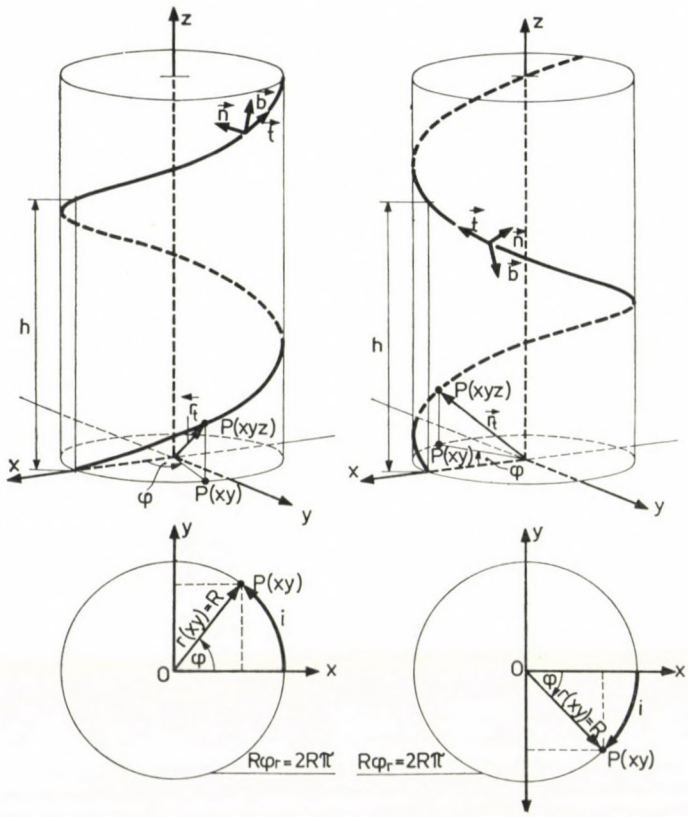

Fig. 1. Generation of the Right-hand and of the left-hand helices

only be positive. The angular displacement ω controlled by the positive or negative sign of the angular velocity φ, therefore, indicates whether a right or a left helix is generated.

The coordinates x and y of the helix are therefore at the time t

$$x = x(t) = R \cdot \cos \varphi = R \cdot \cos (\omega t),$$
$$y = y(t) = R \cdot \sin \varphi = R \cdot \sin (\omega t) \tag{3a}$$

for a right-hand space curve and

$$x = x(t) = R \cdot \cos (-\varphi) = R \cdot \cos \varphi,$$
$$y = y(t) = R \cdot \sin (-\varphi) = -R \cdot \sin \varphi \tag{3b}$$

for a left-hand space curve.

The position of the point $P(x, y, z)$ ordered to the time t according to the coordinates (2) and (3) is thus determined by the position vector

$$\mathbf{r} = \mathbf{r}(t) = x(t)\mathbf{i} + y(t)\mathbf{j} + z(t)\mathbf{k} \tag{4}$$

in the reference system XYZ.

Equations (2) and (3) are differentiable functions of the time t, thus the derivatives of the scalars $x(t)$, $y(t)$, $z(t)$ as well as of the vector $\mathbf{r}(t)$ with respect to the time t can be expressed. Forming the sizes of the velocity vector $\dot{\mathbf{r}}(t)$ and the acceleration vector $\ddot{\mathbf{r}}(t)$, for a right and for a left helix as well, can be expressed in the forms

$$|\dot{\mathbf{r}}(t)| = \sqrt{\dot{x}(t)^2 + \dot{y}(t)^2 + \dot{z}(t)^2} = \sqrt{v^2 + \omega^2 R^2} = \text{const.} \tag{5}$$

$$|\ddot{\mathbf{r}}(t)| = \sqrt{\ddot{x}(t)^2 + \ddot{y}(t)^2 + \ddot{z}(t)^2} = \omega^2 R = \text{const.} \tag{6}$$

The point moving along the helical path during the time dt covers an arc length

$$dS = |\dot{\mathbf{r}}(t)|dt \tag{7}$$

and therefore during the time t, considering (5),

$$S = S(t) = |\dot{\mathbf{r}}(t)| \cdot \int_0^t dt = t\sqrt{v^2 + \omega^2 R^2} = \sqrt{z^2 + \varphi^2 R^2}. \tag{8}$$

If $t = T$, then from (8), taking into consideration (1) and (2)

$$S(t) = \sqrt{h^2 + 4\pi^2 \cdot R^2} = \text{const.} \tag{9}$$

where

$$z(T) = vT = h \tag{10}$$

is the length of lay.

In Eq. (8) we recognize an application of Pythagoras' theorem to a rectangled triangle with cathetes φR and z, and hypotenuse S, according to Fig. 2.

On the base of Fig. 2 are introduced the trigonometrical functions of the pitch angle α and the stranding angle β:

$$\alpha + \beta = \frac{\pi}{2}, \tag{11}$$

$$\sin\alpha = \frac{z}{S} = \frac{h}{S_T} = \frac{v}{\sqrt{v^2 + \omega^2 R^2}} = \cos\beta, \tag{12}$$

$$\cos\alpha = \frac{\varphi R}{S} = \frac{2\pi R}{S_T} = \frac{\omega R}{\sqrt{v^2 + \omega^2 R^2}} = \sin\beta, \tag{13}$$

$$\tan\alpha = \frac{z}{\varphi R} = \frac{h}{2\pi R} = \frac{v}{\omega R} = \frac{1}{\tan\beta}. \tag{14}$$

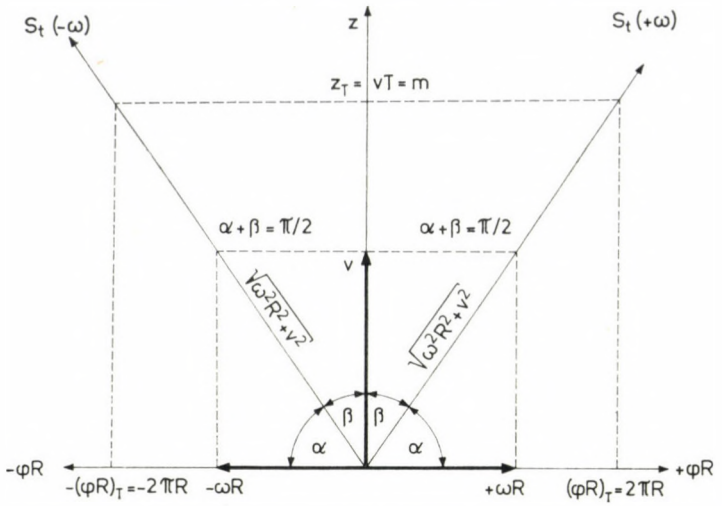

Fig. 2. Development into the plane of the right-hand and the left-hand helices

According to the definition of vector algebra, to the point $P(x, y, z)$ defined by $\mathbf{r}(t)$ of the spatial curve the tangent unit vector $\mathbf{t}$ can be ordered, the normal unit vector $\mathbf{n}$ and the binormal unit vector $\mathbf{b}$:

$$\mathbf{t} = \frac{\dot{\mathbf{r}}(t)}{|\dot{\mathbf{r}}(t)|}, \tag{15}$$

$$\mathbf{n} = \frac{\dot{\mathbf{r}}(t) \times \ddot{\mathbf{r}}(t))}{|\dot{\mathbf{r}}(t) \times \ddot{\mathbf{r}}(t)|} \times \frac{\dot{\mathbf{r}}}{|\dot{\mathbf{r}}|}, \tag{16}$$

$$\mathbf{b} = \frac{\dot{\mathbf{r}}(t) \times \ddot{\mathbf{r}}(t)}{|\dot{\mathbf{r}}(t) \times \ddot{\mathbf{r}}(t)|}. \tag{17}$$

Carrying out the operations prescribed in Eqs (15)–(17) and taking into account (12) and (13), the unit vectors ordered to the points of the right-hand helix, expressed in coordinates of the reference system become

$$\mathbf{t} = \frac{-\omega \cdot R \cdot \sin\varphi \cdot \mathbf{i} + \omega \cdot R \cdot \cos\varphi \cdot \mathbf{j} + v \cdot \mathbf{k}}{\sqrt{v^2 + \omega^2 \cdot R^2}} = \tag{18a}$$

$$= -\cos\alpha \cdot \sin\varphi \cdot \mathbf{i} + \cos\alpha \cdot \cos\varphi \cdot \mathbf{j} + \sin\alpha \cdot \mathbf{k},$$

$$\mathbf{n} = -\cos\varphi \cdot \mathbf{i} - \sin\varphi \cdot \mathbf{j}, \tag{18b}$$

$$\mathbf{b} = \frac{v \cdot \sin\varphi \cdot \mathbf{i} - v \cdot \cos\varphi \cdot \mathbf{j} + \omega \cdot R \cdot \mathbf{k}}{\sqrt{v^2 + \omega^2 R^2}} = \tag{18c}$$

$$= \sin\alpha \cdot \sin\varphi \cdot \mathbf{i} - \sin\alpha \cdot \cos\varphi \cdot \mathbf{j} + \cos\alpha \cdot \mathbf{k}.$$

In a similar way the equations of the unit vectors ordered to the points of the left-hand helix are

$$\mathbf{t} = -\cos\alpha \cdot \sin\varphi \cdot \mathbf{i} - \cos\alpha \cdot \cos\varphi \cdot \mathbf{j} + \sin\alpha \cdot \mathbf{k}, \tag{19a}$$

$$\mathbf{n} = -\cos\varphi \cdot \mathbf{i} + \sin\varphi \cdot \mathbf{j}, \tag{19b}$$

$$\mathbf{b} = -\sin\alpha \cdot \sin\varphi \cdot \mathbf{i} - \sin\alpha \cdot \cos\varphi \cdot \mathbf{j} - \cos\alpha \cdot \mathbf{k}. \tag{19c}$$

The unit vectors $\mathbf{t}, \mathbf{n}, \mathbf{b}$ order a right-angled, right-hand system of axes to the point $P(x, y, z)$ of the spatial curve. The normal plane determined by unit vectors $\mathbf{n}$ and $\mathbf{b}$, is thus always at right angles to the sense of progression of the tangent vector $\mathbf{t}$ belonging to the point in question.

In the geometry of spatial curves an important part is played by the geometrical curvature and the geometrical torsion ordered to a given point of the curve.

According to its definition

$$g = \frac{d\eta}{dS} = \frac{|\dot{\mathbf{r}}(t) \times \ddot{\mathbf{r}}(t)|}{|\dot{\mathbf{r}}(t)|^3}, \tag{20}$$

where η is the measure of direction change of the unit vector $\mathbf{t}$, and

$$c = \frac{d\vartheta}{dS} = \frac{|\dot{\mathbf{r}}(t) \cdot \ddot{\mathbf{r}}(t) \cdot \dddot{\mathbf{r}}(t)|}{|\dot{\mathbf{r}}(t) \times \ddot{\mathbf{r}}(t)|^2}, \tag{21}$$

where ϑ is the measure of direction change of the binormal unit vector $\mathbf{b}$ in the surroundings of the point $P(x, y, z)$ of the spatial curve.

Carrying out the operations prescribed in the Eq. (20) of the geometrical curvature, the curvature ordered to the points of the right-hand and to the left-hand helices becomes

$$g = \frac{\omega^2 R}{v^2 + \omega^2 R^2} = \frac{1}{R}\cos^2\alpha = \text{const.} \tag{22}$$

and the torsion will be

$$\pm c = \frac{\omega v}{v^2 + \omega^2 R^2} = \frac{1}{R}\sin\alpha \cdot \cos\alpha = \text{const.} \tag{23}$$

the sign of the torsion being positive for a right-handed helix, negative for a left-hand helix because of the chosen sign of the angular velocity ($+\omega$ and $-\omega$, respectively).

3. The geometry of the stranded element with circular cross section

Chapter 2 has shown that to a given point $P(x, y, z)$ of the helix the vector triplet **t, n, b** can be ordered and that the plane determined by the unit vectors **n** and **b** is normal to the sense of progression of the helix.

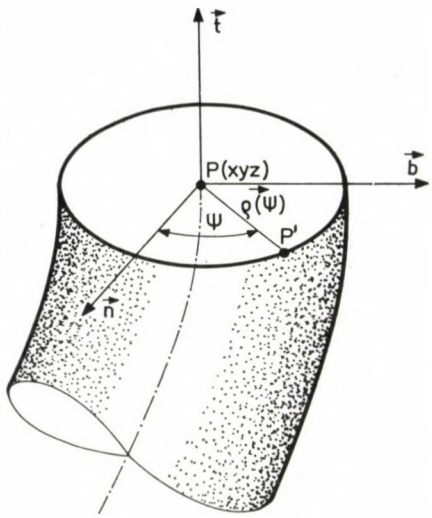

Fig. 3. Marking of the circumferential points of a stranded element of circular cross section

Let us trace into the normal plane a circle with radius R' around the centre $P(x, y, z)$. In the sense of Fig. 3 the position in the normal plane of a point P' on the circumference of the circle with radius R' is defined by

$$\rho(\psi) = R' \cos \psi \cdot \mathbf{n} + R' \sin \psi \cdot \mathbf{b} \tag{24}$$

where $0 \leq \psi \leq 2\pi$.

To the point P' points, according to Fig. 4, in the XYZ system of coordinates the vector

$$\xi(t, \psi) = \mathbf{r}(t) + \rho(\psi) = x(t, \psi) \cdot \mathbf{i} + y(t, \psi) \cdot \mathbf{j} + z(t, \psi) \cdot \mathbf{k}. \tag{25}$$

It can be seen from the figure that the point P' is a point of the surface of the stranded element of diameter $2R' = d$ and that the helix defined by the vector $\mathbf{r}(t)$ is the centroid of this element.

From Eqs (3a), (2), (18b) and (18c) the components of the vector $\xi(t, \psi)$ are for a right-hand element

$$\begin{aligned} x(t, \psi) &= (R - R' \cos \psi) \cos \varphi + R' \sin \alpha \cdot \sin \psi \cdot \sin \varphi, \\ y(t, \psi) &= (R - R' \cos \psi) \sin \varphi - R' \sin \alpha \cdot \sin \psi \cdot \cos \varphi \\ z(t, \psi) &= vt + R' \cos \alpha \cdot \sin \psi \end{aligned} \tag{26}$$

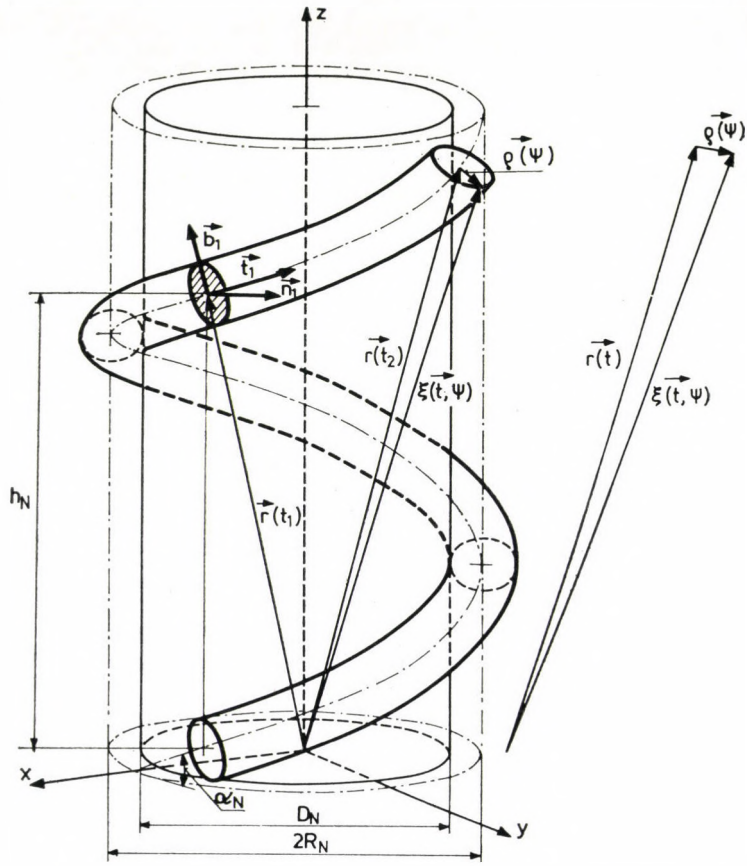

Fig. 4. Generation of the stranded element with circular cross section

and for a left-hand element according to (3b), (2), (19b) and (19c)

$$\begin{aligned} x(t,\psi) &= (R - R'\cos\psi)\cos\varphi - R'\sin\alpha\cdot\sin\psi\cdot\sin\varphi, \\ y(t,\psi) &= -(R - R'\cos\psi)\sin\varphi - R'\sin\alpha\cdot\sin\psi\cdot\cos\varphi, \\ z(t,\psi) &= vt - R'\cos\alpha\cdot\sin\psi. \end{aligned} \tag{27}$$

If $t = \text{const}$, then the scalar functions $x(t = \text{const.}\ \psi)$, $y(t = \text{const.}\ \psi)$, $z(t = \text{const.}\ \psi)$ determine a circle around the point $P(t)$ ordered to the time t of the centroid of the stranded element.

If $\psi = \text{const.}$ the scalar functions $x(t, \psi = \text{const.})$, $y(t, \psi = \text{const.})$, $z(t, \psi = \text{const.})$ determine parameter lines on the surface of the stranded element, which cross the circles $t = \text{const.}$ The circles and the parameter lines form the network of the surface of the stranded element of diameter d.

The arc element of the parameter lines $\psi = \text{const.}$ is

$$dS_\psi = |\dot{\xi}(t, \psi = \text{const.}|\, dt \tag{28}$$

where the components arrive from the differentiation of the components (26) and (27) with respect to the time t

$$|\dot{\xi}(t, \psi = \text{const.})|^2 = \omega^2(R - R' \cos\psi)^2 + \omega^2 R'^2 \sin^2\alpha \cdot \sin^2\psi + \\ + \omega^2 R^2 \tan^2\alpha. \tag{29}$$

The ratio of the arc elements of the stranded element $dS\psi$ and of the centroid dS is therefore from (28) and (7)

$$\left(\frac{dS_\psi}{dS}\right)^2 = \frac{|\dot{\xi}(t, \psi = \text{const.})|^2}{|\dot{\mathbf{r}}(t)|^2}$$

$$= \left(1 - \frac{R'}{R}\cos\psi\right)^2 \cos^2\alpha + \frac{R'^2}{R^2}\sin^2\alpha \cdot \cos^2\alpha \cdot \sin^2\psi + \sin^2\alpha \tag{30}$$

i.e. the ratio $dS\psi/dS$ is not independent of the variable ψ.

The volume element (slice) $dV = A_0 \cdot dS$ of cross section $A_0 = (\pi/4)d^2$ which before stranding was a straight cylinder of height dS, deforms after stranding into the shape according to Fig. 5. The variation of the arc length of the surface parameter lines of the deformed volume element with respect to the arc length of the centroid is in the sense of (30), (22) and (23):

$\psi = 0$:

$$\left(\frac{dS_{\psi=0}}{dS}\right)^2 = 1 - 2\frac{R'}{R}\cos^2\alpha + \frac{R'^2}{R^2}\cos^2\alpha = (1 - gR')^2 + c^2R'^2 < 1, \tag{31a}$$

$\psi = \frac{1}{2}\pi$;

$$\left(\frac{dS_{\psi=\pi/2}}{dS}\right)^2 = 1 + \frac{R'^2}{R^2}\sin^2\alpha \cdot \cos^2\alpha = 1 + c^2R'^2 > 1; \tag{31b}$$

$\psi = \pi$:

$$\left(\frac{dS_{\psi=\pi}}{dS}\right)^2 = 1 + 2\frac{R'}{R}\cos^2\alpha + \frac{R'^2}{R^2}\cos^2\alpha = (1 + gR')^2 + c^2R'^2 > 1, \tag{31c}$$

$\psi = \frac{3}{2}\pi$:

$$\left(\frac{dS_{\psi=3\pi/2}}{dS}\right)^2 = 1 + \frac{R'^2}{R^2}\sin^2\alpha \cdot \cos^2\alpha = 1 + c^2R'^2 > 1. \tag{31d}$$

In the sense of Fig. 5 and Eqs (31a)—(31d) the twisting around the centroid of the slice $dV = A_0 \cdot dS$ twists and also bends the slice $dV = A_0 \cdot dS$. Therefore, in each position of ψ the increase of length of the surface parameter lines

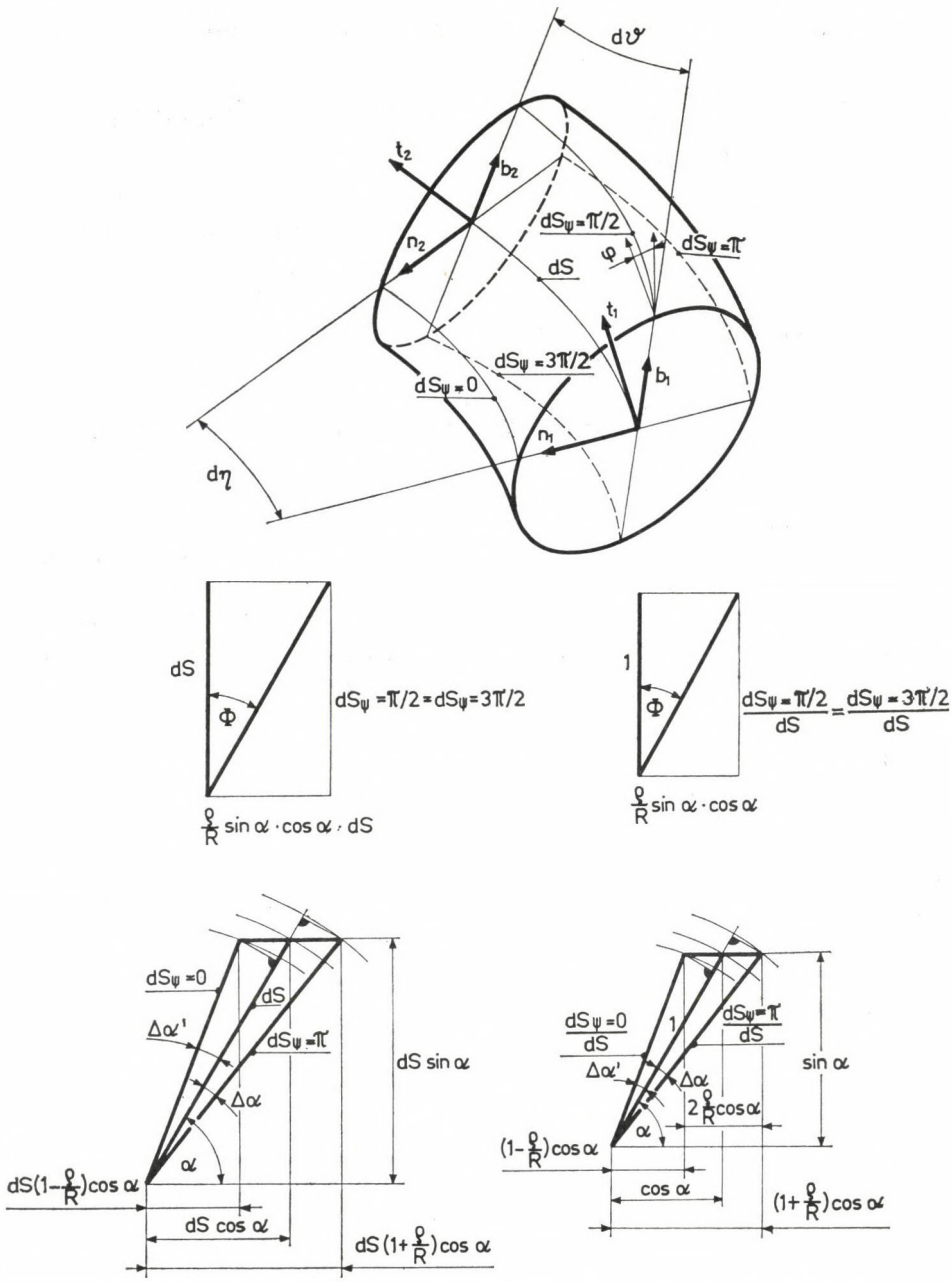

Fig. 5. Deformation of the stranded element with circular cross section

occur caused by the twisting, into which is superposed a maximum shortening in the position $\psi = 0$, in the position $\psi = \pi$ a maximum stretching due to the bending. The twisting of the cross section of the element of finite dimensions is indicated by the angle included by the directions of the tangent vectors $\dot{\xi}(t, \psi = \text{const.})$ of the parameter line $\psi = \text{const.}$ and the centroid $\dot{\mathbf{r}}(t)$ being different from zero.

The direction cosine of the two tangent vectors

$$\cos(\dot{\xi}, \dot{\mathbf{r}}) = \frac{\dot{\xi} \cdot \dot{\mathbf{r}}}{|\dot{\xi} \cdot \dot{\mathbf{r}}|} = \tag{32}$$

$$= \frac{1 - \frac{R'}{R}\cos^2\alpha \cdot \cos\psi}{\sqrt{\left(1 - \frac{R'}{R}\cos\psi\right)^2 \cos^2\alpha + \frac{R'^2}{R^2}\sin^2\alpha \cdot \cos^2\alpha \cdot \sin^2\psi + \sin^2\alpha}}$$

is in the positions $\psi = \pi/2$ and $\psi = 3\pi/2$ where the twisting appears free from the dimensional changes caused by the bending

$$\cos\Phi = \cos(\dot{\xi}, \dot{\mathbf{r}}) = \frac{1}{\sqrt{1 + \frac{R'^2}{R^2}\sin^2\alpha \cdot \cos^2\alpha}} = \frac{1}{\sqrt{1 + c^2R'^2}} \tag{33}$$

In the sense of Fig. 5 the angle Φ can also be expressed in the form

$$\tan\Phi = \frac{R'}{R}\sin\alpha \cdot \cos\alpha = cR' \tag{34}$$

indicating the *pure twisting* of the finite element around its centroid dS.

The *place requirement* of the circular stranded element of diameter d is represented in the reference system XYZ by its section with the planes XY, YZ, XZ.

The shape of the plane section XY is sought for in the plane XY of coordinate $z = \text{const.}$ It is suitable to choose the plane XY defined by the coordinate $z = 0$. The investigations are limited to the section of a right-hand element.

So if $z = 0$, making use of the components of the vector $\xi(t, \psi)$ according to (26)

$$z(t, \psi) = vt + R' \cos\alpha \cdot \sin\psi = 0, \tag{35a}$$

where from

$$-\sin\psi = \frac{vt}{R'\cos\alpha} = \frac{\varphi R \cdot \sin\alpha}{R'\cos^2\alpha} \tag{35b}$$

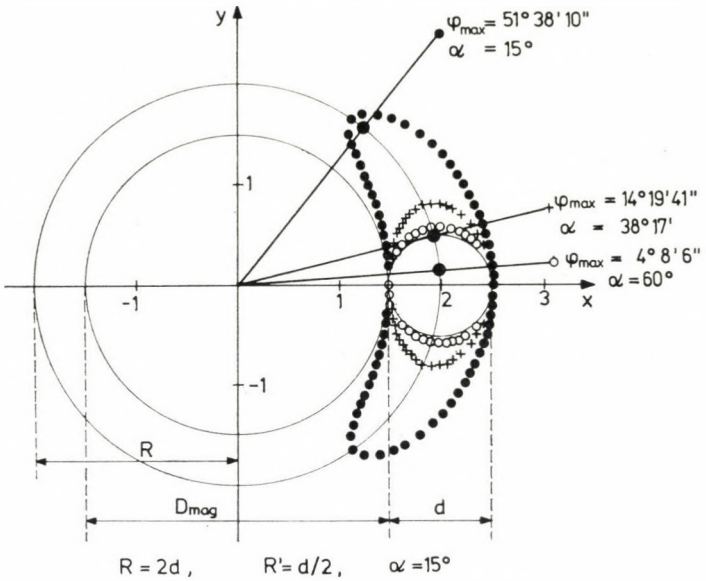

Fig. 6. Section of the stranded element of circular cross section with the plane XY

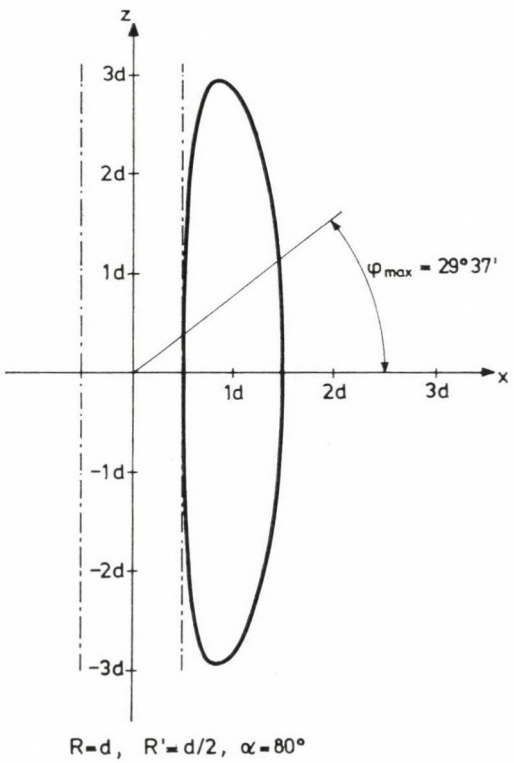

Fig. 7. Section of the stranded element of circular cross section with the plane XZ

and

$$\cos\psi = \pm\sqrt{1-\sin^2\psi} = \pm\sqrt{1-\frac{\varphi^2R^2\sin^2\alpha}{R'^2\cos^4\alpha}} \tag{35c}$$

Substituting Eq. (35b) and (35c) into Eq. (26) of the other two coordinates

$$x(t,\psi) = \left(R \pm \sqrt{R'^2 - \varphi^2R^2\frac{\sin^2\alpha}{\cos^4\alpha}}\right)\cos\varphi - \varphi R\tan^2\alpha\cdot\sin\varphi \tag{36a}$$

and

$$y(t,\psi) = \left(R \pm \sqrt{R'^2 - \varphi^2R^2\frac{\sin^2\alpha}{\cos^4\alpha}}\right)\sin\varphi + \varphi R\tan^2\alpha\cdot\cos\varphi \tag{36b}$$

is obtained. Examining them as functions of the variable it can be seen that they give two pairs of values each, as long as the difference under the root sign does not become zero.

But if

$$R' = \varphi R\frac{\sin\alpha}{\cos^2\alpha} \quad \text{that is, if} \quad \varphi = \varphi^* = \frac{R'}{R}\frac{\cos^2\alpha}{\sin\alpha} \tag{37}$$

then (36a) and (36b) provide one pair of values belonging together, therefore the equations can have real solutions in the range $-\varphi^* \leq \varphi \leq +\varphi^*$.

Calculating the pairs $x(t,\psi)$ and $y(t,\psi)$ belonging together for different angles $\alpha = \text{const.}$ the shapes of Fig. 6 can be constructed. The shape of each plane section XY is for every parameter $0 < \alpha < \pi\,2$ a *degenerated ellipse*, and if $\alpha = \pi/2$ it is a circle of radius R', the cross section of the element of diameter $d = 2R'$.

By a similar method can be produced, choosing $x(t,\psi) = 0$ or $y(t,\psi) = 0$ the plane sections YZ or XZ, respectively of the finite element. Fig. 7 shows the shape of the plane section XZ for given parameters.

The equations describing the shapes — and the equations describing the configurations — of the plane sections are explained by Fig. 8. The plane section XY belonging to the coordinate $z = \text{const.}$ touches or intersects a multitude of circles R' inscribed in the normal plane on the arc length between the points P_1 and P_2 of the centroid ordered to the times t_1 and t_2. Thus, the multitude of the intersected circumference points forms the set of points of the closed curve limiting the plane section.

For an element twisted in the right-hand direction the direction cosines of the angles between the direction **t** normal to the plane of the cross section $A_0 = (\pi/4)d^2$ and the directions **k** normal to the plane XY, **i** normal to YZ and **j** normal to XZ are, considering Eq. (18a)

$$\cos(\mathbf{t},\mathbf{k}) = \mathbf{tk} = \sin\alpha \tag{38a}$$

$$\cos(\mathbf{t},\mathbf{i}) = \mathbf{ti} = -\cos\alpha\cdot\sin\varphi \tag{38b}$$

$$\cos(\mathbf{t},\mathbf{j}) = \mathbf{tj} = \cos\alpha\cdot\cos\varphi. \tag{38c}$$

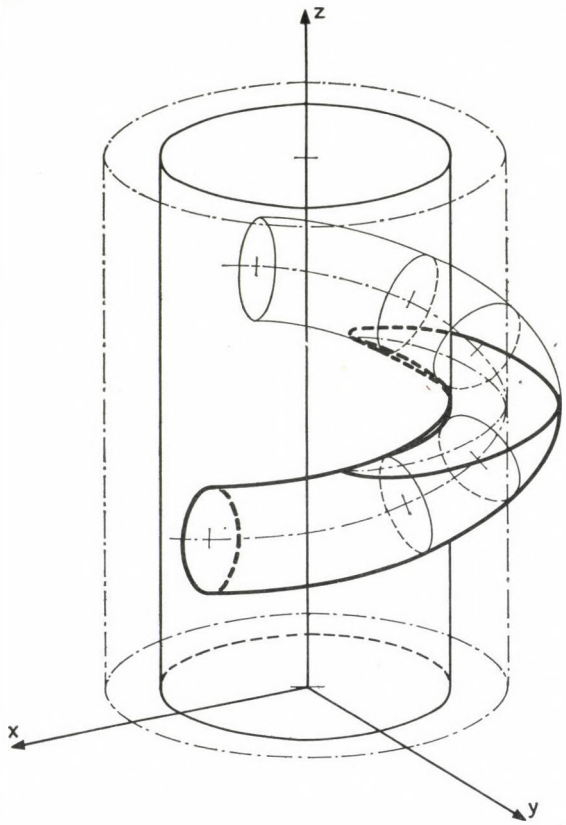

Fig. 8. Interpretation of the plane sections of the stranded element with circular cross section

Therefore, if A_{xy}, A_{yz} and A_{xz} are the areas of the plane sections in the planes XY, YZ — where $\varphi = \pi/2$ — and XZ — where $\varphi = 0$ — so with the projections defined in Fig. 9 the ratios

$$\sin \alpha = \frac{A_0}{A_{xy}}, \quad \text{i.e.} \quad A_{xy} = \frac{A_0}{\sin \alpha}, \tag{39}$$

and

$$\cos \alpha = \frac{A_0}{A_{yz}} = \frac{A_0}{A_{xz}}, \quad \text{i.e.} \quad A_{yz} = A_{xz} = \frac{A_0}{\cos \alpha} \tag{40}$$

are obtained for the ratios of the areas of the cross section of the element and the plane sections.

Carrying out the substitution $R' = \mathrm{d}/2$ in the scalar Eq. $x(t, \psi)$, $y(t, \psi)$ and $z(t, \psi)$, (26) and (27), it can be seen that the difference $R - d/2 \cdot \cos \psi$ as a function of ψ varies between the lower limit $R - d/2$ and the upper limit $R + d/2$. The difference of the two extremum values is the diameter d of the

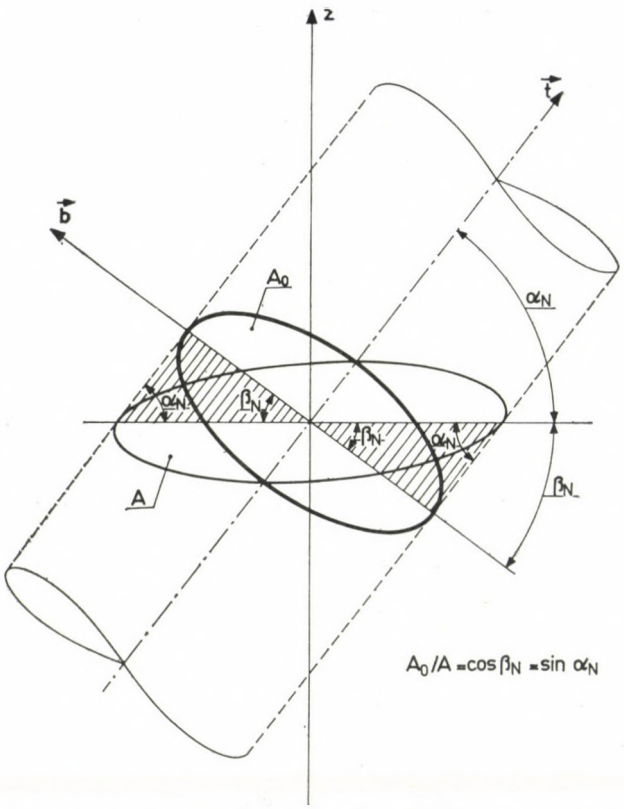

Fig. 9. Projection of the cross section A_0 of the stranded element

stranded element. Therefore, if $R > d/2$, the dimension

$$D = 2R - d > 0 \tag{41a}$$

can be introduced which is the diameter of that *core* onto which the element $d > 0$ is stranded on. By regrouping (41a)

$$R = \frac{D + d}{2} \quad (\text{where } R' = d/2) \tag{41b}$$

and where the radius R can be directly measured as the arithmetical mean of the dimensions D and d.

Carrying out the substitution

$$R - R' \cos\psi = \frac{D}{2} + \frac{d}{2}(1 - \cos\psi)$$

it is obvious that the scalar equations contain, besides the variables t and ψ also the α, d and D factors as parameters, thus they are constants. But the chosen values of the constants may have different values. The pitch angle α can have different values in the range $0 \leq \alpha \leq \pi/2$. The dimensions are defined in the ranges $D \geq 0$ and $d \geq 0$.

Analyzing the manysided applications of the vector Eq. $\xi(t, \psi)$, let us consider the case $\alpha = 0$. The scalar components (26) pass into the form

$$\begin{aligned} x(t, \psi) &= (R - R' \cos\psi) \cos \varphi, \\ y(t, \psi) &= (R - R' \cos \psi) \sin \varphi, \\ z(t, \psi) &= R' \sin \psi, \end{aligned} \tag{42}$$

which are identical with the scalar components of the vector equation of the centrally placed *tore* in the reference system XYZ. Carrying out the substitutions (41b) in the Eq. (42) it also becomes clear that for $D > 0$ they pass into the equations of the annular tore, for $D = 0$ into those of the coreless tore. Finally for $R = 0$ Eq. (42) define spherical coordinates.

4. The geometry of the double twisted helix

Chapter 3 has shown that by the vector $\mathbf{r}(t)$ commanded by the vector $\boldsymbol{\varphi}(\psi)$ — which latter is independent of the time t — the surface points of the element twisted with the pitch angle α can be determined. This element can be considered as the supporting surface of the double twisted helix — the DTH space curve.

Obviously, inasmuch as similarly to the variable $\varphi = \omega t$ determining the vector $\mathbf{r}(t)$ the variable ψ directing the vector $\boldsymbol{\varphi}(\psi)$ is made a variable of the same time t:

$$\psi = \omega' t = 2\pi \frac{t}{T'} = 2\pi \nu' t, \tag{43}$$

so the resulting vector

$$\begin{aligned} \xi(\varphi, \psi) = \xi(t) &= \mathbf{r}(t) + \boldsymbol{\rho}(t) \\ &= x(t) \cdot \mathbf{i} + y(t) \cdot \mathbf{j} + z(t) \cdot \mathbf{k} \end{aligned} \tag{44}$$

points out only a determined sequence of points on the supporting surface and that a multitude of these points forms the DTH space curve.

Chapter 2 has shown that with the vector $\mathbf{r}(t)$ can be generated a right-hand or a left-hand helix according to the chosen sign of the variable φ. Eq. (43) makes the variable ψ also a function of the time t, therefore directing of ψ also becomes necessary. So let there be in the normal plane in question the move of ψ positive if counterclockwise, and of negative sign if clockwise.

Depending on the choice of the signs of the angular displacements φ and ψ the following types of DTH space curves can be generated:

$+\varphi, +\psi$: right hand — right hand thread DTH space curve

$+\varphi, -\psi$: right hand — left hand thread DTH space curve

$-\varphi, +\psi$: left hand — right hand thread DTH space curve

$-\varphi, -\psi$: left hand — left hand thread DTH space curve

As for the right hand — right hand and the left hand — left hand DTH space curves both angular displacements have the same direction, the curves will be named summary DTH space curves of *equal thread sense*, as opposed to the right-left hand and left-right hand curves which will be called *opposing thread direction* DTH space curves.

The coordinates of the component $\mathbf{r}(t)$ of the vector $\xi(t)$ of (44) are determined for a right-hand and a left-hand thread by (2), (3a) and (2), (3b), respectively, while the coordinates of the unit vectors **t, n, b** derived from the vector $\mathbf{r}(t)$ are determined by Eqs (18) and (19). Using these, the equation of the components $\varphi(t)$ of the vector $\xi(t)$ are in the case of $+\psi$

$$\begin{aligned}\rho(t) &= R' \cos\psi \cdot \mathbf{n} + R' \sin\psi \cdot \mathbf{b},\\ &= R' \cos(\omega' t) \cdot \mathbf{n} + R' \sin(\omega' t) \cdot \mathbf{b},\end{aligned} \tag{45}$$

and in the case of $-\psi$

$$\begin{aligned}\rho(t) &= R' \cos(-\psi) \cdot \mathbf{n} + R' \sin(-\psi) \cdot \mathbf{b},\\ &= R' \cos(\omega' t) \cdot \mathbf{n} - R' \sin(\omega' t) \cdot \mathbf{b}.\end{aligned} \tag{46}$$

Thus establishing the equations of the vector components of the resulting vector $\xi(t)$ of (44), the scalar equations of the coordinates $x(t)$, $y(t)$, $z(t)$ of the four DTH space curves are
in the case of a right hand — right hand thread

$$\begin{aligned}x(t) &= (R - R' \cos\psi)\cos\varphi + R' \sin\alpha \cdot \sin\psi \cdot \sin\varphi,\\ y(t) &= (R - R' \cos\psi)\sin\varphi - R' \sin\alpha \cdot \sin\psi \cdot \cos\varphi,\\ z(t) &= vt + R' \cos\alpha \cdot \sin\psi;\end{aligned} \tag{47}$$

in the case of a right — left thread

$$\begin{aligned}x(t) &= (R - R' \cos\psi)\cos\varphi - R' \sin\alpha \cdot \sin\psi \cdot \sin\varphi,\\ y(t) &= (R - R' \cos\psi)\sin\varphi + R' \sin\alpha \cdot \sin\psi \cdot \cos\varphi,\\ z(t) &= vt - R' \cos\alpha \cdot \sin\psi;\end{aligned} \tag{48}$$

in the case of a left-right thread

$$x(t) = (R - R' \cos \psi) \cos \varphi - R' \sin \alpha \cdot \sin \psi \cdot \sin \varphi,$$
$$y(t) = -(R - R' \cos \psi) \sin \varphi - R' \sin \alpha \cdot \sin \psi \cdot \cos \varphi,$$
$$z(t) = vt - R' \cos \alpha \cdot \sin \psi; \tag{49}$$

in the case of a left-left thread

$$x(t) = (R - R' \cos \psi) \cos \varphi + R' \sin \alpha \cdot \sin \psi \cdot \sin \varphi$$
$$y(t) = -(R - R' \cos \psi) \sin \varphi + R' \sin \alpha \cdot \sin \psi \cdot \cos \varphi$$
$$z(t) = vt + R' \cos \alpha \cdot \sin \psi \tag{50}$$

which because of (1) and (43) are functions of the time t defined in the range $0 \leq t \leq \infty$.

The derivatives with respect to the time t of the scalar equations (47)—(50) form the scalar components of the $\dot{\xi}(t)$ velocity, $\ddot{\xi}(t)$ acceleration, ... vectors of the DTH space curves.

The size of the velocity vector $\dot{\xi}(t)$ for the DTH curve of agreeing thread directions is

$$|\dot{\xi}(t)|^2 = v^2 + \omega^2(R - R' \cos \psi)^2 + \\ + (\omega^2 \sin^2 \alpha \cdot \sin^2 \psi + 2\omega\omega' \cdot \sin \alpha + \omega'^2)R'^2, \tag{51}$$

and for the DTH curves of opposing thread directions is

$$|\dot{\xi}(t)|^2 = v^2 + \omega^2(R - R' \cos \psi)^2 + \\ + (\omega^2 \sin^2 \alpha \cdot \sin^2 \psi - 2\omega\omega' \cdot \sin \alpha + \omega'^2)R'^2, \tag{52}$$

that is the magnitudes of the velocity vectors are the same for the right-right and left-left thread as well as for the right-left and the left-right DTH space curves. These identities declare the correspondence of the reflections of the helices twisted in the right-left and in the left-right, as well as of those twisted in the right-right and in the left-left directions, for otherwise identical twisting parameters.

In the same way the magnitudes of the acceleration vectors $\ddot{\xi}(t)$ of the DTH space curves are identical by pairs: for DTH curves of agreeing thread directions

$$|\ddot{\xi}(t)|^2 = [(\omega^2 \sin \alpha + 2\omega\omega' + \omega'^2 \sin \alpha) + \omega'^4 \cos^2 \alpha] R'^2 \sin^2 \psi + \\ + [\omega^2 R - (\omega^2 + 2\omega\omega' \sin \alpha + \omega'^2)R' \cos \psi]^2, \tag{53}$$

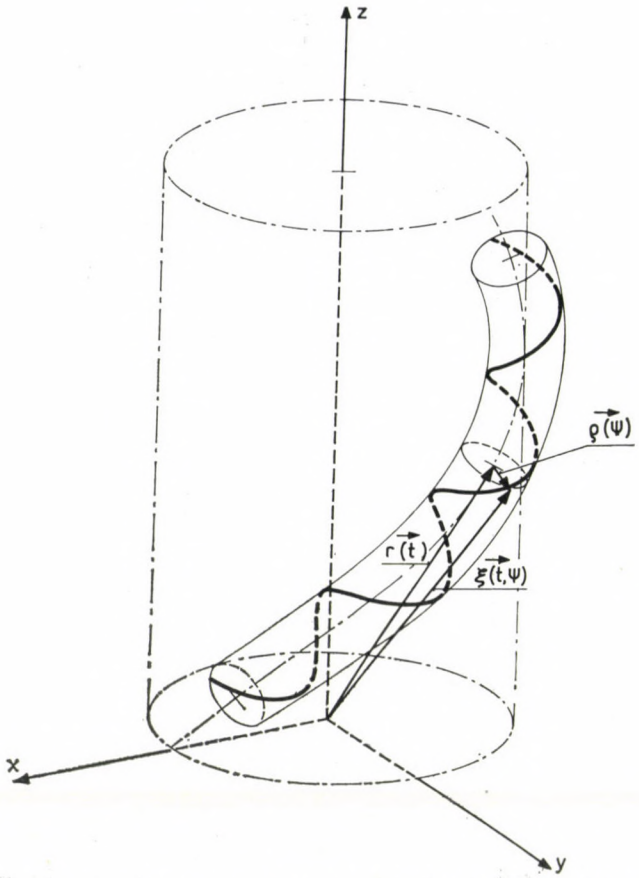

Fig. 10. Generation of the right-hand/right-hand DTH spatial curve

and for the DTH curves of opposing thread directions it is

$$|\ddot{\xi}(t)|^2 = [(\omega^2 \sin\alpha - 2\omega\omega' + \omega'^2 \sin\alpha) + \omega'^4 \cos^2\alpha]\, R'^2 \sin^2\psi + \\ + [\omega^2 R - (\omega^2 - 2\omega\omega' \sin\alpha + \omega'^2) R' \cos\psi]^2. \tag{54}$$

Because of the symmetry identities it is sufficient to limit the further investigations to the right-right space curve according to Fig. 10 and to the right-left space curve of Fig. 11.

On the DTH space curves the mobile point during the time dt covers an arc element of length

$$dS' = |\dot{\xi}(t)|dt \tag{55}$$

In the sense of (7), (8) and (14) belongs to the arc element a centroid length

$$dS = |\dot{\mathbf{r}}(t)|\, dt = \frac{\omega R}{\cos\alpha}\, dt. \tag{56}$$

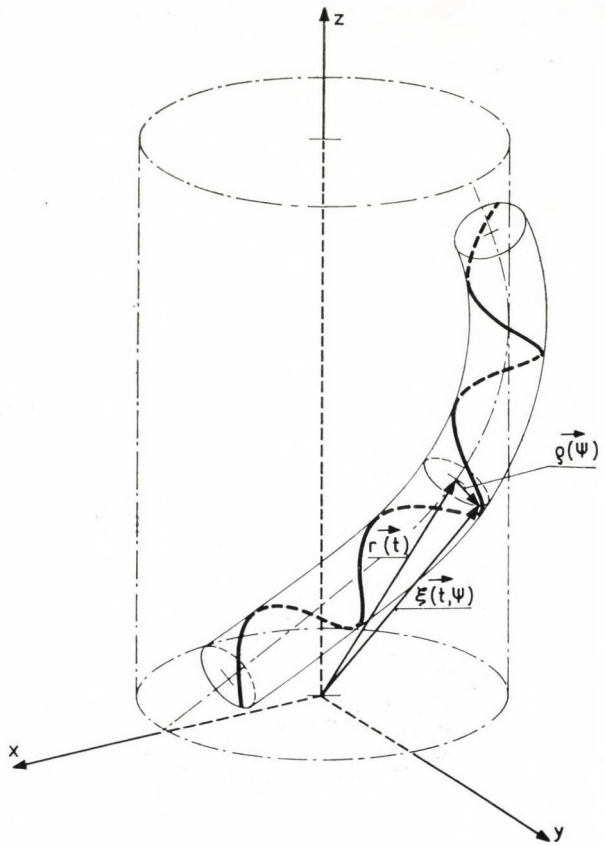

Fig. 11. Generation of the right-hand/left-hand DTH spatial curve

The ratio of the arc element lengths (55) and (56) is thus for space curves with agrreing thread directions, considering (51)

$$\left(\frac{dS'}{dS}\right)^2 = \sin^2\alpha + \left(1 - \frac{R'}{R}\cos\psi\right)^2 \cos^2\alpha +$$

$$+ \left(\sin^2\alpha \cdot \sin^2\psi + 2\frac{\omega'}{\omega}\sin\alpha + \frac{\omega'^2}{\omega^2}\right)\frac{R'^2}{R^2}\cos^2\alpha, \tag{57}$$

for space curves of opposite thread direction this ratio is

$$\left(\frac{dS'}{dS}\right)^2 = \sin^2\alpha + \left(1 - \frac{R'}{R}\cos\psi\right)^2 \cos^2\alpha +$$

$$+ \left(\sin^2\alpha \cdot \sin^2\psi - 2\frac{\omega'}{\omega}\sin\alpha + \frac{\omega'^2}{\omega^2}\right)\frac{R'^2}{R^2}\cos^2\alpha. \tag{58}$$

These Eq. show that the arc length S' varies as a periodical function of the time t along the arc length S.

The velocity vector $\dot{\xi}(t)$ ordered to the chosen point of the DTH space curve includes with the tangent vector $\dot{\mathbf{r}}(t)$ belonging to the corresponding point of the centroid an angle β' determined by the direction cosine

$$\cos(\dot{\xi}, \dot{\mathbf{r}}) = \frac{\dot{\xi}(t) \cdot \dot{\mathbf{r}}(t)}{|\dot{\xi}(t)| \cdot |\dot{\mathbf{r}}(t)|} = \frac{\dot{\xi}(t)}{|\dot{\xi}(t)|}\mathbf{t} = \cos\beta'. \tag{59}$$

The angle β' can be considered as the stranding angle of the DTH space curve with respect to the centroid S, in analogy to the ratio $\cos\beta = z/S = \sin\alpha$ existing between the arc length S of the simple helix and the axis of coordinates z. The complementary angle α' of the angle β' defined in this way can therefore be considered as the pitch angle of the DTH space curve.

Hence between the angles α' and β' exist the connection

$$\alpha' + \beta' = \frac{\pi}{2}, \tag{60}$$

or else $\cos\beta' = \sin\alpha'$ similarly to (11) and (12).

Carrying out the scalar multiplication prescribed in (59), for DTH space curves of agreeing thread directions the periodical time function of the pitch angle α' takes the form

$$\cos\beta' = \sin\alpha' = \tag{61}$$

$$= \frac{1 - \frac{R'}{R}\cos^2\alpha \cdot \cos\psi}{\sqrt{\sin^2\alpha + \left(1 - \frac{R'}{R}\cos\psi\right)^2\cos^2\alpha + \left|\sin^2\alpha \cdot \sin^2\psi + 2\frac{\omega'}{\omega}\sin\alpha + \frac{\omega'^2}{\omega^2}\right|\frac{R'^2}{R^2}\cos^2\alpha}}$$

and for DTH curves of opposing thread directions it becomes

$$\cos\beta' = \sin\alpha' = \tag{62}$$

$$= \frac{1 - \frac{R'}{R}\cos^2\alpha \cdot \cos\psi}{\sqrt{\sin^2\alpha + \left(1 - \frac{R'}{R}\cos\psi\right)^2\cos^2\alpha + \left(\sin^2\alpha \cdot \sin^2\psi - 2\frac{\omega'}{\omega}\sin + \frac{\omega'^2}{\omega^2}\right)\frac{R'^2}{R^2}\cos^2\alpha}}$$

Comparing the cosine (32) of the angle included by the parameter lines $\psi = \text{const.}$ of the surface supporting the DTH space curves and its centroids (32) with the direction cosines (61) and (62) it can be seen that the latter

differ from (32) by the factors

$$C_1 = \left(\frac{\omega'^2}{\omega^2} + 2\frac{\omega'}{\omega}\sin\alpha\right)\frac{R'^2}{R^2}\cos^2\alpha = \tag{63}$$

$$= \left(\frac{\omega'}{\omega} + \sin\alpha\right)^2 \frac{R'^2}{R^2}\cos^2\alpha - \frac{R'^2}{R^2}\sin^2\alpha \cdot \cos^2\alpha = \text{const.}$$

or

$$C_2 = \left(\frac{\omega'^2}{\omega^2} - 2\frac{\omega'}{\omega}\sin\alpha\right)\frac{R'^2}{R^2}\cos^2\alpha = \tag{64}$$

$$= \left(\frac{\omega'}{\omega} - \sin\alpha\right)^2 \frac{R'^2}{R^2}\cos^2\alpha - \frac{R'^2}{R^2}\sin^2\alpha \cdot \cos^2\alpha = \text{const.}$$

respectively. In the same way the arc length ratios according to (30) and to (57) and (58) differ from each other by the constants (63) and (64) independent of the time t.

When explaining the periodicity of the ratio $dS\psi/dS$ according to (30) it has been shown that it is provoked by the deformation at the twisting of the slice $dV = A_0 \cdot dS$ — the twisting and the shortening in the proximity of the core when $\psi = 0$ and the elongation in the opposite position $\psi = \pi$. The deformation of the supporting surface entrains of necessity the variation of the arc length S' and of the pitch angle α', of DTH space curves inscribed on the surface depending on the time t, i.e.

- the double twisted helix twisted twice in agreeing directions suffers an *additional twisting* which increases the arc length S',
- the double twisted helix with opposing thread directions is submitted to a *partial untwisting* which shortens the arc length S',
- in the positions $\psi = 0$ in the vicinity of the core the pitch angle α' of the DTH space curve is reduced,
- in the opposite position $\psi = \pi$ the pitch angle of the DTH space curve increases to its maximum.

The above is illustrated by Figs 12 and 13.

If in the scalar Eqs (47)—(50) for the coordinates of the vector $\dot{\xi}(t)$ determining the DTH space curves

$$R \gg \pm R' \cos\psi$$

and (65)

$$\omega' \gg \omega \sin\alpha,$$

then neglecting the small factors, to the arc S' of the DTH space curve can be ordered such velocity vectors $\dot{\xi}(t)$ the modul of which is for all four types of the curve

$$|\dot{\xi}(t)|^2 = v^2 + \omega^2 R^2 + \omega'^2 R'^2 = \text{const.} \tag{66}$$

and is thus independent of the time t.

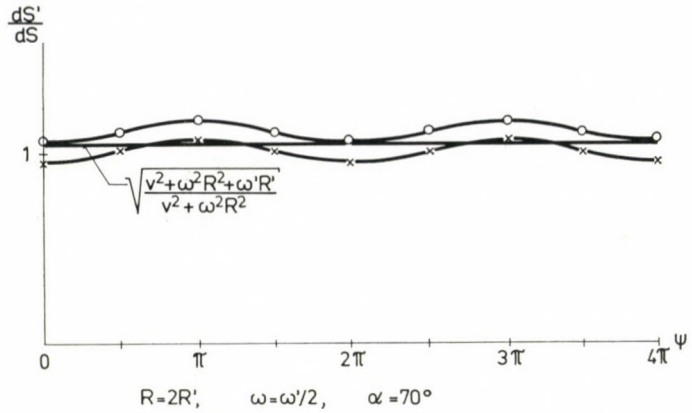

Fig. 12. Variation of the arc length S' of the DTH spatial curves

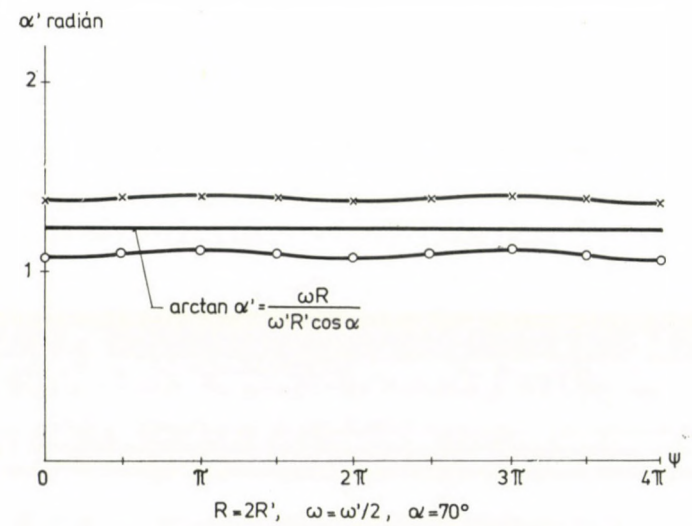

Fig. 13. Variation of the pitch angle α' of the DTH spatial curves

If (66) is fulfilled then Eq. (55) for the arc length of the DTH space curves is easily integrated because

$$S' = |\dot{\xi}(t)| \int_0^t dt = \sqrt{v^2 t^2 + \varphi^2 R^2 + \psi^2 R'^2}\,. \tag{67}$$

In this case also the developments sketched in Figs 14a—14d should be fulfilled and instead of (57), (58)

$$\frac{dS'}{dS} = \sqrt{\frac{v^2 + \omega^2 R^2 + \omega'^2 R'^2}{v^2 + \omega^2 R^2}} = \sqrt{1 + \frac{\omega'^2 R'^2}{\omega^2 R^2} \cos^2 \alpha} = \text{const.} \tag{68}$$

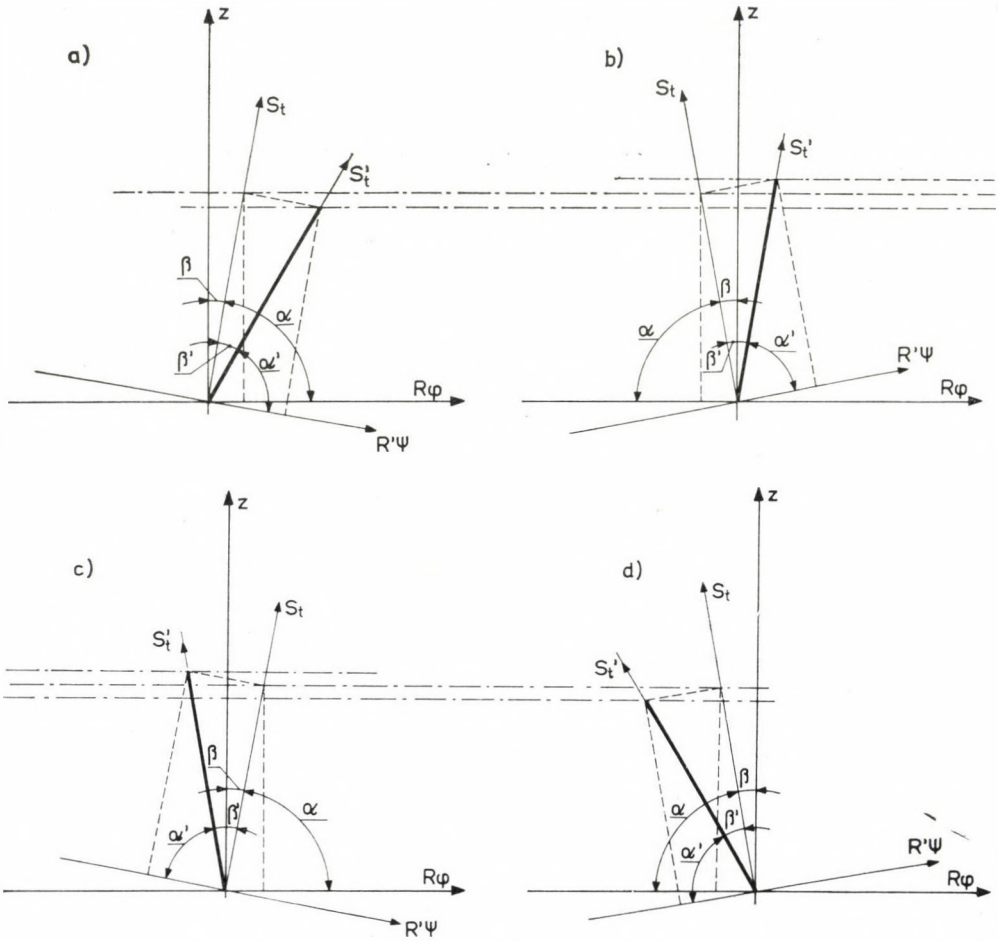

Fig. 14. Approximate calculation of the arc length S' of the DTH spatial curves. *a)* right-hand/right-hand; *b)* right-hand/left-hand; *c)* left-hand/right-hand; *d)* left-hand/left-hand

could characterize the ratio of arc lengths. In the sense of Fig. 14 the reciproca of (68) is equal to the cosine of β' — or according to (60) to the sine of α' — the pitch angle of the DTH curves should therefore be

$$\cos \beta' = \sin \alpha' \equiv \frac{dS}{dS'} \equiv \text{const.} \tag{69}$$

if (65) is complied with.

It is just the obviously impossible character of (69) that indicates that the fulfilment of the conditions (65) cannot be anticipated, therefore the DTH space curves cannot be generated by untwisting from its core, as a first-step the surface of radius R' supporting the DTH curve and then as a second

step the DTH curves themselves would be untwisted. This double development into a plane would make the deformations of the supporting surface disappear, the operation is therefore not permitted.

With the direction **k** of the Z axis of the XYZ reference system the tangent vector $\dot{\xi}(t)$ ordered to the point in question of the DTH space curves includes an angle defined by the direction cosine

$$\cos\left(\mathbf{k}, \dot{\xi}(t)\right) = \frac{\dot{\xi}(t)}{|\dot{\xi}(t)|}\,\mathbf{k}. \tag{70}$$

Carrying out the scalar multiplication prescribed in (70) for a DTH space curve with agreeing thread directions

$$\cos\left(\mathbf{k}, \dot{\xi}\right) = \tag{71}$$

$$= \frac{\sin\alpha + \dfrac{\omega' R'}{\omega R}\cos^2\alpha \cdot \cos\psi}{\sqrt{\sin^2\alpha + \left(1 - \dfrac{R'}{R}\cos\psi\right)^2\cos^2\alpha + \left(\sin^2\alpha \cdot \sin^2\psi + 2\dfrac{\omega'}{\omega}\sin\alpha + \dfrac{\omega'^2}{\omega^2}\right)\dfrac{R'^2}{R^2}\cos^2\alpha}}$$

and for DTH space curves with opposite thread directions

$$\cos\left(\mathbf{k}, \dot{\xi}\right) = \tag{72}$$

$$= \frac{\sin\alpha - \dfrac{\omega' R'}{\omega R}\cos^2\alpha \cdot \cos\psi}{\sqrt{\sin^2\alpha + \left(1 - \dfrac{R'}{R}\cos\psi\right)^2\cos^2\alpha + \left(\sin^2\alpha \cdot \sin^2\psi - 2\dfrac{\omega'}{\omega}\sin\alpha + \dfrac{\omega'^2}{\omega^2}\right)\dfrac{R'^2}{R^2}\cos^2\alpha}}$$

The periodical variations of the angles defined by the direction cosines (71) and (72) as functions of $\psi = \omega' t$ are illustrated by Fig. 15.

Amongst the possible solutions of the direction cosines (71) and (72) corresponding to Figs 10 and 11 the following cases are characteristic:

— for DTH space curves with agreeing thread directions

$$\begin{aligned} &\text{at } \psi = 0 \quad \cos\left(\mathbf{k}, \dot{\xi}\right) = 1, \text{ if } \omega R = R'(\omega - \omega' \sin\alpha), \\ &\text{at } \psi = \pi \quad \cos\left(\mathbf{k}, \dot{\xi}\right) = 0, \text{ if } \omega R = \frac{\cos^2\alpha}{\sin\alpha}\,\omega' R'; \end{aligned} \tag{73}$$

— for DTH curves with opposite thread directions

$$\begin{aligned} &\text{at } \psi = 0 \quad \cos\left(\mathbf{k}, \dot{\xi}\right) = 0, \text{ if } \omega R = \frac{\cos^2\alpha}{\sin\alpha}\,\omega' R' \\ &\text{at } \psi = \pi \quad \cos\left(\mathbf{k}, \dot{\xi}\right) = 1, \text{ if } \omega R = R'(\omega' \sin\alpha - \omega). \end{aligned} \tag{74}$$

If the DTH space curve is the centroid of an elementary strand of a regular cable made from elements of composite structure and the cross section of the

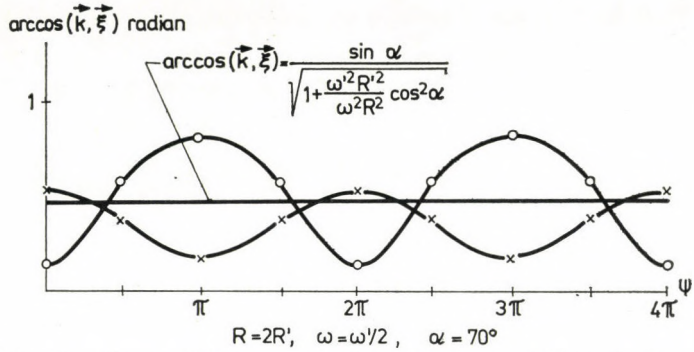

Fig. 15. Direction change of the tangent of the DTH around the axis of coordinates Z

elementary strand is A_0, then in the sense of (39) the area of the plane cross section XY is $A_0/\cos(\mathbf{k}, \dot{\xi})$. Because of the periodical dependence on time of the direction cosines (71) and (72) this ratio varies between a minimum and a maximum, the area of the plane section is therefore

— in the surroundings of the location $\psi = 0$ close to the core:
minimum ($\sim A_0$), for the agreeing thread directions,
maximum ($\geqslant A_0$), for the opposite thread directions;
— in the surroundings of the location $\psi = \pi$:
maximum ($\geqslant A_0$) for the agreeing thread directions,
minimum ($\sim A_0$) for the opposite thread directions

in the case of a double twisted element.

Thus, because of the peculiar space requirements of the elementary strands of finite dimensions there are characteristic differences between the XY plane sections of regular stranded constructions containing double twisted elementary strands, twisted twice in agreeing or in opposing directions. This difference is shown — for the sake of clarity in a somewhat distorted form — in Fig. 16. Obviously, the differences deriving from the structural system structures twice twisted in agreeing or in opposite direction, appear as well in the cross section as in the resulting characteristics of the cables determining the special fields of application of the two types of structures.

According to the definition Eqs (20) and (21) in the immediate vicinity of the chosen point $P(x, y, z)$

$$g' = \frac{|\dot{\xi}(t) \times \ddot{\xi}(t)|}{|\dot{\xi}(t)|^3} = f(\varphi, \psi) \tag{75}$$

determines the geometrical curvature and

$$c' = \frac{\dot{\xi}(t) \cdot \ddot{\xi}(t) \cdot \dddot{\xi}(t)}{|\dot{\xi}(t) \times \ddot{\xi}(t)|^2} = f(\varphi, \psi) \tag{76}$$

determines the geometrical torsion.

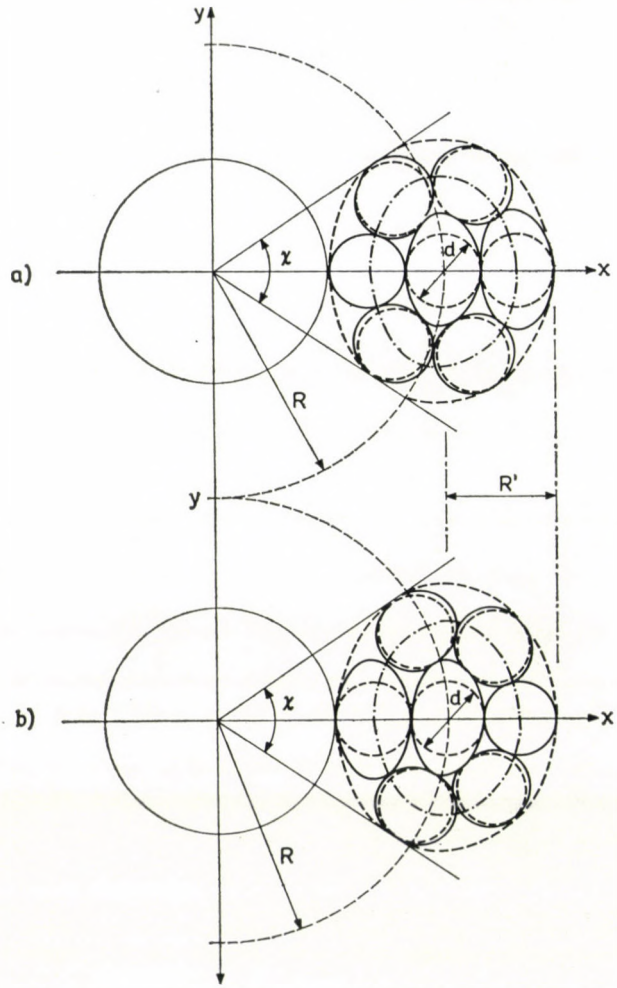

Fig. 16. Plane sections of a stranded bunch. *a)* right-hand/right-hand; *b)* right-hand/left-hand

The vector product from (75) and (76) is calculated by

$$|\dot{\xi}(t)\times\ddot{\xi}(t)| = \sqrt{(\dot{y}\cdot\ddot{z}-\dot{z}\cdot\ddot{y})^2+(\dot{z}\cdot\ddot{x}-\dot{x}\cdot\ddot{z})^2+(\dot{x}\cdot\ddot{y}-\dot{y}\cdot\ddot{x})^2} \qquad (77)$$

the mixed product of (76) is calculated by

$$\dot{\xi}(t)\cdot\ddot{\xi}(t)\cdot\dddot{\xi}(t) = \qquad (78)$$
$$= (\dot{y}\cdot\ddot{z}-\dot{z}\cdot\ddot{y})\cdot\dddot{x}+(\dot{z}\cdot\ddot{x}-\dot{x}\cdot\ddot{z})\cdot\dddot{y}+(\dot{x}\cdot\ddot{y}-\dot{y}\cdot\ddot{x})\cdot\dddot{z}$$

using the derivatives of the coordinates (47)—(50) of the DTH space curve.

Because of the complicate form of the time functions of the scalar components — and especially of its derivatives with respect to the time t —

of the vector $\xi(t)$ the curvature and the torsion of the DTH space curves is not calculated (e.g. in a general form similar to (22) and (23)). But separately every scalar function $\dot{x} = \dot{x}(t), \ldots, \dddot{z} = \dddot{z}(t)$ for (77) and (78) can be calculated

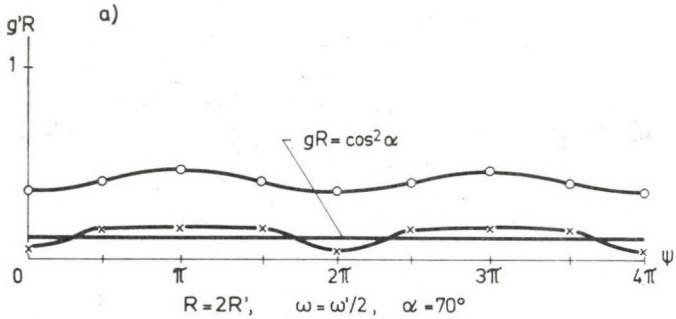

Fig. 17/a. Variation of the geometrical curvature g' of the DTH spatial curves

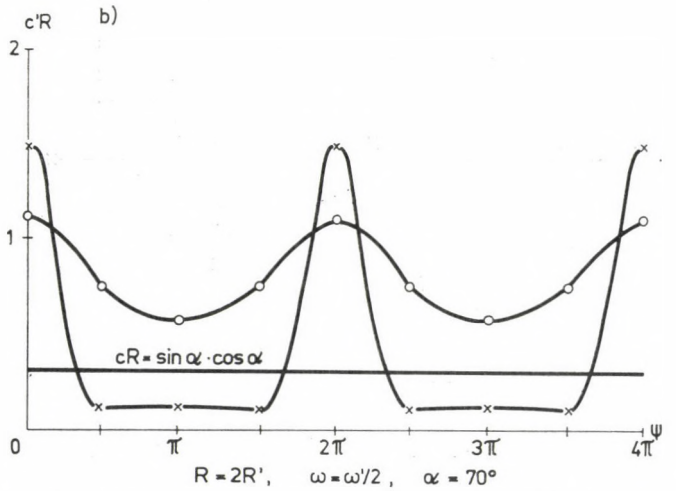

Fig. 17/b. Variation of the geometrical torsion c' of the DTH spatial curves

for given parameters, in possession of this the operations prescribed by (77) and (78) can be carried out and the time functions g' according to (75) and c' according to (76) can be calculated. By this method the curvatures g' and torsions c' belonging to given points of the DTH space curves have been calculated — more exactly the products $g'R$ and $c'R$ — at the characteristic positions $\psi = 0$, $\psi = \pi/2$, $\psi = \pi$ and $\psi = 3\pi/2$. The functions $g'(\varphi, \psi)$ and $c'(\varphi, \psi)$ are presented in Fig. 17, where the curvature $g = \text{const}$ and the torsion $c = \text{const}$ of the centroid of the surface supporting the DTH space curves, are also shown which therefore are straights independent of the time t.

According to Fig. 17 the variation as a function of ψ of the geometrical curvature g' and the geometrical torsion c' of the DTH space curves with an agreeing thread direction being more uniform, but its mean taken for the period $0 \leq \psi \leq 2\pi$ is of higher value than the corresponding characteristics of the DTH space curves of opposite thread directions. The obvious cause of the phenomenon is the additional twisting caused by the double twisting in the agreeing thread directions.

But conspicious are the values of c' for $\psi = 0$, $\psi = 2\pi$, $\psi = 3\pi$, ... of the DTH curves with opposite thread directions showing that in the locations near the core the twisting of the arc section belonging to the arc S' is particularly large.

Hence, while the velocity and acceleration vectors, the pitch angle, the geometrical curvature and the geometrical torsion of the simple helix are constants independent of the time t, the same characteristics of the DTH space curves are periodical functions of time where the "constancy" appears only in the regular repetition of the variations within the periods.

The dependency of the vector $\xi(t)$ of t the DTH space curves according to (44) is defined in the range $0 \leq t \leq \infty$ and it is also known that the pitch angle α can assume a given angle in the range $0 \leq \alpha \leq \pi/2$. Amongst the limit cases $\alpha = 0$ is of special importance, meriting a closer investigation.

Substituting $\alpha = 0$ in the scalar Eqs (47)—(50) of the coordinates of $\xi(t)$, the vectors

$$\xi(t)_{\alpha=0} = (R - R' \cos\psi) \cdot (\cos\varphi \cdot \mathbf{i} + \sin\varphi \cdot \mathbf{j}) + R' \sin\psi \cdot \mathbf{k}, \tag{79a}$$

$$\xi(t)_{\alpha=0} = (R - R' \cos\psi) \cdot (\cos\varphi \cdot \mathbf{i} + \sin\varphi \cdot \mathbf{j}) - R' \sin\psi \cdot \mathbf{k}, \tag{79b}$$

$$\xi(t)_{\alpha=0} = (R - R' \cos\psi) \cdot (\cos\varphi \cdot \mathbf{i} - \sin\varphi \cdot \mathbf{j}) - R' \sin\psi \cdot \mathbf{k}, \tag{79c}$$

$$\xi(t)_{\alpha=0} = (R - R' \cos\psi) \cdot (\cos\varphi \cdot \mathbf{i} - \sin\varphi \cdot \mathbf{j}) + R' \sin\psi \cdot \mathbf{k} \tag{79d}$$

can be calculated for the point movements in right-right, right-left, left-right and left-left thread directions, respectively.

Formerly the Eq. (79) and remembering the Eq. (42) of the vector $\xi(t, \psi)$ determining the surface of the torus, but in (79) the variable ψ being a function $\psi = \omega' t$ of the time t, the Eq. (79) really describe four possible types of the *helix inscribed on the surface of the tore.*

But for a tore supporting surface the angular displacement φ is limited to the range $0 \leq \varphi \leq 2\pi$ and so the definition range of the time t is restricted between the limits $0 \leq t \leq T$ for both variables $\varphi = \omega t$ and $\psi = \omega' t$. So the definition range of the variable ψ can be $0 \leq \psi \leq 2\pi \cdot T/T'$ and the ratio

$$\mu = \frac{T}{T'} = \frac{\omega'}{\omega} = \frac{\psi}{\varphi} \tag{80}$$

can be introduced which shows in how many turns the "bent helix" surrounds its toroid supporting surface.

Carrying out the substitution $\alpha = 0$ in the Eqs (51) and (62) the expression

$$\sin \alpha' = \frac{1 - \frac{R'}{R}\cos\psi}{\sqrt{\left(1 - \frac{R'}{R}\cos\psi\right)^2 + \frac{\omega'^2 R'^2}{\omega^2 R^2}}} = \frac{\omega(R - R'\cos\psi)}{\sqrt{\omega^2(R - R'\cos\psi)^2 + \omega'^2 R'^2}} \tag{81a}$$

describes the thread angle of the helix constructed on the tore surface. By regrouping the periodical time function of the angle α' can be expressed also in the form

$$\tan \alpha' = \frac{\omega}{\omega'}\left(\frac{R}{R'} - \cos\psi\right) = \frac{1}{\mu}\left(\frac{R}{R'} - \cos\psi\right) \tag{81b}$$

the solutions of which for characteristic values of ψ are

$$\text{at the place } \psi = 0\text{: } \tan \alpha' = \frac{1}{\mu}\left(\frac{R}{R'} - 1\right),$$

$$\text{at the place } \psi = \frac{1}{2}\pi\text{: } \tan \alpha' = \frac{1}{\mu}\frac{R}{R'},$$

$$\text{at the place } \psi = \pi \tan \alpha' = \frac{1}{\mu}\left(\frac{R}{R'} + 1\right),$$

$$\text{at the place } \psi = \frac{3\pi}{2}\text{: } \tan \alpha' = \frac{1}{\mu}\frac{R}{R'},$$

i.e. the value of the angle α' decreases to a minimum in the vicinity of the core and increases to a maximum value in the opposite positions. The conditions are shown in Fig. 18. From Fig. 18 can be read the arc length of the parameter lines $S_{\min} = 2\pi(R - R')$ and $S_{\max} = 2\pi(R + R')$, respectively, of the parameter lines on the tore surface which according to (80) are intersected μ-times by the helix inscribed on the surface. Therefore, the distance of two adjacent intersection points at $\psi = 0$ is

$$h'_{\min} = \frac{S_{\min}}{\mu} = 2\pi\frac{R - R'}{\mu} = 2\pi R' \tan \alpha'_{\min}, \tag{82a}$$

and at $\psi = \pi$ it is

$$h'_{\max} = \frac{S_{\max}}{\mu} = 2\pi\frac{R + R'}{\mu} = 2\pi R' \tan \alpha'_{\max}. \tag{82b}$$

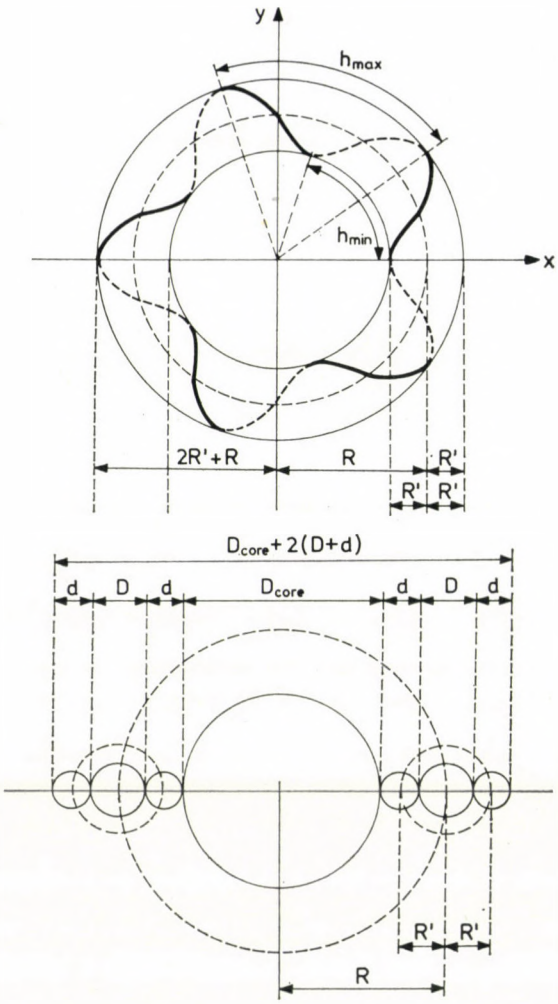

Fig. 18. Bending of a once stranded element around a core of diameter D

The arc length of the parameter lines at $\psi = \pi/2$ and $\psi = 3\pi/2$ is the same as the arc length $S = 2\pi R$ of the centroids of the torus, so these lines are intersected by the helices inscribed on the supporting surface at the distances

$$h' = \frac{S}{\mu} = \frac{2\pi R}{\mu} = 2\pi R' \tan \alpha'. \tag{82c}$$

It is noteworthy that the form of the equations (82) of the arcs h' is similar to the Eq. (14) for the length of lay $h = 2R \tan \alpha$ of the simple helix. But while for the simple helix $\alpha = \text{const.}$ and thus $h = \text{const.}$, for the helix inscribed

on the surface of the torus α' and thus h' also, being periodical functions of the variable $\psi = \omega' t$ vary between an upper and a lower limit.

Thus, it is clear that if on the surface of the torus an element $d > 0$ is wound, because of the place requirement of the finite element the number of possible turns μ is limited or, if from the element of finite dimensions a cable according to Fig. 4 twisted with the pitch angle α' is made, its flexibility around a core of diameter $D > 0$ influences the space requirement of the element, determining the geometrically possible minimum core radius. Therefore, the Eqs (79) permit to geometrically determine the flexibility conditions of the simple stranded constructions.

5. The geometrical conditions of a stranded layer constructed from n > 1 elements of finite dimensions

Knowing the space requirements of the element of finite diameter as discussed in Chapter 3, let us investigate the geometrical conditions for stranding $n > 1$ elements of diameter $d = \text{const}$ upon a core of diameter $D > 0$. Let us prescribe that each element starts the stranding at the moment $t = 0$ and let there be for every element of the layer $v = \text{const}$, $\omega = \text{const}$ and $\alpha = \text{const}$.

The helical centroids of the layer elements are situated on the mantle of a cylinder with radius R, starting at the base circle of circumference $2\pi R$ of the cylinder from n pitch points (pointed out at the time $t = 0$). Let the pitch points be arranged symmetrically, hence

$$i = \frac{2\pi R}{n}, \quad (n = 1, 2, 3, \ldots) \tag{83}$$

arc sections separated from each other.

To the arc sections i of the base circle belongs a central angle

$$\chi = \frac{i}{R} = \frac{2\pi}{n}. \tag{84}$$

It is sufficient to limit the investigations to the layer stranded in right-hand direction.

In accordance with the conditions, the centroids with indices $n = 1, 2, 3, \ldots$ start at the time $t = 0$ from the pitch points with coordinates

$$\begin{aligned} x_1 &= R, & x_2 &= R\cos\chi & \ldots \quad & x_n = R\cos[(n-1)\chi], \\ y_1 &= 0 & y_2 &= R\sin\chi & \ldots \quad & y_n = R\sin[(n-1)\chi], \\ z_1 &= 0, & z_2 &= 0 & \ldots \quad & z_n = 0, \end{aligned} \tag{85}$$

and at the time t they pass through the points with coordinates

$$\begin{aligned} x_{1t} &= R\cos\varphi, \quad x_{2t} = R\cos(\chi+\varphi) \quad \ldots \quad x_{nt} = R\cos[(n-1)\chi+\varphi], \\ y_{1t} &= R\sin\varphi, \quad y_{2t} = R\sin(\chi+\varphi) \quad \ldots \quad y_{nt} = R\sin[(n-1)\chi+\varphi], \\ z_{1t} &= vt, \qquad z_{2t} = vt \qquad\qquad \ldots \quad z_{nt} = vt \end{aligned} \tag{86}$$

In the sense of (25) to the surface points with indices 1, 2, . . ., n and diameter d = const point the vectors

$$\xi_1 = \mathbf{r}_1 + \rho, \quad \xi_2 = \mathbf{r}_2 + \rho, \quad \ldots \quad \xi_n = \mathbf{r}_n + \rho \tag{87}$$

for which $|\rho| = d/2$.

The contact of neighbouring elements is obviously subject to geometrical conditions. In consequence of the centrally symmetrical position of the elements of equal dimensions and equal pitches these conditions can be sought for in the geometrical conditions of any two neighbouring elements. It is suitable to investigate the position of the elements with indices 1 and 2.

In the case of penetration-free contact of the neighbouring elements the locus of their contact points is determined by that vector ξ_P for which $\xi_P = \xi_1 = \xi_2$. It is also obvious that to the common surface points in contact with two elements, two radius vectors of opposite directions point in the corresponding normal planes of the elements with indices 1 and 2, $\rho(\psi)_1$ and $\rho(\psi)_2$.

Finally Figure 19 shows that amongst the contact points of neighbouring elements there exists such a starting point P_k the place being determined by the vector of minimum magnitude ξ_P. There being $|\rho|$ = const., the size of the vector ξ_P — at the time t — can only be influenced by the vector $\mathbf{r}$ also depending on t.

The condition for penetration-free contact of the surfaces of neighbouring elements can therefore be stated by the instruction

$$\begin{aligned} (\xi_p)_{\min} &= (\xi_1)_{\min} = (\xi_2)_{\min} \\ &= (\mathbf{r}_1)_{\min} + \rho = (\mathbf{r}_2)_{\min} - \rho \end{aligned} \tag{88}$$

which can be completed by the instruction

$$\overline{P_1P_2} = d = 2\rho = |\mathbf{r}_1 - \mathbf{r}_2| = 2R' \tag{89}$$

relative to the magnitudes.

In (88) $(\mathbf{r}_2)_{\min}$ is the position vector determining the pitch point P_2 of the element with index 2 situated on the circumference of the base circle

with radius R, which with the coordinates (85) can be written in the form

$$(\mathbf{r}_2)_{\min} = R\cos x \cdot \mathbf{i} + R\sin x \cdot \mathbf{j} \tag{90}$$

To the point $P_1 = P(t^*)$ ordered to the time t of the element with index 1 points the vector

$$(\mathbf{r}_1)_{\min} = R\cos\varphi^* \cdot \mathbf{i} + R\sin\varphi \cdot \mathbf{j} + vt^* \cdot \mathbf{k} \tag{91}$$

with coordinates according to (86).

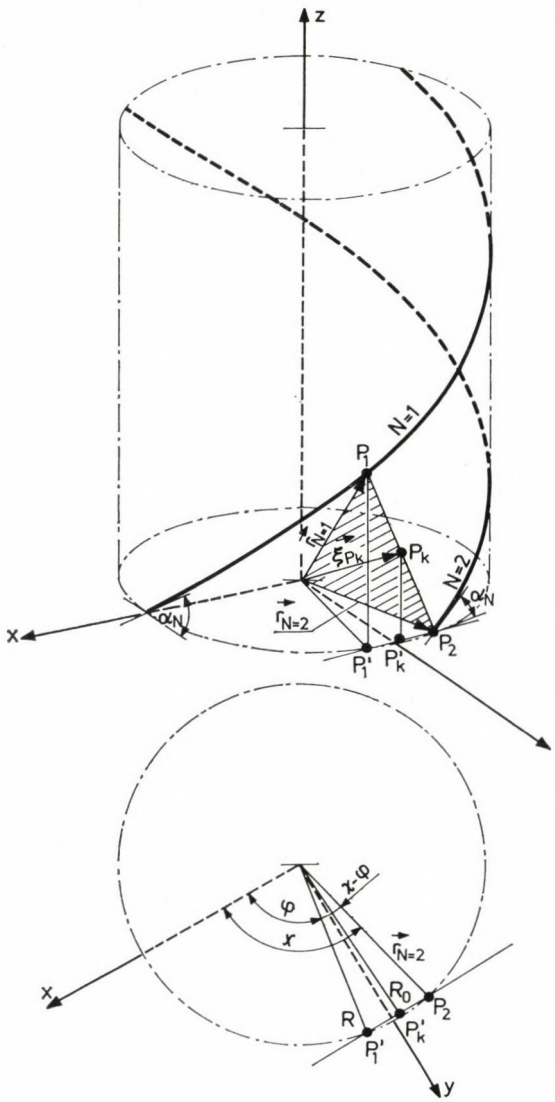

Fig. 19. Conditions of stranding of a layer consisting of $n \geq 1$ elements in case of contact of the elements

Therefore, if into (88) $(\mathbf{r}_1)_{\min}$ is substituted according to (91), and $(\mathbf{r}_2)_{\min}$ according to (90), after rearranging

$$2\boldsymbol{\rho} = (\mathbf{r}_1)_{\min} - (\mathbf{r}_2)_{\min} =$$
$$= R(\cos\varphi^* - \cos\chi)\cdot\mathbf{i} + R(\sin\varphi^* - \sin\chi)\cdot\mathbf{j} + vt^*\cdot\mathbf{k} \tag{92a}$$

is obtained.

The vector $2\boldsymbol{\rho}$ can also be defined by taking into consideration its definition equation (24). In this way deriving the unit vectors $\mathbf{n}$ and $\mathbf{b}$ e.g. from the equation (91) of the vector $(\mathbf{r}_1)_{\min}$ (cf. Eqs (18b) and (18c):

$$\begin{aligned}
2\boldsymbol{\rho} &= 2(R'\cos\psi\cdot\mathbf{n} + R'\sin\psi\cdot\mathbf{b}) = \\
&= -2R'\cos\varphi^*\cdot\cos\psi\cdot\mathbf{i} - 2R'\sin\varphi^*\cdot\cos\psi\cdot\mathbf{j} + \\
&\quad + 2R'\sin\alpha\cdot\sin\varphi^*\cdot\sin\psi\cdot\mathbf{i} - 2R'\sin\alpha\cdot\cos\varphi^*\cdot\sin\psi\cdot\mathbf{j} + \\
&\quad + 2R'\cos\alpha\cdot\sin\psi\cdot\mathbf{k} = \\
&= 2R'(\sin\alpha\cdot\sin\varphi^*\cdot\sin\psi - \cos\varphi^*\cdot\cos\psi)\cdot\mathbf{i} - \\
&\quad - 2R'(\sin\alpha\cdot\cos\varphi^*\cdot\sin\psi + \sin\varphi^*\cdot\cos\psi)\cdot\mathbf{j} + \\
&\quad + 2R'\cos\alpha\cdot\sin\psi\cdot\mathbf{k}.
\end{aligned} \tag{92b}$$

From the identity of the vector Eqs (92a) and (92b) follows the identity of their components

$$\begin{aligned}
R(\cos\varphi^* - \cos\chi) &= \quad 2R'(\sin\alpha\cdot\sin\varphi^*\cdot\sin\psi - \cos\varphi^*\cdot\cos\psi), \\
R(\sin\varphi^* - \sin\chi) &= -2R'(\sin\alpha\cdot\cos\varphi^*\cdot\sin\psi + \sin\varphi^*\cdot\cos\psi), \\
vt^* &= \omega Rt^*\cdot\tan\alpha = \varphi^* R\tan\alpha = 2R'\cos\alpha\cdot\sin\psi.
\end{aligned} \tag{93}$$

Expressing from the first two equations $\cos\psi$, the second sides can be made identical and $\sin\psi$ can be substituted according to the third equation. If therefore from Eqs (93) $\sin\psi$ and $\cos\psi$ are eliminated, the simple expression

$$\tan^2\alpha = \frac{\sin(\chi - \varphi^*)}{\varphi^*} \tag{94}$$

is obtained which because of (84) indeed expresses the functional relation $\alpha = f(n, \varphi)$ of α and n, if the conditions for contact are fulfilled.

From Eqs (89) and (92a)

$$d^2 = |2\boldsymbol{\rho}|^2 = R^2(\cos\varphi^* - \cos\chi)^2 + R^2(\sin\varphi^* - \sin\chi)^2 + (vt^*)^2 =$$
$$= R^2[2 - 2\cos(\chi - \varphi^*) + \varphi^{*2}\tan^2\alpha] \tag{95a}$$

which considering (41b) and (94) can be given the form

$$\frac{D}{d} + 1 = \frac{2}{\sqrt{\varphi^* \sin(\chi - \varphi^*) - 2\cos(\chi - \varphi^*) + 2}} \tag{95b}$$

and which because of (84) can be considered as a functional relation $D/d + 1 = f(n, \varphi)$ between the dimensions D and d and the number of elements n, in case the conditions of the contact are fulfilled.

Examining the relations (94) and (95b) — for given values n — as functions of φ the family of curves Figure 20 can be traced. To give a clearer picture only the curves $n = 1, \ldots, 6$ are shown. The curves $\alpha = f(n, \varphi)$ and $D/d + 1 = f(n, \varphi)$ for $n = 1$ and $n = 2$ are conspicuous because of their characteristic shapes. Later they will be examined in detail.

For given values n and α, φ^* can be calculated from (94). Knowing φ^* to the given values of n and α using (95b) the dimension ratio $(D/d) + 1$

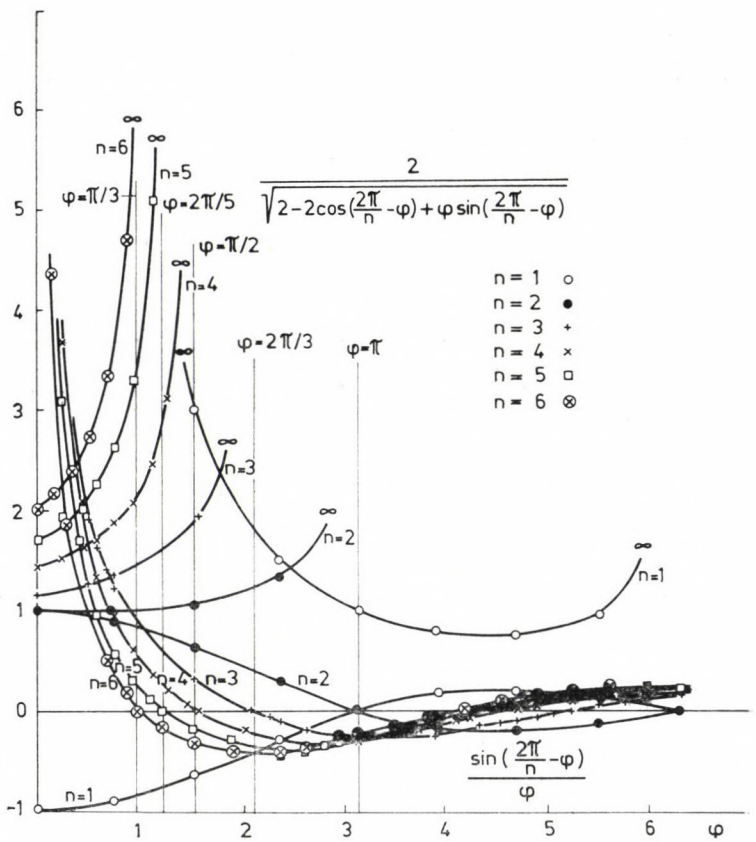

Fig. 20. The functions $D/d + 1 = f(n, \varphi)$ and $\alpha = f/n, \varphi)$

can be ordered. The operations can be carried out on a computer. Table 1 presents from the results of these calculations the dimension ratios $(D/d) + 1$ ordered to the pith angles varying by 5° in the range $0 \leq \alpha \leq \pi/2$ and ordered to the number of elements $n = 1, \ldots, 10$. From the table it is possible to state e.g. that from a number n of elements of diameter d with what — minimum — pitch angle α it is possible to strand a layer.

The two equations (94) and (95b) represent the relations between five parameters — i.e. D, d, α, n and φ^* — therefore from the point of view of geometrical determination the stranded construction has three degrees of freedom. The relatively large number of degrees of freedom permits that conditions are laid down, on the one hand, in the interest of an easier production of the construction, on the other hand, in the interest of resulting physical conditions which can be judged more advantageous (e.g. that for every element of the cable $d = \text{const}$) for conditions to be stipulated.

Applying Eqs (94) and (95b) to the case $n = 1$ it becomes possible to study the contact conditions of an element of diameter $d > 0$ twisted on a core $D \geq 0$ — e.g. the element of a helical spring. Our equations take on

Table 1

Values of $d/(d + 1)$, coordinated to the given angle of pitch and to the elements of number n.

α°	n									
	1	2	3	4	5	6	7	8	9	10
5.0	0.000	1.000	10.956	14.609	18.261	21.913	26.565	29.218	32.870	36.522
10.0	0.000	1.000	5.499	7.330	9.165	10.998	12.831	14.664	16.498	18.331
15.0	0.000	1.000	3.690	4.920	6.147	7.378	8.608	9.838	11.068	12.298
20.0	0.000	1.000	2.793	3.723	4.654	5.582	6.514	7.445	8.376	9.307
25.0	0.000	1.000	2.262	3.015	3.767	4.520	5.271	6.025	6.778	7.532
30.0	0.000	1.000	1.916	2.551	3.187	3.823	4.459	5.093	5.730	6.367
35.0	0.000	1.000	1.677	2.229	2.782	3.335	3.889	4.442	4.997	5.552
40.0	0.000	1.000	1.508	1.996	2.488	2.981	3.475	3.967	4.462	4.957
45.0	0.000	1.000	1.389	1.826	2.270	2.717	3.165	3.613	4.064	4.513
50.0	0.000	1.000	1.306	1.701	2.108	2.517	2.929	3.344	3.757	4.170
55.0	0.000	1.000	1.251	1.610	1.985	2.366	2.750	3.134	3.520	3.906
60.0	0.000	1.000	1.215	1.544	1.894	2.251	2.611	2.974	3.337	3.702
65.0	0.000	1.000	1.191	1.497	1.826	2.164	2.506	2.851	3.197	3.545
70.0	0.000	1.000	1.176	1.463	1.777	2.100	2.428	2.759	3.092	3.424
75.0	0.000	1.000	1.166	1.440	1.742	2.054	2.371	2.692	3.015	3.339
80.0	0.000	1.000	1.159	1.425	1.718	2.023	2.334	2.648	2.964	3.281
85.0	0.000	1.000	1.156	1.417	1.706	2.006	2.312	2.622	2.934	3.247
90.0	0.000	1.000	1.155	1.414	1.701	2.000	2.305	2.613	2.924	3.236

the forms

$$\tan^2 \alpha = \frac{\sin (2\pi - \varphi)}{\varphi} = -\frac{\sin \varphi}{\varphi}, \tag{96}$$

and

$$\frac{D}{d} + 1 = \frac{2}{\sqrt{-\varphi \cdot \sin \varphi - 2 \cdot \cos \varphi + 2}} \tag{97}$$

and their combination results in

$$d^2 = \left(\frac{D+d}{2}\right)^2 [\varphi^2 \tan^2 \alpha + 2(1 - \cos \varphi)] = R^2 \left(\varphi^2 \tan^2 \alpha + 4 \sin^2 \frac{\varphi}{2}\right). \tag{98}$$

This latter was first deduced by R. HARASZTI [24] for describing the compressed state of the cylindrical spring. It is obvious that from (94) and (95b) based on more general principles the self-contact of the threads of the element $n = 1$ can be deduced directly. The conditions characterized by Eq. (98) are shown on Fig. 21.

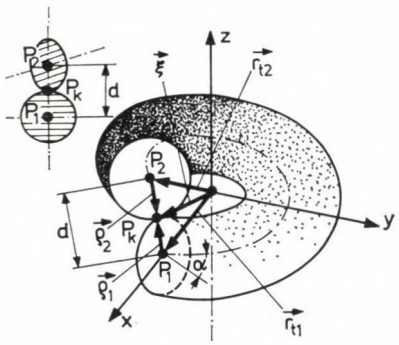

Fig. 21. Self-contact of a stranded element of circular cross section

In the case $n = 2$ from (94) is obtained

$$\tan^2 \alpha = \frac{\sin (\pi - \varphi)}{\varphi} = \frac{\sin \varphi}{\varphi}, \tag{99}$$

and from (95b) is got

$$\frac{D}{d} + 1 = \frac{2}{\sqrt{\varphi \sin \varphi + 2 \cos \varphi + 2}}. \tag{100}$$

According to Fig. 20 for $n = 2$ the curves become $\alpha = f(n, \varphi)$ and the curves $(D/d) + 1 = f(n, \varphi)$ meet at the place $\varphi = 0$, hence there $\tan^2 \alpha = (D/d) + 1 =$

$= 1$. But then $\alpha = \pi/4$ and $D = 0$, the two elements of equal dimensions are twisted upon each other with the pitch angle $\alpha = \pi/4$ securing the most close contact of their threads. This result can be checked experimentally as well.

Experience also shows that the penetration-free contact of the two elements is secured in every case where the thread angle of the twisting is chosen from the range $\pi/4 \leq \alpha \leq \pi/2$. The investigated case shows that obviously (94) and (95b) always order the ratio $(D/d) + 1$ to the minimum value α according to the requirements of penetration-free contact (88).

This statements is also supported by the examination of every limit case $n \geq 3$ showing that the expression

$$\frac{D}{d} + 1 = \frac{2}{\sqrt{\varphi^2 \tan^2 \alpha + 2[1 - \cos(\chi - \varphi)]}} = \frac{2}{\sqrt{\varphi^2 \tan^2 \alpha + 4 \sin^2 (\chi - \varphi)/2}} \tag{101}$$

obtained by combining Eqs (94) and (94b) for $\alpha = \pi/2$ (when $\varphi = 0$) becomes identical with the relation deduced by simple considerations based on Fig. 22.

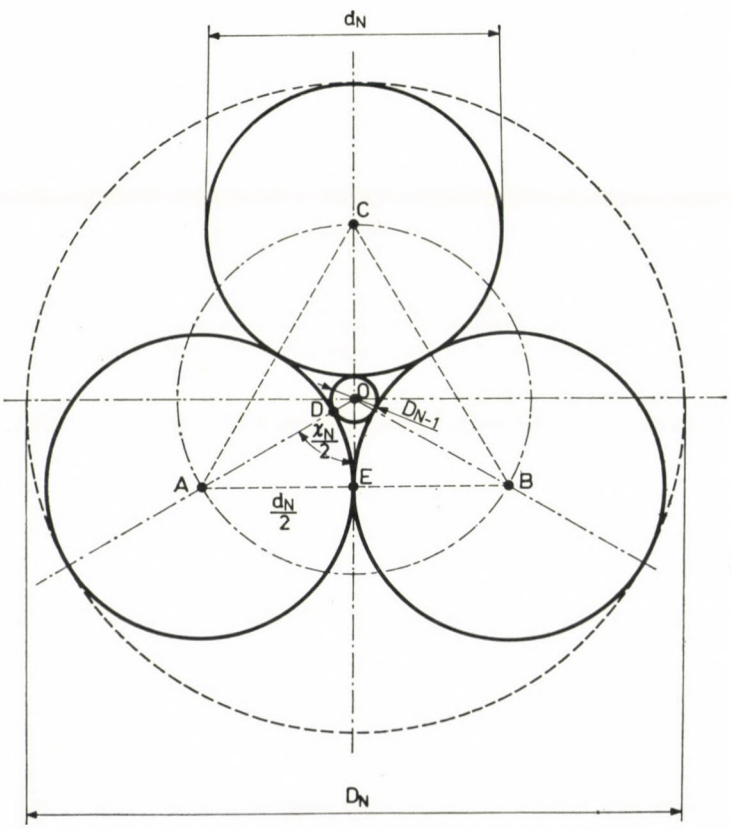

Fig. 22. Contact of the elements of a bunch with parallel elements

Figure 22 shows the cross section of a bundle of three parallel elements in contact with an equal diameter. It can be seen that between the circles in a mutual contact a core of diameter $D > 0$ can be placed.

In the rectangular triangle OAE this figure

$$\frac{\overline{AE}}{\overline{OA}} = \sin\frac{\chi}{2} = \frac{d}{D+d}, \text{ that is } \frac{D}{d} + 1 = \frac{1}{\sin(\chi/2)} \tag{102}$$

It can be seen that substituting $\alpha = \pi/2$ and $\varphi = 0$ into Eq. (101) otherwise obtained passes into the form (102).

If the diameter D of the core fitted between the elements placed in parallel with each other is increased, the contact between them ceases. But it is possible to strand the elements on the core with a pitch angle $\alpha < \pi/2$ whence the contact between the threads is reestablished. Further increasing the diameter D of the core the $n \geq 3$ elements of the layer can be stranded upon the core with ever-decreasing pitch angle, in case of a thread contact. The column for $n \geq 3$ number of elements of Table I shows numerically that in the case of decreasing angle α the ratio $D/(d+1)$ increases.

6. The mechanics of stranding

Figure 4 shows in the reference system XYZ the element of diameter d with the pitch angle α twisted on the core of diameter D. In the sense of the figure the point in question of the centroid of the stranded element is denoted by the position vector $\mathbf{r}(t)$. As has been shown in Chapter 2, the vector triplet **t, n, b** can be ordered to the point in question, so that the cross section A_0 of the element lies in the plane determined by the vectors **n** and **b,** while the vector **t** is normal to the plane of the cross section A_0.

It is furthermore known from Chapter 2 that the acceleration vector $\ddot{\mathbf{r}}(t)$ obtained by derivating $\mathbf{r}(t)$ twice with respect to time, the vector points in the direction of the normal unit vector **n**.

The directions of force and of acceleration provoked by it are in the sense of Newton's 2nd axiom identical, therefore, the vector forcing the stranding of the element can be defined in the form

$$\mathbf{P} = P\mathbf{n}. \tag{103a}$$

The force **P** can also be expressed by coordinates of the XYZ system, if in (103a) **n** is substituted according to Eqs (18b) or (19b). Then for a right-handed element

$$\mathbf{P} = P(-\cos\varphi \cdot \mathbf{i} - \sin\varphi \cdot \mathbf{j}), \tag{103b}$$

for a left-handed element

$$\mathbf{P} = P(-\cos\varphi \cdot \mathbf{i} + \sin\varphi \cdot \mathbf{j}). \tag{103c}$$

The point $P(x, y, z)$ of the centroid of the element, determined by the position vector $\mathbf{r}(t)$ — on which the stranding force $\mathbf{P}$ acts — is in the sense of Fig. 4 at a distance R from the axis of symmetry, therefore the force exerts a torque

$$\mathbf{M} = \mathbf{r}(t) \times \mathbf{P}. \tag{104a}$$

Substituting into the vector product the vectors $\mathbf{r}(t)$ and $\mathbf{P}$ in the case of a right-hand element according to (2), (3a) and (103b)

$$\mathbf{M} = zP(\sin\varphi \cdot \mathbf{i} - \cos\varphi \cdot \mathbf{j}), \tag{104b}$$

for a left-handed element according to (2), (3b) and (103c)

$$\mathbf{M} = zP(-\sin\varphi \cdot \mathbf{i} - \cos\varphi \cdot \mathbf{j}) \tag{104c}$$

the equation of the torque vector can be expressed by the coordinates of the system XYZ.

The equation of the torque vector expressed by the unit vectors **t, n, b** ordered to the chosen point of the centroid is for a right-handed element

$$\mathbf{M} = zP(-\cos\alpha \cdot \mathbf{t} + \sin\alpha \cdot \mathbf{b}), \tag{104d}$$

and for a left-handed element

$$\mathbf{M} = zP(\cos\alpha \cdot \mathbf{t} + \sin\alpha \cdot \mathbf{b}). \tag{104e}$$

In the sense of the vector equations (104d) and (104e) the component $zP\cos\alpha$ of the torque $M = zP$ forces the element to twist around its centroid — the direction $\mathbf{t}$ — therefore the component is a *torque.*

The component $zP\sin\alpha$ bends the element around its binormal $\mathbf{b}$ on the core, therefore it is a *bending moment.*

The twisting and the bending moment thus deforms the straight slice of the element of dS centroid length and A_0 cross section — i.e. of volume $dV = A_0 \cdot dS$ — without change of the elementary volume to twist and bend — to strand — around the core as shown in Fig. 5.

Eqs (23) and (34) give information on the twisting of the slice of elementary volume $dV = A_0 \cdot dS$, and on the sense of the twisting. If the twisting angle Φ is small, then

$$\tan\Phi = \frac{R'}{R}\sin\alpha \cdot \cos\alpha = cR' \sim \Phi, \tag{105}$$

and for an elastic deformation in the sense of Hooke's law a *shearing stress*

$$\tau_\varrho = G\Phi = Gc\varrho \quad (0 \leq \varrho \leq R') \tag{106}$$

arises in the cross section of the element. The proportionality factor G of Eq. (106) is the *modulus of shear* characterizing the material.

As a function of the radius $0 \leq \varrho \leq R'$ the stress τ_ϱ reaches a maximum value at the circumference of the cross section (where $\varrho = R'$), while its zero value is on the centroid (where $\varrho = 0$).

Under the influence of the deformation the arc lengths dS of the parameter lines $\psi = \text{const.}$, forming a network on the surface of the slice $dV = A_0 \cdot dS$ twisted around the axis and bent simultaneously, suffer a change of dimension. The changes of dimensions are determined by the Eq. (31) for the characteristic values of ψ. Considering Eq. (31) the specific arc length reduction provoked by the bending, at $\psi = 0$ is

$$\lambda_{\psi=0} = 1 - \sqrt{\left(\frac{dS_{\psi=0}}{dS}\right)^2 - (cR')^2} = 1 - (1 - gR') = gR' = \frac{R'}{R}\cos^2\alpha, \tag{107a}$$

at the place $\psi = \pi$ the specific arc length increase is

$$\lambda_{\psi=\pi} = \sqrt{\left(\frac{dS_{\psi=\pi}}{dS}\right)^2 - (cR')^2} - 1 = (1 + gR') - 1 = gR' = \frac{R'}{R}\cos^2\alpha, \tag{107b}$$

so the specific values of the contraction at $\psi = 0$ and of the elongation at $\psi = \pi$ are equal.

The deformations (107) rise, if elastic, in the sense of Hooke's law a *tensile/compressive stress*

$$\sigma_\psi = E\lambda_\psi = Eg\varrho \quad (0 \leq \varrho \leq R') \tag{108}$$

in the cross section of the element. The factor of proportionality E of (108) is the *modulus of elasticity* characterizing the quality of the material, $\sigma_{\psi=0}$ is the compressive and $\sigma_{\psi=\pi}$ the tensile stress.

The tensile/compressive stresses as functions of the radius $0 \leq \varrho \leq R'$ are zero at the centroid (where $\varrho = 0$), but assume maximum values at the opposing points $\psi = 0$ and $\psi = \pi$ (where $\varrho = R'$) but in such a way that their mean, taken in respect of the centroid, is zero.

The cross section A_0 of the stranded element is in the sense of (106) and (108) loaded with shear and tensile/compressive stresses. On the surface element dA of the chosen cross section, element dA therefore acts as a *shear force* $\tau_\varrho \cdot dA$ and a *tensile/compressive force* $\sigma_\psi \cdot dA$.

The internal forces $\tau_\varrho \cdot dA$ and $\sigma_\psi \cdot dA$ exert moments $|\varrho \times \tau_\varrho \cdot dA|$ and $|\varrho \times \sigma_\psi \cdot dA|$ which are functions of the radius $0 \leq \varrho \leq R'$ on the directions **t, n, b** ordered to the centre of the cross section A_0.

The vector $\tau_\varrho \cdot dA$ of the shear force is normal to the vector ρ in the plane of the cross section A_0 situated in the same plane and determined by Eq. (24). Thus their vector product points in the direction **t**. In case of the equilibrium of the inner and outer forces and moments

$$zP \cos \alpha = \int_0^{A_0} \rho \times \tau_\varrho \cdot dA' = Gc \int_0^{A_0} \varrho^2 \cdot dA = GcI_p \quad (\text{if } \varrho = R') \tag{109}$$

must be fulfilled. In (109)

$$I_p = I_n + I_b = \frac{\pi}{32} d^4 \tag{110}$$

is the polar moment of second order of the circular cross section $A_0 = (\pi/4) \cdot d^2$ (22).

The vector of the tensile/compression force $\sigma_\psi \cdot dA$ is normal to the cross section A_0 and therefore is also normal to the vector ρ of (24) situated in the plane. The direction of their vector product therefore points in the direction $\pm$ **b**. If the internal and external forces and moments are in eqilibrium then

$$zP \sin \alpha = \int_0^{A_0} |\rho \times \sigma_\psi \cdot dA| = Eg \int_0^{A_0} \varrho^2 \cdot dA = EgI_n \quad (\text{if } \varrho = R') \tag{111}$$

must be fulfilled. In (111)

$$I_n = I_b = \frac{\pi}{64} d^4 \tag{112}$$

is the equatorial moment of second order taken for the directions **n** and **b** of the cross section $A_0 = (\pi/4) \cdot d^2$ (22).

Hence by the Eqs (109) and (111) the moment **M** of (104) can be interpreted as the resultant of "pure twisting" and "pure bending". With these components the magnitude of the moment is

$$|\mathbf{M}| = zP = \sqrt{E^2 g^2 I_n^2 + G^2 c^2 I_p^2} = \frac{\cos \alpha}{R} \sqrt{E^2 I_n^2 \cos^2 \alpha + G^2 I_p^2 \sin^2 \alpha} \tag{113}$$

which determines that force of size P which has forced the cross sectional element to twist characterized by the moduli E and G and by the second order moments I_n and I_p, under the geometrical conditions defined by g, c and z.

In the sense of Eq. (113) the functional connection of the stranding force P and the pitch angle α is defined for the complete range $0 \leq \alpha \leq \pi/2$.

If $\alpha = 0$, (113) takes on the form

$$|\mathbf{M}| = zP = \frac{E\,I_n}{R} \tag{114}$$

known from mechanics, determining the bending moment M and the force requirement P to bend to the radius R of a rod of length z and of the cross section characterized by the second-order moment I_n.

If $\alpha = \pi/2$, then $M = P = 0$, showing that the bending of a straight rod to a radius $R = \infty$ does not need any mechanical stress.

In the intermediate positions $0 \leq \alpha \leq \pi/2$ the component $(EI_n/R) \cos^2 \alpha$ Eq. (113), as a function of α, rapidly drops from the maximum ordered to $\alpha = 0$ to the zero value ordered to $\alpha = \pi/2$, but for the same values of α the component $(GI_p/R) \sin \alpha \cdot \cos \alpha$ is equal to zero, which as a function of α passes through a maximum for the value $\alpha = \pi/4$.

Figure 23 shows the variation of the stranding force P as a function of the pitch angle α for aluminium (Al), copper (Cu) and steel (St) wires (dimensions $d = 1$ mm, $z = 1$ m, core $R = 1$ mm), characterized by their moduli of elasticity and shear.

The discussed behaviour of the components shows that in influencing the variation of force P the importance of the components characteristically

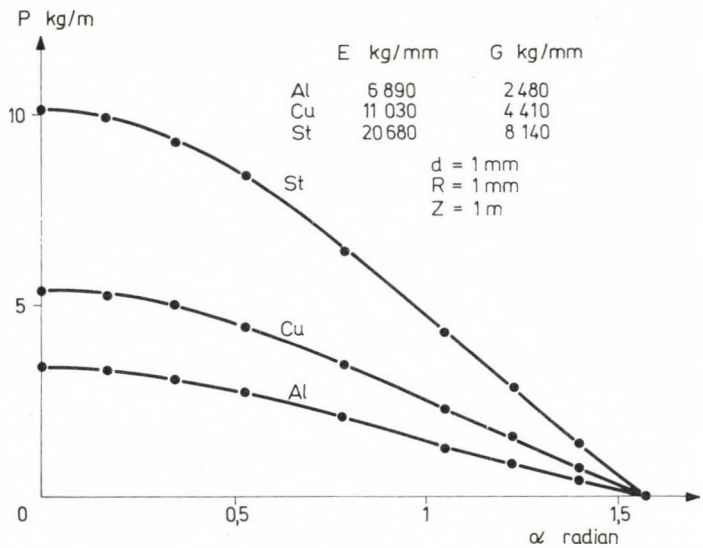

Fig. 23. Force requirement for the stranding of aluminium, copper and steel wires as functions of the pitch angle

differ below and above $\alpha = \pi/4$, nevertheless, the mechanics of stranding of *spring elements* stranded with a pitch angle $\alpha < \pi/4$ and that of *cable elements*, possible to characterize by a pitch angle $\alpha > \pi/4$, can be interpreted by starting out from the same basic principles.

Taking into consideration Eqs (110) and (112) of the moments of second order and Eqs (106) and (108) of the stresses, Eq. (113) can also be expressed in the form

$$\left(\frac{16}{\pi} \cdot \frac{z}{d^3} P\right)^2 = \frac{1}{4}\sigma_\psi^2 + \tau_\varrho^2 \tag{115}$$

if σ_ψ is substituted by its maximum value for $\varrho = R'$ and $\psi = 0$ (or $\psi = \pi$), τ_ϱ is substituted by its maxima for the positions $\varrho = R'$.

Eq. (115) draws the attention to the fact that if it is intended to construct a given stranded construction from wires of increasing diameter — with otherwise unchanged, no number of elements per layer, pitch angle, etc. — then, depending on the material character of the wires, above a certain diameter d so large stresses σ_ψ and τ_ϱ arise on the surface of the wires during stranding which the surface is unable to support without damage.

Eqs (113) and (115) are also suitable for interpreting two well-known technological tests, pointing out at the same time their characteristic difference.

According to the rules for one test the wire of diameter d must be wound on a core of the same diameter with the windings in close contact.

With the other test, gripping the ends the wire folded in two, the branches must be twisted upon each other so that the pitch is gradually reduced and approaches the minimum value $\alpha = \pi/4$.

During the two tests the surface of the wires of determined strength, must not crack.

With the first test the pitch angle of the $n = 1$ elements in contact is $\alpha < \pi/4$ and this means that in the test the bending stress dominates.

With the second test in the case of $\alpha = \pi/4$ the twisting moment is maximum and is, in general, of the same, or approximately the same size as the bending moment.

7. The intrinsic energy accumulating in the stranded conctruction

Knowing the twisting moment (109) and bending moment (111) required for the stranding of the layer element of a regular stranded construction, the *deformation work* L of the element in question can be determined, which in case of elastic deformation can be considered as being equal to the *intrinsic energy* U accumulating in the stranded element.

Replacing the geometrical curvature g of the Eq. (111) of the bending moment by its definition Eq. (20), the differential quotient

$$zP \sin \alpha = EI_n \frac{d\eta}{dS} \tag{116}$$

can be calculated, the integral giving the bending angle

$$\eta = \frac{zP}{EI_n} S \sin \alpha. \tag{117}$$

According to its definition (22) the work L_η of the bending is, considering (117)

$$L_\eta = \frac{1}{2} zP\eta \sin \alpha = \frac{1}{2} \frac{z^2P^2}{EI_n} S \sin^2 \alpha = U_\eta. \tag{118}$$

In the Eq. (109) of the twisting moment replacing the geometrical torsion c by its Eq. (21) and integrating the differential quotient thus obtained, the twisting angle

$$\pm\vartheta = \frac{zP}{GI_p} S \cos \alpha \tag{119}$$

is determined. (23) shows that its sign is positive for a right-handed, negative for a left-handed element.

In the sense of its definition (22) the twisting work L_ν is considering (119)

$$L_\vartheta = \frac{1}{2} zP\vartheta \cos \alpha = \frac{1}{2} \frac{z^2P^2}{GI_p} S \cos^2 \alpha = U_v. \tag{120}$$

Therefore, the determination work of the element of arc length S built into the stranded construction of length z is, using Eqs (109), (111), (118) and (119)

$$L = L_\eta + L_\vartheta = \frac{1}{2}(EI_n g^2 + GI_p c^2)\, S = U_\eta + U_\vartheta = U. \tag{121}$$

Applying (121) to a circular element, the moments of second order can be replace according to (110) and (112). Moreover, considering that the volume of the element of arc length S and diameter d is $V = (1/4)\pi d^2 \cdot S$, then on the base of (106) and (108)

$$L = \frac{V}{4}\left(\frac{Eg^2}{2} + Gc^2\right)\frac{d^2}{4} = \frac{V}{4}\left(\frac{\sigma_\varphi^2}{2E} + \frac{\tau_\varrho^2}{G}\right) = U \tag{122}$$

can be obtained which clearly shows that L is a volumetric work, U a volumetric intrinsic energy.

The internal energy of one single stranded element of circular cross section according to (122) is identical with the concept of *spring energy* known from mechanics.

Using (121) the internal energy accumulating in the whole of the elements built into the chosen layer of the stranded construction can be determined, providing that the stranding stresses do not exceed the limits of elasticity characterizing the material quality of the elements.

So let us discuss the regular stranded construction composed of N layers, the layers containing $n_1, \ldots, n_N$ number of elements with moduli $E_1, \ldots, E_N$, $G_1, \ldots, G_N$ and with pitch angles $\alpha_1, \ldots, \alpha_N$ for each layer. To each element of the chosen N-th layer let there be a cross section A_{0N}, therefore, for its second order moments let there be I_{nN} and I_{pN}.

The deformation work of the element numbered n_N of the N-th layer and its internal energy are in the sense of (121)

$$n_N \cdot L_N = \frac{n_N S_N}{2}(E_N I_{nN} g_N^2 + G_N I_{pN} c_N^2) = n_N U_N \tag{123}$$

the deformation work of all layers built into the stranded construction and their internal energy is

$$L_S = \frac{z}{2} \sum_{N=1}^{N} \frac{n_N}{\sin \alpha_N}(E_N I_{nN} g_N^2 + G_N I_{pN} c_N^2) = U_S \tag{124}$$

where the summation must be carried out for each layer of the construction of length z.

The internal elastic energy accumulated in the layers of the construction left to itself, forces the layers and their elements to *untwist*. Opposing the double character of the stranding, the bending and twisting, the unstranding also has a double character: simultaneously with the untwisting of the layers the untwisting of their elements must also be unhindered during the untwisting as well.

The untwisting of the layers and elements of the construction is triggered, first of all, by the ceasing of the external forces — the stranding forces — equilibrating the internal forces working in the elements, but the design of the stranded construction can also influence the untwisting.

The internal energy provoking the real untwisting of the elements left alone, is obviously the same as the elastic energy according to (124) if every layer of the regular stranded construction is twisted in the same sense.

But if the direction of stranding of the consecutive layers of the regular stranded construction is alternatively right-left-right . . . or left-right-left . . ., then the untwisting of a given layer in a given direction, also the untwisting in a given direction of its elements can be braked by the untwisting in the opposite direction of the layer in direct contact with the layer and its elements

as well as the untwisting in opposite direction of the elements of the layer; the untwisting is provoked, as it were, by an internal energy smaller than the calculated one.

As a consequence of all these considerations the internal energy according to (124) must be considered as the *whole internal energy* accumulating in the stranded construction, (which by the way can be of the same size in stranded constructions of equal material, equal dimensions independently of the equal or opposite thread direction of the layers). But the total internal energy of the stranded construction and its *dynamically not equilibrated internal energy* are equal only if the senses of stranding of all layers of the construction are equal, otherwise for determining the dynamically not equilibrated internal energy one must consider the real direction of untwisting of the individual layers.

Considering the untwisting of a right-hand layer with a negative sign, that of a left-hand layer with a positive sign, introducing furthermore the factors $\mu_1, \ldots, \mu_N$ characterizing the mutual friction of the layers and their elements, the equation for the untwisting of the dynamically unequilibrated internal energy of the stranded construction left alone is

$$\Delta U_S = -\frac{z}{2}\frac{\mu_1 n_1}{\sin \alpha_1}(E_1 I_{n1} g_1^2 + G_1 I_{p1} c_1^2) + \\ + \frac{z}{2}\frac{\mu_2 n_2}{\sin \alpha_2}(E_2 I_{n2} g_2^2 + G_2 I_{p2} c_2^2) - \ldots \tag{125}$$

for right hand — left hand — ... constructions.

The sign obtained for the resulting energy ΔU_S also determines the direction of the initial rotation of the abandoned structure. In an analog way the relation for the energy ΔU_S of the structure constructed from left-right ... thread layers is obtained.

The calculation of all internal energies and of the dynamically not equilibrated ones, is obviously of great importance, especially if it is intended to build the regular stranded construction from elements of composite structure, and if the "Freedom from rotation" of the regular construction is aimed at (without using pre-forming which would certainly exceed the limits of elasticity of the elements).

8. The longitudinal stresses in the stranded construction

Let us consider an element having diameter d stranded with α pitch angle, placed in the XYZ reference system according to Fig. 4. The axis of the — real or imaginary — core coincides with the axis of coordinates Z and let D be the diameter of the core.

Let us assume that the end $Z = 0$ of the element situated in the XY plane is fixed, the opposite end is loaded by the force $\mathbf{P}_t = \mathbf{P}_t \cdot \mathbf{k}$ directed according to $\pm\mathbf{k}$, but the transmission of the force does not influence the displacement of the free end.

According to the assumption to load directed according $\pm\mathbf{k}$ pulls the element, while the load in direction $-\mathbf{k}$ compresses it.

The aim of the investigation is to determine which deformation the $\pm\mathbf{P}_t$ load directed according to Z forces upon the stranded element, the layer formed by n_N stranded elements and the structure formed by N layers.

On the base of Fig. 1 and in the sense of the Eqs (18), (19) of the vector triplet **t, n, b** which can be ordered to the chosen point of the centroid of the stranded element, the equation of the vector $\pm\mathbf{P}_t$ can also be expressed in the coordinates of the system of axes **t, n, b:**
in case of *traction*, for a right-hand thread element:

$$\mathbf{P}_t = P_t \cdot \mathbf{k} = P_t(\sin\alpha \cdot \mathbf{t} + \cos\alpha \cdot \mathbf{b}); \tag{126a}$$

for a left-hand thread element:

$$\mathbf{P}_t = P_t \cdot \mathbf{k} = P_t(\sin\alpha \cdot \mathbf{t} - \cos\alpha \cdot \mathbf{b}); \tag{126b}$$

in case of *compression*, for a right-hand thread element:

$$\mathbf{P}_t = P_t(-\mathbf{k}) = -P_t \cdot \mathbf{k} = P_t(-\sin\alpha \cdot \mathbf{t} - \cos\alpha \cdot \mathbf{b}); \tag{127a}$$

for a left-hand thread element:

$$\mathbf{P}_t = P_t \cdot (-\mathbf{k}) = -P_t \cdot \mathbf{k} = P_t \cdot (-\sin\alpha \cdot \mathbf{t} + \cos\alpha \cdot \mathbf{b}). \tag{127b}$$

The force $\pm\mathbf{P}_t$ acting at the point $P(x, y, z)$ of the centroid situated at distance R of the axis of coordinates, exerts at the point in question a torque given by the vector product

$$\mathbf{M}_t = \mathbf{r}(t) \times \mathbf{P}_t. \tag{128}$$

The vector product (128) is calculated by taking into consideration the components (2) and (3) of the vector $\mathbf{r}(t)$ and the Eqs (126) and (127) of the vector $\mathbf{P}_t$. The equations of the torque vector $\mathbf{M}_t$ are therefore
for *traction* and a right-hand thread element:

$$\begin{aligned}\mathbf{M}_t &= RP_t(\sin\varphi \cdot \mathbf{i} - \cos\varphi \cdot \mathbf{j}) = \\ &= RP_t(-\cos\alpha \cdot \mathbf{t} + \sin\alpha \cdot \mathbf{b});\end{aligned} \tag{129a}$$

for a left-hand thread element:

$$\begin{aligned}\mathbf{M}_t &= RP_t(-\sin\varphi \cdot \mathbf{i} - \cos\varphi \cdot \mathbf{j}) = \\ &= RP_t(\cos\alpha \cdot \mathbf{t} + \sin\alpha \cdot \mathbf{b});\end{aligned} \tag{129b}$$

for *compression* and a right-hand thread element:

$$\mathbf{M}_t = RP_t(-\sin\varphi \cdot \mathbf{i} + \cos\varphi \cdot \mathbf{j}) = \\ = RP_t(\cos\alpha \cdot \mathbf{t} - \sin\alpha \cdot \mathbf{b}); \tag{130a}$$

for a left-hand thread element:

$$\mathbf{M}_t = RP_t(\sin\varphi \cdot \mathbf{i} + \cos\varphi \cdot \mathbf{j}) = \\ = RP_t(-\cos\alpha \cdot \mathbf{t} - \sin\alpha \cdot \mathbf{b}). \tag{130b}$$

Comparing the equations of vector $\mathbf{M}_t$ with those of vector $\mathbf{M}$ (104) responsible for the stranding of the element, it appears that the signs of corresponding components are equal in case of traction, opposite in case of compression. Thus the moments of the traction force induce the element to twist and bend in the same sense as the stranding, the moments of the compression force induce the element to twist and bend in the direction opposite to the stranding.

The *resulting twisting moment* acting upon the stressed element is in case of traction, on the base of (109) and (129):

$$(zP + RP_t)\cos\alpha = \frac{GI_{pt}}{R - \Delta R}\sin(\alpha + \Delta\alpha) \cdot \cos(\alpha + \Delta\alpha) \tag{131a}$$

where

$$RP_t\cos\alpha = \frac{GI_{pt}}{R - \Delta R}\sin(\alpha + \Delta\alpha) \cdot \cos(\alpha + \Delta\alpha) - \frac{GI_p}{R}\sin\alpha \cdot \cos\alpha; \tag{131b}$$

in case of compression, taking into consideration (109) and (130):

$$(zP - RP_t)\cos\alpha = \frac{GI_{pt}}{R + \Delta R}\sin(\alpha - \Delta\alpha) \cdot \cos(\alpha - \Delta\alpha) \tag{132a}$$

where

$$-RP_t\cos\alpha = \frac{GI_{pt}}{R + \Delta R}\sin(\alpha - \Delta\alpha) \cdot \cos(\alpha - \Delta\alpha) - \frac{GI_p}{R}\sin\alpha \cdot \cos\alpha; \tag{132b}$$

and the *resulting bending moment*:
in case of traction in the sense of (111) and (129):

$$(zP + RP_t)\sin\alpha = \frac{EI_{nt}}{R - \Delta R}\cos^2(\alpha + \Delta\alpha) \tag{133a}$$

where

$$RP_t\sin\alpha = \frac{EI_{nt}}{R - \Delta R}\cos^2(\alpha + \Delta\alpha) - \frac{EI_n}{R}\cos^2\alpha; \tag{133b}$$

in case of compression according to (11) and (130):

$$(zP - RP_t) \sin \alpha = \frac{EI_{nt}}{R + \Delta R} \cos^2 (\alpha - \Delta\alpha) \tag{134a}$$

where

$$-RP_t \sin \alpha = \frac{EI_{nt}}{R + \Delta R} \cos^2 (\alpha - \Delta\alpha) - \frac{EI_n}{R} \cos^2 \alpha. \tag{134b}$$

In the sense of Eqs (131)—(134) the moments of the load force change the shape and the location of the centroid of the element, and by this, the geometrical curvatures of the centroid are changed.

The change under the load of the coordinates, determining the choosen point of the element — their transformations — can be defined taking into consideration the elongation and the contraction as well as the rotation in a determined direction due to the torques according to Table 2. The sign of the variation $\Delta\varphi$ of the angle φ also determines the direction of the rotation in the plane XY (right-hand rotation $+\Delta\varphi$, left-hand rotation $-\Delta\varphi'$).

Table 2

Coordinates of the median of the element before and under the application of loading

		Before the application of the loading under	Before the application of the loading under	
			Strain/shrinkage	Rotation
Tension:				
right-hand	x:	$R \cdot \cos \varphi$	$(R - \Delta R) \cdot \cos \varphi$	$(R - \Delta R) \cdot \cos (\varphi + \Delta\varphi)$
element	y:	$R \cdot \sin \varphi$	$(R - \Delta R) \cdot \sin \varphi$	$(R - \Delta R) \cdot \sin (\varphi + \Delta\varphi)$
	z:	z	$z + \Delta z$	$z + \Delta z$
left-hand	x:	$R \cdot \cos \varphi$	$(R - \Delta R) \cdot \cos \varphi$	$(R - \Delta R) \cdot \cos (\varphi + \Delta\varphi)$
element	y:	$-R \cdot \sin \varphi$	$-R(- \Delta R) \cdot \sin \varphi$	$-(R - \Delta R) \cdot \sin (\varphi + \Delta\varphi)$
	z:	z	$z + \Delta z$	$z + \Delta z$
Strain:				
right-hand	x:	$R \cdot \cos \varphi$	$(R + \Delta R) \cdot \cos \varphi$	$(R + \Delta R) \cdot \cos (\varphi - \Delta\varphi)$
element	y:	$R \cdot \sin \varphi$	$(R + \Delta R) \cdot \sin \varphi$	$(R + \Delta R) \cdot \sin (\varphi - \Delta\varphi)$
	z:	z	$z - \Delta z$	$z - \Delta z$
left-hand	x:	$R \cdot \cos \varphi$	$(R + \Delta R) \cdot \cos \varphi$	$(R + \Delta R) \cdot \cos (\varphi - \Delta\varphi)$
element	y:	$-R \cdot \sin \varphi$	$-(R + \Delta R) \cdot \sin \varphi$	$-(R + \Delta R) \cdot \sin (\varphi - \Delta\varphi)$
	z:	z	$z - \Delta z$	$z - \Delta z$

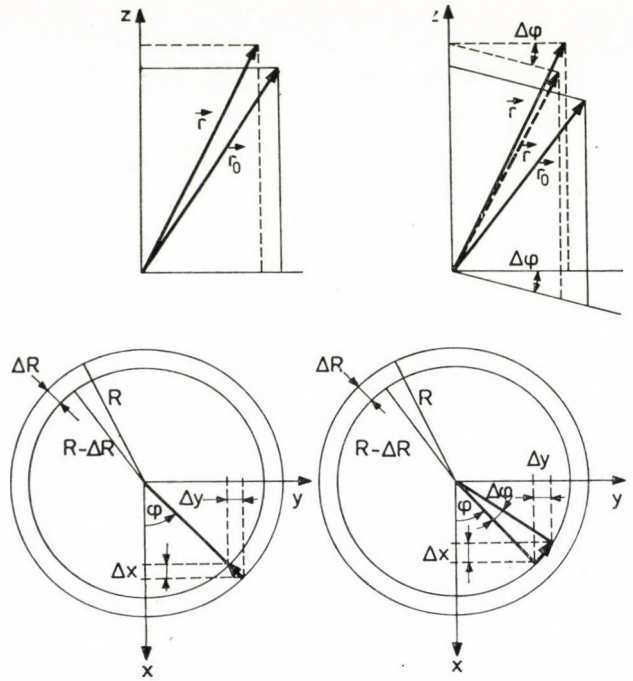

Fig. 24. Elongation and rotation of a stranded element in case of traction

The variations of the coordinates — for the tractive stressing of a right-hand thread element are explained by Fig. 24.

Between the coordinates of Table 2 characterizing the state before loading of the element these exist the connections defined by Eqs (11)—(14). After elongation/compression and rotation these relations are described by

$$\sin(\alpha + \Delta\alpha) = \frac{z + \Delta z}{S + \Delta S} = \frac{\dfrac{z + \Delta z}{z}}{\dfrac{S + \Delta S}{S}} \sin\alpha = \frac{1 + \lambda_z}{1 + \lambda_S} \sin\alpha \qquad (135a)$$

and

$$\cos(\alpha + \Delta\alpha) = \frac{(\varphi + \Delta\varphi) \cdot (R - \Delta R)}{S + \Delta S} = \frac{\dfrac{\varphi + \Delta\varphi}{\varphi} \cdot \dfrac{R - \Delta R}{R}}{\dfrac{S + \Delta S}{S}} \cos\alpha =$$

$$= \frac{\left(1 + \dfrac{\Delta\varphi}{\varphi}\right) \cdot \left(1 - \dfrac{\Delta R}{R}\right)}{1 + \lambda_S} \cos\alpha, \qquad (135b)$$

while in case of compression they are described by the relations

$$\sin(\alpha - \Delta\alpha) = \frac{1 - \lambda_z}{1 - \lambda_S} \sin\alpha \tag{136a}$$

and

$$\cos(\alpha - \Delta\alpha) = \frac{\left(1 - \frac{\Delta\varphi}{\varphi}\right) \cdot \left(1 + \frac{\Delta R}{R}\right)}{1 - \lambda_S} \cos\alpha \tag{136b}$$

which are completed by

$$(\alpha \pm \Delta\alpha) + (\beta \mp \Delta\beta) = \frac{1}{2}\pi \quad \text{where} \quad \Delta\alpha = \Delta\beta \tag{137}$$

In the Eq. (135)

$$\sin(\alpha + \Delta\alpha) > \sin\alpha, \text{ therefore } \lambda_z > \lambda_S \tag{138a}$$

$$\cos(\alpha + \Delta\alpha) < \cos\alpha, \text{ therefore } \left(1 + \frac{\Delta\varphi}{\varphi}\right) \cdot \left(1 - \frac{\Delta R}{R}\right) < 1 - \lambda_S$$

In the Eq. (136)

$$\sin(\alpha - \Delta\alpha) < \sin\alpha, \text{ therefore } \lambda_z > \lambda_S$$

$$\cos(\alpha - \Delta\alpha) > \cos\alpha, \text{ therefore } \left(1 - \frac{\Delta\varphi}{\varphi}\right) \cdot \left(1 + \frac{\Delta R}{R}\right) > 1 - \lambda_S \tag{138b}$$

It can be seen that Eqs (135) and (136) are also defined for the cases $\Delta\varphi = 0$ and $\lambda_S = 0$.

It follows furthermore from Eqs (135) that

$$(1 + \lambda_S)^2 = (1 + \lambda_z)^2 \sin^2\alpha + \left(1 + \frac{\Delta\varphi}{\varphi}\right)^2 \cdot \left(1 - \frac{\Delta R}{R}\right)^2 \cos^2\alpha \tag{139a}$$

and

$$\tan\Delta\alpha = \frac{(z + \Delta z)\cos\alpha - (\varphi + \Delta\varphi) \cdot (R - \Delta R)\sin\alpha}{(z + \Delta z)\sin\alpha + (\varphi + \Delta\varphi) \cdot (R - \Delta R)\cos\alpha}, \tag{139b}$$

while from Eq. (136) it follows that

$$(1 - \lambda_S)^2 = (1 - \lambda_z)^2 \sin^2\alpha + \left(1 - \frac{\Delta\varphi}{\varphi}\right)^2 \cdot \left(1 + \frac{\Delta R}{R}\right)^2 \cos^2\alpha \tag{140a}$$

and

$$\tan\Delta\alpha = -\frac{(z - \Delta z)\cos\alpha - (\varphi - \Delta\varphi) \cdot (R + \Delta R)\sin\alpha}{(z - \Delta z)\sin\alpha + (\varphi - \Delta\varphi) \cdot (R + \Delta R)\cos\alpha} \tag{140b}$$

where the variables $\Delta\varphi$, ΔR and λ_z are quantities which can also be determined experimentally.

In the practical realization of the loading experiments the case $\Delta\varphi = 0$ means that the stranded element or layer, or the stranded construction has both ends fixed, therefore its rotation can neither influence the angular rotation φ nor the twisting Φ.

One of the fixing methods used for the testing of the longitudinal stress of the layer formed by stranded elements or by the stranded construction formed by the layers permit the rotation of one end [12], so here $\Delta\varphi \neq 0$, but even then the fixing does not allow a variation $\pm\Delta\Phi$ of the torsion Φ.

The change of the radius R of the drawn element into $R - \Delta R$, and the change of the radius of the compressed element into $R + \Delta R$ can also be expressed by the ratios of the adequate expressions of the Eqs (131)—(134) for the bending and the twisting moment.

In case of traction from (133b) and (131b):

$$\tan\alpha = \frac{EI_{nt}\, R\cos^2(\alpha+\Delta\alpha) - EI_n(R-\Delta R)\cos^2\alpha}{GI_{pt}R\sin(\alpha+\Delta\alpha)\cos(\alpha+\Delta\alpha) - GI_p(R-\Delta R)\sin\alpha\cdot\cos\alpha} \tag{141a}$$

wherefrom by rearranging

$$-\frac{\Delta R}{R} = \frac{G[I_{pt}\sin(\alpha+\Delta\alpha)\cdot\cos(\alpha+\Delta\alpha) - I_p\sin\alpha\cdot\cos\alpha]\dfrac{\sin\alpha}{\cos\alpha}}{GI_p\sin^2\alpha - EI_n\cos^2\alpha} - \\ - \frac{E[I_{nt}\cos^2(\alpha+\Delta\alpha) - I_n\cos^2\alpha]}{GI_p\sin^2\alpha - EI_n\cos^2\alpha} \tag{141b}$$

determines the amount of reduction of the radius R.

In case of compression from (134b) and (132b):

$$\tan\alpha = \frac{EI_n(R+\Delta R)\cos^2\alpha - EI_{nt}R\cos^2(\alpha-\Delta\alpha)}{GI_p(R+\Delta R)\sin\alpha\cdot\cos\alpha - GI_{pt}R\sin(\alpha-\Delta\alpha)\cdot\cos(\alpha-\Delta\alpha)} \tag{142a}$$

wherefrom by rearranging

$$+\frac{\Delta R}{R} = \frac{G[I_{pt}\sin(\alpha-\Delta\alpha)\cdot\cos(\alpha-\Delta\alpha) - I_p\sin\alpha\cdot\cos\alpha]\dfrac{\sin\alpha}{\cos\alpha}}{GI_p\sin^2\alpha - EI_n\cos^2\alpha} - \\ - \frac{E[I_{nt}\cos^2(\alpha-\Delta\alpha) - I_n\cos^2\alpha]}{GI_p\sin^2\alpha - EI_n\cos^2\alpha} \tag{142b}$$

determines the amount of the increase of R.

When formulating Eqs (131)—(134) the changes in the moments of second order have also been taken into account, caused by the reduction of the cross section of the drawn of the increase of the compressed element, respectively.

If the change in the cross section A_0 of the loaded element is responsible the component $\mathbf{P}_t \sin \alpha$ of the force $\mathbf{P}_t$ acting in the sense of the centroid of the element, which arises in the cross section a tensile/compressive stress

$$\sigma_t = \frac{P_t \sin \alpha}{A_0} = E_0 \lambda_S \tag{143}$$

and elongates/compresses the arc length S of the element according to

$$\lambda_S = \frac{\Delta S}{S} . \tag{144}$$

If $\lambda_S = 0$, then in (141b) and (142b) $I_n = I_{nt}$ and $I_p = I_{pt}$. These identities are complied within the limits of the stressing traction and compression springs [2], but with the stresses of the stranded layer and those of the stranded construction one must also take into consideration the possibility $\lambda_S \neq 0$.

The component $P_t \cos \alpha$ of the force $\mathbf{P}_t$ pointing in the direction $\pm\mathbf{b}$ of the cross section A_0 of the element, arises in the cross section as a shear stress

$$\tau_t = \frac{P_t \cos \alpha}{A_0} \tag{145}$$

of a determined direction.

The ratio of σ_t according to (143) and of τ_t according to (145) is

$$\frac{\sigma_t}{\tau_t} = \tan \alpha \tag{146a}$$

while their square is, considering (39)

$$\sigma_t^2 + \tau_t^2 = \frac{P_t^2}{A_0^2} = \frac{P_t^2}{A_{xy}^2 \sin^2 \alpha} \equiv \frac{\sigma^2}{\sin^2 \alpha} \tag{146b}$$

where σ is that resulting stress which according to the definition of (146b) is formed by relating the force $\mathbf{P}_t$ of direction $\pm\mathbf{k}$ to the plane section A_{xy} of the stranded element situated in plane XY.

As a consequence of (146b) and the Eqs (143) and (145) of the stresses if $\alpha = \pi/2$, i.e. if the centroid of the straight element coincides with the direction of the loading force, then $\tau_t = 0$ and $\sigma_t = \sigma$, in the element arises tracting/compression stress only.

If, on the other hand $o < \alpha < \pi/2$, the traction/compression force $\mathbf{P}_t$ acting upon the stranded element generates the stress σ in the element, which

according to (146b) is decomposed into the stresses σ_t and τ_t and according to the method of fixing of the element they either accumulate as internal stress or are transformed into motive energy provoking the rotation of the element. In the case of a spring element the stress σ according to (146b) is also the total elastic stress of the element, because the stresses σ_ϱ and τ_ϱ arising at the stranding of the element have been liquidated by the permanent deformation of the element (and its heat treatment).

The examination of the longitudinal straining of the layer indexed N constructed from n_N number of elements and the stranded construction formed from N layers (and the core with index $N = 0$) will be limited to the examination of tensile stressing of the layer or construction only. (Practically compressive stressing arises only at the contraction of cables, after thermal dilatation as a phenomenon, provoking the "basketing" of the stranded construction, which but appears locally at certain positions of the cable length and is not distributed uniformly along the complete length).

So let a tensile force $\mathbf{P}_S = P_S \cdot \mathbf{k}$ act in a direction normal to the cross section A_S of the stranded construction consisting of N layers and the core, and let it be divided according to

$$P_S = P_0 + P_1 + \ldots + P_N \tag{147}$$

into partial loads of the core and of the N layers, and let it be divided according to

$$P_N = n_N P_t = n_N P_{0N}, \quad (P_t = P_{0N}) \tag{148}$$

amongst the n_N elements of the N-th layer.

To the analogy of the rule (146b) let us introduce the stress

$$\sigma_N = \frac{P_N}{A_N} = E_N \lambda_z \tag{149}$$

which arises in the cross section A_N of the stranded layer when the length z of the layer increases by λ_z due to the action of the traction force P_N. The factor of proportionality E_N of Eq. (149) is called *apparent modulus of elasticity*.

On the base of Eq. (39) the section A_N in the plane XY of the layer is

$$A_N = n_N A_{xy} = n_N \frac{A_{0N}}{\sin \alpha_N} . \tag{150}$$

Taking into consideration Eqs (143) and (150), from (149) the ratio of the apparent modulus of elasticity E_N and the modulus E_{0N} characterizing the

quality of the layer elements can be expressed by

$$\sigma_N = E_N \lambda_z = \frac{P_N}{A_N} = \frac{P_N}{n_N A_0} \sin \alpha = \frac{P_{0N}}{A_{0N}} \sin \alpha = E_{0N} \lambda_S \tag{151a}$$

i.e.

$$E_N = \frac{\lambda_S}{\lambda_z} \cdot E_{0N} \tag{151b}$$

as functions of the specific elongations of the layer λ_z and of the layer elements λ_s.

Eq. (138a) has shown that $\lambda_z < \lambda_S$, thus of necessity $E_N < E_{0N}$, or else the apparent modulus of elasticity of the stranded layer cannot attain the modulus characteristic for the material quality of the elements in all those cases where $o < \alpha_N < \pi/2$ (on the other hand, if $\alpha_N = \pi/2$, the layer is formed by a bunch of elements really in parallel, then $\lambda_S = \lambda_z$ therefore $E_N = E_{0N}$).

At the traction of the stranded construction made from the core and N layers in the sense of (147)—(151) a stress

$$\sigma_S = \frac{P_S}{A_S} = E_S \lambda_z = \frac{E_0 A_{00} \lambda_z + \ldots + E_{0N} \dfrac{n_N A_{0N}}{\sin \alpha_N} \lambda_{SN}}{A_{00} + \dfrac{n_1 A_{01}}{\sin \alpha_1} + \ldots + \dfrac{n_N A_{0N}}{\sin \alpha_N}} \tag{152a}$$

arises in the cross section A_S of the stranded construction due to its specific elongation λ_z. In Eq. (152a) established for the general case E_S is the apparent modulus of elasticity, $E_0, E_1, \ldots, E_N$ are the moduli of the elements forming the core and the layers (assuming that in the general case the layers of the construction are formed by elements made from different materials).

By transforming Eq. (152a) the relation

$$(E_S - E_0) A_{00} + \left(E_S - E_{01} \frac{\lambda_{S1}}{\lambda_z}\right) \frac{n_1 A_{01}}{\sin \alpha_1} + \ldots + \left(E_S - E_{0N} \frac{\lambda_{SN}}{\lambda_z}\right) \frac{n_N A_{0N}}{\sin \alpha_N} = 0 \tag{152b}$$

reduced to zero can be established and obviously this is fulfilled either when

$$E_0 = E_{01} \frac{\lambda_{S1}}{\lambda_z} = \ldots = E_{0N} \frac{\lambda_{SN}}{\lambda_z}, \tag{153}$$

or in that case when the sum of the positive, negative, maybe zero members is equal to zero.

This latter case obviously represents the inequal distribution of the load P_S stressing the construction when not even the conditions for "moving together" of the layers and their conditions of contact also wanted for the loaded state are fulfilled either.

The adequate design of the construction must therefore be characterized by (153), but in itself (153) only helps in selecting the material qualities of the layer elements, the geometrical conditions for "moving together" must be determined as well.

The required relations are defined by (139a) for tensile loading. Eq. (139a) must be applied to the core and to the layers of the construction.

Therefore, for the stranded construction of length z

$$(1 + \lambda_z)^2 = (1 + \lambda_z)^2 \qquad \text{(for the core, where } \alpha_0 = \pi/2 \text{ and } \lambda_z = \lambda_{S0})$$

$$= \frac{(1 + \lambda_{S1})^2 - \left(1 + \frac{\Delta\varphi_1}{\varphi_1}\right)^2 \cdot \left(1 - \frac{\Delta R_1}{R_1}\right)^2 \cos^2 \alpha_1}{\sin^2 \alpha_1} =$$

$$= \ldots\ldots\ldots\ldots \text{ (for the layers)}$$

$$= \frac{(1 + \lambda_{SN})^2 - \left(1 + \frac{\Delta\varphi_N}{\varphi_N}\right)^2 \cdot \left(1 - \frac{\Delta R_N}{R_N}\right)^2 \cos^2 \alpha_N}{\sin^2 \alpha_N} \tag{154a}$$

according to which for any two neighbouring layers

$$\frac{\sin^2 \alpha_{N+1}}{\sin^2 \alpha_N} = \frac{(1 + \lambda_{S,N+1})^2 - \left(1 + \frac{\Delta\varphi_{N+1}}{\varphi_{N+1}}\right)^2 \cdot \left(1 - \frac{\Delta R_{N+1}}{R_{N+1}}\right)^2 \cos^2 \alpha_{N+1}}{(1 + \lambda_{SN})^2 - \left(1 + \frac{\Delta\varphi_N}{\varphi_N}\right)^2 \cdot \left(1 - \frac{\Delta R_N}{R_N}\right)^2 \cos^2 \alpha_N} \tag{154b}$$

must be complied with.

In the sense of the rule for "moving together" (154b) the increase of length of the layers submitted to a tractive effort is accompanied by a proportionate radial reduction of dimension accompanied by a rotation around the axis of coordinates Z.

Because of a chosen layer element having a constant volume

$$V = \frac{1}{4}\pi d^2 S = \frac{1}{4}\pi(d - \Delta d)^2 (S + \Delta S) \tag{155a}$$

or considering (144), Eq.

$$1 + \lambda_S = \left(\frac{d}{d - \Delta d}\right)^2 \tag{155b}$$

exists between the increase of arc length of the element and its reduction of diameter.

Furthermore, let us remember that in the sense of (41b) under no-load conditions the radius of the N-th layer of the construction is

$$R_N = \frac{D_{N-1} + d_N}{2} \tag{156}$$

where D_{N-1} is the diameter of the — generally composite — core carrying the N-th layer. The dimensional reduction $R_N - \Delta R_N$ due to the elongation λ_z of the construction, in the sense of (156) partly entrains a diameter reduction of the core, partly of the layer element, in (154b) thus neither $\lambda_{S,N+1}$ nor λ_{SN} can be zero.

Figure 24 shows moreover that the angle of rotation around the Z axis, $\Delta\varphi$, is for every layer $\Delta\varphi_N = \Delta\varphi_{N+1} = \text{const}$ and of the same direction; as for the amount of the rotation there must be

$$(\varphi_N + \Delta\varphi_N) \cdot (R_N - \Delta R_N) < (\varphi_{N+1} + \Delta\varphi_{N+1}) \cdot (R_{N+1} - \Delta R_{N+1}).$$

These exigences can be fulfilled only if all the layers of the construction are stranded in the same direction. In a stranded construction made from layers stranded in right hand — left hand — right hand . . ., or left hand — right hand — left hand . . . direction the rotations called forth by the torques of Eq. (129), the friction between the elements of the layers in contact, obviously brakes or even prevents it, in which latter case $\Delta\varphi_N = \Delta\varphi_{N+1} = 0$.

These considerations point on the one hand to the fact that the specific elongations λ_{SN} and $\lambda_{S,N+1}$ in Eq. (154a) must be larger than zero, but the equation is also defined for the case $\Delta\varphi_N = \Delta\varphi_{N+1} = 0$, which occurs either if the fixing of the ends prevents the rotation or when the friction between layers — stranded in opposite direction — prevents the rotations in the opposite direction.

On the other hand, the considerations show that at tensile stressing of the stranded layer and of the stranded construction made from N layers only a small increase of the pitch angle of the layer or layers, respectively — and a small increase Δz of the length z — may be anticipated, thus the *stranded construction* — independent of the material quality of its elements — is a *quasi-unextensible structure*. This peculiar behaviour of the stranded constructions only characterizes those in which the layers directly touch each other and the contact does not occur under the influence of the traction force $\mathbf{P}_t$ (a tractive force acting on the cross section of a loosely stranded construction, in fact increases the apparent pitch angle only by pre-stressing the layers not being previously in contact).

This statement is confirmed by examining the change $\Delta\alpha$ in Eq. (139b) due to the action of the tensile force. Applying (139b) to two adjacent layers with indices N and $N+1$ in case of the length increase $z + \Delta z = \text{const}$

$$\frac{\tan \alpha_N + \tan \Delta\alpha_N}{\tan \alpha_{N+1} + \tan \Delta\alpha_{N+1}} \cdot \frac{1 - \tan \alpha_{N+1} \cdot \tan \Delta\alpha_{N+1}}{1 - \tan \alpha_N \cdot \tan \Delta\alpha_N} = \frac{(\varphi_{N+1} + \Delta\varphi_{N+1}) \cdot (R_{N+1} - \Delta R_{N+1})}{(\varphi_N + \Delta\varphi_N) \cdot (R_N - \Delta R_N)} > 1 \tag{157}$$

must be complied with, the condition for which is

$$\tan \alpha_{N+1} < \frac{1}{\tan \Delta\alpha_{N+1}} \quad \text{and} \quad \tan \alpha_N < \frac{1}{\tan \alpha_N}$$

or

$$\tan \alpha_N + \tan \Delta\alpha_N > \tan \alpha_{N+1} + \tan \Delta\alpha_{N+1} \tag{158}$$

In case the requirements (158) are fulfilled $\alpha_N \geq \alpha_{N+1}$ and that means that it is suitable to choose the arc lengths of the elements built into consecutive layers according to $S_N \geq S_{N+1}$. The correctness of these conclusions is also confirmed by checking the dimensions of practically well proved stranded constructions.

Summary

In this paper, based on the principles of kinematics and using the methods of vector algebra, the equations of the centroid and the surface of the once stranded finite element as well as the equations of the plane cross section of the element thus determining the space requirements of the element also have been formulated.

Being in possession of these relations they have furthermore been determined:

— the number n of elements with diameter $d \geq 0$ which can be stranded around a core of dia. $D \geq 0$ with a pitch angle $\alpha_{\min}$ and the functional relations $\alpha = f(n, \varphi)$ and $(D/d) + 1 = f(n, \varphi)$ between the stranding parameters D, d, h and α assuming contact of the elements without penetration;

— the variation of arc length and location of the parameter lines covering the surface of the element. Determining the amount of these variations the deformation of the elementary-volume slice $dV = A_0 \cdot dS$, the pure bending and the pure twisting have been determined,

as well as the stresses in the cross section σ_ψ and τ_ϱ. Knowing the elastic internal stresses the deformation work of the element characterized by the moduli E and G, then the internal energy accumulating in the stranded layer or in the construction built composed of layers, respectively, distinguishing if from the dynamically unbalanced internal energy causing the decomposition of the core left alone;

— the method for generating the double twisted helix and the equations for the four possible types of DTH space curves have been formulated. By examining the equations of the DTH space curves it has been shown that along the centroid of the double twisted element periodically changing stresses act in the cross section. The places subject to concentrated stress are sources of inhomogeneity in the stranded constructions containing double twisted elements. Examining the cross section of constructions containing double twisted elements of concording and of opposing thread direction, the different shapes of the cross sections of the two types have been determined enhancing how much this influences their possibility of application under conditions also involving conditions of wear.

By the examination of senstivity it has been deduced between what extremum values the parameters in the relations of geometrical and mechanical character are defined. It has been shown that the Eqs (47)—(50) of the DTH space curves pass for $\alpha = 0$ into equations suitable for describing the location of the bent element of the stranded construction. At the same place has been proved that the flexibility of the layer or construction stranded from finite elements, is influenced by the space requirement of its elements. It has been found that the layer or stranded construction which was stranded with the pitch angle $\alpha_{\min}$ belonging to the parameters D, d and n could only be bent at the price of the permanent deformation of its elements.

It also has been shown that the geometrical and mechanical conditions of the traction or compression springs stranded with pitch angle $0 < \alpha < \pi/4$ — as stranded elements — and of the layers or constructions stranded with thread angles $\pi/4 < \alpha < \pi/2$ can be explained starting out from the same principles. Nevertheless the characteristic differences appearing in the behaviour under load of the spring elements and the stranded elements or stranded constructions have been ascribed to the opposite character of the changes in the torques and to the design characteristics which do not influence the displacements provoked by the torques and which brake the displacements or even prevent them.

It has been proved that the twisting torque acting on a single element is proportionate to the product $\sin \alpha \cdot \cos \alpha$ and therefore has a maximum just at the critical angle $\alpha = \pi/4$, thus the directions of the variation occurring

under the influence of tractive or tensile forces, respectively, are opposite for the elements stranded with pitch angles below or above $\alpha = \pi/4$.

On the other hand, obviously the deformation under load of an isolated spring element is limited in space exclusively by the fixing, but the contact of the elements of a stranded layer or construction and their mutual friction hinders the displacement even when the fixing of their ends would otherwise permit the rotation — at least in the XY plane.

By investigating the tensile stress in the twisted element, layer or construction it has been shown that the loading force acting upon an element is split into components $P_t \sin \alpha$ and $P_t \cos \alpha$ raising in the cross section of the element a tensile stress σ_t and a shear stress τ_t. Following the division of the force the apparent moduli of elasticity of the stranded construction E_s and of the stranded layer E_N are of necessity smaller than the modulus E_{0N} characterizing the quality of the elements and assumes a size according to a special average if the layers of the stranded construction are made from materials of different qualities.

Summing up the consequences from the equations characterizing the bending and the longitudinal stressing of the stranded construction it appears that the geometrical conditions of the construction decisively influence the resulting material qualities characterizing the whole of the construction. In the interest of increasing the flexibility the stranded construction must be sacrificed, i.e. the inextensibility of the elements independent of the material, which quality not only characterizes such a construction where the elements are in penetration-free contact mutually as well as with the neighbouring layers.

By the geometrical characterization of the regular stranded constructions as well as of their mechanical qualities the paper wants to make a contribution towards the design and dimensioning practices of the stranded constructions.

Acknowledgements

The author considers it to be his duty of honour to thank Dr. Pál GÁGYOR, former chief engineer of the Cable and Wire Rope Factory who draw his attention to the problems of wire rope design and who as actual general manager of the KG INFORMATIK supported the task of the author.

REFERENCES

1. CZITARY, E.: Seilschwebebahnen. II. Aufl. Springer Verlag, Wien 1962
2. WAHL, A. M.: Mechanical Springs. 2-nd Ed. McGraw-Hill, New York 1963
3. SHITKOW, D. G.—POSPECHOW, I. T.: Drahtseile. VEB Verlag Technik, Berlin 1957
4. DIAMOND, J.: The Twisting of Wire. Principles and Applications. *Wire Journal* (1972), 54—58
5. DIAMOND, J.: Fundamentals of Cabling. *Wire Journal* (1973), 41—45
6. DIAMOND, J.: Design of a Cabling Line. *Wire Journal* (1975), 127—131

7. LILLY, J. C.: The Mathematical Relationship between the Bending Radius of a Cable and the Length of Cable Lay. *Proc. 23-rd Int. Wire and Cable Symp.* 1974
8. LEIDER, M. G.: Untersuchungen über die Zusatzspannungen bei der Biegung von Drahtseilen. *Draht* **24** (1973), 247—255.
9. LEIDER, M. G.: Die Änderung der Zugkraft in den einzelnen Drähten bei der Biegung von mehrlagigen Litzen. *Draht* **35** (1974), 497—501
10. LEIDER, M. G.: Krümmung und Biegespannungen von Drähten in gebogenen Drahtseilen. *Draht* **28** (1977), 1—8
11. LEIDER, M. G.: Mechanismus der Drahtverschiebungen bei der Biegung von Drahtseilen und Berechnung der dadurch hervorgerufenen Beanspruchungen. *Draht* **28** (1977), 148—150, 207—211
12. KOLLROS, W.: Zusammenhang zwischen Torsionsmoment, Zugkraft und Verdrillung in Seilen. *Draht* **26** (1975), 475—480
13. BÜCKNER, W.—PHILLIPPS, W.: Die mechanische Bemessung der Freileitungsseile. *Elektrizitätswirtschaft* **69** (1970), 686—701
14. DI LEONARDO, R.: A Theory of Compact Round Concentric Lay Stranded Electrical Conductors. *Wire Journal* (1977), 56—61
15. BRANDT, E.: Das Verhalten von Aluminium-Stahl Freileitungsseilen statischer Biegeanspruchung. *Energiewirtschaftliche Tagesfragen* **22** (1972), 233—241
16. BRANDT, E.: Ermittelung des Verlegeverhaltens von Freileitungsseilen. *Energiewirtschaftliche Tagesfragen* **23** (1973), 10—19
17—19. WIEK, Ir. L.: Tatsachen und ziffernmäßige Darstellungen der Spannungen in Drahtseilen. Teil I, II, III. Draht **26** (1975), 283—286, Draht **26** (1975), 387—389, Draht **26** (1975), 484—486
20. WIEK, Ir. L.: Computerized Rope Design and Endurance. OIPEEC Round table meeting. Luxembourg, 1977. Oct.
21. PACH Zs. P.—FREY T.: Vektor és tenzor analízis. Műszaki Könyvkiadó, Budapest 1960
22. BUDÓ, Á.: Mechanika. III. kiadás, Tankönyvkiadó, Budapest 1964
23. GOODMAN, A. W.: Analytic Geometry and the Calculus. Collier-McMillan, London, New York 1965
24. HARASZTI, R.: Az archimedesi csavarfelület önérintése. *Miskolci Nehézipari Műszaki Egyetem Közleményei*, **X** (1964), 165—184

Geometrie und Mechanik der regelmäßig verseilten Konstruktionen. Die infolge der bei Herstellung der von den einfach und zweifach gedrehten Elementen aufgebauten regelmäßigen Faserbündel und unter den Zug- und Biegebeanspruchungen des verfertigten Faserbündels auftretenden mechanischen Spannungen werden untersucht. Zur Einführung der mechanischen Spannungen werden die Gleichungen und geometrischen Parameter der einfach und zweifach gedrehten Schraubenlinien, ferner der Raumbedarf und die Oberfläche eines einfach gedrehten Rundelements durch Anwendung der vektoralgebraischen Methoden ermittelt. Bei Kenntnis des Raumbedarfs des gedrehten Elements werden die Beziehungen zwischen der Elementenzahl, der Gewindesteigung und Maßverhältnis der Drehungsschichten des regelmäßigen Faserbündels für den Fall der Durchdringungsfreien formuliert.

Acta Technica Academiae Scientiarum Hungaricae, Tomus 91 (1–2), pp. 203–223 (1980)

GENERALIZATION OF SOUTHWELL'S AND DUNKERLEY'S THEOREMS FOR QUADRATIC EIGENVALUE PROBLEMS

T. TARNAI*

[Manuscript received September 1, 1977]

An approximate method for computing minimum positive eigenvalues of quadratic eigenvalue problems with real spectra is presented, seeking to give lower bounds for the wanted eigenvalue, and to reduce a given problem to simpler problems. Theorems by SOUTHWELL and by DUNKERLEY are generalized, then further relationships giving approximations from below are deduced. Application of the results is illustrated on ateral buckling problems of beams.

1. Introduction

Let us consider linear operators A, B, C defined in a Hilbert space H, occurring in the quadratic eigenvalue problem

$$Au - \lambda Bu - \lambda^2 Cu = 0 \tag{1}$$

where — provided equality (1) is met — number λ is an eigenvalue of Eq. (1), while element $u \in H$, $u \neq 0$ is its eigenelement corresponding to λ.

Let (φ, ψ) $\varphi, \psi \in H$ denote the scalar product defined in the space H, and $D(A)$, $D(B)$, $D(C)$ the domain of definition of operators A, B, C.

Let the following conditions for operators A, B, C be satisfied:

(1.1) Operator A is symmetric, positive definite (there is a number $\alpha > 0$ such that $(Au, u) \geqq \alpha(u, u)$ for every $u \in D(A)$) is of a discrete spectrum (the spectrum consists purely of eigenvalues) and $D(A) \subset D(B) \cap D(C)$.

(1.2) Operator B is symmetric.

(1.3) Operator C is symmetric, positive ($(Cu, u) > 0$ for all $u \in D(C)$, $u \neq 0$).

(1.4) Operators BA^{-1} and CA^{-1} are of finite absolute norm. (Definition of absolute or double norm see e.g. in [10].)

Forming the scalar product of the left-hand side of Eq. (1) and u yields a polynomial whose zeros permit the definition of two functionals (introducing notations $(A\,u, u) = a$, $(B\,u, u) = b$, $(C\,u, u) = c$):

$$\mathfrak{F}^+(u) = \frac{-b + \sqrt{b^2 + 4ac}}{2c}, \tag{2}$$

* Dr. T. TARNAI, Kolostor u. 17. H-1037 Budapest, Hungary.

$$\mathfrak{F}^-(u) = \frac{-b - \sqrt{b^2 + 4ac}}{2c}. \tag{3}$$

Be λ_0 and u_0 the minimum positive eigenvalue of Eq. (1) and the corresponding eigenelement, resp. Provided operators A, B, C satisfy conditions (1.1) to (1.4), it is known [7] to have

$$\lambda_0 = \inf_{u \in D(A) \setminus \{0\}} \mathfrak{F}^+(u) = \mathfrak{F}^+(u_0). \tag{4}$$

If any of operators A, B, C may be produced as sum of operators of identical properties, then each of them is permitted to write an eigenvalue problem of form (1). The aim of this paper is to give a lower bound for the minimum positive eigenvalue of Eq. (1) by means of the minimum positive eigenvalues of the partial problems.

2. Generalization of Southwell's theorem

T h e o r e m 1. *Be A, B, C operators satisfying conditions* (1.1) *to* (1.4). *Be $A = \sum_{i=1}^{n} A_i$. Let operator $A_i (i = 1, 2, \ldots, n)$ have the same properties as A, that is, let it satisfy conditions* (1.1) *to* (1.4) *Be λ_i the minimum positive eigenvalue of equation*

$$A_i u - \lambda B u - \lambda^2 C u = 0 \quad (i = 1, 2, \ldots, n). \tag{5}$$

Then inequality

$$(Bu_0, u_0)\lambda_0 + (Cu_0, u_0)\lambda_0^2 \geq \sum_{i=1}^{n} [(Bu_0, u_0)\lambda_i + (Cu_0, u_0)\lambda_i^2] \tag{6}$$

holds.

P r o o f. Applying notations

$$a_i = (A_i u, u) \quad (i = 1, 2, \ldots, n),$$

$$\mathfrak{F}^+_{A_i}(u) = \frac{-b + \sqrt{b^2 + 4a_i c}}{2c} \qquad (i = 1, 2, \ldots, n) \tag{7}$$

equalities

$$a - \mathfrak{F}^+(u) \cdot b - \mathfrak{F}^{+2}(u) \cdot c = 0,$$

$$a_i - \mathfrak{F}^+_{A_i}(u) \cdot b - \mathfrak{F}^{+2}_{A_i}(u) \cdot c = 0, \qquad (i = 1, 2, \ldots, n),$$

$$a = \sum_{i=1}^{n} a_i$$

imply:

$$\mathfrak{F}^+(u) \cdot b + \mathfrak{F}^{+2}(u) \cdot c = \sum_{i=1}^{n} [\mathfrak{F}^+_{A_i}(u) \cdot b + \mathfrak{F}^{+2}_{A_i}(u) \cdot c]. \tag{8}$$

Be $u = u_0$. Now, according to (4), $\mathcal{F}^+(u_0) = \lambda_0$, and (8) becomes:

$$\lambda_0(Bu_0, u_0) + \lambda_0^2(Cu_0, u_0) = \sum_{i=1}^{n} [\mathcal{F}^+_{A_i}(u_0) \cdot (Bu_0, u_0) + \mathcal{F}^{+2}_{A_i}(u_0) \cdot (Cu_0, u_0)]. \quad (9)$$

Operator $A_i (i = 1, 2, \ldots, n)$ having the same properties as A, for the minimum positive eigenvalue of Eq. (5), a relationship of the form (4) holds:

$$\lambda_i = \inf_{u \in D(A_i)\setminus\{0\}} \mathcal{F}^+_{A_i}(u), \qquad (i = 1, 2, \ldots, n). \quad (10)$$

The right-hand side of equality (9) is reduced by replacing

$$\mathcal{F}^+_{A_i}(u_0)$$

by λ_i, i.e., the infimum of $\mathcal{F}^+_{A_i}(u)$ yielding the inequality (6) to be demonstrated.

1.1 Remark: If in Theorem 1, $B = 0$, inequality (6) will take the form:

$$\lambda_0^2 \geq \sum_{i=1}^{n} \lambda_i^2 . \quad (11)$$

Inequality (11) is identical to Southwell's formula for the eigenvalue problem $Au - \lambda^2 Cu = 0$ linear in λ^2 [5, 6, 9].

Practically, inequality (6) is inefficient for determining the approximate value of λ_0, namely, it requires the knowledge of the eigenelement u_0, corresponding to eigenvalue λ_0. For practical applications, a relationship of the form (11) is convenient, subject to the next theorem.

Theorem 2. *Let all conditions encountered in Theorem* 1 *be satisfied for operators* A, B, C, A_i $(i = 1, 2, \ldots, n)$. *Be* B *a positive semi-definite operator* $((Bu, u) \geq 0,\ u \in D(B))$ *then*:

$$\lambda_0^2 \geq \sum_{i=1}^{n} \lambda_i^2 .$$

Proof. Let equality (8) be rewritten as:

$$\mathcal{F}^{+2}(u) = \sum_{i=1}^{n} \mathcal{F}^{+2}_{A_i}(u) + \frac{b}{c}\left[\sum_{i=1}^{n} \mathcal{F}^+_{A_i}(u) - \mathcal{F}^+(u)\right]. \quad (12)$$

The second term in the right-hand side of (12) has to be shown as being non-negative. Since $b \geq 0$, $c > 0$, the proof will result from realizing

$$\sum_{i=1}^{n} \mathcal{F}^+_{A_i}(u) - \mathcal{F}^+(u) \geq 0 . \quad (13)$$

Demonstration will be by induction. Let $\mathcal{F}^+_{A_1+\ldots+A_k}(u)$ denote functional (2) for the case $A = \sum_{i=1}^{k} A_i$, $(k \leq n)$. Statement (13) is true for $n = 2$ $(A = A_1 + A_2)$

Namely, assuming its opposite:

$$\mathcal{F}^{+}_{A_1 + A_2}(u) > \mathcal{F}^{+}_{A_1}(u) + \mathcal{F}^{+}_{A_2}(u)\,. \tag{14}$$

Substituting (2) and (7) into (14) and multiplying the inequality by $2c$, adding $2b$ to both sides and squaring both sides twice, meanwhile performing simplifications leads to a contradiction. Thus:

$$\mathcal{F}^{+}_{A_1 + A_2}(u) \leqq \mathcal{F}^{+}_{A_1}(u) + \mathcal{F}^{+}_{A_2}(u)\,.$$

Thereby:

$$\mathcal{F}^{+}(u) \leqq \mathcal{F}^{+}_{A_1 + \ldots + A_{n-1}}(u) + \mathcal{F}^{+}_{A_n}(u) \leqq \mathcal{F}^{+}_{A_1 + \ldots + A_{n-2}}(u) + \mathcal{F}^{+}_{A_{n-1}}(u) + \\ + \mathcal{F}^{+}_{A_n}(u) \leqq \ldots \leqq \sum_{i=1}^{n} \mathcal{F}^{+}_{A_i}(u)\,.$$

Relationship (13) is satisfied. Accordingly, the right-hand side of (12) is reduced by omitting its second term:

$$\mathcal{F}^{+2}(u) \geqq \sum_{i=1}^{n} \mathcal{F}^{+2}_{A_i}(u)\,. \tag{15}$$

Be $u = u_0$. Now, because of (4), (15) becomes:

$$\lambda_0^2 \geqq \sum_{i=1}^{n} \mathcal{F}^{+2}_{A_i}(u_0)\,.$$

The right-hand side of this inequality is further reduced by replacing $\mathcal{F}^{+2}_{A_i}(u_0)$ by the square of the infimum of $\mathcal{F}^{+}_{A_i}(u)$ i.e. λ_i^2, the same as the statement in the theorem.

3. Generalization of Dunkerley's theorem

T h e o r e m 3. *Be A, B, C operators satisfying conditions* (1.1) *to* (1.4). *Be* $B = \sum_{i=1}^{n} B_i$. *Let operator* B_i $(i = 1, 2, \ldots, n)$ *have the same properties as* B, *i.e. satisfying conditions* (1.2) *and* (1.4). *Be* λ_i *the minimum positive eigenvalue of equation*

$$Au - \lambda B_i u - \lambda^2 C u = 0 \qquad (i = 1, 2, \ldots, n) \tag{16}$$

giving rise to inequality

$$(Au_0, u_0)\frac{1}{\lambda_0} - (Cu_0, u_0)\lambda_0 \leqq \sum_{i=1}^{n}\left[(Au_0, u_0)\frac{1}{\lambda_i} - (Cu_0, u_0)\lambda_i\right]. \tag{17}$$

Proof. Apply notations

$$b_i = (B_i u, u) \qquad (i = 1, 2, \ldots, n).$$

$$\mathfrak{F}^+_{B_i}(u) = \frac{-b_i + \sqrt{b_i^2 + 4ac}}{2c} \qquad (i = 1, 2, \ldots, n). \tag{18}$$

Equalities

$$\frac{1}{\mathfrak{F}^+(u)} a - b - \mathfrak{F}^+(u) \cdot c = 0,$$

$$\frac{1}{\mathfrak{F}^+_{B_i}(u)} a - b_i - \mathfrak{F}^+_{B_i}(u) \cdot c = 0 \quad (i = 1, 2, \ldots, n),$$

$$b = \sum_{i=1}^{n} b_i$$

yield

$$\frac{1}{\mathfrak{F}^+(u)} \cdot a - \mathfrak{F}^+(u) \cdot c = \sum_{i=1}^{n} \left[\frac{1}{\mathfrak{F}^+_{B_i}(u)} \cdot a - \mathfrak{F}^+_{B_i}(u) \cdot c \right]. \tag{19}$$

Be $u = u_0$. Now, (14) causes (19) to become:

$$\frac{1}{\lambda_0}(Au_0, u_0) - \lambda_0(Cu_0, u_0) = \sum_{i=1}^{n} \left[\frac{1}{\mathfrak{F}^+_{B_i}(u_0)} (Au_0, u_0) - \mathfrak{F}^+_{B_i}(u_0) \cdot (Cu_0, u_0) \right]. \tag{20}$$

Operator B_i $(i = 1, 2, \ldots, n)$ having the same properties as B, for the minimum positive eigenvalue of Eq. (16), a relationship of form (4) holds:

$$\lambda_i = \inf_{u \in D(A) \setminus \{0\}} \mathfrak{F}^+_{B_i}(u). \tag{21}$$

The right-hand side of equality (20) increases upon replacing $\mathfrak{F}^+_{B_i}(u_0)$ by λ_i, i.e. the infimum of $\mathfrak{F}^+_{B_i}(u)$, yielding inequality (17) that was to be proved.

3.1 Remark. If in Theorem 3, $C = 0$, inequality (17) will take the form:

$$\frac{1}{\lambda_0} \leq \sum_{i=1}^{n} \frac{1}{\lambda_i}. \tag{22}$$

Inequality (22) is identical to Dunkerley's theorem for the linear eigenvalue problem $Au - \lambda Bu = 0$ [3, 4, 9]. In this case, B has to be a positive operator.[1]

3.2 Remark. If in Theorem 3, $A = 0$, operator B is negative definite ($-B$ positive definite), of discrete spectrum, and operator CB^{-1} has a finite absolute norm, then inequality (17) becomes:

$$\lambda_0 \geq \sum_{i=1}^{n} \lambda_i. \tag{23}$$

[1] DUNKERLEY [3] arrived empirically to the formula bearing his name, by analysing vibrations of revolving shafts. JEFFCOTT [4] was the first to prove its correctness theoretically, by means of equilibrium equations. Formulation of Dunkerley's formula as a theorem, and its proof based on a simple, variational principle is due to TEMPLE [9].

Inequality (23) is identical to Southwell's theorem for the linear eigenvalue problem $Bu + \lambda Cu = 0$ (with the operator B of indicated properties) [5, 6, 9].

For practical applications, an approximate relationship dispensing with the knowledge of eigenelement u_0 corresponding to eigenvalue λ_0 is more convenient.

T h e o r e m 4. *Under conditions of Theorem* 3, *inequality*

$$\frac{1}{\lambda_0} \leq \sum_{i=1}^{n} \frac{1}{\lambda_i} \tag{24}$$

is true. (This theorem — contrary to Remark 3.1 — does not imply the assumptions $C = 0$ and B positive.)

P r o o f. Rearrange equality (19) as:

$$\frac{1}{\mathfrak{F}^+(u)} = \sum_{i=1}^{n} \frac{1}{\mathfrak{F}^+_{B_i}(u)} + \frac{c}{a}\left[\mathfrak{F}^+(u) - \sum_{i=1}^{n} \mathfrak{F}^+_{B_i}(u)\right]. \tag{25}$$

The second term on the right-hand side of (25) has to be demonstrated as not being positive. Since $c > 0$, $a > 0$ it is sufficient to show:

$$\mathfrak{F}^+(u) - \sum_{i=1}^{n} \mathfrak{F}^+_{B_i}(u) \leq 0. \tag{26}$$

Inequality (26) will be verified by induction. Let $\mathfrak{F}^+_{B_1+\ldots+B_k}(u)$ denote functional (2) for the case where $B = \sum_{i=1}^{k} B_i$, $k \leq n$, a statement true for $n = 2$ ($B = B_1 + B_2$). Namely, assuming its opposite:

$$\mathfrak{F}^+_{B_1+B_2}(u) > \mathfrak{F}^+_{B_1}(u) + \mathfrak{F}^+_{B_2}(u). \tag{27}$$

Substituting (2) and (18) into (27) and multiplying the inequality by $2c$, then adding $(b_1 + b_2)$ to both sides and squaring them twice consecutively leads to a contradiction.

Thus:

$$\mathfrak{F}^+_{B_1+B_2}(u) \leq \mathfrak{F}^+_{B_1}(u) + \mathfrak{F}^+_{B_2}(u).$$

Accordingly:

$$\mathfrak{F}^+(u) \leq \mathfrak{F}^+_{B_1+\ldots+B_{n-1}}(u) + \mathfrak{F}^+_{B_n}(u) \leq \mathfrak{F}^+_{B_1+\ldots+B_{n-1}}(u) + \mathfrak{F}^+_{B_{n-1}}(u) + \mathfrak{F}^+_{B_n}(u) \leq \ldots \leq \sum_{i=1}^{n} \mathfrak{F}^+_{B_i}(u).$$

Thereby (26) has been demonstrated. Because of inequality (26), the right-hand side of (25) is increased by omitting its second term:

$$\frac{1}{\mathfrak{F}^+(u)} \leq \sum_{i=1}^{n} \frac{1}{\mathfrak{F}^+_{B_i}(u)}. \tag{28}$$

Be $u = u_0$. Utilizing (4) renders (28) to:

$$\frac{1}{\lambda_0} \leq \sum_{i=1}^{n} \frac{1}{\mathfrak{F}^+_{B_i}(u_0)}.$$

The right-hand side of this inequality is further increased by replacing $\mathfrak{F}^+_{B_i}(u_0)$ by the infimum of $\mathfrak{F}^+_{B_i}(u)$. Hence, according to (21), the statement in the theorem is arrived at.

T h e o r e m 5. *Be A, B, C operators satisfying conditions* (1.1) *to* (1.4). *Be $B = \sum_{i=1}^{n} B_i$. Let operator $B_i (i = 1, 2, \ldots, n)$ have the same properties as B, i.e. satisfying conditions* (1.2) *and* (1.4). *Be $C = \left(\sum_{i=1}^{n} C_i\right)^2$. Be operator $C_i (i = 1, 2, \ldots, n)$ bounded self-adjoint. (Now, C_i^2 $(i = 1, 2, \ldots, n)$ will have the same properties as C, i.e. satisfying conditions* (1.3) *and* (1.4)). *Let λ_i denote the minimum positive eigenvalue of equation*

$$Au - \lambda B_i u - \lambda^2 C_i^2 u = 0 \qquad (i = 1, 2, \ldots, n) \tag{29}$$

giving rise to the relationship:

$$\frac{1}{\lambda_0} \leq \sum_{i=1}^{n} \frac{1}{\lambda_i}.$$

P r o o f. Apply notations:

$$b_i = (B_i u, u) \qquad (i = 1, 2, \ldots, n),$$

$$\mathfrak{F}^+_i(u) = \frac{-b_i + \sqrt{b_i^2 + 4a(C_i^2 u, u)}}{2(C_i^2 u, u)} \qquad (i = 1, 2, \ldots, n). \tag{30}$$

Equalities

$$\frac{1}{\mathfrak{F}^+(u)} a - b - \mathfrak{F}^+(u) \cdot c = 0,$$

$$\frac{1}{\mathfrak{F}^+_i(u)} a - b_i - \mathfrak{F}^+_i(u)(C_i^2 u, u) = 0 \qquad (i = 1, 2, \ldots, n),$$

$$b = \sum_{i=1}^{n} b_i$$

imply:

$$\frac{1}{\mathcal{F}^+(u)} = \sum_{i=1}^{n} \frac{1}{\mathcal{F}_i^+(u)} + \frac{1}{a}\left[\mathcal{F}^+(u) \cdot c - \sum_{i=1}^{n} \mathcal{F}_i^+(u) \cdot (C_i^2 u, u)\right]. \tag{31}$$

The second term on the right-hand side of (31) has to be shown as being non-positive. Since $a > 0$, it is sufficient to demonstrate

$$\mathcal{F}^+(u) \cdot c \leq \sum_{i=1}^{n} \mathcal{F}_i^+(u) \cdot (C_i^2 u, u). \tag{32}$$

Inequality (32) will be demonstrated by induction. Let $\mathcal{F}_{1,2,\ldots,k}^+(u)$ denote functional (2) for the case $B = \sum_{i=1}^{k} B_i$, $C = \left(\sum_{i=1}^{k} C_i\right)^2$, $k \leq n$. Correctness of (32) will first be demonstrated for $n = 2$ ($B = B_1 + B_2$, $C = (C_1 + C_2)^2$).

It is stated:

$$\mathcal{F}_{1,2}^+(u) \cdot \left((C_1 + C_2)^2 u, u\right) \leq \mathcal{F}_1^+(u)(C_1^2 u, u) + \mathcal{F}_2^+(u) \cdot (C_2^2 u, u). \tag{33}$$

Apply notation:

$$\hat{\mathcal{F}}_{1,2}^+(u) = \frac{-(b_1+b_2) + \left\{(b_1+b_2)^2 + 4a[(C_1^2u,u) + 2(C_1^2u,u)^{\frac{1}{2}}(C_2^2u,u)^{\frac{1}{2}} + (C_2^2u,u)]\right\}^{\frac{1}{2}}}{2\left((C_1 + C_2)^2 u, u\right)}. \tag{34}$$

Because of the Cauchy—Schwarz—Buniakovsky inequality:

$$|(C_1 C_2 u, u)| \leq (C_1^2 u, u)^{\frac{1}{2}}(C_2^2 u, u)^{\frac{1}{2}},$$

thus: $\mathcal{F}_{1,2}^+(u) \leq \hat{\mathcal{F}}_{1,2}^+(u)$. (33) is confirmed by realizing:

$$\hat{\mathcal{F}}_{1,2}^+(u)\left((C_1 + C_2)^2 u, u\right) \leq \mathcal{F}_1^+(u) \cdot (C_1^2 u, u) + \mathcal{F}_2^+(u)(C_2^2 u, u).$$

As an indirect proof, assume

$$\hat{\mathcal{F}}_{1,2}^+(u)\left((C_1 + C_2)^2 u, u\right) > \mathcal{F}_1^+(u) \cdot (C_1^2 u, u) + \mathcal{F}_2^+(u)(C_2^2 u, u). \tag{35}$$

Substitute (34) and (30) into (35). Multiply this inequality by 2 and add $(b_1 + b_2)$ to both sides. Squaring bot sides twice consecutively — simplifying in the meantime — leads to a contradiction. Thus, (33) holds. Accordingly:

$$\mathcal{F}^+(u) \cdot c \leq \mathcal{F}_{1,2,\ldots,n-1}^+(u)\left(\left(\sum_{i=1}^{n-1} C_i\right)^2 u, u\right) + \mathcal{F}_n^+(u) \cdot (C_n^2 u, u) \leq$$

$$\leq \mathcal{F}_{1,2,\ldots,n-2}^+(u)\left(\left(\sum_{i=1}^{n-2} C_i\right)^2 u, u\right) + \mathcal{F}_{n-1}^+(u) \cdot (C_{n-1}^2 u, u) +$$

$$+ \mathcal{F}_n^+(u)(C_n^2 u, u) \leq \ldots \leq \sum_{i=1}^{n} \mathcal{F}_i^+(u) \cdot (C_i^2 u, u).$$

Thereby, (32) has been proved. Due to inequality (32), the right-hand side of (31) becomes increased by omitting its second term:

$$\frac{1}{\mathfrak{F}^+(u)} \leq \sum_{i=1}^{n} \frac{1}{\mathfrak{F}_i^+(u)}. \tag{36}$$

Be $u = u_0$. Utilizing (4) permits (36) to be written as:

$$\frac{1}{\lambda_0} \leq \sum_{i=1}^{n} \frac{1}{\mathfrak{F}_i^+(u_0)}. \tag{37}$$

Operator B_i $(i = 1, 2, \ldots, n)$ having the same properties as B, and operator C_i^2 $(i = 1, 2, \ldots, n)$ as C, the minimum positive eigenvalue of (29) is controlled by a relationship of the form (4):

$$\lambda_i = \inf_{u \in D(A) \setminus \{0\}} \mathfrak{F}_i^+(u). \tag{38}$$

The right-hand side of (37) becomes increased by replacing $\mathfrak{F}_i^+(u_0)$ by the infimum of $\mathfrak{F}_i^+(u)$. Thereby Eq. (38) leads to the statement in the theorem.

3.3. R e m a r k. As to its physical purport. Theorem 5 may be considered as the most direct quadratic generalization of Dunkerley's theorem formulated for an equation having the form $Au - \lambda Bu = 0$ [3, 4, 9].

T h e o r e m 6. *Be A, B, C operators satisfying conditions* (1.1) *to* (1.4). *Be $B = B_1 + B_2$. Let operators B_1 and B_2 have the same properties as operator B, i.e., let them satisfy conditions* (1.2) *and* (1.4). *Also let B_2 be a positive operator* $((B_2u, u) > 0,\ u \in D(B_2),\ u \neq 0)$. *Let λ_1 and λ_2 denote minimum positive eigenvalues of equations*

$$Au - \lambda B_1 u - \lambda^2 Cu = 0 \tag{39}$$

and

$$Au - \lambda B_2 u = 0, \tag{40}$$

respectively. Then inequality

$$\frac{1}{\lambda_0} \leq \frac{1}{\lambda_1} + \frac{1}{\lambda_2} \tag{41}$$

holds.

P r o o f. It is easy to demonstrate the fulfilment of inequality

$$\frac{1}{\mathfrak{F}^+(u)} \leq \frac{1}{\mathfrak{F}_{B_1}^+(u)} + \frac{b_2}{a} \tag{42}$$

where $b_2 = (B_2u, u)$ and $a = (Au, u)$. Namely, assuming its opposite:

$$\frac{1}{\mathfrak{F}^+(u)} > \frac{1}{\mathfrak{F}_{B_1}^+(u)} + \frac{b_2}{a}. \tag{43}$$

Substitute (2) and (18) into (43) considering that $b = b_1 + b_2$, then square both sides of (43) and simplify it. Repeated squaring leads to a contradiction. Be $u = u_0$. Now, (42) may be written as:

$$\frac{1}{\lambda_0} \leq \frac{1}{\mathcal{F}^+_{B_1}(u_0)} + \frac{(B_2 u_0,\ u_0)}{(Au_0,\ u_0)}. \tag{44}$$

The right-hand side of inequality (44) is increased by replacing $\mathcal{F}^+_{B_1}(u_0)$ and $(Au_0, u_0)/(B_2 u_0, u_0)$ by the infima of $\mathcal{F}^+_{B_1}(u)$ and the Rayleigh quotient a/b_2, i.e. λ_1 and λ_2, respectively, leading to the statement in the theorem.

4. Three further theorems

T h e o r e m 7. *Be A, B, C operators satisfying conditions* (1.1) *to* (1.4). *Be B_1 and C_1 operators satisfying conditions* (1.2) *and* (1.4), *and* (1.3) *and* (1.4), *respectively. For each $u \in D(A)$ the inequality*

$$-\frac{b}{c} + \sqrt{\left(\frac{b}{c}\right)^2 + 4\frac{a}{c}} \geq -\frac{b_1}{c_1} + \sqrt{\left(\frac{b_1}{c_1}\right)^2 + 4\frac{a}{c_1}} \tag{45}$$

has to be met, where $b_1 = (B_1 u, u)$, $c_1 = (C_1 u, u)$. Let the minimum positive eigenvalue of

$$Au - \lambda B_1 u - \lambda^2 C_1 u = 0 \tag{46}$$

be denoted by λ_1. Then the inequality

$$\lambda_0 \geq \lambda_1$$

holds.

P r o o f. Denote:

$$\mathcal{F}^+_1(u) = \frac{-b_1 + \sqrt{b_1^2 + 4ac_1}}{2c_1}. \tag{47}$$

Inequality (45) yields:

$$\mathcal{F}^+(u) \geq \mathcal{F}^+_1(u). \tag{48}$$

Operators B_1 and C_1 having the same properties as B and C, λ_1 may be expressed in the form (4):

$$\lambda_1 = \inf_{u \in D(A)\setminus\{0\}} \mathcal{F}^+_1(u). \tag{49}$$

According to (4) and (49), (48) yields the inequalities:

$$\lambda_0 = \mathcal{F}^+(u_0) \geq \mathcal{F}^+_1(u_0) \geq \inf_{u \in D(A)\setminus\{0\}} \mathcal{F}^+_1(u) = \lambda_1.$$

Thus, $\lambda_0 \geq \lambda_1$, q.e.d.

Theorem 8. *Let conditions of Theorem 6, and inequality*

$$b_2 \leqq b_1 + \sqrt{(b_1 + b_2)^2 + 4ac}\,, \qquad u \in D(A) \tag{50}$$

be satisfied.

With notations in Theorem 6, relationship

$$\lambda_2 \geqq \lambda_0$$

holds.

Proof. According to condition (50):

$$\frac{b_2}{a} \leqq \frac{1}{\mathfrak{F}^+(u)}\,. \tag{51}$$

Denote by u_2 the eigenelement of (40) corresponding to λ_2. Be $u = u_2$. Now, (51) may be written as:

$$\frac{1}{\lambda_2} \leqq \frac{1}{\mathfrak{F}^+(u_2)}\,. \tag{52}$$

The right-hand side of (52) is increased by replacing $\mathfrak{F}^+(u_2)$ by λ_0, i.e. infimum of $\mathfrak{F}^+(u)$. Hence:

$$\frac{1}{\lambda_2} \leqq \frac{1}{\lambda_0}\,.$$

Inverse of this inequality corresponds to the statement to be proved.

Theorem 9. *Be A, B, C operators satisfying conditions* (1.1) *to* (1.4). *Be $B = B_1 + B_2$. Let B_1 and B_2 as well as an operator B_3 have the same properties as operator B, i.e., let operators B_1, B_2, B_3 satisfy conditions* (1.2) *and* (1.4). *Also, let condition*

$$b_1 - b_2 + \sqrt{(b_1 + b_2)^2 + 4ac} \leqq 2b_3 \tag{53}$$

be satisfied for any $u \in D(A)$ where $b_i = (B_i u, u)$ $(i = 1, 2, 3)$. Denote by λ_1 the minimum (positive) eigenvalue of

$$Au - \lambda(B_2 + B_3)u = 0. \tag{54}$$

Now, inequality

$$\lambda_0 \geqq \lambda_1$$

holds.

Proof. Condition (53) leads to

$$\mathfrak{F}^+(u) \geqq \frac{a}{b_2 + b_3}\,. \tag{55}$$

Be $u = u_0$. Now, according to (4), (55) may be written as:

$$\lambda_0 \geqq \frac{(Au_0, u_0)}{((B_2 + B_3)u_0, u_0)}. \tag{56}$$

The right-hand side of (56) may be reduced by substituting λ_1, i.e. the infimum of the Rayleigh quotient $a/(b_2 + b_3)$ for $(Au_0, u_0)/((B_2 + B_3)u_0, u_0)$, whence the statement in the theorem follows.

5. Lateral buckling of a beam with forked support at both ends. Examples

Applications of the above theorems will be demonstrated on the lateral buckling of a thin-walled beam of constant, symmetric, open cross section with forked support at both ends, subjected to transverse forces (Fig. 1). In case of small displacements, the differential equation of equilibrium of the buckled beam is [2, 7]:

$$EJ_\omega \vartheta'''' - GJ_c\vartheta'' - \lambda\left[-(r - 2t)(M_{x1}\vartheta')' + (v - t)p_1\vartheta\right] - \lambda^2 \frac{M_{x1}^2}{EJ_y}\vartheta = 0, \tag{57}$$

under boundary conditions:

$$\vartheta(0) = \vartheta(l) = \vartheta''(0) = \vartheta''(l) = 0 \tag{58}$$

where

x, y, z co-ordinates (Fig. 1);
ϑ angle of rotation of the cross section;
t distance from the centroid to the shear centre;
r cross-sectional radius ($r = 1/J_x \cdot \int_F y(x^2 + y^2)dF$, where J_x is the moment of inertia of the cross section referred to the x-axis, and F the cross sectional area);
v distance from the centroid to the point of application of the load;
l span of beam;

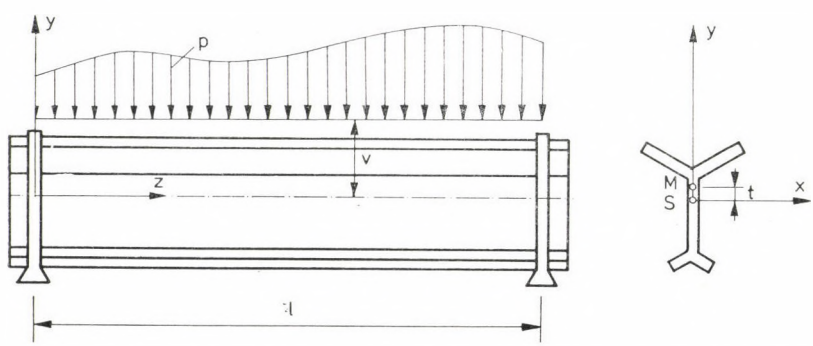

Fig. 1. Beam with forked support at both ends, and characteristic data

J_y moment of inertia of the cross section referred to the y-axis;
J_c torsional constant of the cross section;
J_ω warping constant of the cross section;
E modulus of elasticity;
G modulus of elasticity in shear;
λ load parameter;
p_1 load for $\lambda = 1$ ($p = \lambda p_1$);
M_{x1} bending moment in direction x due to load p_1
$(.)'$ d/dz symbol of differentiation with respect to variable z.

5.1 *Southwell's theorem*

Be the space $L^2\,[0, l]$ of real functions square integrable in the interval $[0, l]$ the Hilbert space H where scalar product of elements $\varphi, \psi \in L^2\,[0, l]$ is defined as:

$$(\varphi,\ \psi) = \int_0^l \varphi(z),\, \psi(z) dz\,.$$

Let us introduce notations

$$A_1\vartheta = EJ_\omega\vartheta'''', \tag{59}$$

$$A_2\vartheta = -GJ_c\vartheta'', \tag{60}$$

$$A\vartheta = EJ_\omega\vartheta'''' - GJ_c\vartheta'', \tag{61}$$

$$B\vartheta = -(r - 2t)(M_{x1}\vartheta')' + (v - t)p_1\vartheta, \tag{62}$$

$$C\vartheta = \frac{M_{x1}^2}{EJ_y}\vartheta. \tag{63}$$

With boundary conditions (58), differential expressions A_1, A_2, A, B, C denote differential operators satisfying conditions of Theorem 1. For a load applied above the shear centre, i.e., $v \geq t$, at the same time $2t \leq r$, or the beam cross section has two axes of symmetry, ($t = r = 0$), then operator B is a positive semi-definite. In this case, Theorem 2 is valid, stating

$$\lambda_0^2 \geq \lambda_1^2 + \lambda_2^2,$$

that is, the square of the critical load of the beam exceeds the sum of squares of critical loads calculated by reckoning either with the warping stiffness or with the torsional stiffness alone.

5.2 *Dunkerley's theorem*

Let us introduce notations

$$B_1\vartheta = -(r - 2t)(M_{x1}\vartheta')', \tag{64}$$

$$B_2\vartheta = (v - t)p_1\vartheta. \tag{65}$$

5.2.1. Operators A, B, C, B_1, B_2 defined by expressions (61), (62), (63), (64), (65), resp., satisfy conditions of Theorem 4, hence:

$$\frac{1}{\lambda_0} \leqq \frac{1}{\lambda_1} + \frac{1}{\lambda_2} \tag{66}$$

where λ_1 is the critical load parameter of the beam for $v = t$, i.e., where the load acts on the beam at the shear centre, λ_2 being the critical load parameter of a beam with a cross section of two axes of symmetry ($r = t = 0$) but all the stiffness data are the same as those of the reference beam, and so is the distance of the load application point from the shear centre (Fig. 2).

5.2.2. Be operator B_2 according to (65) positive, i.e., let the load act above the shear centre. Now, the conditions of Theorem 6 are satisfied, and — following a suggestion by KOLLÁR — the buckling load of the beam may be estimated as follows: Let us first determine the critical load of the beam for the case where the load acts at the shear centre ($B_2 = 0$, load position 1 in Fig. 3). λ_1 is the critical load parameter for this case. Thereafter the critical

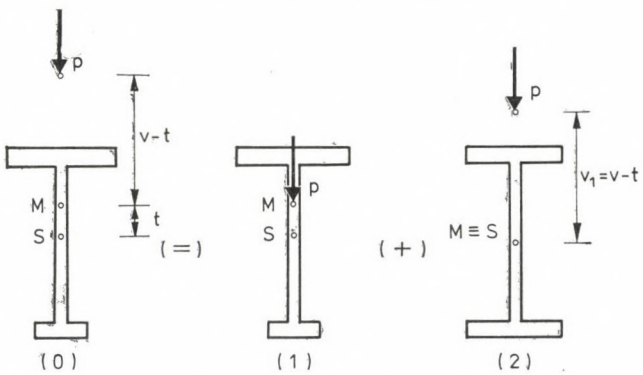

Fig. 2. Application of Dunkerley's theorem symmetrizing the beam cross section in imagination

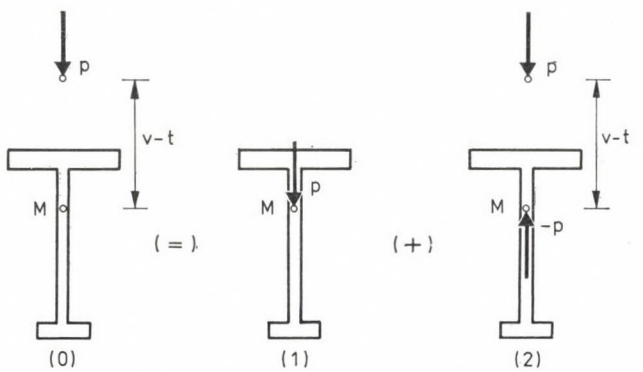

Fig. 3. Application of Dunkerley's theorem supporting the beam in imagination

load of the beam is determined for the case where, in addition to the load acting at the original point, another load of the same value, but of opposite direction, acts at the shear centre ($B_1 = 0$, $C = 0$, load position 2 in Fig. 3). This is equivalent to a hinged support of the beam along its axis passing through the shear centre. This support does not prevent beam deformations, the beam striving to rotate around this axis anyway. The critical load parameter for this case is λ_2. The critical load parameter λ_0 of the beam is subject to the inequality

$$\frac{1}{\lambda_0} \leq \frac{1}{\lambda_1} + \frac{1}{\lambda_2}.$$

5.2.3. Let the load system acting on the beam consist of n parts. Be p_{i1} the function of the basic value of the ith partial load and v_i the distance of its point of application from the centroid. Be the function of the basic value of the complete force system acting on the beam $p_1 = \sum_{i=1}^{n} p_{i1}$. Now, the application point of basic load p_1 is at a distance $v = \sum_{i=1}^{n} v_i p_{i1}/p_1$ from the centroid, and the bending moment in direction x due to load p_1 will be $M_{x1} = \sum_{i=1}^{n} M_{xi1}$ where M_{xi1} is the bending moment in direction x due to load p_{i1}. It should be noted that — as against Fig. 1 — distances v_i and v may vary along the beam.

Let us introduce notations

$$B_i\vartheta = -(r - 2t)(M_{xi1}\vartheta')' + (v_i - t)p_{i1}\vartheta \qquad (i = 1, 2, \ldots, n), \tag{67}$$

$$C_i\vartheta = \frac{M_{xi1}}{\sqrt{EJ_y}}\vartheta \qquad (i = 1, 2, \ldots, n), \tag{68}$$

and from (68):

$$C_i^2\vartheta = \frac{M_{xi1}^2}{EJ_y}\vartheta \qquad (i = 1, 2, \ldots, n) \tag{69}$$

where B_i and C_i^2 are operators under the validity of boundary conditions (58), satisfying conditions (1.2) to (1.4). Operator C_i is bounded and self-adjoint because of the boundedness of function M_{xi1}. Obviously,

$$B = \sum_{i=1}^{n} B_i \quad \text{and} \quad C = \left(\sum_{i=1}^{n} C_i\right)^2.$$

Thus, operators A, B, C, B_i, C_i and C_i^2 $(i = 1, 2, \ldots, n)$ defined by relationships (61), (62), (63), (67), (68) and (69), resp., satisfy conditions of Theorem 5, therefore, the critical load parameter λ_0 ($p_{kr} = \lambda_0 p_1$) of the complete force

system on the beam meets Dunkerley's formula

$$\frac{1}{\lambda_0} \leq \sum_{i=1}^{n} \frac{1}{\lambda_i} \tag{70}$$

λ_i being the critical parameter of the ith load ($p_{ikr} = \lambda_i p_{i1}$).

Relationship (70) contains critical load parameters rather than critical loads. This should be stressed, namely in case of concentrated loads, the two concepts often intermingle. In cases under 5.1, 5.2.1 and 5.2.2, only little trouble arises from an indistinct handling of the concepts, since in partial problems the basic load values are invariable. Not loads, but beam properties are modified. Actually, however, the beam is the same in any partial problem, but the basic value of partial loads differ for each partial problem. Not the beam, but the loads are modified.

The error due to exchanging the two concepts will be illustrated in a simple example. Let a I-beam of bisymmetrical cross section, with a forked support at both ends, be subjected to a single concentrated load at a point of the span. Let the buckling load value be assumed as being known for the two cases of application on the upper and on the lower flange. Let us estimate the ciritcal value of the load acting at the centroid of the cross section. Let us denote the critical value, the basic value, and the critical parameter, of the load acting at the centroid, the upper flange and the lower flange by P_{kr}, P_{1kr}, P_{2kr}; P_1, P_{11}, P_{21} and λ_0, λ_1, λ_2, respectively. Be $P_1 = 1$. Resultant of forces P_{11} and P_{21} acts at the centroid and equality $P = P_{11} + P_{21}$ holds if $P_{11} = P_{21} = 1/2$. Now $P_{kr} = \lambda_0$, $P_{1kr} = \lambda_1/2$, $P_{2kr} = \lambda_2/2$ and

$$\frac{1}{P_{kr}} = \frac{1}{\lambda_0} \leq \frac{1}{\lambda_1} + \frac{1}{\lambda_2}. \tag{71}$$

Replacing critical load parameters by critical load values in (71) leads to

$$\frac{1}{P_{kr}} \leq \frac{1}{P_{1kr}} + \frac{1}{P_{2kr}} = \frac{2}{\lambda_1} + \frac{2}{\lambda_2}$$

yielding for the critical force wanted, half the value of that given by the correct relationship (71).

5.3 *Replacement of a given load type by another one*

No solutions have been published on the lateral buckling of beams with a forked support, except for some special load cases. Practically, however, several load systems different from those in question are encountered. Let

us determine the buckling load of a beam loaded in a different manner, by means of a load type of known solution, at an approximation on the safe side. One load type will be replaced by another one.

The lateral buckling equation of a beam under the examined load type will be:

$$A\vartheta - \lambda B\vartheta - \lambda^2 C\vartheta = 0,$$

where A, B, C are operators defined by (61), (62), (63), respectively. The lateral buckling equation of the substituting beam of known critical load will be:

$$A\vartheta - \lambda B_1\,\vartheta - \lambda^2 C_1\vartheta = 0,$$

where

$$B_1\vartheta = -(r - 2t)(\overline{M}_{x1}\vartheta')' + (\bar{v} - t)\,\bar{p}_1\vartheta, \tag{72}$$

$$C_1\vartheta = \frac{\overline{M}_{x1}^2}{EJ_y}\,\vartheta \tag{73}$$

where $\bar{p}_1$ is the basic value of the substituting load, $\overline{M}_{x1}$ the bending moment in direction x, and $\bar{v}$ the distance from centroid to the point of application. Be λ_0 and λ_1 the critical load parameters of substituted and substituting load, resp. In order to meet inequality

$$\lambda_0 \geqq \lambda_1$$

fulfilment of condition (45) is needed, in conformity with Theorem 7. (Namely operators A, B, C, B_1, C_1 satisfy conditions (1.1) to (1.4)). Obviously, condition (45) is always satisfied for any $\vartheta \in D(A)$, $(C_1\vartheta, \vartheta) \geqq (C\vartheta, \vartheta)$ and $(B_1\vartheta, \vartheta)/(C_1\vartheta, \vartheta) \geqq (B\vartheta, \vartheta)/(C\vartheta, \vartheta)$. Beams of a bisymmetrical cross section always satisfy these conditions, if e.g., on the one hand, moment diagram $\overline{M}_{x1}$ of the substituting basic load fully contains the moment diagram M_{x1} of the substituted basic load, on the other hand, the specific torque $\bar{v} \cdot \bar{p}_1$ calculated from unit twist of the substituting basic load $\bar{p}_1$ exceeds the product of the specific torque $v \cdot p_1$ for the substituted basic load by a constant not less than the supremum of the quotient $(C_1\vartheta, \vartheta)/(C\vartheta, \vartheta)$. For $\lambda_1 = 1$, that is, if basic value of the substituting load is thus assumed as to put the beam into an indifferent state of equilibrium, $\lambda_0 \geqq 1$. It means that the critical value of the substituted load is not less than the basic value p_1.

5.4 *Reduction of critical load by additional supports*

Cases are known to exist [1] where critical loads of a beam decrease in spite of an increased number of supports. An example of I-beams with hinged cross section and torsion-free flanges (trusses) was discussed in [8].

The following will be a rather general treatment of the problem of the variation of the critical lateral buckling load of a thin-walled beam of symmetric, open, and indeformable cross section with a forked support at both

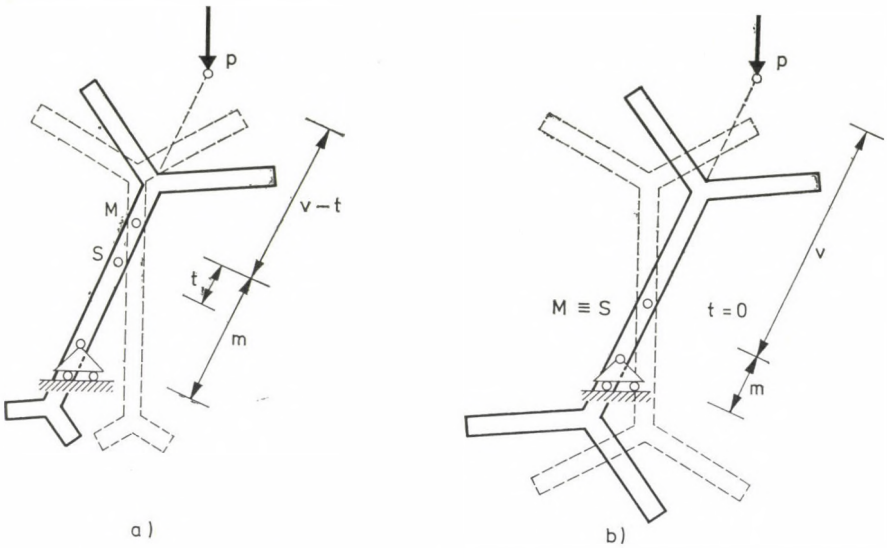

Fig. 4. Cross section of the beam supported on rollers all along its length: *a)* symmetrical cross section; *b)* bisymmetrical cross section

ends, under transverse loads, when the beam is supported by rollers all along an axis in the plane of symmetry, parallel to the centroidal axis. This constraint permits rotation and lateral displacement of beam cross sections but prevents vertical displacement (Fig. 4).

For the sake of simplicity, first, constant beam cross sections with *two axes of symmetry* will be considered (Fig. 4b). Now, operator B_1 according to (64) is zero. Lateral buckling equation of the beam with no roller support takes the form:

$$A\vartheta - \lambda B_2\vartheta - \lambda^2 C\vartheta = 0 \tag{74}$$

where operators A, B_2, C are defined by expressions (61), (65), (63), respectively. Supporting the beam on rollers along the longitudinal axis passing through the shear centre because of $M_{x1} = 0$ will cause the lateral buckling equation to have the form:

$$A\vartheta - \lambda B_2\vartheta = 0. \tag{75}$$

Let a load be applied above shear centre i.e. be B_2 a positive (definite) operator; since $B_1 = 0$, hence $b_1 = 0$, condition (50) is satisfied. According to Theorem 8:

$$\lambda_2 \geqq \lambda_0,$$

i.e. the roller support raised the critical load of the beam (λ_0 and λ_2 being ciritcal load parameters of beams without, and with roller support, respectively).

Assuming the roller support to be below the shear centre, the equation of equilibrium of the beam in laterally buckled state will be:

$$A\vartheta - \lambda(B_2 + B_3)\vartheta = 0 \tag{76}$$

where

$$B_3\vartheta = mp_1\vartheta \tag{77}$$

where m is the distance between the shear centre and the support (Fig. 4)· (m is positive if the support is below the shear centre.) Assuming the support to be ever deeper below the shear centre, then operator B_3, i.e. distance m may have a value m_0 beyond that m satisfies condition (53). Then Theorem 9 implies that the minimum positive eigenvalue λ_0 of (74) exceeds the minimum (positive) eigenvalue λ_1 of (76), that is, the beam with an unsupported flange has the higher critical load, hence, in spite of the additional support, the critical load decreases.

Assuming a uniformly distributed load and a constant load application point ($v = \text{const.}$), let us determine an m_0 value, beyond that the roller support destabilizes, and below that, stabilizes the beam equilibrium. No stipulation is made on the sign of v. The load may act either at, or below, or over the shear centre, deduced relationships remain valid. The following will not be restricted in the case of a bisymmetrical beam cross section. In general, the beam cross section is assumed to have a *single axis of symmetry* (in the direction of the external loads, Fig. 4a).

Lateral buckling equation of the unsupported beam is:

$$A\vartheta - \lambda(B_1 + B_2)\vartheta - \lambda^2 C\vartheta = 0, \tag{78}$$

and of the supported one:

$$A\vartheta - \lambda(B_2 + B_3)\vartheta = 0 \tag{79}$$

where A, B_1, B_2, B_3, C are operators defined by expressions (61), (64), (65), (77), (63), respectively. Be $p_1 = 1$. Now, $B_2 = v - t$, $B_3 = m$. Eq. (79) has positive eigenvalues if $v - t + m > 0$.

Obviously, the minimum positive eigenvalue of (79) is

$$\lambda_1 = \frac{\lambda_A}{v - t + m}, \tag{80}$$

where λ_A denotes the minimum (positive) eigenvalue of operator A according to (61). Let us find the supporting depth value $m = m_0$ where the critical loads of supported and unsupported beams are equal, i.e., where λ_1 equals the minimum positive eigenvalue λ_0 of (78). From (80) and from equalities

$\lambda_1 = \lambda_0$ and $m = m_0$ it ensues:

$$m_0 = \frac{\lambda_A}{\lambda_0} - v + t, \tag{81}$$

the distance m_0 sought for. If the exact value of λ_0 is missing, then m_0 may be estimated as follows. In the actual case, $B = B_1 + B_2$ and $b = b_1 + b_2$ hence, from Eqs (2) and (4):

$$m_0 \geqq \frac{b_1 + b_2 + \sqrt{(b_1 + b_2)^2 + 4ac}}{2a} \cdot \lambda_A - v + t, \tag{82}$$

where

$$a = (A\vartheta, \vartheta), \tag{83}$$

$$b_1 = (B_1\vartheta, \vartheta), \tag{84}$$

$$b_2 = (v - t)(\vartheta, \vartheta), \tag{85}$$

$$c = (C\vartheta, \vartheta). \tag{86}$$

Let ϑ_A denote the eigenelement corresponding to the minimum eigenvalue λ_A of operator A according to (61). Clearly:

$$\lambda_A = EJ_\omega \left(\frac{\pi}{l}\right)^4 + GJ_c \left(\frac{\pi}{l}\right)^2, \tag{87}$$

$$\vartheta_A = \sin \frac{\pi z}{l}. \tag{88}$$

Be $\vartheta = \vartheta_A$. Now — since $M_{x1} = (z/l)(l - z)$ — according to [7], (83), (84), (85), (86) become:

$$a = \lambda_A \cdot \frac{l}{2}, \tag{89}$$

$$b_1 = (r - 2t)l \frac{\pi^2 - 3}{24}, \tag{90}$$

$$b_2 = (v - t) \cdot \frac{l}{2}, \tag{91}$$

$$c = \frac{l^5}{16\, EJ_y \pi^4} \cdot \frac{\pi^4 + 45}{15}. \tag{92}$$

Substituting (87), (89), (90), (91), (92) into (82) yields for m_0 the lower bound:

$$m_0 \geqq \frac{1}{2}\left\{(r - 2t)\frac{\pi^2 - 3}{12} - v + t + \left\{\left[(r - 2t)\frac{\pi^2 - 3}{12} + v - t\right]^2 + \right.\right.$$

$$\left.\left. + \frac{EJ_\omega + GJ_c (l/\pi)^2}{EJ_y} \cdot \frac{\pi^4 + 45}{30}\right\}^{\frac{1}{2}}\right\}.$$

Finally, it should be mentioned that from Eqs (80) and (81) it is directly recognized that $\lambda_0 \leqq \lambda_1$ for $m \leqq m_0$, and $\lambda_0 \geqq \lambda_1$ for $m \geqq m_0$.

REFERENCES

1. BARTA, J.: Über stabilisierende und destabilisierende Wirkungen. *Acta Techn. Hung.* **68** (1970), 311—317
2. CHWALLA, E.: Kippung von Trägern mit einfach-symmetrischen, dünnwandigen und offenen Querschnitten. *Sitzungsberichte der Akademie der Wissenschaften Wien IIa*, **153** (1944), 47—60
3. DUNKERLEY, S.: On the Whirling and Vibration of Shafts. *Philosophical Transactions of the Royal Society of London. Ser. A.* **185** (1894), 279—360
4. JEFFCOTT, H. H.: The Periods of Lateral Vibration of Loaded Shafts. — The Rational Derivation of Dunkerley's Empirical Rule for Determining Whirling Speeds. *Proceedings of the Royal Society of London. Ser. A.* **95** (1919), 106—115
5. LAMB, H.— SOUTHWELL, R. V.: The Vibrations of a Spinning Disk. *Proceedings of the Royal Society of London. Ser. A.* **99** (1921), 272—280
6. SOUTHWELL, R. V.: On the Free Transverse Vibrations of a Uniform Circular Disc Clamped at its Centre; and on the Effects of Rotation. *Proceedings of the Royal Society of London. Ser. A.* **101** (1922), 133—153
7. TARNAI, T.: Lateral Buckling Analysis of Beams by the Theory of Quadratic Operator Pencils. *Acta Techn. Hung.* **87** (1978), 233—254
8. TARNAI, T.: Lateral Buckling of Plane Trusses with Parallel Chords, Hinged Joints, Simple Forked Support at Both Ends. *Acta Techn. Hung.* **87** (1978), 425—439
9. TEMPLE, G.: The Computation of Characteristic Numbers and Characteristic Functions. *Proceedings of the London Mathematical Society. Ser.* 2. **29** (1929), 257—280
10. ZAANEN, A. C.: Linear Analysis. North-Holland Pub. Co. Amsterdam 1960

Über die Verallgemeinerung der Theoreme von Southwell and Dunkerley für quadratische Eigenwertaufgaben. In diesem Aufsatz wird die Näherungsberechnung des kleinsten Eigenwertes positiven von quadratischen Eigenwertaufgaben mit reellem Spektrum behandelt. Es wird untersucht, wie untere Schranken für den gesuchten Eigenwert gegeben werden können, bzw. wie sich eine gegebene Aufgabe auf einfachere Aufgaben zurückführen läßt. Die Theorems von Southwell und Dunkerley werden verallgemeinert, dann weitere, untere Annäherungen ergebende Zusammenhänge deduziert. Die Anwendung der erhaltenen Ergebnisse wird an Trägerkippungsaufgaben veranschaulicht.

Acta Technica Academiae Scientiarum Hungaricae, Tomus 91 (1—2), pp. 225—240 (1980)

JOHN CSONKA AND THE PRECISION MACHINE INDUSTRY OF HUNGARY

P. VAJDA*

[Manuscript received March 5, 1980]

John CSONKA is generally known to have been together with Donát BÁNKI the original inventor of the modern carburetor for the gasoline engines. His great pioneering achievements in the national automobile and general manufacturing industries are fully acknowledged in his biographies and the popular literature. His work as designer and independent manufacturer left an important mark on the Hungarian machine industry. As a teacher of machine shop skills and practice he maintained an exceptionally high standard which in many respects was higher than could typically be found in the colleges of that period.

Biography

John CSONKA was born on January 22, 1852 in Szeged, Hungary into a family of noted craftsmen. His father, Vincent TSONKA was a well-known mechanic and the last Master of the Guild of Mechanics and Smiths, in whose shop every kind of machines and instruments than in use, were made. Father Vincent directed his workshop in the old-fashioned patriarchal manner. No doubt, John was greatly influenced by this approach and also acquired his basic technical knowledge there. After the elementary school years his ambitious father enrolled him in a high-school and simultaneously took him into his workshop. When the work in this rather agricultural community became too narrow for John, he obtained employment in the shop of the Szeged-Fiume Railway in his home town and later in the round-house shop of the Hungarian National Railways in Budapest, the country's capital. Here, indeed he could acquire knowledge referring to current machine shops. In 1874 he undertok a long trip abroad studying in Vienna, Korneuburg, St. Poelten, and in 1875 in Paris. It must have been of extraordinary importance for him that in Paris he could familiarize himself with the Lenoir gas engine which was already in widespread use in France. From there he moved to England then returned to Paris again. Finally in 1877 after stopping in Zurich, Milano and Vienna, he returned to Hungary.

* Dr. P. VAJDA, Alkotás u. 1/a, H-1123 Budapest, Hungary.

While these studies abroad represented much hardship and sacrifice, it was mainly due to the experience that out of the thirty-two applicants and even having given in his application after the closing date, that on February 11, 1877 he, the youngest applicant was appointed as instructor-manager of the machine shop of the Department of Mechanical Engineering at the Technical University of Budapest. In order to improve the quality of teaching from the beginning, he introduced the employment of fully qualified machineshop personnel as instructors, who could guide the students, plus carry out practical machine shop work. John Csonka remained in this teaching position for forty-eight years and during this line two generations of mechanical engineers were brought up.

During the great changes and rapid development of technology it proved that in the management of a mechnical workshop theoretical knowledge is not sufficient, but well founded practical experience is also absolutely necessary for the production of quality goods. To be able to compete on the world market this is essential both in respect to the quality of the goods and their cost. He quickly realized, that next to the work at the drafting board the need for precise estimates, the planning and organising of the production are the basis of a prosperous undertaking.

Today all this is generally recognized, and in fact, it became the subject of an independent detailed branch of engineering. The trained worker fully accepts the need of leadership by a qualified mechanical engineer and the best results can only be achieved by such cooperation.

The particular value of John CSONKA's sixty years of teaching is the realization of this change in shop management, and that, decade after decade he put these principles into practice.

Before retiring from his teaching post at the Technical University he had established five basic shop machines: a lathe, a milling machine, a drill-press, a shaper, and a sawing machine. In 1925 he installed these machines in the basement of the apartment house (at 31 Béla Bartók Street), Budapest and started his own independent machine shop. He did this as his son, Prof. Dr. Paul CSONKA later quoted about him: "without financial backing but with a great deal of moral capital". First he did repair work only, but soon he was able to turn to his favorite field, the manufacturing of engines. In the middle of the nineteen thirties a much larger shop was established on the Budafoki Street. During his last year, in 1939, with considerable increase in work volume and facilities his thoughts turned to a properly designed factory building. By this time he employed three hundred skilled workers including many mechanical engineers. He did not live to be present at the inauguration, of the new plant. Even right before being taken to the hospital he completed the design of a new small engine, which in fact was later put on the market. He passed away on October 27, 1939 — after only two weeks illness at the

hospital. The John Csonka Machine Factory, Inc. (Csonka János Gépgyára, R.T.) and its successor, The Small Engine and Machine Factory, Inc. are carrying on the spirit of the Founder.

Gas and petroleum engines

Already as a young man, John CSONKA could foresee the great future of the internal combustion engine as the generator of mechanical power. At the World Fair of 1878 in Paris seventy-five gas engines of various construction were exhibited by thirty-two manufacturers. The ancestor of those engines was the Lenoir engine of 1860, a type operated without compression. This was followed by various other compressionless engines of similar design, like those of HUGON, BISSHOP, AIMULLER, GILLES, LANGEN—OTTO and others. All these atmospheric engines became obsolete when BRAYTON's compression engine (USA 1873) made its appearance. The first four-stroke compression engine of the new era was produced by OTTO in 1878. The "petroleum motor" as it was called in those days, became widely used in the nineties. For the training shop of the Technical University CSONKA first made some water-column machines. Later he replaced them by a vertical cylinder steam engine. Finally, after recognizing the many short-comings of the Langen—Otto gas-engine, the Swidorski petroleum engine and of the slide-valve governed engine, he himself designed and produced his own engine: *the very first Hungarian gas engine*. This indeed was a remarkable accomplishment both in respect to the design and of the actual building of the engine: particularly since only very poor shop facilities were available to him. In this way he became *one of the very first pioneers of the gasoline engine.*

CSONKA's next triumph was the creation of an engine which could be operated on two different fuels, either by city-gas or kerosene. This again was an original invention both in design and concept. He designed this engine in 1882 and built it in the following year. His patent application was filed on November 26, 1884 under the title "Gas and Petroleum Motor". The significant novelty and improvement in this engine was the exclusive application of poppet valves. This solution had not only a definite price adventage over the slide valve governed approach, but was also easier and cheaper to produce and repair. It not only eliminated the need for lubrication, but also made a higher compression possible. The effect of the inlet and exhaust poppet valves was excellent. It was DAIMLER who first recognized the superiority of this design. The other manufacturers, like OTTO and BENZ, retained the old method: the slide valve control, which was an inheritance from the steam engine. However, by the end of the century the new solution was generally accepted by most manufacturers.

The ignition was carried out by a governed circuit breaker, and was later replaced by the more practical Bosch ignition system. Though electric devices were an almost unknown area for most mechanics in those days, this somewhat complicated ignition system, if kept clean and properly maintained, worked very well. On the CSONKA engine, the suction was governed by a centrifugal regulator which assured the even running of the engine.

By the simple turning of two valves, the fuel could be changed from city gas to kerosene. This was made possible by using the exhaust gases for increasing the temperature of the "petroleum" rendering it more volatile. In those early years, city gas was used mainly for illumination, and it happened that sometimes during the day — the gas supply was discontinued. One can see the great advantage of being able to change the fuel from gas to kerosene. There was no other engine on which this fuel change could easily be made. The engines on market ran either on gas or on kerosene. With this important feature, the Csonka engine was more advanced than any other design. The emphasis here was on the easy conversion from one fuel to the other. In principle, any gas engine could be operated on kerosene, with the help of a fuel evaporator. As early as 1862 it was demonstrated that the Lenoir engine could be made to run on kerosene, but it was complicated and unreliable. A great number of patents were obtained for such "vaporizers", but not one of them proved to be of practical value.

Comparing it to the other engines of those years, the Csonka engine was definitely the best engine, and in fact, it compared favourably with all other four-stroke engines. CSONKA independently solved the problem of the construction of an engine, and the problem of changing the fuel from gas to kerosene

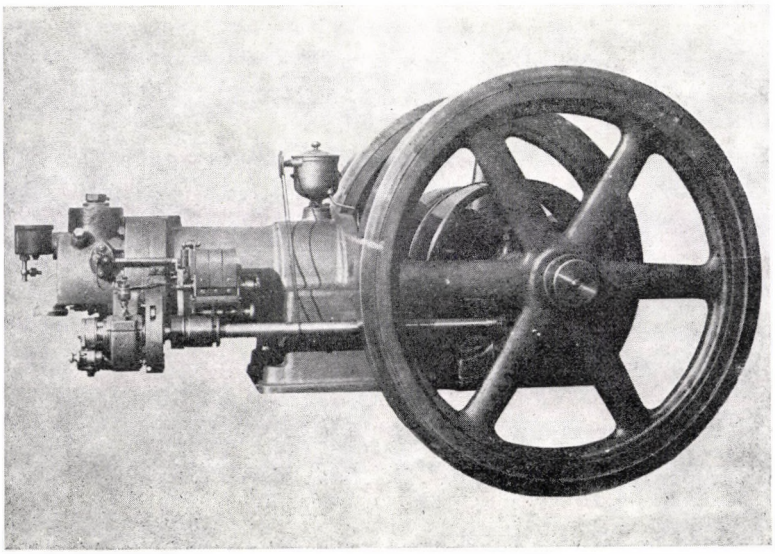

in an original and unique way. Even in its outer appearance, the valve engine came the nearest to the later developed internal combustion engines.

In order to be able to appreciate the importance of John CSONKA's great accomplishments, a few words are needed to explain the technical development during his life. The last third of the nineteenth century was an extraordinary period of prosperity all over Europe, as well as in Hungary. The Hungarian machine industry was still in its infancy. The industrial statistics of 1884 give a few typical figures. In this country, girded by the Carpathian Mountains, only 3414 plants had a mechanical power source. Of these, — 92% were steam engines amounting to sixty-four thousand H. P. (In France the total amounted to 683 000 H.P., and in Germany over a million.) Only twelve thousand workers were employed in mechanized factories, and only 5,4% of the population was employed in industry. Out of those industries, 63% were operated solely by the owner, 33,7% had one to five employees and a meager 2,5% had more than five employees. Consequently, the workshop at the Technical University with as many as twenty-five employees was of considerable size for those time. Apart from actual teaching hours, CSONKA used his team for regular production. Considering the great amount of work and care involved in designing and building internal combustion engines, one can appreciate CSONKA's outstanding accomplishment over the many years in carrying out this work single-handed, and under pioneering conditions. In addition, he also had to train his workers in this new field, including the casting of the parts which they mostly carried out themselves.

The Bánki—Csonka engine and the carburetor

By this time CSONKA's name was well-known in his country. He sold the license for his patented engine to the big machine plant: Ganz & Co. Budapest. At that time Ganz was overrun by orders. Therefore, CSONKA produced his own engines for Ganz & Co. which were sold as: "Ganz engines". In 1887 Andreas MECHWART, president of the Ganz Company asked him to join their staff with the assignment to redesign the engines of the recently acquired "Leobersdorf Motor Factory". This project was started by a young Ganz engineer, the brilliant Donat BÁNKI who was obtaining minimal result because of inadequate facilities at the Ganz plant. MECHWART agreed to the transfer of two engines to CSONKA's shop at the Technical University in Budapest. This began the very successful cooperation of many years between CSONKA and BÁNKI which resulted in several important joint patents. These included a number of innovations on gas and kerosene engines and their control mechanisms. (January 19, 1888. Vd. XXII. No. 1889: Improvements on Gas Engines; April 11, 1888. Vd. XXII. No. 1581: Control Mechanism on Four-

Stroke Kerosene Engines and the same in Germany, DRP No. 51854. April 11, 1889.)

The engines redesigned and produced for Ganz Co. were named "Ganz engines" with the patent of BÁNKI—CSONKA clearly indicated on them. These engines were not identical with the later marketed famous "Bánki—Csonka engines" which were the first industrially produced engines in Hungary. These were four-stroke, watercooled, Otto-cycle ones. The horizontal engines put out 1 to 8 H.P., and the output of the vertical designs was 6 to 30 H.P. The central axis of the cylinder at this engine did not meet the center of the driving shaft. Through this construction, the higher jacket pressure of the piston during expansion was considerably reduced. The intake and the exhaust were

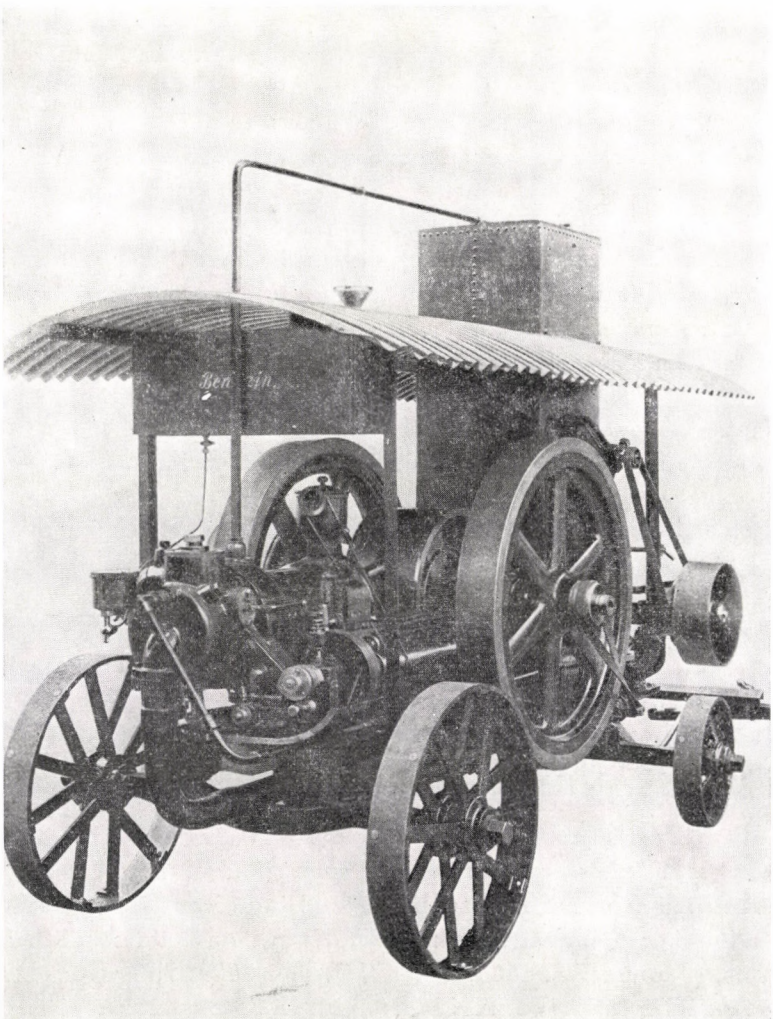

governed by poppet valves. This was definitely a great improvement over the sliding valve method, which had been adapted from the steam engine. It took some time, however, before the poppet valve generally replaced the old system.

On the horizontal engines up to 6 H.P. and on the two cylinder vertical engines up to 16 H.P. an automatic intake valve system was used. Larger engines were equipped with controlled intake valves. The exhaust valve was of the "hit and miss" governing type described in the Bánki—Csonka patent. These engines used the closed ignition tubes first, automatic up to 1 H.P. and was governed on the higher output engines. The very reliable closed ignition tube was indeed a truly important innovation and up to the time of the later

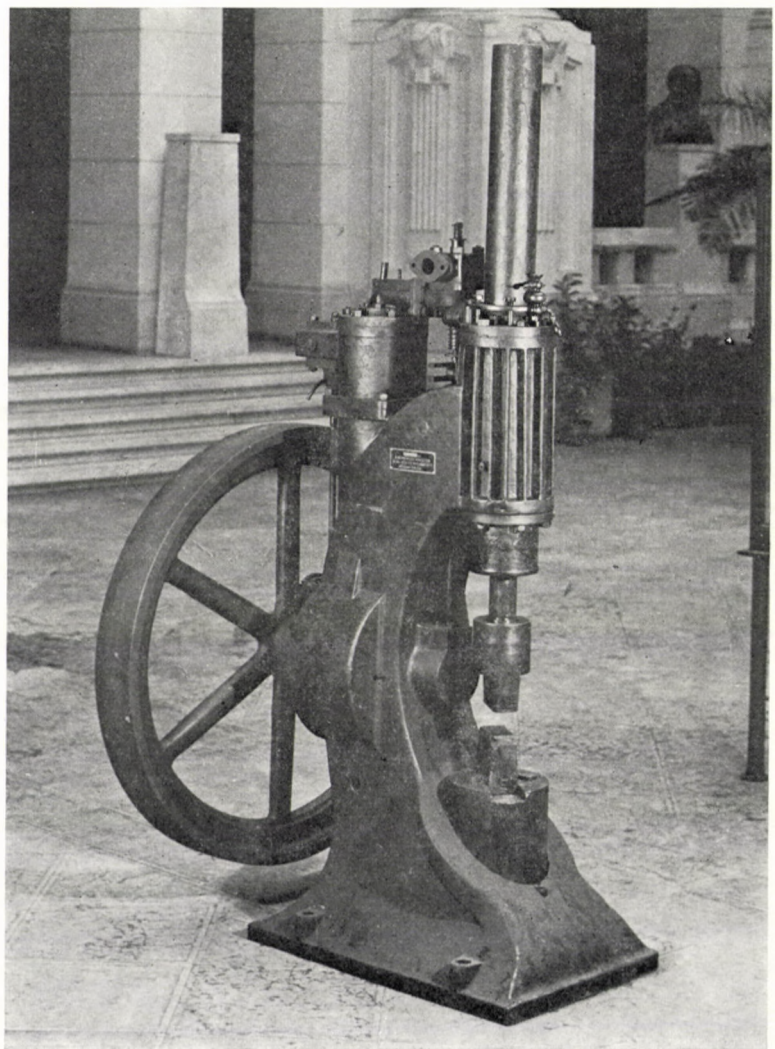

electric ignition systems was almost universally used. These engines were very reliable and their fuel economy was bout 20 % better than the original engines made by OTTO, commonly used in other countries.

The high explosion pressure of these engines found further application in operating mechanical hammers. The basic idea was drawn from the design of the Robson gas hammer, but its automatic independent construction was far superior to it. This engine was capable of carrying out two different functions. It could drive the transmission system of a shop, and could also be used as a forging hammer. The complicated foreign forging machines gradually disappeared from the market, but the Bánki—Csonka gas hammer made by

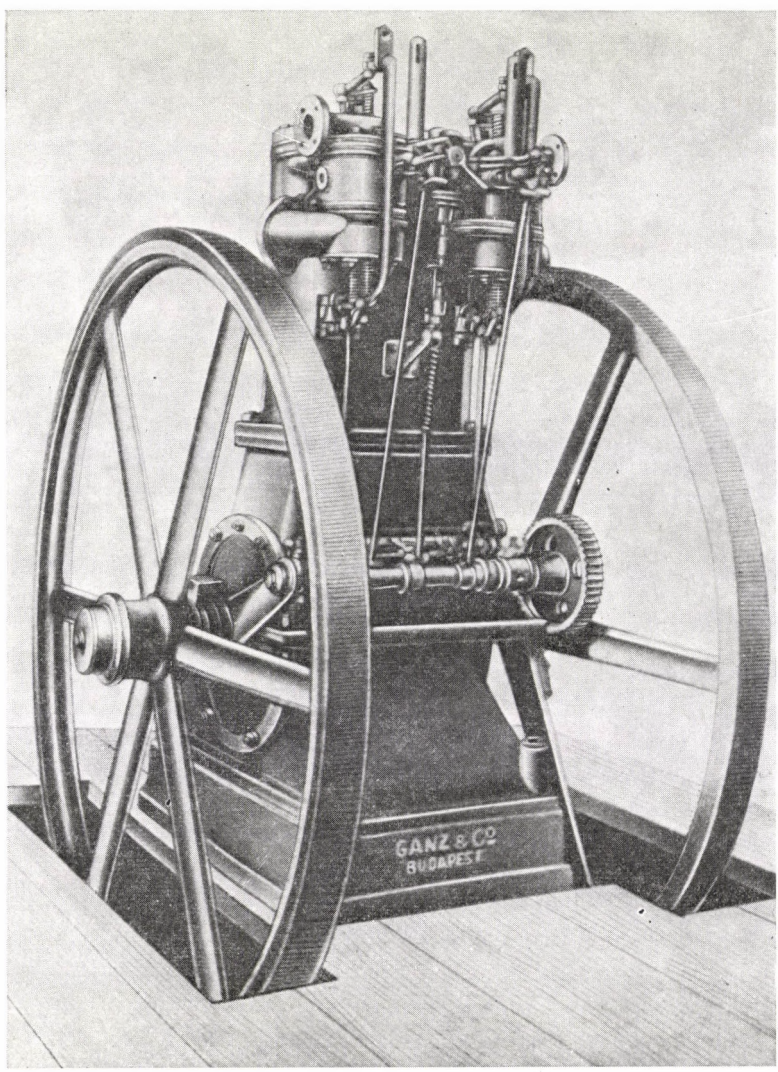

the Ganz Factory in Budapest, and later by the Berlin-Anhaltische Maschinenbau A.G. — also, remained the much sought for engine and hammer, for several decades. The first 2 H.P. hammer was regularly marketed by the Ganz Factory in Hungary and later by other factories in Germany as well.

After this most successful undertaking, CSONKA and BÁNKI turned their attention to the construction of small engines for industrial and agricultural purposes. Based on their joint design, CSONKA built the first 3/4 H.P. experimental engine which became the prototype of all later Bánki—Csonka engines.

After a long search, fifty years later, this first experimental engine with its flame ignition tube and the world's first atomizing carburetor was found in

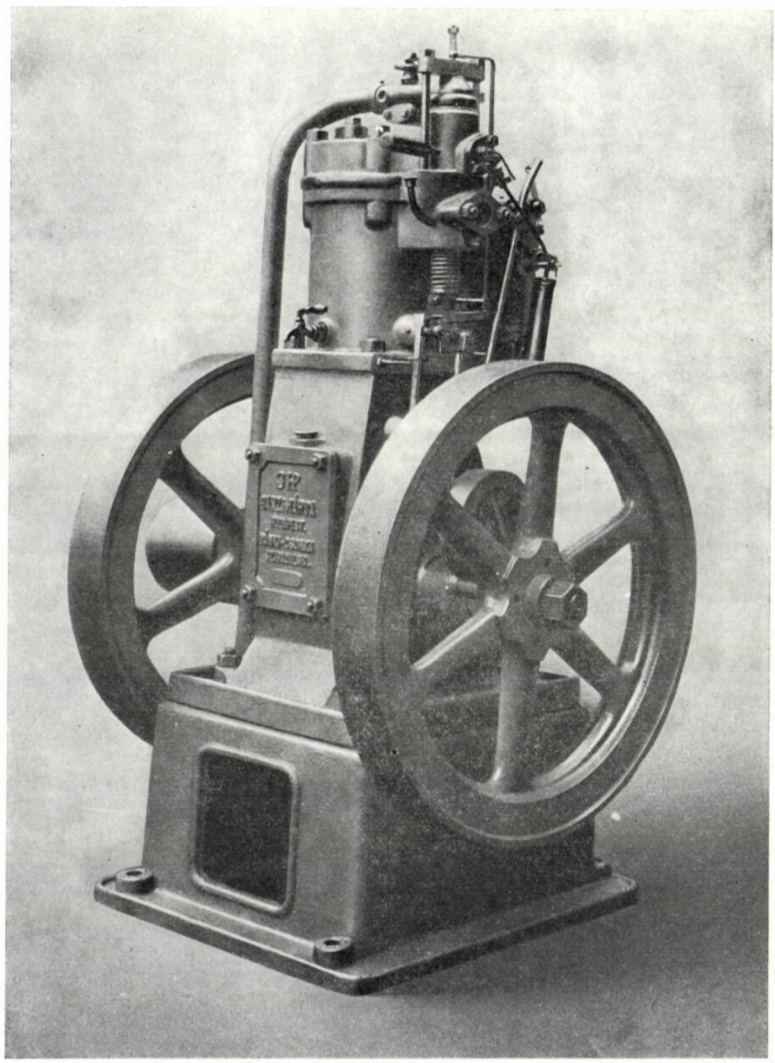

the shop of its twelfth owner still in regular use. The former owners sold it when their shop became larger, and they purchased larger engines. It was the same engine which was exhibited in its final form in —1891. Soon engines with further improvements were rapidly becoming popular in Hungary, manufactured by Ganz factory and marketed under the name "Bánki—Csonka engine". They were vertical engines with closed crank shaft and with an open flame red hot ignition tube. An engine with further improvements which was exhibited in 1893 became even more popular and was widely used in Hungary for the next 20÷30 years. We quote from one of its appraisers: ". . . this engine is an outstandingly successful Hungarian invention, second to none of the famous engines of its class abroad."

As stated before, the best known invention of the two brilliant inventors "the atomizing carburetor" made its first appearance on the Bánki—Csonka engines. The formation of a fuel spray by a rapid airstream was John CSONKA's idea. It is described in detail in the patent application (submitted February 11, 1893) for the engine and all its components. An independent carburetor application was made on October 18, 1893. In the literature of technical history the name of W. MAYBACH is usually given as the first inventor of the atomizing carburetor and the date of his patent application is given as August 17, 1893. The "priority" of MAYBACH is a mistake. Not only was the patent application of BÁNKI and CSONKA submitted a half year earlier, but in fact their engine with a perfectly well functioning carburetor was publicly exhibited earlier, in 1891. According to Oscar GLATZ, a foreman of CSONKA, who was still alive in 1941, the carburetor was completed after a year and half experimenting and preparatory work including the carburetor's float-valve chamber and the float-valve fuel level control by the autumn of 1891. He was able to pinpoint this time so accurately from memory since it was in the autumn of 1891 that Oscar GLATZ was called up for military service and by then, with the carburetor satisfactorily completed, the two inventors had already turned their attention to the improvement of the ignition system.

We can see that the design described in the patent application of February 11, 1893 is in fact the basic construction of the modern carburetor now used and manufactured in great number. The description and the drawings attached clearly show even the arrangement of the parts as it is used today.

The Ganz factory bought the patents of the Bánki—Csonka engine together with that of the fuel level controlled carburetor. Unfortunately, the patent clerk of the Ganz factory on one occasion failed to pay the required annual fee to the Patent Office and the patent-protection expired. By the end of the century the French produced such carburetors by the hundred thousands.

As referred to before, it was only on August 17, 1893 that MAYBACH applied for the French patent (Brevet No. 232230), six month after the application of BÁNKI and CSONKA. MAYBACH's description is similar to the Bánki—

Csonka's patent of February 1893. In spite of this it is astonishing and regrettable that BÁNKI and CSONKA are not generally known as the inventors of the carburetor.

Since CSONKA's first engine the theory and practical knowledge concerning the internal combustion engine have enormously developed, BÁNKI himself carried out a great deal of pioneer theoretical work. He achieved the first results while a student at the Technical University to Budapest. Soon attention turned more and more to the theory of the internal combustion engines. In Germany alone, twenty-five factories made "kerosene" (later gasoline) engines, during the early nineties. In the description of these engines it was emphasized that kerosene distilled for illumination, is not flammable and is not hazardous, it does not even burn without a wick. But the later engines used gasoline more and more . . . that meant an explicit danger. Fortunately the inventors of the carburetor found, the gasoline can be harmlessly atomized in the carburetors. So the gasoline which was first considered as a very harmful "worthless" byproduct, now was quite commonly used.

At this stage it was not any longer sufficient that the engine should run reliably with speed regulation and moderate fuel consumption. It became a matter of great importance that agricultural workers with no mechanical knowledge should be able to operate it. With its low fuel consumption, extreme durability, minimal repair requirements, the Bánki—Csonka engines were among the bests on the market, in spite of the great competition and the high quality of the German products. In one of the descriptions of Ganz these engines were stated without any reservation as being the best on the market. The Ganz factory had very definite advantages: BÁNKI was an outstanding theoretician and CSONKA was able to turn their ideas into realization amazingly fast. In this way the Bánki—Csonka engines were always up-to-date and

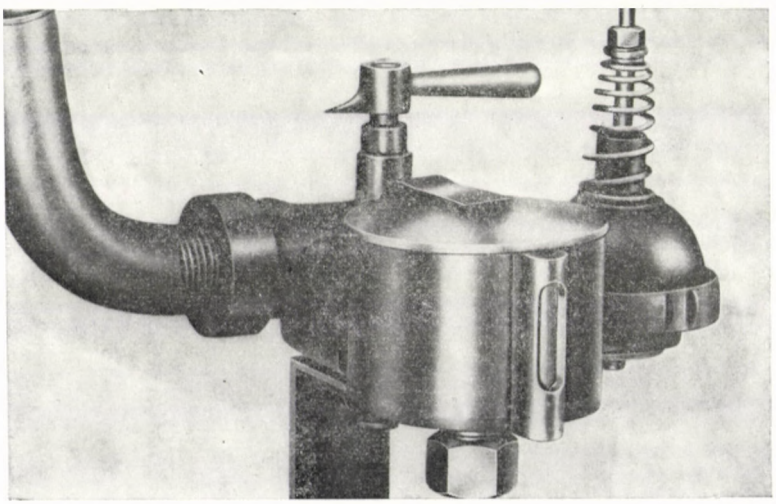

ahead of the heavy foreign competition. Comparing the highly advanced engines of BÁNKI and CSONKA many other contemporary engines were rather outdated.

Motorized vehicles and automobiles

Early in the century the activity of John CSONKA took a new direction. The Hungarian Postal Services invited bidders for the building of twenty-two, three-wheeler postal vehicles. Twenty original De Dion-Bouton made units were purchased from the Velodrom Automobil Garage and two from the Ganz factory. Ganz used the design and construction of CSONKA. He made the engines himself at the Technical University. These tricycles gave excellent service for over two decades. In fact, these were the world's first motorized postal vehicles. According to the book: Henry's Wonderful Model "T", the American Postal Service started by using motorized vehicles only in 1917 and 1918.

While the cooperation between CSONKA and BÁNKI had proved itself most successful, later the two engineers followed different interests. In 1902

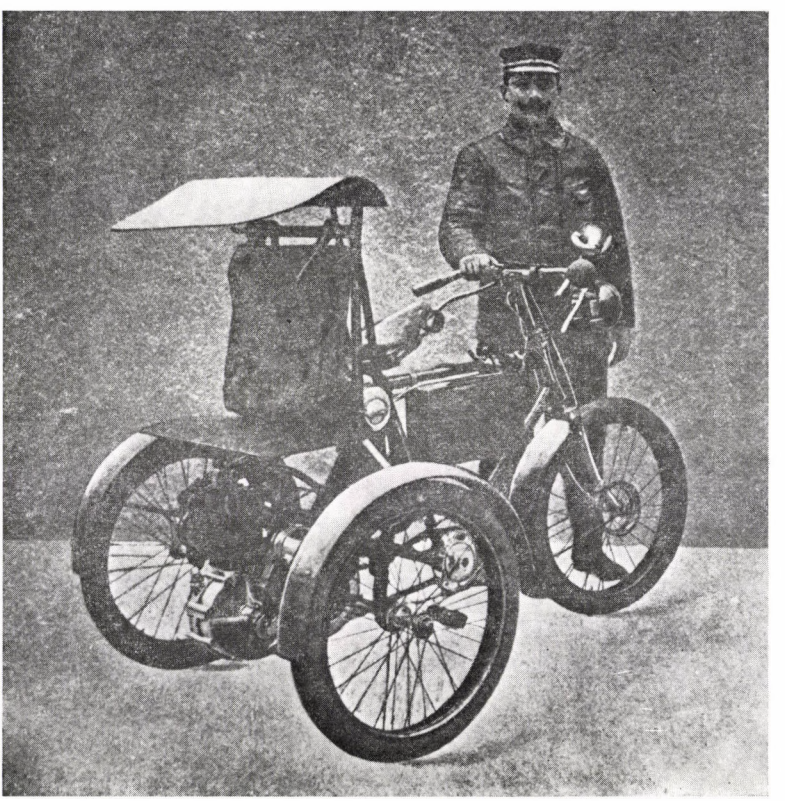

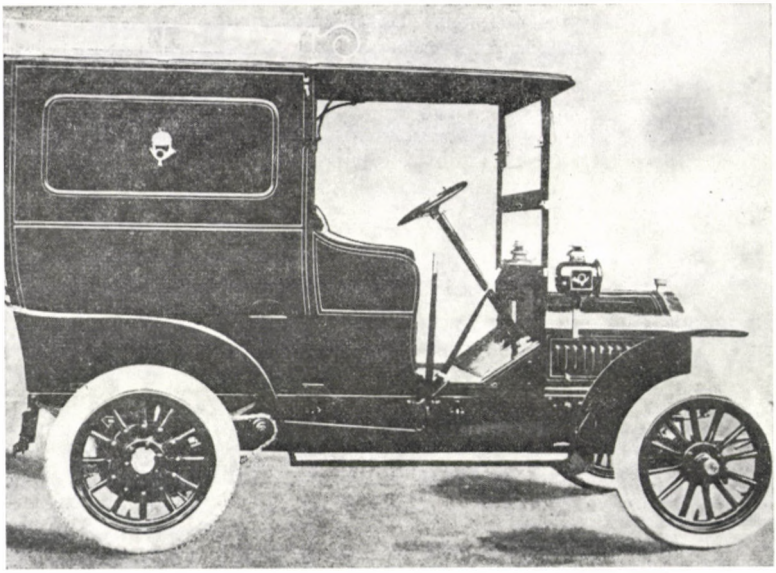

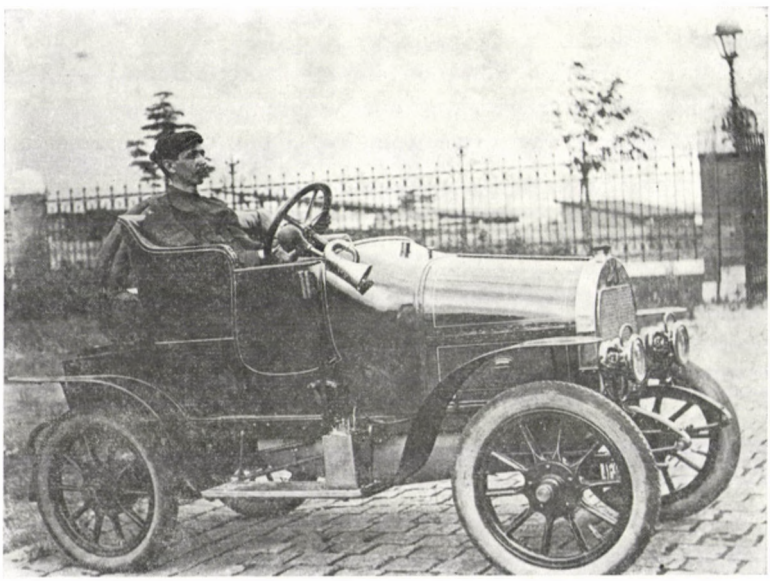

CSONKA started to build two-cylinder water cooled motor vehicles. But since he himself was not satisfied with the two-cylinder engines for automobiles, he did not finish the cars, he only sold the engines. In 1904 the Hungarian Postal Services called for bids for motorized four-wheel vehicles. Both the Hungarian Wagon and Machine Factory and the Machine Factory of István Röck submitted designs made by János CSONKA. There were also six foreign compe-

titors. After careful evaluation the Postal Services found the CSONKA design[8] to be the superior ones. Thus, the first eight postal automobiles were designed and also partly built by CSONKA. A test run of 2000 Km. was carried out on an experimental vehicle in which it stood up without any trouble. The Postal Services now placed an order for ninety Csonka vehicles. These automobiles were mainly used for the transportation of parcels and remained in service with minor maintenance for twenty-five years. Considerable interest was shown in the Bosch ignition system of his automobiles. CSONKA was almost the very first, who applied high tension ignition. Surprisingly enough, the majority of the experts distrusted this new electric system, though of course, time fully justified the choice of both BOSCH and CSONKA.

Later CSONKA designed several other postal vehicles, in 1906 he also built a 26—28 H.P. automobile for the Zsolnay-ceramic factory in Pécs. From 1909 on he designed and made a number of small cars. The first one was a small, one-cylinder model which was light enough for two men to lift. Only three such vehicles were built Another design for a four-cylinder, water cooled system small car design was purchased by a Canadian firm.

Following the success of the previous CSONKA vehicles, the Hungarian Postal Services ordered two bigger, 16 H.P. Csonka cars from the István Röck Machine Factory. These two automobiles took part in the "Prince Heinrich Tour", where they were rivals of over one hundred renowned automobiles, the products of world-famed big companies. One of these completed the track without any fault and was awarded a placing and a plaque, the other after a flawless run stopped a few yards before the finishing line. (Believed to have

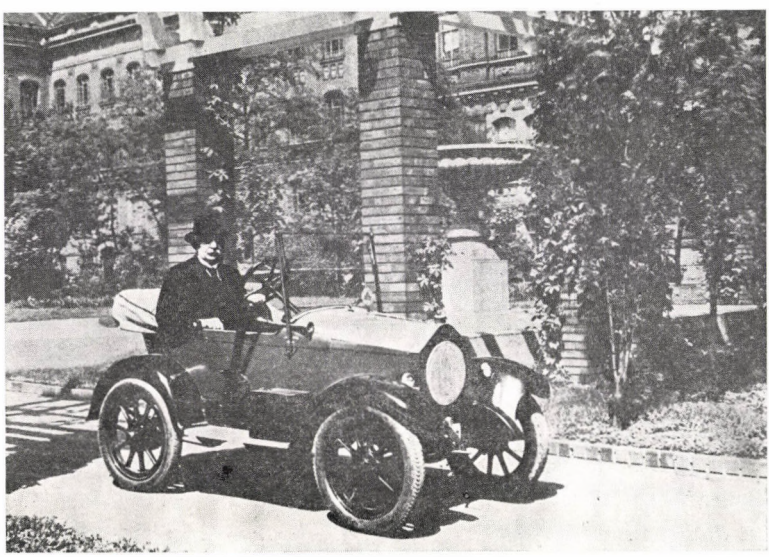

been caused by dirt in the fuel.) These successes greatly enhanced the confidence in the Hungarian machine industry as did other later achievements, like the outstanding results of Ágost BENÁRD M.D. at the International Small-Auto Competition in 1912 with one of CSONKA's four-cylinder engine automobiles.

Standardization and material testing

John CSONKA quite early recognized the importance of manufacturing the engine and vehicle parts in standardized types. For the five different types and sized vehicles which he designed and made for the Hungarian Postal Services he specified a standardized type of 16 H.P. engine. Also the carriages of the five different models were made of standard components. Identical specifications were used for the four types, while the front wheels on foreign cars were smaller than the rear wheels, as was customary on the horse drawn vehicles of that time. On the Csonka models all four wheels were of the same size and specification, already in 1905. He systematically designed all the major parts and components on carefully specified standards which made both the manufacture and the maintenance easier and cheaper. Nothing more vividly shows the excellent reputation of the Csonka engines than one particularly important application: during the First World War the wireless communication between the Central Powers and Bulgaria could be maintained only through generators powered by Csonka engines.

CSONKA fully understood the need to manufacture according to strict specifications. He had an amazing perception in these matters long before this was generally understood. It was typical of him in his seventies, before retiring from the Technical University, to encourage his two sons John und Béla both mechanical engineers, to make for themselves the basic machine tools for their own use. In the absence of standardized measuring units they even made the etalons for themselves. Later when CSONKA manufactured machine tools for the British market, it was found that *all the measurements were entirely within the tolerances of the strict meticulous German Standards.*

He made a number of testing machines for the Technical University. Particularly those he made together with Prof. Sándor REJTŐ for testing the strength of paper and cloth became well known. The very same testing machines were used at the Government Institute of Standards and Measures and in the laboratory of the Hungarian State Railways. He also made a number of machine models for the Museum of Transportation in Budapest, for the Technical University and for trade exhibitions.

During the Millenium Exhibition in 1896 he built a small railway and locomotive for the public. The diversity of his many undertaking were truly amazing.

The serious economic conditions which followed the First World War effected the rapidly developing motor vehicle industry in Hungary. But CSONKA's creativity had not diminished even in his seventies and eighties. In his own machine shop he started manufacturing excellent four stroke, two-cylinder "Boxer" engines. These were widely used as a power source for portable X-ray equipments, fire fighting water pumps, generators of electricity and for outboard motor purposes. He was eighty-eight when his last assignment came from the Turkish government to design a very light engine which one man could carry in his back-pack. He passed away while working on this project, which was brought to completion by his assistant Paul TOPERCZER.

This was the rich life of a diligent pioneer engineer and inventor who had many outstanding accomplishments. He was a quiet, modest man, devoted to his family and to his vocation. Had be been the son of a great Western industrial country, his name would be a by-word in his chosen field: that of the development of motorized, liquid fuel transportation. He made great contributions to the industrial development and comforts of our modern age. His intellectual legacy now belongs both to his own country and the whole world.

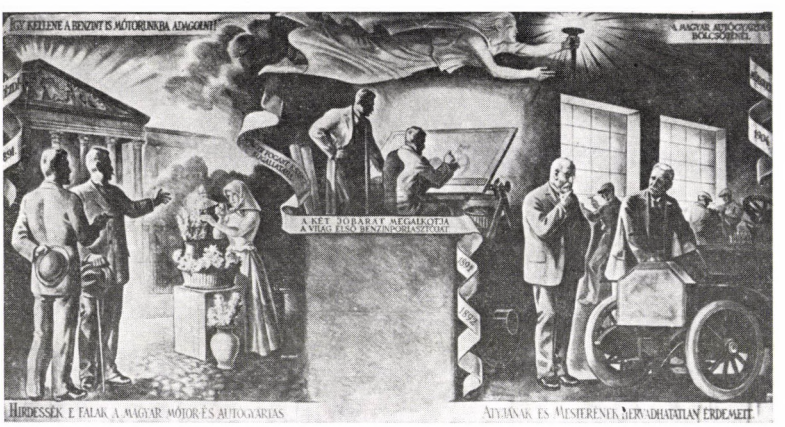

INDEX

Printed in Hungary

A kiadásért felel az Akadémiai Kiadó igazgatója. Műszaki szerkesztő: Zacsik Annamária

A kézirat nyomdába érkezett: 1980. VIII. 15. — Terjedelem: 21,35 (A/5) ív, 86 ábra

81.8631 Akadémiai Nyomda, Budapest — Felelős vezető: Bernát György

Acta Techn. Hung. **91** (1980) pp. 3—18

KOVÁCS, K. P.—GEYSEN, W.—PFAFF, G.: *Huntings in 3-phase Machines*

This article is dealing with a new simple method of determining of damping factor in synchronous and induction 3-phase machines. We do calculate the damping factor in two steps: at first one calculates this factor with stator resistances neglected (m_s^d; $R_s = 0$), at second we are making the same process with supposinly negligible rotor resistances (m_d^r; $R_r = 0$). The real damping factor of machine will be given as the algebraic sum of both component damping factors ($m_d^s + m_d^r = m_d$). We are showing that this simple method makes a good approximation at supplying frequencies close to the rated frequency only. By using this superposition method we are determining stabilitq limiting curves in some special cases. In last part we are dealing with oscillations of a synchronous machine supplying a passive (inductive) network.

Acta Techn. Hung. **91** (1980) pp. 19—56

JANKÓ, L.: *Comparison of the Membrane and Bending Theory of Shallow Saddle-shaped Hypar Shells, Supported by Shear Diaphragms, under Uniform Load*

The paper is the first part of a series consisting of three parts. The 2nd and 3rd chapters deal with the phenomena of the stability of the saddle-shaped hypar shells which are supported along the lines of the principal curvature by edge arches possessing flexural and torsional rigidity being negligible in the horizontal plane. In the paper at hand, prior to the investigations of the stability, the following problems will be discussed: the problem of existence and uniqueness of the *membrane solution*; the difficulties emerging from the *kinematic uncertainty* of the shell and the problem what are the geometric parameters on the basis of which these shells, with a close approximation, as *membrane shells* could be considered.

Acta Techn. Hung. **91** (1980) pp. 57—80

KOZÁK, I.—SZEIDL, GY.: *The Field Equations and Boundary Conditions with Force Stresses and Couple Stresses in the Linearized Theory of Micropolar Elastostatics*

Authors determined in two different ways the independent, necessary and sufficient conditions of the compatibility of the strain fields i.e. the six field equations of compatibility to be selected in various ways as well as the boundary conditions of compatibility; first based on the conditions of the single-valued displacements and rotations on the boundary surface, second, on the basis of the principle of minimum complementary energy. The field equations and boundary conditions written to the stress fields of the linearized theory of the micropolar elastostatics are summed up, then, on the basis of the uniqueness of the solutions the necessity and sufficiency of the field equations and boundary conditions justified.

Acta Techn. Hung. **91** (1980), pp. 81—110

TARNAI, T.: *Existence and Uniqueness Criteria of the Membrane State of Shells*

In this paper the problem is dealt with, what sort of boundary conditions are to be prescribed on the edge of a shell that is to be in a statically determinate membrane state. Existence and uniqueness criteria of the solution of the membrane-shell equation are investigated, on the basis of the partial differential equations' theory, for various boundary conditions. This part of the paper implies the results obtained for hyperbolic shells.

Acta Techn. Hung. **91** (1980), pp. 111—119

SITKEI, GY.—FEHÉR, J.: *Regularities of the Clod Comminution at the Preparation of Seed Beds*

On the basis of the experiments performed with a soil bin a relationship has been established between the clod size, critical value of the tool velocity and the moisture content of the soil. By making use of a simplified theory, the specific power demand for the clod comminution has been determined. Also the effect of the internal porosity on the power demand has been investigated On the basis of the experiments could be pointed out that by increasing the tool velocity over about 11 or 12 km/h does not seem to be convenient, because it leads, in this region only to a further clod comminution of inferior value.

Acta Techn. Hung. **91** (1980), pp. 121—135

FARKAS, J.—SZABÓ, L.: *Optimum Design of Beams and Frames of Welded I-Sections by Means of Backtrack Programming*

A brief description of backtrack programming method is given. This combinatorial discrete programming method can be succesfully applied to optimization problems with nonlinear objective function and constraints if the number of unknowns is not too large. This method is advantageous in the case of welded beams, mainly because the thicknesses of the plates should be rounded. The paper presents the application of a backtrack method for the following optimization problems. 1) Suboptimization of welded I-sections subjected to bending and compression. The application of these suboptimized I-sections to the elastic minimum weight design of frames is demonstrated by a numerical example of a single-bay pitched-roof portal frame. 2) Minimum cost design of welded homogeneous and hybrid I-beams, simply supported and loaded with an uniformly distributed normal load. In the objective functions the cost of materials, welding and painting are taken into account. The constraints of bending and shear stresses as well as those of local buckling of web and flange are considered. The lowering of flange thickness with a welded splice is also taken into consideration.

Acta Techn. Hung. **91** (1980), pp. 137—202

HOFFMANN, P.: *Geometry and Mechanics of Regular Stranded Constructions*

The mechanical stresses are investigated which are generated during the manufacturing of regular strands which are built up from simple and double stranded elements and by the tensile and flexural loading of the ready-made strands. In order to introduce the mechanical stresses, the equations and geometric parameters of the simple and double stranded helicoidal lines as well as the space requirement and surface area of the simple stranded elements of circular cross section are determined by making use of the methods of the vector algebra. With the known value of the space requirement of the stranded element, the relationships between the number of the elements in each layer, the height of thread and size relation of the regular strand are determined in the case of the penetration-free contact of the layers and elements.

Acta Techn. Hung. **91** (1980), pp. 203—223

TARNAI, T.: *Generalization of Southwells and Dunkerley's Theorems for Quadratic Eigenvalue Problems*

An approximate method for computing minimum positive eigenvalues of quadratic eigenvalue problems with real spectra is presented, seeking to give lower bounds for the wanted eigenvalue, and to reduce a given problem to simpler problems. Theorems by SOUTHWELL and by DUNKERLEY are generalized, then further relationships giving approximations from below are deduced. Application of the results is illustrated on lateral buckling problems of beams.

Acta Techn. Hung. **91** (1980), pp. 225—240

VAJDA, P.: *John Csonka and the Precision Machine Industry of Hungary*

John CSONKA is generally known to have been together with Donát BÁNKI the original inventor of the modern carburetor for the gasoline engines. His great pioneering achievements in the national automobile and general manufacturing industries are fully acknowledged in his biographies and the popular literature. His work as designer and independent manufacturer left an important mark on the Hungarian machine industry. As a teacher of machine shop skills and practice he maintained an exceptionally high standard which in many respects was higher than could typically be found in the colleges of that period.

The *Acta Technica* publish papers on technical subjects in English, French, German and Russian.

The *Acta Technica* appear in parts of varying size, making up one volume.

Manuscripts should be addressed to

Acta Technica
H-1051 Budapest
Münnich Ferenc u. 7.
Hungary

Correspondence with the editors and publishers should be sent to the same addres

Orders may be placed with "Kultura" Foreign Trading Company (H-1389 Budapest 62, P.O.B. 149. Account No. 218-10990) or its representatives abroad.

Les *Acta Technica* paraissent en français, allemand, anglais et russe et publient des travaux du domaine des sciences techniques.

Les *Acta Technica* sont publiés sous forme de fascicules qui seront réunis en volumes.

On est prié d'envoyer les manuscrits destinés à la rédaction à l'adresse suivante:

Acta Technica
H-1051 Budapest
Münnich Ferenc u. 7.
Hongrie

Toute correspondance doit être envoyée à cette même adresse.

On peut s'abonner à l'Entreprise du Commerce Extérieur «Kultura» (H-1389 Budapest 62, P.O.B. 149. Compte courant No. 218-10990) ou chez représentants à l'étranger.

«*Acta Technica*» публикуют трактаты из области технических наук на русском-немецком, английском и французском языках.

«*Acta Technica*» выходят отдельными выпусками разного объема. Несколько вы пусков составляют один том.

Предназначенные для публикации рускописи следует направлять по адресу:

Acta Technica
H-1051 Budapest
Münnich Ferenc u. 7.
Венгрия

По этому же адресу направлять всякую корреспонденцию для редакции и администрации.

Заказы принимает предприятие по внешней торговле «Kultura» (H-1389 Budapest 62, P.O.B. 149. Текущий счет № 218-10990) или его заграничные представительства и уполномоченные.

Reviews of the Hungarian Academy of Sciences are obtainable at the following addresses:

AUSTRALIA
C.B.D. LIBRARY AND SUBSCRIPTION SERVICE, Box 4886, G.P.O., *Sydney N.S.W. 2001*
COSMOS BOOKSHOP, 145 Ackland Street, *St. Kilda (Melbourne), Victoria 3182*

AUSTRIA
GLOBUS, Höchstädtplatz 3, *1200 Wien XX*

BELGIUM
OFFICE INTERNATIONAL DE LIBRAIRIE, 30 Avenue Marnix, *1050 Bruxelles*
LIBRAIRIE DU MONDE ENTIER, 162 Rue du Midi, *1000 Bruxelles*

BULGARIA
HEMUS, Bulvar Ruszki 6, *Sofia*

CANADA
PANNONIA BOOKS, P.O. Box 1017, Postal Station "B", *Toronto, Ontario M5T 2T8*

CHINA
CNPICOR, Periodical Department, P.O. Box 50, *Peking*

CZECHOSLOVAKIA
MAD'ARSKÁ KULTURA, Národní třida 22, *115 66 Praha*
PNS DOVOZ TISKU, Vinohradská 46, *Praha 2*
PNS DOVOZ TLAČE, *Bratislava!*

DENMARK
EJNAR MUNKSGAARD, Norregade 6, *1165 Copenhagen*

FINLAND
AKATEEMINEN KIRJAKAUPPA, P.O. Box 128 *SF-00101 Helsinki 10*

FRANCE
EUROPÉRIODIQUES S.- A., 31 Avenue de Versailles, *78170 La Celle St.-Cloud*
LIBRAIRIE LAVOISIER, 11 rue Lavoisier, *75008 Paris*
OFFICE INTERNATIONAL DE DOCUMENTATION ET LIBRAIRIE, 38 rue Gay Lussac, *75240 Paris Cedex 05*

GERMAN DEMOCRATIC REPUBLIC
HAUS DER UNGARISCHEN KULTUR, Karl-Liebknecht-Strasse 9, *DDR-102 Berlin*
DEUTSCHE POST ZEITUNGSVERTRIEBSAMT, Strasse der Pariser Kommüne 3—4, *DDR-104 Berlin*

GERMAN FEDERAL REPUBLIC
KUNST UND WISSEN ERICH BIEBER, Postfach 46, *7000 Stuttgart 1*

GREAT BRITAIN
BLACKWELL'S PERIODICALS DIVISION, Hythe Bridge Street, *Oxford OX1 2ET*
BUMPUS, HALDANE AND MAXWELL LTD., Cowper Works, *Olney, Bucks MK46 4BN*
COLLET'S HOLDINGS LTD., Denington Estate, *Wellingborough, Northants NN8 2QT*
W.M. DAWSON AND SONS LTD., Cannon House, *Folkestone, Kent CT19 5EE*
H. K. LEWIS AND CO., 136 Gower Street, *London WC1E 6BS*

GREECE
KOSTARAKIS BROTHERS, International Booksellers, 2 Hippokratous Street, *Athens-143*

HOLLAND
MEULENHOFF-BRUNA B.V., Beulingstraat 2, *Amsterdam*
MARTINUS NIJHOFF B.V., Lange Voorhout 9—11, *Den Haag*
SWETS SUBSCRIPTION SERVICE, 347b Heereweg, *Lisse*

INDIA
ALLIED PUBLISHING PRIVATE LTD, 13/14 Asaf Ali Road, *New Delhi 110001*
150 B-6 Mount Road, *Madras 600002*
INTERNATIONAL BOOK HOUSE PVT. LTD., Madame Cama Road, *Bombay 400039*
THE STATE TRADING CORPORATION OF INDIA LTD., Books Import Division, Chandralok, 36 Janpath, *New Delhi 110001*

ITALY
EUGENIO CARLUCCI, P.O. Box 252. *70100 Bari*
INTERSCIENTIA, Via Mazzé 28, *10149 Torino*
LIBRERIA COMMISSIONARIA SANSONI, Via Lamarmora 45, *50121 Firenze*
SANTO VANASIA, Via M. Macchi 58, *20124 Milano*
D. E. A., Via Lima 28, *00198 Roma*

JAPAN
KINOKUNIYA BOOK-STORE CO. LTD., 17-7 Shinjuku-ku 3 chome, Shinjuku-ku, *Tokyo 160-91*
MARUZEN COMPANY LTD., Book Dpartment, P.O. Box 5056 Tokyo International, *Tokyo 100-31*
NAUKA LTD. IMPORT DEPARTMENT, 2-30-11 Minami Ikebukuro, Toshima-ku, *Tokyo 171*

KOREA
CHULPANMUL, *Phenjan*

NORWAY
TANUM-CAMMERMEYER, Karl Johansgatan 41—43, *1000 Oslo*

POLAND
WĘGIERSKI INSTYTUT KULTURY, Marszałkowska 80, *Warszawa*
CKP I W ul. Towarowa 28 *00-958 Warszawa*

ROMANIA
D. E. P., *Bucureşti*
ROMLIBRI, Str. Biserica Amzei 7, *Bucureşti*

SOVIET UNION
SOJUZPETCHATJ — IMPORT, *Moscow*
and the post offices in each town
MEZHDUNARODNAYA KNIGA, *Moscow G-200*

SPAIN
DIAZ DE SANTOS, Lagasca 95, *Madrid 6*

SWEDEN
ALMQVIST AND WIKSELL, Gamla Brogatan 26, *101 20 Stockholm*
GUMPERTS UNIVERSITETSBOKHANDEL AB, Box 346, *401 25 Göteborg 1*

SWITZERLAND
KARGER LIBRI AG, Petersgraben 31, *4011 Basel*

USA
EBSCO SUBSCRIPTION SERVICES, P.O. Box 1943, *Birmingham, Alabama 35201*
F. W. FAXON COMPANY, INC., 15 Southwest Park, *Westwood, Mass. 02090*
THE MOORE-COTTRELL SUBSCRIPTION AGENCIES, *North Cohocton, N. Y. 14868*
READ-MORE PUBLICATIONS, INC., 140 Cedar Street, *New York, N. Y. 10006*
STECHERT-MACMILLAN, INC., 7250 Westfield Avenue, *Pennsauken, N. J. 080110*

VIETNAM
XUNHASABA, 32, Hai 3a Trung, *Hanoi*

YUGOSLAVIA
JUGOSLAVENSKA KNJIGA, Terazije 27, *Beograd*
FORUM, Vojvode Mišiča 1, *21000 Novi Sad*

10. XII. 1981. HU ISSN 0001—7035 Index: 26.025

ACTA TECHNICA

ACADEMIAE SCIENTIARUM HUNGARICAE

REDIGIT: M. MAJOR

TOMUS 91
FASCICULI 3—4

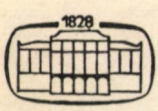

AKADÉMIAI KIADÓ, BUDAPEST 1980

ACTA TECHNICA

Az *Acta Technica* angol, francia, német és orosz nyelven közöl értekezéseket a műszaki tudományok köréből.

Az *Acta Technica* változó terjedelmű füzetekben jelenik meg, több füzet alkot egy kötetet.

A közlésre szánt kéziratok a következő címre küldendők:

Acta Technica
1051 Budapest, Münnich Ferenc u. 7.

Ugyanerre a címre küldendő minden szerkesztőségi és kiadóhivatali levelezés.

Megrendelhető a belföld számára az „Akadémiai Kiadó"-nál (1363 Budapest Pf. 24. Bankszámla 215-11448), a külföld számára pedig a „Kultura" Külkereskedelmi Vállalatnál (1389 Budapest 62, P.O.B. 149 Bankszámla: 218-10990) vagy annak külföldi képviseleteinél és bizományosainál.

Die *Acta Technica* veröffentlichen Abhandlungen aus dem Bereiche der technischen Wissenschaften in deutscher, englischer, französischer und russischer Sprache.

Die *Acta Technica* erscheinen in Heften wechselnden Umfanges. Vier Hefte bilden einen Band.

Die zur Veröffentlichung bestimmten Manuskripte sind an folgende Adresse zu senden:

Acta Technica
H-1051 Budapest
Münnich Ferenc u. 7.
Ungarn

An die gleiche Anschrift ist auch jede für die Schriftleitung und den Verlag bestimmte Korrespondenz zu richten.

Bestellbar bei »Kultura« Außenhandelsunternehmen (H-1389 Budapest 62, P.O.B. 149, Bankkonto Nr. 218-10990) oder seinen Auslandsvertretungen.

Acta Technica Academiae Scientiarum Hungaricae, Tomus 91 (3—4), pp. 239—245 (1980)

LIMIT ANALYSIS OF CONCRETE TUBES, REINFORCED BY A SET OF THIN SHELLS

M. HEINLOO*
CAND. OF PHYS. AND MATH. SCI.

[Manuscript received: 21 March 1980]

The paper deals with limit analysis of thick-walled concrete tubes, reinforced by a set of thin cylindrical membrane shells and loaded by internal pressure. The exact solution of the problem is obtained and the influence of the location of the shells to the limit pressure is analysed.

1. Introduction

The aim of this paper is to present the limit analysis of thick-walled concrete tubes, reinforced by a set of thin coaxial cylindrical membrane shells and loaded by internal pressure (Fig. 1). In our investigations the concrete is considered as a perfectly plastic material, which obeys the Tresca yield condition, but its tensile strength is equal to zero. It is assumed, that the tube is restrained from motion in the axial direction and the thin shells are made of perfectly plastic material. It is convenient to introduce the following non-dimensional quantities:

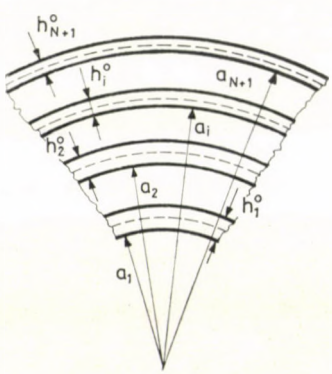

Fig. 1

* M. HEINLOO, Struve 5—47, Tartu, Estenian SSR, USSR

$$\sigma_i^* = \frac{\sigma_i^{*o}}{\sigma_c^{*o}}; \; \sigma_{\theta i}^s = \frac{\sigma_{\theta i}^{so}}{\sigma_c^{*o}}; \; \sigma_{\theta,N+1}^s = \frac{\sigma_{\theta,N+1}^{so}}{\sigma_c^{*o}}; \; \sigma_{\theta i} = \frac{\sigma_{\theta i}^o}{\sigma_c^{*o}};$$

$$\sigma_{ri} = \frac{\sigma_{ri}^o}{\sigma_c^{*o}}; \; \alpha_i = \frac{a_i}{a_1}; \; \alpha_{N+1} = \frac{a_{N+1}}{a_1}; \; p_i = \frac{p_i^o}{\sigma_c^{*o}};$$

$$p_i' = \frac{p_i^{o\prime}}{\sigma_c^{*o}}; \; r_i = \frac{\varrho_i}{a_1}; \; h_i = \frac{h_i^o}{a_1},$$

where σ_c^{*o}, σ_i^{*o} — strength of concrete in compression and the yield points for the material of the shells, respectively; $\sigma_{\theta i}^o$, σ_{ri}^o, $\sigma_{\theta i}^{so}$, $\sigma_{\theta,N+1}^{so}$ — components of stresses in the layers of concrete and in the shells, respectively; a_i — internal radii of the layers of concrete; a_{N+1}, p_1^o — external radius and internal pressure of the reinforced concrete tube; $p_2^o, p_3^o, \ldots, p_N^o$ and $p_2^{o\prime}, p_3^{o\prime}, \ldots, p_N^{o\prime}$ — contact pressures on the internal and external surfaces of the shells, respectively (Fig. 2); $\varrho_i (a_i \leq \varrho_i \leq a_{i+1})$ — running radii; h_i^o, h_{N+1}^o — thicknesses of the shells.

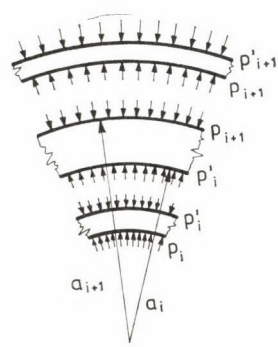

Fig. 2

2. Investigation of a single layer

For the layer i of concrete the equilibrium equation takes the form [1]:

$$\frac{d\sigma_{ri}}{d_{ri}} + \frac{\sigma_{ri} - \sigma_{\theta i}}{r_i} = 0 \tag{1}$$

with the boundary conditions (Fig. 2):

$$\sigma_{ri}(\alpha_i) = -p_i'; \quad \sigma_{ri}(\alpha_{i+1}) = -p_{i+1}. \tag{2}$$

Let us assume, as in the paper [2], that from the point of view of yielding the tube has two different regions, which are separated by the unknown radius $r_i = x_i$:

In the outer part ($x_i \leq r_i \leq \alpha_{i+1}$)

$$\sigma_{\theta i} = 0. \tag{3}$$

In the inner part ($\alpha_i \leq r_i \leq x_i$)

$$\sigma_{\theta i} - \sigma_{ri} = 1. \tag{4}$$

Substituting Eqs (3) and (4) into Eq. (1), we obtain the differential equations

$$\frac{d\sigma_{ri}}{dr_i} + \frac{\sigma_{ri}}{r_i} = 0, \tag{5}$$

if $x_i \leq r_i \leq \alpha_{i+1}$ and

$$\frac{d\sigma_{ri}}{dr_i} - \frac{1}{r_i} = 0, \tag{6}$$

if $\alpha_i \leq r_i \leq x_i$.

Now, taking into account the second boundary condition of (2) and considering the fact, that at the radius $r_i = x_i$ value σ_{ri} must be continuous, we can solve the differential equations (5) and (6). Hence, the stress distribution in the layer i is given by the formulae

$$\sigma_{ri} = -\frac{p_{i+1}\alpha_{i+1}}{r_i}\ ;\ \sigma_{\theta i} = 0, \tag{7}$$

if $x_i \leq r_i \leq \alpha_{i+1}$ and

$$\sigma_{ri} = -\left(\frac{p_{i+1}\alpha_{i+1}}{x_i} + \ln\frac{x_i}{r_i}\right),\ \sigma_{\theta i} = 1 + \sigma_{ri} \tag{8}$$

if $\alpha_i \leq r_i \leq x_i$.

Finally, using Eq. (8) and the first boundary condition of (2), the value of the pressure, acting on the inner radius of layer i, can be obtained at which the stress field in layer i is statically admissible:

$$p_i' = \frac{p_{i+1}\alpha_{i+1}}{x_i} + \ln\frac{x_i}{\alpha_i}. \tag{9}$$

However, the problem has not been solved yet, because Eqs (7) $\div$ (9) contain the unknown parameters x_i, p_i', p_{i+1}. For the determination of the parameters p_i' and p_{i+1}, notice, that the tangential stresses in the thin membrane shells may be expressed by the formulas

$$\sigma_{\theta i}^s = \frac{\alpha_i}{h_i}(p_i - p_i');\ \sigma_{\theta,N+1}^s = \frac{\alpha_{N+1}}{h_{N+1}} p_{N+1}. \tag{10}$$

Let us assume, that the yielding condition for the shells may be written in the form

$$\sigma_{\theta i}^{s} = \sigma_i^* \ (i = 1, 2, \ldots, N); \ \sigma_{\theta, N+1}^{s} = \sigma_{N+1}^* . \tag{11}$$

Substituting Eq. (10) into Eq. (11), we get

$$p_i = \frac{m_i}{\alpha_i} + p_i' ; \ p_{N+1} = \frac{m_{N+1}}{\alpha_{N+1}} , \tag{12}$$

where $m_i = \sigma_i^* h_i, m_{N+1} = \sigma_{N+1}^* h_{N+1}$.

Finally, substituting Eq. (9) into Eq. (12), we obtain

$$\begin{aligned} p_i &= \frac{m_i}{\alpha_i} + \frac{p_{i+1}\alpha_{i+1}}{x_i} + \ln \frac{x_i}{\alpha_i} ; \\ p_{N+1} &= \frac{m_{N+1}}{\alpha_{N+1}} ; (i = 1, 2, \ldots, N) . \end{aligned} \tag{13}$$

3. Investigation of the whole tube

When considering the whole tube using the recursive formula (13) the statically admissible load multiplier p_1 can be expressed in the term of parameter x_i. This parameter can be obtained by considering the condition, that $\sigma_{\theta i}$ must be continuous at the radius $x_i (\alpha_i \leq x_i \leq \alpha_{i+1})$. Using (7) and (8) this condition leads to the equation $x_i = p_{i+1}\alpha_{i+1}$. If $\alpha_{i+1}p_{i+1} \leq \alpha_i$, then we must take $x_i = \alpha_i$ and if $\alpha_{i+1}p_{i+1} \geq \alpha_{i+1}$, then $- \ x_i = \alpha_{i+1}$.

Notice, that the continuous condition for $\sigma_{\theta i}$ leads to the minimum condition for p_1 and vice versa. Hence, the last condition may be used instead of the continuous condition for $\sigma_{\theta i}$.

In the case of two layers i.e., when the concrete tube is reinforced by three shells, if

$$\alpha_3 p_3 \leq \alpha_2 , \tag{14}$$

then $x_2 = \alpha_2$ and from Eq. (13) we obtain

$$p_2 = \frac{m_2 + m_3}{\alpha_2} , \tag{15}$$

if

$$\alpha_2 \leq \alpha_3 p_3 \leq \alpha_3 , \tag{16}$$

then $x_2 = m_3$ and from Eq. (13) we obtain

$$p_2 = 1 + \frac{m_2}{\alpha_2} + \ln \frac{m_3}{\alpha_2}, \tag{17}$$

if

$$\alpha_3 p_3 \geq \alpha_3, \tag{18}$$

then $x_2 = \alpha_3$ and from Eq. (13) we obtain

$$p_2 = \frac{m_2}{\alpha_2} + \frac{m_3}{\alpha_3} + \ln \frac{\alpha_3}{\alpha_2}, \tag{19}$$

if

$$\alpha_2 p_2 \leq 1, \tag{20}$$

then $x_1 = 1$ and from Eq. (13) we obtain

$$p_1 = m_1 + p_2 \alpha_2, \tag{21}$$

if

$$1 \leq \alpha_2 p_2 \leq \alpha_2, \tag{22}$$

then $x_1 = \alpha_2 p_2$ and from Eq. (13) we obtain

$$p_1 = 1 + m_1 + \ln (\alpha_2 p_2), \tag{23}$$

if

$$\alpha_2 p_2 \geq \alpha_2 \tag{24}$$

then $x_1 = \alpha_2$ and from Eq. (13) we obtain

$$p_1 = m_1 + p_2 + \ln \alpha_2 . \tag{25}$$

It can be seen, that the systems of inequalities (16), (20); (16), (22); (18), (22); (18), (20) are impossible. For example, in the case of the system (16), (20) we have

$$\begin{gathered} \alpha_2 \leq \alpha_3 p_3 \leq \alpha_3 ; \\ \alpha_2 p_2 \leq 1 \end{gathered} \tag{26}$$

Using the second of Eqs (13) and Eq. (17), we obtain

$$\begin{gathered} \alpha_2 \leq m_3 \leq \alpha_3 \\ \alpha_2 + m_2 + \alpha_2 \ln \frac{m_3}{\alpha_2} \leq 1 . \end{gathered} \tag{27}$$

So far as $\alpha_2 \geq 1$, $m_2 \geq 0$ and from the first of Inequality (27) we have $\ln (m_3/\alpha_2) \geq 0$, then the second inequality of (27) is impossible.

Thus, combining (14)÷(19) with (20)÷(25) we can find, that only five cases are possible:

A. If $m_3 \leq \alpha_2$, $m_2 + m_3 \leq 1$, then $x_1 = 1$, $x_2 = \alpha_2$ and $p_1 = m_1 + m_2 + m_3$.

B. If $m_3 \leq \alpha_2$, $1 \leq m_2 + m_3 \leq \alpha_2$, then $x_1 = m_2 + m_3$, $x_2 = \alpha_2$ and $p_1 = 1 + m_1 + \ln(m_2 + m_3)$.

C. If $m_3 \leq \alpha_2$, $m_2 + m_3 \geq \alpha_2$, then $x_1 = x_2 = \alpha_2$ and $p_1 = m_1 + (m_2 + m)/\alpha_2 + \ln \alpha_2$.

D. If $\alpha_2 \leq m_3 \leq \alpha_3$, then $x_1 = \alpha_2$, $x_2 = m_3$ and $p_1 = 1 + m_1 + m_2/\alpha_2 + \ln m_3$.

E. If $m_3 \geq \alpha_3$, then $x_1 = \alpha_2$, $x_2 = \alpha_3$ and $p_1 = m_1 + m_2/\alpha_2 + m_3/\alpha_3 + \ln \alpha_3$.

The kinematically admissible solution can be constructed for each layer of concrete and, hence, for the whole tube by analogy with the paper [2] and also coincides with the statical admissible solution. Consequently, it can be stated, that Eqs (8) and (13) together with the continuous condition for $\sigma_{\theta i}$ (minimum condition for p_1) represent the complete solution of the problem. Similarly to paper [2] it may be shown, that in the inner part of the layer i ($\alpha_i \leq r_i \leq x_i$) there are shear lines in 45° direction to the radius, while in the outer part ($x_i \leq r_i \leq \alpha_{i+1}$) crack develops in the radial direction. This is illustrated for the case of two layers on Fig. 3. For example, in case *A* cracks develop in both layers, while in case *B* here are shear lines in the inner part of the first layer and cracks develop in the outer part of the first layer and in the second layer.

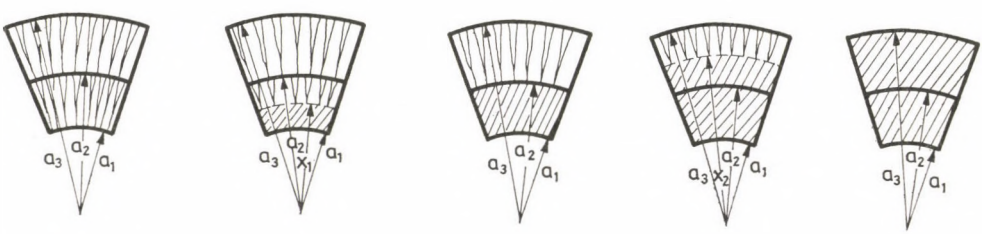

Fig. 3

4. Remarks

Let us investigate the dependence of p_1 on α_2 in the case when the concrete tube is reinforced by three shells. In full investigation we must consider six cases:

1. $m_3 \leq 1, \quad m_2 + m_3 \leq 1$,
2. $m_3 \leq 1, \quad 1 \leq m_2 + m_3 \leq \alpha_3$,
3. $m_3 \leq 1, \quad m_2 + m_3 \geq \alpha_3$,
4. $1 \leq m_3 \leq \alpha_3, \quad 1 \leq m_2 + m_3 \leq \alpha_3$,
5. $1 \leq m_3 \leq \alpha_3, \quad m_2 + m_3 \geq \alpha_3$,
6. $m_3 \geq \alpha_3$.

The dependence of p_1 on α_2 in case 4 is illustrated on Fig. 4. The regions $1 \leq \leq \alpha_2 \leq m_3$, $m_3 \leq \alpha_2 \leq m_2 + m_3$ and $m_2 + m_3 \leq \alpha_2 \leq \alpha_3$ correspond to the cases D, C and B, respectively. On the Fig. 4. $M = 1 + m_1 + m_2 + \ln m_3$, $L = m_1 + m_2 + m_3 + \ln m_3$, $N = 1 + m_1 + \ln (m_2 + m_3)$. In this case p_1 has the maximum value if $\alpha_2 = 1$, i.e. if the tube is reinforced on the internal and external surfaces. The analogical result can be obtained in the cases 2, 3, 5, 6. Case 1 corresponds to case A in all region $1 \leq \alpha_2 \leq \alpha_3$ and p_1 is not depend on α_2.

Thus, in cases $2 \div 6$ the maximum value of p_1 has the tube reinforced only on the external and internal surfaces.

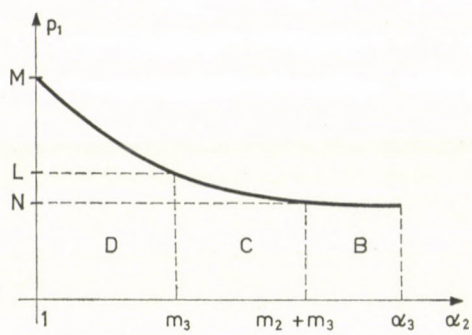

Fig. 4

Acknowledgement

The author benefited greatly from discussion with prof. S. Kaliszky to vhom he is very grateful.

REFERENCES

1. Prager, W.—Hodge, P. G.: Theory of Perfectly Plastic Solids. New York, J. Wiley 1951
2. Kaliszky, S.: Limit Analysis of Post-Stressed Thick-Walled Concrete Tubes. *Acta Techn. Hung.* **75** (1973), 193—202

Grenztragfähigkeit von mehrschichtigen, auf Innendruck beanspruchten Betonrohren. — Der Aufsatz beschäftigt sich mit der plastischen Analyse von dickwandigen Betonrohren, die aus einer Schar zylindrischer Innenschalen bestehen. Es wird die exakte Lösung des Problems angegeben, und die Beanspruchung der einzelnen Schalenschichten im plastischen Grenzzustand besprochen.

Acta Technica Academiae Scientiarum Hungaricae, Tomus 91 (3—4), pp. 247—256 (1980)

SECTORIAL SHELL WITHOUT TIES WITH UNBENT EDGE ARCHES AND DIVIDING RIBS

P. CSONKA*
DOCTOR OF THE TECHN. SC.

[Manuscript received 8th April, 1980]

The stress pattern generated by uniformly distributed vertical load in special shaped sectorial shells is analysed in the framework of the membrane theory. It is proved that the edge members (edge arches in horizontal and dividing ribs in vertical planes) of these shells do not undergo bending and torsional effects, but are only affected by axial (funicular) forces. The lateral tension of the dividing ribs is cancelled by the lateral tensile forces of the edge arches. That is why for this type of shells no ties or struts are to be applied between the abutment points of the ribs.

1. Introduction

In the following sectorial shell structures of a particular shape and behaviour erected on regular ground plan are dealt with which may be applied in constructing festival or exhibition halls and pavilions (Fig. 1).

The sectors of the shell in question are of elliptic paraboloid shape. The lower edges of the sectors are bordered by elliptically arched edgebeams *(edge arches)* lying in the horizontal plane and propped by a wall throughout the whole length. Each sector is bordered at both sides by arch beams of parabolic axis *(deviding ribs)* in the vertical plane.

The load applied on the shell is taken into account as a system of vertical forces of intensity $\bar{p}_0$ uniformly distributed over the ground plan of the shell. The dead weight of the dividing ribs is neglected in the calculations.

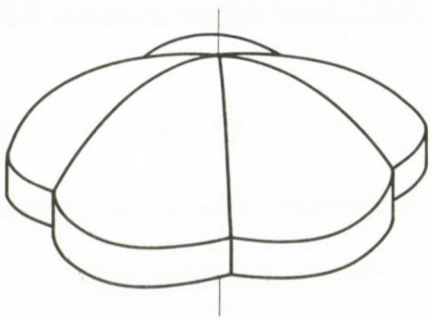

Fig. 1

* Prof. Dr. P. Csonka, Bartók B. út 31., H-1114 Budapest, Hungary

The purpose of the paper is to determine the stress pattern induced in the shell. This problem is treated in the framework of the membrane theory of shells. The flexural-torsional moments disturbing the membrane-like stress distribution, generated at the joints of the shell and edge beams, are also left out of consideration.

The following shows that no flexural-torsional forces are induced either in the edge arches or in the dividing ribs; in these members only axial forces, that is, funicular forces are present. Further, it will be proved that the abutments of the dividing ribs do not exert anything but vertical efforts on the supports. In consequence, the abutments of the dividing ribs need neither tie rods nor bracing members.

2. Geometrical data

The investigations concern the sector of the shell marked by dotting in Fig. 2. The equation of the elliptical arc bordering the ground plan figure of the shell sector in question is

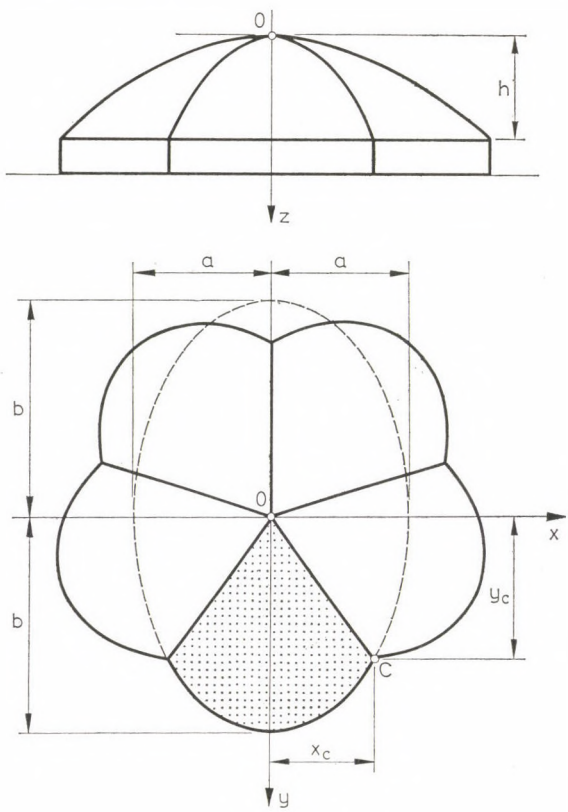

Fig. 2

$$\frac{x^2}{a^2} + \frac{y^2}{b^2} - 1 = 0\,,$$

and the equation of the middle surface of the shell sector is

$$z = h\left(\frac{x^2}{a^2} + \frac{y^2}{b^2} - 1\right). \tag{1}$$

In case where the shell consists of m sectors, the angle at the centre, denoted with γ, is

$$\gamma = \frac{\pi}{m}\,. \tag{2}$$

The coordinates of the abutment point C of the dividing rib OC are as follows

$$x_C = \frac{ab\tan\gamma}{\sqrt{a^2 + b^2\tan^2\gamma}}\,, \tag{3}$$

$$y_C = \frac{ab}{\sqrt{a^2 + b^2\tan^2\gamma}}\,. \tag{4}$$

The length of the ground plan projection of the dividing rib is:

$$v_C = \frac{ab\sqrt{1 + \tan^2\gamma}}{\sqrt{a^2 + b^2\tan^2\gamma}} = \frac{ab}{\cos\gamma\sqrt{a^2 + b^2\tan^2\gamma}}\,. \tag{5}$$

The slope of the tangent at point C of the elliptic arc bordering the investigated shell sector is the following

$$\tan\varepsilon = -\frac{b}{a}\cdot\frac{x_C}{\sqrt{a^2 - x_C^2}}\,,$$

or, by replacing the value of x_C given in (3):

$$\tan\varepsilon = -\frac{b^2}{a^2}\tan\gamma\,.$$

Thus, with the symbols of Fig. 3,

$$\tan\alpha = -\tan\varepsilon = \frac{b^2}{a^2}\tan\gamma \tag{6}$$

and

$$\tan\beta = \frac{1}{\tan\alpha} = \frac{a^2}{b^2\tan\gamma}\,. \tag{7}$$

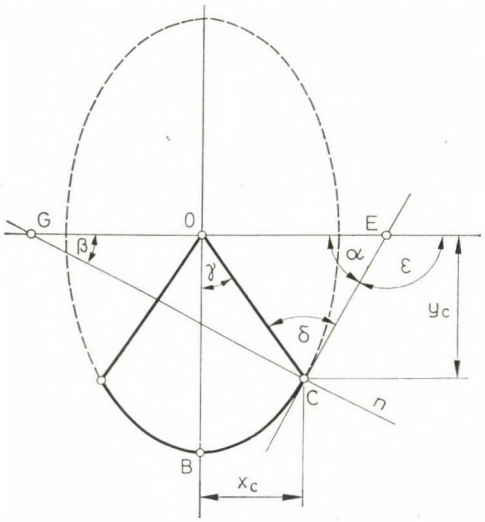

Fig. 3

In Fig. 3 the straight line CE is the tangent of the elliptic arc at point C and the straight line CG is the normal of the elliptic arc at the point C.

3. The stress pattern of the shell

The stress pattern of the shell sector investigated may be expressed by the stress function $F = F(x, y)$. This function, on the one hand, has to satisfy Pucher's differential equation of membrane shells [1, 2]

$$\frac{\partial^2 z}{\partial x^2} \cdot \frac{\partial^2 F}{\partial y^2} - 2\frac{\partial^2 z}{\partial x \cdot \partial y} + \frac{\partial^2 z}{\partial y^2} \cdot \frac{\partial^2 F}{\partial x^2} + \bar{p}_0 = 0\,, \tag{8}$$

and, on the other hand, it has to fulfil the boundary condition

$$F = 0 \tag{9}$$

relating to shells which have edge arches supported by wall [4, 5].

The stress function which satisfies both of the above two conditions may readily be described as

$$F = -\bar{p}_0 \frac{a^2 b^2}{8h}\left(\frac{x^2}{a^2} + \frac{y^2}{b^2} - 1\right). \tag{10}$$

The stress function F being familiar, the x, y directed projected stress resultants may be determined from the following formulae:

$$\bar{N}_x = \frac{\partial^2 F}{\partial y^2} = -\bar{p}_0 \frac{a^2}{4h},$$

$$\bar{N}_{xy} = -\frac{\partial^2 F}{\partial x \cdot \partial y} = 0,$$

$$\bar{N}_y = \frac{\partial^2 F}{\partial x^2} = -\bar{p}_0 \frac{b^2}{4h}. \tag{11}$$

4. The stress pattern of the edge arch

The horizontal component of the funicular force generated in the edge arch of a membrane shell with wall support — in the present problem the funicular force itself — can be determined by the formula

$$H = -\frac{\partial F}{\partial n} = -\frac{\partial F}{\partial x} \cdot \frac{dx}{dn} - \frac{\partial F}{\partial y} \cdot \frac{dx}{dn}. \tag{12}$$

In this formula, n designates the direction of the ground plan projection of the external normal of the edge arch at the point of investigation.

By taking (7) into account one obtains at point C of the edge arch

$$\frac{dx}{dn} = \cos\beta = \frac{1}{\sqrt{1 + \tan^2\beta}} = \frac{b^2 \tan\gamma}{\sqrt{a^4 + b^4 \tan^2\gamma}},$$

$$\frac{dy}{dn} = \sin\beta = \frac{\tan\beta}{\sqrt{1 + \tan^2\beta}} = \frac{a^2}{\sqrt{a^4 + b^4 \tan^2\gamma}},$$

thus, by making use of formula (12), the funicular force at point C is

$$H = -\frac{1}{\sqrt{a^4 + b^4 \tan^2\gamma}} \left(\frac{\partial F}{\partial x} b^2 \tan\gamma + \frac{\partial F}{\partial y} a^2 \right). \tag{13}$$

However, taking (3) and (4) into account, one obtains

$$\frac{\partial F}{\partial x} = -\bar{p}_0 \frac{b^2}{4h} x_C = -\bar{p}_0 \frac{ab}{4h} \cdot \frac{b^2 \tan\gamma}{\sqrt{a^2 + b^2 \tan^2\gamma}},$$

$$\frac{\partial F}{\partial y} = -\bar{p}_0 \frac{a^2}{4h} y_C = -\bar{p}_0 \frac{ab}{4h} \frac{a^2}{\sqrt{a^2 + b^2 \tan^2\gamma}}.$$

By replacing these values into Eq. (13), the funicular force acting in the cross section of the edge arch at point C is

$$H = \bar{p}_0 \frac{ab}{4h} \frac{a^4 + b^4 \tan^2 \gamma}{\sqrt{a^4 + b^4 \tan^2 \gamma}\ \sqrt{a^2 + b^2 \tan^2 \gamma}}$$

which, after reduction may be written in the simplified form:

$$H = \bar{p}_0 \frac{ab}{4h} \frac{\sqrt{a^4 + b^4 \tan^2 \gamma}}{\sqrt{a^2 + b^2 \tan^2 \gamma}} \,. \tag{14}$$

The component of this tensile force H directed towards point 0 (Fig. 4) is

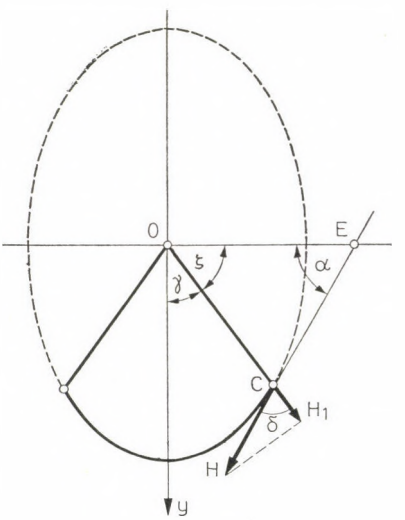

Fig. 4

$$H_1 = H \cos \delta. \tag{15}$$

The angle δ entering in the formula (15) can be determined from triangle *OCE:*

$$\delta = 180° - \alpha - \zeta = 180° - \alpha - (90° - \gamma) = 90° - (\alpha - \gamma) \,.$$

In the case of this angle

$$\cos \delta = \sin (\alpha - \gamma) = \sin \alpha \cdot \cos \gamma - \cos \alpha \cdot \sin \gamma =$$

$$= \frac{\tan \alpha}{\sqrt{1 + \tan^2 \alpha}} \cdot \cos \gamma - \frac{1}{\sqrt{1 + \tan^2 \alpha}} \sin \gamma \,,$$

and making use of (6) yields

$$\cos \delta = \frac{b^2 \tan \gamma}{\sqrt{a^4 + b^4 \tan^2 \gamma}} \cos \gamma - \frac{a^2}{\sqrt{a^4 + b^4 \tan^2 \gamma}} \cdot \sin \gamma \, .$$

After simplifying the above relationship one obtains

$$\cos \delta = \frac{(b^2 - a^2) \sin \gamma}{\sqrt{a^4 + b^4 \tan^2 \gamma}} \, . \tag{16}$$

Eventually, replacement of Eqs (14) and (16) into Eq. (16) yields for the component of the one-sided funicular force at point C directed towards the point O the formula

$$H_1 = \bar{p}_0 \frac{ab}{4h} \cdot \frac{\sqrt{a^4 + b^4 \tan^2 \gamma}}{\sqrt{a^2 + b^2 \tan^2 \gamma}} \cdot \frac{(b^2 - a^2) \sin \gamma}{\sqrt{a^4 + b^4 \tan^2 \gamma}}$$

which, after reduction, can be written in form:

$$H_1 = \bar{p}_0 \frac{ab}{4h} \frac{(b^2 - a^2) \sin \gamma}{\sqrt{a^2 + b^2 \tan^2 \gamma}} \, . \tag{17}$$

5. The stress state of the dividing rib

For the determination of the forces exerted by the shell sector on the dividing rib, a triangle shaped element joined to the dividing rib, should be cut out of the shell.

The projection of the shell element on the ground plan and the specific values of the *horizontal* components of the forces applied on the shell element are depicted in Fig. 5. From among these force components the values of $\bar{N}_x$ and $\bar{N}_y$ are familiar from formula (11), it remains only to determine the values of the components $\bar{N}_u$ and $\bar{N}_{wv}$ which may readily be carried out by making use of the equilibrium equations

$$\bar{N}_u = \bar{N}_x \cos^2 \gamma + \bar{N}_y \sin^2 \gamma \, ,$$
$$\bar{N}_{uv} = (\bar{N}_x - \bar{N}_y) \sin \gamma \cdot \cos \gamma \, ,$$

whence, by making use of formulae (11):

$$\bar{N}_u = - \frac{\bar{p}_0}{4h} (a^2 \cos^2 \gamma + b^2 \sin^2 \gamma) \, , \tag{18}$$

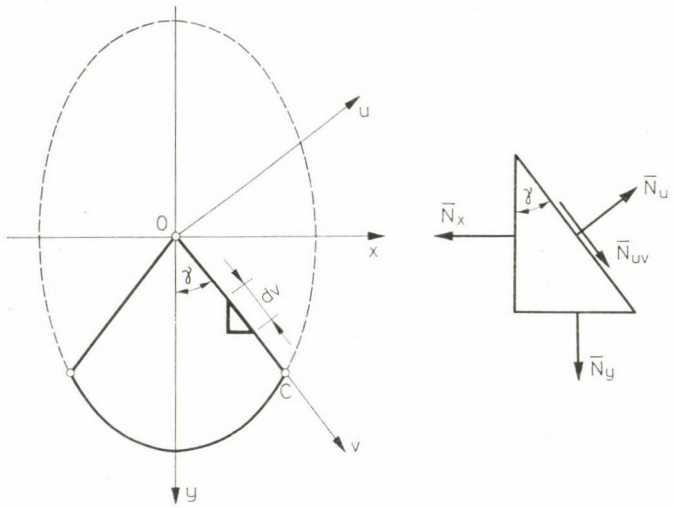

Fig. 5

$$\overline{N}_{uv} = -\frac{\overline{p}_0}{4h}(a^2 - b^2)\sin\gamma \cdot \cos\gamma). \tag{19}$$

The side of the triangle shaped shell element is also submitted to ***vertical*** forces. The specific value of these forces is

$$N_z = \overline{N}_u \frac{\partial z}{\partial u} + \overline{N}_{uv} \frac{\partial z}{\partial v}, \tag{20}$$

wherein:

$$\frac{\partial z}{\partial u} = -\frac{2hv}{a^2 b^2}(b^2 - a^2)\sin\gamma \cdot \cos\gamma,$$

$$\frac{\partial z}{\partial v} = +\frac{2hv}{a^2 b^2}(a^2\cos^2\gamma + b^2\sin^2\gamma).$$

Replacement of (18) and (19) into Eq. (20) yields

$$N_z = \frac{\overline{p}_0}{a^2 b^2}(b^2 - a^2)(a^2\cos^2\gamma - b^2\sin^2\gamma) \cdot \sin\gamma \cdot \cos\gamma. \tag{21}$$

The forces $\overline{N}_u$ attacking the dividing rib OB from both sides mutually equipoise each other, so that, concerning the loading forces acting on the dividing rib OC, only the forces $\overline{N}_{uv}$ and N_z are to be considered.

It can be readily proved that the force components $\overline{N}_{uv}$ and N_z acting on both sides on the dividing rib OC, do not generate anything but axial (funicular) forces in the rib. Namely, along the segment of the dividing rib from $v = 0$ to v (Fig. 6) the sum of the forces N_z acting on both sides, can be determined, taking Eq. (21) into consideration, by formula

$$2\int_0^v N_z\,dv = \frac{2\overline{P}_0}{a^2 b^2}(b^2 - a^2)\,(a^2\cos^2\gamma + b^2\sin^2\gamma)\cdot\sin\gamma\cdot\cos\gamma\cdot\frac{v^2}{2} \qquad (22)$$

and the sum of the forces $\overline{N}_{uv}$ acting on both sides, may be expressed considering Eq. (19), by formula

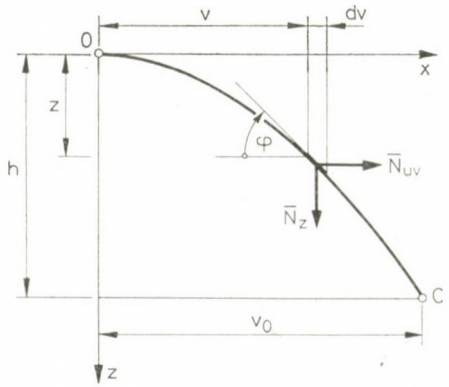

Fig. 6

$$2\int_0^v \overline{N}_{uv}\,dv = \frac{\overline{P}_0}{2h}(b^2 - a^2)\,v\sin\gamma\cdot\cos\gamma\cdot v\,. \qquad (23)$$

The quotient of these two latter values is equal to the derivative of the centre line of the dividing rib OC at point v, that is, to the tangent of the angle φ:

$$\frac{\partial z}{\partial v} = \frac{2hv}{a^2 b^2}(a^2\cos^2\gamma + b^2\sin^2\gamma)\,. \qquad (24)$$

This means that the centre line of the rib OC is really the funicular curve of the forces attacking the rib. Thus, it is evident, that under the effect of the load no flexural-torsional forces are generated in the dividing rib OC.

6. Equilibrium of the points of abutment of the ribs

By a simple consideration it is easy to prove that the v-directed horizontal forces acting on the abutment point of the rib OC constitute within themselves a set of forces in equilibrium, and so, the abutment point C need not be fixed against a v-directed displacement by a tie rod nor with any other device.

Namely, according to formula (17), the v-directed force acting from both sides *outwards* upon the abutment point C is

$$2\,H_1 = \bar{p}_0 \frac{ab}{2h} \frac{(b^2 - a^2)\sin\gamma}{\sqrt{a^2 + b^2\tan^2\gamma}} \tag{25}$$

and considering formulae (5) and (19), the v-directed force exerted *inwards* by the sectioning rib on point C is

$$2\bar{N}_{uv}\,v_C = 2\frac{\bar{p}_0}{4h}(b^2 - a^2)\sin\gamma\cdot\cos\gamma\frac{ab}{\cos\gamma\sqrt{a^2 + b^2\tan^2\gamma}}$$

which, after simplification, reads

$$2\bar{N}_{uv}\,v_C = \bar{p}_0\frac{ab}{2h}\cdot\frac{(b^2 - a^2)\sin\gamma}{\sqrt{a^2 + b^2\tan^2\gamma}}\,. \tag{26}$$

Since the force (25) directed outwards and that (26) directed inwards, are opposed to each other, point C in the horizontal direction needs no particular support, as it is equipoised. The equilibrium of point C is realized in direction u by the existing symmetry, and in direction z by the fact of being wall supported.

REFERENCES

1. PUCHER, A.: Über den Spannungszustand in gekrümmten Flächen. *Beton und Eisen* **33** (1934), 298
2. CSONKA, P.: Membranschalen. *Bauingenieur-Praxis* No. 16. Verlag von Wilhelm Ernst u. Sohn, Berlin—München 1966, pp. 61—69
3. DULÁCSKA E.: Muschelformige Schalenkonstruktion. *Acta Techn. Hung.* **29** (1960), 397—405
4. CSONKA P.: Composite Shells Polygonal in Plan with Free Front Edge and Unbent Dividing Ribs. *Theorie und Praxis des Stahlbaues.* Festschrift zum 65. Geburtstag von Herrn Dr.-Ing. Gotthard Franz, Karlsruhe. Verlag von Wilhelm Ernst u. Sohn, Berlin—München 1969, pp. 160—165
5. CSONKA P.: Kuppelschalen über Polygonalgrundrissen. *Schalen in Beton und Kunststoff.* Entwurf—Bemessung—Ausführung. Published by S. Polónyi with contributions of A. M. Haas, H. Rühle, P. Csonka, H. Isler, F. Candela. Bauverlag GmbH., Wiesbaden u. Berlin 1970, pp. 88—95

Segmentenschale ohne Zugstangen mit biegungsfreien Randbogen und Rippen. — Segmentenschalen von außergewöhnlicher Form und speziellen Eigenschaften werden im Rahmen der Membrantheorie behandelt. Als Belastung wird ein gleichmäßig verteiltes, vertikales Kraftsystem in Betracht gezogen. Es wird bewiesen, daß in den Begrenzungsträgern der einzelnen Schalensegmente keine Biege- bzw. Torsionskräfte auftreten und der Seitenzug der Verteilungsrippen durch den Seitenzug der Randbogen ausgeglichen, bzw. behoben wird. Aus diesem Grunde sind bei den behandelten Schalen keine Zugstangen bzw. Strebebalken erforderlich.

Acta Technica Academiae Scientiarum Hungaricae, Tomus 91 (3—4), pp. 257—263 (1980)

HIGH-ACCURACY INTERPOLATION OF STRESSES

E. BÉRES*
DR. OF TECHN. SCI.

[Manuscript received January 3, 1980]

Dividing a solid into elements by parallel and perpendicular planes, the accuracy of stress distribution may be improved by extending the required fitting of the approximative polynomial, in addition to the element corners, also to neighbouring nodes, meaning 32 fittings in space, 12 in the plane, and 4 along the straight line. The suggested three-variable polynomial of 32 terms will be presented to change in plane and along the straight line into two-variable and single-variable polynomials of 12 and 4 terms, respectively. Distribution is uniform at element interfaces, showing the approximation to be continuous and unambiguous throughout the solid.

As a difference from approximate functions for single elements as is assumed in the finite element method, where fitting points may only be on the boundary of, or inside, the element (see e.g. HUEBNER [1]), approximate functions fitted to element corners and neighbouring nodes may be convenient [2]. These approximate functions are also required to fit into some order along the element boundaries. In our case these functions will only be required to be of identical value at the element interfaces, that is, the approximate function has to be continuous troughout the domain in an order C°. In the case of approximating by polynomials, the geometric isotropy is conditioned by

a) completeness of the polynomial of order n, or

b) symmetry of an incomplete polynomial of order n.

As referred to in [1] and appearing from a paper by DUNNE [3] and comments [4], for points exclusively on boundaries, a complete polynomial can be only exeptionally applied. Since the examined case is restricted to element corners, application of complete polynomials has been disregarded and symmetrical polynomials taken as approximate functions. In the following, these will be demonstrated to provide continuous approximation throughout the domain in order C°,

a) *Three-variable functions of each stress component belonging to the elements can be assumed so that stress distributions along element interfaces are uniform throughout.*

b) *If properly assumed, three-variable functions belonging to elements meeting along one edge are reduced along that edge to the same single-variable function.*

*Dr. E. BÉRES, Hunyadi János u. 11, H-1011 Budapest, Hungary

Detailed analysis and demonstration will refer to the special case where four points are considered along each straight line parallel to the coordinate axis, that is, the single-variable approximate polynomial is of order three. Namely, partly, a higher-order approximation is generally needless, and partly, on this basis the assumption and the demonstration are easily performed for a polynomial of arbitrary order (e.g. 5 or 7). These functions entering in definite integrals, assumption of odd-order polynomials is advisable.

Assuming a coordinate system according to Fig. 1 leads to a third-order polynomial fitting points 9, 1, 4 and 18:

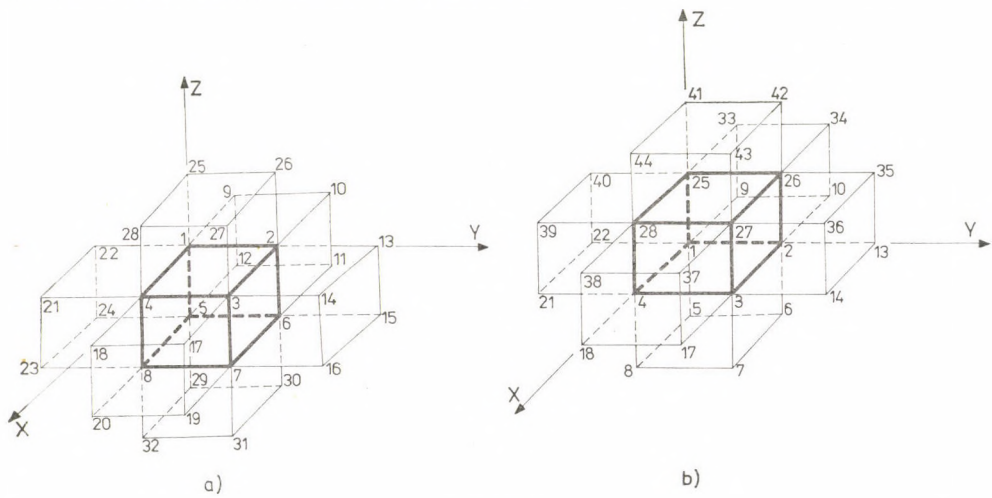

Fig. 1

$$g(x) = ax^3 + bx^2 + cx + d\ , \tag{1}$$

with unknown coefficients a, b, c, d, to be expressed by function values belonging to the four points.

Thereafter the two-variable polynomial belonging to the plane x, y has to be assumed to yield function (1) for the section $y = 0$. Obviously, two-variable polynomial (1) in [2]

$$f(x, y) = Ax^3 + Bx^2 + Cx + Dy^3 + Ey^2 + Fy + Gx^3y + Hxy^3 + Jx^2y + Kxy^2 + Lxy + M \tag{2}$$

meets this condition, namely

$$f(x, 0) = Ax^3 + Bx^2 + Cx + M. \tag{3}$$

Obviously, function values belonging to points 9, 1, 4 and 18 determine constants of both (1) and (3), hence

$$f(x, 0) \equiv g(x), \tag{4}$$

that is to say, $A = a$, $B = b$, $C = c$, and $M = d$.
Also,

$$f(x, b) = a_1x^3 + b_1x^2 + c_1x + d_1 = g_1(x) \ ,$$

where $g_1(x)$ is a polynomial of order three, fitting points 10, 2, 3, 17.

(2) approximates stress distribution over a rectangle with corners 1, 2, 3, 4. The approximation has been improved by prescribing equality in other corners of the four adjacent rectangles, equivalent to having indicated 12 points in all, that is, assuming a polynomial of 12 terms. In assuming the polynomial, care has been taken to be symmetrical in x and y, and to have nothing but terms occurring in (1) in case of $y = 0$. Symmetry provides for a similar expression to result for $x = 0$. (2) is the lowest-order expression meeting these conditions.

According to the same train of thought, it is easy to assume a three-variable polynomial leading to two-variable polynomials of form (2) along prism faces, and to single-variable polynomials of form (1) along its edges. Namely, if the approximate polynomial is to be written for the prism outlined in a thick line in Fig. 1/a so that it equals the given function values even in the neighbouring points, then fitting will affect 32 points in all, thus, a polynomial of 32 terms will be assumed. In this case, also variables x, y and z are required to have symmetric expressions, and of course, to have them reduced to expressions of form (2) along each face. The three-variable polynomial of lowest order, also meeting the condition of geometric isotropy, is:

$$\begin{aligned} h(x, y, z) = {} & a_0 + a_1 x + a_2 y + a_3 z + a_4 x^2 + a_5 xy + a_6 xz + a_7 y^2 + \\ & + a_8 yz + a_9 z^2 + a_{10} x^3 + a_{11} x^2 y + a_{12} x^2 z + a_{13} xy^2 + \\ & + a_{14} xyz + a_{15} xz^2 + a_{16} y^3 + a_{17} y^2 z + a_{18} yz^2 + a_{19} z^3 + \\ & + a_{20} x^3 y + a_{21} x^3 z + a_{22} x^2 yz + a_{23} xy^2 z + a_{24} xyz^2 + \\ & + a_{25} xy^3 + a_{26} xz^3 + a_{27} y^3 z + a_{28} yz^3 + a_{29} x^3 yz + \\ & + a_{30} xy^3 z + a_{31} xyz^3 \ . \end{aligned} \tag{5}$$

Apparently, in fact:

$$h(x, y, 0) = f(x, y) \tag{6}$$

and

$$h(x, 0, 0) = g(x) \ . \tag{7}$$

Although (5) is not the only polynomial meeting the assumptions, it unambiguously contributed to defining a suitable polynomial.

Now, it is easy to demonstrate that three-variable functions referring to different prisms are reduced to the same two-variable and single-variable functions along the interfaces and the common edges, respectively. Figs 1/a and 1/b show two adjacent prisms with their surroundings applied to the interpolating polynomials. Fig. 1/a refers to elements with points 1, 2, 3, 4, 5, 6, 7, 8, and Fig. 1/b to those with 1, 2, 3, 4, 25, 26, 27, 28. Face 1, 2, 3, 4 is common to both. Among 32 points each of both elements and their surroundings, 20 are common, and 12 each are different. Therefore, polynomials $h(x, y, z)$ referring to the two elements and their constants are different, but functions $f(x, y)$ belonging to the common face 1, 2, 3, 4 are identical. Namely, let us assume the coordinate system according to Figs 1/a and 1/b. Let function $h(x, y, z)$ belonging to Fig. *a* be $h_a(x, y, z)$ and that belonging to *b*, $h_b(x, y, z)$ then:

$$h_a(x, y, 0) = h_b(x, y, 0) = f(x, y) , \tag{8}$$

where $f(x, y)$ is a two-variable polynomial fitting points 1, 2, 3, 4, 9, 10, 13, 14, 17, 18, 21, 22. Eq. (5) being symmetrical about variables x, y, z, the proof is valid to all faces of the prism. Thereby theorem a) has been adequately demonstrated.

Each internal edge belongs to four elements, each two contacting only along this edge. Theorem b) stating the three-variable function $h(x, y, z)$ belonging to all four elements, to reduce to the same single-variable function $g(\xi)$ ($\xi = x, y, z$) along the edge, might also be proved relying on theorem a), but there is a still simpler demonstration.

Let us consider line 1—4 in Fig. 1. It is a common edge of elements with corners 1, 2, 3, 4, 5, 6, 7, 8; 1, 2, 3, 4, 25, 26, 27, 28; 1, 4, 21, 22, 25, 28, 39, 40 and 1, 4, 21, 22, 5, 8, 23, 24 having polynomials $h_1(x, y, z)$, $h_2(x, y, z)$, $h_3(x, y, z)$ and $h_4(x, y, z)$, respectively. According to (5) and (7), obviously,

$$h_1(x, 0, 0) = h_2(x, 0, 0) = h_3(x, 0, 0) = h_4(x, 0, 0) = g(x) , \tag{9}$$

where $g(x)$ is a third-order polynomial fitting points 9, 1, 4, 8. Because of the letter symmetry, also this proof is valid to any edge. Thereby theorem *b)* has been proved.

Up till now, only inner elements have been considered, thus, partly, there was a neighbouring point in any direction, and partly, all surfaces were plane, and all lines straight. Along boundary surfaces of solids, however, cases other than that, hence not plane surfaces and curved lines are possible. The simplest is to demonstrate graphically that the preceding statements, that is, Eq. (5) and the theorems are invariably valid for these cases. First of all, Figs 2, 3 and 4 illustrate alternatives for assuming the 32 points in different cases, then Fig. 3 explains why the theorems are valid in different special cases.

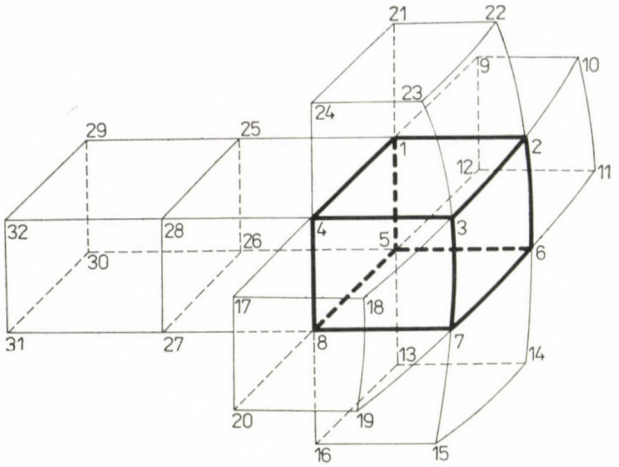

Fig. 2

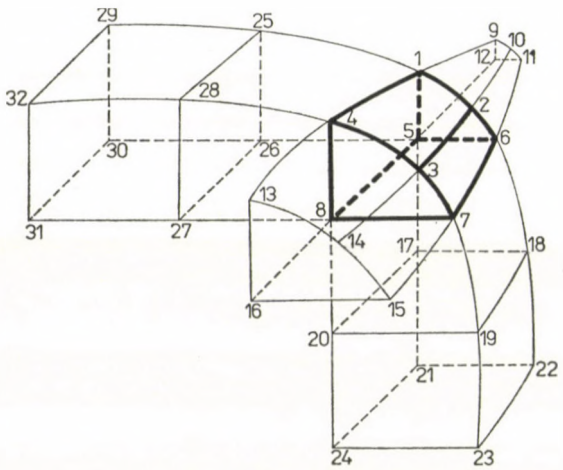

Fig. 3

The figures show the possibility to always assume 32 points of an element to have 12 points each in the plane sections, providing for the three-variable function of form (5) to take form (2) in the section. They may be less regular arrangement of the 32 points in the space or of the 12 points in the plane than seen in Fig. 1 has no principial difference.

At a first glance, the difference seems more marked for elements joining along curved edges, the fundamental case referring only to straight edges, a fact entering in the proof. Fig. 3 referring to various cases, illustration will be taken therefrom.

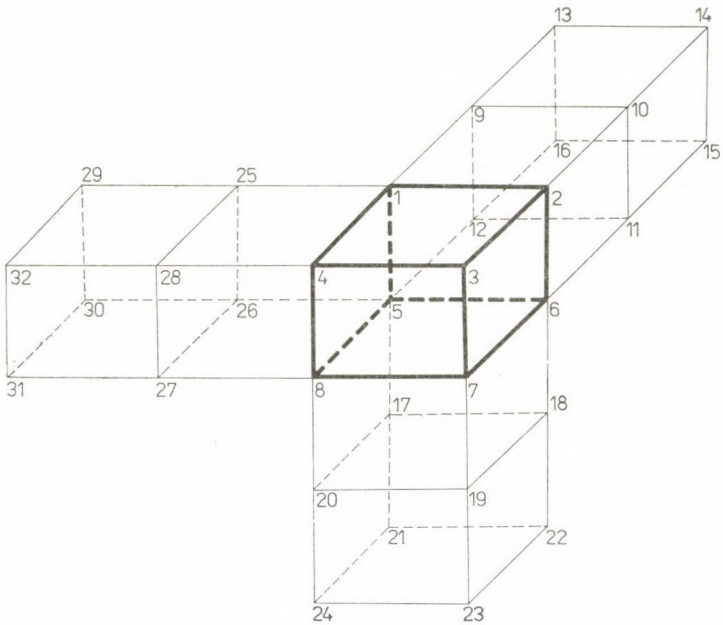

Fig. 4

Lines in the solid such as 5—8 or 7—8 are straight, hence under the direct validity of the former proof, irrespective of the irregularity of the element.

The line of intersection between the solid surface and the planes is a plane curve, that is, however, a common edge only between two elements, having a plane interface along which function values for both elements are the same. This identity refers, of course, also to the entire face, hence, also to its boundary line. Such lines in Fig. 3 are 1—2, 2—6, 1—4, 4—3, 3—7, 6—7. Line 2—3 needs no special consideration, it belonging to a single element, self-intended to have a continuous function.

Thus, it has been demonstrated, that decomposing the solid into elements by means of parallel and normal planes permits to indicate element-wise distribution of element corner stresses uniform along element interfaces and common edges, that is, element-wise interpolation may be applied, assuming continuous stress distribution throughout the solid. Inside each element, this distribution may be expressed by a polynomial of form (5), equivalent to a third-order polynomial approximation along the edges, while stress distribution along the interfaces is described by two-variable polynomials.

At the same time it has been proved that, while equilibrium conditions have only been approximated by double integrals referring to the element surfaces in [2], and this by involving only two-variable integrands in each

integral, while approximation of the continuity conditions involved only linear integrals, this method leaves the tridimensional, hence three-variable character of the general case unaffected.

REFERENCES

1. HUEBNER, K. H.: The Finite Element Method for Engineers, John Wiley et Sons, New York—London—Sydney—Toronto, 1975
2. BÉRES, E.: Three-dimensional Stress Analysis by Means of a Continuum Sub-Space. *Acta Techn. Hung.* **79** (1974), 239—266
3. DUNNE, P. C.: Complete Polynomial Displacement Fields for Finite Element Method. *The Aeronautical Journal*, **72** (1968), 245—246
4. IRONS, B. M.—ERGATOUDIS, J.—ZIENKIEWICZ, O. C.: Comments on Complete Polynomial Displacement Fields for Finite Element Method. *The Aeronautical Journal*, **72** (1968).

Hochgenaue Interpolation von Spannungen. — Wird ein Körper mittels gleichlaufenden bzw. senkrechten Ebenen zu Elementen verschnitten, so kann die Genauigkeit der Näherung der Spannungsverteilung über den einzelnen Elementen dadurch erhöht werden, daß die Anpassung des Annäherungspolynoms außer zu den Elementenspitzen, auch zu den benachbarten Knotenpunkten erfordert wird. Das bedeutet im Raum 32, in der Ebene 12, und längs einer Geraden 4 Punktanpassungen. Es wird gezeigt, daß das vorgeschlagene 32-gliedrige Polynom mit drei Veränderlichen in der Ebene zu einem 12-gliedrigen, und längs einer Geraden zu einem 4-gliedrigen Polynom mit zwei bzw. einem Veränderlichen übergeht. Der Wert der elementenweise Verteilungen ist gleich bei den Elementenanschlüsse, also ist die Annäherung im ganzen Körper kontinuierlich und eindeutig.

Acta Technica Academiae Scientiarum Hungaricae, Tomus 91 (3—4), pp. 265—301 (1980)

UNTERSUCHUNG DER STABILITÄT SATTELFÖRMIGER, FLACHER, NORMALKRAFTFREI GELAGERTER HP-SCHALEN UNTER GLEICHMÄSSIG VERTEILTER BELASTUNG

L. JANKÓ*

[Eingegangen am 28. Dezember 1978]

Diese Abhandlung bildet den zweiten Teil einer dreiteiligen Artikel-Serie. Im ersten Teil waren die theoretischen Fragen der Existenz und der Eindeutigkeit der Membranlösung, sowie der kinematischen Unbestimmtheit von HP-Schalen behandelt worden. Auf Grund dessen wird in diesem Teil die Erscheinung der *Verzweigung* aus dem *unverformten* Grundzustand erörtert. Im Laufe der Analyse wird auch der Untersuchung der *dehnungslosen Beulungsmöglichkeit* eine große Bedeutung zugemessen.

BEZEICHNUNGEN

$C_{ij} = \cos\frac{i\pi}{2a}x \cdot \cos\frac{j\pi}{2b}y$;

$C_{mn} = \cos\frac{m\pi}{2a}x \cdot \cos\frac{n\pi}{2b}y$;

$D = \frac{Eh}{1-\mu^2}$ spezifische Dehnungssteifigkeit;

E Elastizitätsmodul;
F Spannungsfunktion der Mittelflächenkräfte ($F'' = N_x$, $F'' = -N_{xy}$, $F'' = N_y$);
F_0 Spannungsfunktion des Grundzustandes;
$\bar{F} \equiv \delta F$ erste Variation der Funktion F_0 ($F = F_0 + \bar{F}$);

$B = \frac{Eh^3}{12(1-\mu^2)}$ spezifische Biegesteifigkeit;

M_x, M_y bzw. $M_{xy} = M_{yx}$ Biege- bzw. Drillmomente;
N_x, N_{xy}, N_y Mittelflächenkräfte;
N_{xb}, N_{xyb}, N_{yb} Mittelflächenkräfte nach der Biegetheorie;
N_{xm}, N_{xym}, N_{ym} Membrankräfte;

$S_{ij} = \sin\frac{i\pi}{2a}x \cdot \sin\frac{j\pi}{2b}y$;

$S_{mn} = \sin\frac{m\pi}{2a}x \cdot \sin\frac{n\pi}{2b}y$;

U_b Potential der Biegeschnittkräfte;
U_m Potential der Mittelflächenkräfte;
V Potential der äußeren Kräfte;
$2a$, $2b$ Spannweiten der Randbogen in den x- bzw. y-Richtungen;
f_a, f_b Pfeilhöhen der in den x- bzw. y-Richtungen liegenden Randbogen;
h Schalendicke;

* Dr.-Ing. L. JANKÓ, Lajos u. 142., H-1036 Budapest, Ungarn

i, j	Halbwellenzahlen in den x- bzw. y-Richtungen (der Index n weist auf dehnungslose Verformung hin);
p	Intensität der gleichmäßig verteilten, in Richtung der Achse z wirkenden, symmetrischen Belastung (bezogen auf die Flächeneinheit der Grundrißprojektion);
p_{kr}^{lin}	lineare kritische Last;
$\bar{p}_{\text{kr}}$	kritische Durchschlagslast;
$p_{kr,v}^{\text{lin}}$	lineare kritische Last der Verzweigung aus dem verformten Grundzustand;
u, v	Verschiebungen in Richtungen der Flächentangenten parallel zur $x-z$- bzw. $y-z$-Ebene;
$z(x, y)$; $\bar{z}(\bar{x}, \bar{y})$	Ordinaten der Schalenmittelfläche;
w	Verschiebung eines Mittelflächenpunktes in Richtung der Flächennormale ($w = w_0 + \bar{w}$);
w_0	im Grundzustand entstehende Verschiebung eines Mittelflächenpunktes in Richtung der Flächennormale;
$\bar{w}$	erste Variation der Verschiebung w_0 (im Nachbarzustand);
w_a	Vorbeulamplitude (Anfangsausmittigkeit);
$\alpha = f_a/f_b$	Pfeilhöhenverhältnis;
$\beta = a/h$	Schalenparameter;
$\gamma = a/b$	Steinverhältnis;
$\delta \equiv (\bar{\ })$	Symbol der Variationsbildung;
η	Koordinate in Richtung einer der beiden geraden Erzeugenden vom Punkt $x = a$, $y = b$ (verläuft parallel zur zweiten Leitebene);
$\lambda = p_{kr}^{\text{lin}}/E$	Eigenwert;
μ	Querdehnungszahl (in den Berechnungen: $\mu = 0{,}2$);
ξ	Koordinate in Richtung einer der beiden geraden Erzeugenden vom Punkt $x = a$, $y = b$ (ξ verläuft parallel zur ersten Leitebene);
Π	Gesamtpotential;
$\varrho = f_b/b$	Schalenparameter;
ω	Hälfte des Winkels zwischen den Leitebenen;

$\Delta\Delta(\ ) = (\ )^{IV} + 2(\ )^{II} + (\ )^{::}$ der biharmonische Differentialoperator;

$L_p(f_1, f_2) = f_1^{II} f_2^{::} - 2 f_1^{'} f_2^{'} + f_1^{::} f_2^{II}$ der Puchersche-Differentialoperator.

1. Einleitung. Zweckbestimmung

Wegen ihrer gefälligen Form und der günstigen Ausführungsmöglichkeiten, die die geraden Erzeugenden bieten, werden immer häufiger Schalenkonstruktionen in Form des hyperbolischen Paraboloids (im weiteren HP-Schalen) gebaut.

Die HP-Schalen sind im allgemeinen entlang ihren Flächenerzeugenden oder den Hauptkrümmungslinien auf Randträgern gelagert.

Die statischen Probleme der längs der Erzeugenden abgestützten HP-Schalen sind sowohl nach der Theorie I. Ordnung, als auch nach der Theorie II. Ordnung ausführlich erörtert werden [5], [7], [15], [19], [21].

Im Falle der sattelförmigen HP-Schalen (Bild 1) jedoch, die entlang der Hauptkrümmungslinien durch Randbogen abgestützt sind, die in der horizontalen Richtung eine vernachlässigbare Biege- bzw. Drillsteifigkeit besitzen (im weiteren »normalkraftfreie« oder »halbsteife« Randträger), liegen die Dinge anders. Die Ausarbeitung des (»linearen« und »nichtlinearen«) Stabilitätsverhaltens der erwähnten Schalen steht jedoch noch aus.

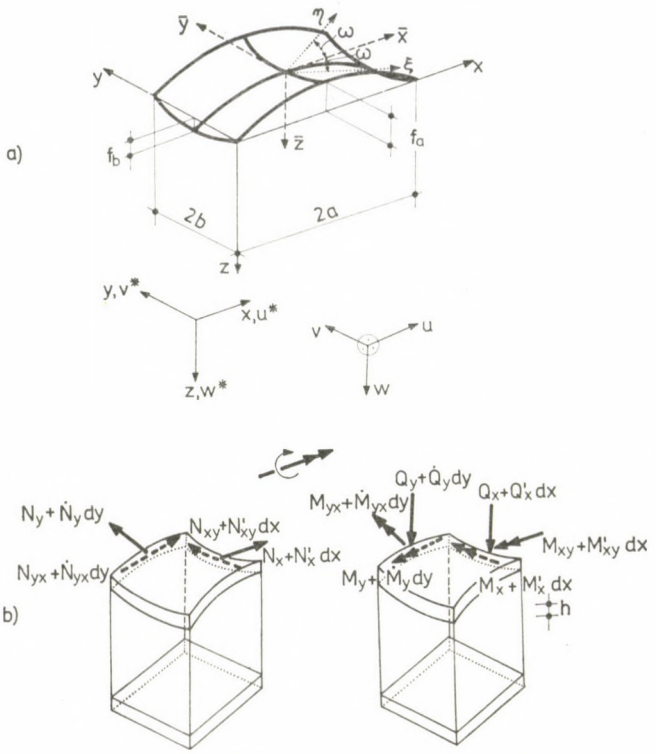

Bild 1. Geometrische Angaben der sattelförmigen HP-Schale. Vorzeichenregel der inneren Kräfte und der Verschiebungen

Mihailescu [16] hat die Verzweigungserscheinung der sattelförmigen HP-Schalen ($w_0 = 0$) auf Grund der Beulgleichung der ebenen Platten untersucht. Er hat angenommen, daß die Beulung durch eingliedrige, symmetrische Beulformen gekennzeichnet werden kann.

Die kritische Druckkraft hat sich dadurch ergeben, daß die konstanten Membrandruckkräfte in Richtung der Erzeugenden, die im mittleren Gebiet der Schale auftreten, vom Verfasser in die Beulgleichung einer »Ersatzplatte« eingesetzt worden sind.

Die in Betracht gezogenen Beulformen sind nicht die maßgebenden Beulformen der HP-Schale. Die Anwendung dieser Lösung führt zu einer recht unwirtschaftlichen Bemessung.

Apeland [1] hat unter Zugrundelegung eingliedriger Beulformen die Verzweigungserscheinung von flachen Paraboloidschalen mit auch in horizontaler Richtung biegesteifen und drillsteifen Randträgern behandelt. Die hergeleiteten Zusammenhänge sind für Schalen gültig, die ihre Lasten in der einen Richtung (x: von oben betrachtet konvexe Bogen) durch konstante Druckkräfte, in der anderen Richtung (y: von oben betrachtet konkave Bogen)

durch konstante Zugkräfte tragen. Dieses schubkraftlose Kräftespiel läßt sich praktisch kaum verwirklichen. Seine Randbedingungen und das angenommene willkürliche Kräftespiel beziehen sich nicht auf den Fall, der von uns untersucht werden soll.

GIONCU [9] hat das Kräftespiel von APELAND zugrunde gelegt. Er hat angenommen, daß die HP-Schale in Richtung x vielen Wellen beult. Unter diesen Annahmen hat die Berechnung zu folgender Schlußfolgerung geführt: die lineare kritische Last der sattelförmigen HP-Schale ist der kritischen Last derjenigen windschief-viereckigen HP-Schale gleich, die gleichen Krümmungsverhältnisse besitzt wie die sattelförmige HP-Schale.

Seine Annahmen, bezogen sowohl auf die Membranlösung, als auf die (eingliedrige) Beulform, sind willkürlich, deswegen läßt sich dieses Resultat ohne Kritik nicht annehmen.

TSUBOI [23] hat sich mit der Beulung der normalkraftfrei gelagerten, flachen Paraboloidschalen befaßt. Diese Berechnungen, die mit Hilfe eingliedriger Beulformen durchgeführt worden sind, beziehen sich auf HP-Schalen mit quadratischem Grundriß.

Die Analyse der Wirkung der Möglichkeit der Bildung von dehnungslosen Verformungen wurde nicht behandelt.

Die allgemeine Theorie der Stabilitäts- und Schwingungserscheinungen von anisotropen flachen Schalen ist von DULÁCSKA [6] ausführlich bearbeitet worden.

Im Rahmen dieser Bearbeitung ist auch die Verzweigungserscheinung von zweimal gekrümmten Kuppelschalen mit unterschiedlichen Krümmungsverhältnissen behandelt worden [6], [12].

Der als Berechnungsgrundlage dienende Membranzustand ist durch die Zusammenhänge $N_{xm} = \text{konst.}$, $N_{ym} = \text{konst.}$, $N_{xym} = 0$ gekennzeichnet. Die Herleitung hat die (versteifende) Wirkung der Ränder unberücksichtigt gelassen, die Ergebnisse haben demnach für die Schalen Gültigkeit, die in mehreren Wellen ausbeulen, bei denen also die Randbedingungen praktisch keine Rolle mehr spielen. Bei derart ausbeulenden Schalen ist auch die Voraussetzung erfüllt, daß sie innerhalb der entstehenden Beulwelle als flach angesehen werden dürfen.

Von großer Bedeutung ist auch seine Feststellung, daß die untere Schranke der linearen kritischen Last der HP-Schale und die lineare kritische Last der in identischer Form ausbeulenden ebenen Platte einander gleich sind.

Tatsache ist, daß im Zusammenhang mit den Stabilitätserscheinungen der an ihren Rändern normalkraftfreien hyperbolischen Sattelparaboloidschalen nur einige Ergebnisse sind. Nach Ansicht des Verfassers erklärt sich dies

— aus dem Problem der *Existenz und Eindeutigkeit der Membranlösung* und

— aus den Schwierigkeiten, die sich aus der *kinematischen Unbestimmtheit* (dehnungslose Verformungen) der Fläche ergeben.

Diese Abhandlung hat sich die theoretische Untersuchung der Verzweigung aus dem unverformten Grundzustand ($w_0 = 0$) der an ihren Rändern normalkraftfreien, sattelförmigen HP-Schalen *zum grundlegenden Ziel gesetzt.*

Aus den erwähnten Gründen sind diese Themenkreise vor den Stabilitätsuntersuchungen in [10] ausführlich behandelt worden. Es sind die Schalenparameterbereiche ermittelt worden, in welchem der Effekt der Biege- und Drillmomente im Vergleich zum Effekt der Mittelflächenkräfte nach der Biegetheorie vernachlässigbar klein ist.

Unter solchen geometrischen Verhältnissen genügt es die HP-Schalen bloß nach der Membrantheorie zu bemessen. Im gegebenen Fall muß man sich mit den Biegeeffekten nur in den Randbereichen befassen. In solchen Fällen ist es richtig auch den Verlauf des Stabilitätsverlustes nach der »linearen« Stabilitätstheorie zu untersuchen. Es handelt sich nämlich um eine *Verzweigungserscheinung*, die aus dem unverformten (membranartigen) Grundzustand ($w_0 = 0$) erfolgt (Bild 2).

Im Laufe der Erörterungen wird auch darauf eingegangen, wie die Entwicklungsmöglichkeit der dehnungslosen Verformungen [8], [10], [12], [13] den Verlauf des Stabilitätsverlustes beeinflußt.

Zur Erleichterung der praktischen Anwendung sind die zur Bemessung gut geeigneten Resultate in Formeln und Schaubildern bzw. Tafeln dargelegt.

2. Kennzeichnung des Grundzustandes. Grundannahmen

In [10] wurden die Ausdrücke für die inneren Kräfte der HP-Schalen unter Belastung p = konst. nach der Theorie I. Ordnung der flachen Schalen aufgeschrieben:

$$p(x, y) = \frac{16}{\pi^2} p \sum_{m}^{M} \sum_{n}^{N} \frac{1}{mn} \sin \frac{m\pi}{2a} x \sin \frac{n\pi}{2b} y \,, \qquad (2.1)$$

$$m = 1, 3, 5, \ldots, M \,,$$

$$n = 1, 3, 5, \ldots, N$$

$$\alpha = \frac{f_a}{f_b} \,, \beta = \frac{a}{h} \,, \qquad (2.2\text{a}-\text{d})$$

$$\gamma = \frac{a}{b} \,, \varrho = \frac{f_b}{b} \,,$$

$$A_{mn} = \frac{768(1 - \mu^2)}{\pi^4} (\varrho\beta\gamma)^2 (m^2 - \alpha n^2), \qquad (2.3)$$

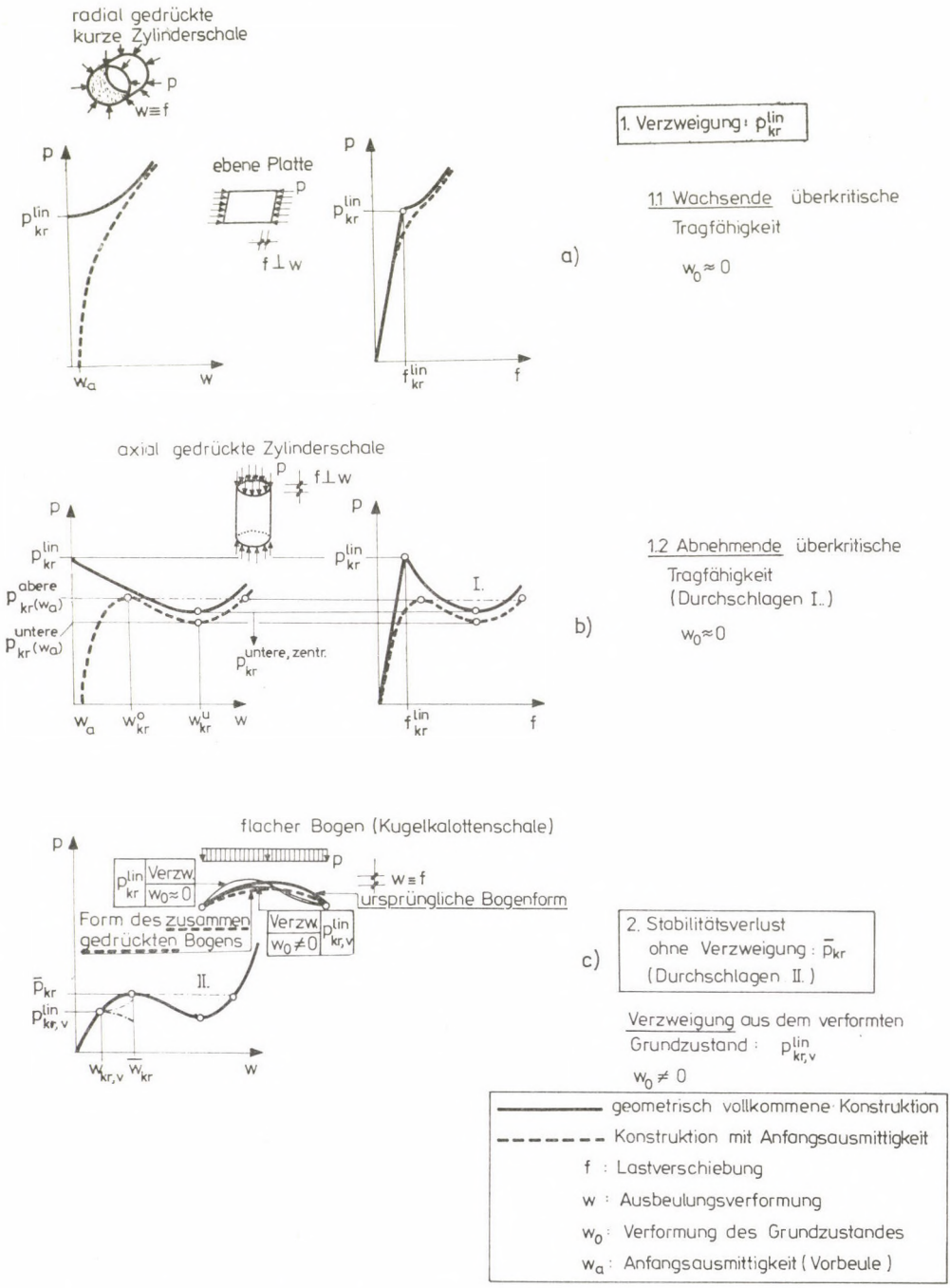

Bild 2. Einige charakteristischen Tragverhaltenskurven der Stabilitätserscheinungen

$$B_{mn} = (m^2 + \gamma^2 n^2)^2 , \tag{2.4}$$

$$N_{mn} = - \frac{A_{mn}}{A_{mn}(m^2 - \alpha n^2) + B_{mn}^2} , \tag{2.5}$$

$$S_{mn} = \sin \frac{m\pi}{2a} x \cdot \sin \frac{n\pi}{2b} y ,$$

$$C_{mn} = \cos \frac{m\pi}{2a} x \cdot \cos \frac{n\pi}{2b} y , \tag{2.6a—b}$$

$$\left.\begin{aligned} n_x^0 &= - \frac{8}{\pi^2} \sum_m^M \sum_n^N \frac{n}{m} N_{mn} S_{mn}, \\ n_{xy}^0 &= - \frac{8}{\pi^2 \gamma} \sum_m^M \sum_n^N N_{mn} C_{mn}, \\ n_y^0 &= - \frac{8}{\pi^2 \gamma^2} \sum_m^M \sum_n^N \frac{m}{n} N_{mn} S_{mn}, \\ m &= 1, 3, 5, \ldots, M \\ n &= 1, 3, 5, \ldots, N \end{aligned}\right\} \tag{2.7a—c}$$

$$\left.\begin{aligned} m_x^0 &= - \frac{64}{\pi^4} \sum_m^M \sum_n^N \frac{m}{n} \frac{B_{mn}}{A_{mn}} N_{mn} S_{mn}, \\ m_{xy}^0 &= - \frac{64\,(1-\mu)}{\pi^4} \gamma \sum_m^M \sum_n^N \frac{B_{mn}}{A_{mn}} N_{mn} C_{mn}, \\ m_y^0 &= - \frac{64}{\pi^4} \gamma^2 \sum_m^M \sum_n^N \frac{n}{m} \frac{B_{mn}}{A_{mn}} N_{mn} S_{mn}, \\ w^0 &= - \frac{3072\,(1-\mu^2)}{\pi^6} \beta^4 \sum_m^M \sum_n^N \frac{1}{mn} \frac{B_{mn}}{A_{mn}} N_{mn} S_{mn}, \\ m &= 1, 3, 5, \ldots, M \\ n &= 1, 3, 5, \ldots, N \end{aligned}\right\} \tag{2.8 a—d}$$

$$\left.\begin{aligned} N_{xb} &= n_x^0 \frac{pa^2}{f_b} , \\ N_{xyb} &= n_{xy}^0 \frac{pa^2}{f_b} , \\ N_{yb} &= n_y^0 \frac{pa^2}{f_b} , \end{aligned}\right\} \tag{2.9 a—c}$$

$$\begin{aligned} M_x &= (m_x^0 + \mu m_y^0)\, pa^2 , \\ M_{xy} &= \quad m_{xy}^0\, pa^2 , \\ M_y &= (m_y^0 + \mu m_x^0)\, pa^2 , \\ w &= \frac{ph}{E} w^0 . \end{aligned} \tag{2.10a—d}$$

Die angegebenen Zusammenhänge entsprechen der Lösung von [2].

Es wird der kritische Lastwert gesucht, bei dem für die ausgebeulte Schale eine Gleichgewichtslage entstehen kann, die der unausgebeulten Schale unendlich nahe liegt.

Die Untersuchung der Verzweigungserscheinung braucht nur die ersten Potenzen der unendlich kleinen Verschiebungskomponenten, bzw. ihrer Ableitungen zu berücksichtigen, da die zweiten Potenzen schon um eine Größenordnung kleiner und somit vernachlässigbar sind. Dieses Verfahren wird im weiteren als die Berechnungsweise nach der *linearen Theorie* genannt. Der vor der Verzweigung sich gebildete unverformte *Grundzustand wird als Membranzustand betrachtet.*

Dies ist dadurch zu begründen, daß es in [10] nachgewiesen wurde: *die Biegewirkungen sind* für die Fälle der geometrischen Verhältnisse $f_a/f_b = (1{,}5 \div 2) \div 4$ *gegenüber der Mittelflächenwirkungen* nach der Biegetheorie der behandelten sattelförmigen HP-Schalen *verschwindend gering.* Demnach sind in diesem Parameterbereich die sattelförmigen HP-Schalen als Membranschalen und infolgedessen die durch die *stetigen* Gleichungen (2.9a—c) bestimmten Normal- und Schubkräfte als Membrankräfte zu betrachten bzw. anzunehmen.

Die Verwendung der unstetigen Membranlösung wäre einerseits unbequem, anderseits ist eine solche Lösung nur unter gewissen speziellen Verhältnissen f_a/f_b möglich.

Die Durchbiegungen des vor der Verzweigung existierenden Grundzustandes sind — wie es in der Fachliteratur [3], [12], [17], [22], [25] allgemein angenommen wird — zu vernachlässigen, also

$$w_0 = 0 . \tag{2.11}$$

Der sogenannte *unverformte Grundzustand* wird durch die Gleichung (2.11) definiert.

Im Hinblick darauf, daß der Grenzwert f_a/f_b, bei dem die Schale nicht mehr als Membranschale betrachtet werden kann, sich nicht genau definieren läßt, werden die linearen kritischen Lasten für den in [10] untersuchten gesamten Parameterbereich ($f_a/f_b = 1 \div 4$) bestimmt.

Selbstverständlich ist schon im voraus bekannt, daß die zu den Verhältnissen $f_a/f_b = 1 - (1{,}5 \div 2)$ gehörigen linearen kritischen Lasten nur theoretische Bedeutung haben.

In diesem Bereich darf man die HP-Schalen unter Berücksichtigung der Biege- und Drillmomente nur nach *der (nichtlinearen) Theorie der großen Verformungen* behandeln.

Die nichtlineare Untersuchung wird in [11] vorgenommen.

Mit Hilfe der in diesem Abschnitt bestimmten linearen kritischen Lasten und der Last-Durchbiegungskurven nach der (nichtlinearen) Theorie der großen Verformungen kann man das gesamte Stabilitätsverhalten der behandelten HP-Schalen ermitteln.

Die Schalen werden als *flach* und geometrisch *vollkommen* und ihr Werkstoff wird als *linear-elastisch* betrachtet. Es werden die sich auf die ganze Fläche ausbreitenden Beulformen untersucht.

Die von den äußeren Lasten unabhängigen Schub-Eigenspannungen werden gleich Null betrachtet.

3. Grundgleichungen

Falls die Beulung der Schalenkonstruktion aus unverformtem Grundzustand ($w_0 = 0$) stattfindet, kann die zweite Variation der potentiellen Energie der Mittelflächenkräfte U_{m0} und jene der potentiellen Energie der Biegeschnittkräfte U_{b0} des Grundzustandes (mit Indizes »o«) in der Form

$$\delta^2 U_{m0} = \frac{1}{Eh}\int_0^{2a}\int_0^{2b} [\bar{F}^{\prime\prime 2} - 2\mu\bar{F}^{\prime\prime}\bar{F}^{\cdot\cdot} + \bar{F}^{\cdot\cdot 2} + 2(1+\mu)\,\bar{F}^{\cdot\prime 2} + \\ + (F_0^{\prime\prime}\bar{w}^{\cdot 2} - 2F_0^{\cdot\prime}\bar{w}^{\cdot}\bar{w}^{\prime} + F_0^{\cdot\cdot}\bar{w}^{\prime 2})Eh\,]\,dx\,dy\,, \tag{3.1}$$

$$\delta^2 U_{b0} = B\int_0^{2a}\int_0^{2b} [\bar{w}^{\prime\prime 2} + 2\mu\,\bar{w}^{\cdot\cdot}\,\bar{w}^{\prime\prime} + \bar{w}^{\prime\prime 2} + 2(1-\mu)\,\bar{w}^{\cdot\prime 2}]\,dx\,dy \tag{3.2}$$

aufgeschrieben werden.

Die beim Übergang vom Grundzustand zum Nachbarzustand auftretenden Durchbiegungsvariationen $\bar{w} \equiv \delta w_0$ und die Spannungsfunktionsvariationen $\bar{F}(\bar{w}) = \delta F_0$ sind durch Querstriche bezeichnet.

Die zweite Variation der potentiellen Energie V_0 der äußeren Belastung p ist in diesem Fall gleich Null:

$$\delta^2 V_0 = 0\,. \tag{3.3}$$

Es sei der spezifische Wert der zweiten Variation der inneren, bzw. der vollständigen potentiellen Energie mit u_0, bzw. mit π_0 bezeichnet.

Die zweite Variation der vollständigen Energie des Grundzustandes Π_0 ist letzten Endes durch die Zusammenhänge

$$\delta^2 U_0 = \int_0^{2a} \int_0^{2b} u_0 \, dx \, dy = \delta^2 U_{m0} + \delta^2 U_{b0}, \tag{3.4}$$

$$\delta^2 \Pi_0 = \int_0^{2a} \int_0^{2b} \pi_0 \, dx \, dy = \delta^2 U_0 + \delta^2 V_0 \tag{3.5}$$

gegeben. Der Energieausdruck (3.5) ist doppelt so groß, wie die Differenz der vollständigen potentiellen Energie nach und vor der Beulung.

Bekanntlich ist das Kriterium des indifferenten Gleichgewichtzustandes wie folgt abzufassen: die vollständige potentielle Energie Π_0 muß (vorausgesetzt, daß die Lasten des Systems unverändert bleiben) mindestens eine spezielle zweite Variation besitzen, deren jede erste Variation gleich Null ist. Mit anderen Worten: zur Bestimmung der linearen kritischen Last p_{kr}^{lin} hat man die Variationsaufgabe

$$\delta(\delta^2 \Pi_0) = 0 \tag{3.6}$$

zu lösen.

Die Extremalfunktion $\bar{w}$, welche das erwähnte Funktional $\delta^2 \Pi_0$ zu einem stationären Wert (Extremwert) macht, wird durch die Lösung der folgenden Euler-Lagrangeschen Differentialgleichung geliefert:

$$\frac{\partial \pi_0}{\partial \bar{w}} - \left(\frac{\partial \pi_0}{\partial \bar{w}'}\right)' - \left(\frac{\partial \pi_0}{\partial \dot{\bar{w}}}\right)^{\cdot} + \left(\frac{\partial \pi_0}{\partial \bar{w}''}\right)'' + \left(\frac{\partial \pi_0}{\partial \dot{\bar{w}}'}\right)^{\cdot\prime} + \left(\frac{\partial \pi_0}{\partial \bar{w}''}\right)^{\cdot\cdot} = 0 \,. \tag{3.7}$$

Werden die Ableitungen der Spannungsfunktion $\bar{F}$ in der zweiten Variation der potentiellen Energie U_{m0} der Mittelflächenkräfte in Abhängigkeit von den Verschiebungsvariationen $\bar{u}$, $\bar{v}$, $\bar{w}$ aufgeschrieben und dann die durch die Gleichung (3.7) vorgeschriebenen Operationen durchgeführt, so gelangt man zur Gleichung

$$B \Delta\Delta \bar{w} - L_p(\bar{F}, z) - L_p(F_0, \bar{w}) = 0 \,. \tag{3.8}$$

Wie bekannt, ist die Beziehung (3.8) die Gleichgewichtsgleichung der aus dem unverformten Grundzustand auftretenden Verzweigungserscheinung der flachen Schalen [6], [7].

Schreiben wir den Ausdruck (3.1) in die folgende Form um:

$$\begin{aligned} \delta^2 U_{m0} = \int_0^{2a} \int_0^{2b} & [2\big(\bar{F}''(\bar{v}^{\cdot} - \bar{w}z^{\cdot\cdot}) - \bar{F}^{\cdot\prime}(\bar{u}^{\cdot} + \bar{v}') + \bar{F}^{\cdot\cdot}(\bar{u}' - \bar{w}z'')\big) - \\ & - \frac{1}{Eh}(\bar{F}''^2 - 2\mu \bar{F}^{\cdot\cdot} \bar{F}'' + \bar{F}^{\cdot\cdot 2} + 2(1+\mu)\bar{F}^{\cdot\prime 2}) + \\ & + F_0'' \bar{w}^{\cdot 2} - 2F^{\cdot\prime} \bar{w}^{\cdot} \bar{w}' + F_0^{\cdot\cdot} \bar{w}'^2] \, dx \, dy \,. \end{aligned} \tag{3.9}$$

Wird jetzt die Variationsbildung des Funktionals $\delta^2 U_0$ nach dem Prinzip vom stationären Wert der Ergänzungsenergie (Minimumsatz der Formänderungsarbeit, bzw. Satz III. von Castigliano) nach $\bar{F}$ durchgeführt, so erhält man die Kompatibilitätsgleichung der Verzweigungsaufgabe der flachen Schalen [6], [7] mit Hilfe der Euler-Lagrangeschen Differentialgleichung

$$\left(\frac{\partial u_0}{\partial \bar{F}^{\prime\prime}}\right)^{\prime\prime} + \left(\frac{\partial u_0}{\partial \bar{F}^{\cdot\prime}}\right)^{\cdot\prime} + \left(\frac{\partial u_0}{\partial \bar{F}^{\cdot\cdot}}\right)^{\cdot\cdot} = 0 \tag{3.10}$$

wie folgt:

$$\Delta\Delta\bar{F} + D(1-\mu^2) L_p(\bar{w}, z) = 0\,. \tag{3.11}$$

Später werden die Gleichungen (3.8) und (3.11) nach dem Galerkinschen Verfahren gelöst. Vor der Bekanntgabe der exakten Lösung ist es zweckmäßig eine Näherungslösung zu suchen, welche die wesentlichsten Züge der behandelten Verzweigungserscheinung mit einfachen Mitteln beschreiben kann.

4. Näherungsverfahren

Auf Grund der allgemeinen Beulgleichungen von DULÁCSKA [6] (die unter Zugrundelegung eingliedriger Beulformen aufgestellt wurden) läßt sich nachweisen, daß die lineare kritische Last der sattelförmigen HP-Schalen (s. Bild 3, oberhalb), die ihre gleichmäßig verteilte Last p mit dem Kräftesystem

$$N_{x0} = -\frac{pa^2}{2fa}$$

tragen, nach der Formel

$$p_{cr,h}^{\text{lin}} = \frac{E\pi^2}{24(1-\mu^2)} \frac{\alpha\varrho}{\gamma\beta^3} \frac{1}{i^2}(i^2+\gamma^2 j^2)^2 + \frac{E32}{\pi^2} \frac{\alpha\gamma\varrho^3}{\beta} \frac{1}{i^2}\left(\frac{\alpha j^2 - i^2}{i^2+\gamma^2 j^2}\right)^2 \tag{4.1}$$

berechenbar ist. Das erste Glied drückt die Biegewirkung, das zweite Glied die Wirkung der Mittelflächendehnungen aus. Im Falle einer dehnungslosen Verformung gibt der Ausdruck (4.1) die kritische Last der durch die Randkräfte der HP-Schale belasteten *ebenen Platte* mit der Beulform der Schale an [6], [12].

Im folgenden wird bewiesen, daß die lineare kritische Last nach der Beziehung (4.1) *die obere Schranke* der linearen kritischen Last der sattelförmigen, an ihren Rändern normalkraftfreien HP-Schalen liefert:

$$p_{cr}^{\text{lin}} < p_{cr,h}^{\text{lin}}\,. \tag{4.2}$$

Im weiteren wird die erwähnte, bogenartig wirkende Schale als *Schale von homogenem Spannungszustand* genannt.

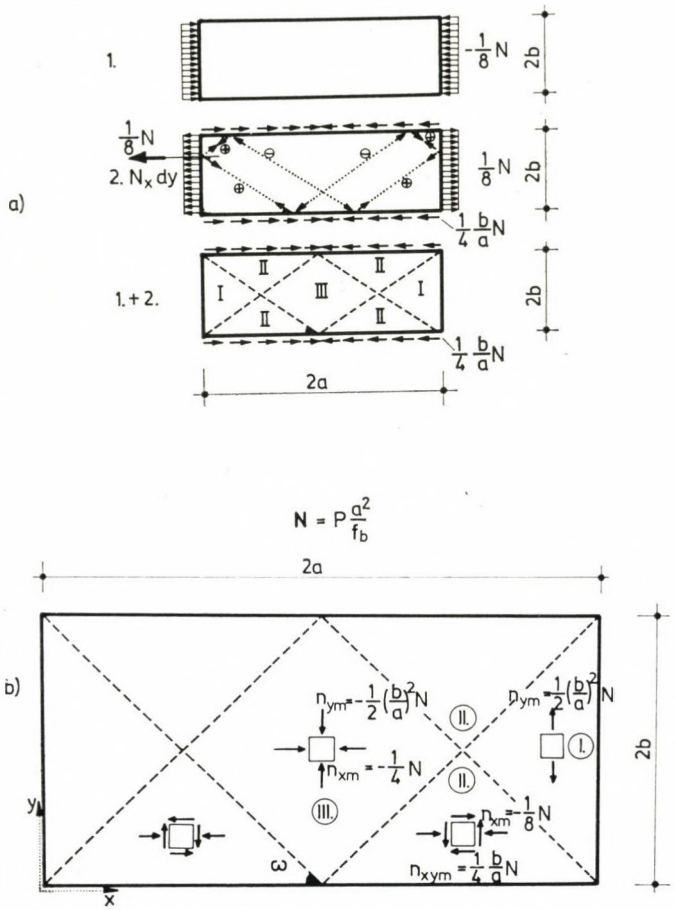

Bild 3. Membrankräfte der »normalen« HP-Schale (»voile normal«)

4.1 *Dehnungslose Beulung*

In den in diesem Abschnitt erörterten Fällen muß das Kriterium der dehnungslosen Verformung [10]

$$\frac{f_a}{f_b} = \frac{i_n^2}{j_n^2} \tag{4.3}$$

erfüllt werden.

Würde die Schale ihre Belastungen mit den Kräften $N_{x0} = \text{konst.}$, $N_{xy0} = N_{y0} = 0$ tragen, so hätte die Eigenfunktion $\bar{w}$ der Differentialgleichungen mit konstanten Koeffizienten (3.8) und (3.11) — unabhängig davon, ob sich die Mittelfläche im Laufe der Beulung dehnt oder nicht dehnt — die folgende Form:

$$w_{ij} S_{ij} = w_{ij} \sin \frac{i\pi}{2a} x \cdot \sin \frac{j\pi}{2b} y .$$

Bei einer dehnungslosen Verzweigungserscheinung besteht zwischen den Beulhalbwellenzahlen i_n, j_n ein durch die Beziehung (4.3) bestimmter Zusammenhang:

$$\bar{w} = w_{i_n j_n} S_{i_n j_n} ,$$

$$S_{i_n j_n} = \sin \frac{i_n \pi}{2a} x \sin \frac{j_n \pi}{2b} y . \tag{4.4a—b}$$

Die Membrankräfte nach der »geometrischen« Theorie von AIMOND sind zwar konstant, aber die Schubkräfte sind im ganzen Bereich nicht gleich Null. Im Falle eines solchen Kräftespieles kann also die eingliedrige Funktion $w_{i_n j_n} \cdot S_{i_n j_n}$ keine exakte Eigenfunktion sein.

Sind die Mittelflächenkräfte durch die stetigen Funktionen (2.9a—c) bestimmt, so kann der Ausdruck (4.4a—b) keine exakte Lösung für die Differentialgleichungen mit variablen Koeffizienten (3.8) und (3.11) liefern.

Die Erfüllung der Ungleichung (4.2) wird durch folgende Untersuchungen bewiesen. Erstens werden eingliedrige Beulformen zugrunde gelegt, weil wenn für diese die Ungleichung erfüllt wird, dann wird diese für die exakten Beulform von Kombinationen sinusförmiger Funktionen noch mehr erfüllt.

Der Grund hierfür liegt darin, daß der partielle Differentialoperator, der das Gleichgewicht der Aufgabe beschreibt, positiv definit ist. In diesem Fall nähert das Galerkinsche Verfahren von oben, also ergibt sich ein kleinerer Eigenwert für mehr Glieder.

Falls *die Schale von homogenem Spannungszustand* in Form der Gln. (4.4a—b) dehnungslos ausbeult, so gelangt man mit Hilfe des Galerkinschen Verfahrens — gekennzeichnet durch die Gleichungen

$$X = B \Delta\Delta \bar{w} - L_p(F_0, \bar{w}) , \tag{4.5}$$

$$\int_0^{2a} \int_0^{2b} X \cdot S_{i_n j_n} \, dx \, dy = 0 \tag{4.6}$$

zu folgenden Zusammenhängen:

$$\frac{\pi^4}{16} B \frac{b}{a^3} (i_n^2 + \gamma^2 j_n^2)^2 - \frac{\pi^2}{8} p_{cr,h}^{\text{lin}} \frac{ab}{f_a} i_n^2 = 0 , \tag{4.7}$$

$$p_{cr,h}^{\text{lin}} = \frac{E\pi^2}{24(1-\mu^2)} \frac{\alpha\varrho}{\gamma\beta^3} \frac{1}{i_n^2} (i_n^2 + \gamma^2 j_n^2)^2 . \tag{4.8}$$

Dieses Ergebnis entspricht selbstverständlich der Gleichung (4.1).

Das Produktintegral der *an ihren Rändern normalkraftfreien* »normalen« HP-Schale ($f_a/f_b = 4$) aus der Funktion $L_p(F_0, \bar{w})$ und der zueinander orthogonalen Funktionen $S_{i_n j_n}$ — unter Annahme der Existenz der in jedem Bereich konstanten Membrankräfte nach der Aimondschen geometrischen Theorie (Bild 3) — ist dem Wert gleich, der für den *homogenen Spannungszustand* bestimmt wurde:

$$\int_0^{2a}\int_0^{2b} L_p(F_0, \bar{w}) \cdot S_{i_n j_n}\, dx\, dy = \frac{\pi^2}{8}\, p\, \frac{ab}{f_a}\, i_n^2 . \tag{4.9}$$

Vergleicht man das soeben erhaltene Ergebnis mit den Gleichungen (4.7) und (4.8), so ist feststellbar, daß die lineare kritische Last der *dehnungslos* ausbeulenden, *an ihren Rändern normalkraftfreien*, »*normalen*« HP-Schale ($f_a/f_b = 4$) *gleich* der kritischen Last der *HP-Schale von homogenem Spannungszustand* von der Beulform der an ihren Rändern normalkraftfreien Schale ist (eingliedrige Funktion $\bar{w}$).

Die Berechnung bezogen auf die *Schale mit einem Pfeilhöhenverhältnis* $f_a/f_b = 9/4$ *ergibt*, daß sich die Zahl 8 im Nenner des Ausdruckes (4.9) unter Zugrundelegung eines an den Rändern normalkraftfreien unstetigen Spannungszustandes auf den Wert von 4.8 verändert, während diese sich bei homogenem Spannungszustand weiterhin zu 8 ergibt.

Es läßt sich in gleicher Weise beweisen, daß der Ausdruck (4.9) für jede in dehnungsloser Form ausbeulende HP-Schale — deren unstetiger Membranzustand nach AIMOND existiert — durch den homogenen Spannungszustand einen Minimalwert annehmen wird.

Daraus folgt die Erfüllung der Ungleichung (4.2) für die bisher behandelten Fälle, unter Zugrundelegung eingliedriger Funktionen $\bar{w}$.

Beachtung verdient die Tatsache, daß, wenn die »normale« HP-Schale zu dehnungsloser Beulung fähig ist, dann ist die Größe ihrer linearen kritischen Last von der Verteilung in x bzw. y Richtungen der vor der Beulung entstehenden inneren Kräfte unabhängig.

Wir gelangten unter anderen zum Resultat [10], daß die nach den doppelten Fourierschen Reihen (2.9a—c) bestimmten Verteilung der inneren Kräfte durch die Kräfteverteilung, die die »geometrische« Theorie liefert, sehr gut angenähert wird, wenn man im Bereich von f_a/f_b bleibt, wo die Biegewirkungen vernachlässigbar klein sind.

Dementsprechend gibt der Ausdruck (4.8) auch dann *die obere Schranke der kritischen Lasten* der dehnungslosen ausbeulenden HP-Schale an, wenn die Mittelflächenkräfte nicht konstant sind. Diese Feststellung wird durch das Bild 4 bekräftigt, auf dem die Girlandenkurve nach dem Ausdruck (4.1) und die exakte Girlandenkurve, die im Abschnitt 5 unter Zugrundelegung *eingliedriger*

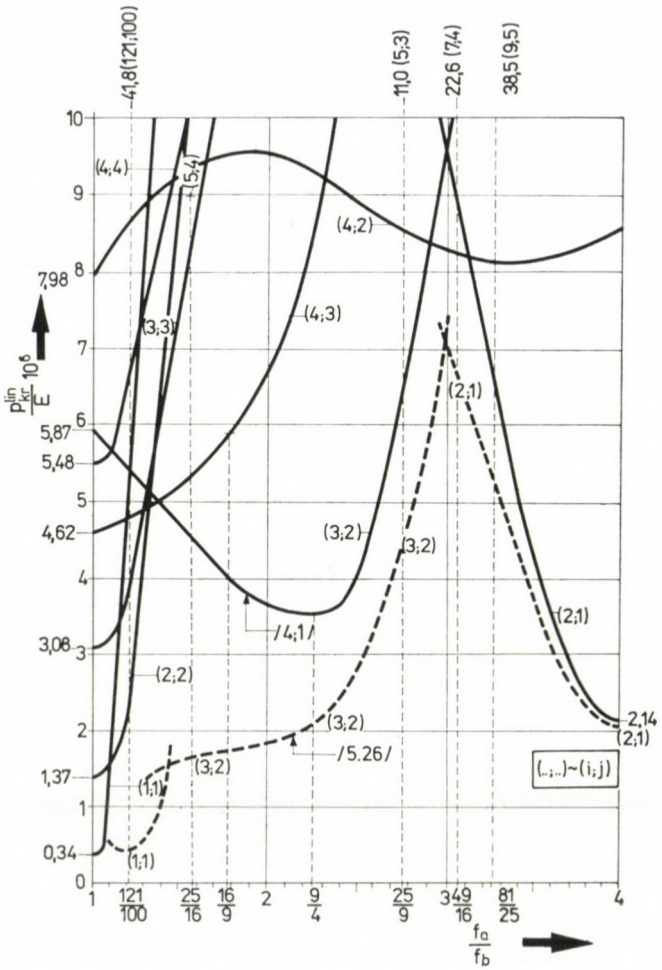

Bild 4. Vergleich der nach der Gleichung (4.1) bestimmten Girlandenkurve mit der exakten Lösung (5.26) ($a/h = 100$, $a/b = 1$, $f_b/b = 0{,}2$; die Funktion $\bar{w}$ besteht aus einem Glied)

Beulformen $\bar{w}$ bestimmt wurde, dargestellt sind. Die Ungleichung (4.2) erfüllt sich unbedingt, denn die Berechnung der Eigenwertaufgabe mit Hilfe einer *mehrgliedrigen* (exakten) *Beulform* liefert eine Girlandenkurve (s. Bild 6), die unter der (im Bild 4 gestrichelt dargestellten) durch *eingliedrige* Beulformen bestimmten Girlandenkurve verläuft.

Auf Grund des Bildes 4 sind die Formen derjenigen dehnungslosen Beulfunktionen, die zu den HP-Schalen mit dehnungsloser Verformungsmöglichkeit (gestrichelte vertikale Linien) gehören, mit Hilfe des Zusammenhanges (4.3) zu bestimmen.

4.2 *Beulung mit Dehnungen*

Die folgende Annahme scheint auf der Hand zu liegen: die mit Hilfe dehnungsloser Beulform berechnete lineare kritische Last der an ihren Rändern normalkraftfreien HP-Schale ist kleiner als diejenige, die durch Dehnungsverformung (Verformung mit Verzerrungen) bestimmt werden kann. Diese Behauptung ist nur für gewisse spezielle Verhältnisse f_a/f_b richtig. Auf Grund der Beziehung (4.3) ist leicht einzusehen, daß wenn das Verhältnis f_a/f_b z. B. dem Wert von 49/25 gleich wäre, so würde die eingliedrige dehnungslose Beulform in der x Richtung 7, in der y Richtung 5 Halbwellen bilden.

Aller Wahrscheinlichkeit nach gehört zu einer anderen Beulform mit weniger Halbwellenzahlen *verbunden mit den Verzerrungen der Mittelfläche* eine kleinere kritische Last. Das Gesagte wird noch anschaulicher, wenn die dehnungslose Verformung nach der Geylingschen »Reflexions-Theorie« [8] behandelt wird. Je größer die Zahl der zum Ausgangspunkt zurückführenden Umläufe entlang den Erzeugenden ist, um so kürzer sind die Wellenlängen, mit denen die Schale zur dehnungslosen Verformung gezwungen wird. In solchen Fällen wird also einerseits die Verformung praktisch schon durch die Biegesteifigkeit B allein verhindert, anderseits wird sie, wenn es dazu kommt, in weit dichteren Wellen auftreten, als die Beulform der Schale, weshalb sie auch weniger Gefahren in sich birgt, als die Beulform von größeren Halbwellenlängen, verbunden mit Mittelflächenverzerrungen [12].

Falls sich die Mittelfläche während der Beulung verzerrt, so addiert sich zum Produktintegral [s. (4.6)] des Faktors S_{ij} der Beulfunktion

$$\bar{w} = w_{ij} S_{ij} ,$$
$$S_{ij} = \sin \frac{i\pi}{2a} x \cdot \sin \frac{j\pi}{2b} y \qquad (4.10\text{a}-\text{b})$$

und der Funktion $L_p(F_0, \bar{w})$ noch ein Glied: das Produktintegral aus den Funktionen $L_p(\bar{F}, z)$ und S_{ij}.

In der gleichen Weise, wie im Abschnitt 4.1, ist zu beweisen: die Ungleichung (4.2) erfüllt sich auch bei Anwendung einer *eingliedrigen, mit Verzerrungen verbundenen Beulform.*

Die Ergebnisse der Berechnungen mit eingliedrigen Beulformen sind auch im Bild 4 dargestellt. Durch vertikale, gestrichelte Linien wurden die HP-Schalen mit dehnungsloser Verformungsmöglichkeit gezeichnet. Wie gut ersichtlich, ist die dehnungslose Verformung *nur bei gewissen speziellen Pfeilhöhenverhältnissen* ($f_a/f_b = 1,\ 9/4,\ 4$) maßgebend.

Für die *sonstigen* Pfeilhöhenverhältnisse ($f_a/f_b = 121/100,\ 25/16,\ 16/9,\ 25/9,\ 49/16,\ 81/25$) — welche ebenfalls die HP-Schalen mit dehnungsloser Verformungsmöglichkeit kennzeichnen — sind die Beulformen gefährlicher, die

mit Mittelflächenverzerrungen verbunden sind, aber *größere Halbwellenlängen* besitzen als die entsprechenden dehnungslosen Durchbiegungsformen.

Interessant ist zu beobachten, daß diese Beulformen mit größeren Halbwellenlängen gerade diejenigen sind, die in Fällen der Verhältnisse $f_a/f_b = 1$, 9/4 und 4 dehnungslose Verformungen bilden ($i_n = j_n = 1$; $i_n = 3, j_n = 2, i_n = 2, j_n = 1$). Die exakte Beulform wird sich aus der linearen Kombination der Funktionen von Typen (4.4a—b) und (4.10a—b) zusammensetzen.

Im Falle einer Kombination wird die Ungleichung (4.2) *noch mehr erfüllt.*

Bezüglich der »halbnormalen« HP-Schale ($f_a/f_b = 1$) erfüllt sich die Ungleichung (4.2) nicht, weil diese Schale und die Schalen vom gleichen Tragverhalten (mit den Parametern $f_a/f_b \approx 1 \div 1{,}5$) auf keine Weise als Membranschalen zu betrachten sind [10]. Diese Konstruktionen tragen ihre Belastungen überwiegend durch Biegeschnittkräfte. Ihre (fiktiven) linearen kritischen Lasten wurden nur der Vollständigkeit halber bestimmt.

Von großem Nutzen ist, daß die Formel (4.1) (bzw. (4.8)) für den Fall der »*normalen*« *HP-Schale* ($f_a/f_b = 4$) einen nur um etwa 4% höheren Wert als die exakte Lösung (5.26) bezogen auf eingliedrige Beulformen (für Parameter des Bildes) liefert.

Der Fehler beträgt bei Verwendung einer 24 gliedrigen Beulform etwa 10%. Für den Vorentwurf ist auch die lineare kritische Last der HP-Schalen mit dem Verhältnis $f_a/f_b = 9/4$ aus einer der Gln. (4.8) sehr ähnlichen Gleichung zu bestimmen. Die Abweichung besteht bloß darin, daß im Nenner statt der Zahl 24 die Zahl 40 steht. Dieses Ergebnis wurde unter Zugrundelegung des unstetigen Membrankräftespieles bestimmt. Vergleicht man die Abweichung zwischen der Näherungslösung (4.8) und der exakten Lösung im Bild 6, so sieht man, daß dieser Fehler eine ähnliche Größe wie der auf die »normale« Schale bezogene besitzt.

5. Exakte Lösung des Eigenwertproblems

5.1 *Beulform*

Bekanntlich besitzt der Verzweigungsvorgang von unendlich kleine Verformungen leistenden Stäben und ebenen Platten eine wichtige Annahme: die Stabachse, bzw. Mittelfläche bleibt dehnungslos (bzw. unverzerrt) [3], [17], [22].

Bei Bestimmung der linearen kritischen Lasten der Schalen kann die Dehnungslosigkeit der Mittelfläche nicht allgemein angenommen werden [3], [12], [17], [22], [25]. Die Mittelfläche der Schalen kann nur dann dehnungslos bleiben, wenn die geometrischen Verhältnisse und die Lagerungsart der Konstruktion den dehnungslosen Verformungsvorgang ermöglichen [8], [10], [13].

Die dehnungslose Beulform der Schale kann in gewissen Fällen gefährlicher sein, als die mit den Verzerrungen der Mittelfläche verbundene Beulform mit größerer Halbwellenlänge. Auf Grund des Abschnitts 4 liefert zu den zählbaren unendlichen Elementenmengen f_a/f_b ($f_a/f_b = 1, 9/4, 4 \ldots$) der Schale mit dehnungsloser Verformungsmöglichkeit die eingliedrige dehnungslose Beulform und zu anderen zählbaren unendlichen Elementenmengen f_a/f_b ($f_a/f_b =$ $= 121/100, 25/16, 16/9, 25/9, 49/16, 81/25 \ldots$) die eingliedrige Beulform mit Verzerrungen der Mittelfläche die kleinere lineare kritische Last.

Natürlich existieren in Wirklichkeit keine dehnungslosen und keine mit Dehnungen (Verzerrungen) verbundenen Beulformen, sondern es gibt verschiedene Beulhalbwellenlängen, die die Konstruktion selbst — der Bedingung (3.6) entsprechend — wählt.

Auf Grund der obigen Ausführungen wird die Beuleigenfunktion in Form der folgenden leicht zu handhabenden trigonometrischen Reihe angenommen:

$$\bar{w} = \sum_{i}^{I_0} \sum_{j}^{J_0} w_{ij} S_{ij} = \sum_{i}^{I_0} \sum_{j}^{J_0} \bar{w}_{ij} . \tag{5.1}$$

In Bezug auf die Beulhalbwellenzahlen i und j wird nicht festgesetzt, daß diese miteinander in dem durch die Beziehung (4.3) beschriebenen Zusammenhang stehen müssen. Diese Möglichkeit ist aber nicht ausgeschlossen. Der später erläuterte Algorithmus wird selbst, automatisch die dehnungslosen und nichtdehnungslosen Komponenten der Beulform auswählen.

Jedes Glied der die exakte Eigenfunktion $\bar{w}_e$ ersetzenden Ansatzfunktion $\bar{w}$ erfüllt die folgenden geometrischen (bzw. »künstlichen«, s. z. B. [17]) und statischen (bzw. »natürlichen«, s. z. B. [17]) Randbedingungen der Aufgabe:

$$\bar{w}_{ij}\Big|_{\substack{x=0 \\ x=2a}} = 0 , \quad \bar{w}_{ij}\Big|_{\substack{y=0 \\ y=2b}} = 0 , \tag{5.2a—d}$$

$$\bar{w}''_{ij}\Big|_{\substack{x=0 \\ x=2a}} = 0 , \quad \bar{w}''_{ij}\Big|_{\substack{y=0 \\ y=2b}} = 0 . \tag{5.3a—d}$$

Die die exakte Eigenfunktion $\bar{F}_e$ ersetzende Funktion $\bar{F}$ wird durch die trigonometrische Reihe

$$\bar{F} = \sum_{i}^{I_0} \sum_{j}^{J_0} F_{ij} \cdot S_{ij} = \sum_{i}^{I_0} \sum_{j}^{J_0} \bar{F}_{ij} \tag{5.4}$$

beschrieben. Jedes Glied dieser Reihe erfüllt die Bedingungen der Aufgabe bezogen auf die Randnormalkräfte:

$$\bar{F}_{ij}^{\,|\,}\Big|_{\substack{y=0\\y=2b}} = 0,\ \bar{F}_{ij}^{\,\cdot\cdot}\Big|_{\substack{x=0\\x=2a}} = 0\ . \qquad (5.5a-d)$$

Bekanntlich muß jedes Glied der Ansatzfunktionen beim Galerkinschen Verfahren die sämtlichen Randbedingungen, d. h. sowohl die geometrischen (»künstlerischen«) als auch die statischen (»natürlichen«), erfüllen.

5.2 *Lösung nach dem Galerkinschen Verfahren*

Vor allem soll die Verbindungen zwischen je einem Glied der Beulfunktion (5.1) und je einem Glied der Spannungsfunktion (5.4) auf Grund der Gleichung (3.11) bestimmt werden:

$$F_{ij} = w_{ij} \frac{8}{\pi^2} Eh a\gamma\varrho \frac{(\alpha j^2 - i^2)}{(i^2 + \gamma^2 j^2)^2}\ . \qquad (5.6)$$

Setzt man in die Gleichgewichtsgleichung (3.8) die Funktionen der Mittelflächenkräfte vom Grundzustand (2.9a—c) sowie die Ausdrücke (5.1), (5.4), (5.6) ein, so läßt sich die linke Seite der Gleichgewichtsgleichung (X), wie folgt, aufschreiben:

$$\begin{aligned}\frac{4a\,X}{\pi^2 E} = {} & \frac{\pi^2}{48(1-\mu^2)} \frac{1}{\beta^3} \sum_i^{I_0} \sum_j^{J_0} w_{ij}(i^2 + \gamma^2 j^2)^2 \cdot S_{ij} + \\ & + \frac{16}{\pi^2} \cdot \frac{\varrho^2\gamma^2}{\beta} \sum_i^{I_0} \sum_j^{J_0} w_{ij} \frac{(\alpha j^2 - i^2)^2}{(i^2 + \gamma^2 j^2)^2} S_{ij} + \\ & + \frac{p}{E} \frac{\gamma}{\varrho} \Bigg[n_x^0 \sum_i^{I_0} \sum_j^{J_0} w_{ij}\, i^2 \cdot S_{ij} - \\ & - 2\, n_{xy}^0 \gamma \sum_i^{I_0} \sum_j^{J_0} w_{ij}\, ij\, C_{ij} + n_y^0 \gamma^2 \sum_i^{I_0} \sum_j^{J_0} w_{ij}\, j^2\, S_{ij} \Bigg].\end{aligned} \qquad (5.7)$$

Die *Fehlerfunktion* X wäre dann gleich Null, wenn die Ansatzfunktion (5.1) die exakte Beulfunktion mit völliger Genauigkeit bestimmen würde.

Der Ausdruck (5.1) setzt sich aus linear unabhängigen Komponenten zusammen. Ferner werden sämtliche geometrische und statische Randbedingungen der Aufgabe erfüllt. Daher erfüllen sich die Bedingungen der Anwendbarkeit des Galerkinschen Verfahrens [4], [17], [18], [25].

Stellt man sich die Fehlerfunktion X als eine Reihe vor, die nach den zueinander orthogonalen Faktoren S_{ij} der Komponenten der Funktion $\bar{w}$ entwickelt ist, so stellt sich heraus, daß die folgende Definitionsgleichung des Galerkinschen Verfahrens (vom Prinzip der virtuellen Verschiebungen mit dem

Werkstoffsgesetz (Elastizitätsgesetz) durch Variationsberechnung abgeleitet [25])

$$\int_0^{2a}\int_0^{2b} XS_{i'j'}\,dx\,dy = 0 \tag{5.8}$$

$$i' = 1, 2, \ldots, I_0$$
$$j' = 1, 2, \ldots, J_0$$

die Tendenz der Funktion X nach Verschwinden ausdrückt (d. h. X muß gegen Null streben, wenn $I_0 \to \infty$, $J_0 \to \infty$). Die Fehlerfunktion X ist also zu dem Faktor S_{ij} jeder Komponente der Funktion $\bar{w}$ orthogonal.

Sind die Operatoren positiv definit, so werden die Eigenwerte p_{kr}^{lin} durch das Galerkinsche-Verfahren von oben angenähert [4]. Dies folgt auch daraus, daß dieses Verfahren nicht nur eine der approximativen Lösungsmethoden bezogen auf die Differentialgleichungen der angewandten Elastizitätstheorie ist, sondern auch als eine Version der Energiemethode betrachtet werden kann.

Bei Auflösung des Gleichungssystems (5.8) muß man die verallgemeinerte Orthogonalität der in ihm befindlichen trigonometrischen Funktionen zu den Gewichtsfunktionen (2.9a—c) aufschreiben. Das Gleichungssystem (5.8) führt zur folgenden Eigenwertaufgabe:

$$\mathbf{A}w = \lambda w\,. \tag{5.9}$$

Diese Gleichung sieht in ausführlicherer Form so aus:

$$\lambda = \frac{E}{p_{kr}^{\text{lin}}}, \tag{5.10}$$

$$\left.\begin{aligned}
&\underset{(N_0\times N_0)}{\mathbf{A}} = \underset{(N_0\times N_0)}{\mathbf{D}^{-1}}\ \underset{(N_0\times N_0)}{\mathbf{B}}\,,\\
&\mathbf{D} = \langle d_{11}, d_{22}, \ldots, d_{kk}, \ldots, d_{N_0N_0}\rangle\\
&N_0 = I_0 \cdot J_0\,,\\
&d_{kk} = \frac{\pi^2}{48(1-\mu^2)}\,\frac{(i'^2+\gamma^2 j'^2)^2}{\beta^3} + \frac{16}{\pi^2}\,\frac{\varrho^2\gamma^2}{\beta}\,\frac{(\alpha j'^2 - i'^2)^2}{(i'^2+\gamma^2 j'^2)^2}\,,
\end{aligned}\right\} \quad (5.11a—d)$$

$$\left.\begin{aligned}
&\mathbf{B} = \{b_{kl}\}\,,\\
&b_{kl} = -\frac{\gamma}{\varrho ab}\int_0^{2a}\int_0^{2b}\Bigg[n_x^0\sum_i^{I_0}\sum_j^{J_0} i^2 S_{ij} - 2n_{xy}^0\gamma\sum_i^{I_0}\sum_j^{I_0} ijC_{ij} +\\
&\quad + n_y^0\gamma^2\sum_i^{I_0}\sum_j^{J_0} j^2 S_{ij}\Bigg] S_{i'j'}\,dx\,dy,\\
&i' = 1, 2, \ldots, I_0, \qquad j' = 1, 2, \ldots, J_0\\
&k = j' + J_0(i' - 1), \qquad l = j + J_0(i - 1)\,.
\end{aligned}\right\} \quad (5.12a—e)$$

Die Matrix **B** ist keine Diagonalmatrix, weil auch die aus den Funktionen der inneren Kräfte stammenden Funktionen S_{mn}, C_{mn} — als Gewichte — im Laufe der Bildung von **B** hinter das Integralzeichen gelangen. (Verallgemeinerte Orthogonalität.)

Die Untersuchungen werden im konservativen Kraftfeld und in demjenigen unendlich kleinen Bereich durchgeführt, der sich in der nächsten Nähe des Grundzustandes befindet. Daher ist die zweite Variation der potentiellen Energie des Systems (der Energiezuwachs $2\,\Delta\Pi$) eine homogene quadratische Form der verallgemeinerten Koordinaten $(\bar{w}, \bar{w}', \bar{w}^{\cdot}, \bar{w}'', \bar{w}^{\cdot\prime}, \bar{w}^{\cdot\cdot})$. Daraus folgt, daß die Matrix **B** (die aus der mit den Dehnungs- und Gleitungszuwachsen $1/2\,\bar{w}'^2$, $1/2\,\bar{w}^{\cdot 2}$, $\bar{w}^{\cdot}\bar{w}'$ geleisteten Arbeit der Spannungen des Grundzustandes stammt) *reel symmetrisch ist.*

Es läßt sich leicht einsehen, daß die Matrix **D** eine *reelle, positive definite Diagonalmatrix ist.* Bekanntlich können die reellen symmetrischen Matrizen mit Hilfe einer Ähnlichkeitstransformation — als ein spezieller Fall der unitären Transformation von normalen Matrizen — in die Diagonalform transformiert werden [20, 24]. Ferner sind ihre Eigenwerte und Eigenvektoren reell. Die Matrix $\mathbf{A} = \mathbf{D}^{-1}\mathbf{B}$ ist nicht symmetrisch. Daher ist es zweckmäßig, *die verallgemeinerte Eigenwertaufgabe* (5.9) unter Anwendung der Zerlegung $\mathbf{D} = \mathbf{D}^{1/2}\mathbf{D}^{1/2}$ auf eine *Eigenwertaufgabe zurückzuführen*, deren Matrix **C** reel symmetrisch ist.

Die aus den Matrizen **B** und **D** abgeleitete Matrix **C** hat nach wie vor nur reelle Eigenwerte und Eigenvektoren. Die erwähnte Zerlegung der Matrix **D** ist ein spezieller Fall der Choleskyschen Zerlegung. Die Schritte der Bildung der Matrix **C** sind folgende:

$$\mathbf{B}\underline{w} = \lambda \mathbf{D}^{1/2}\,\mathbf{D}^{1/2}\,w\,. \tag{5.13}$$

Die Gleichung (5.13) soll von links durch $\mathbf{D}^{1/2}$ multipliziert werden:

$$\mathbf{D}^{-1/2}\,\mathbf{B}\,\underline{w} = \lambda\,\mathbf{D}^{1/2}\underline{w}\,. \tag{5.14}$$

Durch die Transformation

$$\underline{w} = \mathbf{D}^{-1/2}\underline{x} \tag{5.15}$$

wird die Gleichung (5.13) die folgende Form annehmen:

$$\mathbf{D}^{-1/2}\,\mathbf{B}\mathbf{D}^{-1/2}\underline{x} = \lambda\underline{x}\,. \tag{5.16}$$

Die der in der Gleichung (5.16) vorkommenden reellen symmetrischen Matrix

$$\mathbf{C} = \mathbf{D}^{-1/2}\,\mathbf{B}\mathbf{D}^{-1/2} \tag{5.17}$$

zugeordnete Eigenwertaufgabe

$$(\mathbf{C} - \lambda \mathbf{E})\underline{x} = 0 \tag{5.18}$$

ist schon die wohlbekannte *gewöhnliche (spezielle) Eigenwertaufgabe.*

Ein allgemeines Element der Matrix **C** läßt sich aus den entsprechenden Elementen der Matrizen **B** und **D** bilden:

$$c_{kl} = \frac{b_{kl}}{+\sqrt{d_{kk}\, d_{ll}}} \,. \tag{5.19}$$

Nach Durchführung der durch die Gleichung (5.8) vorgeschriebenen Integrationen erhält man die folgenden Beziehungen:

$$d_{kk} = \frac{\pi^6}{12\,288\,(1-\mu^2)} \frac{\varrho}{\gamma\beta^3} (i'^2 + \gamma^2 j'^2)^2 + \frac{\pi^2}{16} \frac{\varrho^3\gamma}{\beta} \frac{(\alpha j'^2 - i'^2)^2}{(i'^2 + \gamma^2 j'^2)^2}, \tag{5.20}$$

$$SZ = ij i'j' \,[2(m^2 j^2 + n^2 i^2) - (m^2 + i^2 - i'^2)(n^2 + j^2 - j'^2)] \,, \tag{5.21}$$

$$NE = [m^2 - (i + i')^2][m^2 - (i - i')^2][n^2 - (j + j')^2][n^2 - (j - j')^2], \tag{5.22}$$

$$b_{kl} = \sum_m^M \sum_n^N N_{mn} \frac{SZ}{NE} \,, \tag{5.23}$$

$$\begin{aligned} &i = 1, 2, \ldots, I_0, \quad j = 1, 2, \ldots, J_0, \quad m = 1, 3, \ldots, M, \quad n = 1, 3, \ldots, N, \\ &\qquad i' = 1, 2, \ldots, I_0, \quad j' = 1, 2, \ldots, J_0 \,, \\ &\qquad k = j' + J_0(i' - 1), \\ &\qquad l = j + J_0(i - 1). \end{aligned}$$

Daraus ist leicht zu erkennen, daß die reelle Matrix **D** positiv definit und die reelle Matrix **B** symmetrisch ist.

Infolge der verallgemeinerten Orthogonalität mit den Gewichtsfunktionen S_{mn} befinden sich Elemente mit *von Null verschiedenen* Werten an jenen Stellen der Matrix **B**, die den Bedingungen

$$\begin{aligned} i \pm i' &= 0, \pm 2, \pm 4, \ldots, \\ j \pm j' &= 0, \pm 2, \pm 4, \ldots \end{aligned} \tag{5.24a—b}$$

entsprechen. Die Strukturen der Matrizen **D** und **B** können, wie folgt, dargestellt werden (es seien z. B. I_0 und J_0 gerade Zahlen):

Wenn einer Näherungslösung nur eingliedrige Beulformen zugrunde gelegt werden, dann kann man den Ausdruck

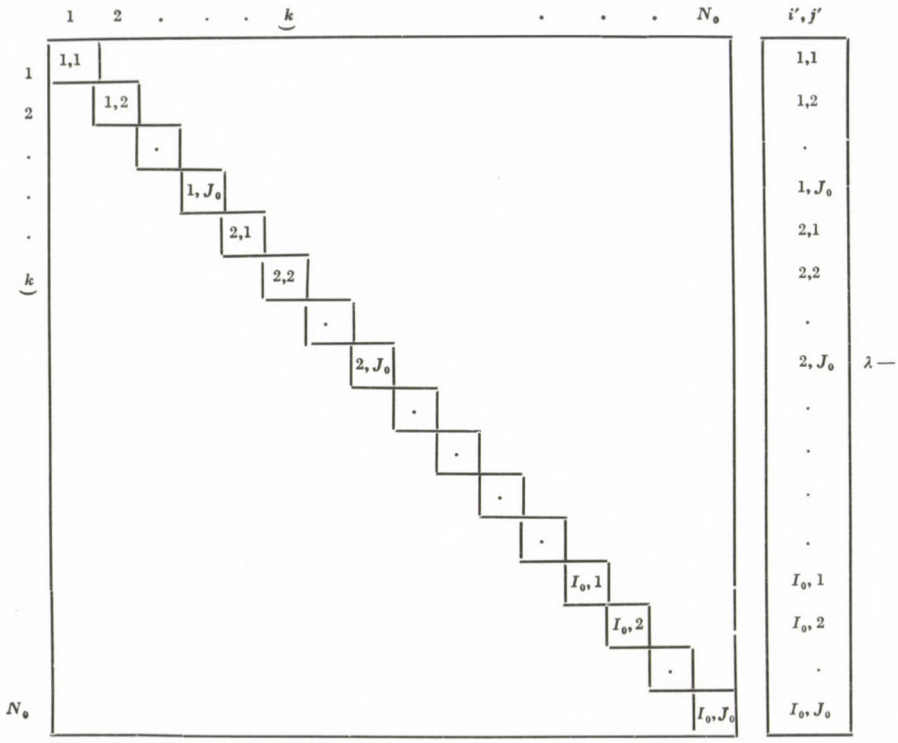
1 2 . . . k . . . N0
i', j'
1,1
1,2
1, J0
2,1
2,2
2, J0
I0, 1
I0, 2
I0, J0
λ —
D

(5.25)

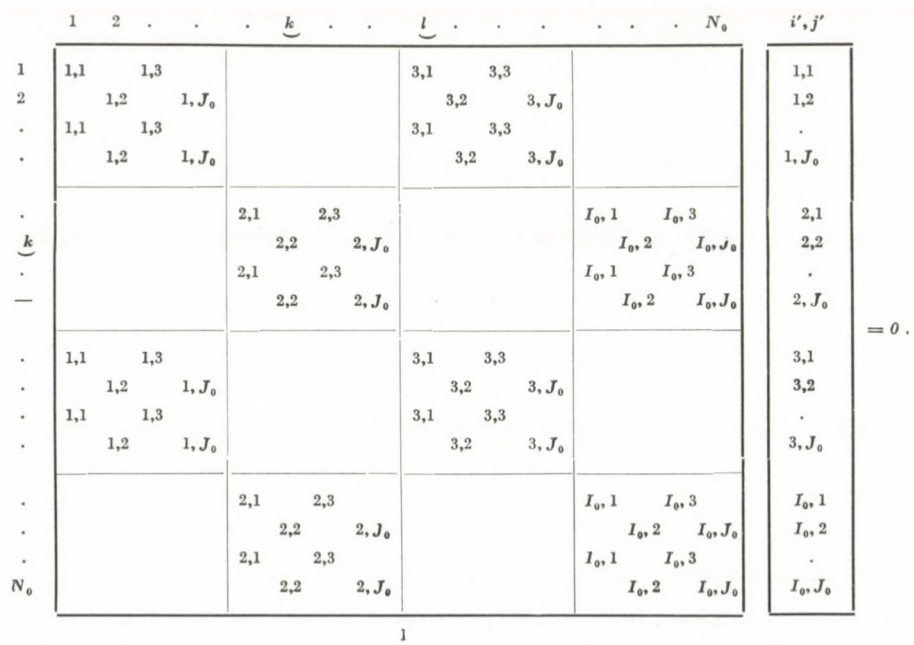
1 2 . . . k . . l N0
i', j'
1,1 1,3 3,1 3,3
1,2 1, J0 3,2 3, J0
2,1 2,3 I0, 1 I0, 3
2,2 2, J0 I0, 2 I0, J0
— = 0 .
1
4
Acta Technica Academiae Scientiarum Hungaricae 91, 1980

$$\frac{p_{kr}^{\text{lin}}}{E} = \frac{d_{11}}{b_{11}} \tag{5.26}$$

anwenden.

Es lohnt sich die Struktur der in Gleichung (5.25) dargestellten Matrix **B** zu untersuchen. Die Matrix **B** ist als eine Übermatrix (Kästchenmatrix) aufzufassen, in der sich die *Kästchen* mit nicht Null-Werten »*schachbrettartig*« befinden. *Dies folgt aus der verallgemeinerten Orthogonalität* (5.24a—b).

Falls sich die Beulwellen in den Richtungen x und y mit gleichen Zahlen gestalten — also, wenn $I_0 = J_0$ ist —, so hat die Matrix **B** 4 unabhängige Zeilen. Dies ersieht man daraus, daß — wegen der »schachbrettartigen« Struktur — zwei unabhängige Zeilen zu einer Kästchenzeile gehören, und daß sich in der Übermatrix zwei unabhängige Kästchenzeilen wiederholen. Aus dem Gesagten folgt nicht, daß die Matrix **B** keine »einfache« Struktur hat, denn jede reelle symmetrische Matrix hat N_0-zählige unabhängige (links- oder rechtsseitige) Eigenvektoren (so kann auch die Matrix **B** in die Diagonalform transformiert werden). Es handelt sich bloß darum, daß sich jeder der (unabhängigen) Eigenvektoren $\overline{w}_k$ (Anzahl $= N_0$) aus den Gliedern (Anzahl variabel) einer der 4 verschiedenen, bestimmten Gruppen der trigonometrischen Summe (5.1) zusammensetzt.

Falls z. B. $I_0 = J_0 = 5$ ist, so setzen sich die zu den Eigenwerten λ_1, λ_2, λ_3, λ_4, λ_5 gehörigen Eigenvektoren bloß aus den linearen Kombinationen von variablen Verhältnissen der Komponenten S_{11}, S_{13}, S_{15}, S_{31}, S_{33}, S_{35}, S_{51}, S_{53}, S_{55} zusammen.

Diese Tatsache hat einen *sehr bedeutenden rechentechnischen* Vorteil: statt das vollständige charakteristische Polynom $\text{Det}(\lambda) = |\lambda\mathbf{E} - \mathbf{C}|$ der Matrix **C** aufzuschreiben, genügt es die der erwähnten 4 Gruppen entsprechenden 4 Polynome von wesentlich niedrigeren Grade als von Det (λ) zu bestimmen. Dieser Vorteil ist selbstverständlich auch bei Anwendung einer numerischen Methode wesentlich. Physikalisch läßt sich die Unabhängigkeit der erwähnten 4 Gruppen S_{ij} daraus erklären, daß *die Beulfunktionen vier unterschiedliche charakteristische Formen haben*:

- die Schnitte der Beulformen in den $\bar{x}$, bzw. $\bar{y}$ Richtungen liegen in bezug auf die $\bar{x} - \bar{z}$-, bzw. $\bar{y} - \bar{z}$ — Ebenen symmetrisch,
- diese Schnitte liegen in bezug auf die $\bar{x} - \bar{z}$-, bzw. $\bar{y} - \bar{z}$ — Ebenen antimetrisch,
- die Schnitte in der $\bar{x}$ Richtung befinden sich zu der $\bar{x} - \bar{z}$ — Ebene symmetrisch und die Schnitte in der $\bar{y}$ Richtung befinden sich zu der $\bar{y} - \bar{z}$ — Ebene antimetrisch,
- die Schnitte in der $\bar{x}$ Richtung befinden sich in bezug auf die $\bar{x} - \bar{z} =$ Ebene antimetrisch und die Schnitte in der $\bar{y}$ Richtung befinden sich in bezug auf die $\bar{y} - \bar{z}$ — Ebene symmetrisch.

Die N_0-zähligen Eigenvektoren können sich bloß aus den Gliedern eines der obigen vier Fällen zusammensetzen.

Falls $I_0 \neq J_0$ ist — d. h. die Anzahl der Glieder der Beulfunktion in den Richtungen x und y verschieden ist —, so hat die Matrix **B** 2 oder 4 unabhängige Zeilen. In diesem Fall werden nämlich aus den 4 Kombinationen der Symmetrie und der Antimetrie 2 ($J_0 = 1$) oder 4 bleiben. Die zweierlei Kombination ist nur eine theoretische Möglichkeit, denn die Größe J_0 muß im Interesse der höheren Genauigkeit größer als 1 sein. Es soll zuletzt darauf verwiesen werden, daß die abgeleiteten Zusammenhänge durch geringe Umformung auch für die Untersuchung *der Tonnenschalen mit parabolischen Leitkurven* ($f_b \to 0$) und für die *elliptischen Paraboloidschalen* ($f_b \to -f_b$) verwendet werden können.

5.3 *Numerische Untersuchungen*

Für Bestimmung der Eigenwerte und Eigenvektoren der Matrix **C** (bzw. der mit Hilfe der entsprechenden Permutation erhaltenen 4 unabhängigen Kästchen (Blöcke)) wurde die mit der Wielandtschen Iteration verbundene Variante des von J. G. Francis vorgeschlagenen, numerisch außerordentlich stabilen, *QR-Algorithmus* angewandt [20], [24].

Die Girlandenkurven der Bilder 5—13 wurden für die geometrischen Verhältnisse bestimmt, die die Mehrheit der Stahlbetonschalen gut kennzeichnen [10].

Die Beulfunktion setzte sich im allgemeinen aus 27 Gliedern ($I_0 J_0 = N_0 = 9 \times 3 = 27$) zusammen. Die Berechnungen lieferten das interessante und vom Gesichtspunkt der Praxis nützliche Resultat, daß die Beulfunktion in jedem Fall *ein dominantes Glied* hatte. Besonders für die geometrischen Verhältnisse $f_a/f_b = 9/4$ und $f_a/f_b = 4$ (»normale« HP-Schale) spielte je ein Glied eine dominante Rolle, und zwar gerade jenes, das *keine Verzerrungen* verursacht (d. h. gerade das dehnungslose Glied).

Wir gelangten zu folgender Feststellung: wenn die Stabilität *der Schale mit dem Pfeilhöhenverhältnis* $f_a/f_b = 9/4$ durch die vollständige mehrgliedrige Beulform untersucht wird, dann wird die lineare kritische Last im allgemeinen um weniger, als 25% niedriger als die, welche mit Hilfe des eine dehnungslose Beulung verursachenden dominanten Gliedes (seine Form ist durch die Zahlen $i_n = 3$, $j_n = 2$ bestimmt) berechnet wird.

Bei Beulung der »normalen« Schale ist das durch die Zahlen $i_n = 2, j_n = 1$ charakterisierbare *dehnungslose* Glied dominant. Die Abweichung zwischen den zu der eingliedrigen und der mehrgliedrigen Beulform gehörigen linearen kritischen Lasten beträgt im allgemeinen weniger als 15%.

Diese Resultate stehen mit der Feststellung der Abschnitte 4.1 und 4.2 in Einklang, nämlich daß die linearen kritischen Lasten für den Vorentwurf

Tafel I

$\frac{p_{kr}^{lin}}{E}\,10^6$				wenn $\frac{f_{a_1}}{f_{b_1}}=\frac{f_{a_2}}{f_{b_2}}$, $\frac{a_1}{b_1}=\frac{a_2}{b_2}$, $\frac{a_1\cdot f_{b_1}}{h_1\cdot b_1}=\frac{a_2\cdot f_{b_2}}{h_2\cdot b_2}$, dann $\frac{p_{kr_2}^{lin}}{p_{kr_1}^{lin}}=\left(\frac{a_1/h_1}{a_2/h_2}\right)^4$								
$a/h=$				100			150			200		
$f_b/b=$				0,1	0,2	0,3	0,1	0,2	0,3	0,1	0,2	0,3
$\frac{a}{b}$	1	$\frac{f_a}{f_b}$	$\frac{25}{16}=1{,}5625$	0,500	1,440	3,483	0,176	0,688	1,817	0,090	0,425	1,258
			$\frac{9}{4}=2{,}2500$	0,876	1,840	2,911	0,272	0,575	0,881	0,115	0,242	0,372
			$\frac{25}{9}=2{,}7777$	1,300	3,712	7,500	0,480	1,481	3,800	0,232	0,880	2,450
			3,0000	1,130	5,008	11,97	0,594	2,364	6,279	0,313	1,480	4,136
			$\frac{81}{25}=3{,}2400$	1,000	4,640	13,57	0,460	2,680	8,320	0,290	1,900	6,303
			4,0000	0,865	1,920	2,984	0,275	0,589	0,900	0,120	0,250	0,386
	2		$\frac{25}{16}=1{,}5625$	0,620	2,032	3,606	0,270	0,712	1,543	0,127	0,386	0,920
			$\frac{9}{4}=2{,}2500$	1,400	3,248	5,205	0,438	1,028	1,600	0,203	0,449	0,685
			$\frac{25}{9}=2{,}7777$	1,330	4,752	9,300	0,625	1,837	3,800	0,297	0,930	2,050
			3,0000	1,195	5,600	11,47	0,547	2,266	5,281	0,350	1,299	3,265
			$\frac{81}{25}=3{,}2400$	1,100	4,320	11,74	0,468	2,319	6,850	0,270	1,600	4,800
			4,0000	1,105	2,448	3,791	0,350	0,749	1,120	0,153	0,321	0,490

$\frac{a}{b}$	3	$\frac{f_a}{f_b}$	$\frac{25}{16} = 1{,}5625$	2,400	3,216	5,483	0,510	1,083	2,319	0,201	0,590	1,025
			$\frac{4}{9} = 2{,}2500$	2,200	6,608	10,38	0,760	2,050	3,340	0,413	0,924	1,446
			$\frac{25}{9} = 2{,}7777$	1,920	5,584	13,20	0,640	2,607	5,000	0,349	1,340	2,500
			3,0000	1,880	5,168	11,70	0,610	2,311	5,690	0,323	1,473	3,061
			$\frac{81}{25} = 3{,}2400$	1,860	4,624	9,690	0,590	1,914	4,870	0,289	1,180	3,320
			4,0000	2,000	4,224	6,440	0,610	1,272	1,998	0,264	0,550	0,850

der soeben behandelten zwei Schalentypen mit eingliedrigen Beulformen mit guter Näherung aus der Formel (4.8) berechnet werden können. In den Nenner der *der unstetigen Membranlösung entsprechenden* Formel (4.8) ist im Falle von $f_a/f_b = 9/4$ statt der Zahl 24 die Zahl 40 zu schreiben. (Vgl. mit der Bemerkung am Ende des Abschnittes 4.2.)

In den Fällen der Pfeilhöhenverhältnisse $f_a/f_b = 9/4 \div 4$ bildet entweder die Sinusfunktion mit Halbwellenzahlen $i_n = 3$, $j_n = 2$ oder jene mit $i_n = 2$, $j_n = 1$ das dominante Glied der Beulform.

Die zu den eingliedrigen (in diesen Fällen schon auch Mittelflächenverzerrungen verursachenden) Beulformen gehörigen linearen kritischen Lasten sind im allgemeinen weniger als 30% größer als die genauen Werte. *Die Mini-*

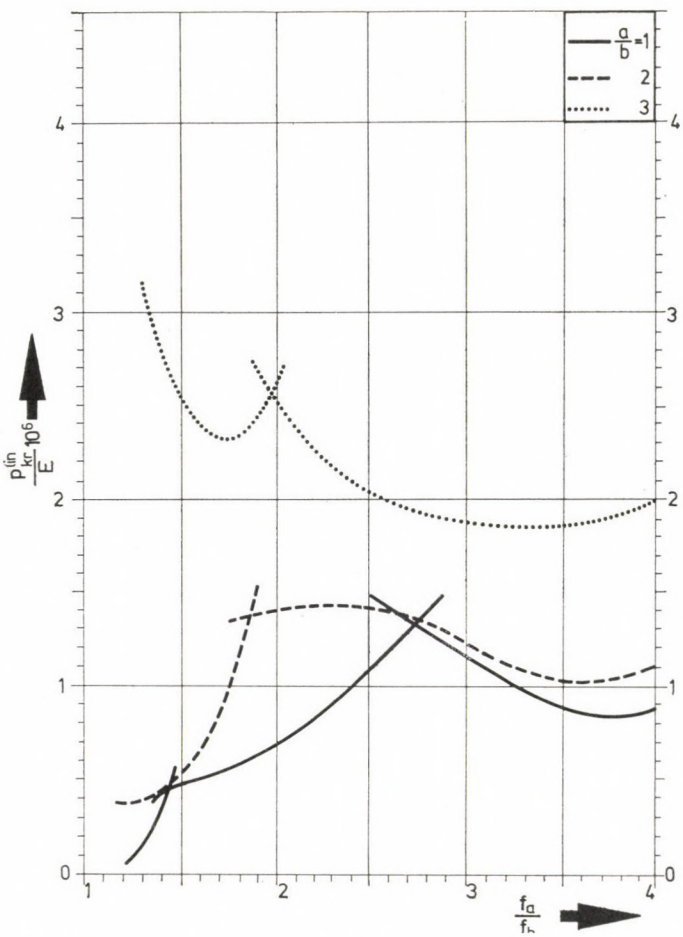

Bild 5. Lineare kritische Last der HP-Schale ($a/h = 100$, $f_b/b = 0{,}1$)

malwerte der erhaltenen Girlandenkurven liegen in der Nähe der Pfeilhöhenverhältnisse f_a/f_b der im wesentlichen dehnungslosen ausbeulenden HP-Schalen ($f_a/f_b = 9/4,\ 4$). Im untersuchten Bereich ($f_a/f_b = 1 \div 4$) befinden sich die Maximalwerte der linearen kritischen Lasten etwa in der Umgebung des Verhältnisses $f_a/f_b = 3$. Diese Lasten übersteigen wesentlich diejenige, die zu den Schalen mit den Pfeilhöhenverhältnissen $f_a/f_b = 4$ bzw. $9/4$ gehören. Es ist ersichtlich, daß die Kurven etwa beim Pfeilhöhenverhältnis $f_a/f_b = 3$ sehr steil verlaufen. Daher erscheint es als sehr wahrscheinlich, daß diese Schalen *gegen geometrische Unvollkommenheiten* (Vorbeulen oder kleine Änderung des Verhältnisses f_a/f_b) ziemlich *empfindlich sind.* Aus dem Verlauf der Kurven ist auch darauf zu folgern, daß wenn sich das Verhältnis f_a/f_b ändert, die kritische Last sowohl *abnehmen* als auch zunehmen *kann.*

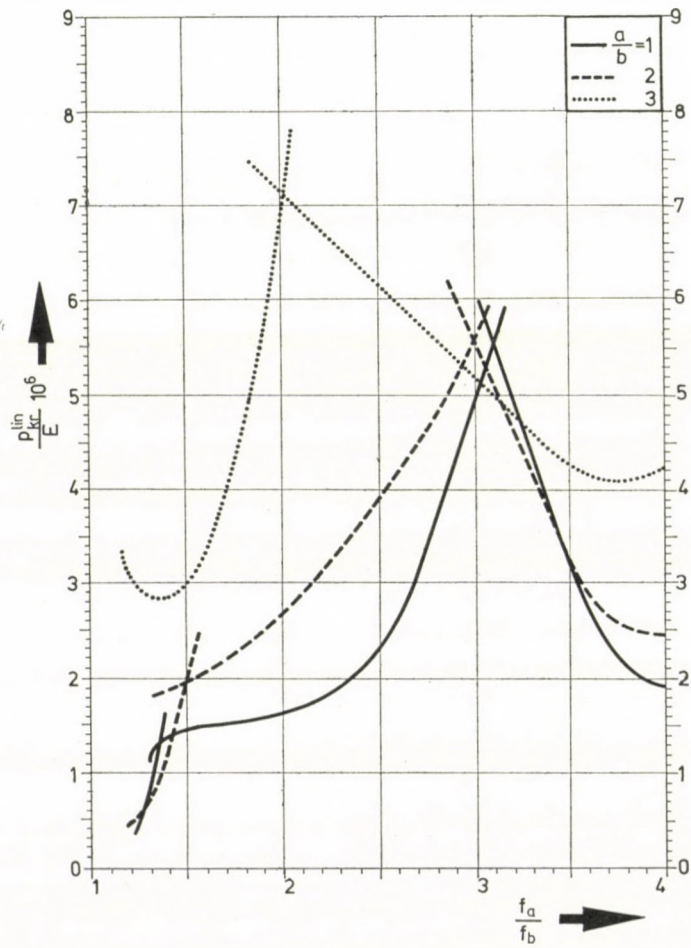

Bild 6. Lineare kritische Last der HP-Schale ($a/h = 100, f_b/b = 0{,}2$)

Etwa im Bereich von $f_a/f_b = 1{,}5 \div 2{,}25$ ist für die meisten Fälle (im allgemeinen, wenn $f_a/f_b \neq 3$ ist) die zum Parameter $f_a/f_b = 9/4$ gehörige Beulform maßgebend.

In der Umgebung der *»halbnormalen«* Schale (etwa $f_a/f_b = 1 \div 1{,}5$) wurden die berechneten linearen kritischen Lasten nur der Vollständigkeit halber dargestellt, denn diese Schalen dürfen nur nach der Theorie der großen Verformungen (im weiteren: nichtlineare Theorie) behandelt werden.

Das läßt sich damit erklären, daß z. B. die »halbnormale« Schale ihre Lasten überwiegend durch Biegeschnittkräfte trägt. Mittelflächenkräfte werden in ihr bloß durch die Lastkomponenten verursacht, deren Formen von den dehnungslosen Durchbiegungformen abweichen: $m \neq n$ [10].

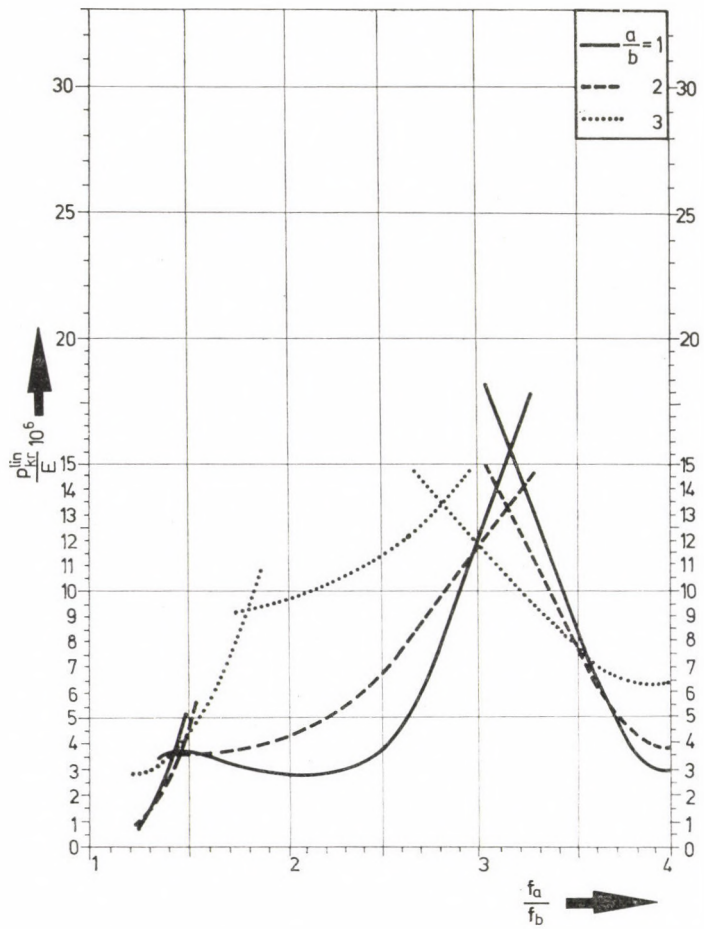

Bild 7. Lineare kritische Last der HP-Schale ($a/h = 100, f_b/b = 0{,}3$)

Die berechneten linearen kritischen Lasten für »halbnormale« Schalen ($f_a/f_b = 1$) sind auch nicht dargestellt, denn *diese sehr großen fiktiven Werte haben keine praktische Bedeutung.* Es soll noch bemerkt werden, daß etwa bei den Verhältnissen $f_a/f_b = 1 \div 1{,}5$ *das dehnungslose Glied* mit Halbwellenzahlen $i_n = j_n = 1$ die dominante Komponente der Beulform bildet.

Der Fehler der zu den eingliedrigen Beulformen gehörigen linearen kritischen Lasten ist im Vergleich zu den genauen Werten wesentlich größer, als die erwähnte Abweichung bezogen auf die sonstigen Schalen.

Selbstverständlich gibt es keine bestimmte Grenze f_a/f_b, von der an es berechtigt wäre die Schale nach der linearen Theorie zu behandeln. Diese nicht bestimmte Grenze befindet sich etwa zwischen den Werten $f_a/f_b = 1{,}5$ und 2 [10].

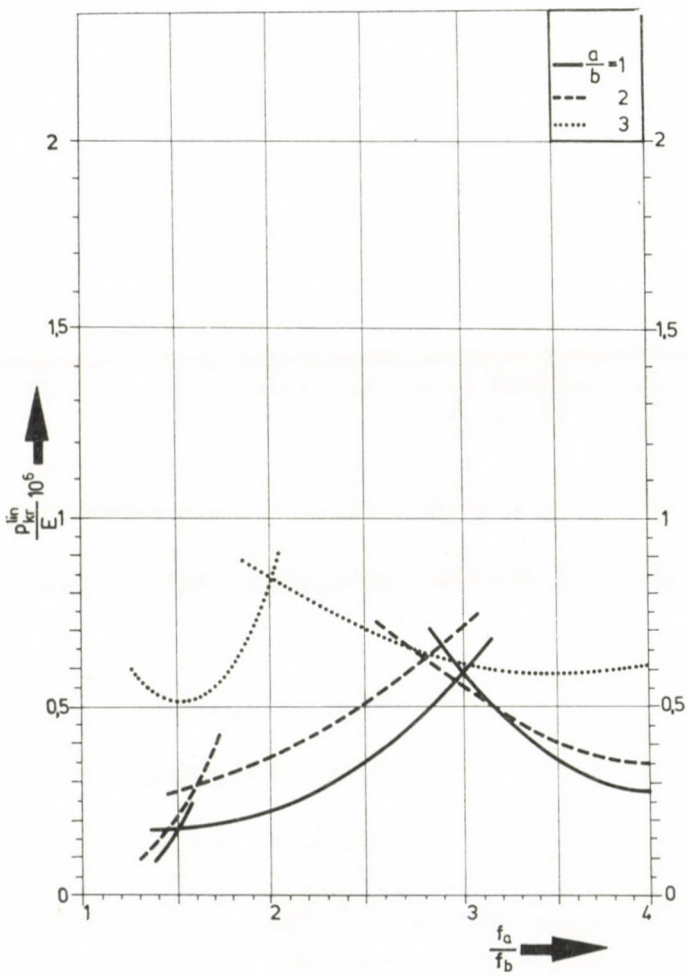

Bild 8. Lineare kritische Last der HP-Schale ($a/h = 150, f_b/b = 0{,}1$)

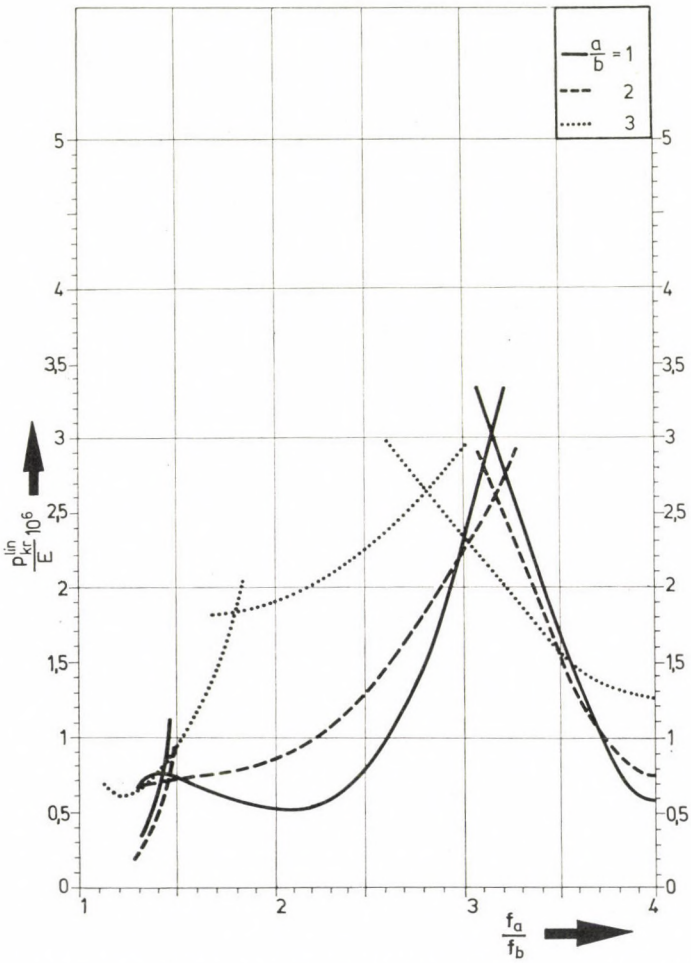

Bild 9. Lineare kritische Last der HP-Schale ($a/h = 150, f_b/b = 0{,}2$)

6. Zusammenfassung

In diesem Artikel wurde die aus dem unverformten Grundzustand ($w_0 = 0$) erfolgende *Verzweigungserscheinung* der flachen, sattelförmigen, unter gleichmäßig verteilter Belastung stehenden HP-Schalen erörtert.

In [10] wurde gezeigt, bei welchen geometrischen Verhältnissen es gerechtfertigt ist, die Stabilitätsuntersuchung dieser Schalen nach der linearen Theorie durchzuführen. Dieser Bereich kann näherungsweise durch die Pfeilhöhenverhältnisse $f_a/f_b = (1{,}5 \div 2) \div 4$ gekennzeichnet werden. In diesen Fällen sind die *Membranwirkungen* gegenüber der Biegewirkungen vernachlässigbar klein.

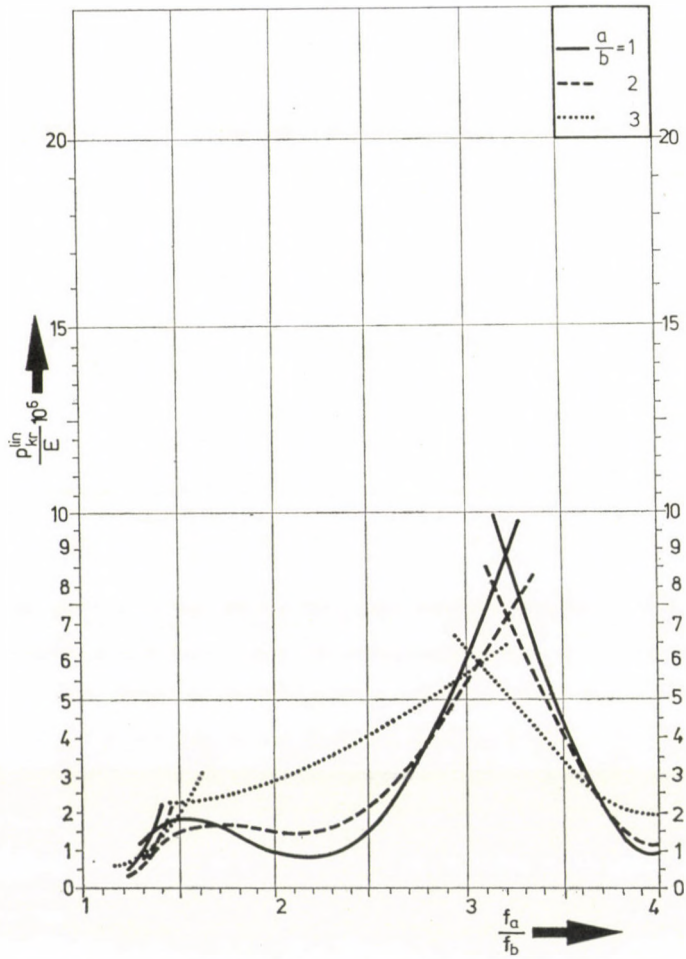

Bild 10. Lineare kritische Last der HP-Schale ($a/h = 150, f_b/b = 0{,}3$)

Im Laufe der Analyse wurde auch der Untersuchung der *dehnungslosen Beulungsmöglichkeit* eine große Bedeutung zugemessen.

Vor der exakten Lösung wurde auch ein *Näherungsverfahren* erarbeitet. Das Resultat lautet: die lineare kritische Last der bogenartig wirkenden HP-Schale bildet *die obere Schranke* der linearen kritischen Last der an ihren Rändern normalkraftfreien HP-Schale.

Die Eigenwertgleichung des Problems wurde nach dem Galerkinschen Verfahren aufgeschrieben. Vor den numerischen Untersuchungen wurde an Hand der speziellen Struktur der Matrizen festgestellt, daß sich irgendeine Beulform nur aus denjenigen Gliedern zusammensetzen kann, die einer der vier Kombinationen der Symmetrie und Antimetrie entsprechen. Unter diesen

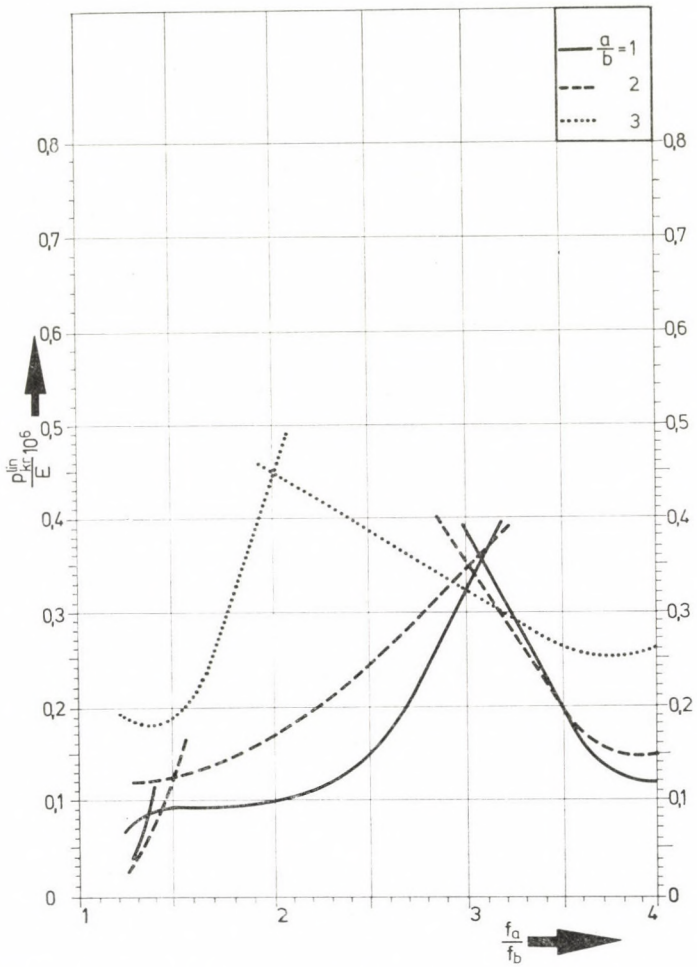

Bild 11. Lineare kritische Last der HP-Schale ($a/h = 200, f_b/b = 0{,}1$)

Gliedern befinden sich sowohl dehnungslose als auch nicht-dehnungslose (mit Verzerrungen verbundene) Komponenten. Es läßt sich an Hand der numerischen Ergebnisse feststellen, daß in jeder Beulform ein *dominantes Glied* vorhanden ist. Dieses Glied ist in Fällen der »*halbnormalen*« HP-Schalen ($f_a/f_b = 1$), der HP-Schalen mit dem Pfeilhöhenverhältnis $f_a/f_b = 9/4$ sowie der »*normalen*« HP-Schalen ($f_a/f_b = 4$) ihrer *dehnungslosen Durchbiegungsform* gleich.

Das dominante Glied der Beulform der übrigen Schalen stimmt entweder mit jenen der »halbnormalen« oder der »normalen« HP-Schale oder mit jenen der HP-Schale mit dem Pfeilhöhenverhältnis $f_a/f_b = 9/4$ überein. Diese dominanten Glieder verursachen auch Mittelflächenverzerrungen.

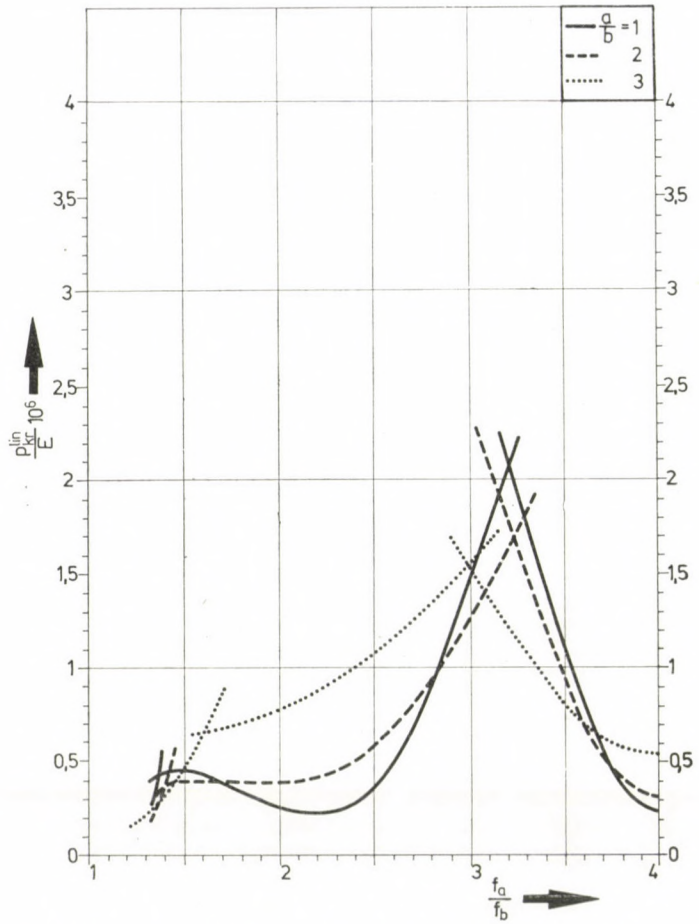

Bild 12. Lineare kritische Last der HP-Schale ($a/h = 200, f_b/b = 0{,}2$)

Die Minimalwerte der erhaltenen Girlandkurven befinden sich in der Nähe der Pfeilhöhenverhältnisse f_a/f_b der *im wesentlichen dehnungslos* beulenden HP-Schalen (z. B. $f_a/f_b = 9/4, 4$).

Die Maximalwerte der linearen kritischen Lasten gehören in meisten Fällen zu den Verhältnissen f_a/f_b, die in der Nähe des Parameterwertes $f_a/f_b = 3$ liegen ($f_a/f_b = 1 \div 4$).

Der Vollständigkeit halber wurden auch diejenigen *fiktiven* linearen kritischen Lasten bestimmt, die zu den Parametern f_a/f_b gehören, die nahe zum Wert f_a/f_b der »halbnormalen« Schale liegen.

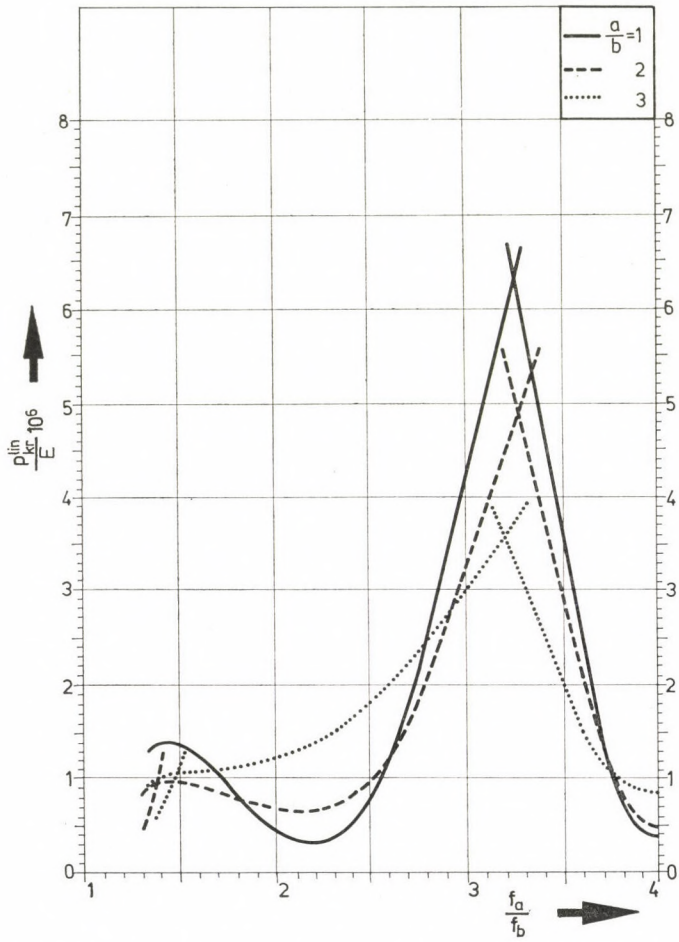

Bild 13. Lineare kritische Last der HP-Schale ($a/h = 200, f_b/b = 0{,}3_1$

Diese Schalen tragen ihre Lasten überwiegend durch Biegeschnittkräfte. Deshalb muß man ihre Stabilitätsuntersuchungen nach der (nichtlinearen) Theorie der großen Verformungen durchführen.

In unserem folgenden Artikel wird das nichtlineare Stabilitätsverhalten der bisher erörterten HP-Schalen behandelt [11].

SCHRIFTTUM

1. Apeland, K.: A Note on the Stability Problem of Shallow Translational Shells. *Journal of Applied Mechanics.* Sept. (1960), 586—588
2. Beleș, A.—Soare, M.: Das elliptische und hyperbolische Paraboloid im Bauwesen. VEB Verlag für Bauwesen, Berlin-Akademie-Verlag, Bukarest 1970
3. Bürgermeister, G.—Steup, H.—Kretzschmar, H.: Stabilitätstheorie II. Akademie-Verlag, Berlin 1957

4. COLLATZ, L.: Eigenwertaufgaben mit technischen Anwendungen. Akademische Verlagsgesellschaft Geest & Portig K.-G., Leipzig 1949
5. DAYARATNAM, P.—GERSTLE, K. H.: Buckling of Hyperbolic Paraboloids. *Proc. World Conference on Shell Shell Structures, San Francisco* 1962. 289—296
6. DULÁCSKA, E.: Vibration and Stability of Anisotropic Shallow Shells. *Acta Techn. Hung.* **65** (1969), 225—260
7. DULÁCSKA, E.: Stability of Anisotropic Hyperbolic Paraboloid Shells. *Acta Techn. Hung.* **59** (1967), 123—130
8. FLÜGGE, W.—GEYLING, F. T.: A General Theory of Deformations of Membrane Shells. *International Association for Bridge and Structural Engineering.* **17** (1957), 23—46
9. GIONCU, V.—IVAN, M.: Instabilitatea structurilor diu Placi Curbe Subţiri. Editura Ac. Rep. Socialiste România, 1978
10. JANKÓ, L.: Analyse des Verhältnisses zwischen Membran- und Biegeschnittkräften in sattelförmigen flachen, normalkraftfrei gelagerten HP-Schalen unter gleichmäßig verteilter Belastung. *Acta Techn. Hung.* 91 (1980), 19—55
11. JANKÓ, L.: Untersuchung der Gleichgewichtszustände sattelförmiger, flacher, normalkraftfrei gelagerter HP-Schalen unter gleichmäßig verteilter Belastung, mit besonderer Berücksichtigung des Durchschlagens und der Abzweigung. *Acta Techn. Hung.* 91 (1980)
12. KOLLÁR, L.—DULÁCSKA, E.: Schalenbeulung. Werner, Düsseldorf — Akadémiai Kiadó, Budapest 1974
13. KOLLÁR, L.: Héjak nyúlásmentes alakváltozásai. *Építés- és Építészettudomány* (1971), 19—38 (auf ungarisch) [Dehnungslose Verformungen der Schalen]
14. KOLLÁR, L.: Schalenkonstruktionen. Sonderdruck aus dem *Beton-Kalender* 1974. Verlag von Wilhelm Ernst und Sohn, Berlin—München—Düsseldorf 1974
15. LEET, K. M.: Study of Stability in the Hyperbolic Paraboloid. *Journ. Eng. Mech. Divis. Proc. ASCE*, **92** (1966) No 1, 121—142
16. MIHAILESCU, M.: Despre stabilitatea invelitorilor subtiri in formă de paraboloizi hiperbolici. *Industria constructiilor şi a materialelor de construcţii.* **2** (1954), 66—70
17. PFLÜGER, A.: Stabilitätsprobleme der Elastostatik. 2. Aufl. Springer-Verlag, Berlin—Göttingen—Heidelberg—New York 1964
18. PONOMARJOV, Sz. D.: Szilárdsági számítások a gépészetben. I. kötet. Műszaki Könyvkiadó, Budapest 1963, 357—381. (auf. ung.) [Festigkeitsberechnungen im Maschinenbau]
19. RALSTON, A.: On the Problem of Buckling of a Hyperbolic Paraboloidal Shell Loaded by Its Own Weight. *Journ. Math. Phys.* **35** (1956), 53—59
20 RALSTON, A.: A First Course in Numerical Analysis. McGraw-Hill Book Company, New York—Toronto—London 1963
21 REISSNER, E.: On Some Aspects of the Theory of Thin Elastic Shells. *Boston Society of Civil Engineers* (1955), 100—133
22. TIMOSHENKO, S. P.—GERE, J. M.: Theory of Elastic Stability. McGraw-Hill Book Company, New York—Toronto—London 1961
23. TSUBOI, Y.: Parametric Study of Buckling of Shells with Reference to Gaussian Curvature. *IASS World Congress on Space Enclosures.* Building Research Centre. Concordia University Montreal (1976), July, 343—363
24. WILKINSON, J. H.—REINSCH, C.: Linear Algebra. Springer-Verlag, Berlin 1971
25. WOLMIR, A. S.: Biegsame Platten und Schalen. VEB Verlag für Bauwesen, Berlin 1962

Stability of Shallow Saddle-shaped Hypar Shells, Supported by Shear Diaphragms, under Uniform Load. This paper is the second part of a series consisting of three parts, the first of which treated theoretical problems (i.e., existence and uniqueness of the membrane solution, kinematic uncertainity) the response to which assures a suitable fundament for performing the present stability analyses. In the paper, the phenomenon of branching from the undeformed state of the saddle-shaped flat hypar shells without lateral thrust is dealt with. In this connection also the question is analysed what influence has the possibility of the development of an inextensional deformation on the process of losing stability.

Acta Technica Academiae Scientiarum Hungaricae, Tomus 91 (3—4), pp. 303—319 (1980)

ON THE EFFECT OF STOCHASTIC ROAD PROFILES ON VEHICLES TRAVELLING AT VARYING SPEED

M. FARKAS,* J. FRITZ,** P. MICHELBERGER***

[Manuscript received 15 March 1979]

Vehicles participating in mass transportation are frequently constrained to change their velocities due to traffic and other reasons. It is assumed that the road profile, as a function of the distance from the origin, is a steady state stochastic process and the distance covered by time-dependent variable speed is a process of steady-state increment. Assuming them to be independent processes, it is pointed out that the complex process, i.e., the road profile as a time-dependent function is a steady-state process. The particular case of the bus applied in town traffic is detailed which, between two stops runs with uniform speed, decelerates and accelerates uniformly at the stopping places while it is assumed that the placement of the stations might be simulated by a kind of Poisson's processes.

1. Introduction

The swinging of vehicles due to the excitation of stochastic road profiles has attracted much attention and has been a main research problem in the past few years. While previously, first of all, the swinging comfort and the stability of the motion had been studied, recently some work has started on the study of stress affecting the vehicle structure. While in the first case the idealization and the drastic simplification of the conditions among which the investigations are carried through are justified, in the latter the actual operational conditions are to be approximated as well as possible. In spite of the fact that in designing, naturally, several simplifying assumptions are to be applied even in this latter case. The labour consumption of the investigations is influenced, first of all, by the model of the swinging system. The computations are considerably simplified if some linear approximation of the originally non-linear model can be used, since then in possession of the spectral density function of the excitation, the spectrum and other statistical data of the investigated outputs can be determined analytically.

The spectral method can be applied if the excitation of the road is stationary. The measured statistical characteristics of the road irregularities show that this condition is fulfilled if the road profile is considered a stochastic

* Prof. M. FARKAS 1111 Budapest, Műegyetem rkp. 3. Hungary
** J. FRITZ H-1053 Budapest, Reáltanoda u. 13—15. Hungary
*** Prof. P. MICHELBERGER 1111 Budapest, Műegyetem rkp. 3. Hungary

process depending on *distance*. It is easy to see that travelling at a constant speed on realizing the road profile the excitation will remain stationary as a function of *time*, too.

However, a large number of vehicles are working in cities, where due to traffic density and the traffic light system, all vehicles have frequently to change speed. The frequent variation of speed is still more characteristic for municipal buses the drivers of which have to brake and accelerate not only as a consequence of the traffic situation but also because of the bus stops. This characteristic kind of operation is, in general, considered to be unstationary. As a consequence, the spectral method is not applied even for the case of linear models; in most cases the equations of motion are solved over the time domain, instead. However, if the representative road or time interval is as long as necessary then the amount of computational work increases beyond admissible limits. It is worth while to find conditions under which the operation with varying speed stays stationary.

In the phases of braking and accelerating some pitching oscillations arise which are due to the inertial forces and the position of the centre of gravity of the vehicle. However, this phenomenon is independent of the excitation due to the irregularities of the road profile [2] since it arises on a theoretically smooth road, too. Therefore, we do not account for this pitching oscillation in our investigations (its effect can be taken into consideration afterwards).

The frequency of the irregularities of the road profile varies as a consequence of varying velocity. Due to this variation of the frequency of the irregularities the spectrum of the excitation also changes and this is important from the point of view of our investigation. This phenomenon can be best grasped by analysing the travelling, through a realization of the road profile with constant and varying speed, respectively.

On Figure 1a a part of a realization of the road profile as a function of distance a can be seen. Travelling through this section at constant velocity v_1 means that by the simple linear transformation $s = v_1 t$ the horizontal axis can be turned into the time axis without altering the picture. Assume that v_1 is the maximal speed in city traffic and the road profile is drawn on arubber band of varying width. On sections where the velocity is v_1 the band is stiff, on sections where the actual speed v is less than v_1 the band is streched by the ratio v_1/v (Fig. 1b, 1c). In this way a new distance s' is defined by $= sv_1/v$ ("the stretch of road covered with a lower speed v seems to be longer"). Travelling with constant speed v_1 on the road whose profile is considered as a function of the new distance s' (Fig. 1c) yields the same excitation as if the original road with profile as a function of s had been covered at varying speed. The main problem is whether the irregularities remain stationary after such a deformation, or more precisely, under what conditions imposed on the distribution of the stretched sections does the process remain stationary.

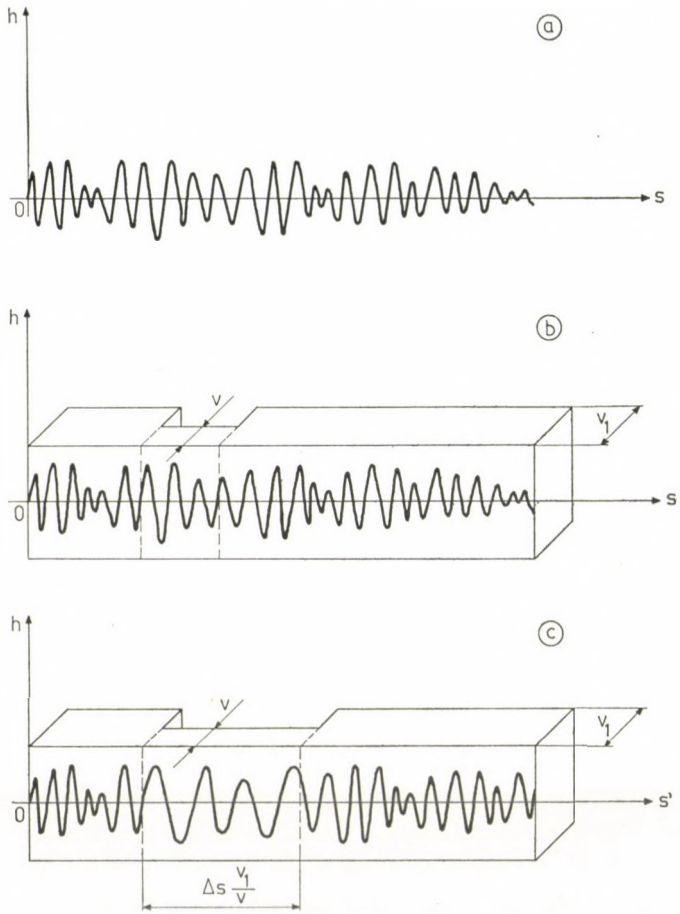

Fig. 1

A further problem is whether these conditions hold in practice. A positive answer to these questions makes the spectral method applicable to the investigation of the operation at varying velocity (apart from the pitching motion). In this case the excitation has a spectral density function which, of course, is to be statistically determined by separate measurement (road profile testing at a varying velocity).

The municipal bus operation has some further characteristics which may make the modification of the known spectrum of excitation corresponding to constant speed possible, thus making the varying speed measurements superfluous.

A characteristic velocity-time diagram of a municipal service is shown of Fig. 2. The lengths of the trapeziums are random variables (they depend on the distances of bus stops, on traffic lights, on traffic jams etc.). The sections

corresponding to accelerating and braking may be considered to be deterministic and of unit length (Fig. 2a). From the point of view of the stresses on the vehicle structure the time intervals in which the bus is not moving could be disregarded, assuming that the acceleration starts without delay at the instant when the bus was brought to a stop. Thus instead of Fig. 2a we might consider the diagram on Fig. 2b. In this way we have neglected those few damped oscillations which are made by the vehicle after having been brought to a halt. The number of these oscillations are, clearly, small compared to the frequency of swinging while the vehicle is moving. We further assume that the time required for bringing the vehicle to a halt from maximal velocity or vice versa is small compared to the mathematical expectation of the distance of two stops $\varrho_i - \varrho_{i-1}$. The value of the velocity as a function of time is then given by

$$v(t) = \begin{cases} 2v_1 t\,, & \left[0, \dfrac{1}{2}\right] \\ v_1\,, & \left[\dfrac{1}{2}, \varrho_1\right] \\ -2v_1 t + v_1(1 + 2\varrho_1)\,, & \left[\varrho_1, \varrho_1 + \dfrac{1}{2}\right] \\ 2v_1 t - v_1(1 + 2\varrho_1)\,, & \left[\varrho_1 + \dfrac{1}{2}, \varrho_1 + 1\right] \\ \vdots & \cdot \end{cases}$$

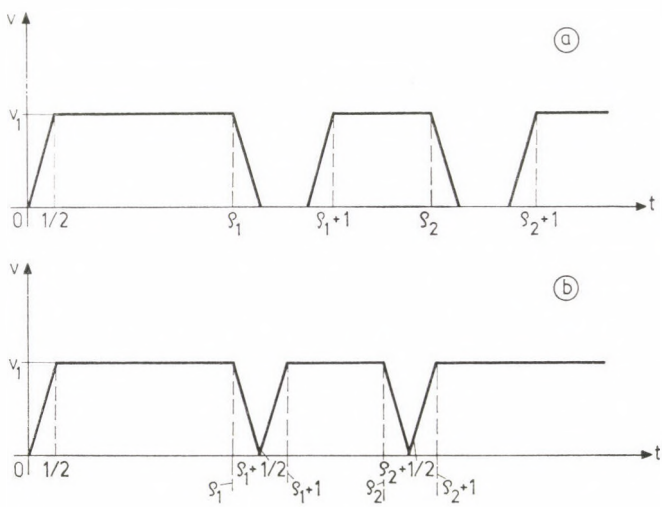

Fig. 2

A realization of the road profile has been shown on Fig. 1a. Since we consider the road profile as a random process, this realization has to be given as a function of time. The role of the deformed distance s' of the rubber band model is now played by the time t. The density of the ratio of deformations is given by

$$\frac{v(t)}{v_1} = ds/dt = \lim_{\Delta t \to 0} \Delta s/\Delta t$$

If we denote the realization of the road profile as a function of time by h, we have

$$\tilde{h}(t) = h(s(t))$$

and (Fig. 2)

$$\frac{d\tilde{h}}{dt} = \frac{dh}{ds}\frac{ds}{dt} = \frac{dh}{ds}\frac{v}{v_1} = \begin{cases} \dfrac{dh}{ds} 2t, & 0 \le t \le \dfrac{1}{2} \\ \dfrac{dh}{ds}, & \dfrac{1}{2} \le t \le \varrho_1 \\ \dfrac{dh}{ds}[-2t + 1 + 2\varrho_1], & \varrho_1 \le t \le \varrho_1 + \dfrac{1}{2} \\ \dfrac{dh}{ds}[2t - 1 - 2\varrho_1], & \varrho_1 + \dfrac{1}{2} \le t \le \varrho_1 + 1 \\ \vdots & \end{cases}$$

If the distance of stops is assumed to follow an exponential distribution, a further task is to generate the spectrum of the deformed process $h(t)$ provided that the spectrum of the original process $h(s)$ is given.

2. Auto correlation and spectral density of composed stochastic processes

As was discussed above, we are facing the following problem. The profile of the road as a function of distance s from the starting point is described by a stationary process $h = \eta(s)$, and the distance s travelled by our vehicle in the period $(0, t)$ of time is again a stochastic process $s = \xi(t)$. Thus, the random forces acting on the system can be expressed in terms of the composed process as

$$\tilde{h} = \tilde{\eta}(t) = \eta(\xi(t)) .$$

As usual in the literature [1], we assume that $\eta(s)$ is a second order stationary process of zero mean and spectral density $f(\omega)$; i.e. the autocorrelation $K(s) = E[\eta_r \eta_{r+s}]$ does not depend on r and

$$K(s) = \int_{-\infty}^{\infty} e^{i\omega s} f(\omega)\, d\omega \,. \tag{1}$$

Here and in what follows we assume that $f(\omega)$ is a given nonnegative and integrable real function. Since $\eta(s)$ is a real process, $f(-\omega) = f(\omega)$ for each $\omega \in (-\infty, +\infty)$. For $\xi(t)$ we have a natural representation

$$\xi(t) = \int_0^t v(u)\, du \,, \tag{2}$$

where the velocity process $v = v(t)$ can be considered as a strictly stationary stochastic process. Hence, it directly follows (see [1]) that $\xi(t)$ is a process with stationary increments, i.e. the joint distribution of the differences

$$\xi(t + t_2) - \xi(t + t_1), \quad \xi(t + t_3) - \xi(t + t_2), \ldots, \quad \xi(t + t_n) - \xi(t + t_{n-1})$$

is independent of t. Therefore, it is reasonable to expect that the composed process $\tilde{\eta}(t) = \eta(\xi(t))$ will again be stationary.

Before proving such a statement we have to specify the coupling (joint-distribution) of our processes $\eta(s)$ and $\xi(t)$, since the problem is not well-posed otherwise. On a city road the driving strategy depends mainly on such external conditions as traffic lights, stops, other vehicles etc., so that the driver can not take or does not want to take into account road inequalities. Therefore, it is quite natural to assume that $v(t)$ and $\eta(s)$ are independent stochastic processes; i.e. any group $v(t_1), v(t_2), \ldots, v(t_n)$ of variables is independent of any group $\eta(s_1), \eta(s_2), \ldots, \eta(s_m)$. Hence, it directly follows that $\xi(t)$ and $\eta(s)$ are independent processes, too. In particular, the conditional distribution of the product $\eta(r)\eta(r + s)$ for given $\xi(u) = r$, $\xi(u + t) = r + s$ is the same as the unconditioned, therefore

$$\begin{aligned} E[\tilde{\eta}(u)\, \tilde{\eta}(u + t)] &= E[\eta(\xi(u))\, \eta(\xi(u + t))] = \\ &= E[E(\eta(\xi(u))\, \eta(\xi(u + t)) \mid \xi(u), \quad \xi(u + t))] \\ &= E[K(\xi(u + t) - \xi(u))] \,. \end{aligned} \tag{3}$$

Let

$$F_t(s) = P(\xi(u + t) - \xi(u) < s) \tag{4}$$

denote the distribution function of the increment $\xi(u+t) - \xi(u)$. Since $\xi(t)$ has stationary increments, F does not really depend on u. Therefore, the autocorrelation function

$$E\big(\tilde{\eta}(u)\,\tilde{\eta}\,(u+t)\big) = \int_{-\infty}^{\infty} K(s) F_t(ds) = R(t) \tag{5}$$

of the composed process $\tilde{\eta}(t)$ is again independent of u, which proves that $\tilde{\eta}(t)$ is a second order stationary process.

Let us remark that $\xi(u+t) = \xi(u)$ is possible with a positive probability, thus $F_t(s)$ is not necessarily absolutely continuous. On the other hand, it is reasonable to assume that $\xi(u+t) \geq \xi(u)$ if $t \geq 0$, and $R(t)$ is integrable; then $\tilde{\eta}(t)$ has a continuous spectral density $g(\tilde{\omega})$ given by

$$g(\tilde{\omega}) = \frac{1}{2\pi}\int_{-\infty}^{\infty} R(t) e^{-i\tilde{\omega}t} dt = \frac{1}{\pi}\,\mathrm{Re}\int_0^{\infty} R(t)\, e^{-i\tilde{\omega}t}\, dt\,. \tag{6}$$

Hence

$$g(\tilde{\omega}) = \frac{1}{\pi}\,\mathrm{Re}\int_0^{\infty}\int_0^{\infty} e^{-i\tilde{\omega}t}\, K(s)\, F_t(ds) dt =$$

$$= \frac{1}{\pi}\,\mathrm{Re}\int_{-\infty}^{\infty}\int_0^{\infty}\int_0^{\infty} e^{i\omega s - i\tilde{\omega}t}\, f(\omega) F_t\,(ds)\, dt\, d\omega = \tag{7}$$

$$= \frac{2}{\pi}\int_0^{\infty} \hat{F}\,(\omega, \tilde{\omega})\, f(\omega)\, d\omega\,,$$

where

$$\hat{F}(\omega, \tilde{\omega}) = \mathrm{Re}\int_0^{\infty}\int_0^{\infty} e^{i\omega s - i\tilde{\omega}t}\, F_t\,(ds)\, dt\,. \tag{8}$$

Since the spectral density $f(\omega)$ of $\eta(s)$ is assumed to be known, we have only to determine the kernel function $\hat{F}(\omega, \tilde{\omega})$ defined in (8). This calculation will be carried out for the model $\xi(t)$ for city traffic outlined in the first section.

3. Calculation of the kernel function $\hat{F}$ for a Poissonian model of city traffic

In this model, apart from some nonoverlapping braking-accelerating periods, our vehicle travels at a constant velocity v_1. Although many more realistic (and more sophisticated) models could have been treated with the same methods, for convenience sake we assume that the velocity-time diagram has the same shape in each braking-accelerating interval, and the unit of time is chosen as the common length of these intervals. Our main assumption is that the waiting times between consecutive braking-accelerating intervals are

independent and exponentially distributed random variables with the common parameter $\lambda = 0$. Further parameters of the model are those specifying the shape of the velocity diagram in the braking-accelerating intervals. Let $v_0(t)$ denote the velocity diagram in the particular case when (0, 1) is the only braking-accelerating interval; for convenience sake we put $v_0(t) = v_1 - \varphi(t)$, where $\varphi(t)$ may be an arbitrary continuous function, such, that $\varphi(t) = 0$ if $t \leq 0$ or $t \geq 1$. Then the velocity process $v(t)$ is constructed as

$$v(t) = v_1 - \sum_{n=1}^{\infty} \varphi(t - \varrho_n)\,, \tag{9}$$

where $0 \leq \varrho_1 < \varrho_2 < \ldots < \varrho_n < \ldots$ is the sequence of starting points of braking-accelerating intervals; i.e.

$$\varrho_{n+1} > \varrho_n + 1 \qquad \text{for each } n: \quad \Delta_n = \varrho_{n+1} - \varrho_n - 1$$

$n = 1, 2, \ldots$, is a sequence of independent and exponentially distributed random variables of parameter $\lambda > 0$, and $\{\varrho_n\}$ is a stationary point process in $(0, +\infty)$. The example of

$$\varphi(t) = \begin{cases} 0 & \text{if} \quad t \leq 0 \\ a_1 t & \text{if} \quad 0 \leq t \leq \dfrac{v_1}{a_1} \\ v_1 & \text{if} \quad \dfrac{v_1}{a_1} \leq t \leq \dfrac{a_2 - v_1}{a_2} \\ a_2 - a_2 t & \text{if} \quad \dfrac{a_2 - v_1}{a_2} \leq t \leq 1 \\ 0 & \text{if} \quad t \geq 1 \end{cases} \tag{10}$$

where $v_1/a_1 < (a_2 - v_1)/a_2$ will be explicitly solved later. (See Fig 3a; Fig 3b shows the graph in case

$$\frac{v_1}{a_1} > \frac{a_2 - v_1}{a_2}\,.$$

The basic object of our study is the stationary point process $\{\varrho_n\}$ often referred to as the Poisson hard-core process; it can be constructed as follows. Let $\gamma_1, \gamma_2, \ldots, \gamma_n, \ldots$ denote a sequence of independent exponential random variables with a common parameter $\lambda > 0$, and put $\zeta = 0$, $\zeta_1 = \gamma_1, \ldots, \zeta_n = \gamma_1 + \gamma_2 + \ldots + \gamma_n, \ldots$; then $\{\zeta_n\}$ forms a Poisson process of intensity λ in $(0, +\infty)$. Then $\tau_n = \zeta_n + n$, $n = 0, 1, 2, \ldots$ are the points of a new point

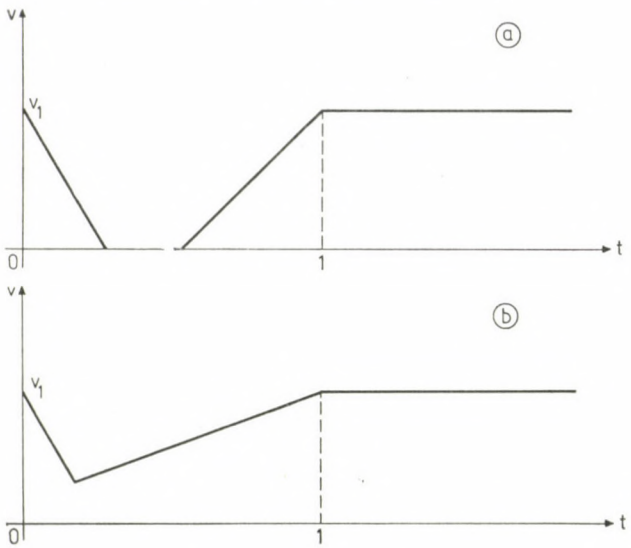

Fig. 3

process, such, that $\tau_{n+1} > \tau_n + 1$ and the differences $\tau_{n+1} - \tau_n - 1$ are independent exponential variables of common parameter λ. Unfortunately $\{\tau_n\}$ does not form a stationary point process, but near infinity it behaves as a stationary one. Indeed, let $N_0(t) = \max \{n \mid \tau_n < t < \tau_{n+1}\}$ and $N_u(t) = N_0(u + t) - N_0(u)$, then $N_0(t)$ and $N_u(t)$ have jumps exactly at the points of $\{\tau_n\} \cap (u, +\infty)$. If u is large then $N_u(t)$ describes the behaviour of the point process $\{\tau_n\}$ near infinity. It is easy to check that $N_0(t)$ is a strongly mixing process, so that there exists the weak limit $N_\infty(t) = \lim_{u \to \infty} N_u(t)$ and it is a stationary point process, see [1]. Let us remember that weak convergence of stochastic processes means convergence of the underlying probability measures in the sense that the expectation of any continuous and bounded function converges. The points of the point process $\{\varrho_n\}$ we need are located just at the jumps of the limiting process $N_\infty(t)$, thus the velocity process

$$v(t) = v_1 - \sum_{n=1}^{\infty} \varphi(t - \varrho_n)$$

is a well defined stochastic process.

Comparing (4), (8) and the definition of $\{\varrho_n\}$ we obtain that

$$\begin{aligned} \hat{F}(\omega, \tilde{\omega}) &= \operatorname{Re} \int_0^\infty E\left[\exp\left(i\omega \int_0^t v(x)\,dx - i\tilde{\omega}t\right)\right] dt = \\ &= \operatorname{Re} \int_0^\infty \lim_{u \to \infty} E\left[\exp\left(i\omega\, \xi_u(t) - i\tilde{\omega}t\right)\right] dt\,, \end{aligned} \tag{11}$$

where

$$\xi_u(t) = \int_u^{u+t} \left(v_1 - \sum_{n=1}^{\infty} \varphi(x - \tau) \right) dx = v_1 t - \sum_{n=1}^{\infty} \int_0^{u+t} \varphi(x - \tau_n)\, dx \,. \quad (12)$$

The evaluation of the above, rather complicated expression will be based on the following trivial remarks. Since $\varphi(x) = 0$ if $x \leq 0$ or $x \geq 1$, the value of

$$\int_u^{u+t} \varphi(x - \tau_n)\, dx$$

depends on τ_n only if $u - 1 \leq \tau_n < u$ or $u + t - 1 < \tau_n \leq u + t$, and

$$\int_u^{u+t} \varphi(x - \tau_n)\, dx = \begin{cases} 0 & \text{if} \quad \tau_n \leq u - 1 \quad \text{or} \quad \tau_n \geq u + t, \\ \delta & \text{if} \quad u \leq \tau_n \leq u + t - 1\,, \\ \psi(1 - y + t) - \psi(1 - y) & \text{if} \quad \tau_n = u - 1 + y, 0 \leq y < 1, \\ \psi(z) - \psi(z - t) & \text{if} \quad \tau_n = u + t - z, \quad 0 \leq z < 1, \end{cases} \quad (13)$$

where

$$\psi(x) = \int_{-\infty}^{x} \varphi(t) dt \,, \quad (14)$$

$$\delta = \psi(1) = \int_0^t \varphi(t)\, dt \,. \quad (15)$$

Therefore, we have only to determine the joint distribution of the number of points in $(u, u + t - 1)$ and the location of points (if any) in the critical intervals $(u - 1, u)$ and $(u + t - 1, u + t)$. Let us remark that neither of the critical intervals can contain two or more points of $\{\tau_n\}$, thus we have the following five possibilities only, which exclude each other, with a probability $1 - O(\varepsilon)$ as $\varepsilon > 0$ goes to zero. The contribution of the k-th case to the integral in (11) will be denoted by I_k, i.e.

$$\hat{F}(\omega, \tilde{\omega}) = \mathrm{Re}\,[I_1 + I_2 + I_3 + I_4 + I_5] \,. \quad (16)$$

Here and in what follows, $\varepsilon > 0$, $u > 0$, $t > 0$, $y \geq 0$, $z \geq 0$ are real numbers, m denotes a nonnegative integer, and the abbreviations $(x)_+ = \max\{0, x\}$, and $\beta = \omega v_1 - \tilde{\omega}$ are used.

(i) $N_{u-1}(1) = 0$, $N_u((t-1)_+) = m$, $N_{u+t-1}(1) = 0$. The probability of this event is denoted by

$$p_m^{(u)}(t) \quad \text{and} \quad p_m(t) = \lim_{u \to \infty} p_m^u(t) \,.$$

Then $\eta_u(t) = v_1 t - m\delta$, thus

$$I_1 = \int_0^\infty \sum_{m=0}^{\infty} \exp\left[i\beta t - i\omega m\delta\right] p_m(t) dt\,.$$

(ii) $N_{u-1+y}(\varepsilon) = 1$ for $t \leq y < 1$. The probability of this event is

$$p^{(u,\varepsilon)}(y, t) \quad \text{and} \quad p(y, t) = \lim_{u\to\infty} \lim_{\varepsilon\to 0} \frac{1}{\varepsilon} p^{(u,\varepsilon)}(y, t)\,.$$

Then

$$\eta_u(t) = v_1 t - \psi(1 - y + t) + \psi(1 - y)\,,$$

thus

$$I_2 = \int_0^1 \int_t^1 \exp\left[i\beta t - i\omega\psi(1 - y + t) + i\omega\psi(1 - y)\right] p(y, t)\, dy dt\,.$$

(iii) $N_{u-1+y}(\varepsilon) = 1$, $N_u((t-1)_+) = m$, $N_{u+t-1}(1) = 0$ for $0 \leq y \leq$ $\leq \min\{1, t\}$. The probability of this event is

$$p_m^{(u,\varepsilon)}(y, t) \quad \text{and} \quad p_m(y, t) = \lim_{u\to\infty} \lim_{\varepsilon\to 0} \frac{1}{\varepsilon} p^{(u,\varepsilon)}(y, t)\,.$$

Then

$$\eta_u(t) = v_1 t - m\delta - \delta + \psi(1 - y)\,,$$

thus

$$I_3 = \int_0^\infty \left[\sum_{m=0}^{\infty} \int_0^{\min\{1,t\}} \exp\left[i\beta t - i\omega(m+1)\delta + i\omega\psi(1-y)\right] p_m(y,t)\, dy \right] dt\,.$$

(iv) $N_{u-1}(1) = 0$, $N_u((t-1)_+) = m$, $N_{u+t-z}(\varepsilon) = 1$ for $0 \leq z <$ $< \min\{1, t\}$. The probability of this event is

$$p^{(u,\varepsilon)}(z, t) \quad \text{and} \quad p_m(z, t) = \lim_{u\to\infty} \lim_{\varepsilon\to 0} \frac{1}{\varepsilon} p_m^{(u,\varepsilon)}(z, t)\,.$$

Then

$$\eta_u(t) = v_1 t - m\delta - \psi(z)\,,$$

thus

$$I_4 = \int_0^\infty \left[\sum_{m=0}^{\infty} \int_0^{\min\{1,t\}} \exp\left[i\beta t - i\omega m\delta - i\omega\psi(z)\right] p_m(z, t) dz \right] dt\,.$$

(v) $N_{u-1+y}(\varepsilon) = 1$, $N_u((t-1)_+) = m$, $N_{u+t-z}(\varepsilon) = 1$ for $0 \leq y < 1$, $0 \leq z < 1$ and $y + z < t$. The probability of this event is denoted by

$$p_m^{(u,\varepsilon)}(y, z, t) \quad \text{and} \quad p_m(y, z, t) = \lim_{u\to\infty} \lim_{\varepsilon\to 0} \frac{1}{\varepsilon^2} p_m^{(u,\varepsilon)}(y, z, t).$$

Then

$$\eta_u(t) = v_1 t - m\delta - \delta + \psi(1-y) - \psi(z),$$

thus

$$I_5 = \int_0^\infty \left[\sum_{m=0}^{\infty} \int_0^1 \int_0^{\min\{1, t+z\}} \exp\left[i\beta t - i\omega(m+1)\delta + i\omega\psi(1-y) - i\omega\psi(z)\right] p_m(y, z, t)\, dy\, dz \right] dt .$$

The next step is to determine the functions $p_m(t)$, $p(y, t)$, $p_m(y, t)$ $p_m(z, t)$ and $p_m(y, z, t)$. Let $q(x)$ denote the probability of $N_x(1) = 0$. Since $N_x(1) = 0$ if and only if $\tau_n < x < x + 1 < \tau_{n+1}$ for some n, i.e. $\zeta_n < x - n < \zeta_{n+1}$, we have

$$q(x) = \sum_{0 \le n < x} (x-n)^n \frac{\lambda^n}{n!} e^{-\lambda(x-n)} \tag{17}$$

for each $x > 0$, and

$$\lim_{x \to \infty} q(x) = \frac{1}{1+\lambda} . \tag{18}$$

Indeed, as τ_n is a sum of n independent summands, the law of large numbers implies that

$$\lim_{n \to \infty} \frac{\tau_n}{n} = \lim_{n \to \infty} \frac{1}{n} E(\tau_n) = 1 + \frac{1}{\lambda} ,$$

thus,

$$\lim_{x \to \infty} \frac{1}{x} N_0(x) = \frac{1}{1 + \frac{1}{\lambda}} = \lim_{x \to \infty} E\big(N_x(1)\big) .$$

On the other hand, $N_x(1) \le 1$ implies $E(N_x(1)) = 1 - q(x)$, which proves (18). As we shall soon see, (18) implies the existence of limits appearing in (i)—(v) and in (11). Now we are in a position to calculate the above functions.

Since (i) means that $\tau_n < u - 1 < u < \tau_{n+1}$ and $\tau_{n+m} < u + t - 1 < u + t < \tau_{n+m+1}$ for some n, i.e. $\zeta_n < u - n - 1 < \zeta_{n+1}$ and $\zeta_{n+m} < u + t - n - m - 1 < \zeta_{n+m+1}$, we have

$$p_m^{(u)}(t) = q(u-1)(t-m)^m \frac{\lambda^m}{m!} e^{-\lambda(t-m)}$$

for $0 \le m \le t$, while otherwise $p_m^{(u)}(t) = 0$. Thus,

$$p_m(t) = \frac{1}{1+\lambda} (t-m)^m \frac{\lambda^m}{m!} e^{-\lambda(t-m)} \tag{19}$$

if $0 \ge m < t$, and $p_m(t) = 0$ if $m \ge t$.

(ii) holds if and only if $u-1+y<\tau_n\leq u-1+y+\varepsilon$ for some n, i.e. $u-1+y-n<\zeta_n\leq u-1+y+\varepsilon-n$, thus $p^{(u,\varepsilon)}(y,t)=q(u-2+y)\lambda\varepsilon+o(\varepsilon)$,

whence

$$p(y,t)=\frac{\lambda}{1+\lambda}\,. \tag{20}$$

In the third case $t\leq 1$ implies that $m=0$, thus (iii) holds if and only if $u-1+y<\tau_n\leq u-1+y+\varepsilon$ and $\tau_{n+m}<u+t-1<u+t\leq\leq\tau_{n+m+1}$ for some n, i.e. $u-1+y-n<\zeta_n<u-1+y+\varepsilon-n$ and $\zeta_{n+m}<u+t-1-n-m\leq\zeta_{n+m+1}$, whence

$$p_m^{(u,\varepsilon)}(y,t)=q(u-2+y)\,\lambda\varepsilon(t-m-y)^m\frac{\lambda^m}{m!}\,e^{-\lambda(t-m-y)}+o(\varepsilon)$$

if $0\leq m<t-y$ and otherwise it equals zero, consequently

$$p_m(y,t)=\frac{\lambda}{1+\lambda}(t-m-y)^m\frac{\lambda^m}{m!}\,e^{-\lambda(t-m-y)} \tag{21}$$

if $0\leq m<t-y$ and $p_m(y,t)=0$ if $m\geq t-y$.

Similarly, (iv) means that $\tau_n<u-1<u-\tau_{n+1}$ and $u+t-z<\leq\tau_{n+m+1}\leq u+t-z+\varepsilon$ for some n, i.e. $\zeta_n<u-1-n<\zeta_{n+1}$ and $u+t-z-n-m-1<\zeta_{n+m+1}\leq u+t-z-n-m-1+\varepsilon$,

whence

$$p_m^{(u,\varepsilon)}(z,t)=q(u-1)(t-m-z)^m\frac{\lambda^m}{m!}\,e^{-\lambda(t-m-z)}\,\lambda\varepsilon+o(\varepsilon)$$

if $0\leq m<t-z$ and otherwise it equals zero, thus

$$p_m(z,t)=\frac{\lambda}{1+\lambda}(t-m-z)^m\frac{\lambda^m}{m!}\,e^{-\lambda(t-m-z)} \tag{22}$$

if $0\leq m<t-z$ and $p_m(z,t)=0$ if $m\geq t-z$.

Finally, (v) means that $u-1+y<\tau_n\leq u-1+y+\varepsilon$ and $u+t-\leq\tau_{n+m+1}\leq u+t-z+\varepsilon$ for some n, i.e. $u-1+y-n<\zeta_n\leq u-\leq-1+y-n+\varepsilon$ and $u+t-z-n-m-1<\zeta_{n+m+1}\leq u+t-z-\leq-n-m-1+\varepsilon$, thus

$$p_m^{(u,\varepsilon)}(y,z,t)=q(u-2+y)\lambda\varepsilon(t-m-z-y)^m\frac{\lambda^m}{m!}\,e^{-\lambda(t-m-y-z)}\,\lambda\varepsilon+o(\varepsilon^2)$$

if $0 \leq m < t - y - z$ and otherwise it is zero,
whence

$$p_m(y, z, t) = \frac{\lambda^2}{1 + \lambda} (t - m - y - z)^m \frac{\lambda^m}{m!} e^{-\lambda(t-m-y-z)} \tag{23}$$

if $0 \leq m < t - y - z$ and $p_m(y, z, t) = 0$ if $m \geq t - y - z$.

To calculate I_1, I_3, I_4 and I_5,

$$I = \int_0^\infty \left[\sum_{0 \leq m < t-x}^{\infty} \exp\,[i\beta t - i\omega m\delta](t - m - x)^m \frac{\lambda^m}{m!} e^{-\lambda(t-m-x)} \right] dt,$$

is a common factor in each of them with $x = 0$ or $x = y$ or $x = z$ or $x = y + z$.
Interchanging the summation and integration it follows that

$$I = \sum_{m=0}^{\infty} \int_{m+x}^{\infty} \exp\,[i\beta t - i\omega m\delta]\,(t - m - x)^m \frac{\lambda^m}{m!} e^{-\lambda(t-m-x)}\, dt =$$

$$= \sum_{m=0}^{\infty} \int_0^{\infty} \exp\,[i\beta(t + m + x) - i\omega m\delta] \frac{(\lambda t)^m}{m!} e^{-\lambda t}\, dt = \tag{24}$$

$$= \int_0^{\infty} \exp\,[i\beta(t + x) + \lambda t(e^{i\alpha} - 1)]\, dt = \frac{e^{i\beta x}}{\lambda(1 - e^{i\alpha}) - i\beta},$$

where $\alpha = \beta - \omega\delta = \omega v_1 - \tilde{\omega} - \omega\delta$.

Using this identity it follows that

$$I_1 = \frac{1}{1 + \lambda} \frac{1}{\lambda(1 - e^{i\alpha}) - i\beta,}, \tag{25}$$

$$I_3 = \frac{\lambda}{1 + \lambda} \frac{e^{-i\omega\delta}}{\lambda(1 - e^{i\alpha}) - i\beta} \int_0^1 \exp\,[i\beta y + i\omega\psi(1 - y)]dy =$$

$$= \frac{\lambda}{1 + \lambda} \frac{e^{i\alpha}}{\lambda(1 - e^{i\alpha}) - i\beta} \int_0^1 \exp\,[-i\beta x + i\omega\psi(x)]\, dx = \tag{26}$$

$$= \frac{\lambda}{1 + \lambda} \frac{e^{i\alpha}}{\lambda(1 - e^{i\alpha}) - i\beta} \overline{J(1)},$$

where

$$J(u) = \int_0^u \exp\,[i\beta x - i\omega\psi(x)]\, dx, \tag{27}$$

and the bar denotes complex conjugation. Similarly,

$$I_4 = \frac{\lambda}{1+\lambda} \frac{1}{\lambda(1-e^{i\alpha}) - i\beta} J(1), \tag{28}$$

and

$$I_5 = \frac{\lambda^2}{1+\lambda} \frac{e^{i\alpha}}{\lambda(1-e^{i\alpha}) - i\beta} |J(1)|^2. \tag{29}$$

Finally, by interchanging the order of integration and substituting $1 - y = u$ and $1 - y + t = x$, it follows that

$$I_2 = \frac{\lambda}{1+\lambda} \int_0^1 \int_0^y \exp\left[i\beta t - i\omega\psi(1-y+t) + i\omega\psi(1-y)\right] dt\,dy =$$

$$= \frac{\lambda}{1+\lambda} \int_0^1 \int_0^y \exp\left[i\beta x - i\omega\psi(x) - i\beta u + i\omega\psi(u)\right] du\,dx =$$

$$= \frac{\lambda}{1+\lambda} \int_0^1 \overline{J(x)}\, J'(x)\, dx,$$

whence

$$\operatorname{Re} I_2 = \frac{\lambda}{2+2\lambda} |J(1)|^2 . \tag{30}$$

Consequently,

$$\hat{F}(\tilde{\omega}, \omega) = \operatorname{Re} I_1 + \operatorname{Re} I_2 + \operatorname{Re} I_3 + \operatorname{Re} I_4 + \operatorname{Re} I_5 =$$

$$= \frac{\lambda}{2+2\lambda} \frac{[2\lambda^2(1-\cos\alpha) + \beta^2]\,|J(1)|^2}{2\lambda^2(1-\cos\alpha) + \beta^2 + 2\beta\lambda\sin\alpha} + \tag{31}$$

$$+ \frac{\lambda}{1+\lambda} \frac{1 - \cos\alpha + (\lambda - \lambda\cos\alpha - \beta\sin\alpha) \operatorname{Re} J(1) - \beta(1-\cos\alpha) \operatorname{Im} J(1)}{2\lambda^2(1-\cos\alpha) + \beta^2 + 2\beta\lambda\sin\alpha}$$

where $\alpha = \omega v_1 - \tilde{\omega} - \omega\delta$, $\beta = \omega v_1 - \tilde{\omega}$ and $J(1)$ is a function of β and ω given by (27), while $\lambda > 0$, $v_1 > 0$, $\delta > 0$ are parameters of the model.

4. Piecewise linear velocity diagrams

Here we consider the example defined in (10); we have to calculate the integral

$$J(1) = \int_0^1 \exp\left[i\beta x - i\omega\psi(x)\right] dx \tag{32}$$

for

$$\varphi(x) = \begin{cases} \dfrac{1}{2} a_1 x^2 & \text{if} \quad 0 \leq x \leq \dfrac{v_1}{a_1}, \\ v_1 x - \dfrac{1}{2} \dfrac{v_1^2}{a_1} & \text{if} \quad \dfrac{v_1}{a_1} \leq x \leq 1 - \dfrac{v_1}{a_2}, \\ \delta - \dfrac{a_2}{2}(1-x)^2 & \text{if} \quad 1 - \dfrac{v_1}{a_2} \leq x \leq 1, \end{cases} \tag{33}$$

where $v_1/a_1 < 1 - v_1/a_2$, and

$$\delta = v_1 \left(1 - \frac{v_1}{2a_1} - \frac{v_1}{2a_2}\right). \tag{34}$$

We shall see that the following method applies for arbitrary piecewise linear φ. Unfortunately, $J(1)$ cannot be expressed in terms of elementary functions even in this simple case; we need the transcendent function

$$\Psi(u) = \int_0^u e^{ix^2}\, dx. \tag{35}$$

Then

$$\int_0^{\vartheta_1/a_1} \exp\left[i\beta x - i\frac{a_1\omega}{2} x^2\right] dx =$$

$$= \sqrt{\frac{2}{a_1\omega}} \exp\left(i\frac{\beta^2}{2a_1\omega}\right) \left[\overline{\Psi\left(\sqrt{\frac{\tilde{\omega}^2}{2a_1\omega}}\right)} - \overline{\Psi\left(\sqrt{\frac{\beta^2}{2a_1\omega}}\right)}\right], \tag{36}$$

and

$$\int_0^{\vartheta_2/a_2} \exp\left[-i\beta x + i\frac{a_2\omega}{2} x^2\right] dx =$$

$$= \sqrt{\frac{2}{a_2\omega}} \exp\left(-i\frac{\beta^2}{2a_2\omega}\right) \left[\Psi\left(\sqrt{\frac{\tilde{\omega}^2}{2a^2\omega}}\right) - \Psi\left(\sqrt{\frac{\beta^2}{2a_2\omega}}\right)\right], \tag{37}$$

whence

$$J(1) = \sqrt{\frac{2}{a_1\omega}} \exp\left(i\frac{\beta^2}{2a_1\omega}\right) \left[\overline{\Psi\left(\sqrt{\frac{\tilde{\omega}^2}{2a_1\omega}}\right)} - \overline{\Psi\left(\sqrt{\frac{\beta^2}{2a_1\omega}}\right)}\right] +$$

$$+ \sqrt{\frac{2}{a_2\omega}} \exp\left(i\alpha - i\frac{\beta^2}{2a_2\omega}\right) \left[\Psi\left(\sqrt{\frac{\tilde{\omega}^2}{2a_2\omega}}\right) - \Psi\left(\sqrt{\frac{\beta^2}{2a_2\omega}}\right)\right] + \tag{38}$$

$$+ \frac{i}{\tilde{\omega}} \left[\exp\left[i\left(\frac{\tilde{\omega}v_1}{a_2} - \omega\delta - \tilde{\omega}\right)\right] - \exp\left[-i\frac{\tilde{\omega}v_1}{a_2} - i\omega\delta\right]\right].$$

Substituting (38) into (32) we obtain $\hat{F}(\omega, \tilde{\omega})$ in a final form.

REFERENCES

1. FELLER, W.: An Introduction to Probability Theory and its Applications II., Wiley, New York 1966
2. ZASCHEL, J. M.: Die Analyse und Beschreibung von Betriebsbeanspruchungen zur Lebensdauerbeurteilung, *Fatigue Life under Random Load Conference*, Trieste 5—6 October 1978, Università degli Studii di Trieste

Wirkung der stochastischen Straßenbahnprofile auf die mit veränderlicher Geschwindigkeit fahrenden Fahrzeuge. — Die im städtischen Verkehr angewandten Fahrzeuge sind infolge von Verkehrsumständen oder von anderen Ursachen oftmals zur Änderung ihrer Geschwindigkeit gezwungen. Man setzt voraus, daß das Straßenbahnprofil als eine Funktion der Länge des vom Ausgangspunkt gemessenen Weges, ein stochastischer Vorgang von stationärem Inkrement ist. Vorausgesetzt, daß derselbe ein unabhängiger Vorgang ist, es wird bewiesen, daß der zusammengesetzte Vorgang, d.h., das Straßenbahnprofil, als Funktion der Zeit, stationär ist. Der Spezialfall des in den Städten angewandten Autobusses wird behandelt, welcher zwischen zwei Haltestellen mit konstanter Geschwindigkeit fährt, bremst, und später beschleunigt gleichermaßen an den Haltestellen, wobei es voraussetzt wird, daß die Anordnung der Haltestellen durch einen Poissonschen Vorgang modelliert werden kann.

Acta Technica Academiae Scientiarum Hungaricae, Tomus 91 (3—4), pp. 321—333 (1980)

ERWÄRMUNGEN UND VERLUSTE IN STREUFELDERN VON TRANSFORMATOREN

K. KARSAI*

DOKTOR DER TECHN. WISSENSCHAFTEN.

[Eingegangen am 29. April 1980]

Die Arbeit beschäftigt sich mit der Bedeutung der Verluste und der Erwärmungen in Streufeldern. Es werden die Stellen im Transformator angegeben, wo Verluste und Erwärmungen auftreten; im Eisenkern, im Kessel und im Deckel, in den Schrauben zwischen dem Kessel und dem Deckel, in der Umgebung der Durchführungen und in der Jochklemmkonstruktion. Es werden Methoden, die die unerwünschten Auswirkungen der Streufelder beschränken, diskutiert und für blanke und auch isolierte Konstruktionsteile Temperaturschranken empfohlen. Als letztes werden verschiedene Methoden diskutiert, mit deren Hilfe die durch das Streufeld verursachten gefährlichen Erwärmungen bestimmt werden können.

1. Einführung

Bis das heutige System der elektrischen Energieverteilung besteht, werden immer Großtransformatoren gebraucht. Prognosen sehen gegenwärtig eine höchstmögliche Einheitsleistungsgrenze der Großtransformatoren von etwa 3000 MVA vor. Bis diese Höchstleistung erreicht wird, werden Verluste und die Erwärmungen, verursacht durch die in Transformatoren entstehenden Streufelder, immer mehr schwierige Probleme bedeuten. Dies ist der Fall, weil mit der Leistungserhöhung auch die Streufelder sich verbreiten, da die mögliche Abmessungen, das heißt das Transportprofil der Transformatoren eingeschränkt ist. Infolge der hohen Feldstärken entstehen höhere Verluste, die schon selbst unwirtschaftlich sind, das Hauptproblem liegt aber darin, daß es auch starke lokale Erwärmungen entstehen. Die Erwärmungen vermindern die Betriebszuverlässigkeit der Transformatoren, und machen sie mehr empfindlich gegenüber den im Betrieb früher oder später unvermeidlichen Überbelastungen. Diese Probleme der Streufelder treten im allgemeinen erst ab Leistungen von 100 MVA pro Säule auf.

Im Rahmen dieser Veröffentlichung sollen bezüglich dieser Problematik einige Gesichtspunkte diskutiert werden. Unter dem Begriff Streufluß verstehen wir im weiteren alle diejenige magnetische Felder, die zum Teil, oder ganz, außerhalb des Eisenkerns verlaufen.

* K. Karsai Árpádfejedelem útja 47, H—1023 Budapest, Ungarn

2. Allgemeines über die in Streufeldern entstandenen Verluste und lokalen Erwärmungen

Das erste Bild zeigt die Stellen des Transformators, wo Verluste und Erwärmungen auftreten. Dies sind die Folgenden: Mit der Nummer 1 sind die Kraftlinien, die aus der Spule austreten und in den Kern eintreten bezeichnet worden; dieser Fluß ändert sich stark in Abhängigkeit der Betriebsart des Transformators. Diesbezüglich möchten wir darauf hinweisen, daß die in den Eisenkern eindringenden Feldlinien — wie es auch dem Bild 2a zu entnehmen ist — im Falle, wenn die innere Spule gespeist und die äußere kurzgeschlossen ist, sich hauptsächlich über die Säule schließen. Wird aber dagegen die äußere Spule gespeist und die innere kurzgeschlossen, schließt sich der größte Teil des Streuflusses nicht über die Säule, sondern er berührt das Joch, den Kessel und auch weitere Konstruktionsteile. Daraus ergibt sich, daß das Hauptfluß beim Kurzschluß der inneren Spule im unteren und im oberen Joch, beim Kurzschluß der äußeren Spule in der Säule des Eisenkerns den Nennwert übersteigt. Dies selbst verursacht im Eisenkern eine zusätzliche

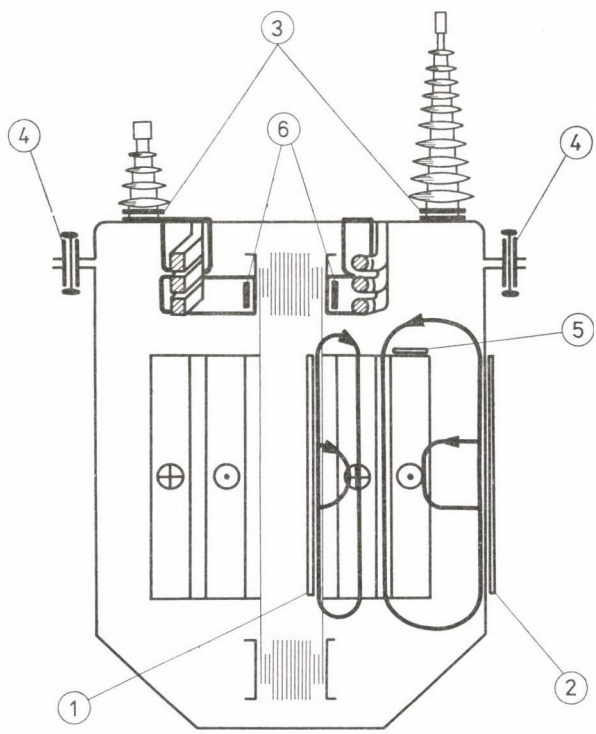

Bild 1. Die verschiedenen Stellen des Transformators, wo die in Streufeldern entstehenden Verluste und Erwärmungen auftreten

Erwärmung. Die Gefahr derartiger Situationen tritt an den Stellen des Joches oder der Säule auf, wo die Induktionslinien senkrecht auf die Lamellen verlaufen. [1]

Bezüglich dieser Erscheinung sollte an der Stelle die Anwendbarkeit der Ersatzschaltungen des Transformators behandelt werden. Für die treue Abbildung eines Transformators sind die mit 3 a, b und c bezeichneten Ersatzschaltungen des dritten Bildes alle gleich geeignet. Im Hinblick auf die Feldverhältnisse aber entspricht das Bild 3a nicht den im Bild 2 gezeichneten Verhältnissen. Diesbezüglich gibt das Bild 3c eine richtige und das Bild 3b eine angenähert gute Abbildung. Auf Bild 3 sind X_{si} und X_{sa} die mit der inneren beziehungsweise der äußeren Spule verbundenen Streufelder.

X_n der Hauptfluß, sowie X_{hs} und X_{hj} bedeuten die resultierenden Flüsse in der Säule und im Joch. Die Größe des Hauptflusses in der Säule kann nach Messungen entweder den Wert 0,1 Φ_n oder den Wert von 1,1 Φ_n erreichen.

Derartige große Änderungen des Hauptflusses können anhand der folgenden Überlegungen erläutert werden:

— Nimmt man an, daß außer der zwei Spulen der im Bild 2 gezeigten Transformatoren eine zusätzliche fiktive Spule direkt am Eisenkern vorhanden ist. Ihre Abmessung in Radialrichtung kann vernachlässigt werden und ist also die in ihr induzierte Spannung U_{hs} proportional dem Wert des Flusses Φ_{hs} in der Säule. Schreibt man zunächst die für diesen Transformator gültigen Gleichungen zur Bestimmung der Streureaktanzen auf, so können die Streureaktanzen der inneren und der äußeren Spule X_{si} bzw. X_{sa} bestimmt werden. Für Transformatoren mit konzentrischer Spulenanordnung ist X_{si} mit einer Größenordnung kleiner als X_{sa}. Im Bild 3c

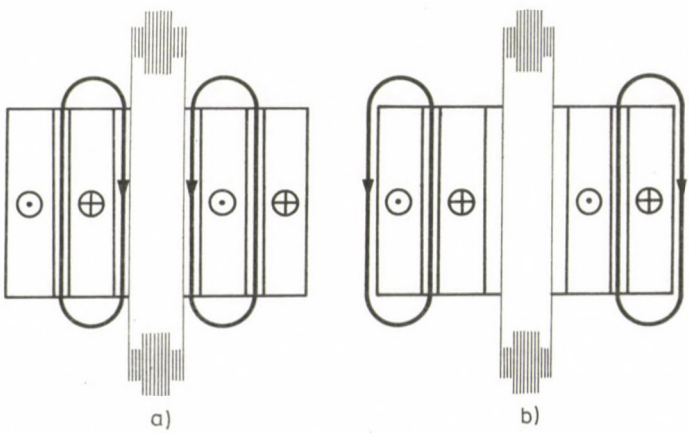

Bild 2. Die in den Eisenkern eindringenden Feldlinien im Falle wenn *a)* die innere Spule gespeist und die äußere kurzgeschlossen, *b)* die äußere Spule gespeist und die innere kurzgeschlossen sind

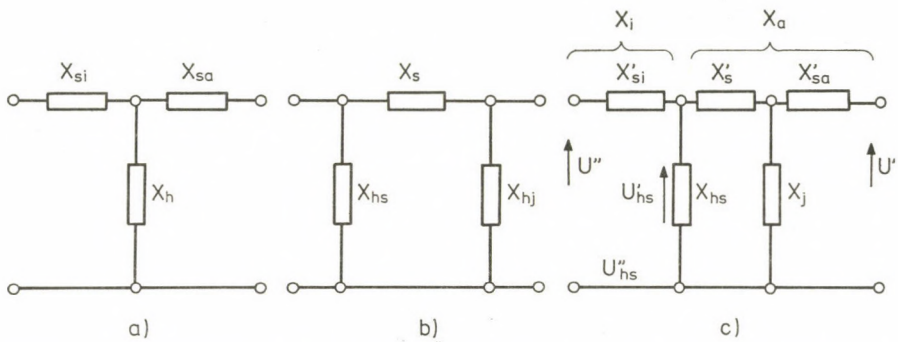

Bild 3. Drei Ersatzschaltungen eines Transformators: *a)* konventionelle T Schaltung; *b)* π Schaltung; *c)* kombinierte π Schaltung

entsprechen X_{si} der Reaktanz X_i und $(X_s + X_{sa})$ der Reaktanz X_a. (Siehe unten.)

— Für einen zweispuligen Transformator, wo die äußere Spule gespeist wird, ergeben sich die an der Reaktanz X_{hs} meßbaren Spannungsänderungen U'_{hs} (Bild 3c) nach Gleichung (1). (Die Reaktanz $X_j \cong X_{hs} \gg X_a$.)

$$\mathbf{U}'_{hs} = \mathbf{U}' \frac{\mathbf{Z}_b - \mathbf{X}_i}{\mathbf{Z}_b - \mathbf{X}_i + \mathbf{X}_a} = \mathbf{C}\boldsymbol{\Phi}_{hs} \tag{1}$$

wo U' die Speisespannung,
Z_b die Lastimpedanz und
c eine Konstante sind.

Nach Gleichung (1) kann festgestellt werden, daß im Leerlauf des Transformators $U'_{hs} = U$ ist und im Kurzschluß ergibt sich der Wert von U'_{hs} mit einer Größenordnung kleiner als der von U und wird ein negatives Vorzeichen haben.

— Gleichung (2) gibt die Spannungsänderungen U''_{hs} für einen zweispuligen, durch die innere Spule gespeisten Transformator an:

$$\mathbf{U}''_{hs} = \mathbf{U}'' \frac{\mathbf{X}_a + \mathbf{Z}_b}{\mathbf{X}_a + \mathbf{Z}_b - \mathbf{X}_i} = \mathbf{C}\boldsymbol{\Phi}_{hs} \tag{2}$$

wo U'' die Speisespannung ist.

In diesem Fall gilt im Leerlauf genauso daß $U''_{hs} = U$ ist, es werden aber im Kurzschluß sowohl U_{hs} als auch der Fluß in der Säule größer als im Leerlauf sein.

Mit der Nummer 2 im Bild 1 wurde das Streufeld im Kessel bezeichnet. Da aber hier der Fluß einen wesentlich längeren Weg im Öl hat, kann der maximale Induktionswert höchstens einige hunderstel Tesla betragen [2].

Dennoch können die durch diesen Fluß im Kessel hervorgerufenen Verluste wegen der großen Fläche bedeutende Werte erreichen.

Das Streufeld, das bei den Ausführungen im Deckel entsteht, wird mit Nummer 3 auf dem ersten Bild bezeichnet. Dieses Feld wird durch den Erregerstrom der Durchführung hervorgerufen, dessen Größe auch in der Größenordnung 10^4 A/m liegen kann. Die Nummer 4 im Bild 1 bezeichnet die Verluste, die durch Ströme verursacht werden, welche durch die zwischen dem Deckel und dem Kessel angebrachten Schrauben fließen. Die Ursache dieser Erscheinung liegt darin, daß der Streufluß der Spulen, das Streufeld der stromführenden Schienen und die Erregungswirkung der Durchführungen im Deckel und im Kessel ein Potentialfeld induzieren, dessen Ausgleichströme durch die zwischen dem Deckel und dem Kessel angebrachten Schrauben fließen können. Diese Ströme können Werte von 10 bis 100 A erreichen, wodurch die erwärmten Schrauben die Dichtungen zerstören können. Diese Wirkung der Streufelder läßt sich ganz vermeiden. Die erste Möglichkeit dafür ist es den Deckel abzuschweißen, infolge dessen die Stromdichte, wegen der erhöhten, geschweißten Fläche, kleiner wird. Eine zweite Möglichkeit bietet uns die galvanische Abtrennung des Deckels vom Kessel, wobei wegen der Festhaltung des Potentials eine einzige galvanische Verbindung angemacht wird. In diesem Fall können dann keine Ströme fließen.

Mit der Nummer 5 im Bild 1 wird der Wirbelstrom in den vollen Metallteilen, die zu den Wicklungsenden oder den Abschirmelektroden der Spule die Verbindung darstellen, bezeichnet [3]. Die Induktion kann an dieser Stelle den Wert von 0,1 T erreichen. Als letztes ist im Bild 1 das Streufeld in der Jochpreßkonstruktion mit der Nummer 6 bezeichnet. Der Induktionswert liegt hier in der Größenordnung von 0,01 T.

3. Maßnahmen zur Ermäßigung der ungünstigen Auswirkungen der Streufelder

Die Streufelder verursachen in den aktiven und inaktiven Teilen des Transformators weitere Verluste und lokale Erwärmungen. Die Größe dieser Mehrverluste kann in der Größenordnung der in den Spulen entstehenden Verluste liegen; die lokalen Erwärmungen verringern die Betriebssicherheit des Transformators. Im letzten Jahrzehnt beschäftigte man sich sehr viel mit der möglichen Ermäßigung der negativen Wirkungen der Streufelder und wurden dafür die folgenden Methoden entwickelt:

— Elektromagnetische Abschirmung mit Kupfer- oder Aluminiumplatte (Bild 4). Die Theorie dieser Methode ist gut bekannt. Diesbezüglich kann in erster Linie soviel festgestellt werden, daß die Methode nur bei einer an

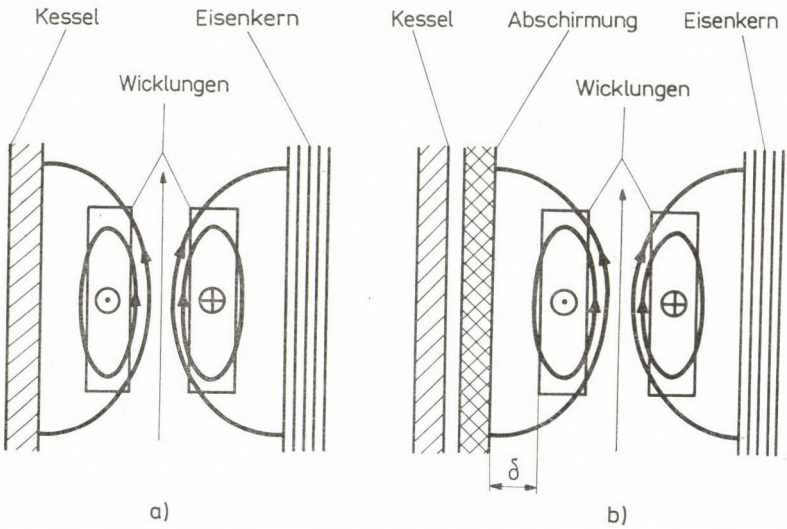

Bild 4. Die Streuflußwege zwischen den Wicklungen und Kesselwänden. *a)* ohne elektromagnetische Abschirmung; *b)* mit elektromagnetischer Abschirmung

der Plattenoberfläche unveränderlichen, durch die Rückwirkung der Wirbelströme nicht beeinflußten Induktion, dann wirksam ist, wenn die Dicke der Abschirmplatten die Eindringstiefe (bei Kupfer 9,5 mm bei Aluminium 12 mm) erreichen. Dicke Platten sind schwer zu bearbeiten, sie sind teuer und auch in dem Platten selbst entstehen Verluste. Bei größeren Induktionen können sogar auch gefährliche Erwärmungen auftreten.

— Eine gut bewährte Methode ist die Anwendung von magnetischen Schunts. Die theoretische Grundlage dieser Methode beruht darauf, daß der Fluß über die angemessen gestalteten Transformatorkernplatten geführt wird und dadurch die Feldlinien den großen zusammenhängenden Metallteilen ausweichen (Bild 5).

— Die Anwendung von nichtmagnetischen Metallen, vor allem in der Umgebung der Durchführungen im Deckel, aber auch bei den Preßplatten des Eisenkerns und genauso bei der Jochpreßplatte. Zur Information soll hier erwähnt werden, daß der Baustahl bei der Untersuchung einer Jochpreßplattenmodells, das Aluminium mit gleicher mechanischen Festigkeit, und der antimagnetische Stahl, ein Verhältnis der Verluste von 1—0,5—0,05 und ein Verhältnis der Höchsterwärmungen von 1—0,5—0,05 aufweisen.

— Die Anwendung von Nichtmetallen. Auf diesem Gebiet werden weitverbreitet glasfaserverstärkte Epoxydharze (Deckel, Spulenklemmkonstruktionen) und geschichtete Holzplatten (Klemmringe und das Gerüst der Abschirmringe, worauf der Metallbezug aufgebracht wird) verwendet.

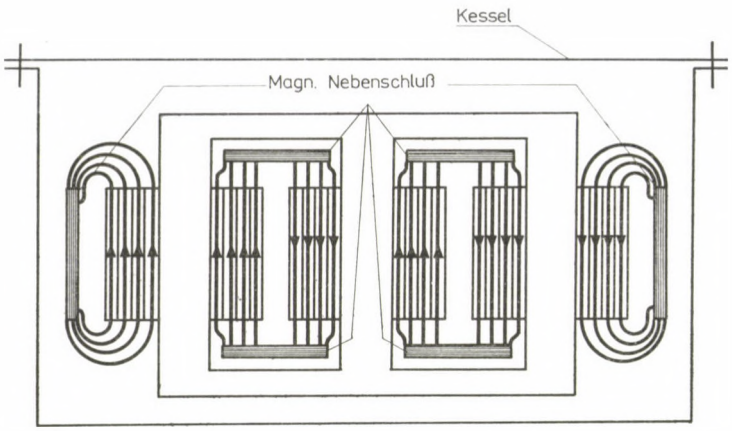

Bild 5. Die Anwendung von magnetischem Nebenschluß

4. Das Vermeiden von gefährlichen Erwärmungen

Die maximal konsequente Anwendung der vorher besprochenen Maßnahmen wird doch nicht dazu führen, daß in Transformatoren keine weitere Erwärmungen auftreten werden. Die wichtige Frage ist es die Größe der Erwärmung zu erkennen und festlegen zu können, welche Erwärmungen noch zugelassen werden. Zur Berechnung der Beanspruchungen sind zahlreiche Methoden bekannt. Sie alle beruhen darauf, daß zuerst die Verteilung des magnetischen Feldes, und daraus der Verlust berechnet wird [4]. In Kenntnis der Verlustverteilung kann die zu erwartende lokale Erwärmung bestimmt werden. Das andere Verfahren beruht darauf, daß die Temperatur des gefragten Teils im Transformator oder an einem entsprechend konstruierten Modell gemessen wird. An internationaler Ebene wird immer mehr die Problematik der zulässigen Beanspruchungen diskutiert. Diesbezüglich haben wir eine Umgebungstemperatur von 313 K zugrunde gelegt und das folgende festgestellt:

— Die maximale Dauertemperatur des Öls von einem größeren Volumen (> 10 cm^3) darf 368 K nicht überschreiten.
— Die Temperatur von größeren (> 10 cm^2) blanken oder lackierten Metalloberflächen darf nicht höher als 413 K steigen. Laut unserer Versuchsergebnisse konnte festgestellt werden, daß die Bewegung des Öls in der Umgebung einer Metalloberfläche von 413 K Temperatur immer schneller wird, das Öl hat »keine Zeit« sich zu erwärmen und können deshalb weder Blasenentstehung noch Entstehung von anderen Alterungsprodukten wahrgenommen werden.

— Die mit Papier isolierten Metallteile dürfen an einer kleinen Fläche keine höhere Temperaturen als 393 K haben. (*IEC Publ*, N° 354).
— Die kurzzeitigen (in der Größenordnung von Sekunden) thermischen Überbelastungen sind ausschließlich aus metallographischen Gründen eingeschränkt. Die zulässigen Temperaturgrenzen sind für Kupfer 523 K und für Aluminium 473 K. Eine Bemessung der Transformatoren nach den lokalen Erwärmungen infolge der Streufelder besteht also darin, daß die berechneten oder die gemessenen Temperaturen die vorher erwähnten Grenzen nicht überschreiten dürfen [5]. Ein Beispiel zur Anwendung dieser Methode zeigt das Bild 6. Auf dem Bild werden die wärmsten Punkte einer 20 mm dicken 140×85 mm breiten Kupferplatte in Abhängigkeit der Induktion aufgezeichnet. Die Kraftlinien verlaufen aus beiden Richtungen senkrecht auf die Platte. Der Prüfling ist im Öl und ist entweder blank, oder mit einer 1 mm dicken geschichteten Papierisolierung versehen. Aus dem Diagramm kann ersehen werden, daß es bei dem blanken Prüfling die maximal zulässige Induktion 0,098 T beträgt. Erhöht sich nämlich die 368 K Öltemperatur mit 45 K, dann ist die vorher angegebene 413 K maximale Temperaturschranke erreicht worden. Beim papierisolierten Prüfling kann aber nur eine Induktion von 0,0225 T zugelassen werden, da infolge der hier auftretenden Erwärmung von 25 K — wenn es auch noch in der Umgebung der höchsten Öltemperatur passiert — schon die höchstzulässige Temperatur von 393 K erreicht wurde.

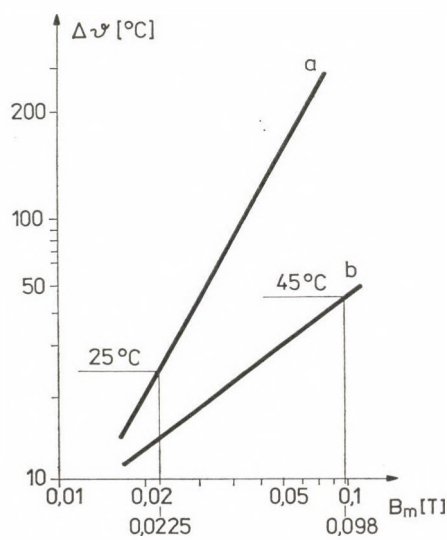

Bild 6. Die wärmsten Punkte einer 20 mm dicken und 140×85 mm breiten Platte aus Kupfer in Abhängigkeit der Induktion. Die Kurve *a* zeigt die Erwärmung der isolierten Platte, die Kurve *b* die der blanken Platte

Ein weiteres Beispiel zeigt die wärmsten Punkte der schichteten Säule im Streufeld.

Die Erwärmungsdiagramme von fünf verschiedenen Anordnungen, die auf Bild 7 gezeigt werden, sind dem Bild 8 zu entnehmen. Bei den hier gezeigten Varianten sind die zulässigen Induktionswerte recht unterschiedlich. Im Falle eines Eisenkerns ergibt sich der Wert von 25 K so, daß die Temperatur des Eisenkerns mit 20 K höher liegt als die höchste Öltemperatur von 368 K, und so wird eine weitere Temperaturerhöhung von 25 K möglich um die zulässige 413 K-Schranke zu erreichen.

Bild 9 zeigt die Geschwindigkeiten der Erwärmungen für die schon kennengelernten Anordnungen, die dann auftreten, wenn der Induktionswert des Streufeldes, infolge einer Überbelastung des Transformators, sich mit ΔB erhöht. Betrachte man als Beispiel die Variante *C*. Hier beträgt die Induktion des Streufeldes den Dauerwert $B = 0{,}05$ T. Dazu gehört — aufgrund des Bildes 8 — eine Erwärmung von 13 K. Angenommen, daß die Temperatur des Eisenkerns 20 K über die Öltemperatur von 368 K liegt, ergibt sich eine lokale

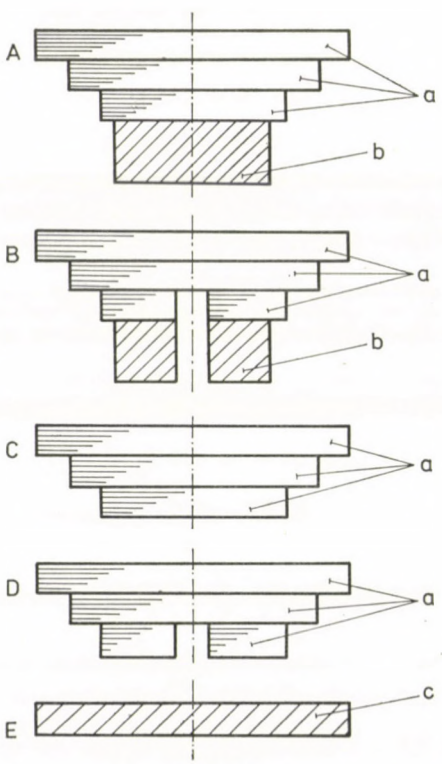

Bild 7. Verschiedene Anordnungen: *a* Blechpakete; *b* Antimagnetische Zugsplatte; *c* kesselwand

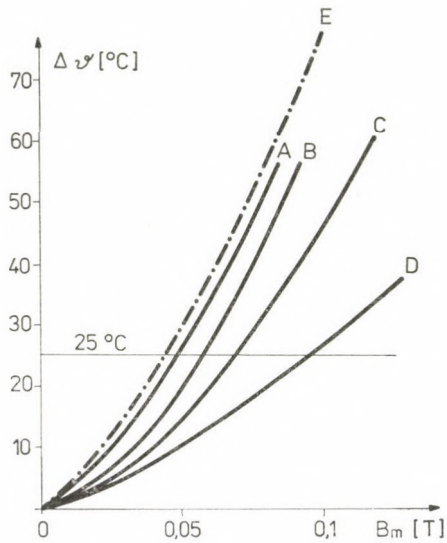

Bild 8. Die Erwärmungsdiagramme von fünf verschiedenen, Anordnungen die auf Bild 7 gezeigt sind

Erwärmung von 401 K (368 + 20 + 13 K). Wird der Transformator in diesem Zustand so weit überbelastet, daß die Induktion sich mit $\Delta B = 0{,}02$ T erhöht, dann wird die Anfangsgeschwindigkeit der transienten Erwärmung des wärmsten Punktes den Wert von 0,053 K/sec betragen. Dies heißt, daß die Überbelastung noch für weitere vier Minuten mit Sicherheit zugelassen werden kann, da die Erwärmung bestimmt kleiner wird, als etwa 12 K ($4 \times 60 \times 0{,}053$), womit die Temperatur des ursprünglich an 401 K Temperatur liegenden Eisenkerns sich erhöhen darf.

Stehen aber keine transiente Erwärmungskurven zur Verfügung (Bild 9), so können die transienten Erwärmungswerte aufgrund der folgenden Überlegungen bestimmt werden [5]: Für ein Körper mit der Masse m, mit der Wärmeübertragungsoberfläche A gilt im stationären Zustand:

$$p_0 m \cdot dt = \alpha A(\vartheta_m - \vartheta_s)dt \tag{3}$$

wo p_0 der in der Masseneinheit entstehende Verlust,
α die Wärmeübertragungszahl der Oberfläche,
ϑ_m die mittlere Temperatur des Körpers und
ϑ_s die Umgebungstemperatur sind.

Erhöht sich der spezifische Verlust p_0 auf $(p_0 + p_1)$, dann ist die Anfangsgeschwindigkeit der Temperaturerhöhung:

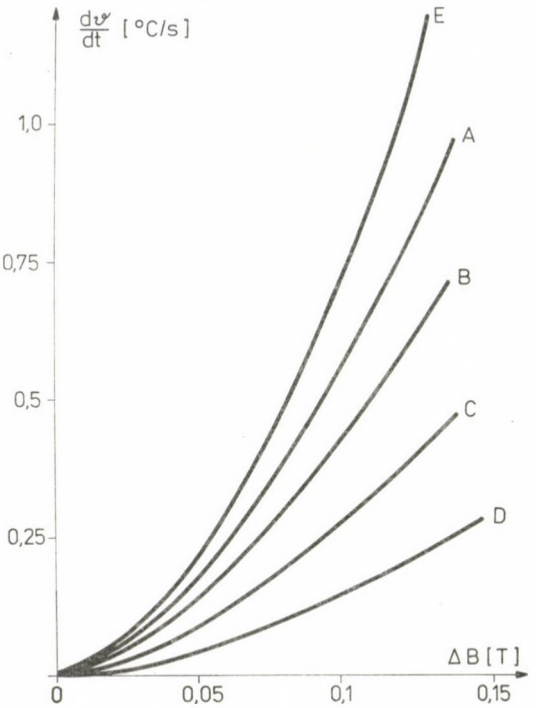

Bild 9. Die Geschwindigkeit der Erwärmung für die auf Bild 7 gezeigten Anordnungen

$$\frac{d\vartheta}{dt} = \frac{p_1}{c}, \tag{4}$$

wobei c die spezifische Wärme des Körpers ist. Da zum Verlust p_0 eine Induktion B_0, zum $(p_0 + p_1)$ die Induktion $(B_0 + B_1)$ gehören, so können die folgenden Näherungsgleichungen formuliert werden:

$$p_0 = kB_0^2 \quad \text{und} \quad p_0 + p_1 = k(B_0 + B_1)^2 \tag{5}$$

Für Gleichung (4) erhält man damit (bei Vernachlässigung der Wärmeabgabe der Oberfläche)

$$\frac{d\vartheta}{dt} = \frac{p_0}{c}\left[\left(1 + \frac{B_1}{B_0}\right)^2 - 1\right]. \tag{6}$$

In diesem Zusammenhang drückt p_0/c die dem Anfangszustand vorangehende transiente Erwärmung aus. Mit Hilfe der Gleichung (6) kann zu jeder Induktionsänderung ein Erwärmungswert zugeordnet werden.

5. Schlußfolgerungen

In Rahmen dieser Veröffentlichung wurde eine Methode dargestellt, deren Grundgedanke ist, daß Temperaturgrenzen festgelegt werden und zunächst kontrolliert wird, ob Temperaturen, die entweder mit Berechnungen oder mit Messungen bestimmt werden, in der Konstruktion gefährliche Erwärmungen verursachen. Die nächste Frage ist, wie weit diese Methode anwendbar ist?

Selbstverständlich sollte man bei der Anwendung einer Methode mit Umsicht vorgehen, auch dann, wenn die zur Verfügung stehenden Grunddaten — ob sie aus Berechnungen oder Messungen gewonnen wurden — mit der heute gekannten maximal zuverlässigsten Methode ermittelt wurden. Diese Vorsicht ist damit zu begründen, daß selbst die Feldberechnung des magnetischen Kreises, der nichtlineare Strecken enthält, nicht ohne weiteres durchführbar ist. Die selbe Erscheinung kommt bei der Wärmeverteilung von in Öl getauchten Metallgegenständen vor. Alle diese Umstände wirken unter verschiedenen Belastungen gegenseitig aufeinander, die ihrerseits Parameter des magnetischen Kreises und der Wärmeabfuhr bewirken. Die Methode ist aber zur Orientation, oder zum Vergleich von Konstruktionsteilen gut geeignet. Es sollte hier betont werden, daß trotz der modernsten, neusten rechen- und meßtechnischen Möglichkeiten, die große Erfahrung des Forschers zur Erkennung der Gefahr der Streufelder, das Kenntnis dieses Problemkreises und eine gewisse Intuition unentbehrlich sind. Trotz allem gibt es verschiedene Möglichkeiten der Kontrolle fabrikfertiger Konstruktionen. Auf diesem Gebiet

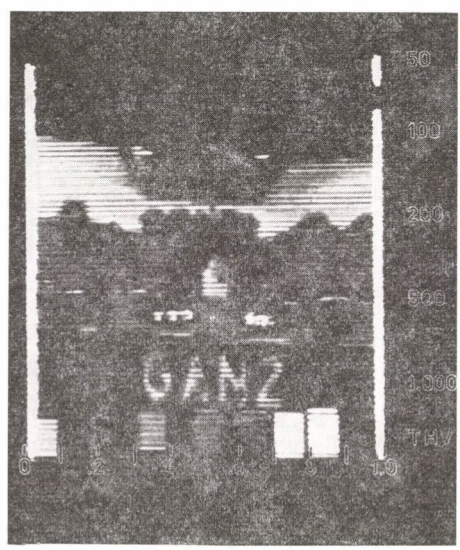

Bild 10. Fotographische Aufnahme mit Thermovision. Die hellen Objekte sind die Kesselschrauben, durch die Ströme zwischen dem Kessel und dem Deckel fließen

können der Vergleich der Verluste, die bei ausgenommenem Transformator und beim Transformator im Kessel bestimmt waren, sowie auch Messungen in beiden Fällen mit Thermovision empfohlen werden. Dies letztere ist — wie es auch im Bild 10 gezeigt wird — zur Darlegung der durch die Kesselschrauben fließenden Ströme ausgezeichnet geeignet.

Gegenwärtig laufen weitere Forschungsarbeiten über Gasanalysen, die vor und nach den Erwärmungsprüfungen, mit 1 bis 1,2-fachem Nennstrom, durchgeführt werden. Charakteristisch für diese Untersuchungen ist das, daß die Gasanalysen vor und nach der Erwärmung auch in fehlerhafteten Fällen wie auch in fehlerfreien Fällen beträchtlich unterschiedliche Ergebnisse liefern. Es ist bis jetzt noch nicht gelungen für jeden in der Praxis vorkommenen Fall eine allgemeine Aussage zu treffen.

SCHRIFTTUM

1. Bose, A. K.—Kroon, C.—Wildeboer, J.: The Loading of the Magnetic Circuit. 12-09 CIGRE report, 1978
2. Karsai K.—Kerényi D.—Kertész V.: Transzformátorok szórt mágneses terében keletkező veszteségek. *Elektrotechnika* **68** (1975), 299—309
3. Karsai K.—Kerényi D.—Kertész V.: Transzformátor sugárirányú terében keletkező veszteségek és melegedések. *Elektrotechnika* **70** (1977), 237—246
4. Kerényi, D.: Approximate Formula for the Eddy-Current Losses Induced in Rectangular Metal Blocks by Magnetic Field. *GANZ Electrical Review* (1977), No. 16
5. Karsai K.—Kerényi D.—Kiss L.: Some Aspects of Design Associated with the Operation Reliability of Large and EHV Transformers. CIGRE 1978 Session, No 12-04, Paris

Heatings and Losses Occurring in the Magnetic Stray Fields of Transformers. — Heatings and losses being produced in the magnetic stray fields of transformers are treated. The places of production of heating and losses: the magnetic core, tank, cover, screws between cover and tank, zone of the bushings and yoke-clamp device are detailed. Methods reducing the detrimental consequences of stray fields are dealt with. Admissible heating values are recommended both to bare and insulated surfaces. Eventually, different methods are evaluated which are suitable to the determination of dangerou heating having beeп produced in the stray field.

Acta Technica Academiae Scientiarum Hungaricae, Tomus 91 (3—4), pp. 335—353 (1980)

UTILISATION DES SOUS-PRODUITS INDUSTRIELS DANS LE DOMAINE DE LA CONSTRUCTION DE ROUTES EN HONGRIE

L. GÁSPÁR*

[Présenté le 15 Mars 1980]

L'utilisation des cendres volantes, du laitier et des déchets de manière telle qu'elle est écrite dans cette étude, est très significative du point de vue de l'économie nationale. Afin d'accélérer l'introduction générale de l'utilisation complexe des sous-produits industriels, ce qui fait le sujet de cette étude, les centrales thermiques, les hauts fourneaux, l'industrie de carrières et de ballastières ainsi que les départements routiers et l'industrie de matériaux de construction devraient développer d'activités plus intenses. Une tâche à exécuter tout d'abord est la fabrication de chaux hydratée en quantité suffisante parce que la manque de cette matière retarde la construction des couches d'assise à liants en quantité exigée. La suppression des entraves de l'introduction générale des procédés en question voudrait favoriser efficacement une économie poussée en matériaux et en énergie qui est actuellement lourde de signification.

Les exigences d'économie en matériaux et en énergie ainsi que celle de la préservation d'environnement ont donné la naissance à l'utilisation de certains sous-produits industriels dans la construction routière. Dans la construction de routes, à l'assise constituant la majeur partie du corps de chaussée (fig. 1) et aux remblais l'occasion se présente pour l'utilisation de tels sous-produits.

Il y a environ une décennie et demi que les essais ont pris naissance en Hongrie aussi, pour l'utilisation de plusieurs sous-produits industriels dans le domaine de la construction de routes. Ce sont surtout les expériences françaises [1], soviétiques [2] et polonaises [3] sur la base desquelles quelques sous-produits de l'industrie hongroise ont été avérés à l'application dans ce domaine.

On pourrait utiliser convenablement les *cendres volantes des centrales thermiques* et le *laitier granulé de hauts fourneaux* au lieu des liants classiques,

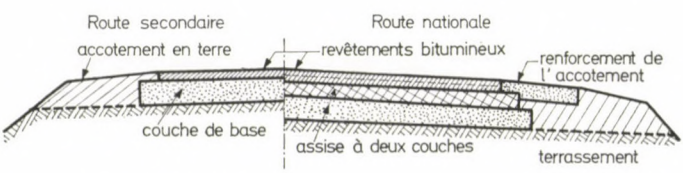

Fig. 1. Profil schématique des corps de chaussée

* L. GÁSPÁR, Beloiannisz-u, 11, H—1054 Budapest, Hongrie

le bitume et le ciment. Les produits de pierre concassée de haute qualité et le gravier sableux bien gradué peuvent être remplacés par des *déchets de carrières et de ballastières* dans les assises des revêtements.

Dans l'incinérateur de résidus urbains en construction à Budapest, à partir de l'année 1982 il se produit des mâchefers annuels de 120 000 tonnes. D'après les expériences étrangères ces màchefers d'incinération peuvent être utilisés avantageusement pour l'assise de revêtement seul ou stabilisés par des liants. L'application de ce matériau permet la construction économique de routes en terre d'une longueur de 50 à 60 km dans la capitale.

Dans des années prochaines, dans notre pays, deux hauts fourneaux introduiront la fabrication d'acier à convertisseur d'oxygène d'où on obtient comme sous-produit de 270 000 tonnes de laitier LD par an de bonne qualité. Cela peut être le matériau granulé non seulement des couches de base et couches de fondation, mais aussi celui des revêtements.

L'utilisation des cendres volantes

Dans les centrales thermiques en Hongrie, actuellement *il se produit près de cinq millions de tonnes de cendres volantes et des scories fines par an.*

Les dépôts des cendres volantes non exploitées de 65 millions de tonnes occupent une surface d'environ 1000 hectares. Plusieurs centrales thermiques font transporter leurs cendres volantes et scories mélangées avec beaucoup de l'eau, par des canaux et conduits de tuyaux aux bassins de décantation.

Les dépenses d'investissement de tels ouvrages s'élèvent en cas d'un dépôt de demi millions tonnes de cendres par an, à cinquant millions Ft, tandis que les frais généraux d'opération annuels montent à dix millions Ft environ. A l'ambiance des bassins de décantation déséchés, en temps venteux, la pollution d'air est importante.

Du point de vue de la préservation d'environnement et de l'économie on porte ses efforts dans le monde entier à *l'utilisation des cendres volantes sèches.* Les cendres séparées ou leur majorité peuvent être utilisées comme «produit disponible». Les cendres volantes obtenues sont stockées dans des silos, d'où on les met sur le marché par voie ferrée ou sur route, le cas échéant, mises en sac.

Des dispositifs d'extraction des cendres volantes sont actuellement opérés à Bánhida (210), à Pécs (280), à Dorog (34), à Berente (280) et à Visonta (350). (Les chiffres entre les paranthèses représentent les quantités en mille tonnes des cendres volantes produites aux endroits indiqués, par an.) La crise du pétrole augmentait la signification du chauffage au charbon. A la centrale thermique en construction à Bicske, la production des cendres volantes se montera à deux millions tonnes par an.

Les cendres volantes sont utilisées actuellement par l'industrie de ciment et par l'usine de béton léger à Kazincbarcika en une quantité totale de 300 000 tonnes environ par an.

Essais en Hongrie

Il y a quinze ans environ que des essais de laboratoire ont été instaurés en Hongrie aussi, en vue de l'utilisation de cendres volantes dans le domaine de construction de routes. L'entreprise hongroise de construction de routes en asphalte a construit en 1966 des sections d'essai en utilisant l'une des sortes de cendres volantes basiques provenant de la centrale thermique de Ajka, sur la voie d'accès de la coopérative agricole de production Egyetértés à Bedegkér (comitat Tolna) ainsi que dans deux rues à Gárdony. La couche de base de revêtement bitumineux est en sol de cohésion moyenne (limon), d'origine locale stabilisé avec de cendres volantes, respectivement avec un mélange de cendres volantes et de ciment [4].

L'Institut de Recherches Scientifiques de la Circulation Routière (Közúti Tudományos Kutató Intézet, dans la suite KÖTUKI) au cours de réalisation d'un grand nombre de séries d'essais de laboratoire examinait l'applicabilité de plusieurs genres de cendres volantes et des agrégats d'origine du pays. D'après les résultats de ces essais il a été établi qu'il est possible d'obtenir un matériau pour l'assise de revêtement résistante à l'eau et à gel, à partir de l'agrégat concassé et de débris de dolomite d'une granularité convenable avec le dosage pas plus de 2 à 3 pour cent de chaux hydratée et de cendres volantes neutres de 8 à 12 pour cent. En cas de l'utilisation de graviers sableux et des déchets de carrières le dosage de 3 à 4 pour cent de chaux et de 12 à 16 pour cent de cendres volantes est nécessaire.

Étant donné que le mélange est de prise lente, il peut être mis en place encore le jour ou le troisième après la préparation, par conséquent, on en peut transporter aussi à des chantiers éloignés. Le mélange à consistence de l'humidité optimale est répendu par un profileur de route et compacté avec des rouleaux. La couche compacte peut être mise en circulation immédiatement (le trafic ne doit pas être dévié pendant des semaines, comme en cas des assises à liant de ciment). C'est particulièrement avantageux en cas de renforcement de la chaussée des routes de faible portance sans suspension du trafic [5].

La direction des routes à Tatabánya a réalisé en 1975 sur trois tronçons de route, à titre d'essai, une nouvelle couche de base, c'est-à-dire, une élargissement de chaussée en utilisant les cendres volantes de Bánhida.

Avant de commencer la réalisation, la Direction a consulté le département de la chaussée du KÖTUKI, et fait entreprendre des séries d'essais.

Sur le tronçon d'environ 2 km de long de la route de jonction de Mór—Kocs près de Dad, la nouvelle couche de base d'une épaisseur de 18 cm a été construite par la stabilisation du gravier sableux local avec de cendres volantes

et de chaux. Des cendres volantes de Bánhida des taux de 10 à 14 pour cent, tandis que de la chaux de 4 à 5 pour cent ont été additionnés. A l'un des tronçons la chaux fut remplacée par 20 pour cent de sous-produit de chaux hidratée de l'origine de Dorog. Le mélange a été préparé par une chaîne de machines à motoculteur à fraise rotative. Selon les mesures de contrôle la résistance et la portance de la couche de base est favorable. Les frais généraux de construction n'ont été montés qu'aux 68 pour cent de ceux de l'assise en pierres concassées classique.

Sur le tronçon d'un km et demi environ de la route de jonction de Szőny—Kocs la chaussée étroite a été élargie par la construction d'une assise traitée par cendres volantes et par chaux. Le mélange a été préparé de gravier de Mócsa à un centre de malaxage de béton. Le trafic n'a pas été dévié de la bande d'élargissement frais de l'assise. Sur toute la largeur de la chaussée élargie on a posé un revêtement de grave-bitume en une épaisseur de 4 cm. La résistance à la compression des cubes d'essai découpés au printemps de l'année 1976, était de 10 à 14 N/mm^2. La portance de la bande de l'élargissement est plus favorable que celle de la chaussée ancienne.

La troisième section d'essai a été construite sur la voie d'accès de Koppánymonostor. La nouvelle couche de base a été construite du mélange mentionné ci-dessus. Avant que la saison hivernale fut venue, l'assise a été couverte d'une couche de revêtement bitumineux d'épaisseur de 4 cm. La portance mesurée au printemps de 1976 était sur le tronçon dont l'assise a été construite, plus favorable que celle de la section se raccordant à la précédente, construite avec une assise de liant de ciment, c'est-à-dire, de béton maigre, un matériau classique [6].

Élaboration des prescriptions techniques et des normes de profession de ministère

L'étude des méthodes étrangères ainsi que les expériences favorables acquises au cours des essais de laboratoire et sur des tronçons de route d'essai ont permis la réglementation des différents domaines de l'utilisation des cendres volantes en Hongrie.

Sur mandat du Département Routier du Ministère des Communications, le KÖTUKI commença en 1975 l'élaboration des prescriptions techniques y relatives.

Pour commencer les *prescriptions techniques provisoires* (P.T.P.) *des assises en graves-cendres volantes-chaux* ont été établies en avril 1976. Ces directives envisagent les prescriptions concernant les matériaux, les projets, la réalisation et le contrôle d'exécution des couches d'assise. Des tronçons de route plus récemment construits sur les territoires des comitats Komárom, Szolnok, Heves, Nógrád et Borsod et autre part, ont été réalisés conformément à ces prescriptions.

Les *prescriptions techniques provisoires visant la construction des assises de revêtement et des remblais de routes stabilisées avec les matériaux des bassins de décantation des cendres volantes* ont été établies en 1977. Ces prescriptions facilitent aussi l'appréciation du fait que dans l'ambiance des centrales thermiques l'utilisation des matériaux des bassins de décantation pour la construction des remblais et des chaussées est-elle économique ou non. Des grandes quantités des matériaux des bassins de décantation sont accumulées aux endroits suivants (en millions de tonnes): Pécs 11,7, Tiszapalkonya 8,3, dans la région de la montagne Mátra (à Lőrinci) 8,3, Berente 7,0, Oroszlány 6,8, Visonta 3,0, Komló 2,5, Tatabánya 2,3, Bánhida 1,5, Dorog 0,5 et Kispest 0,5.

Le premier remblai construit de cendres volantes-scories se trouve sur un tronçon de correction de la route de jonction Oroszlány—Bokod, en 1979. La portance de ce remblai et de la couche de base de graves-cendres volantes-chaux posée sur le remblai est très favorable.

Le second remblai est réalisé sur le tronçon de correction de longueur de 1,7 km de la route nationale No. 36 près de Polgár par l'utilisation de cendres volantes-scories de Tiszapalkonya.

Une troisième spécification des prescriptions techniques provisoires est celle visant la *stabilisation des sables à l'aide de cendres volantes*. Les sables d'origine hongroise peuvent être stabilisés par l'addition de 3 à 7 pour cent de chaux et de 15 à 30 pour cent de cendres volantes.

L'entreprise pour la construction de routes en béton construisit une couche de base d'épaisseur de 20 cm et d'une longueur de 600 m.c. en mai 1978 à Hatvan dans la rue Elefánt József du sable de dessablage des matériaux de la ballastière à Hatvan, stabilisée avec de 18 pour cent de cendres volantes humides de l'origine de Visonta et de 5 pour cent de chaux.

Les prescriptions techniques provisoires qui étaient les dernières de la série, visant la réglementation de la *stabilisation de sols par l'addition de cendres volantes*, ont été publiées en 1978.

D'après les recherches du KÖTUKI le limon qui se trouve à l'emplacement de la centrale thermique en construction à Bicske peut être stabilisé par l'addition de 5 pour cent de chaux et de 20 pour cent de cendres sèches d'origine de Bánhida (ou de 25 pour cent de cendres humides de bassin de décantation).

La Commission Nationale de Développement Technique a aussi examiné plusieur fois à partir de 1963 les possibilités de l'utilisation des cendres volantes. Le projet de conception fut publié en 1977 [7].

Le KÖTUKI a établi en 1979 les normes de profession de ministère des *projets des assises traitées* [8]. Bien entendu, celles-ci visent aussi la réglementation des projets des assises produites par l'utilisation de liants de cendre volantes et de laitier granulé.

Au cours des essais de laboratoire préparatoires la résistance à compression de 60 jours d'une éprouvette cilindrique de l'élancement d'un et demi est déterminante.

Les limites inférieures de cette résistance sont:

— en cas de la couche de renforcement marquée PE: 7 N/mm^2
— pour les graves-cendre volantes-chaux marquées PK: 5 N/mm^2
— pour le sol stabilisé marqué PT: 3 N/mm^2.

Comme le liant non seulement des cendres volantes sèches mais aussi des cendres volantes et des scories neutre accumulées aux bassins de décantation peuvent être utilisées. Mais ces dernières doivent être additionnées en une quantité élevée de 20 pour cent environ, à cause de ces teneurs en scories.

Les données technologiques des couches d'assise à liant de cendres volantes et de chaux sont indiquées sur la figure 2.

Introduction générale de l'utilisation des cendres volantes

Par conséquent de la réglementation de la technologie il se présente la possibilité que les cendres volantes et la matière des bassins de décantation peuvent être largement utilisées dans les différents domaines de la construction routière.

Actuellement les cendres volantes fines de Pécs, de Bánhida et de Visonta on facilite l'utilisation des cendres volantes par la mécanisation de l'humectation ou du mélange avec de chaux.

La préparation d'un nombre d'autres utilisations des cendres volantes dans le domaine de la construction routière sont en cours. Il est particulièrement avantageux de produire de mélanges de marque PE ou PK de certains déchets de carrière et de ballastières avec l'addition de cendres volantes et d'un peu de chaux.

A Érd, par exemple, de nouvelles routes en une longueur de 20 km sont en construction avec de telles couches d'assise.

Outre la construction de nouvelles assises il est un problème très opportun d'élargir les chaussées étroites et de renforcer les corps de chaussée de très faible portance. A ces opérations dans les régions où les lieux de production des granulats convenables sont de fréquence suffisante, le mélange aux cendres volantes peut être aisément réalisé, en utilisant des malaxeurs de relativement petites dimensions.

Les entreprises du trust de construction de routes s'installent aussi à la construction des assises à liants de cendres volantes et de chaux.

L'introduction générale est actuellement retardée par le défaut de chaux hidratée.

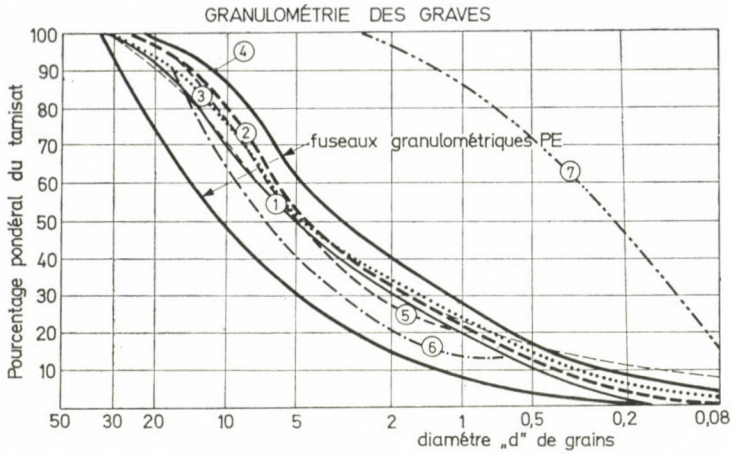

No.	Indication	Le lieu d'origine; bassin de décantation	Désignation
1	———	Nyékládháza	gravier sableux
2	– – – –	Sástó 55% 0/5 ; 45% 5/20	gravillon avec déchets
3	·····	Szár - Kányavölgy	débris de dolomite
4	———	Mocsa	gravier sableux
5	– – – –	Komló	gravillon avec déchets
6	–·–·–	Zsámbék 70% 0/5 ; 30% 5/20	débris de dolomite
7	–··–·–	bassin de décantation d'Oroszlány	cendres volantes humides

DONNÉES TECHNOLOGIQUES

Marque de la couche de assise	No. du grave	Le liant						Teneur en eau de fabrication w %	La limite inférieure de la densité sèche t/m³
		chaux (hydratée)		cendres volantes		laitier granulé			
		%	kg/m³	%	kg/m³	%	kg/m³		
PE	1	4	78	16 a)	310			12	1,92
PK	1	2,5	50	10 a)	200			11	2,00
PK	2	3	58	12 a)	230			12	1,92
PE	3	2	44	8 b)	175			7	2,18
PE	4	4	83	25 c)	510			9	2,04
PK	4	20 e)	390	20 c)	390			11	1,95
PK	5	4	75	12 d)	225			11	1,87
PE	6	2,5	53	10 d)	210			10	2,10

a) Cendres volantes humide de Visonta
b) Cendres volantes sèches de Bánhida
c) Bassin de décantation d' Oroszlány (cendres volantes humides)
d) Cendres volantes sèches de Pécs
e) Sous-produit de chaux hytratée de Dorog (éteinte)

Fig. 2. Données technologiques des graves-cendres volantes-chaux

Simultanément avec la construction du séparateur de cendres volantes fines envisagée à la *centrale thermique de Ajka*, il est expédient de donner la solution de *l'extraction des cendres volantes*. Les cendres volantes basiques sont aussi en elles-mêmes des liants convenables. En éteignant les cendres volantes

encore à haute température avec vaporisation d'eau, le pouvoir liant peut être augmenté d'avantage. De tels matériaux peuvent remplacer une sorte de ciment de résistance réduite. Les résultats d'essai du KÖTUKI sont bien favorables.

L'utilisation du laitier granulé

Le laitier est le sous-produit de la fabrication de la fonte brute. Refroidit-on rapidement le laitier incandescent avec de l'eau, il devient un granulat. Ce matériau métastable de structure vitreuse est de propriété puzzolanique: en présence de l'eau elle fixe de chauc et devient un liant hydraulique.

A Ózd, à Diósgyőr et à Dunaújváros il se produit à chacun de ces lieux une quantité annuelle de laitier de 0,5 million tonnes environ. Le laitier granulé est utilisé par quelques cimenteries comme matériau de remplissage. En France on le met à profit comme de liant des assises avec succès.

Sur la base de quatre constituants les plus significatifs, la composition chimique de deux laitiers français et de trois laitiers hongrois est comme suit:

	Hauts fourneaux français		Usines métallurgiques Lenin	Usines métallurgiques à Ózd	Usine sidérurgique de Duna
CaO	p.c. 35 à 45	40 à 45	40 à 44	44 à 46	38 à 45
SiO_2	p.c. 31 à 35	32 à 36	37 à 40	37 à 40	36 à 42
Al_2O_3	p.c. 15 à 25	11 à 17	10 à 11	7 à 8	8 à 10
MgO	p.c. 4 à 11	5 à 7	5 à 6	3 à 8	6 à 9

Comme le montrent les chiffres du tableau ci-dessus, la teneur en SiO_2 est un peu plus haute dans des laitiers hongrois que celle dans des laitiers français au désavantage de l'Al_2O_3.

Le KÖTUKI étudiait en détail les expériences françaises et instaurait des séries d'essais en laboratoire avec les granulats hongrois. En vertu des résultats obtenus il a établi que les granulats disponibles en Hongrie sont de trop gros grains et par conséquent ne sont pas suffisamment actifs [9]. Les mêmes expériences ont été acquises sur les tronçons de route d'essai construits en 1974 et 1975 aux alentours de Komárom, Hosszúpereszteg, Székesfehérvár et Szeged [10].

Sur mandat du Département des Routes du Ministère des Communications, le KÖTUKI a établi dans les années 1976/1977 les prescriptions techniques provisoires visant l'utilisation et la préparation des assises et des sables stabilisés construits par l'application de liants de laitiers granulés et de chaux.

L'entreprise de construction des routes en béton a construit en 1978 la couche de base d'une rue à Hatvan en utilisant de sables de 0/5 mm, stabilisée avec de laitier granulé d'origine de Ózd.

Les hauts fourneaux de la Hongrie ne peuvent pas granuler le laitier à finesse suffisante, c'est pourquoi il ne restait que le broyage du granulat. Le KÖTUKI a vérifié sur la base des essais de laboratoire exécutés par lui-même, que ces laitiers granulés prébroyés d'origine de notre pays répondent à toutes les exigences, comme le montre clairement le diagramme la figure 3. Les granulats doivent être broyés de manière qu'ils contiennent une quantité de fraction inférieure de 0,08 mm d'au moins de 10 pour cent.

L'entreprise de construction de routes en béton a installé aussi une broyeuse de granulat à sa station de malaxage à Dunaújváros. Ici, il utilise comme agrégat granulaire de laitier cristallisé et classifié. Avec de telle mélange construit-on les assises et la couche de renforcement des chaussées neuves respectivement des routes de faible portance dans ces parages. Le trust de construction de routes envisage aussi l'acquisition d'une telle broyeuse.

La norme [8] de projet d'assises traitées vise aussi la construction des assises avec des liants de laitier granulé et de chaux. Les limites inférieures de la résistance à compression de 60 jours sont comme suit:

— en cas de la couche de renforcement de marque GE 5 N/mm²
— pour les graves-laitier-chaux de marque GK 2,5 N/mm²
— pour le sable stabilisé de marque GH 2 N/mm²

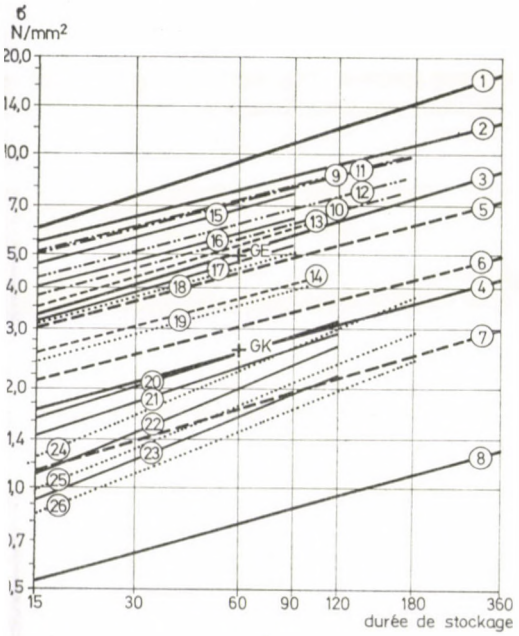

No.	Désignation du matériau	Fractions 0/6 : 6/20	Lieu d'origine	En dessous de 0,08 mm % du granulat	Dosage %	Chaux %
1	Débris de dolomite de Zsámbék	30 : 70	Ózd	52	20	3
2				35	20	
3					10	
4					5	
5				21	20	
6					15	
7					10	
8				0 (original)	20	
9	Débris de dolomite de Litér	45 : 55	Dunaújváros	23	20	3
10					15	2
11	Débris de dolomite de Iszkaszentgyörgy	50 : 50			20	3
12					15	2
13	Graves-sable d'Adony	77 : 23			20	3
14					15	3
15	Sables-grave de Győr	67 : 33			20	2
16					15	2
17					10	3
18	Sables gros de Fehérvárcsurgó	100 : 0			25	3
19					15	2
20	Graves-sable de Nyékládháza et de Mály	50 : 50	Diósgyőr	8	25	3
21					20	
22					15	
23					10	
24	Sable fin	100 % (0/0,5)	Ózd	52	20	2
25					15	2
26					10	3

Fig. 3. Changement de la résistance de compression des éprouvettes cylindriques d'élancement d'un et demi, produites des mélanges de liants de laitier prébroyé à des différentes granularités et de chaux en fonction de la durée de stockage

Les données technologiques des assises traitées avec de laitier granulé et de chaux sont présentées sur la figure 4.

Les résultats obtenus en Hongrie par l'utilisation des cendres volantes et du laitier granulé dans le domaine de la construction de routes ont été reportés aussi par des publications françaises [11].

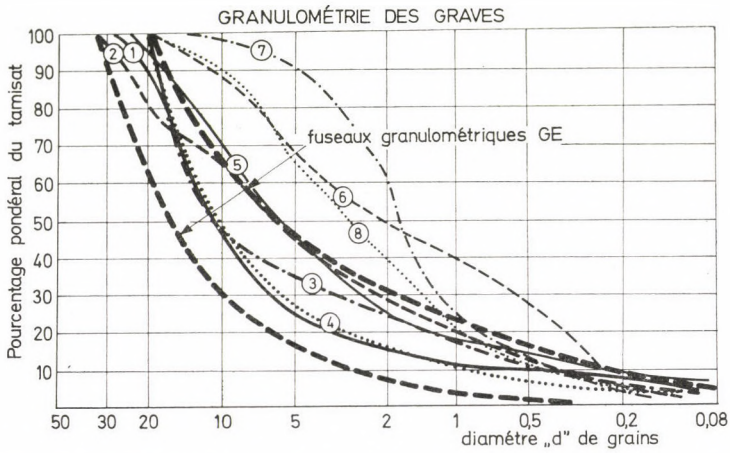

No.	Indication	Le lieu d' origine	Désignation
1	———	Carrière de Szob (andésite)	gravillon avec déchets
2	– – – –	Miskolc	gravier sableux
3	—·—·—	Ózd 35% 0/5; 75% 5/20	laitier cristalisé concassé et classé
4	·····	Zsámbék 30% 0/6; 70% 6/20	débris-dolomite
5	———	Iszkaszentgyörgy	débris-dolomite
6	– – – – –	Adony	gravier sableux
7	—·—·—	Dunaújváros	laitier granulé
8	·····	Ózd	laitier granulé

DONNÉES TECHNOLOGIQUES

Marque de couche d' assise	No. de granulat	Le liant						Teneur en eau de fabrication	La limite inférieure de la densité sèche t/m³
		chaux (hydratée)		cendres volantes		laitier granulé			
		%	kg/m³	%	kg/m³	%	kg/m³		
GK	1	2	43			20 D	430	8	2,15
GK	2	2	44			20 Ó	440	9	2,20
GK	3	3	55			20 D	365	10	1,82
GE	4	3	68			10 Ó *)	225	7	2,23
GK	4	2	45			6 Ó *)	135	6	2,24
GE	5	2	45			15 D **)	335	6	2,23
GE	6	3	60			15 D **)	300	6	2,00

D: Dunaújváros
Ó: Ózd

*) 35 p.c. au-dessous de 0,08 mm (broyé)
**) 25 p.c. au-dessous de 0,08 mm (broyé)

Fig. 4. Données technologiques des couches d'assise aux liants graves-laitier-chaux

Utilisation des déchets des carrières et des ballastières

Les prétentions formulées à l'agrégat minéral des corps de chaussée ont été, dans les années récentes, polarisées. Pour produire des revêtements, on requiert de gravillons de haute qualité (de marque NZ et KZ) tandis que dans les couches d'assise (fig. 1) en applicant des technologies convenables, roches de qualité relativement faible, ainsi que des déchets des carrières et des ballastières peuvent être aussi utilisés.

De telle manière on économise la roche de haute qualité et il devient possible d'éventer par anticipation des nouvelles carrières. D'autre part, l'exploitation des déchets est d'importance du point de vue tant de l'exploitation des mines que de préservation d'environnement.

A l'étranger on a reconnu auparavant la signification de l'économie de la richesse minérale de bonne qualité. Dans des plusieurs pays occidentaux on produit aussi des matériaux granulaires de relativement faible qualité dans le cadre de la technologie des grosses entreprises et on en met en vente à des prix modérés. Dans certains pays socialistes l'utilisation des déchets des carrières et des ballastières dans les couches de l'assise des chaussées est retardée par des presciption de construction trop sevères actuellement valides ainsi que de certains régulateurs d'économie. Cependant, les exigences actuelles de l'économie de la richesse minérale stimulant de plus en plus d'un nombre de pays d'entreprendre des essais à l'élaboration des technologies qui favoriseraient l'utilisation des matériaux granulaires de qualité inférieure.

La pratique hongroise

Afin d'encourager l'utilisation des matériaux mentionnés ci-dessus dans le domaine de la construction de routes en Hongrie, les organs routiers et l'industrie d'exploitation des carrières développent depuis 1972 une activité intense. Sous l'effet des publications y relatives [12] et d'une conférence ayant eu lieu à l'usine de carrière à Szob, septembre, 1973, l'utilisation des déchets des carrières à la construction et à l'entretien de routes commença à s'épanouir. L'industrie de carrières met en vente actuellement à partir de différentes usine environ 350 000 tonnes de déchets par an. Les domaines de l'utilisation sont: couches d'assises neuves; élargissement des chaussées étroites; sous-couches; renforcement des accotements, etc . . .

La couche de fondation au-dessous du revêtement en béton de l'autoroute M 7, par exemple, a été construite de déchets de calcaire de Polgárdi, de débris d'aplite de Kisfalud et de débris de dolomite de Litér, d'une part, comme stabilisation mécanique, d'autre part, stabilisée avec de ciment. L'élargissement des chaussées étroites et le renforcement des accotements des routes de grande circulation du réseau routier national, dans toutes les régions de

l'administration routière à l'exception de trois comitats sont exécutés pour la plupart en utilisant des déchets de carrière et de ballastière ou de débris [13].

Sur mandat du Département de Routes du Ministère des Communications le KÖTUKI a élaboré les prescriptions techniques provisoires de titre: «Construction des assises de chaussée en utilisant de déchets de carrières et de ballastières et de débris» (KPM KF IMI I/79) dont les prescriptions les plus significatives peuvent être résumées dans ce qui suit:

Les déchets de carrières

Au cours de l'exploitation de la carrière et de la production de pierres concassées il se produit des déchets de découverte, des déchets d'exploitation et des déchets de concassage. La quantité des déchets annuelle se produisant dans nos grandes carrières atteint les deux millions tonnes et la quantité accumulée peut être estimée à 20 millions tonnes. Du point de vue de possibilité d'utilisation dans le domaine de construction de routes, deux produits de valeur sont obtenus: pierres concassées avec déchets et gravillons avec déchets. Toutes les deux espèces contiennent aussi une certaine quantité des pierres de bonne qualité.

Les pierres concassées avec de déchets sont séparées à l'avant ou après le préconcasseur aux fractions de 0/50 ou 0/80 mm; ce sont les déchets d'exploitation qui peuvent être utilisés pour la stabilisation mécanique.

Les gravillons avec déchets sont, du point de vue de la granulométrie et de la qualité, de propriété plus stable étant, d'une part, de déchets de concassage de 0/5, 0/12 ou 0/20 mm et, d'autre part, de déchets d'exploitation de fraction de 0/30 mm. Celles-ci peuvent être utilisées convenablement surtout à la construction des couches d'assises traitées.

En cas où la partie fine de déchets de 0/20 et de 0/30 varient irrégulièrement et entre des larges limites, elle doit être séparé pour les couches d'assises traitées à des fractions 0/5 et 5/D mm. La granulométrie requise (voir les fuseaux granulométriques des figures 2 et 4) peut être réalisée par le mélange de dosage convenable de ces fractions. Les quantités estimées de déchets accumulées et se produisant annuellement dans des grandes carrières sont indiquées dans le tableau 1.

Les déchets de ballastières

Au cours de l'exploitation des ballastières il se produit des matériaux de découverte ainsi que de déchets gros de séparation, tandis que, au cours de production du gravier sableux on obtient de sables de dessablage.

Les matériaux de découverte sont le gravier sableux et le sable limoneux déshumifiés couvrant le gravier sableux à exploiter. Ce sont applicables également à la production de stabilisation à liant et mécanique.

Tableau 1.

	Désignation des carrières	Dimensions approchées des grains de déchets	Déchets stockés (en mille tonnes)	Déchets se produisant annuellement (tonnes/an)
Carrière de nord	Tarcal	0-20 (35)	1200	150
	Tállya	0-12 (35)	2000	300
	Recsk	0-20 (35)	800	100
	Nógrádkövesd			
	Szanda	0-40 (60)	3000	150
	Bercel	0-30	2000	100
	Szob	0-20 (40)	5000	150
	Keszeg	0-20 (40)	500	100
Carrière de sud	Komló	0-20	300	100
	Nagyharsány	0-20 (40)	200	150
	Polgárdi	0-20	100	150
	Uzsa	0-12 (20)	3000	300
	Zalahaláp	0-20	600	100

Les déchets gros de séparation sont des matériaux de granularité mixte qui seront éloignés ensemble avec des mottes d'argile, mais ils contiennent aussi de fraction fine. De tels matériaux proviennent de la ballastière d'Ártánd. De ces matériaux peut-on produire le matériau de stabilisation mécanique mais, préalablement, les mottes d'argile sont à éloignées à partir du matériau répendu en se servant d'une fourche à ce but.

Le sable de dessablage est un matériau passé au tamis à grains de 0/5, de granularité mixte du gravier sableux contenant un certain excès de sable qui peut être stabilisé par l'addition de liant.

Les quantités annuelles estimées de déchets des grandes ballastières sont indiquées dans le tableau 2.

Tableau 2.

Désignation des ballastières	Déchets de découverte sans la couche de l'humus		Déchets de séparation gros (avec des mottes d'argile)		Sable de dessablage 0/5 mille m^3
	mille m^3	désignation	mille m^3	D_{max} m/m	
Ártánd	100	sable limoneux	50	60	30
Zsolna	50	graves-sable limoneux	-	-	50
Nyékládháza	150	sable limoneux	30	60 (150)	-
Hatvan	60	sable peu limoneux	-	-	15
Ócsa	200	sable fin	-	-	40
Délegyháza	60	sable moyen	-	-	20
Kiskunlacháza	40	sable	-	-	
Gyékényes	120	gravier sableux limoneux	-	-	-
Szombathely	75	sable argileux	(10)	(100)	
Hegyeshalom	20	sable moyen	-	-	-

La stabilisation mécanique

La stabilisation mécanique est une couche de chaussée produite par compactage à partir des matériaux granulaires de consistence de terre humide et de granulométrie continue. On l'appelle aussi béton minéral.

La production de cette stabilisation est un procédé économique surtout en cas d'utilisation à ce but de déchets de l'exploitation de carrière à des fractions de 0/50 à 0/80 mm et de déchets de séparation des ballastières. En effet, celles-ci peuvent satisfaire les prescriptions concernant la granulométrie de la couche d'assise marquée M 50. Dans la proximité des carrières, la construction de la stabilisation mécanique de marque M 20 peut être économique si on se sert de gravillons aves déchets à fractions de 0/20 à 0/30 mm [8]. Le fuseau granulométrique de deux couches d'assise ainsi que les courbes granulométriques des pierres concassées et des gravillons avec déchets de quelques carrières sont montrées sur la figure 5.

Les déchets de grains plus gros se segrègent à un certain point pendant le stockage et le transport. Par conséquent, après leur répandage les parties fines ou gros nécessaires manquent à certains endroits. Néanmoins, la couche compactée peut être mise en circulation qui, de sa part, découvre les endroits défectueux. Ceux-ci seraient réparés couramment par l'addition des grains fins ou gros suivant qu'il est requis.

Couches d'assise traitées

D'après les résultats des séries d'essais de laboratoire du KÖTUKI et sur la base des expériences acquises sur plusieurs tronçons de route construits, les couches d'assise peuvent être construites en utilisant de gravillons avec déchets de matériaux de découverte et de sable de dessablage:

— béton marqués B 70,
— graves-ciment marqués CK,
— sol et sables-ciment marqués CT,
— couche de renforcement, graves-cendres volantes-chaux marqués PE,
— graves-cendres volantes-chaux marqués PK,
— sol et sables-cendres volantes-chaux marqués PT,
— couche de renforcement de graves-laitier marquée GE,
— graves-laitier marqués GK,
— sables-laitier marqués GH,
— sable stabilisé avec émulsion de bitume (sable-émulsion) marqué BH.

Les quantités de ciment de marque 350 nécessitées à la construction de couche d'assise en utilisant de quelques déchets de carrière (définis d'après les

spécifications concernant les couches d'assise de marques CK et B 70) sont comme suit:

	CK	B 70
andésite de Szob 0/20	150 kg/m³	200 kg/m³
gravillon avec déchet de Szob	90 kg/m³	110 kg/m³
andésite de Nógrádkövesd 0/10	120 kg/m³	230 kg/m³
andésite de Komló 0/10	150 kg/m³	200 kg/m³
calcaire de Polgárdi 0/20	70 kg/m³	130 kg/m³
gravillon avec déchets de Polgárdi	100 kg/m³	150 kg/m³

Les données technologiques concernant les mélanges produits par l'utilisation des déchets avec de liants de cendres volantes ou de laitier granulé et de chaux sont résumées sur les figures 2 et 4.

Les couches d'assises construites par l'utilisation des sous-produits industriels mentionnés plus haut interviennent aussi dans les nouvelles normes professionnelles de ministère des couches d'assise.

Organisation de l'utilisation complexe des sous-produits industriels

La situation géographique des carrières et des ballastières le plus importantes, des usines métallurgiques et des centrales thermiques de chauffage à charbon pulvérisé est représentée sur la carte schématique de la figure 6.

Il est recommandable d'installer des stations de malaxage régionales aux dépôts de déchets des grandes carrières. Particulièrement économiques sont les couches d'assise construites par l'application de liants à cendres volantes et à laitier granulé, parce qu'elles permettent à la fois l'utilisation de deux genres de sous-produits industriels polluant l'ambiance. Les tronçons de route construits avec de telles assises s'avèrent favorables tant de point de vue technique que économique.

L'application de ces mélanges est aussi avantageuse à la construction des assises de corps de chaussées neuves ainsi que pour élargissement des chaussées étroites. Ces mélanges sont aussi appropriés pour revêtir des voies en terre rejoignantes, des accotements en terre, des routes de mise en chantier, des surfaces des usines et de stockage de matériaux de construction.

Comme il a été signalé plus haut, la Direction des Routes de Tatabánya commença en 1975 dans le comitat Komárom la construction des couches de

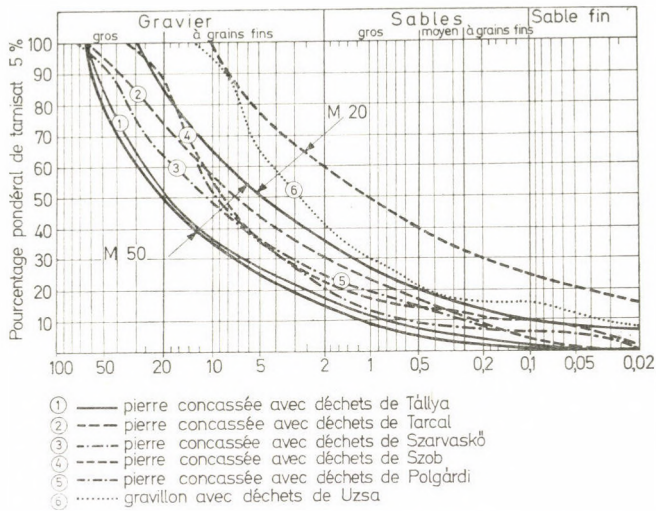

Fig. 5. Fuseaux granulométriques de la stabilisation mécanique et granulométrie de déchets de quelques carrières

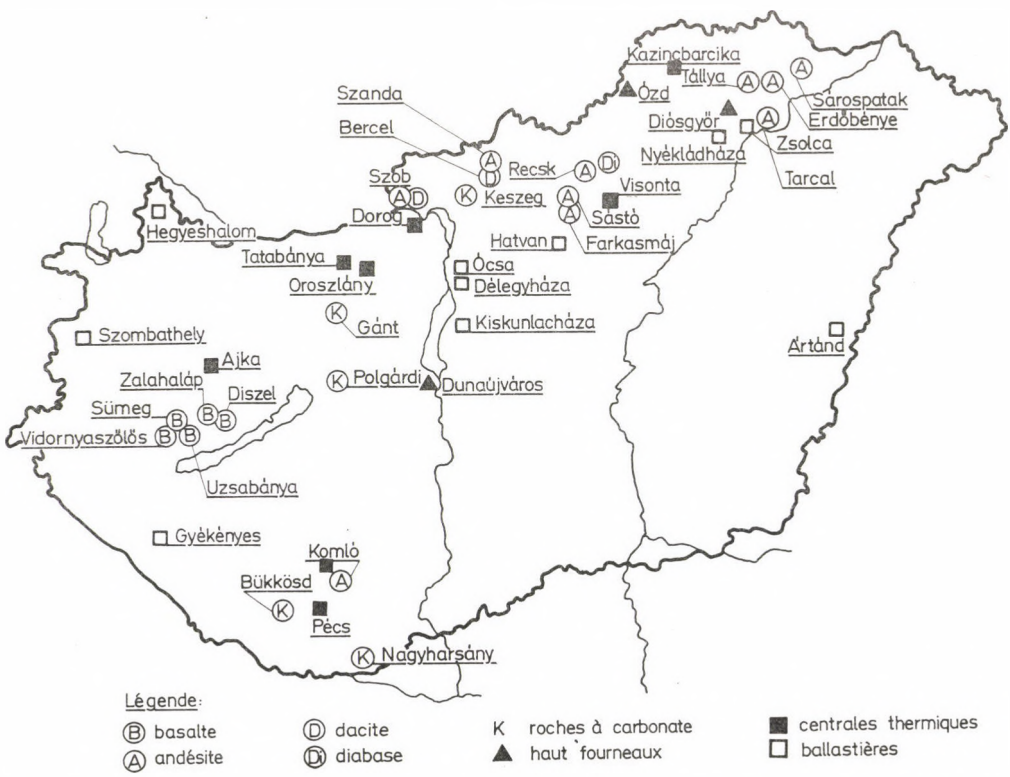

Fig. 6. Situation géographique des carrières, ballastières, hauts fourneaux et des centrales thermiques de chauffage à charbon pulvérisé en Hongrie

base par utilisation des cendres volantes et de chaux comme liants. A sa station de malaxage stable établie à la ballastières de Mocsa, elle produit déjà annuellement de mélange pour cent mille mètre carré de couches d'assise.

Des tronçons de route de longueur réduite ont été construits aussi dans les comitats Heves, Szolnok, Borsod et Nógrád. A ce propos il convient de faire allusion à deux rues de Hatvan signalées plus haut, dont les couches de base furent construites en 1978 par l'entreprise de construction de routes en béton par la stabilisation du sable de désablage de la ballastière de Hatvan.

La Direction de Routes de Salgótarján construisit en 1978 des tronçons de route d'essai courtes par stabilisation avec cendres volantes et de chaux des déchets des carrières de Nógrádkövesd et Keszeg. Sur la base des expériences y acquises, la direction en question a installé en été de 1979 à la *carrière de calcaire de Keszeg* un centre de malaxage d'exploitation continue.

Les déchets 0/20 de la carrière à Keszeg contiennent une quantité excessive de fins. C'est pourquoi on n'obtient qu'une couche de fondation PK par addition de 12 pour cent de cendres volantes de Visonta et de 3 pour cent de chaux. Ces déchets ne deviennent apte à la construction de la couche de renforcement de marque PE que par l'éloignement de la partie majeure de la fraction fine.

Le mélange stocké au dépôt fut transporté avant trois jours pour en utiliser à l'élargissement de la chaussée étroite du tronçon de km 5,6 à 10,2 de la route d'accès de Legénd et au renforcement de la chaussée élargie. La chaussée renforcée a été couverte d'un enduit superficiel bicouche d'émulsion de bitume. La résistance de la couche de base et la portance de la chaussée seront contrôlées régulièrement. Les premier résultats sont favorables. Le Ministère des Communications présentait l'ouvrage de caractère d'essai le 26^{ième} septembre 1979 aux experts. En utilisant les déchets de Keszeg de granularité améliorée on construit depuis cette année (1980) un grand nombre de couche de marque PE et PK. A ce centre de malaxage il a été réalisé le principe d'après lequel les deux sortes de sous-produits industriels, notamment les déchets et les cendres volantes peuvent être utilisés en même temps économiquement.

Une réalisation similaire à celle de Keszeg est envisagée par l'entreprise de construction de routes en béton par l'utilisation de déchets de la fraction 0/25 mm de la carrière de dolomite de Gánt. A la station de malaxage à Bicske de cette entreprise on produira pour la construction de l'autoroute M 1 un mélange de marque PK pour l'application audessous de la couche de base de grave-bitume pour la couche de fondation. La portance et la résistance de ces stabilisations réalisées à titre d'essais en utilisant de sable et de débris de dolomite, d'une très faible teneur en terre végétale, ont avéré favorables.

La Direction de Routes de Miskolc envisage l'installation d'un centre de malaxage similaire à celui à la carrière de Tarcal. On y produira à partir de déchets de la carrière une sorte de mélange avec de liants de cendres volantes

et de chaux pour mettre en oeuvre à l'élargissement des chaussées étroites et au renforcement des structures de chaussée de faible portance de cette région.

Il est recommandable d'examiner les possibilités de l'établissement des centres de malaxage similaires aussi aux autres carrières.

Là où des déchets de différentes fractions se mélangent, d'abord, la fraction grosse (au-dessus de 30 mm) devrait être séparée et en récupérée de pierre concassée de marque Z. Contient le reste de déchets 0/30 de fraction fine en excès, la granularité pourrait être améliorée par une classification imparfaite à 5 mm (en éliminant les fins superflus).

BIBLIOGRAPHIE

1. GÁSPÁR, L.: (L'utilisation des cendres volantes sur le domaine de la construction de routes en France.) *Informations Techniques Françaises* No. 74. 2A. Útügyi szakközlemények. OMKDK (Centre de Documentation de la Bibliothèque Technique Nationale) 1974. (Avec une liste détaillée de la litérature y relative.)
2. JEGOROV, SZ. V.—KUZMICSEV, V. T.—VOLODKO, V. P.: Zolü unosza TEC v dorozsnom sztroityelsztve Ukrainü. Avtomobilnüje Dorogi 1974. november
3. PACHOWSKI, J.: (Stabilisation de sol par l'utilisation de cendres volantes de lignite en construction routière dans la Pologne). *Mélyépítéstudományi Szemle*, mars, 1972
4. FÜLÖP, I.: (Essais de stabilisation de sol par l'utilisation de cendres volantes de lignite basiques.) *Mélyépítéstudományi Szemle*, août, 1967
5. GÁSPÁR L.: (Utilisation en construction routière des cendres volantes et des matériaux des bassins de décantation des centrales thermiques.) *Mélyépítéstudományi Szemle*, mai, 1977
6. LACHNER L.: (Les expérience récentes acquises pendant la circulation concernant la réalisation des stabilisations avec des cendres volantes sèches.) *Mélyépítéstudományi Szemle*, août, 1977
7. (Utilisation des cendres volantes — laitier des centrales thermiques et des poussières de l'industrie des silicates.) Projet de conception de la Commission Nationale de Développement Technique, 20-10-7323 K, 1977
8. *MSZ* (Normes Hongroises) -07.3703-80. (Projets des couches d'assises stabilisées)
9. GÁSPÁR, L.: (Assises traitées avec de laitier granulé) *Mélyépítéstudományi Szemle*, novembre, 1976
10. PRÄGER, I.—POLÁNYI, L.: (Essais de construction routière en utilisant de laitiers granulés) *Mélyépítéstudományi Szemle*, juin, 1976
11. GÁSPÁR, L.: Emploie des cendres volantes et du laitier granulé en construction routière. *Bulletin de Liaison des Laboratoires des Ponts et chaussées*, No. 86, novembre—décembre 1976 (la seconde partie a été publié dans le numéro 89, mai—juin, 1977)
12. GÁSPÁR, L.: (Possibilités d'utilisation des déchets et des débris stockés aux haldes de carrières.) *Mélyépítéstudományi Szemle*, mars, 1973
13. GÁSPÁR, L.: Construction d'assise de chaussée par l'utilistion de déchets des carrières et des ballastières. *Építőanyag*, juillet, 1979

Making Use of the Industrial By-products in the Field of Road Construction in Hungary. — Utilization of the fly ash, blast furnace cinder and waste rock in the way written in the paper is, from the viewpoint of people's economy very significant. With the view of the earliest possible overall introduction of the combined utilization of the industrial by-products, the thermal power plants, ironworks, stone and gravel industry, as well as the highway departments and the construction material industry should develop further efforts. — One of the most urgent tasks is the production of a sufficient quantity of the calcium hydrate, because the lack of this material keeps back the large-scale construction of the base courses. — Surmounting the difficulties of the introduction of the measures proposed would efficiently foster the economy on material and energy which is very much on the carpet at present.

Benutzung der industriellen Nebenprodukte durch den Straßenbau in Ungarn. — Die Nutzbarmachung der Flugasche, Hochofenschlacke und Taubgesteine auf die in der Abhandlung beschriebene Art ist von dem volkswirtschaftlichen Gesichtspunkt äußerst wichtig. — Um die in der Abhandlung vorgeführte komplexe Benutzung der industriellen Nebenprodukte baldmöglichst einführen zu können, müssen die Wärmekraftwerke, Hochofenhütten, die Stein- und Kiesindustrie, sowie die Straßenverkehrsbehörden und die Baustoffindustrie weitere Schritte machen. — Eine der schleunigsten Aufgaben ist die Herstellung des Kalkhydrats in einer ausreichenden Menge, die der Mangel dieses Materials einen umfangreichen Bau von gebundenen Tragschichten behindert. — Die Abwehr der Hindernisse der allgemeinen Einführung würde die Materialersparnisse, die derzeit zeitgemäß sind, wirksam erhöhen.

Acta Technica Academiae Scientiarum Hungaricae, Tomus 91 (3—4), pp. 355—371 (1980)

APPLYING ABSTRACT ALGEBRAIC STRUCTURES TO STRUCTURAL DESIGNING*

D. HOLNAPY**
CANDIDATE OF TECHN. SCI.

[Manuscript received 2. Jan. 1980]

Previously, in the process of the computerized designing technique in connection with system construction, the design of objects was defined by a selection of the system components according to a given policy. In this paper, this method of designing based on the selection of the system components will be formulated by using abstract algebraic structures. Although this principle is of general validity, yet the concepts as discussed in the present paper, are restricted to beam structures only.

1. Introduction

In this paper a new approach-evolving way for the formulation of building-industrial (automated) designing method, realized with the use of system components, is presented. The paper deals with the partial results of current research investigation on the computer technics. The utilization of the results might be expected the soonest in the field of structural designing (i.e., in statics) but the theory is also suitable for the development of mechanical (automated) designing of such projects as can be produced by connecting abstract elements i.e., system components (for example, dwelling functions).

The structural engineers above so far used from mathematics almost only the field of reals (as an algebraic stucture) and its continuous and derivable functions. The recognition of the discreteness of some phenomena and the claim to simulate these phenomena by models also required the knowledge of other fields of mathematics. Recently, as is shown by the research work in the field of theoretical physics, also the application of the stock of means of abstract algebra seems to be necessary [2, 3, 12].

The aspect of the researcher is strongly influenced by its mathematical grounding. The phenomenon investigated is covered up by a "mask" from the researcher through which only those aspects are visible to the mathematical formulation of which he is capable of applying. By embracing a wider spectrum of the stock of means of mathematics it may be expected that the mentioned "mask" perhaps disguises less of the significant aspects.

* Lecture held on the 3rd Hungarian Mechanical Conference.

** Dr. D. HOLNAPY, Építéstudományi Intézet Dávid F. u. 6, H-1113 Budapest, Hungary

The purpose of this paper is to develop a mathematical apparatus which permits the investigation of the most significant aspects of system building and with whose aid it can easily be described.

2. Beginning of the algebraic presentation of the process of designing

In the last 20 years, the spreading of the matrix calculation could be observed. The introduction of the matrix calculation meant practically the intrusion of a new algebraic structure to the field of engineering calculations. The quadratic matrices together with the operations interpreted on them, in contrast to the *field of reals*, constitute a *ring*. Thus, the method of the calculation mentioned and already widely spread broke the exclusive way of thinking in the world of the field of reals.

However, the engineering practice of calculation also used far more definitely algebraic operations for producing constructions (lattice girders, chemical engineering systems) consisting of system elements (beams, appliances) diverging from those currently used.

2.1 Beam structure as an assembly of beam elements

The beam structures are produced by connecting beam elements; the composition of such structures is realized by algebraic operations. A first example is presented from the book of J. SZABÓ and B. ROLLER [15] to demonstrate the idea of the author (Fig. 1). In this example, the relationship is investigated which is valid to the joint movements of the separate and connected beams.

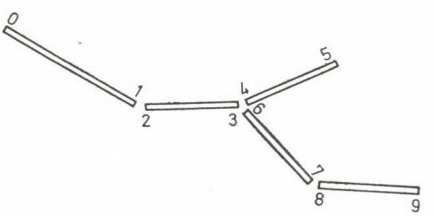

Fig. 1. Beam structure. Connection of beams

In deducting the set of equations describing the stationary conditions of trussed beams, one proceeds by the description of a set of beams which are independent of each other, then one connects them in a convenient way. The rigid connection in the nodes of beams is characterized, that in each node the displacement vectors of the beam ends connected to that node, are the same.

Thus, in case of connection: $u_1 = u_2$, $u_3 = u_4 = u_6$, $u_7 = u_8$. In the following relationship (1) which describes the rigid connection of the beams in the node, the connection to build up a structure is realized by the projector matrix **P**.

$$u_r = \begin{bmatrix} u_0 \\ u_1 \\ u_2 \\ u_3 \\ u_4 \\ u_5 \\ u_6 \\ u_7 \\ u_8 \\ u_9 \end{bmatrix} = \begin{bmatrix} \overset{0}{\smile} & \overset{1}{\smile} & \overset{3}{\smile} & \overset{5}{\smile} & \overset{7}{\smile} & \overset{9}{\smile} \\ E & & & & & \\ & E & & & & \\ & E & & & & \\ & & E & & & \\ & & E & & & \\ & & & E & & \\ & & E & & & \\ & & & & E & \\ & & & & E & \\ & & & & & E \end{bmatrix} \cdot \begin{bmatrix} u_0 \\ u_1 \\ u_3 \\ u_5 \\ u_7 \\ u_9 \end{bmatrix} = P \cdot u_c \,, \tag{1}$$

wherein:

u_r : vector containing displacement vectors,
u_c : vector containing displacement vectors of a connected system.

Designing the shown above structure was at the beginning only a trick of calculation and this step of calculation has been avoided in the practice due to economic reasons. From the viewpoint of the days of evolution of the system construction, in the organizing step mentioned above, one should notice the core of the idea that the *composition of beams into structures is an algebraic operation on the set of the system components* (i.e., system-component symbols).

In designing the system buildings, the above mentioned creation of connections was formed by a calculating trick of the operator of the connection of structural parts, wherefore, the above description may be interpreted as the beginning of the algebraic formulation of the designing process.

2.2 System of the chemical-engineering operations as the assembly of appliances

The chemical-engineering operations system is produced by the connection of appliances, and this composition is carried out by an algebraic operation. From the book of T. BLICKLE [1] the 2nd example is shown in Fig. 2 for the demonstration of the idea discussed. In this example, the appliances constitute, in their physical reality, a basic set and the corresponding symbol set (of one-to-one correspondance) constitute the basic set in the mathematical sense. The set of symbols of the appliances (system components) consists of the symbols produced, according to Fig. 2. In this figure, above the ingoing materials, below the outgoing ones separated with circles are listed. The

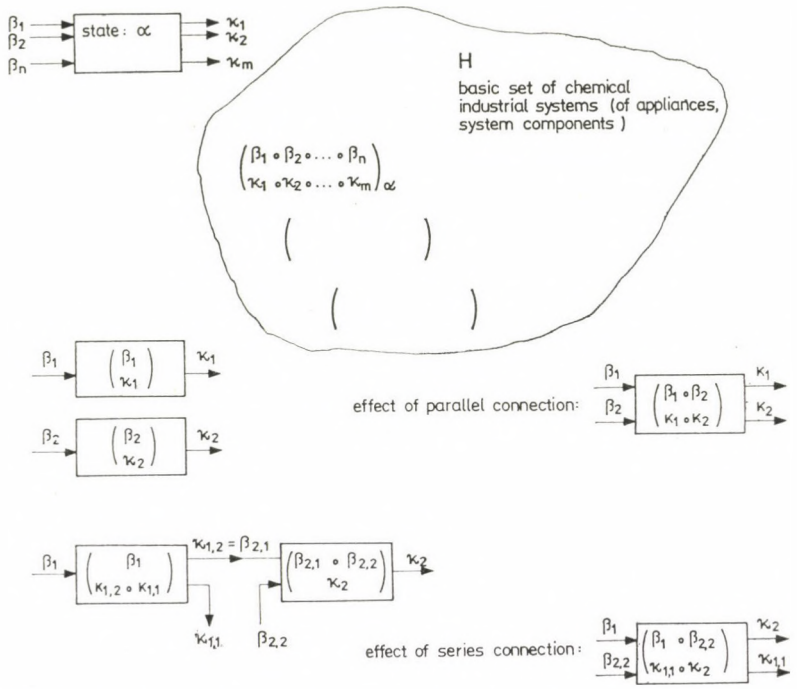

Fig. 2. Operation system in the chemical industry. Connection of appliances

subscript characterizes the state of the appliance (i.e., that of the system component).

Even without the knowledge and knowning the details in fields which are far from the building industry, it may be understood that the parallel connection of the appliances is symbolized by the operation

$$\begin{pmatrix} \beta_1 \\ \varkappa_1 \end{pmatrix} \bigcirc \begin{pmatrix} \beta_2 \\ \varkappa_2 \end{pmatrix} = \begin{pmatrix} \beta_1 \circ \beta_2 \\ \varkappa_1 \circ \varkappa_2 \end{pmatrix} \tag{2}$$

and the series connection by the operation

$$\begin{pmatrix} \beta_1 \\ \varkappa_{1,2} \circ \varkappa_{1,1} \end{pmatrix} \oplus \begin{pmatrix} \varkappa_{1,2} \circ \beta_{2,2} \\ \varkappa_2 \end{pmatrix} = \begin{pmatrix} \beta_1 \circ \beta_{2,2} \\ \varkappa_{1,1} \circ \varkappa_2 \end{pmatrix} \tag{3}$$

($\bigcirc$ is commutative and associative, $\oplus$ associative but *not* commutative).

By the above mentioned method also applied in the practice is already deliberately expressed the fact that ***the composition of the appliances to a chemical engineering operation system is an algebraic operation of the set of the appliances*** (i.e., of the symbols of the appliances).

The automated design technique developed in the chemical industry applying algebraic means may also be the model of system building.

3. Gradual development of the algebraic structure isomorphic to the system construction

In this part of the paper one has tried to describe, as far as possible, in an exact way the details of the realisation of system-building. The concepts taken from mathematics [4, 11, 14, 16] written in capitals at the first place of their use are emphasized in order to make the reader conscious of how the familiar concepts of designing often to be found trivial, become step-by-step exact describable in the language of mathematics.

3.1 Representation of the concept of the set $\langle H \rangle$ in the system construction

The totality of the system components constitutes a SET and each of the system components is the ELEMENT of the SET. GIVING the totality, i.e., the SET of the system components may take place by listing the elements of the system components (in the catalogue of the system components) or by describing some of their characteristic properties (case of the generated catalogue). It is evident that the above said holds true for the set of the system components taken in the physical sense (by the use of which construction of a building may effectively be carried out), but also holds true with respect to their mathematical representation, i.e., to the set of symbols and to the sets of the codes of the elements (Fig. 3). The example is taken from one of the lightweight structure building systems developed in Hungary named ÉTISZERK [10]. Due to the close connection between the above mentioned two sets (physical system components and the representation or them), in the following they will not be sharply distinguished from each other.

In the course of the automated design the selection of the objects does not always take place from the system components. In many cases, it is con-

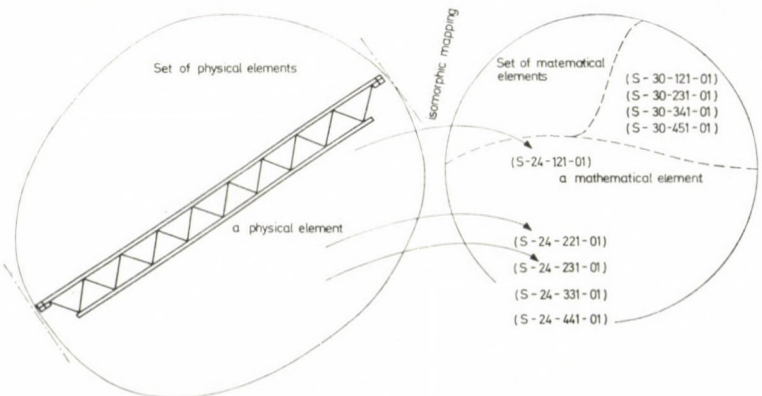

Fig. 3. Set of system components

venient to form design units [17] from the system components and in making the decision, to adopt or to reject the ensemble of the system components, as a whole.

In such cases the elements of the set which are the subject of selection are sets themselves. Thus, it is convenient to introduce the concept of the DEGREE OF SETS. Accordingly, the set of the system components is a set of first degree, and the set of the design units produced from the system components is a set of second degree, etc. Thus, by forming sets by $n - 1$ steps one obtains a set of nth degree which, in the case treated of, for example, might be sets of the objects, buildings, constructions to be realized (Fig. 4).

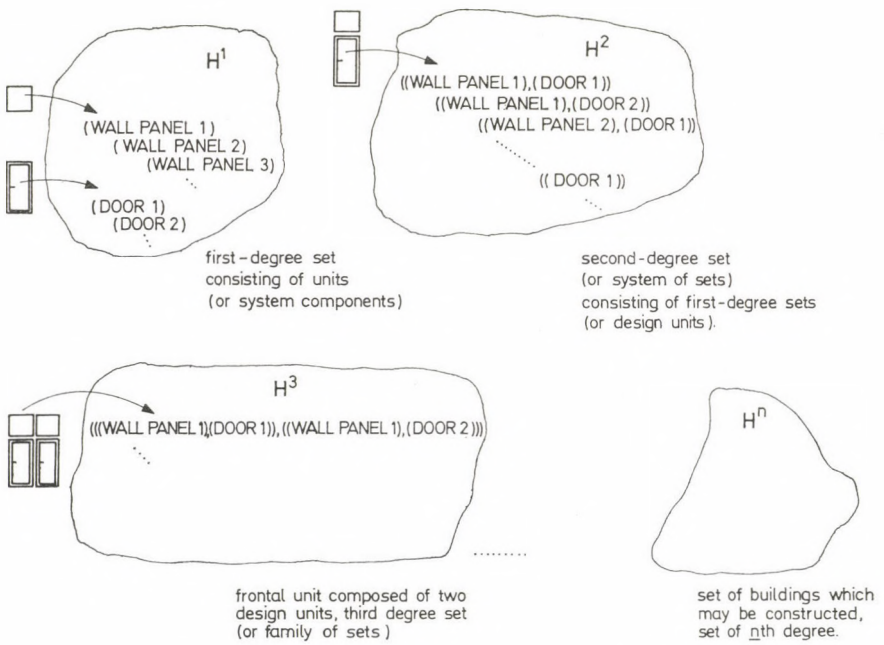

Fig. 4. Hierarchic construction of buildings

One speaks about the EQUALITY OF THE SETS of the system components in the case where the elements of the sets are identical. If one considers only one selected part of the set of the system components, say, right handed doors, then all of these selected elements constitute a SUBSET. The part of the set of the system components which does not contain the subset of the right-handed doors selected as mentioned above, is named COMPLEMENTARY SET or more exactly, complementary set related to the set of system components of the right-handed doors. Using several catalogues in selecting the elements or units for the construction of an object is, as if one would use a basic set accomplished

by UNITING OF THE SETS. The subset of 6,0 m long lattice girders may be produced as the INTERSECTION (or common part) OF THE SUB-SET containing those of 6,0 m length and the lattice girders. The DIFFERENCE OF SETS should be formed of certain elements from among those of the basic set which should be excluded with the view of carrying out the rest of the work.

The terminology so far are, so to say, quite the same as those used in everyday parlance. Their recollection is essentially necessary when in the case of contestable interpretation, the concepts should be interpreted according to their exact definition.

3.2 Representations of the concept of the model $\langle H, < \rangle$ in the system construction

Nothing can be done with the set of system components by itself. In the opinion of the author for carrying out the automated designing, besides the system component also the policy of assembling is needed [8]. The system components without the strategy of purposeful policy of their arrangement and assembling as if they were tiny stone pieces in bulk prepared for the composition of a mosaic work without an artistic conception. The first stage of working out the policy of assembling is to define the relationship of the elements. Below, these concepts will be presented according to their exact mathematical definitions.

The concept of the PRODUCT OF SETS makes it easier to understand what follows. Be U the number of the columns and V the set of the beams to be applied. The structures to be produced from the above elements should be characterized by such an ORDERED PAIR (Fig. 5) wherein, in the first place the symbol of the column, and in the second place that of the beam is put. If one produces all of the similar practicable structures (ordered pairs), so these ordered pairs will constitute a set which will be the product (Cartesian product)

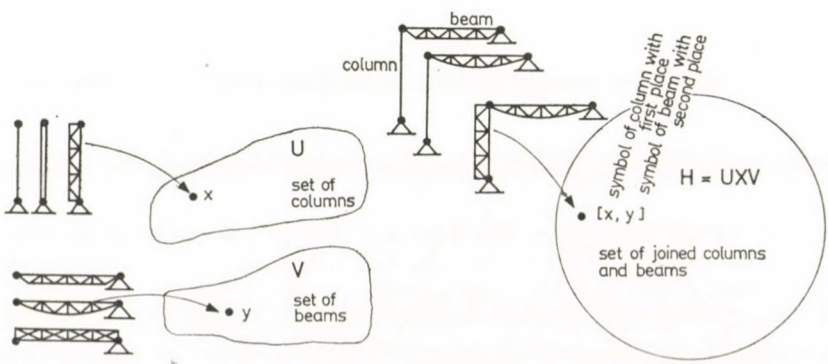

Fig. 5. Cartesian product

of the set of structures to be accomplished in this way. Obviously, the structures consist, in general, not only of two but n system-components (and it is not all the same whether which is placed where), therefore, the set which represents them, will be produced by several multiplications (Cartesian multiplications) of the sets, and its elements are ORDERED n-TUPLES.

When, in the example treated above, the set of products $H = UXV$ or, more simply expressed, the ordered pairs have been established, essentially, to an element $u \in U$, one or more $v \in V$ elements have been added. In such cases, it is customary to speak of MAPPING, i.e., to assume that the second element of the ordered pair is coordinated to the first one of the ordered pair. The mapping is such a commonly used concept which is also customary in a case where to the *first element* (primary element) several elements (mapped elements) considered as second ones are associated, but a selected particular mapped element may also be coordinated to several primary elements. Mapping was mentioned above in this paper when, according to Fig. 3, to the physical system components their symbols in one-to-one have been coordinated. On the basis of this very close mapping becomes possible, bearing physical components in mind, one works with mathematical symbols. The mapping does not necessarily concern all the elements of the sets U and V. In this case the mapping is realized as the product set of an $U_{\ddot{o}}$ subset of the set U and of a V_k subset of the set V. If the set of the ordered pairs U, V is characterized by a particular property R or, in other words, the property R defines the set of products, so one speaks of BINARY RELATION. Such a relation-defining property might be, for example, "being of equal length". Then a subset of the product-set $H \times H$, i.e., the product-set of the system-component set H multiplied with itself was defined, implying those ordered pairs the lengths of which are equal to each other.

According to Fig. 3, for example, (S-24-121-01) "$R^{\text{equal length}}$" (S-24-221-01), is in relation i.e., both are 240 cm long. In the very same relation belong the elements (S-30-121-01) and (S-30-231-01) because both of them are 300 cm long. A convenient aid for the demonstrative representation is the directed graph representation [7]. It is evident that on the basis of identical properties not only pairs but also n-tuples may be formed. These n-ARY RELATIONS, as sets, might also be interpreted as a subset of the Cartesian product of n sets For the sake of completeness it should be noted that the results of mapping may be submitted to further mappings and because the relation is a special case of mapping, also the elements of the set of relations may be brought into relation with other set-elements. Such kinds of chaining can be carried out with the aid of the PRODUCTS OF MAPPINGS, RELATIONS.

The relation mentioned "being of equal length" is reflexive and symmetrical. Reflexive, because (S-24-121-01) "$R^{\text{equal length}}$" (S-24-121-01), i.e., it is equal in length to itself and, in case of (S-30-213-01) "$R^{\text{equal length}}$" (S-30-

231-01) also the statement (S-30-231-01) "$R^{\text{equal length}}$" (S-30-121-1) holds true. In general, the sequence of the elements in the ordered pairs are not interchangeable. A non-interchangeable binary relation is, for example, "being an element of".

On the basis of the PROPERTIES OF BINARY RELATIONS general validity laws may be stated.

From among the KINDS OF BINARY RELATIONS one of the most significant property, concerning the subject matter of the paper, is the equivalence relation which, in comparison with those mentioned above, is also transitive. A good example may be there to the relation "being 300 cm long". It is evident that if

(S-30-121-01) "$R^{300\ \text{long}}$" (S-30-231-01)

and

(S-30-231-01) "$R^{300\ \text{long}}$" (S-30-341-01)

so

(S-30-121-01) "$R^{300\ \text{long}}$" (S-30-341-01)

is also in relation.

The last of the above relations might be assumed as *unary* (one-variable) relation. Also a significant relation is the ordering relation. The irreflexive ordering relation which is less specific, is irreflexive, asymmetrical and of transitive behaviour. The relation "being the element of" is as follows:

a) neither of the elements is a part of itself (i.e., it is irreflexive or, in other words, antireflexive),

b) in case where an element is the part of an element of higher order (design unit), its follows that it is not true inversely (i.e., it is asymmetrical),

c) the part of a part of an element of higher order (object, building) is also the part of the whole object (i.e., it is transitive).

Such an (irreflexive) ordering relation produces an ORDERING on a set. In the case where the basic set and the relations defined on it are given, one can speak in an algebraic sense about a MODEL [11]. In the title of this chapter, with $\langle H, < \rangle$, where the less than sign, symbolically means, all relations defined on the set H. An example, to the construction of a model taken in such a mathematical sense has been given by MÜLLER [13], wherefrom the details which are, in principle, essential and interesting from the viewpoint of the treated subject are depicted in Fig. 6. The Cartesian product of the subsets U, V of the system-component H involves all of pairings. The subsets of this set of products are, by definition, relation sets, namely, those possessing the properties "being apt for assembling according to function", "being apt for assembling according to dimensions, modular coordination".

From the above is to be seen that on the side of practical designing, the first experiments have been undertaken in order to try to describe the dif-

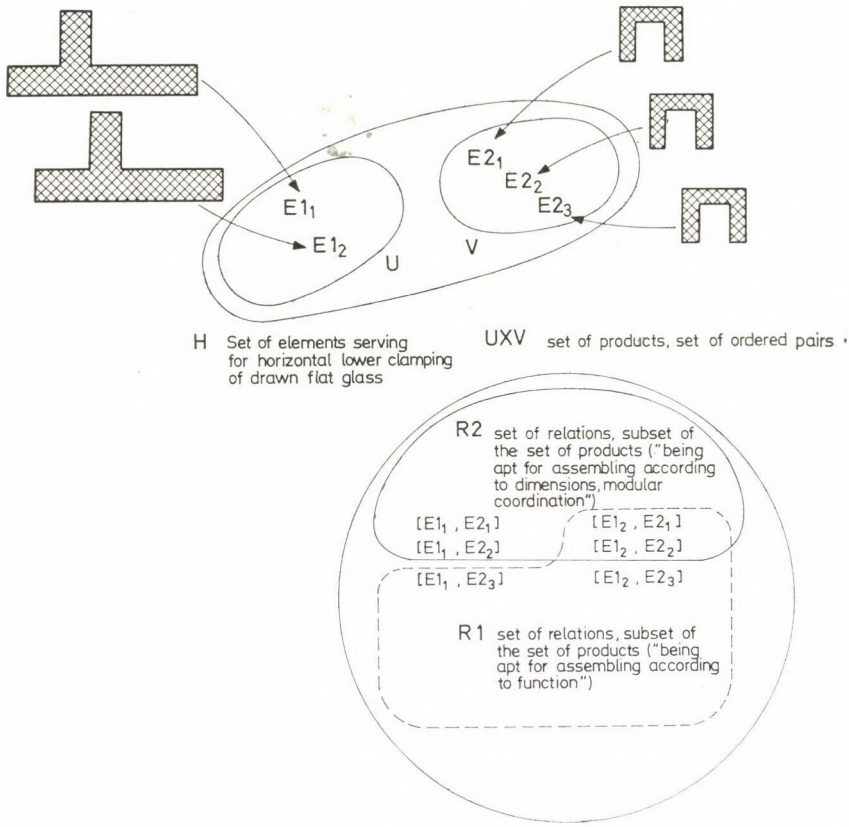

Fig. 6. A fictitious example for the relationship between elements serving for horizontal lower clamping of drawn flat glass according to MÜLLER

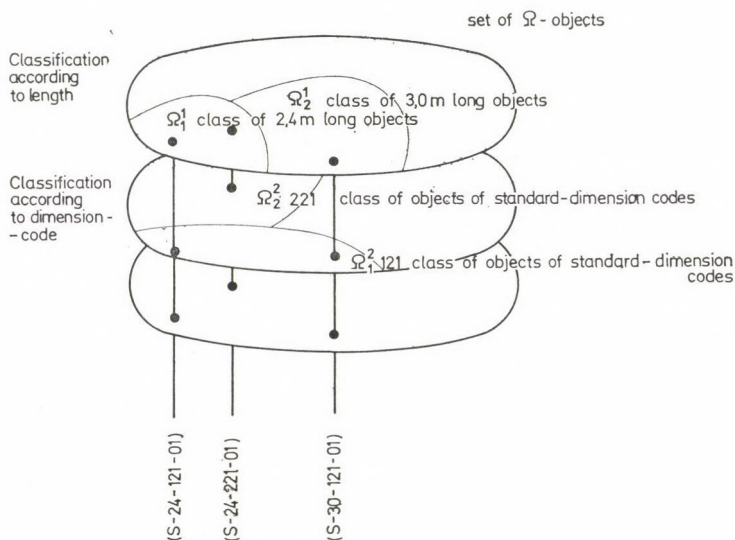

Fig. 7. Forming of equivalence classes on the basis of equivalue relations

ferent steps of designing with the means of algebra, by making use of models taken in abstract algebraic conception (i.e., of relation structures).

CLASSIFICATION, EQUIVALENCE CLASSES may be produced by specifying equivalence relations. As is known, the equivalence relations are reflexive, symmetrical and transitive relations. Such is the relation "being 300 cm long", mentioned above, as an example. The classes induced by the equivalence relations are disjunct from each other. Several equivalence relations produce, in general, several kinds of classifications on a basic set. Some design problems can be solved by finding the element which satisfies all equivalence relations. A demonstrative example on this subject is presented in Fig. 7. This selection, especially having languages of mathematical-logical base, may be extraordinary by simply programmed.

3.3 The representations of the concept $\langle H, <, \bigcirc \rangle$ of the algebraic structure in the system construction

It has been seen that the concept of mapping and that of the relation lie very close to each other. In neither of them is the uniqueness stipulated in either direction. If, say, mapping of the set of system components is carried out onto the set of the real numbers (for example, to that meaning the cost of the components), one obtains an unique mapping (Fig. 8). This kind of mapping is called in algebra FUNCTION, or more exactly, function of a single variable. One speaks of FUNCTION OF n VARIABLES if the cost of a design unit is calculated. Namely, the cost of a unit assembled from the system components of a higher level, depends on the costs of the system components and on the parameters reflecting the manner of assembling. Structural engineers already know these concepts from mathematical analysis. However, in most cases, the internal image formed from the function is connected to the continuous functions. From this image one should free oneself. In the mathematical models of the

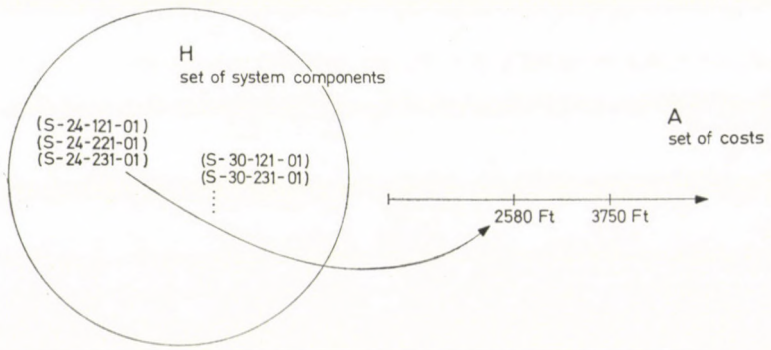

Fig. 8. Demonstration of the concept of the function by concepts used in the system construction

system construction, the continuous functions and, consequently, the derivations will have a reduced role in comparison to the earlier models [8].

The concept of INVERSE FUNCTION or the invertibility of the functions is also comparable to that known from analysis, only the definition should be given in a form also suitable for discreet elements. The elements of the set of the physical system components and the symbols of the system components are connected by such an invertible functional connection to each other as mentioned above. One speaks of OPERATION in case of functions mapping the basic set into itself. The concept of the algebraic operation is the same as those known from arithmetic. The addition usually carried out in the field of reals, is such a function of two variables as those of the set of values (the domain of maps) which is identical with the domain of the variables (of the primary maps). Operations may not only be defined between two elements. The mapping into itself, defined as a function of n elements of the set is an n-ARY OPERATION. In particular, in describing the system construction being so far in the maturing stage, perhaps a great many operations may be defined over the system components. Also the totality of these operations themselves are sets which are called OPERATORS' region. A part of the PROPERTIES OF OPERATIONS have a particular name. Most of these properties are also to be found in the system construction. The operation of "putting on" is associative (not quite such as the addition in the field of reals, because that one is also commutative). Namely, the foundation block is "put on" the ground, and upon this one, one puts on the column, while upon this latter the beam is put on. This operation of the putting of elements on each other, may be grouped (being associative), namely, on the foundation the ensemble of the beam put upon the column may be placed but, upon the ensemble of the beam with the column below it placed on the foundation, the beam might be placed; the results is the very same in every case. The above said may be considered as the "bracketing" of the construction. The above mentioned operation is not commutative. That is to say, it is not all the same if a beam is put upon the column or to put the column upon the beam. Defining operations on the basic set of the model taken in the above developed algebraic sense, yields an ALGEBRAIC STRUCTURE. Such an algebraic structure is also the field of reals, the best known algebraic structure.

Algebra deals substantially with the investigation of algebraic structures. At this point it is clearly seen that to the design built up on the system components an appropriate algebraic structure should be found to have an apparatus of the algebraic description of the design processes.

The WELL KNOWN ALGEBRAIC STRUCTURES are those whose application should be first of all tried to the description of the system construction in the course of research for the most convenient algebraic structure. But, to do this, the internal structure of the system construction should be better known.

Hereby, the point is attained where the explanation of the title of the paper became possible. Namely, the establishment of the algebraic structure is required which is isomorphic to the system construction. Among the MORPHISM, the mapping realized in an operation preserving way between two sets, i.e., in a relation preserving way that is one-to-one, this is isomorphism.

In this paper one has tried to carry out the set of system-component symbols of the set of the actual physical system components, to formulate the relations on the set of symbols in an operation preserving way and on the model shaped in this way (relation structure), to define operations which can be treated with the aid of algebraic apparatus and correspond to the actual assembly of the system components. That is why, that algebraic structure is sought for which is isomorphic to the system construction.

The system construction may also be imagined from the system components which are considered to be a GENERATOR SYSTEM, the object to be constructed is produced gradually by operations. However, in that case, in the basic set H of the structure $\langle H, <, \bigcirc \rangle$ not only the system components but also all the objects which may be generated from them, are involved. But, because these objects may be produced from all the generating elements of the structure, it is not necessary to store all elements of the H. (On practical grounds it is convenient to store the design units, i.e., not to keep only the minimum basic stock of the generator system.) In case of modelling, the system construction in this way, the algebraic structure which is isomorphic to the system construction will be an algebraic structure to be finitely generated.

4. Ideas and work-hypotheses concerning the algebraic structure isomorphic to the system construction

In the course of studying the algebraic description of the system construction one came to the point where to the system components actually existing a *set of symbols* has been coordinated. The *relation* between the physical system components were also defined on the set of symbols, and to the construction activities as *operations*, operations have been corresponded on the set of symbols. It is to be seen that thereby an *algebraic structure* is coordinated to the system construction. The question arises what are the relations and what operations can be thought out? What can be considered as work hypotheses in the course of working out the algebraic structure isomorphic to the system construction? As an answer to those questions the construction of a frame of a building has been detailed to go as deep as is possible at all, at the present stage of the study. Nowadays, to the automated designing realized by the system components, the discreet mathematical programming is used [5, 6, 8, 9]. For characterizing the system applied in the structure (now only beams) or objects, the notation demonstrated in Fig. 9 is introduced.

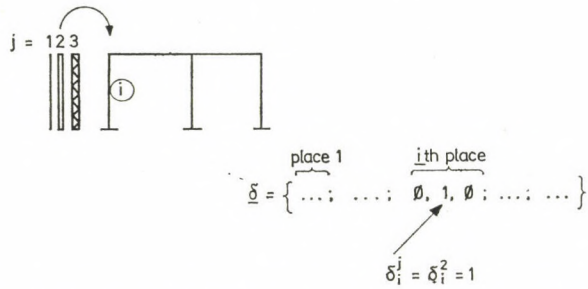

Fig. 9. **Definition of the vector δ characterizing the object**

In case of the vector component δ_j^i, the subscript i denotes that the beam, to be selected to replace the ith beam, the subscript j is the serial number of the bars to be selected to the ith place.

$$\delta_j^i \begin{cases} 0 \text{ in the case where at the } i\text{th place not the beam No. } j \text{ is placed} \\ \text{otherwise } 1 \end{cases}$$

It is evident that in the group of elements of the same subscript only one element may be used differing from zero (in the model possibly another may be permissible), i.e., to one place only one element can be placed.

Be Ω the set of the system components. Let us characterize its elements by a code number and coordinate, by relations defined on Ω, to each element a subset of property T.

Let, on the above mentioned algebraic structure (probably on a network) a function which, on the specified geometrical and feasibility conditions, generates from the elements of Ω the δ-vectors of the realizable buildings (Fig. 10).

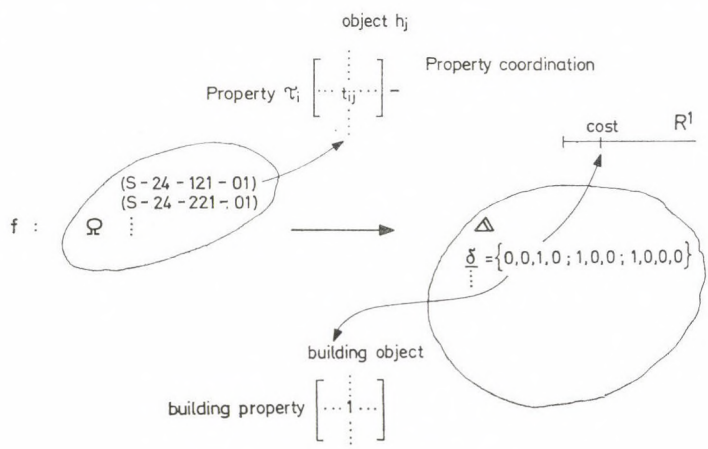

Fig. 10. **Generation of buildings**

Also to the δ-vectors a set of properties are associated which may be produced from the set of properties of the system components.

In case where an answer should be given to the question which from among the objects, otherwise satisfying the static and strength requirements, for example, the less expensive (the details of static and strength calculations are here not dealt with), it is sufficient for property coordination to define on the set Δ a function, say r, which maps onto R^1 (onto the one-dimension Euclidian space, i.e., the real numbers).

(The above example needed to demonstrate the formulation of the algebraic structure, and not wish to give a semblance that all problems of the optimum structural designing was or could be solved in that way.)

Let us define between δ_1 and δ_2 a "min" operation as follows

$$\min(\delta_1, \delta_2) = \begin{cases} \delta_1 & \text{if} \quad r(\delta_1) \leq r(\delta_2) \\ \delta_2 & \text{if} \quad r(\delta_1) > r(\delta_2) \,. \end{cases}$$

Let us again define the "max" operation on similar principles. These operations are:

— associative,
— commutative,
— max. with respect to min. is distributive,
— min. with respect to max. is distributive,
— idempotent, and
— the absorptional identities are fulfilled.

Let us denote the vector containing the 1s be put at the places of the most expensive elements with 1 and the vector containing the 1s at the places of the less expensive elements with 0. Then:

$$\max(\delta, 1) = 1 \,,$$

$$\max(\delta, 0) = 1 \,,$$

$$\min(\delta, 0) = 0 \,,$$

$$\min(\delta, 1) = \delta \,.$$

This is the way we could form the "unit" and the "zero" element in the algebraic structure developed above which is a *distributive net.*

The above overall-view was reasonable and justified because it was connected to the customary way of thinking and the cost which was coordinated by the mapping (or, more exactly the *function)* "r" to the object assured a

total ordering (chain) over the set Δ. The real advantages show themselves in case where one should not appreciate only according to a single parameter (for example the cost) and the appreciations according to different parameters may also be contradictory. Such viewpoints of appreciation, partially ordering relations, might be as follows:

— being less expensive,
— being realizable sooner,
— being labour-absorbing,
— being more simply mountable, etc.

In this case, the *supremum* and *infimum* takes over the function, the role of the preceding (max., min.) operations. Although not every object can be compared to each other, however, about some of them something could be said still in connection with the definition of the supremum and infimum which could be considered as an appreciation. It could be expected that the apparatus which describes the system construction is a net (function) defined on the nets of the system components involving the above partial ideas [2].

REFERENCES

1. Blickle, T.: Mathematical Models of Heat and Material Transfer Systems. Műszaki Könyvkiadó, Budapest 1977
2. Fáy, Gy.—Tőrös, R.: Quantum Logics. Gondolat Könyvkiadó, Budapest 1978
3. Galambos, S.: Quantum-Logical Structure for Designing Industrialized System Construction. Építéstudományi Intézet (Hungarian Institute for Building Science), Budapest 1979
4. Görke, L.: Sets, Relations, Functions. Tankönyvkiadó, Budapest 1969
5. Grósz, M.: Automated Designing with Integer Programming. *Műszaki Tudomány* **53** (1977), 207—216
6. Grósz, M.— Holnapy, D.: Fundamental Mathematical Model of the Automated Engineering Designing and its Application to Planning Water-Supply Systems. Hungarian Hydrological Society, *National Itinerary Congress*, Keszthely, May 17—18, 1979
7. Hámori, M.: Relations. Tankönyvkiadó, Budapest 1972
8. Holnapy, D.: Computers in the Industrialized Building Designing. Műszaki Könyvkiadó, Budapest 1979
9. Holnapy, D.—Grósz, M.: Structural Designing of Foundation Block Systems by Selection. *Systems Theory Conference* '79 Sopron, September 3—5, 1979
10. Kiszelya, L.: Designing of ÉGT-Steel Frames. *Publication of the Hungarian Institute for Building Science* (Építéstudományi Intézet), Budapest 1977
11. Maurer, Gy.—Virág, I.: Introduction into the Theory of Structures. Dácia Könyvkiadó, Kolozsvár—Napoca 1976
12. Molnár, L.: System-Approach Mathematical Investigation of Building Systems. *Publication of Hungarian Institute for Building Science* (Építéstudományi Intézet), Budapest 1978
13. Müller, F.: Information Theory in Planning I. *Publication of the Pollack Mihály Technical Highschool*, Pécs 1975
14. Rédei, L.: Algebra I. Akadémiai Kiadó, Budapest 1954
15. Szabó, J.—Roller, B.: Theory and Calculation of Beam Structures. Műszaki Könyvkiadó, Budapest 1971
16. Szász, G.: Theory of Networks. Tankönyvkiadó, Budapest 1975
17. Takács, I.: Computerized Aid for Designing Buildings to be Constructed from Prefabricated Units. *SZÁMGÉP-publication*, Budapest 1973

Anwendung abstrakter algebraischer Strukturen im Konstruktionsentwurf. — Früher wurde der Entwurf der Bauobjekten im sich an die Systemarchitektur anknüpfenden rechenautomatischen entwurftechnologischen Prozeß als eine Auswahl der Systemkomponenten für Zusammenbau nach einer bestimmten Strategie betrachtet. In der vorhandenen Abhandlung wird dieser auf die Auswahl der Systemkomponenten basierende Entwurf mit Hilfe von abstrakten algebraischen Strukturen formuliert. Ist zwar dieses Prinzip von allgemeiner Gültigkeit, werden jedoch die in der Abhandlung behandelten Erwägungen nur auf die Stabkonstruktionen begrenzt.

Acta Technica Academiae Scientiarum Hungaricae, Tomus 91 (3—4), pp. 373—391 (1980)

SATURATED PHASE ENTHALPY RELATIONSHIPS FOR SOLID CO_2 IN CH_4 AT CRYOGENIC PHASE BEHAVIOR

M. A. I. BUKHARI*

[Manuscript received 31 Juli, 1978]

With low temperature processing of CO_2 contaminated natural gas becoming an established practice, the design of cryogenic installations for freezing out solid CO_2 produces, economically, much more refined natural gas than is now offered by more conventional techniques. Although the cryogenic phase behaviour of the CH_4—CO_2 system has been extensively investigated. The full potential of low-temperature processing cannot be realized until reliable thermodynamic data has become available. The main purpose of this paper is to present, analytically, some usefull data, based on reliable correlations, for use in the design of cryogenic processes involving solid CO_2 in CH_4.

Notation

A	Exchange energy density
A_0, B_0, C_0, a, b, c, α, ν	parameters of the BWR equation of state
F	molal Gibbs free energy
H	molal enthalpy, heat content
M	molecular weight
P	pressure
R	universal gas constant
S	molal entropy
T	temperature
V	molal volume
d	density
f	fugacity
ln	natural logarithm (base e)
k_{12}	parameter characterizing deviation from the geometric mean assumption for characteristic temperature
l_{12}	parameter characterizing deviation from the geometric mean assumption for cohesive energy
x	mole fraction, liquid-phase
Δ	increment, a differential function
Λ_{ij}	temperature-dependent Wilson parameter
α	coefficient of thermal expansion
α_1, α_2	empirical constants in Wilson's equation
β_1, β_2	empirical constants in Wilson's equation
ν	activity coefficient
δ	solubility parameter
Φ	volume fraction
λ_{ii}, λ_{ij}	parameter representing energies of i—i or i—j molecular interactions
$(\lambda_{ij} - \lambda_{ii})$	temperature-independent Wilson parameter
ξ_{ii}, ξ_{ij}	local volume fraction of species i about a central segment of type i and j. respectively

* Present address: M. A. I. BUKHARI, P.O. Box 2408, Khartoum, Sudan

Superscripts

E	excess (over ideal)
M	mixing
VAP	vaporization
L	liquid-phase
S	solid-phase
g	gas
O	standard state
—	partial quantity

Subscripts

c	critical point
i, j	general indices, components

Introduction

Increasing demand for energy has necessitated the utilization of the huge reserves of natural gas previously considered uneconomical because of high carbon dioxide contamination. CH_4-CO_2 system equilibria extend to low temperatures over the larger portion of the composition range and over a wide range of pressures. CO_2 starts to separate as a solid at temperatures below its triple point (−56.6 °C) and at pressures below 50 atmospheres. With low temperature processing of natural gas becoming an established practice, the design of cryogenic installations for freezing out solid CO_2 produces, economically, much more refined natural gas than is now offered by more conventional techniques. Although the cryogenic phase behaviour of the system has been extensively investigated. The full potential of low-temperature processing cannot be realized until reliable thermodynamic data has become available. The main purpose of this paper is to present, analytically, some useful data, based on reliable correlations, for use in the design of cryogenic processes involving solid CO_2 in CH_4. In formulating the thermodynamic data analysis, some of the most recent concepts of "regular" solution theory of SCATCHARD, HILDEBRAND and coworkers [1, 2] and WILSON's semi-empirical extension of the FLORY—HUGGINS treatment of "athermal" mixing [3—5], together with the BENEDICT, WEBB and RUBIN equation of state [6—9] are applied.

Thermodynamic Models

Solution theories aim at the prediction of mixture properties from properties of their own pure components. The thermodynamics of solid-liquid equilibria become complicated if a solid solution is formed, but equilibria here are those for which the solid-phase CO_2 (referred to by index 2) is a pure solute, and the liquid-phase a saturated solution of the salute in the liquid solvent

CH_4 (referred to by index 1). The activity of the solidphase must be expressed as the ratio of its fugacity to the fugacity it would have as a pure subcooled liquid. The equation of equilibrium at constant temperature and pressure which relates the fugacity of the pure solid solute to properties of the liquid mixture is

$$a_2^s = f_2^s / f_2^{0L} = \nu_2 x_2 \tag{1}$$

where x_2 is the molal fraction of component 2 in solution, and ν_2 is the activity coefficient of the solute in solution referred to the hypothetical pure liquid subcooled below its melting point, all at the temperature T of the system. The sum of the free energy changes in the hypothetically separate processes of melting the solid to form a pure subcooled liquid, and then mixing the subcooled liquid with the liquid solvent to the equilibrium concentration must be zero. This molal free energy change is related to the activity of the solute by

$$\overline{\Delta F}_2^M = RT \quad \text{In} \quad a_2^s = RT \text{ In } \nu_2 x_2 . \tag{2}$$

Deviations of this term from the ideal may be expressed in terms of the excess enthalpy and entropy of mixing as follows:

$$F^E = H^E - TS^E . \tag{3}$$

If $F^E = 0$ the solution is ideal. Assuming zero excess entropy of mixing ($S^E = 0$) leads to the concept of "regular" solutions. On the other hand, assuming zero excess enthalpy of mixing ($H^E = 0$) leads to the concept of "athermal" solutions.

The Scatchard-Hildebrand Equation

This equation attempts to quantify the excess enthalpy of mixing and takes the form

$$\overline{\Delta H}^M = (x_1 v_1 + x_2 v_2) \Phi_1 \Phi_2 A_{12} . \tag{4}$$

Volume fractions Φ_1 are defined in terms of molar volumes of components i as

$$\Phi_i = \frac{x_i v_i}{\sum_i x_i v_i} . \tag{5}$$

The interchange cohesive energy density A_{12} is related to the cohesive energy densities C by

$$A_{12} = C_1 + C_2 - 2C_{12} . \tag{6}$$

The cohesive energy density for unlike molecular interaction is defined as

$$C_{12} = (C_{11} C_{22})^{1/2} 1 \times 2(1 - l_{12}) . \tag{7}$$

Where l_{12} is a binary constant characteristic of a given solute-solvent pair and to a good approximation is independent of composition and varies little with temperature.

The expressions for the activity coefficients and partial molal heats of mixing of solute and solvent are then

$$\overline{\Delta H}_2^M = RT \ln \nu_2 = v_2 \Phi_1^2 ((\delta_1 - \delta_2)^2 + 2 l_{12} \delta_1 \delta_2) , \tag{8}$$

$$\overline{\Delta H}_1^M = RT \ln \nu_1 = v_1 \Phi_2^2 ((\delta_1 - \delta_2)^2 + 2 l_{12} \delta_1 \delta_2) . \tag{9}$$

Solubility parameters δ are defined by

$$\delta = C^{1/2} . \tag{10}$$

In the original Scatchard-Hildebrand theory $l_{12} = 0$. While l_{12} may be positive or negative, its magnitude is always small compared to unity. CHEUNG and ZANDER [10] and PRESTON and PRAUSNITZ [11] in their studies of solubilities in cryogenic solvents have indicated that even a small l_{12} on the order of 10^{-2} can have a large effect on ν_1 and ν_2, and hence on $\overline{H\Delta}^M$, especially if δ_1 and δ_2 are nearly the same. Later workers [12] have used experimental solubility data to calculate l_{12} values for twelve binary systems including the CH_4—CO_2 system.

Cohesive energy densities and solubility parameters can be estimated from

$$\delta = C^{1/2} = \left(\frac{(\Delta H^{VAP} - RT)^{1/2}}{V^L} \right) . \tag{11}$$

Equation (11) is truly valid only at relatively low temperatures where vapour pressures are low enough so that the vapour in equilibrium with the liquid is essentially ideal. This is true for CO_2 below its triple point but for CH_4, vapour pressures are considerable, and the effect of temperature has to be taken into account. CHEUNG and ZANDER [10] have expressed this temperature dependence in the form

$$\delta = C^{1/2} = (De^{-BT})^{1/2} \tag{12}$$

and have determined the constants D and B for CH_4. For heats of vaporization at different temperatures they have used the work of SILVERBERG and WENZEL [13] who fitted them on the basis of Nutting equation for latent heats:

$$\Delta H^{VAP} = KM(T_C - T)^n . \tag{13}$$

Table I lists the values of the various constants used in equations (12) and (13).

Table I

Constants for the determination of physical properties

Compound	M gm/g-mol	T_c °k	K cal/g(°K)^n	n	D cal/CC	B °K^{-1}
CH_4	16,04	191,1	26,94	0,347	4,394	0,003635
CO_2	44,01	304,2	14,43	0,392		

The Wilson Equation

As an alternative to regular solution approach which takes into account the non-randomness in liquid mixtures, WILSON [5] has introduced "Local volume fractions", and has obtained his expression for F^E as a logarithmic function of composition by arbitrarily substituting "local volume fractions" ξ_{ii} for overall volume fractions Φ_i in the Flory-Huggins equation for F^E. The equation is suitable for representing the excess free energy of mixing of completely miscible nonelectrolytes, with two or four activity coefficients and then the corresponding excess enthalpy and entropy may be conveniently derived. Heats of mixing are expressed as

$$\begin{aligned}\Delta\dot{H}^M = x_1 x_2 &\left[\frac{\Lambda_{12}}{x_1 + \Lambda_{12}x_2}(\lambda_{12} - \lambda_{11}) + \frac{\Lambda_{21}}{x_2 + \Lambda_{21}x_1}(\lambda_{12} - \lambda_{22})\right] - \\ &- x_1 x_2 T\left[\frac{\Lambda_{12}}{x_1 + \Lambda_{12}x_2} \cdot \frac{\partial}{\partial T}(\lambda_{12} - \lambda_{11}) + \right. \\ &\left. + \frac{\Lambda_{21}}{x_2 + \Lambda_{21}x_1} \cdot \frac{\partial}{\partial T}(\lambda_{12} - \lambda_{22})\right] + \\ &+ x_1 x_2 RT^2\left[\frac{\Lambda_{12}}{x_1 \times \Lambda_{12}x_2} - \frac{\Lambda_{21}}{x_2 + \Lambda_{21}x_1}\right] \times \\ &\times \left[\frac{1}{v_2}\left(\frac{\partial v_2}{\partial T}\right) - \frac{1}{v_1}\left(\frac{\partial v_1}{\partial T}\right)\right].\end{aligned} \tag{14}$$

Equation (14) may be split into three specific parts, whereby

$$\Delta H^M = \Delta H^M_* + \Delta H^M + \Delta H^M_V. \tag{15}$$

The term ΔH^M_* represents the heat of mixing when the energy parameters $(\lambda_{ij} - \lambda_{ii})$ and other variables are independent of temperature. ΔH^M_λ represents the correction for ΔH^M arising from the temperature dependence of the param-

eters $(\lambda_{ij} - \lambda_{ii})$. ΔH_V^M is the correction introduced by the variation with temperature of the volume ratio V_j/V_i.

ORYE and PRAUSNITZ [14] have introduced the two adjustable parameters Λ_{12} and Λ_{21} into the Wilson equation defined by

$$\Lambda_{12} = (V_2^L/V_1^L) \exp. [-(\lambda_{12} - \lambda_{11})/RT], \tag{16}$$

$$\Lambda_{21} = (V_1^L/V_2^L) \exp. [-(\lambda_{12} - \lambda_{22})/RT]. \tag{17}$$

JENSEN and KURATA [15] have shown that the Wilson equation is an excellent model for solid CO_2 solubility in liquid methane, ethane and n-butane, and that it provides a better model than do correlations based on regular solution theory. The authors have formulated fourth-order polynomials in temperature by the method of linear least squares to calculate solute and solvent liquid molal volumes.

$$V = D_0 + D_1 T + D_2 T^2 + D_3 T^3 + D_4 T^4 \tag{18}$$

least-square values of the constants are listed in Table II.

Table II

*Least-square constant to compute liquid molal volumes**

Component	D_0	D_1	D_2	D_3	D_4
CH_4	216,55	5,9317	$7{,}1338 \times 10^{-2}$	$-3{,}7484 \times 10^{-4}$	$7{,}4579 \times 10^{-7}$
CO_2	27,712	$-5{,}0755 \times 10^{-2}$	$9{,}7244 \times 10^{-4}$	$-4{,}3568 \times 10^{-6}$	$8{,}7729 \times 10^{-9}$

Volume cc/g-mol

* For CO_2 constants are valid from the liquid freezing point to 220 °K; for CH_4 constants are valid only to 180 °K.

JENSEN and KURATA have also used a nonlinear least squares analysis to fit experimental solid CO_2 solubility in liquid CH_4 to the Wilson equation for solubility and have found values of $(\lambda_{12} - \lambda_{11})$ and $(\lambda_{12} - \lambda_{22})$ which minimize the weighted sum of the squares of the difference between observed and calculated variables. The authors have found better agreement by considering temperature-dependence of the Wilson parameters expressed in terms of empirical constants α and β:

$$(\lambda_{12} - \lambda_{11}) = \alpha_1 + \alpha_2/RT, \tag{19}$$

$$(\lambda_{12} - \lambda_{22}) = \beta_1 + \beta_2/RT. \tag{20}$$

Equations (16) and (17) now become

$$\Lambda_{12} = (V_2^L/V_1^L) \exp. [-\alpha_1/RT - \beta_2/(RT)^2] , \quad (21)$$

$$\Lambda_{21} = (V_1^L/V_2^L) \exp. [-\beta_1/RT - \beta_2/(RT)^2] . \quad (22)$$

Least square values of the parameters and empirical constants are given in Table III.

Table III

Wilson equation parameters for solid CO_2 solubility in liquid CH_4

System	Two-parameter equation		Four-parameter equation			
	$(\lambda_{12}-\lambda_{11})$ cal/g-mol	$(\lambda_{12}-\lambda_{22})$ cal/g-mol	α_1 cal/g-mol	$\alpha_2 \times 10^{-3}$ cal/(g-mol)^2	β_1 cal/g-mol	β_2 cal/(g-mol)^2
CH_4-CO_2	521,05	661,32	739,99	−100,80	667,33	4,4382

Since equation (18) becomes invalid as the methane temperature, 191,1 K, is approached. JENSEN and KURATA have assumed the ratio V_i/V_j in equations (16), (17), (21) and (22) to be equal to the ratio at 180 K for temperatures greater than 180 K.

The BWR Equation

The Benedict, Webb and Rubin equation of state [6—9] was originally developed, primarily to permit the description of the phase behaviour of multicomponent hydrocarbon mixtures of relatively low molecular weight, is traditionally associated with these compounds and is considered to be the best available presently for the hydrocarbon system. The equation has appeared to researchers to be the most promising method for obtaining precise thermal data on mixtures. However, earlier workers [16—21], and others, have reported difficulties in the prediction of properties of hydrocarbon mixtures containing non-hydrocarbons, and in low-temperature applications.

The most recent, and perhaps so far the most significant contribution in the evolution process of developing the BWR equation of state is that afforded by BISHNOI and ROBINSON [22—24]. The authors have assimilated the observations of previous workers to formulate and test new mixing rules for the BWR parameters. In their development, they have followed a system of logic similar to that used by GUN [25] and CHUEH and PRAUSNITZ [26]. The rules contain a binary interaction parameter k_{ij} readily obtainable from information on binary interactions or other data available in the literature, namely, from experimental values of the second virial cross-coefficients. BISHNOI and

ROBINSON have also concluded in their study that their revised BWR parameters for CH_4, C_2H_6, C_3H_8 and H_2S, obtained by choosing specific volume as the dependent variable, rather than pressure (or compressibility factor) are more useful to correlate the volumetric properties and to calculate the fugacities of the liquid and gas phase at the saturation points.

Densities are calculated using the BWR equation of state

$$P = RTd + \left(B_0 RT - A_0 - \frac{C_0}{T^2}\right) d + (bRT - a)d^3 + \\ + a\alpha d^6 + \frac{cd^3(1 + \nu d^2) - \exp(-\nu d^2)}{T^2} . \tag{23}$$

Isothermal enthalpy departures are henceforth evaluated from

$$(H - H^0) = \left(B_0 RT - 2A_0 - \frac{4Co}{T^2}\right) d + (2bRT - 3a)\frac{d^2}{2} + \\ + 6a\alpha\frac{d^3}{5} + \frac{cd^2}{T^2}\left[3 \cdot \frac{1 - \exp(-\nu d^2)}{\nu d^2} - \right. \\ \left. - \frac{\exp(-\nu d^2)}{2} + \nu d^2 \exp(-\nu d^2)\right] . \tag{24}$$

In the ideal gas state there is no change in enthalpy upon mixing and hence

$$\Delta H^M = (H - H^0) - x_1(H - H^0)_1 - x_2(H - H^0)_2 . \tag{25}$$

Mixture enthalpies are then given by

$$H = (H - H^0) + x_1 H_1^0 + x_2 H_2^0 \tag{26}$$

where H_1^0 is the hypothetical ideal gas enthalpy of pure component i at a reference pressure of 1 atmosphere, based on the data of Din (27).

The revised mixing rules, for a binary mixture:

$$B_0 = [x_1 B_{01}^{1/2} + x_2 B_{02}^{1/2}] ,$$

$$A_0 = x_1^2 A_{01} + x_2^2 A_{02} + 2x_1 x_2 (A_{01} A_{02})^{1/2}(1 - k_{12}) ,$$

$$C_0 = x_1^2 C_{01} + x_2^2 C_{02} + 2x_1 x_2 (C_{01} C_{02})^{1/2}(1 - k_{12})^3 ,$$

$$b = (x_1 b_1^{1/3} + x_2 b_2^{1/2})^3 , \tag{27}$$

$$a = x_1 3a_1 + x_2 3a_2 + 3x_1 x_2(x_1 a_1^{1/3} + x_2 a_2^{1/3})(1 - k_{12})^{2/3} \cdot a_1^{1/3} a_2^{1/3},$$

$$c = x_1^3 c_1 + c_2^3 c_2 + 3x_1 x_2(x_1 c_1^{1/3} + x_2 c_2^{1/3})(1 - k_{12})^2 \cdot c_1^{1/3} c_2^{1/3},$$

$$\alpha = [x_1 \alpha_1^{1/3} + x_2 \alpha_2^{1/3}]^3,$$

$$v = [x_1 v_1^{1/2} + x_2 v_2^{1/2}]^2.$$

Bishnoi and Robinson's parameters for the BWR equation are given in Table IV.

Table IV

Parameters for the BWR Equation

Parameter	CH_4	CO_2
$B_0 \times 10^2$	4,3203053	3,2014927
A_0	1,8712416	1,8367101
$C_0 = 10^{-5}$	0,23500139	1,7602805
$b \times 10^3$	3,9787382	6,2536078
a	0,069197996	0,24204855
$c \times 10^{-4}$	0,30179295	1,9008120
$\alpha \times 10^5$	9,6835765	4,8784066
$v \times 10^3$	5,7118125	4,2808218
$R = 0{,}0825$		

Units: Atm, °K, lit/g-mol

Heat of mixing calculations

The Wilson Equation

The original two-parameter Wilson equation and the modified four-parameter equation are here used to compute heats of mixing of saturated liquid solutions of solid CO_2 in CH_4. Volume ratios V_j/V_i and coefficients of volume expansion $(dV_j/dt)/V_j$ are calculated from equation (18). As CH_4 approaches its critical temperature, 191.1 K, the temperature derivative dV/dT approaches infinity (Fig. 1). This difficulty is overcome by assuming the ratio $(dV/dT)/V$ to be constant for temperatures equal to or greater than 180 K, i.e.

$$\frac{1}{V} \cdot \frac{dV}{dT} = \alpha_0, \qquad T \geq 180 \text{ K}. \tag{28}$$

Integrating

$$V = V_0 \exp \alpha_0(T - 180), \qquad T \geq 180 \text{ K}. \tag{29}$$

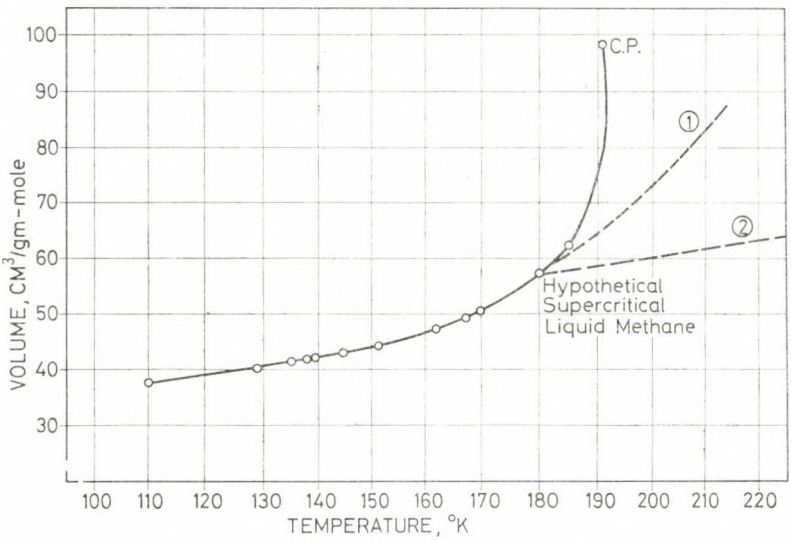

Fig. 1. Saturated liquid volumes of methane

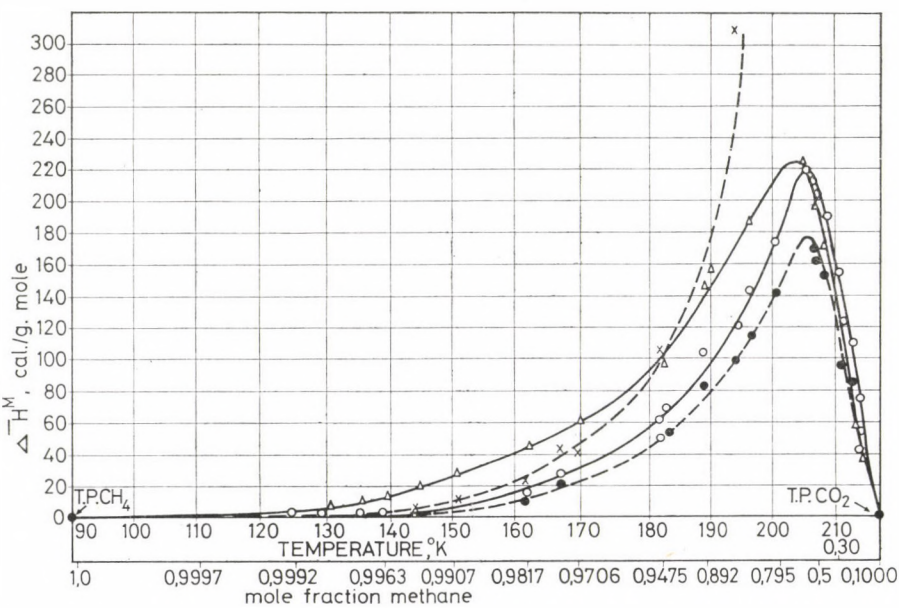

Fig. 2. Heat of mixing for the saturated liquid solution of carbon dioxide in methane in the three-phase region. ▲ Computed from the BWR equation of state; ○ Two-parameter Wilson equation; • Four parameter Wilson equation; × Modified Scatchard–Hildebrand equation $l_{12} = -0.02$

Where $\alpha_0 = 1.25063 \times 10^{-2}\ K^{-1}$
and $V_0 = 57.0288\ cm^3/g\text{-mol}$

are respectively the coefficient of volume expansion and the molal volume of liquid methane at 180 K. This assumption produces curve *1*, (Fig. 1), and this extension for temperatures above 180 K makes a better fit with the general shape of the curve compared to curve *2*, drawn on the assumption that the volume ratio of CH_4 with respect to CO_2 is constant. Calculated results are listed in Table V and plotted in Fig. 2. There is a marked similarity between these curves and the locus of triple points, (Fig. 3).

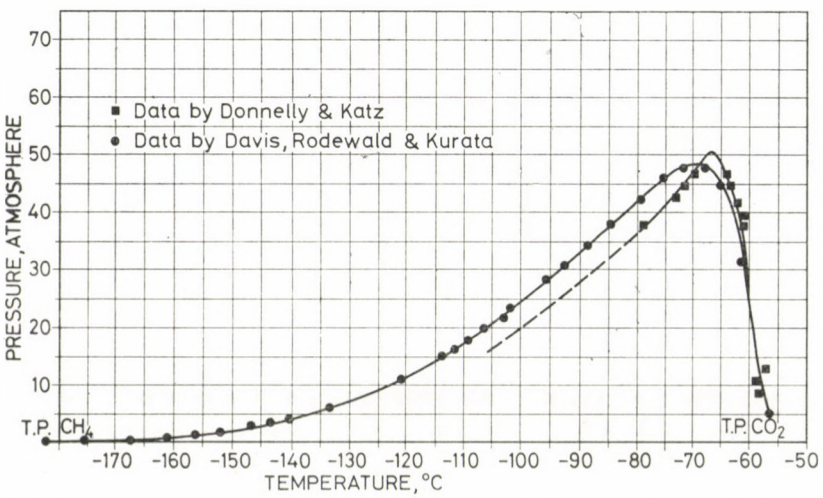

Fig. 3. Locus of triple points (solid-liquid-vapour) of the methane-carbon dioxide system

Modified Scatchard—Hildebrand Equation

For temperatures greater than 180 K equations (12) and (29) are respectively used to estimate solubility parameters and molal liquid volumes of hypothetical supercritical liquid CH_4. Mixing heats are calculated from partial quantities by

$$\Delta H^M = x_1 \overline{\Delta H}_1^M + x_2 \overline{\Delta H}_2^M . \tag{30}$$

Calculated values are listed in Table V. Figures 4 and 5 illustrate the variation with temperatures of the calculated solubility parameters and partial molal heats of mixing of both solute and solvent.

Table V

Heats of Mixing of Saturated Liquid Solutions of Solid CO_2 in CH_4

T °K	P Atm.	X M. F. CH_4	ΔH^M cal/g-mol				
			WILSON Eq.		MOD. SC.-Hild. Eq.		BWR
			a	b	l_{12} 0,03	l_{12} —0,02	k_{12} 0,05
110,7		0,9997	0,1022	0,2201	0,3544	0,2774	
124,9		0,9992	0,3298	0,6105	0,9824	0,7929	
125,2		0,9992	0,3309	0,6110	0,9833	0,7942	
129,6	3,54	0,9984	0,6882	1,227	1,994	1,626	7,543
135,2	5,00	0,9975	1,132	1,938	3,176	2,623	9,528
138,7		0,9971	1,360	2,273	3,734	3,108	
139,4	6,30	0,9963	1,738	2,892	4,775	3,981	14,04
144,5	7,80	0,9942	2,856	4,593	7,646	6,452	20,53
150,4	10,00	0,9907	4,875	7,531	12,62	10,80	28,43
151,4		0,9901	5,254	8,061	13,50	11,59	
162,0	17,00	0,9817	11,33	16,13	26,81	23,69	45,31
167,2		0,9686	20,57	28,34	47,98	43,05	
169,9	22,00	0,9706	20,77	28,07	46,41	41,98	61,27
180,0		0,9450			100,09	93,67	
182,2	32,50	0,9415	49,18	62,28	160,2	157,2	92,21
183,2		0,9340	54,63	69,07	179,2	175,8	
183,2		0,9415	49,72	62,77	159,6	156,5	
189,3	38,50	0,8920	83,71	104,71	278,3	272,9	145,43
194,6		0,8740	98,80	122,09	313,8	307,7	
196,9	45,00	0,8461	114,89	141,60	372,8	365,5	186,57
199,8	46,95	0,8030					201,24
201,3	48,00	0,7950	141,52	173,45	471,1	461,7	240,14
206,2	47,50	0,574	176,15	217,97	798,8	782,6	217,18
207,3	46,20	0,5000	169,65	210,97	859,0	841,6	198,50
207,6	46,00	0,4570	161,69	201,92	880,5	862,6	189,34
209,0	43,50	0,4000	151,17	189,36	888,6	870,5	170,60
210,4	40,00	0,3000	121,38	153,79	846,6	829,3	130,90
211,2	35,00	0,2320	95,79	122,84	766,1	750,4	178,90
212,6	27,50	0,2000	84,72	108,97	710,4	695,8	172,60
213,7	24,00	0,1350	56,36	73,91	556,7	545,2	54,94
214,3	15,50	0,1000	40,52	54,00	447,2	438,0	39,50

(*a*) Four-Parameter Wilson Equation
(*b*) Two-Parameter Wilson Equation

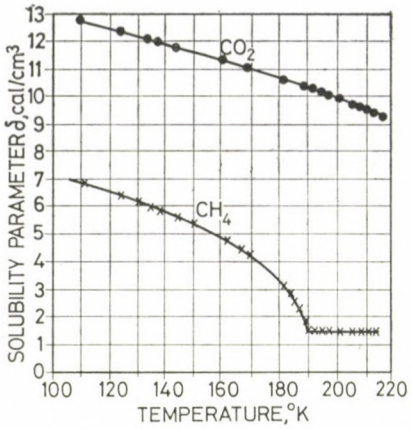

Fig. 4. Solubility parameters

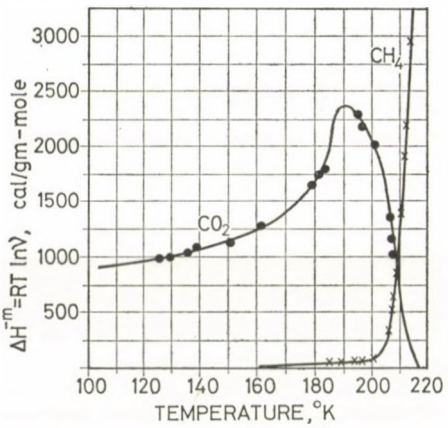

Fig. 5. Partial molal enthalpies

The BWR Equation

For CH_4 above its critical temperature, direct application of the BWR equation has resulted in an abrupt reversal in the sign of V, from + to − values, inducating that the properties of pure CH_4, as such, do not really represent the actual behaviour of this component in the mixture as far as the equation is concerned. As a first attempt to improve the equations ability to estimate excess enthalpies in this region, the gas has been assumed to behave as a hypothetical supercritical liquid with vapour pressures extrapolated from the plot of ln P^0 VS $1/T$. This has produced an improvement. However, far better results have been obtained by the use of equation (29) to calculate the densities

Table VI

Saturated phase enthalpies in the Three-phase

T °C	P Atm.	X M. F. CH_4	cal/gm-mole				
			$(H-H_0)$	$H°$		H	
			Mixture	CH_4	CO_2	SOL'N	
T. P.							
−182,48	0,1154	1,000				820	
−143,55	3,54	0,9984	−1989	3210	7050	1227	
−137,95	5,00	0,9975	−1919	3250	7100	1341	
−133,75	6,30	0,9963	−1872	3280	7120	1422	
−128,65	7,80	0,9942	−1821	3340	7150	1541	
−122,75	10,0	0,9907	−1768	3370	7210	1638	
−111,15	17,0	0,9817	−1671	3470	7310	1869	
−103,25	22,0	0,9706	−1612	3560	7400	2061	
−90,95	32,5	0,9415	−1523	3640	7500	2343	
−83,85	38,5	0,8920	−1541	3700	7550	2575	Liquid-
−82,94	39,26	0,8780	−1565	3710	7570	2616	phase
−76,25	45,0	0,8461	−1537	3750	7620	2809	
−73,33	46,95	0,803	−1620	3770	7650	2914	
−71,85	48,0	0,795	−1588	3800	7670	3005	
−67,94	47,84	0,655	−1992	3820	7700	3167	
−66,95	47,5	0,574	−2248	3830	7710	3235	
−65,85	46,2	0,500	−2478	3840	7720	3302	
−65,55	46,0	0,457	−2619	3845	7725	3333	
−64,15	43,5	0,400	−2792	3900	7740	3412	
−62,75	40,0	0,300	−3120	3855	7745	3458	
−63,06	39,47	0,260	−3269	3860	7750	3470	
−61,95	35,0	0,232	−3270	3870	7760	3588	

of hypothetical liquid CH_4. These values (Table V) fit well with the rest of the data, produce a smooth curve, and are in qualitative agreement with values predicted by the Wilson equation (Fig. 2).

Saturated phase enthalpy diagrams

In Table VI are tabulated the saturated liquid and vapour phase enthalpies using the BWR equation of state. The data are plotted as an enthalpy-temperature, and enthalpy composition diagrams in the univariant $S-L-V$ equilibrium region (Figs 6 and 7).

region computed by the BWR Equation of state

T °C	P Atm.	X M. F. CH_4	cal/gm-mole				
			$(H-H^\circ)$	H_θ		H	
			Mixture	CH_4	CO_2	SOL'N	
−60,55	27,5	0,200	−3348	3875	7770	3643	
−59,45	24,0	0,135	−3646	3900	7780	3610	
−58,85	15,5	0,100	−3759	3910	7785	3639	
−56,6	5,112	0,000				4000	
−182,48	0,1154	1,000				2900	
−132,22	6,70	0,9988	−127,34	3300	7150	3177	
−107,56	19,0	0,9937	−292,22	3500	7650	3234	
−97,28	27,0	0,9892	−399,83	3600	7450	3242	
−95,56	28,0	0,9828	−412,41	3610	7460	3264	
−89,17	34,0	0,9730	−506,06	3650	7510	3248	
−84,44	38,2	0,9633	−569,41	3700	7550	3272	
−79,50	42,66	0,9435	−654,4	3720	7600	3285	Vapour-
−67,44	48,0	0,8827	−656,11	3820	7700	3619	phase
−63,06	39,47	0,825	−477,53	3850	7750	4055	
−60,05	27,22	0,80	−288,31	3870	7770	4362	
−59,0	16,6	0,70	−187,08	3900	7780	4876	
−58,5	12,5	0,60	−158,30	3905	7790	5301	
−58,0	10,21	0,50	−146,75	3910	7800	5708	
−57,5	8,17	0,40	−132,73	3910	7800	6111	
−57,3	6,80	0,30	−125,37	3915	7805	6513	
−57,0	5,78	0,20	−120,41	3915	7810	6911	
−56,8	5,44	0,10	−128,60	3920	7815	7297	
−56,6	5,112	0,00				7663	

Conclusions

Figure 2 is a graphical comparison of the predicted heats of mixing of the saturated liquid-phase in the $S-L-V$ equilibrium region. Their degree of accuracy may not be fully determined until experimental data at these low temperatures become available. Until then, the high engineering accuracy with which both thermodynamic models have been used to predict the solubility of solid CO_2 in CH_4, and the relative qualitative agreement between the differently-predicted values, lend further confidence to the feasibility of utilizing the BWR equation in its new form, to correlate volumetric and thermo-

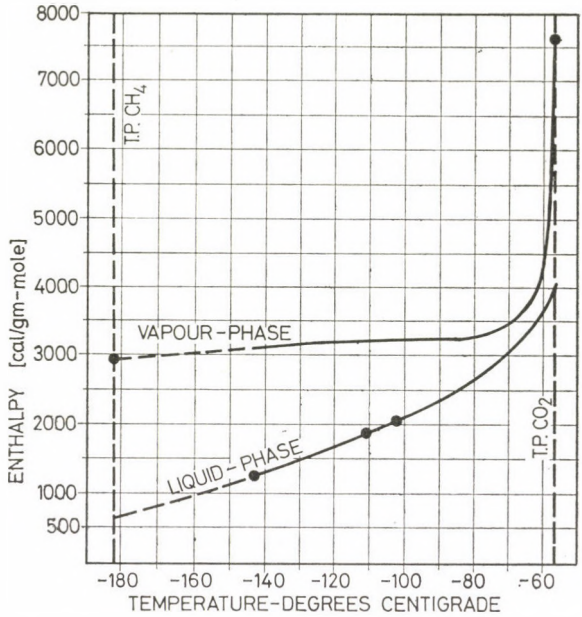

Fig. 6. Enthalpy-temperature relationship in the three-phase region of the CH_4-CO_2 system

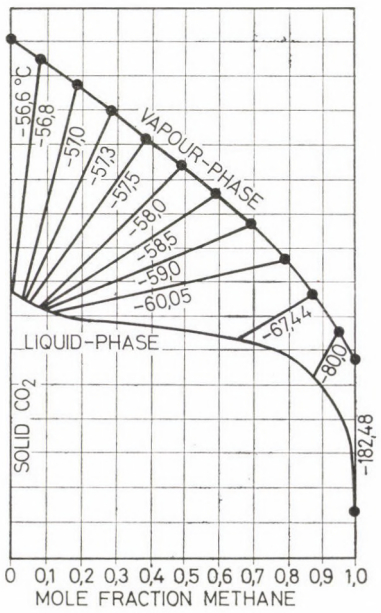

Fig. 7. Enthalpy-composition diagram for the CH_4-CO_2 system in the three-phase region

dynamic properties of light hydrocarbons, including non-hydrocarbon constituents, at such low temperatures. For CH_4 above its critical temperature, equations (8) and (9), derived for solutions of liquids mixing with no volume change, predict heats of mixing (Fig. 2) jumping to high values for two major limitations:

1 — The volume of the gas decreases enormously on mixing isothermally with the liquid

2 — The definition of activity coefficient as given is not directly applicable to a component above its critical temperature (see Appendix).

APPENDIX

Regular Solution Theory for Gas-solid Heats of Mixing

Various authors [28—31] and others have succesfully attempted to use regular solution theory to generalize correlations for the solubility of gases in liquids. From these correlations it is possible to make estimates of the heat of solution of gases in liquids, as may be required in enthalpy balance calculations in certain phase separation problems. These correlations may be further generalized to obtain an interpretation of the behaviour of gases in equilibria where solids, liquids and gases are involved.

For CH_4 above its critical temperature, component *1* is now a gas, while pure component *2* is in the solid state. For the two components to form a liquid mixture it is necessary to consider the mixing between a hypothetical subcooled liquid CO_2 with a hypothetical supercritical liquid CH_4. The difficulty encountered when applying regular solution theory (which assumes no volume change) may be circumvented by considering the mixing process as an isothermal, isobaric thermodynamic process in a series of two hypothetically separate steps:

Step I

1. In the first hypothetically separate process the gas is compressed isothermally at temperature T from the initial pressure P and molar volume V_1^g to a hypothetical state having a liquid-like volume $V_{1'}^L$, which is practically equal to its partial molar volume $\overline{V}_1^L$ in the liquid solution and to pressure P_1 corresponding to its partial pressure in the mixture.

2. This change is accompanied by an isothermally small expansion of the solvent from the initial pressure P and molar volume V_2^L to its partial molar volume, $\overline{V}_2^L$ in the liquid solution, and its partial pressure P_2.

3. These hypothetically separate processes occur with an overall net result that the sum of the partial pressures of solute and solvent is equal to the initial pressure or the pressure P of the equilibrium solution, i.e.

$$P_1 + P_2 = P. \tag{31}$$

Step II

The hypothetical liquid-like fluid is dissolved into the hypothetical liquid solvent isothermally at temperature T and isobarically at pressure P to the equilibrium mixture.

Step I is accompanied by free energy and enthalpy changes of the solute:

$$\Delta F_1(\mathrm{I}) = F_{1'}^L - F_1^g \int_P^{P_1} = V_1 dP = RT \ln f_1^{0L}(P_1)/f_0^{0g}(P), \tag{32}$$

$$\Delta H_1(\mathrm{I}) = H_{1'}^L - H_1^g = \Delta F_1(\mathrm{I}) + T\Delta S_1(\mathrm{I}). \tag{33}$$

Step (II) is also accompanied by a free energy and an enthalpy change:

$$\overline{\Delta F}_1^M(\mathrm{II}) = \overline{F}_1^L - F_1^L = RT \ln \nu_1 x_1 = RT \ln f_1^L(P_1)/f_1^{0L}(P_1) \tag{34}$$

where x_1 is the mole fraction of the gaseous solute in the liquid solvent, and ν_1 is its activity coefficient referred to the pure hypothetical liquid as a standard state. The equation of equilibrium is thus

$$\Delta F_1(\mathrm{I}) + \overline{\Delta F}_1^M(\mathrm{II}) = 0\,. \tag{35}$$

The activity coefficient of the gaseous solute referred to the pure hypothetical liquid must now be expressed in terms of partial molar volumes

$$\mathrm{RT} \ln \nu_1 = \overline{V}_1^L \Phi_2^2 \left[(\delta_1 - \delta_2)^2 + 2l_{12}\,\delta_1\delta_2\right] = \overline{\Delta H}_1^M(\mathrm{II}) \tag{36}$$

where Φ_2 is the volume fraction expressed in terms of the partial molar volumes.

The gas-phase and condensed fluid properties can be obtained from tabulated properties of the pure component, etc.

PRAUSNITZ [29] has suggested a method for estimating partial molar volumes. Even when a gas is condensed to a liquid-like volume, it will, upon dissolution in at least some solvents, experience a furher small volume change. However, this volume change is very much smaller than that corresponding to step I, may be neglected, and for estimation purposes equation (29) may be used.

The partial molal heat of mixing of the gas is now given by

$$\overline{\Delta H}_1^M = H_1^{-L} - H_1^g = \Delta H_1(\mathrm{I}) + \overline{\Delta H}_1^M(\mathrm{II})\,. \tag{37}$$

$\overline{\Delta H}_1^M(\mathrm{II})$ is always positive (endothermic), but the enthalpy change ΔH_1 (I) accompanying the isothermal compression of the gas to a liquid-like volume is negative and has the effect of reducing the partial molal enthalpies of CH_4 predicted by equation (9).

REFERENCES

1. HILDEBRAND, J. H.—SCOTT, R. L.: The Solubility of Non-Electrolytes. Third ed., Reinhold Publishing Corporation, New York 1950
2. HILDEBRAND, J. H.—PRAUSNITZ, J. M.—SCOTT, R. L.: Regular and Related Solutions. The Solubility of Gases, Liquids and Solids. Van Nostrand Reinhold Company, New York 1970
3. FLORY, P. J.: *J. Chem. Phys.* **10** (1942), 51
4. HUGGINS, M. L.: *Ann. N. Y. Acad. Sci.* **43** (1942), 1
5. WILSON, G. M.: *J. Am. Chem. Soc.* **86** (1964), 127
6. BENEDICT, M.—WEBB, G. B.—RUBIN, L. C.: *J. Chem. Phys.* **8** (1940), 334
7. BENEDICT, M.—WEBB, G. B.—RUBIN, L. G.: *J. Chem. Phys.* **8** (1942), 747
8. BENEDICT, M.—WEBB, G. B.—RUBIN, L. C.: *Chem. Eng. Prog.* **47** (1951), 449
9. BENEDICT, M.—WEBB, G. B.—RUBIN, L. C.: *Chem. Eng. Prog.* **47** (1951), 571
10. CHEUNG, H.—ZANDER, E.: *Chem. Eng. Prog. Symp.* Series **88** (1968), 64
11. PRESTON, G. T.—PRAUSNITZ, J. M.: *Ind. and Eng. Chem. Process.* Des. Dev. **9** (1970), 264
12. PRESTON, G. T.—FUNK, E. W.—PRAUSNITZ, J. M.: *J. Phys. Chem.* **75** (1971), 2345
13. SILVERBERG, P. M.—WENZEL, L. A.: *J. Chem. Eng. Data* **10** (1965), 363
14. ORYE, R. V.—PRAUSNITZ, J. M.: *Ind. Eng. Chem.* **57** (1965), 18
15. JENSEN, R. H.—KURATA, F.: *A IChEJ.* **17** (1971), 357
16. EAKIN, B. E.—ELLINGTON, R. T.: Thermodynamics and Transport Properties of Gases Liquids and Solids (Symposium on Thermodynamic Properties). Am. Soc. Mech. Eng., McGraw-Hill, New York, February 1959
17. STOTLER, H. H.—BENEDICT, M.: *Chem. Eng. Prog. Symp. Ser.* **49** (1953), 25
18. CULLEN, E. J.—KOBE, K. A.: *A. IChEJ.* **1** (1955), 452
19. BARNER, H. E.—ADLER, S. B.: *Hydrocarbon Process* **47** (1968), 150
20. KAMINISHI, G. I.— ARAI, Y.—MAEDA, S.: *J. Chem. Eng. Japan* **1** (1968), 109
21. ORYE, R. V.: *Ind. and Eng. Chem. Process Design and Dev.* **8** (1969), 579
22. BISHNOI, P. R.—ROBINSON, D. B.: *Canadian J. Chem. Eng.* **49** (1971), 642
23. BISHNOI, P. R.—ROBINSON, D. B.: *Ind. and Eng. Chem. Process, Design and Dev.* **50** (1972), 101
24. BISHNOI, P. R.—ROBINSON, D. B.: *Ind. and Eng. Chem. Process, Design and Dev.* **50** (1972), 506
25. GUN R. D.: M. Sc. Thesis, Chem. Eng. Dept. Univ. of California, 1958
26. CHUEH, P. L.—PRAUSNITZ, J. M.: *Ind. Eng. Chem. Fund.* **6** (1967), 492
27. DIN, F.: Thermodynamic Functions of Gases, Volumes 1 and 3. Butterworths Scientific Publications, London 1956 and 1961

28. Chao, K. C.—Seader, J. D.: *AIChEJ.* **1** (4): (1961)
29. Prausnitz, J. M.: *AIChEJ.* **4** (1958), 269
30. Prausnitz, J. M.—Edmister, W. C.—Chao, K. C.: *AIChEJ.* **6** (1960), 214
31. Prausnitz J. M. Shair, F. H.: *AIChEJ.* **7** (1961), 682

Enthalpiebeziehungen für ein festes Kohlendioxid enthaltendes gesättigtes Methan-Kohlendioxid System von Kryogenphasenkennwerten. — Das mit CO_2 verunreinigte Erdgas kann durch Behandlung bei niedriger Temperatur — durch Ausfrieren des CO_2 — wirtschaft lich gereinigt werden. Die Ausfrierungstechnik ergibt eine bessere Raffinage, als andere übliche Raffinationsverfahren. Deshalb wurde das System CH_4-CO_2 bei den Kryogenphasenkennwerten eingehend untersucht. Die in der Behandlung bei niedriger Temperatur immanenten potentiellen Möglichkeiten können nur im Fall ausgenützt werden, wo die gültigen reellen thermodynamischen Angaben im Behandlungsbereich zur Verfügung stehen. Das Hauptanliegen der Abhandlung ist die Demonstration einiger brauchbaren thermodynamischen Angaben. Dieselben wurden analytisch ermittelt unter Berücksichtigung der reellen Beziehungen, die zur Berechnung der Ausfrierungstechnik geeignet sind.

Acta Technica Academiae Scientiarum Hungaricae, Tomus 91 (3—4), pp. 393—397 (1980)

SOME SPECIAL CASES OF INEXTENSIONAL DEFORMATIONS OF SHALLOW SHELLS

P. CSONKA*
DOCTOR OF TECHN. SC.

[Manuscript received 8th April, 1980]

Certain instances for the inextensional deformations of shallow shells are dealt with, where the differential equations and the functions characterizing the deformations are of extraordinarily simple form in spite of the fact that the flexural rigidity of the shell wall is also taken into consideration.

1. Introduction

Based on the theory of shallows shells certain cases are treated in the following where the differential equations and the functions describing the inextensional deformation pattern of the shell are of extraordinarily simple structure.

In analysing the problem it is assumed that the shell material cannot expand in the lateral direction and the flexural rigidity of the shell is constant along the whole extent of the shell.

2. Fundamental relationships

The investigations are carried out in an orthogonal system of coordinates $O(x, y, z)$ whose z-axis is vertical with downwards positive direction. In this system of coordinates the form of the shell is characterized by shape function

$$z = z(x, y), \tag{1}$$

the specific projective value of the uniformly distributed vertical load acting on the shell by load function

$$\overline{p} = p(x, y), \tag{2}$$

the stress pattern of the shell by stress function

* Prof. Dr. P. Csonka, Bartók B. út 31, H-1114 Budapest, Hungary

$$F = F(x, y)\,, \tag{3}$$

and the vertical displacement of points of the middle surface of the shell by displacement function

$$w = w(x, y)\,. \tag{4}$$

Let us denote the wall thickness of the shell with t, the Young's modulus of elasticity of the shell material with E, the tensile stiffness of the shell with D, and the bending stiffness with K where

$$D = Et, \qquad K = \frac{Et^3}{12}\,. \tag{5}$$

The projected stress resultants $\overline{N}_x$, $\overline{N}_{xy}$, $\overline{N}_y$ of the x, y direction are in relation with the second derivatives of the stress function F

$$\overline{N}_x = \frac{\partial^2 F}{\partial y^2}\,, \qquad \overline{N}_{xy} = -\frac{\partial^2 F}{\partial x \cdot \partial y}\,, \qquad \overline{N}_y = \frac{\partial^2 F}{\partial x^2}\,, \tag{6}$$

and the projected moments $\overline{M}_x$, $\overline{M}_{xy}$, $\overline{M}_y$ are in relation with the second derivatives of the displacement function w:

$$M_x = K\frac{\partial^2 w}{\partial x^2}\,, \qquad M_{xy} = K\frac{\partial^2 w}{\partial x \cdot \partial y}\,, \qquad M_y = K\frac{\partial^2 w}{\partial y^2}\,. \tag{7}$$

According to Wlassow's theory on shallow shells the statical behaviour of shells subjected only to vertical loads can be described by two fourth-order differential equations. These equations read as follows

$$\begin{aligned} &\Box F - K\triangle\triangle F + \overline{p} = 0\,, \\ &\Box w + \triangle\triangle F = 0 \end{aligned} \tag{8}$$

wherein the meaning of the operators $\triangle$ and $\Box$ are as follows

$$\begin{aligned} \triangle &= \frac{\partial^2}{\partial x^2} + \frac{\partial^2}{\partial y^2}\,, \\ \Box &= \frac{\partial^2 z}{\partial x^2} \cdot \frac{\partial^2 z}{\partial y^2} - 2\,\frac{\partial^2 z}{\partial x \cdot oy} \cdot \frac{\partial^2}{\partial x \cdot \partial y} + \frac{\partial^2 z}{\partial y^2} \cdot \frac{\partial^2}{\partial x^2}\,, \end{aligned} \tag{9}$$

respectively.

In solving the differential equations (7), two conditions can and should be satisfied along the shell edge.

3. Basic formulae of the inextensional deformation

The deformation of the shell may be considered as inextensional when the linear elements of the middle surface do not undergo any change in length under the effect of the load. In such cases, it is evident that:

$$\overline{N}_x = 0\,, \quad \overline{N}_{xy} = 0\,, \quad \overline{N}_y = 0\,, \tag{10}$$

Since, in accordance with formulae (6), the membrane forces $\overline{N}_x$, $\overline{N}_{xy}$, $\overline{N}_y$ are the second derivatives of the stress function F, from Eq. (10) follows that in case of inextensional deformation the function F cannot be but the linear function of the place coordinates. Consequently, the preliminary condition of an inextensional deformation is that the stress function should be of the form

$$F = Ax + By + C \tag{11}$$

which, by omitting the linear terms as insignificant from the point of view of the membrane forces, reads

$$F = 0\,. \tag{12}$$

When inextensional deformation is present, the differential equations (8) of the theory of the shallow shells can be put into the following simpler form:

$$\begin{aligned} -K \triangle\triangle w + \overline{p} &= 0\,, \\ \square w &= 0\,. \end{aligned} \tag{13}$$

In cases where the shell surface is not subjected to any load, that is, if

$$\overline{p} = 0\,,$$

the conditions (13) of the inextensional deformation get a still simpler form:

$$\begin{aligned} \triangle\triangle w &= 0\,, \\ \square w &= 0\,. \end{aligned} \tag{14}$$

In such cases only the edge of the shell structure is attacked by loads, namely, by couples.

The formulae (13) and (14) hold true also for finite K-values.

4. Examples

Below, a few simple examples of inextensional deformation are presented. For all of these examples it is assumed that

$$\bar{p} = 0\,, \tag{15}$$

thus, the conditions of the deformation are controlled by formulae (14).

Example 1

If the shape function of the shell has the form

$$z = Ax^2 + Bxy + Cy^2$$

wherein A, B and C are constant values, the displacement functions satisfying condition (14) are as follows:

$$w = Bx^2 + 2(A + C)xy + By^2$$

and

$$w = (B^2 - AC)x^3 + 3(A^2 + BC)x^2y + (C^2 + AB)xy^2 + (B^2 - AC)y^3.$$

It is evident that the linear combinations of the above displacement functions also satisfy conditions (14).

Example 2

If the shape function of the shell is

$$z = A(x^2 + y^2), \qquad A = \text{const.},$$

so, the conditions of the inextensional deformation (14) will be fulfilled in all cases where the displacement function w is biharmonic.

Example 3

In case where the form of the shape function is

$$z = Ax^3 + 3Bx^2y + 3Cxy^2 + Dy^3$$

wherein A, B, C and D are constant, conditions (14) of the inextensional deformation satisfy the following displacement functions and also their combinations:

$$w = (B^2 - AC)^2 + (BC - AD)xy + (C^2 - BD)y^2$$

and

$$w = (3ABC - 2B^3 - A^2D) + 3(2AC^2 - B^2C - 2ABD)x^2y -$$
$$- 3(2B^2D - BC^2 - ACD)xy^2 + (3BCD - 2C^3 - AD^2)y^3\,.$$

Example 4

In cases where the form of the shape function is

$$z = A(x^4 + y^4), \qquad A = \text{const.},$$

the displacement function satisfying conditions (14) is as follows:

$$w = B(x^4 - y^4), \qquad B = \text{const.}$$

Note

In all cases of the above examples the conditions (14) of inextensional deformation will also be fulfilled if the functions z and w interchange their roles.

REFERENCES

1. Flügge, W.: Statik und Dynamik der Schalen. Springer Verlag, Berlin—Göttingen—Heidelberg 1934
2. Wlassow, W. S.: Allgemeine Schalentheorie und ihre Anwendung in der Technik, Akademie Verlag, Berlin 1958
3. Bölcskei, E.: Theory of Shallow Shells and its Use in Practice. *Scientific Publications of the Technical University of Building Industry and Transportation* **6** (1966), No. 5/6 (In Hungarian)
4. Kollár, L.: Inextensional Deformations of Shells. *Építés- és Építészettudomány* **3** (1971), 19—38 (In Hungarian)

Einige Spezialfälle der dehnungslosen Formänderung von flachen Schalen. — Es werden einige Fälle der dehnungslosen Formänderung flacher Schalen behandelt, wo sich die den Formänderungszustand beschreibenden Funktionen und Differentialgleichungen außergewöhnlich einfach gestalten, obwohl die Biegefestigkeit der Schalen nicht vernachlässigt wird.

Acta Technica Academiae Scientiarum Hungaricae, Tomus 91 (3—4), pp. 399—409 (1980)

ADAPTIVE PLANNING OF ELECTRIC POWER DISTRIBUTION NETWORKS AND OF THEIR COMPLEX CONTROL ENGINEERING SUBSYSTEMS; INTERACTIVE EFFECTS

M. SZANISZLÓ*
CAND. OF TECHN. SCI.

[Manuscript received April 8, 1980]

The paper presents an integrated planning system of distribution network, operation control and control engineering system. A new adaptive method for long-term planning of distribution network and control engineering is described which is adaptable to external and internal changes. Adaptivity is extended to process, model, algorithm, network and control engineering. As a model for planning a distribution network control engineering system — as a practical example — the planning of computerized telecontrol systems of regional dispatching centres is presented. Based on the analysis of interactions an increasing interaction between network and control engineering is experienced. The new control engineering subsystems have a reducing effect on the overall costs, and outage duration, result in increased network utilization and reliability and, finally, accomplish complex system control of distribution networks. The consideration of interactions yield improved system parameters.

1. Introduction, cybernetics of distribution networks

Significant achievements have taken plan in the methods of solving certain tasks encountered in the planning of power distribution networks, mainly in the field of deterministic optimization methods. A detailed survey of publications was given in previous papers (21, 23), where also the basic concepts of the "development and planning system" have been defined:

$$DP_N = \{I, G, M, P\}$$

consisting of the following subsystems:

I = basic investigations,
G = guiding principles,
M = methods,
P = process of planning.

So far, few publications have dealt with the complete planning system and, within this scope, with the process of planning, which is of great practical and theoretical importance owing to the constraints imposed by the restricted

* Dr. M. Szaniszló, Institute for Electrical Power Research, H—1368 Budapest, POB 233, Hungary

capacities available for planning, execution and operation, therefore, our scientific research work has partly been carried out in this direction.

In order to obtain a complex and coordinated development of a network, also the development and planning of operation control and its new control engineering subsystems (complex automation, telecontrol, telecommunication, computer, ripple control) are required.

Based on the recognition of the ever increasing interactive effects, instead of sequential planning of associated subsystems, the aim of integrated planning has been set, together with the elaboration of the DP (development and planning system) for the mentioned subsystems.

A power distribution network, operation control and control equipment are regarded as constituting a cybernetic system. The planning system is investigated from the viewpoint of long-term planning.

With the aim of improving the "satisfactory" and "optimizing" methods followed in the planning of distribution networks and control equipment, a new method termed "adaptive planning" has been formulated, which takes into consideration the uncertainties of the input data, and adapts itself rationally to the external and internal changes. The terms "adaptive planning" and "adaptivity" are equally referred to processes, models, algorithms, networks and control engineering.

The interactions of network and control engineering are analysed, with special respect to new elements which reduce the resultant cost and increase the reliability of operation.

In the case of steadily developing systems, the adaptivity of a system can be increased by improving the adaptivity of the planning system itself, whereby a dynamic equilibrium is ensured.

The bases of the research-development planning system of the distribution network control system are like to FT_H.

2. Planning system

Plans covering different periods of time satisfying different functions and of different orientations have to be prepared, systemized according to groups, based on their interrelations.

Based on Figure 1, the integrated planning system ("S") is defined in the following way:

$$S = \{DP, CP, IP, IE\}$$

where

DP = set of elements of development and planning system,
CP = set of concrete long-term plans,
IP = set of investment-oriented plans,
IE = set of interrelations (connections).

Further:

$$DP = \{DP_N, DP_O, DP_C, DP_M\}$$

and

$$CP = \{CP_N, CP_O, CP_C, CP_M\}$$

where

$$KT = \{SE, PP\},$$

SE = set of concrete long-term plans,
PP = set of project-oriented plans.

In order to analyse the interaction and feedback effects, in Figure 1 the realization (RE), the concrete systems already in service (CS) and the environmental system (E) are shown.

It is appropriate to prepare the plans for the control system (system plans) with a dynamical approach, according to and simultaneously with the long-term network development plan. This means the elaboration of new models and methods: see Section 4.

3. Adaptive planning

Three main types of planning are distinguished: satisfactory, optimizing and adaptive.

The *satisfactory* type of planning does not use any mathematical models, planning is based on professional skill. Although the analyses are usually aided by computer background.

The *optimizing* type of planning applies mathematical models and methods based on simplifying assumptions and solve partial planning tasks by searching for the extreme values of target functions usually minimizing present-value costs).

As early as in the preparation stage, several uncertainties and changes may occur preparing the plans for a concrete project especially in more advanced stages, of planning, e.g.

— uncertainties of basic data,
— environmental changes,
— variations within the investigated system.

The *adaptive* planning is a synthesis of already developed planning methods, but additionally, it contains new elements in order to enhance adaptability and ensure dynamic equilibrium of the plan.

By adaptability the capability of reacting to external or internal changes by a suitable response is understood. The degree of adaptivity may be different,

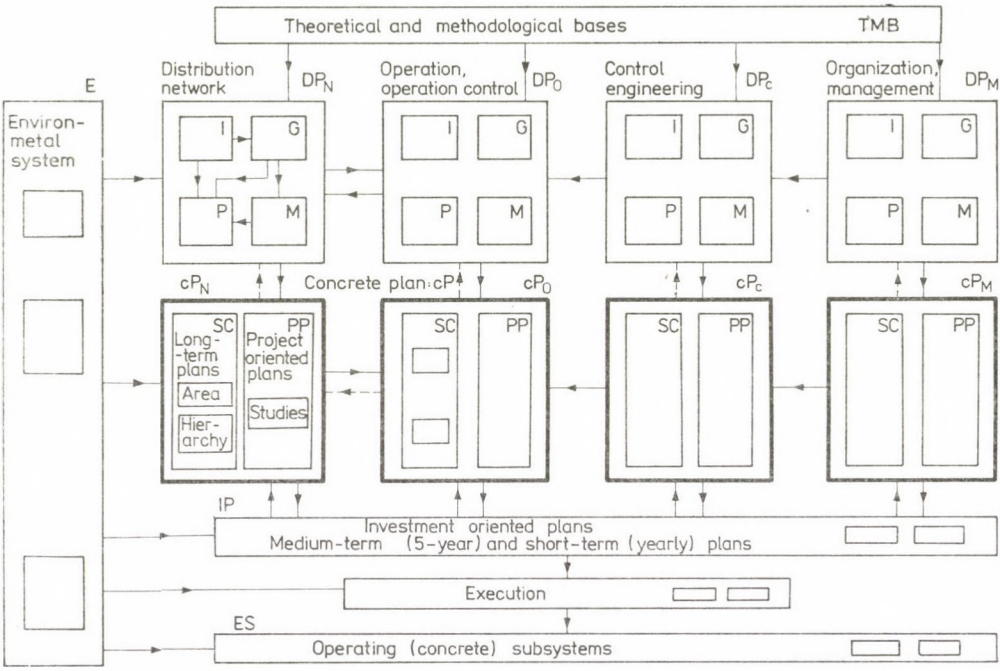

Fig. 1

ranging from simple passive adaptation to active internal and external (structural, functional, interrelative) modifications and influences. An adaptivity of the highest degree is capable of changing the system structure and influencing the environment.

As new feature appearing in the system of adaptive planning is the emphasis placed on the rational adaptation to changes, both in the process of planning and in the models and methods.

In adaptive planning the following essential tasks can be formulated:

1) taking into account the uncertainty of basic data as early as in the first phase of planning (adaptive model);

2) recognition in due time (adaptive information subsystem);

3) evaluation (cyclical or initiated by a change), elaboration of new elements, re-planning (adaptive method and control subsystem);

(4) preparation of decisions and assuring efficient execution (decision and control subsystem) ranging from long-range planning to implementation.

The adaptive planning process, its subsystems, modules and interrelations thereof are shown in Figure 2.

With a view to adaptivity, the following subsystems and modules are placed in the foreground:

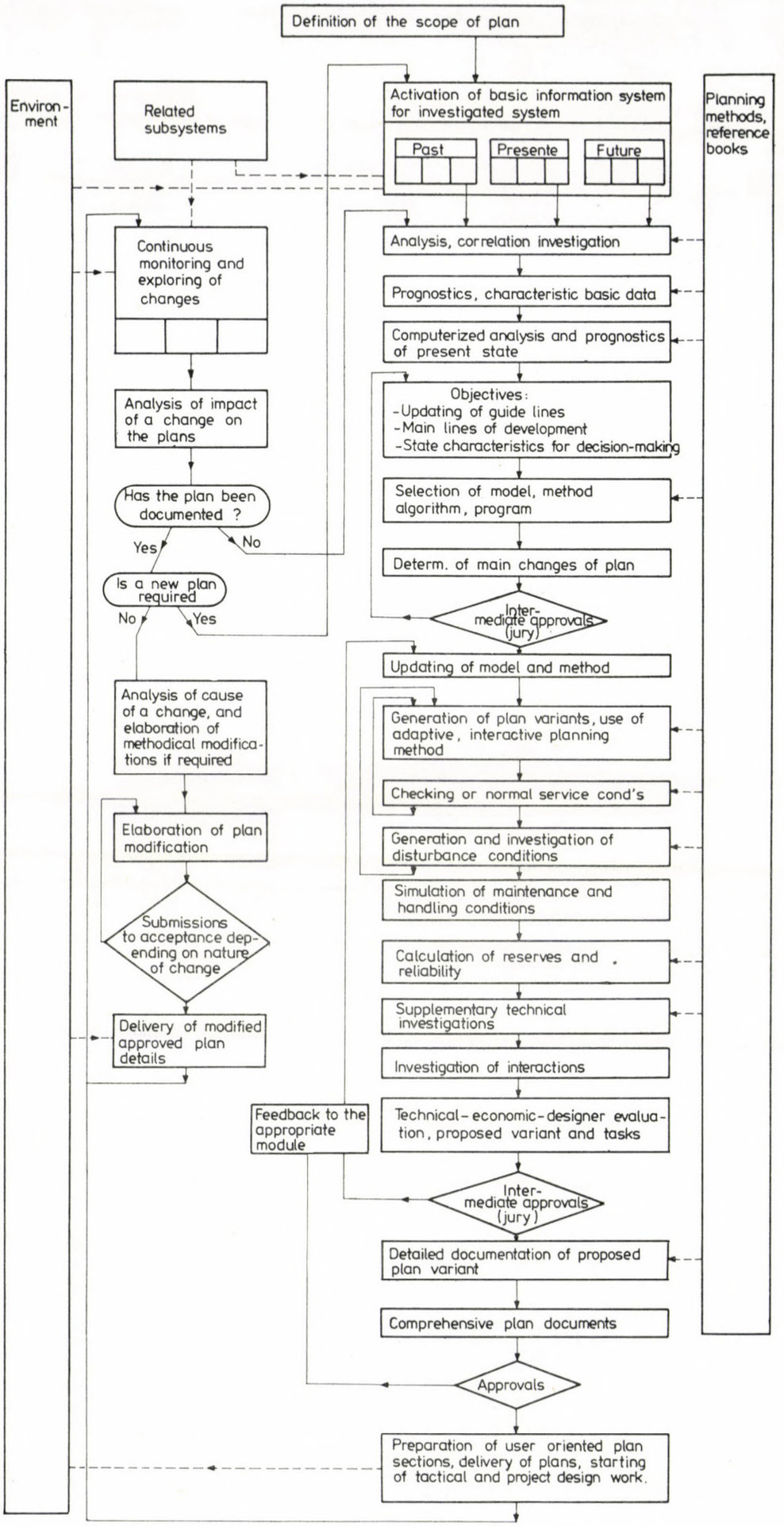
Definition of the scope of plan
Environ-ment
Related subsystems
Activation of basic information system for investigated system
Past
Presente
Future
Planning methods, reference books
Continuous monitoring and exploring of changes
Analysis, correlation investigation
Prognostics, characteristic basic data
Computerized analysis and prognostics of present state
Analysis of impact of a change on the plans
Objectives:
-Updating of guide lines
-Main lines of development
-State characteristics for decision-making
Has the plan been documented ?
Yes
No
Selection of model, method algorithm, program
Determ. of main changes of plan
Is a new plan required
No
Yes
Inter-mediate approvals (jury)
Updating of model and method
Analysis of cause of a change, and elaboration of methodical modifica-tions if required
Generation of plan variants, use of adaptive, interactive planning method
Checking or normal service cond's
Elaboration of plan modification
Generation and investigation of disturbance conditions
Simulation of maintenance and handling conditions
Submissions to acceptance dep-ending on nature of change
Calculation of reserves and reliability
Supplementary technical investigations
Delivery of modified approved plan details
Investigation of interactions
Feedback to the appropriate module
Technical-economic-designer evalua-tion, proposed variant and tasks
Inter-mediate approvals (jury)
Detailed documentation of proposed plan variant
Comprehensive plan documents
Approvals
Preparation of user oriented plan sections, delivery of plans, starting of tactical and project design work.

Fig. 2

— adaptive planning subsystem: model, method, algorithm;
— adaptive control system, information subsystem to monitor and search for changes;
— control subsystem; subsystem of expertise and management (jury = decision node);
— subsystem to investigate interrelations.

The adaptive planning is "environment and interrelation" oriented.

A continuous planning process and the resulting control on development, directed by the planning activity is, in fact, a "planning process control".

With respect to feedback, three time phases are accentuated: plan making, realization of plans, and operation.

In the course of a continuous feedback-type plan making and checking, based on continuous processing of acquired experiences, a certain degree of learning is also taking place. This is, in effect, an elementary form of adaptive learning, control and planning.

In addition to synthetizing the experiences, learning can be enhanced by simulation. The simulation results in a considerably shorter and more economical learning.

The adaptive planning system, the module system of the planning process is also suitable for being used in the planning of distribution networks, operation control and new control systems. The contents of modules has been worked out in details for distribution networks and for their control methods.

The planning process includes modules, which can be modelled mathematically, and for which appropriate algorithms can be constructed, permitting these modules to be treated by means of a computer. These modules belong to the automated technical planning: ATP.

The models can be divided into three main groups: deterministic, stochastic, adaptive (uncertain basic data).

The most suitable means for taking into account the adaptive, dynamic models with uncertain basic data. For those operation control and control engineering modules, which can be modelled, it is suitable to elaborate first, the deterministic methods, and, then, the adaptive ones.

A synthesis of the network model (M_N), the operation control model (M_0O) and the system control model (M_C) establishes the basis for integrated planning, *viz.* the cybernetic model (M) of a distribution network:

$$M = \{M_N, M_0O, M_C^*\} .$$

New elements are introduced for modelling, e.g.: hyper-, hierarchic-, hybrid-, Petri-graphs.

The supervision and control of state variables (S), such as power (P), current (I), voltage (U), frequency, operating states (g), temperature (t).

$$S\ (P, I, U, f, g, t)$$

are accomplished (in space and time) by system control methods.

4. Distribution network control system

The hierarchic network, operation control and system engineering subsystems are shown in Figure 3.

The evolution tendencies of protective relays and automata for distribution networks (e.g. protection, automation, telecontrol, telecommunication, computers, ripple-control), can be investigated in several aspects: complexity, function, hardware elements, software, planning demands.

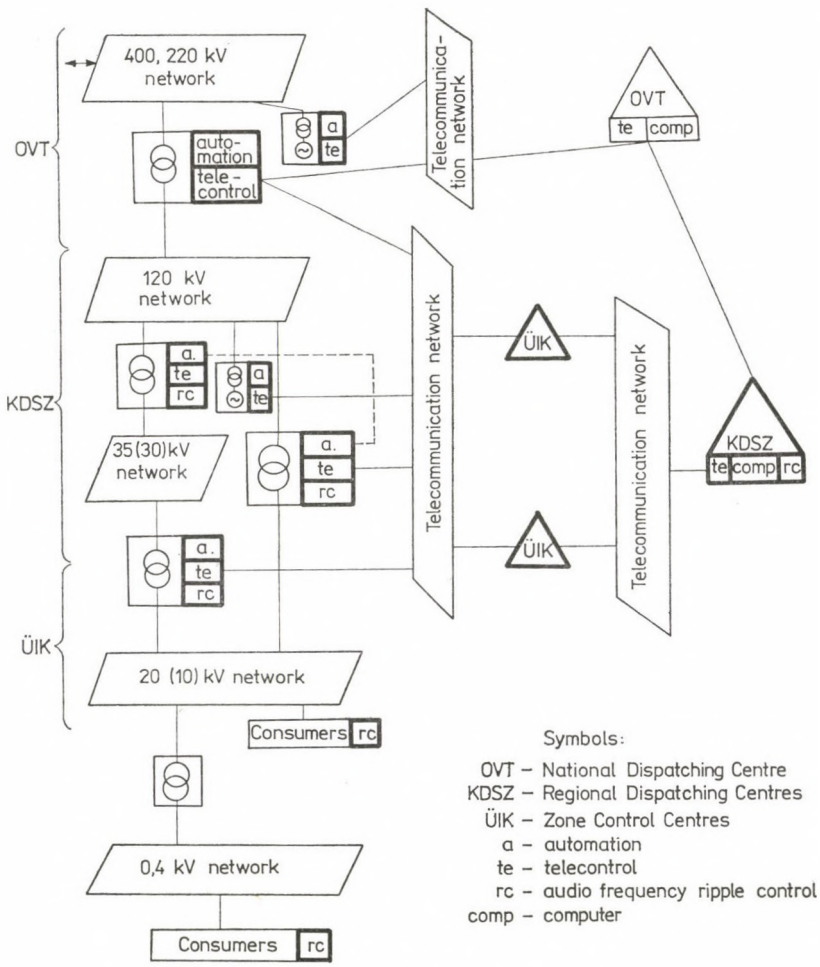

Fig. 3

The automata and protective relays are developing in the direction of complex automation and protective systems. E.g.: complexity on circuit (bay) level. For reliability or economic reasons it seems appropriate, on the long term — to develop so-called intelligent "grouped complex" automation systems: for busbar sections, transformers, etc.

The complexity or intricacy of a telecontrol system or a ripple control system is considerable even in the initial stages of development and implementation, since, due to the function and structure of such systems, they form a great contiguous system covering a whole regional dispatching area.

Regarding the functions, both quantitative and qualitative progress is to be expected here too, e.g. functions of remote supervision, telecommand and system regulation. The adaptive control engineering system is considered as the most up-to-date.

For medium- and low-voltage networks and consumers new control engineering methods (automation, ripple ON-OFF control of individual loads) have come into prominance.

As regards hardware, the change of generation (in electronics) becomes a common phenomenon together with the appearance of programmed elements and computer systems.

All the above mentioned features necessitate long-term and continuous planning of control engineering (cybernetic) systems. Individual, ad hoc plans are no longer sufficient.

The planning of control engineering systems is performed on the basis of adaptive planning process shown in Figure 2. Several system plans have been prepared for the computer and telecontrol systems of regional dispatching centres (3, 12).

Due to the special requirements and characteristics, the determination of models of formulizable modules have raised new tasks. According to the principle of progressivity, in this field, first, the deterministic models have to be elaborated and applied, and later they can be developed into adaptive models.

As an example, for the telecontrol system of a regional dispatching, the main elements of a possible combinatorical model are shown:

$$M_I = \{R, T, C, F, PG\}$$

where

R = topographic domain of interpretation and set of basic data,
T = target function(s) and evaluation criteria,
C = set of constraints,
F = set of functional and information-flow relations,
PG = planning guide lines and further stipulations.

The elements of set R are:

$$R = \{G_{pn}, G_{oc}, G_{tn}, I_m, I_s, I_{tc}, I_e, B\}$$

where

G_{pn} = graph of power network (hierarchic graph),
G_{oc} = graph of operation control system,
G_{tn} = maximum graph of telecommunication network,
I_m = set of measured data requirements,
I_s = set of signalled data requirements,
I_{tc} = set of telecommand requirements,
I_e = set of man-machine relations requirements,
B = set of specification data and costs of telecontrol equipment.

The evaluation criterion of target function (T) can be e.g.:

— cost minimum (absolute or present-value),
— maximalization of service continuity and reliability (in the case of investment constraint).

Elements of the set of constraints C are e.g.:

— constraints imposed by equipment information capacity,
— maximum permissible information up-dating time.

The elements of sets F and PG are being determined during the development of the system and gradual evolution of the planning guide lines.

I_m, I_j, I_p can be given with minimum and maximum values (adaptive model).

5. Interactions between network and control engineering

In the previous sections already described some interactions within the complex system of operation control and control engineering. In this section the interactions between network and control engineering system (subsystems) will be investigated.

For the sake of completeness and as the best example let the interaction between network and protective relays be mentioned first, which is well known and considered in the plans.

A similar close interrelation exists between network and automata. The "*n*-1" planning principle is achieved by the adoption of automata. Along with the development of automatic devices restoring service continuity in conjunction with a fault and those performing certain regulation tasks, new automated functions are added, whereby interaction increases to the extent of causing repercussions on network planning and critical characteristic state

parameters. Implementation of extensive automation systems creates new possibilities.

In the case of distribution network transformers and lines (on voltage levels of 120, 20, 10, 0.4 kV) one of the following reserve principles can be applied: no standby is installed, individual standby is available, a common standby is provided.

Introducing new automatic means a so-called "common system standby" can be established for an interconnected, topologically contiguous distribution network, which reacts on the planning of the power network and results in considerable cost savings.

The overload supported by the network elements at forced outages may be further increased by shortening the time required by the transposition of loads. This is an important achievement, because the state of the network during a forced outage is the critical factor, it is a planning constraint, to be considered in network planning, it is just the load transposition time that can be reduced by appropriate application of suitable automatic equipments, telecontrol means and audio-fraquency remote (ripple) control methods.

Using common standby lines and automation, the degree of reliability of radial (tree) distribution networks can be improved, and, in addition, by meshed networks the utilization factor of lines is increased.

The cost effects of interactions are such as to render more complicated and extensive control engineering systems economical (besides technical necessity).

Automation and telecontrol permit the implementation and exploitation of unattended distribution transformer stations at a satisfactory reliability level of operation.

When calculating the operation reliability (V) of a network, in addition to the network (N), the control engineering subsystems (C) and operation control (OC) have to be considered:

$$V_r = f(N, C, OC).$$

E.g.: switch-over times: manual 30 to 60 min., by telecontrol 1 to 3 min. local automation 1 to 10 s. protective relays 0.1 to 0.5 s.

The ripple control is an important subsystem of operation control, which renders the control system complete and "closed" from generating plant to consumer. A close interrelation exists between the distribution network control engineering subsystems as well.

By increasing the interactions between the network and control encineering (by introducing new control engineering means) the following advantages are achieved:

— savings in investment costs,
— increased equipment utilization,
— improved reliability, reduced outage durations.

By considering the interactions improved system parameters can be determined:
V_r, P_r, where P_r is the reliably available capacity (power) of the distribution system:

$$P_r = f(P_{trf}, P_h, C, m, P(t), M, I, Ü).$$

Where

P_{trf} = capacity of transformers.
P_h = reserve power,
C = overload carrying capacity,
m = number of connections,
P(t) = load *vs.* time curve,
M = set of warming-up parameters.
P(t) can be given with minimum and maximum values.

The concrete results of quantitative investigations will be published in a separate paper.

REFERENCES

1. ACKOFF, R. L.: A concept of corporate planning. Wiley, New York, 1970
2. ASHBY, W. R.: An introduction to cybernetics, London, 1964
3. BENKŐ, K.—HADIK, Z.—MADASNÉ, D. M.— SZANISZLÓ, M.: A DÉDÁSz üzemirányítási rendszerének korszerűsítése. Telemechanikai és számítógépes alrendszer rendszerterve. I. kötet. VEIKI kutatási jelentés, Budapest 1978
4. BOARDMAN, S. T.—WILDE, R. S.: Interactive Design of Electricity-Distribution Networks. *Power Record* (1973), sept.
5. BOHNE, M.—BÜRGEL, K.—SCHLEDE, J.: Planung elektrischer Netze. *Elektrizitätwirtschaft* (1976), 88—93
6. GESZTI, P. O.—BENKÓ, I.—REGULY, Z.: Villamos hálózatok I. Egyetemi jegyzet, Tankönyvkiadó, Budapest 1974
7. GESZTI, P. O.—BENKÓ, I.—BÓKAY, B.—KISS, L.—REGULY, Z.—VARJÚ, GY.: Villamos hálózatok II. Egyetemi jegyzet. Tankönyvkiadó, Budapest 1969
8. HAJNAL, A.: Az adaptív népgazdasági tervező rendszer. OT Tervgazdasági Intézet. Budapest 1972
9. HENAULT, P. M.—EASTVEDT, R. B.—PESCHON, I.—HAJDU, L. P.: Power System Long-Term Planning in the Presence of Uncertainty. *IEEE Transactions on Power Apparatus and Systems.* No. 1. (1970), 156—163
10. JÁNDY, G.: Operációkutatás a kapacitások tervezésében és irányításában. Műszaki Könyvkiadó, Budapest 1971
11. JUGYIN, D. B.— BEREZNYERA, T. D.: Statikus és dinamikus sztohasztikus programozási modellek. Közgazdasági Operációkutatási alkalmazások. Budapest 1976
12. MADASNÉ, D. M.—PAPP, GY.—SZANISZLÓ, M.—ZARÁNDI, L.-NÉ: A DÉMÁSz Körzeti Teherelosztó telemechanikai és számítógépes alrendszerének rendszerterve. *VEIKI, RTF* **14** (1975) Budapest, 1975 november
13. MADASNÉ, D. M.—SZANISZLÓ, M.: Körzeti Villamos Teherelosztók számítógépes folyamatirányítása (előtanulmány). *VEIKI, RTF* **8** 74, Budapest (1974)

14. MADASNÉ, D. M.—SZANISZLÓ, M.: Az ELMÜ BVTSz Telherelosztó és az Északpesti Üzemigazgatóság telemechanikai rendszerének kialakítása. *VEIKI, RTF* 7/76, Budapest (1976)
15. MITYUSKIN, K. G.: Adaptive System for Collection and Transmission of Operational Dispatcher Information in Power Systems. CIGRE. 1976. 35—02
16. MÜNKER, H.: Planung elektrischer Versorgungsnetze. *AEG-Telefunken Technische Mitteilungen.* (1977) 209—217
17. NYIKOS, J.: Budakörnyék 20 kV-os hálózatának fejlesztési terve. MVMT—ELMÜ tervtanulmány, Budapest 1972
18. RÁCZ, L.—REGULY, Z.: Rendszerelmélet és operációkutatás alkalmazása villamos energiarendszerekben. Budapesti Műszaki Egyetem. Villamosmérnöki Kar, Tankönyvkiadó, Budapest 1976
19. SASVÁRI, S.—SZANISZLÓ, M.—SZEMEREI, Z.: Villamos hálózatfejlesztési tanulmányok, tervek tartalma, formája és kidolgozásának metodikája. ELMÜ tanulmány, Budapest 1970
20. SZANISZLÓ, M.: The Design of Distribution Networks with Several Rings by Branch and Bound Method. Acta Technika, 1972. (1—2) pp. 95—115
21. SZANISZLÓ, M.: Városi villamos elosztóhálózati rendszerek tervezése szintézis módszerrel. Kandidátusi értekezés. (VEIKI tanulmány) Budapest 1977
22. SZANISZLÓ, M.: Villamos elosztóhálózatok és új elosztóhálózati irányítástechnikai rendszerek integrált tervkészítési folyamata, adaptív tervezése, kölcsönhatások. Budapest, VEIKI tanulmány, 1978
23. SZANISZLÓ, M.: Power Network Design by the Branch and Bound Method. *Periodika* 17 (1973) No. 3
24. SZENDY, K.: Korszerű hálózatszámítási módszerek. Akadémiai Kiadó, Budapest 1967
25. VÁGÓ, I.: Grámelmélet alkalmazása villamos hálózatok számításában. Műszaki könyvkiadó, Budapest 1976
26. VITEK, V.: VYZKUMNÉ ZPRÁVA k DU P-04-125-021-01 o hlavni etapé E 06 „Koncepce rizeni elektrizacni soustavy po roce 1980" (PE EGU c. 10 02-1 07). (Kutatási jelentés a DU P 04-125-021-01-hez „Villamos energiarendszer irányításának koncepciója 1980 után" E 06 főütemről. Kutatási jelentés.)
27. Automatizálási Irányelvek a nagy- és a középfeszültségű elosztóhálózatok üzemére. Magyar Villamos Művek Tröszt, Budapest 1965
28. Hálózatfejlesztési irányelvek nagyfeszültségű szabadvezetékes elosztóhálózatok kialakítására. MVMT Hálózati Igazgatósága, Budapest 1967
29. KDSz üzemirányítás fejlesztési koncepció. MVMT Budapest 1974

Charakteristiken des infolge der Schaltüberspannung auftretenden Durchschlags der großen Fernleitungsmast-Leiter Luftabstände. — Die Abhandlung berichtet über eine Serie von umfassenden Untersuchungen von verschiedenen Isolationsmodellen der Fernleitungsmaste, die mit Impulsspannung durchgeführt wurden. Die Einwirkung der Wellenform auf die elektrische Festigkeit gegen die Schaltüberspannung von positiver Polarität wird durch Anwendung von Spannungswellen einer Stirnzeit von 35 bis 1200 μs. Die Untersuchungsergebnisse umfassen und erweitern die Anhäufung der zur Verfügung stehenden Daten und infolgedessen kann eine verallgemeinerte Kennlinie der Spannung-Wellenform des Durchschlags ermittelt werden. Der Autor führte besondere Untersuchungen durch um eine ausreichende Menge von Experimentenresultate zusammen zu bringen, die für die Aufstellung eines den Durchschlag von großen Luftabständen representierenden Modells notwendig sind. Aufgrund der Messungen wurden die Parameter des Übergangs von der Koronaentladung zur Leaderentladung und dieselben der Entwicklung der Leaderentladung ausgewertet. Die Gegenüberstellung der Ergebnisse der theoretischen Rechnungen mit denselben der Experimente bewies, daß in der Modellierung des Entladungsprozesses ein Fortschritt erreicht werden konnte.

Acta Technica Academiae Scientiarum Hungaricae, Tomus 91 (3—4), pp. 411—417 (1980)

BUCKLING OF THE SADDLE-SHAPED HYPAR SHELL ACTING LIKE AN ARCH

E. DULÁCSKA*
CAND. OF TECHN. SCI.

[Manuscript received May 2, 1980]

The paper presents the determination of the linear critical load of the uniformly loaded saddle-shaped hyperbolic paraboloid shell stiffened along two opposite edges by diaphragms rigid only in their own planes, while rigidly supported in all directions along the other two edges. The buckled shape always consists of a combination of two sine functions which make the displacement vanish along the rigidly supported edges. The numerical values of the coefficient necessary to compute the critical loads are given in a table, facilitating practical computations.

1. Introduction

Saddle-shaped shells are willingly used to cover large areas bacause of their pleasant form, and since their formwork can be assembled of straight sheets (Fig. 1). This type of shells is mostly supported in either of the two following ways:

The shell might be supported along all its four edges ($x = 0$, $x = L_x$, $y = \pm L_y/2$) by diaphragms (or arches) rigid only in their own planes, unable to resist lateral thrust ("semi-rigid diaphragms", see Fig. 1a). The membrane stress state of the uniformly loaded saddle-shaped shell corresponding to this kind of support was determined by AIMOND [1]. The validity of the membrane

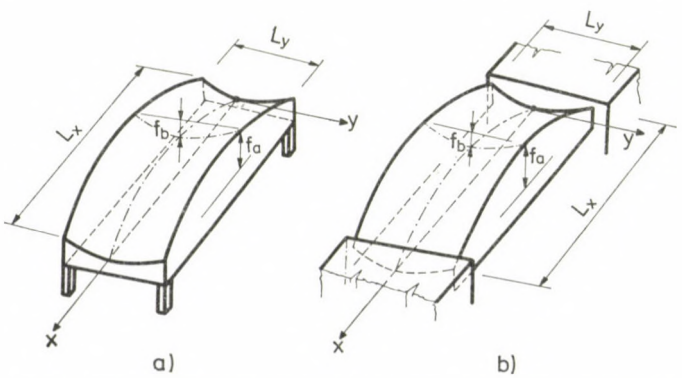

Fig. 1. The usual support conditions of the saddle-shaped shell

* Dr. DULÁCSKA Endre, II. Kitaibel Pál u. 12 H-1022 Budapest, Hungary

theory was investigated by JANKÓ [6] who found that in the range $2 \leq f_a/f_b \leq 4$ the shell carries at least 95 per cent of the load by membrane forces.

In the second case the shell is rigidly supported along the edges $x = 0$ and $x = L_x$, while the two other edges are stiffened by "semi-rigid diaphragms". It is generally assumed that the shell carries the uniform load by x-directed compressive membrane forces only, i.e. it acts like a simple arch in the x direction. HRUBAN presents an example for this case in [5]. However, this kind of support is statically indeterminate, even in the frame of membrane theory. Moreover, the edge conditions can be met by the bending theory only. We made investigations on numerical examples, referring to the extreme cases $f_a/f_b = 1$ and 4, to what extent the internal forces of the shell supported this way, obtained by the bending theory, differ from the assumed simple arch-like action. We found that the shell carries at least 98 per cent of the uniform load by membrane forces like an arch, and that the modification of the membrane forces due to the edge disturbances is less tham 1 per cent. Hence, we may state that the assumed simple arch-like action approximates rather well the actual state of stress.

In the first period of application of saddle-shaped shells it was assumed that, since the hypar shell has an undevelopable middle surface, it has a high critical load, not to be analysed any further. However, it turned out in practical applications that buckling may cause the collapse of large hypar shells [2]. It has also been established that the saddle-shaped shell supported by four "semi-rigid diaphragms" is capable of developing an inextensional deformation [4]. The tensile stiffness of the shell plays no role during inextensional deformations, so that the shell does not become stiffer than a flat plate of the same dimensions. Thus, the critical load pertaining to an inextensional buckling shape is to be expected as being rather low.

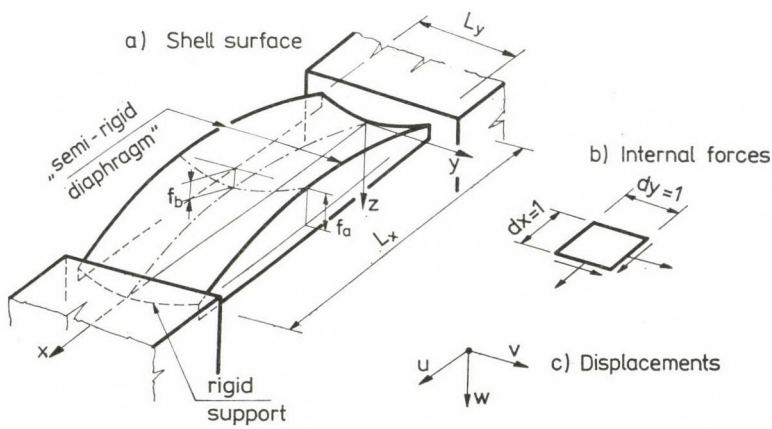

Fig. 2. The saddle-shaped shell with prevented edge displacement. Notations

The stability behaviour of shells supported by four "semi-rigid diaphragms" has ben clarified by JANKÓ in two papers [7], [8].

The critical load of the saddle-shaped shell supported in the second way (i.e. rigid supports, at $x = 0$ and $x = L_x$ while "semi-rigid diaphragms" along the edges $y = \pm L_y/2$, and assuming a pure arch-like action) is expected to be higher than that valid for the previous case, since the rigid support of two edges excludes the possibility of inextensional deformation. Since this case has not been solved yet, we want to deal with the derivation of the linear critical load for this type of shells.

2. Assumptions

In the analysis we assume that the shell is shallow and its material is linearly elastic.

We derive the critical load on the basis of the linear (classical) buckling theory. The notation is to be seen in Fig. 2. We neglect the deformations caused by the membrane forces prior to buckling.

Be the shell subjected to a uniform load p acting in the z direction. We assume that the shell is in a pure membrane stress state and has the specific internal forces:

$$n_x = \frac{pL_x^2}{8f_a}; \quad n_y = 0; \quad n_{xy} = 0, \tag{1}$$

i.e. it acts like an arch in the x direction.

The middle surface of the shell is described by the equation:

$$z = \frac{x^2}{2R_x} - \frac{y^2}{2R_y} - \frac{xL_x}{2R_x}. \tag{2}$$

The boundary conditions are:

$$\begin{aligned} &\text{along } y = \pm L_y/2: && w = w'' = n_y = u' = 0; \\ &\text{along } x = 0 \text{ and } x = L_x: && w = w^{II} = u = v^{\cdot} = 0. \end{aligned}$$

Here, $'$ and $^{\cdot}$ denote differentiation with respect to x and y, while u, v and w are displacement components as shown in Fig. 2.

3. The equations of buckling

The differential equation of buckling of the shell in question is, according to [3]:

$$B\triangle\triangle\triangle\triangle w + p\triangle\triangle w + D\left(\frac{w^{::}}{R_x^2} - \frac{2w^{II\cdot\cdot}}{R_xR_y} + \frac{w^{IV}}{R_y^2}\right) = 0, \tag{3}$$

where B and D are the bending and tensile stiffnesses, respectively, and $\triangle$ is the *Laplace* operator.

This equation is satisfied by a product consisting of sine and cosine functions in the x and y directions, respectively. In order to satisfy the boundary conditions along the rigidly supported edges, we have to choose two such products, because the displacement due to one product has to cancel that due to the other one. Hence, the eigenfunctions of the differential equation (3), satisfying the boundary conditions $u = 0$ along the edges $x = 0$ and $x = L_x$, are as follows:

$$w = \cos \frac{n\pi}{L_y} y \left(A_1 \sin \frac{m_1 \pi}{L_x} x + A_2 \sin \frac{m_2 \pi}{L_x} x \right), \tag{4}$$

where m_1, m_2 and n are whole numbers, to be specified later, and A_1, A_2 are the buckling amplitudes.

The stress function belonging to (4) has the shape:

$$F = D \cos \frac{n\pi}{L_y} y \left(A_1 F_1 \sin \frac{m_1 \pi}{L_x} x + A_2 F_2 \sin \frac{m_2 \pi}{L_x} x \right), \tag{5}$$

with F_1 and F_2 as for the time being unspecified constants.

The membrane forces are to be computed from F, according to the expressions:

$$n_x = F'' ; \quad n_y = F^{II}; \quad n_{xy} = -F^{I'}. \tag{6}$$

Introducing the expressions (4) and (5) for w and F into the compatibility equation of the shell:

$$F^{IV} + 2F^{II''} + F^{::} = -D \left(\frac{w^{II}}{R_y} + \frac{w''}{R_x} \right), \tag{7}$$

and considering that $R_x = L_x^2/8f_a$ and $R_y = L_y^2/8f_b$, we can express F_1 and F_2 by the other constants as follows:

$$F_1 = \frac{\dfrac{m_1^2 \pi^2 8 f_b}{L_x^2 L_y^2} - \dfrac{n^2 \pi^2 8 f_a}{L_y^2 L_x^2}}{\left(\dfrac{m_1^2 \pi^2}{L_x^2} + \dfrac{n^2 \pi^2}{L_y^2} \right)^2}, \tag{8}$$

$$F_2 = \frac{\dfrac{m_2^2 \pi^2 8 f_b}{L_x^2 L_y^2} - \dfrac{n^2 \pi^2 8 f_a}{L_y^2 L_x^2}}{\left(\dfrac{m_2^2 \pi^2}{L_x^2} + \dfrac{n^2 \pi^2}{L_y^2} \right)^2}. \tag{9}$$

The related values of the amplitudes A_1 and A_2 have to be determined from the boundary condition

$$u \mid x = \frac{0}{L_x} = 0 ,$$

which yields the equation [3]:

$$u = \int \left(\frac{F''}{D} - \frac{xw'}{R_x} \right) dx = 0 . \tag{10}$$

Introducing the derivatives of F and w we obtain the relation:

$$\frac{A_2}{A_1} = - \frac{m_2}{m_1} \cdot \frac{m_1^2 \pi^2 F_1 - 1}{m_2^2 \pi^2 F_2 - 1} . \tag{11}$$

All the other boundary conditions are automatically satisfied by the functions assumed for w and F.

4. Determination of the critical load

We can proceed by determining the critical load as follows. Let us assume the values $n = 1, 2, 3, \ldots$, and a pair of values for m_1 and m_2, namely, $m = 1, 3, 5, \ldots$, for the symmetric shape and $m = 2, 4, 6, \ldots$, for the antimetric shape. We compute F_1 and F_2 from Eqs (8) and (9), using these assumed n, m_1 and m_2 values, then we determine A_2/A_1 from (11). Assuming an optional value (preferably unity) for A_1, w will be determined by Eq. (4). Introducing the necessary derivatives in the differential equation (3), the critical load pertaining to the assumed values n, m_1 and m_2 can be computed.

The calculation described above has to be repeated with several n, m_1 and m_2 values. Among the critical loads obtained in this way, the minimum one will be the actual critical load of the shell.

The critical load can be written in the form

$$p_{cr}^{lin} = c \sqrt{12} \frac{\sqrt{BD}}{R_x R_y} \approx c \sqrt{BD} \frac{222 f_a f_b}{L_x^2 L_y^2} . \tag{12}$$

Neglecting Poisson's ratio, and confining our investigation to shells with a homogeneous wall, Eq. (12) can be rewritten with $B = Et^3/12$ and $D = Et$ as follows:

$$p_{cr}^{lin} = c \frac{Et^2}{R_x R_y} . \tag{13}$$

Table I

Values of c

$8f_b/t$	100					
$L_x/L_y =$	0,5	1,0	1,5	2,0	2,5	3,0
$f_a/f_b =$ 0,5	0,564	0,344	0,282	0,195	0,166	0,182
1,0	0,580	0,412	0,266	0,246	0,191	0,141
1,5	0,585	0,421	0,276	0,233	0,233	0,163
2,0	0,586	0,444	0,318	0,224	0,215	0,192
2,5	0,585	0,464	0,331	0,228	0,202	0,211
3,0	0,585	0,479	0,345	0,237	0,199	0,198
3,5	0,585	0,492	0,369	0,261	0,201	0,196
4,0	0,584	0,501	0,379	0,260	0,205	0,186

$8f_b/t$	200					
$L_x/L_y =$	0,5	1,0	1,5	2,0	2,5	3,0
$f_a/f_b =$ 0,5	0,481	0,294	0,200	0,188	0,129	0,113
1,0	0,516	0,339	0,227	0,157	0,159	0,133
1,5	0,535	0,355	0,231	0,175	0,141	0,150
2.0	0,546	0,390	0,234	0,194	0,139	0,135
2,5	0,552	0,395	0,262	0,202	0,144	0,129
3,0	0,557	0,409	0,266	0,198	0,163	0,130
3 5	0,560	0,423	0,276	0,210	0,167	0,130
4,0	0,563	0,437	0,295	0,207	0,186	0,129

$8_b f/t$	300					
$L_x/L_y =$	0,5	1,0	1,5	2,0	2,5	3,0
$f_a/f_b =$ 0,5	0,459	0,259	0,182	0,141	0,137	0,094
1,0	0,497	0,282	0,180	0,143	0,126	0,158
1,5	0,519	0,310	0,202	0,158	0,120	0,112
2,0	0,533	0,344	0,220	0,161	0,127	0,105
2,5	0,543	0,353	0,230	0,163	0,144	0,113
3,0	0,549	0,374	0,251	0,165	0,141	0,121
3,5	0,554	0,395	0,248	0,184	0,139	0,121
4,0	0,558	0,416	0,259	0,184	0,147	0,126

$$p_{cr}^{\text{lin}} = c\frac{Et^2}{R_x R_y} = cEt^2\frac{64 f_a f_b}{L_x^2 L_y^2}$$

In order to facilitate stability analysis, we performed the above computations and determined the factor c of the critical load. These values are compiled in Table 1. These values correspond to points of a festoon curve which bulges downwards, so that a linear interpolation is unsafe. We thus recommend to draw the section of the curve passing through the computed neighbouring values and to read off the sought value from this curve.

Comparing the critical load of the shell rigidly supported at $x = 0$ and $x = L_x$, acting like an arch, with that of a shell exerting no lateral thrust [7], we can conclude that the rigid supports raise the critical load considerably.

Beulung der bogenartig wirkenden, sattelförmigen Hyparschale. — Der Verfasser bestimmt die lineare kritische Intensität der gleichmäßig verteilten Last der sattelförmigen, entlang zwei gegenseitigen Ränder durch »halbstarre« Diaphragmen versteiften, an den verbleibenden zwei Rändern starr gestützten hyperbolischen Paraboloidenschale. Die Beulfigur setzt sich immer aus der Kombination zwei Sinuswellen zusammen, die die Unverschieblichkeit der starr gestützten Ränder gewährleisten. Der zur Bestimmung der kritischen Last erforderliche Koeffizient wird für die am häufigsten vorkommenden geometrischen Verhältnisse numerisch bestimmt und tabellarisch angegeben, um den einfachen Stabilitätsnachweis zu fördern

REFERENCES

1. Aimond, F.: Etude statique des voiles minces paraboloïde hyperbolique travaillant sans flexion. *AIPC Mémoires*, *4* (1936)
2. Beleş, A. A.—Soare, M.: Paraboloidul eliptic şi hiperbolic in construcţii. Editura Acad. R. S. R. Bucuresti 1964
3. Dulácska, E.: Vibration and Stability of Anisotrop Shallow Shells. *Acta Techn. Hung. 65* (1969), 225—260
4. Geyling, F. T.: A General Theory of Deformations of Membrane Shells. Diss. Stanford University, Stanford, Calif. 1953
5. Hruban, K.: Die Biegetheorie der Translations-flächen und ihre Anwendung im Hallenbau. *Acta Techn. Hung.* 7 (1953), 425—464
6. Jankó, L.: Analyse des Verhältnisses zwischen Membran- und Biegeschnittkräften in sattelförmigen flachen, normalkraftfrei gelagerten HP-Schalen unter unter gleichmäßig verteilter Belastung. *Acta Techn. Hung.* (**91** 1980).
7. Jankó, L.: Untersuchung der Statbilität sattelförmiger, flacher, normalkraftfrei gelagerter HP-Schalen unter gleichmäßig verteilter Belastung. *Acta Techn. Hung.* (**91** 1980).
8. Jankó, L.: Untersuchung der Gleichgewichtzustände sattelförmiger, flacher, normalkraftfrei gelagerter HP-Schalen unter gleichmäßig verteilter Belastung, mit besonderer Berücksichtigung des Durchschlagens und der Abzweigung. *Acta Techn. Hung.* (**91** 1980).

Acta Technica Academiae Scientiarum Hungaricae, Tomus 91 (3—4), pp. 419—467 (1980)

UNTERSUCHUNG DER GLEICHGEWICHTSZUSTÄNDE SATTELFÖRMIGER, FLACHER, NORMALKRAFTFREI GELAGERTER HP-SCHALEN UNTER GLEICHMÄSSIG VERTEILTER BELASTUNG, MIT BESONDERER BERÜCKSICHTIGUNG DES DURCHSCHLAGENS UND DER ABZWEIGUNG

L. JANKÓ*

[Eingegangen am 28. Dezember 1978]

Diese Abhandlung bildet den letzten Teil einer dreiteiligen Artikel-Serie. Im ersten Teil waren die theoretischen Fragen der Existenz und der Eindeutigkeit der Membranlösung, sowie der kinematischen Unbestimmtheit von HP-Schalen behandelt worden. Auf Grund dessen wurde die Erscheinung der *Verzweigung* aus dem *unverformten* Grundzustand im zweiten Teil erörtert. In der vorliegenden Arbeit werden die *charakteristische Tragverhaltenskurven* der HP-Schalen bestimmt und es wird untersucht, ob das Stabilitätsversagen als Folgerung eines *Durchschlagens* auftreten kann. Wir werden auch auf die näherungsweise Untersuchung der Verzweigung aus dem *verformten* Grundzustand eingehen. Dies bietet die Möglichkeit den wachsenden oder abnehmenden Charakter des *überkritischen* Tragverhaltens zu bestimmen.

Bezeichnungen

$C_{ij} = \cos\frac{i\pi}{2a}x \cdot \cos\frac{j\pi}{2b}y$;

$D = \frac{Eh}{1-\mu^2}$ spezifische Dehnungssteifigkeit;

E Elastizitätsmodul;

F Spannungsfunktion der Mittelflächenkräfte ($F'' = N_x, F'' = -N_{xy}, F'' = N_y$);

F_0 Spannungsfunktion des Grundzustandes;

$\overline{F} \equiv \delta F$ erste Variation der Funktion $F_0 (F = F_0 + \overline{F})$;

$B = \frac{Eh^3}{12(1-\mu^2)}$ spezifische Biegesteifigkeit;

M_x, M_y bzw. $M_{xy} = M_{yx}$ Biege- bzw. Drillmomente;

N_x, N_{xy}, N_y Mittelflächenkräfte;

$S_{ij} = \sin\frac{i\pi}{2a}x \cdot \sin\frac{j\pi}{2b}y$;

U_b Potential der Biegeschnittkräfte;

U_m Potential der Mittelflächenkräfte;

V Potential der äußeren Kräfte;

$2a, 2b$ Spannweiten der Randbogen in den x- bzw. y-Richtungen;

f_a, f_b Pfeilhöhen der in den x- bzw. y-Richtungen liegenden Randbogen;

h Schalendicke;

i, j Halbwellenzahlen in den x- bzw. y-Richtungen (der Index n verweist auf dehnungslose Verformung);

* Dr.-Ing. L. JANKÓ, Lajos u. 142, H-1036 Budapest, Ungarn

p — Intensität der gleichmäßig verteilten, in Richtung der Achse z wirkenden, symmetrischen Belastung (bezogen auf die Flächeneinheit der Grundrißprojektion):

p_{kr}^{lin} — lineare kritische Last;

$\bar{p}_{kr}$ — kritische Durchschlagslast;

$p_{kr,v}^{\text{lin}}$ — lineare kritische Last der Verzweigung aus dem verformten Grundzustand;

u, v — Verschiebungen in Richtungen der Flächentangenten parallel zur $x-z$- bzw. $y-z$-Ebene;

$z(x, y)$; $\bar{z}(\bar{x}, \bar{y})$ — Ordinaten der Schalenmittelfläche;

w — Verschiebung eines Mittelflächenpunktes in Richtung der Flächennormale ($w = w_0 + \bar{w}$);

w_0 — im Grundzustand entstehende Verschiebung eines Mittelflächenpunktes in Richtung der Flächennormale;

$\bar{w}$ — erste Variation der Verschiebung w_0 (im Nachbarzustand);

w_a — Vorbeulamplitude (Anfangsausmittigkeit);

$\alpha = \dfrac{f_a}{f_b}$ — Pfeilhöhenverhältnis;

$\beta = \dfrac{a}{h}$ — Schalenparameter;

$\gamma = \dfrac{a}{b}$ — Seitenverhältnis;

$\delta \equiv (-)$ — Symbol der Variationsbildung;

η — Koordinate in Richtung einer der beiden geraden Erzeugenden vom Punkt $x = a, y = b$ (η verläuft parallel zur zweiten Leitebene);

μ — Querdehnungszahl (in den Berechnungen: $\mu = 0{,}2$);

ξ — Koordinate in Richtung einer der beiden geraden Erzeugenden vom Punkt $x = a, y = b$ (ξ verläuft parallel zur ersten Leitebenen);

Π — Gesamtpotential;

$\varrho = \dfrac{f_b}{b}$ — Schalenparameter;

ω — Hälfte des Winkels zwischen den Leitebenen;

$\triangle\triangle(\ ) = (\ )^{IV} + 2(\ )^{II\cdot\cdot} + (\ )^{\cdot\cdot\cdot\cdot}$ — der biharmonische Differentialoperator;

$L_p(f_1, f_2) = f_1^{II} f_2^{\cdot\cdot} - 2f_1^{\cdot I} f_2^{\cdot I} + f_1^{\cdot\cdot} f_2^{II}$ — der Puchersche-Differentialoperator.

1. Einleitung. Zweckbestimmung

Wegen ihrer gefälligen Form und der günstigen Ausführungsmöglichkeiten, die die geraden Erzeugenden bieten, werden immer häufiger Schalenkonstruktionen in Form des hyperbolischen Paraboloids (im weiteren HP-Schalen) gebaut.

Diese Abhandlung beschäftigt sich mit den Eigenheiten der *Gleichgewichtszustände von großen Verformungen* von sattelförmigen, unter gleichmäßig verteilter Belastung stehenden HP-Schalen. Diese Schalen sind längs der Hauptkrümmungslinien durch Randbogen abgestützt, die in der horizon-

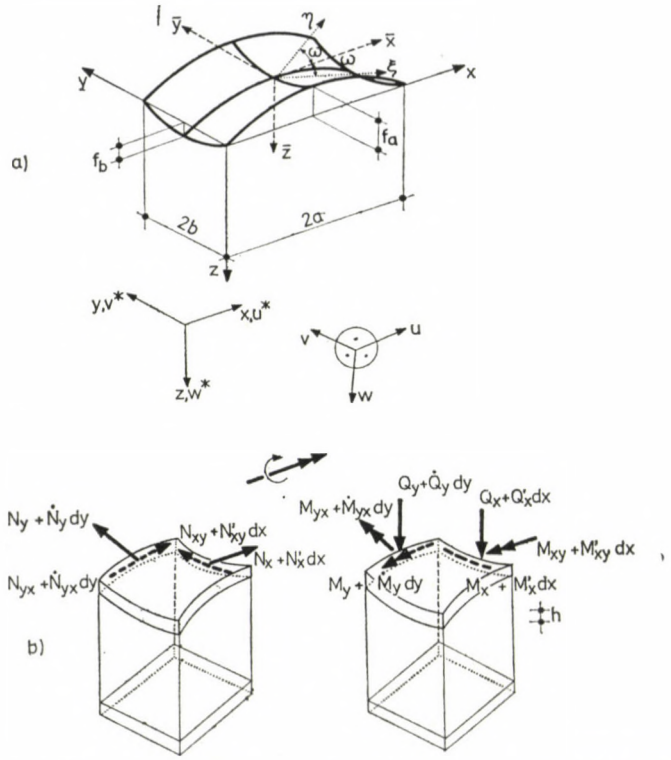

Bild 1. Geometrische Angaben der sattelförmigen HP-Schale. Vorzeichenregel der inneren Kräften und der Verschiebungen

talen Richtung vernachlässigbare Biege- bzw. Drillsteifigkeiten besitzen (im weiteren »normalkraftfreie« Randträger).

Dieser Aufsatz bildet eine Fortsetzung zweier Veröffentlichungen vom Verfasser. Vor den Stabilitätsuntersuchungen wurden die Schalenparameterbereiche in [5] ermittelt, in welchen *der Effekt der Biege- und Drillmomente* (mit den zugehörigen Querkräften) im Vergleich zum Effekt der Mittelflächenkräfte nach der Biegetheorie *vernachlässigbar* klein ist. Bei diesen Parametern darf die HP-Schale als *Membranschale* angesehen werden. In solchen Fällen ist es richtig auch den Verlauf des Stabilitätsverlustes nach der »linearen« Stabilitätstheorie zu untersuchen. Es handelt sich nämlich um eine *Verzweigungserscheinung*, die aus dem unverformten (membranartigen) Grundzustand ($w_0 = 0$) erfolgt. Für die geometrischen Verhältnisse, die die meisten Stahlbetonschalen gut kennzeichnen, wurden vom Verfasser in [6] die Girlandenkurven der linearen kritischen Lasten bestimmt.

Die »halbnormale« HP-Schale ($f_a/f_b = 1$) und die Schalen, deren Pfeilhöhenverhältnisse mit dem f_a/f_b-Wert von 1 lediglich geringfügig abweichen, tragen den überwiegenden Teil ihrer Belastung durch Biegeschnittkräfte.

Es stellte sich heraus, daß Mittelflächenkräfte in diesen Schalen ausschließlich durch die Lastkomponenten hervorgerufen werden, deren Form von der dehnungslosen Durchbiegungsform der »halbnormalen« HP-Schalen abweichen [5].

Nach dem bisher Gesagten liegt es auf der Hand, daß das Stabilitätsverhalten dieser Schalen ausschließlich nach der (nichtlinearen) Theorie der großen Verformungen ermittelt werden kann.

Naturgemäß braucht man zur Bemessung die verschiedenen Gleichgewichtszustände von großen Verformungen auch für den Fall der HP-Schalen zu kennen, die mit guter Annäherung als Membranschalen betrachtet werden können.

Als Fortsetzung der erwähnten Untersuchungen der Verzweigung [6] soll in der vorliegenden Arbeit auch die Frage bentwortet werden: Was für charakteristische Tragverhaltenskurven haben die erwähnten HP-Schalen? Dazu werden die ermittelten Tragverhaltenskurven mit den im Bild 2 dargestellten verglichen.

Es wird untersucht, ob das Stabilitätsversagen infolge von *Durchschlagen* auftreten kann.

Es kann aber auch vorkommen, daß die Konstruktion unter der Belastung eine symmetrische Zusammendrückung erleidet, die zwar nicht genügt, um sie zum symmetrischen Durchschlagen zu bringen, jedoch dazu ausreicht, daß die Druckkraft, die infolge der Zusammendrückung angestiegen ist, sie antimetrisch ausbeulen läßt. Wir müssen also die Frage stellen: ob die behandelten HP-Schalen zum Überspringen in eine antimetrische Beulung neigen. Es wird auf die näherungsweise Untersuchung dieser Erscheinung eingegangen.

Dieses Näherungsverfahren bietet die Möglichkeit, den *wachsenden* oder *abnehmenden* Charakter des überkritischen Tragverhaltens zu bestimmen.

Zur Erleichterung der praktischen Anwendung sind die zur Bemessung gut geeigneten Resultate in Formeln und Schaubildern sowie Tabellen dargestellt.

2. Grundannahmen

Nach der Theorie der großen Verformungen (im weiteren: nichtlineare Theorie) hat man auch die höheren Potenzen der Ableitungen derjenigen Verschiebungskomponenten in die Berechnung einzubeziehen, die die Durchbiegungsform bestimmen (»geometrische Nichtlinearität«).

Aus dieser Potenzreihe werden so viele Glieder beibehalten, wie es die Berechnungsmöglichkeiten erlauben. Auf diese Weise läßt sich der Beulvorgang nicht nur bis zum benachbarten Gleichgewichtszustand der unausgebeulten Form, sondern selbst bis zu den Deformationen w verfolgen, die das Mehrfache der Wanddicke erreichen.

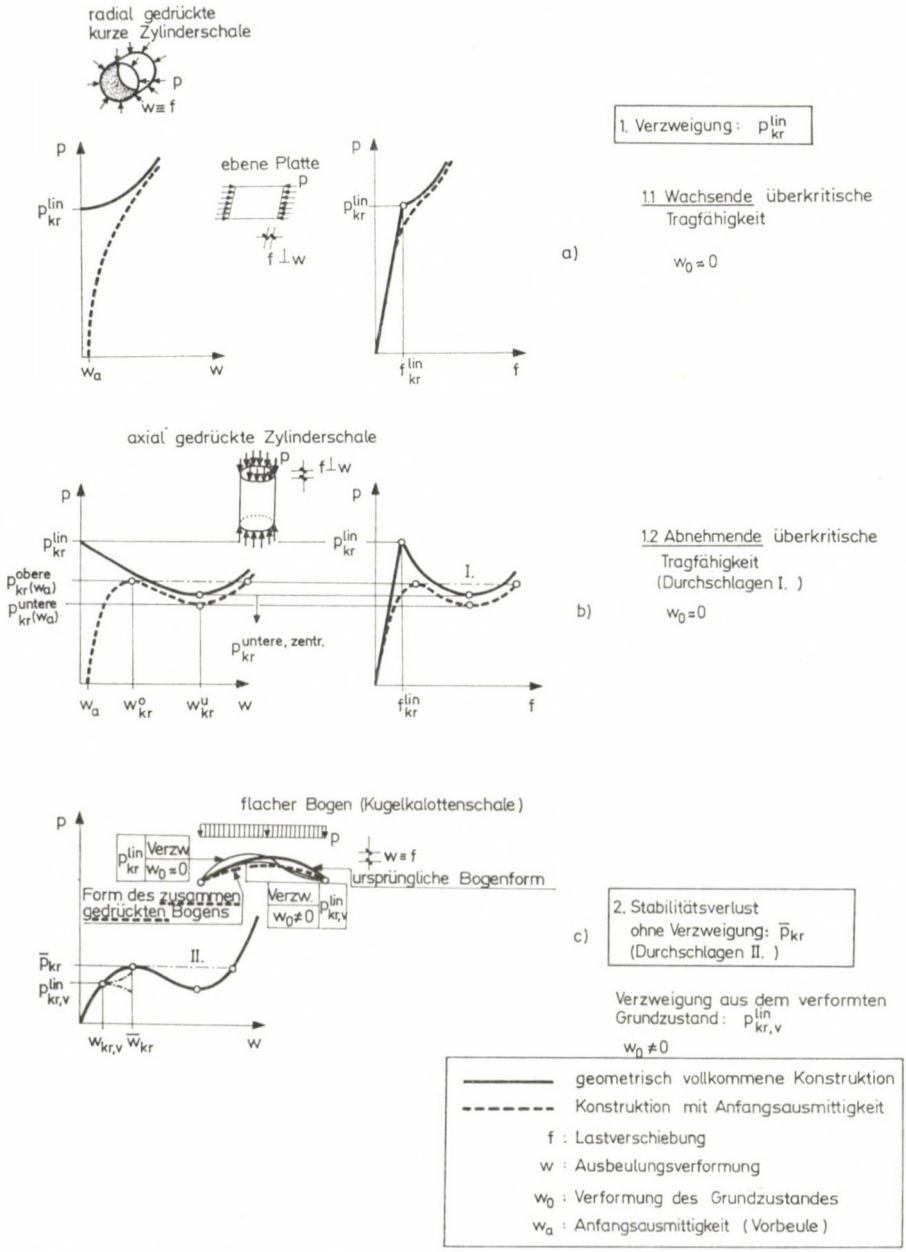

Bild 2. **Einige charakteristische Tragverhaltenskurven der Stabilitätserscheinungen**

Von der sog. *linearen Theorie* weicht die *nichtlineare Theorie* insofern ab, als sie sich nicht auf unendlich kleine Verschiebungen beschränkt, sondern von den in den Deformationsgleichungen auftretenden Gliedern höherer Ordnung die quadratischen Glieder der Ableitungen der auf die Schalenfläche senkrechten Verschiebung w berücksichtigt.

Wir beschränken uns jetzt — wie üblich — auf die *Genauigkeit bis auf Glieder zweiter Ordnung* (beschränkte große Verformungen). (Das Quadrat der Verschiebung w ist etwa von der gleichen Größenordnung wie selbst die Verschiebungen u und v).

Die charakteristischen Tragverhaltenskurven werden nach der nichtlinearen Gleichgewichts- und Verträglichkeitsgleichung der *flachen* Schalen [12], [18] bestimmt.

Zur Lösung des Problems wird das Galerkinsche Verfahren angewandt.

Von der Mittelfläche der Schale wird angenommen, daß sie geometrisch vollkommen ist.

Wir beschäftigen uns mit den Durchbiegungsformen, die sich auf die ganze Fläche erstrecken.

Die näherungsweise Art des angewandten Verfahrens besteht darin, daß sich die als Durchbiegungs- bzw. Spannungsfunktion angesetzten trigonometrischen Reihen — je nach der erforderlichen Genauigkeit — bloß aus je zwei Gliedern zusammensetzen.

In Kenntnis der Tragfähigkeitskurven können wir auch die Frage stellen: ob die behandelten HP-Schalen zum Überspringen in eine antimetrische Beulung neigen.

3. Die Tragfähigkeitskurven

3.1 Grundgleichungen

Die innere potentielle Energie U der unter der gleichmäßig verteilten Belastung $p = p(x, y)$ stehenden Schale läßt sich als eine Summe der potentiellen Energie der Mittelflächen- und der Biegeschnittkräfte (U_m und U_b) wie folgt, aufschreiben [13], [18]:

$$U_m = \frac{1}{2Eh}\int_0^{2a}\int_0^{2b} [F^{\prime\prime 2} - 2\mu\, F^{\cdot\cdot} F^{\prime\prime} + F^{\cdot\cdot 2} + 2(1+\mu)F^{\cdot 2}]\, dx\, dy\,, \tag{3.1}$$

$$U_b = \frac{B}{2}\int_0^{2a}\int_0^{2b} [w^{\prime\prime 2} + 2\,\mu w^{\cdot\cdot} w^{\prime\prime} + w^{\prime\prime 2} + 2(1-\mu)\, w^{\cdot 2}]\, dx\, dy\,, \tag{3.2}$$

$$U = \int_0^{2a}\int_0^{2b} u_0\, dx\, dy = U_m + U_b\,. \tag{3.3}$$

Hierbei ist u_0 die spezifische innere potentielle Energie.

Für den Ausdruck der potentiellen Energie der äußeren Kräfte gilt:

$$V = -\int_0^{2a}\int_0^{2b} pw\,dx\,dy\,. \tag{3.4}$$

Die Beziehung für das elastische Potential (bzw. Gesamtpotential) lautet also:

$$\Pi = \int_0^{2a}\int_0^{2b} \pi\,dx\,dy = U + V. \tag{3.5}$$

Hier ist π die spezifische vollständige potentielle Energie.

Nach dem Prinzip vom stationären Wert des elastischen Potentials muß die erste Variation des elastischen Potentials im Gleichgewichtszustand Null werden

$$\delta\Pi = 0\,. \tag{3.6}$$

Wenn der Gleichgewichtszustand stabil ist, dann nimmt das elastische Potential einen Minimalwert auf. Die diesem Minimalwert zugehörige Funktion w ist die Extremalfunktion.

Zur obigen Variationsaufgabe gehört die folgende Euler-Lagrangesche Differentialgleichung:

$$\frac{\partial\pi}{\partial w} - \left(\frac{\partial\pi}{\partial w'}\right)' - \left(\frac{\partial\pi}{\partial \dot{w}}\right)^{\cdot} + \left(\frac{\partial\pi}{\partial w''}\right)'' + \left(\frac{\partial\pi}{\partial \dot{w}'}\right)^{\cdot\prime} + \left(\frac{\partial\pi}{\partial \ddot{w}}\right)^{\cdot\cdot} = 0\,. \tag{3.7}$$

Nach Durchführung der vorgeschriebenen Operationen ($F = F(w)$) gelangt man zu der wohlbekannten Gleichgewichtsgleichung der Aufgabe [12], [18]:

$$B\Delta\Delta w - L_p(F, z) - L_p(F, w) - p = 0\,. \tag{3.8}$$

Es soll die Gleichung der potentiellen Energie der Mittelflächenkräfte in der Form

$$\begin{aligned} U_m = \int_0^{2a}\int_0^{2b} \Bigg\{ & F''(v^{\cdot} - w z^{\cdot\cdot} + \frac{1}{2} w^{\cdot 2}) - F^{\cdot\prime}(u^{\cdot} + v' + w' w^{\cdot}) + \\ & + F^{\cdot\cdot}\left(u' - w z'' + \frac{1}{2} w'^2\right) - \frac{1}{2Eh}\left[F''^2 - 2\mu\, F^{\cdot\cdot} F'' + \right. \\ & \left. + F^{\cdot\cdot 2} + 2(1+\mu) F^{\cdot\prime 2}\right] \Bigg\} dx\,dy \end{aligned} \tag{3.9}$$

geschrieben werden.

Mit Hilfe dieser — nach dem Prinzip vom Minimalwert der Ergänzungsenergie (Satz III von Castigliano) — erhält man aus der folgenden Variationsaufgabe nach F

$$\delta U = 0 \tag{3.10}$$

bei Anwendung der Euler—Lagrangesche Differentialgleichung

$$\left(\frac{\partial u_0}{\partial F^{\prime\prime}}\right)^{\prime\prime} + \left(\frac{\partial u_0}{\partial F^{\cdot\prime}}\right)^{\cdot\prime} + \left(\frac{\partial u_0}{\partial F^{\cdot\cdot}}\right)^{\cdot\cdot} = 0 \tag{3.11}$$

die Gleichung [12], [18]:

$$\Delta\Delta F + D(1-\mu^2)\left[L_p(w,z) + \frac{1}{2}L_p(w,w)\right] = 0\,, \tag{3.12}$$

die die Verträglichkeit der Mittelflächenverzerrungen ausdrückt.

Die Gleichungen (3.8) und (3.12) sind identisch mit den Gleichungen DONNELLS, die er aus der exakten (die Flachheit der Schale nicht voraussetzen den) Ableitung erhielt, indem er die im Vergleich zu den anderen unwichtigen Gliedern vernachlässigte. Die Donnellschen Gleichungen sind durch zwei Eigenheiten gekennzeichnet: einerseits setzen sie die Flachheit der Schale voraus, anderseits berücksichtigen sie aus der Reihe der Glieder höheren Grades nur die in Gl. (3.9) vorkommenden $\frac{1}{2}w^{\cdot 2}, w^{\prime}w^{\cdot}, \frac{1}{2}w^{\prime 2}$. Sie sind aber nur dann gültig, wenn die Schale *innerhalb einer Beulwelle* als *flach* angesehen werden kann.

3.2 Durchbiegungsform und Spannungsfunktion

Bekanntlich kann man das Galerkinsche Verfahren auch so anwenden, daß sowohl die Durchbiegungsform als auch die Spannungsfunktion F *gleichzeitig* als je eine Summe von linearen unabhängigen Gliedern dargestellt wird [18].

Jedes Glied der Funktion w muß den folgenden geometrischen (»künstlichen«) und statischen (»natürlichen«) Randbedingungen der Aufgabe genügen:

$$w_{ij0}\Big|_{\substack{x=0\\x=2a}} = 0\,, \qquad w_{ij0}\Big|_{\substack{y=0\\y=2b}} = 0\,, \tag{3.13a—d}$$

$$w^{\prime\prime}_{ij0}\Big|_{\substack{x=0\\x=2a}} = 0\,, \qquad w^{\cdot\cdot}_{ij0}\Big|_{\substack{y=0\\y=2b}} = 0\,. \tag{3.14a—d}$$

Jedes Glied der Spannungsfunktion F hat die folgenden statischen Randbedingungen zu erfüllen:

$$F''_{ij0}\Big|_{\substack{y=0\\y=0b}} = 0\,, \qquad F''_{ij0}\Big|_{\substack{x=0\\x=2a}} = 0\,. \tag{3.15a—d}$$

Diese letzteren Zusammenhänge formulieren die Bedingungen der *normalkraftfreien Abstützung*, es handelt sich nämlich um Randbogen, die bloß Schubkräfte aufnehmen können.

Demnach sind die Funktionen w und F durch die trigonometrischen Reihen

$$w = \sum_{i}^{I_1}\sum_{j}^{J_1} w_{ij}\cdot S_{ij} = \sum_{i}^{I_1}\sum_{j}^{J_1} w_{ij0}\,, \tag{3.16}$$

$$i = 1, 3, 5, ..., I_1$$

$$j = 1, 3, 5, ,.., J_1$$

$$F = \sum_{i}^{I_2}\sum_{j}^{J_2} F_{ij}\cdot S_{ij} = \sum_{i}^{I_2}\sum_{j}^{J_2} F_{ij0} \tag{3.17}$$

$$i = 1, 3, 5, ..., I_2$$

$$j = 1, 3, 5, ..., J_2$$

darzustellen. Hier gilt die Abkürzung:

$$S_{ij} = \sin\frac{i\pi}{2a}x\cdot \sin\frac{j\pi}{2b}y. \tag{3.18}$$

3.3 *Auflösung nach dem Galerkinschen Verfahren*

Die folgenden zwei Definitionsgleichungen dieser Variante des Galerkinschen Verfahrens sind aus dem Prinzip der virtuellen Verrückungen bzw. der virtuellen Änderungen des Spannungszustandes — unter Anwendung des Hookeschen Gesetzes — durch Variationsrechnung herzuleiten [18]:

$$\int_0^{2a}\int_0^{2b} X\,S_{i'j'}\,dx\,dy = 0\,, \tag{3.19}$$

$$i' = 1, 2, 3, ..., I_1$$

$$j' = 1, 2, 3, ..., J_1$$

$$\int_0^{2a}\int_0^{2b} Y\, S_{i'j'}\, dx\, dy = 0\,. \tag{3.20}$$

$$i' = 1, 2, 3, \ldots, I_2$$

$$j' = 1, 2, 3, \ldots, J_2$$

Die in der ersten Gleichung befindliche Fehlerfunktion X erhält man so, daß man die Ausdrücke (3.16) und (3.17) in die Gleichgewichtsgleichung (3.8) einsetzt.

Nach Einsetzen der Funktionen (3.16) und (3.17) in die Verträglichkeitsgleichung (3.12) ergibt sich die Fehlerfunktion Y.

Die Fehlerfunktionen X bzw. Y wären nur dann genau gleich Null, wenn die Ansatzfunktionen (3.16) bzw. (3.17) mit den exakten Lösungsfunktionen identisch wären.

Stellt man sich die Fehlerfunktion X (bzw. Y) in Form einer trigonometrischen Reihe vor, die nach den Faktoren S_{ij} der Funktion w (bzw. F) entwickelt ist, so stellt sich heraus, daß die Gleichung (3.19) (bzw. (3.20)) die Forderung nach dem Verschwinden der Funktion X (bzw. Y) ausdrückt (X und Y sind zu S_{ij} orthogonal).

Im vorliegenden Fall setzt sich sowohl die Funktion w als auch die Funktion F aus zwei Gliedern zusammen (mit Index $i_1 j_1$ bzw. $i_2 j_2$).

Unter Durchführung der durch die Gln. (3.19) und (3.20) vorgeschriebenen Operationen ergibt sich das folgende System von nichtlinearen Differentialgleichungen:

$$a_{11}\frac{w_{i_1j_1}}{h} + a_{12}\frac{w_{i_1j_1}}{h}\frac{F_{i_1j_1}}{E} + a_{13}\frac{w_{i_2j_2}}{h}\frac{F_{i_2j_2}}{E} + a_{14}\frac{w_{i_1j_1}}{h}\frac{F_{i_2j_2}}{E} +$$

$$+ a_{15}\frac{w_{i_2j_2}}{h}\frac{F_{i_1j_1}}{E} + a_{16}\frac{F_{i_1j_1}}{E} + a_{17}\frac{p}{E} = 0\,,$$

$$a_{21}\frac{w_{i_2j_2}}{h} + a_{22}\frac{w_{i_1j_1}}{h}\frac{F_{i_1j_1}}{E} + a_{23}\frac{w_{i_2j_2}}{h}\frac{F_{i_2j_2}}{E} + a_{24}\frac{w_{i_1j_1}}{h}\frac{F_{i_2j_2}}{E} +$$

$$+ a_{25}\frac{w_{i_2j_2}}{h}\frac{F_{i_1j_1}}{E} + a_{26}\frac{F_{i_2j_2}}{E} + a_{27}\frac{p}{E} = 0\,, \tag{3.21a–d}$$

$$a_{31}\frac{F_{i_1j_1}}{E} + a_{32}\frac{w_{i_1j_1}}{h} + a_{33}\left(\frac{w_{i_1j_1}}{h}\right)^2 + a_{34}\frac{w_{i_1j_1}}{h}\frac{w_{i_2j_2}}{h} + a_{35}\left(\frac{w_{i_2j_2}}{h}\right)^2 = 0\,,$$

$$a_{41}\frac{F_{i_2j_2}}{E} + a_{42}\frac{w_{i_2j_2}}{h} + a_{43}\left(\frac{w_{i_1j_1}}{h}\right)^2 + a_{44}\frac{w_{i_1j_1}}{h}\frac{w_{i_2j_2}}{h} + a_{45}\left(\frac{w_{i_2j_2}}{h}\right)^2 = 0\,.$$

Für die Koeffizienten des Gleichungssystems gelten die Zusammenhänge:

$$
\begin{aligned}
&a_{11} = \frac{\pi^4}{192(1-\mu^2)} \frac{Ebh}{\beta^3} \frac{1}{a_{i_1 j_1}}, \quad a_{12} = -\frac{2}{3}\pi^2 \frac{Eh}{ab} i_1 j_1, \quad a_{13} = a_{24} \\
&a_{14} = 2\pi^2 \frac{Eh}{ab} c_{i_2 j_2 i_1 j_1} = a_{15}, \quad a_{16} = \frac{\pi^2}{2} \frac{Ef_b}{ab} b_{i_1 j_1}, \quad a_{17} = -\frac{16}{\pi^2} Eab \frac{1}{i_1 j_1}, \\
&a_{21} = \frac{\pi^4}{192(1-\mu^2)} \frac{Ebh}{\beta^3} \frac{1}{a_{i_2 j_2}}, \quad a_{22} = a_{14}, \quad a_{23} = -\frac{2}{3}\pi^2 \frac{Eh}{ab} i_2 j_2, \\
&a_{24} = 2\pi^2 \frac{Eh}{ab} c_{i_1 j_1 i_2 j_2} = a_{25}, \quad a_{26} = \frac{\pi^2}{2} \frac{Ef_b}{ab} b_{i_2 j_2}, \quad a_{27} = -\frac{16}{\pi^2} Eab \frac{1}{i_2 j_2}, \\
&a_{31} = \frac{\pi^4}{16} \frac{Eb}{a^3} \frac{1}{a_{i_1 j_1}}, \quad a_{32} = -\frac{\pi^2}{2} \frac{Eh^2 f_b}{ab} b_{i_1 j_1}, \quad a_{33} = \frac{\pi^2}{3} \frac{Eh^3}{ab} i_1 j_1, \\
&a_{34} = -2\pi^2 \frac{Eh^3}{ab} c_{i_2 j_2 i_1 j_1}, \quad a_{35} = \frac{a_{44}}{2}, \\
&a_{41} = \frac{\pi^4}{16} \frac{Eb}{a^3} \frac{1}{a_{i_2 j_2}}, \quad a_{42} = -\frac{\pi^2}{2} \frac{Eh^2 f_b}{ab} b_{i_2 j_2}, \quad a_{43} = \frac{a_{34}}{2}, \\
&a_{44} = -2\pi^2 \frac{Eh^3}{ab} c_{i_1 j_1 i_2 j_2}, \quad a_{45} = \frac{\pi^2}{3} \frac{Eh^3}{ab} i_2 j_2.
\end{aligned}
\tag{3.22a–z}
$$

In den obigen Ausdrücken kommen folgende Hilfsgrößen vor:

$$
\begin{aligned}
a_{i_1 j_1} &= \frac{1}{(i_1^2 + \gamma^2 j_1^2)^2}, \quad b_{i_1 j_1} = \alpha j_1^2 - i_1^2, \\
c_{i_1 j_1 i_2 j_2} &= \frac{i_2^2 j_2^2 (i_1^2 j_1^2 - 2(i_1^2 j_2^2 + i_2^2 j_1^2))}{i_1 j_1 (4i_2^2 - i_1^2)(4j_2^2 - j_1^2)}.
\end{aligned}
\tag{3.23a–c}
$$

Die Hilfsgrößen $a_{i_2 j_2}$, $b_{i_2 j_2}$, $c_{i_2 j_2 i_1 j_1}$ sind so zu berechnen, daß man statt der Zahl i_1 die Zahl i_2 und statt der Zahl j_1 die Zahl j_2 schreibt und umgekehrt.

Das Gleichungssystem (3.21a–d) ist auf eine gemischte Gleichung dritten Grades zu reduzieren. Drückt man $F_{i_1 j_1}/E$ und $F_{i_2 j_2}/E$ aus den Gleichungen (3.21c–d) aus und setzt man diese in die Gleichungen (3.21a–b) ein, so läßt sich die Gleichung (3.21a) in Gestalt einer gemischten Gleichung dritten Grades aufschreiben:

$$A_0 \frac{w_{i_1 j_1}}{h} + B_0 \frac{w_{i_1 j_1}}{h} \frac{w_{i_2 j_2}}{h} + C_0 \left(\frac{w_{i_1 j_1}}{h}\right)^2 +$$

$$+ D_0 \left(\frac{w_{i_1 j_1}}{h}\right)^2 \frac{w_{i_2 j_2}}{h} + E_0 \left(\frac{w_{i_1 j_1}}{h}\right)^3 + F_0 \frac{w_{i_2 j_2}}{h} + G_0 \left(\frac{w_{i_2 j_2}}{h}\right)^2 + \quad (3.24)$$

$$+ H_0 \frac{w_{i_1 j_1}}{h} \left(\frac{w_{i_2 j_2}}{h}\right)^2 + I_0 \left(\frac{w_{i_2 j_2}}{h}\right)^3 = -\frac{p}{E} .$$

Die Koeffizienten *der Gleichung von der Struktur der Gl.* (3.24), die aus der Gl. (3.21b) stammt, werden mit $-A_{00}$, $-B_{00}$, ..., $-I_{00}$, bezeichnet. Durch Subtraktion dieser Gleichung mit Koeffizienten $-A_{00}$, B_{00}, ..., $-I_{00}$ aus der Gl. (3.24) erhält man *die »charakteristische« Gleichung* der Aufgabe:

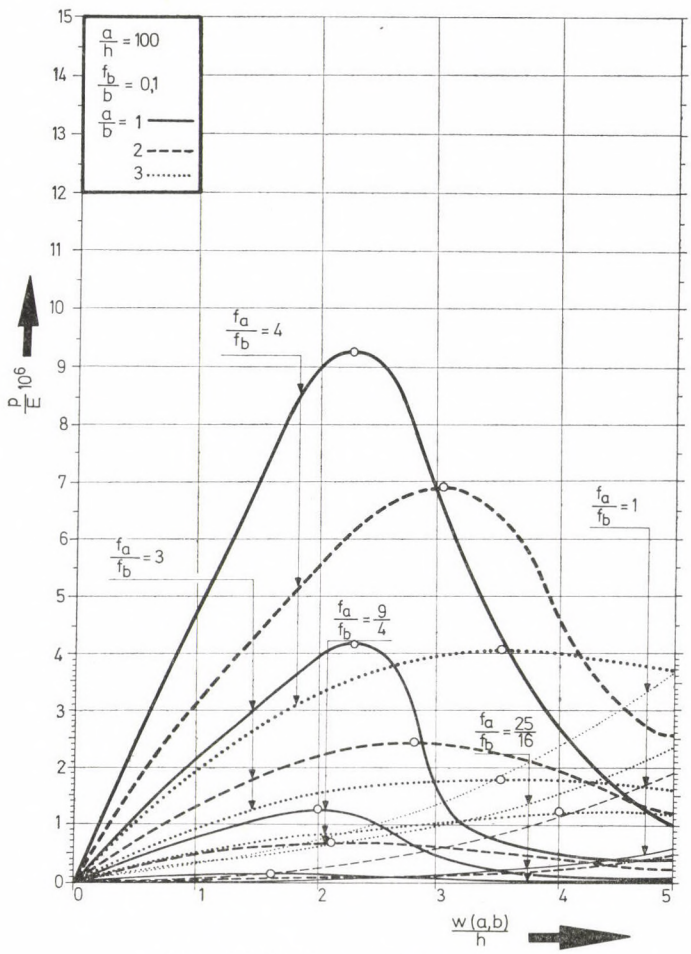

Bild 3. Nichtlineares Tragverhalten

$$A\frac{w_{i_1 j_1}}{h} + B\frac{w_{i_1 j_1}}{h}\frac{w_{i_2 j_2}}{h} + C\left(\frac{w_{i_1 j_1}}{h}\right)^2 + D\left(\frac{w_{i_1 j_1}}{h}\right)^2\frac{w_{i_2 j_2}}{h} +$$

$$+ E\left(\frac{w_{i_1 j_1}}{h}\right)^3 + F\frac{w_{i_2 j_2}}{h} + G\left(\frac{w_{i_2 j_2}}{h}\right)^2 + \tag{3.25}$$

$$+ H\frac{w_{i_1 j_1}}{h}\left(\frac{w_{i_2 j_2}}{h}\right)^2 + I\left(\frac{w_{i_2 j_2}}{h}\right)^3 = 0\,.$$

Die Koeffizienten der Gl. (3.25) lauten:

$$A = A_0 + A_{00}\,, \quad B = B_0 + B_{00}, \ \ldots, \quad I = I_0 + I_{00}, \tag{3.26}$$

$$A_0 = -i_1 j_1\left[\frac{\pi^6}{3072(1-\mu^2)}\frac{1}{a_{i_1 j_1}}\frac{1}{\beta^4} + \frac{\pi^2}{4}\left(\frac{\gamma\varrho}{\beta}\right)^2 b^2_{i_1 j_1}\, a_{i_1 jj}\right],$$

$$A_{00} = 0\,,$$

$$B_0 = -\pi^2\left(\frac{\gamma}{\beta}\right)^3 \varrho i_1 j_1\,[2a_{i_1 j_1}\, b_{i_1 j_1} + a_{i_2 j_2} b_{i_2 j_2}]\, c_{i_2 j_2 i_1 j_1}\,,$$

$$B_{00} = \pi^2\left(\frac{\gamma}{\beta}\right)^3 \varrho\, i_2 j_2\,[2a_{i_2 j_2}\, b_{i_2 j_2} + a_{i_1 j_1}\, b_{i_1 j_1}] c_{i_1 j_1 i_2 j_2}\,,$$

$$C_0 = \frac{\pi^2}{2}\left(\frac{\gamma}{\beta}\right)^3 \varrho\, i_1^2 j_1^2\, a_{i_1 j_1}\, b_{i_1 j_1}\,,$$

$$C_{00} = \pi^2\left(\frac{\gamma}{\beta}\right)^3 \varrho\, i_2 j_2\left[a_{i_1 j_1}\, b_{i_1 j_1} + \frac{1}{2}\, a_{i_2 j_2}\, b_{i_2 j_2}\right] c_{i_2 j_2 i_1 j_1}\,,$$

$$D_0 = \pi^2\left(\frac{\gamma}{\beta}\right)^4 i_1 j_1\,[2i_1 j_1\, a_{i_1 j_1} - 6c_{i_1 j_1 i_2 j_2}\, a_{i_2 j_2}]\, c_{i_2 j_2 i_1 j_1}\,,$$

$$D_{00} = \pi^2\left(\frac{\gamma}{\beta}\right)^4 i_2 j_2\left[-2\left(-2\, c^2_{i_2 j_2 i_1 j_1} + \frac{1}{3}\, i_1 j_1\, c_{i_1 j_1 i_2 j_2}\right) a_{i_1 j_1} + \right.$$

$$\left. + \left(-\frac{2}{3}\, i_2 j_2\, c_{i_2 j_2 i_1 j_1} + 4\, c^2_{i_1 j_1 i_2 j_2}\right) a_{i_2 j_2}\right],$$

$$E_0 = -2\,\pi^2\left(\frac{\gamma}{\beta}\right)^4 i_1 j_1\left[a_{i_2 j_2}\, c^2_{i_2 j_2 i_1 j_1} + \frac{1}{9}\, i_1^2 j_1^2\, a_{i_1 j_1}\right],$$

$$E_{00} = -2\,\pi^2\left(\frac{\gamma}{\beta}\right)^4 i_2 j_2\left[\frac{1}{3}\, i_1 j_1\, a_{i_1 j_1} - a_{i_2 j_2}\, c_{i_1 j_1 i_2 j_2}\right] c_{i_2 j_2 i_1 j_1}\,, \tag{3.27a–j}$$

$$
\left.
\begin{aligned}
F_0 &= 0\,, \\
F_{00}(i_2, j_2, i_1, j_1) &= -A_0(i_1, j_1, i_2, j_2)\,, \\
G_0(i_2, j_2, i_1, j_1) &= -C_{00}(i_1, j_1, i_2, j_2)\,, \\
G_{00}(i_2, j_2, i_1, j_1) &= -C_0(i_1, j_1, i_2, j_2)\,, \\
H_0(i_2, j_2, i_1, j_1) &= -D_{00}(i_1, j_1, i_2, j_2)\,, \\
H_{00}(i_2, j_2, i_1, j_1) &= -D_0(i_1, j_1, i_2, j_2)\,, \\
I_0(i_2, j_2, i_1, j_1) &= -E_{00}(i_1, j_1, i_2, j_2)\,, \\
I_{00}(i_2, j_2, i_1, j_1) &= -E_0(i_1, j_1, i_2, j_2)\,.
\end{aligned}
\right\} \quad (3.28\text{a}-\text{h})
$$

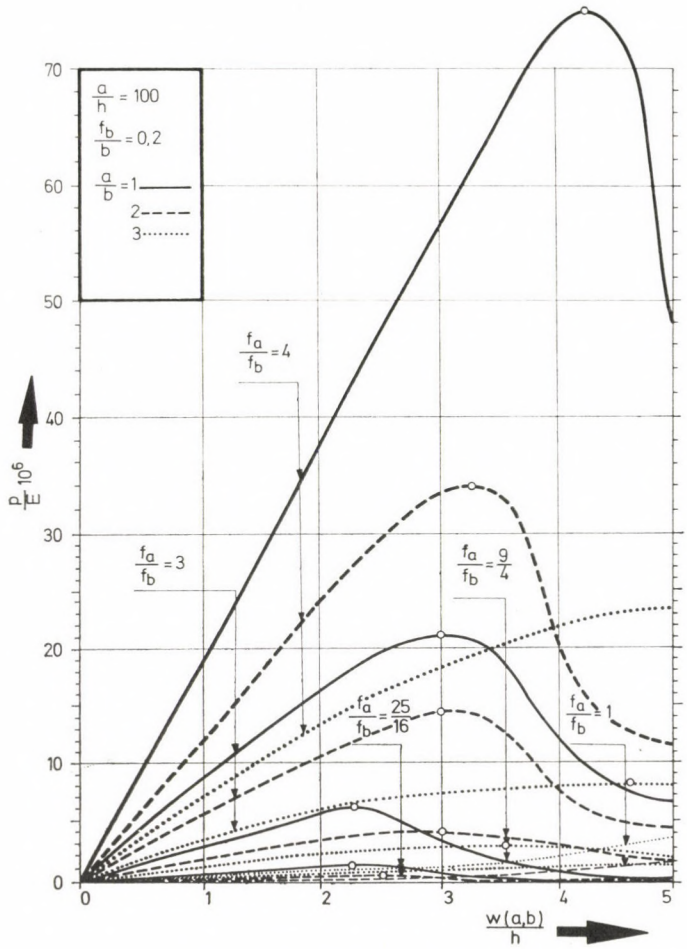

Bild 4. Nichtlineares Tragverhalten

Die in den Gln. (3.28a—h) befindlichen Symbole in Klammern verweisen darauf, daß man die Größen F_{00}, G_0, ..., I_{00} aus den Funktionen $-A_0$, $-C_{00}$, ..., $-E_0$ durch den Austausch der Variablen ($i_1 \to i_2$, $j_1 \to j_2$, $i_2 \to i_1$, $j_2 \to j_1$) erhalten kann.

Durch Einführung der Hilfsgröße

$$\frac{w(a,b)}{h} = \frac{w}{h} = \frac{w_{i_1 j_1}}{h} S^0_{i_1 j_1} + \frac{w_{i_2 j_2}}{h} S^0_{i_2 j_2} \tag{3.29}$$

gelangt man zur »*charakteristischen*« *Gleichung* in Form von

$$a_0 + a_1 \frac{w_{i_1 j_1}}{h} + a_2 \left(\frac{w_{i_1 j_1}}{h}\right)^2 + a_3 \left(\frac{w_{i_1 j_1}}{h}\right)^3 = 0, \tag{3.30}$$

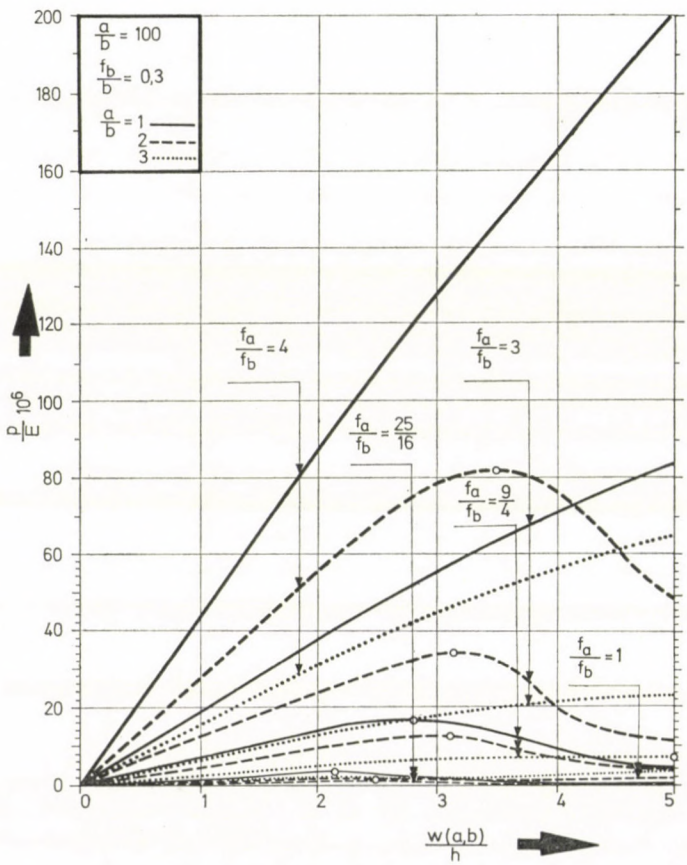

Bild 5. Nichtlineares Tragverhalten

wobei:

$$S^0_{i_1 j_1} = \sin\frac{i_1\pi}{2} \cdot \sin\frac{j_1\pi}{2}, \quad S^0_{i_2 j_2} = \sin\frac{i_2\pi}{2} \cdot \sin\frac{j_2\pi}{2}, \qquad (3.31a-b)$$

$$a_0 = \frac{F}{S^0_{i_2 j_2}}\frac{w}{h} + G\left(\frac{w}{h}\right)^2 + \frac{I}{S^0_{i_2 j_2}}\left(\frac{w}{h}\right)^3,$$

$$a_1 = A - \frac{F}{S^0_{i_2 j_2}} S^0_{i_1 j_1} + \left(\frac{B}{S^0_{i_2 j_2}} - 2GS^0_{i_1 j_1}\right)\frac{w}{h} + \left(H - \frac{3I}{S^0_{i_2 j_2}} S^0_{i_1 j_1}\right)\left(\frac{w}{h}\right)^2,$$

$$a_2 = -\frac{B}{S^0_{i_2 j_2}} S^0_{i_1 j_1} + C + G + \left(\frac{D}{S^0_{i_2 j_2}} - 2HS^0_{i_1 j_1} + 3\frac{I}{S_{i_2 j_2}}\right)\frac{w}{h}, \qquad (3.32a-d)$$

$$a_3 = -\frac{D}{S^0_{i_2 j_2}} S^0_{i_1 j_1} + E + H - \frac{I}{S^0_{i_2 j_2}} S^0_{i_1 j_1}$$

bedeuten.

3.4 Numerische Untersuchungen

Die numerisch bestimmten $p - w$ Tragverhaltenskurven sind in den Bildern 3—13. dargestellt. Das Tragverhalten nach der Theorie der großen Verformungen wird im weiteren »nichtlineares Tragverhalten« genannt (vgl. mit Abschn. 2). In der Tabelle I sind die kennzeichnenden Ordinaten der erwähnten Kurven zusammengefaßt.

Eine Komponente der Durchbiegungsfunktion kann durch die Zahlen $i_1 = j_1 = 1$, die andere hingegen durch die Zahlen $i_2 = 3$, $j_2 = 1$ oder $i_2 = 3$, $j_2 = 3$ gekennzeichnet werden.

Es handelt sich um eine Belastung, die sowohl in Bezug auf die $\bar{x}$-Achse als auch die $\bar{y}$-Achse symmetrisch verteilt ist, folglich sollen bei dieser Untersuchung keine antimetrischen Durchbiegungsformen berücksichtigt werden. Antimetrische Komponenten werden nur im Falle einer Ausbeulung angesetzt, die aus dem verformten Grundzustand abzweigt (s. im Punkt 4.).

Von den zwei Werten i_2 bzw. j_2 wurde mit demjenigen gerechnet, dem eine kleinere Tragfähigkeit zugeordnet ist. Eine bedeutendere Abweichung zwischen der Wirkung dieser letzteren Komponenten erwies sich in den Bereichen nach den Scheitelpunkten der Schalen.

Um die nach dem Durchschlagen auftretenden größeren Verformungen der endlich dünnwandigen Schale verfolgen zu können, müßten noch weitere, und zwar auch Glieder höherer Ordnung, in die Berechnung einbezogen werden.

Für die Bemessung der Schale werden in erster Reihe die Maximalwerte der Kurven benötigt, und deshalb betrachten wir diese genauere Untersuchung — im Rahmen dieser Abhandlung — nicht als unsere Aufgabe.

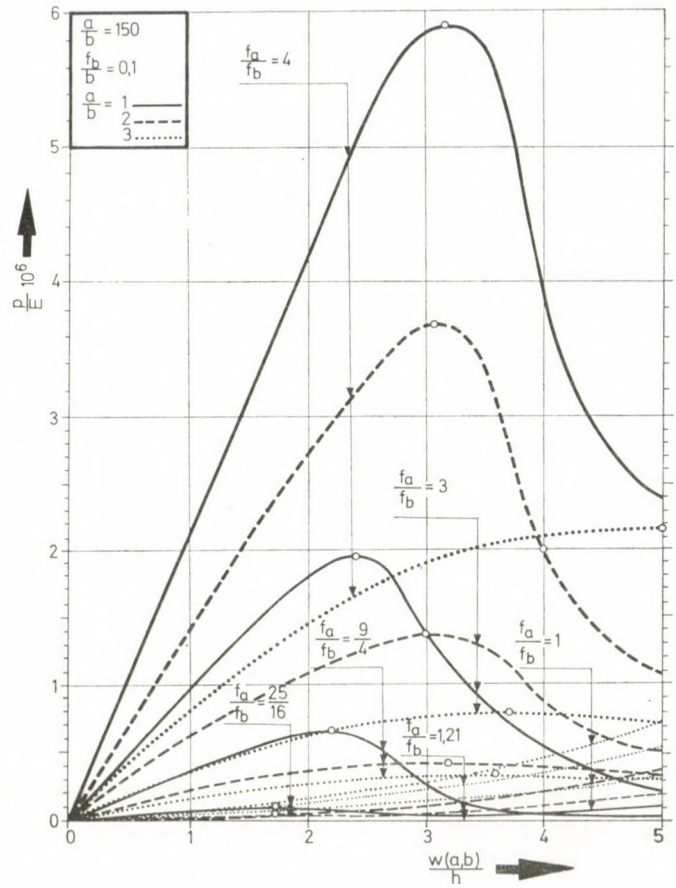

Bild 6. Nichtlineares Tragverhalten

Die Berechnungen wurden so vorgenommen, daß die relativen Amplituden $w_{i_1 j_1}/h$, $w_{i_2 j_2}/h$ der Komponenten der Funktion w für im voraus angesetzte Größen $w(a, b)/h$ bestimmt wurden, sodann wurde der Tragfähigkeitsparameter p/E aus dem Zusammenhang (3.24) berechnet.

Wie die Schaubilder deutlich erkennen lassen, kann (nach der Theorie der großen Verformungen) *das nichtlineare Tragverhalten* derjenigen HP-Schalen, die nach der Theorie I. Ordnung als Membranschalen zu betrachten sind ([5], $f_a/f_b = (1{,}5-2) \div 4$), *durch die charakteristische Tragverhaltenskurve von Bild* 2.*c* gekennzeichnet werden. Diese Art des Tragverhaltens wird im weiteren »*schalenartiges*« Tragverhalten genannt. Das läßt sich am besten durch die Kurven der »*normalen*« Schale ($f_a/f_b = 4$) oder *der Schale mit dem Pfeilhöhenverhältnis* $f_a/f_b = 9/4$ veranschaulichen. In diesen Fällen ist zu beobachten,

daß sich die Tragfähigkeit bei wachsender Durchbiegung eine Zeitlang monoton vergrößert (stabiler Gleichgewichtszustand), aber dann, nach Erreichen der Lastintensität $\overline{p}_{kr}$ (bei Beginn des *labilen* Gleichgewichtszustandes), tritt das *Durchschlagen* in einer Lage mit niedrigerem Potential auf. Auf die *abnehmende* Tragfähigkeit folgt eine *zunehmende* Tragfähigkeit (stabiler Gleichgewichtszustand).

Da die Konstruktion bei Erreichen des Durchschlagens — vom Gesichtspunkt der Ingenieurs-Praxis — als zu Bruch gegangen anzusehen ist, wurden die Kurvenzweige mit wieder wachsendem Bereich gar nicht dargestellt.

Ein System von Erzeugenden der translationalen HP-Schalen bildet eine von oben gesehen konkave Parabelschar, folglich kann man daran denken, daß diese Schalen eine monoton zunehmende (nichtlineare) Tragfähigkeit aufweisen. Aber diese ist — mit Ausnahme der »halbnormalen« HP-Schale, die sich plattenartig verhält — nur dann möglich, wenn die HP-Schale *entlang der*

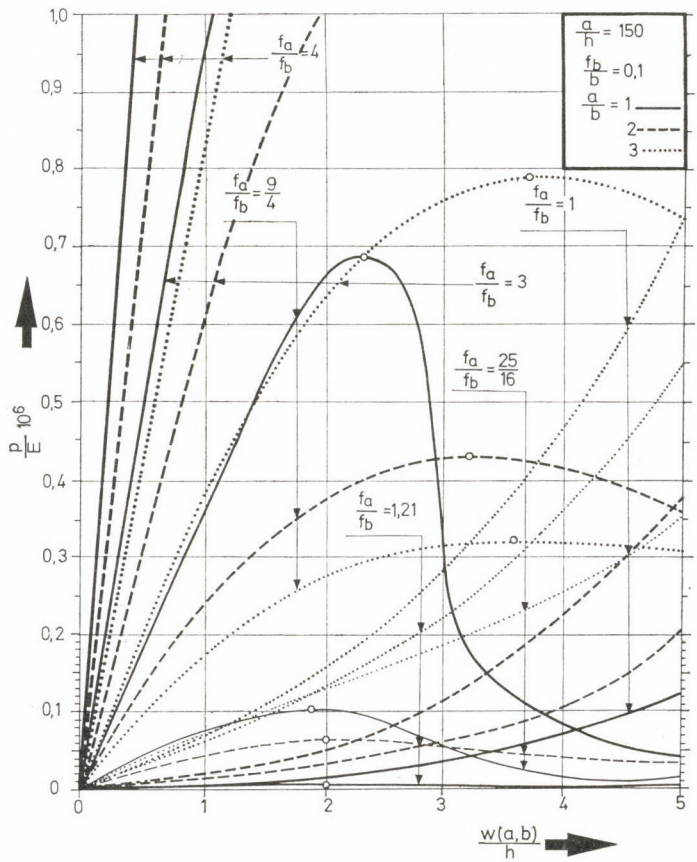

Bild 7. Nichtlineares Tragverhalten

asimptotischen Linien (die die an der Fläche befindlichen Entsprechenden der Charakteristiken sind) abgestützt ist [9].

Der Grund hiefür liegt darin, daß mindestens diejenige Zugfaser von der von oben gesehen konkaven Fasern, die die Eckpunkte miteinander verbindet, gewissermaßen als Aufhängung der sich ausbeulenden gedrückten Fasern wirkt [8].

Jede von oben gesehen konkave Faser der sattelförmigen, an ihren Rändern normalkraftfreien HP-Schale schließt sich solchen Randbogen an, die in Seitenrichtung *frei verschiebbar* sind (die Wirkung der Faser bei den Lagerungen ist vernachlässigbar). Deshalb tritt die erwähnte Aufhängungswirkung nicht ein.

Ein weiteres Anwachsen der Tragfähigkeit nach dem Durchschlagen ist nur nach Auftreten von Verformungen in sehr großem Ausmaß möglich. In diesem Fall finden sich die Bogen in x-Richtung schon in einer von oben

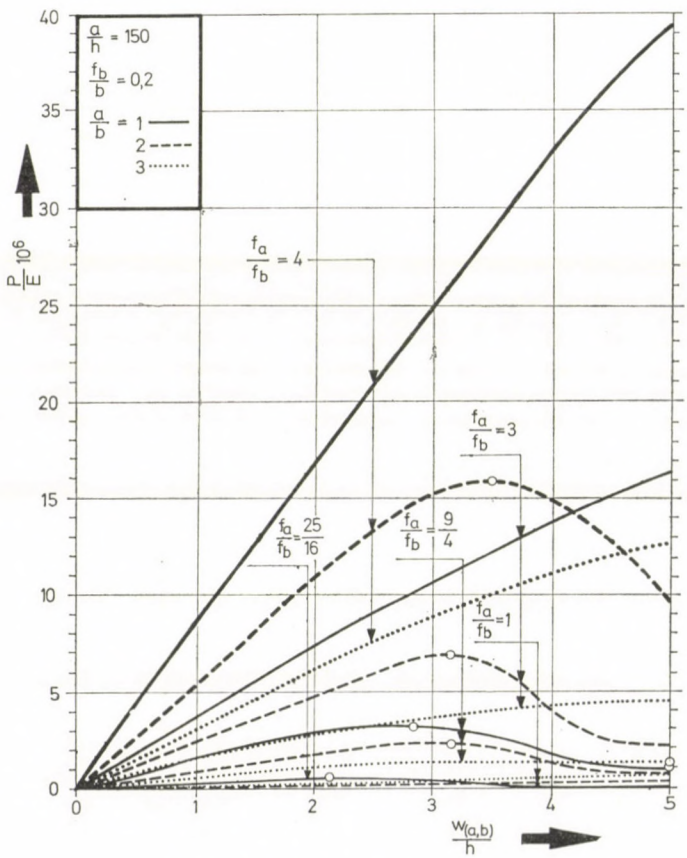

Bild 8. Nichtlineares Tragverhalten

gesehen konkaven Lage, folglich wurde dieser in praktischer Ansicht nicht interessante Zustand in den Bildern 3—13 auch nicht dargestellt.

Die *»halbnormale«* HP-Schale ($f_a/f_b = 1$) weist ein Tragverhalten auf, das von dem bisher behandelten schalenartigen Verhalten vollständig abweicht. Es soll daran erinnert werden, daß diese Schale ihre Lasten nach der Theorie I. Ordnung zum überwiegenden Teil durch Biegeschnittkräfte trägt [5].

Diese *plattenartige*, monoton zunehmende Tragverhaltensart geht auch aus den Bildern 3—13 hervor. Es stimmt zwar, daß die Tragfähigkeit der »halbnormalen« HP-Schale mit zunehmender Durchbiegung immer größer wird, aber *die Last*, die sie auf diese Weise tragen vermag, *ist zu klein*.

In Einklang mit den Resultaten nach der Theorie I. Ordnung [5] läßt sich auch jetzt feststellen, daß die »halbnormale« Schale und die HP-Schalen, deren Pfeilhöhenverhältnisse von dem f_a/f_b-Wert von 1 nur geringfügig abweichen

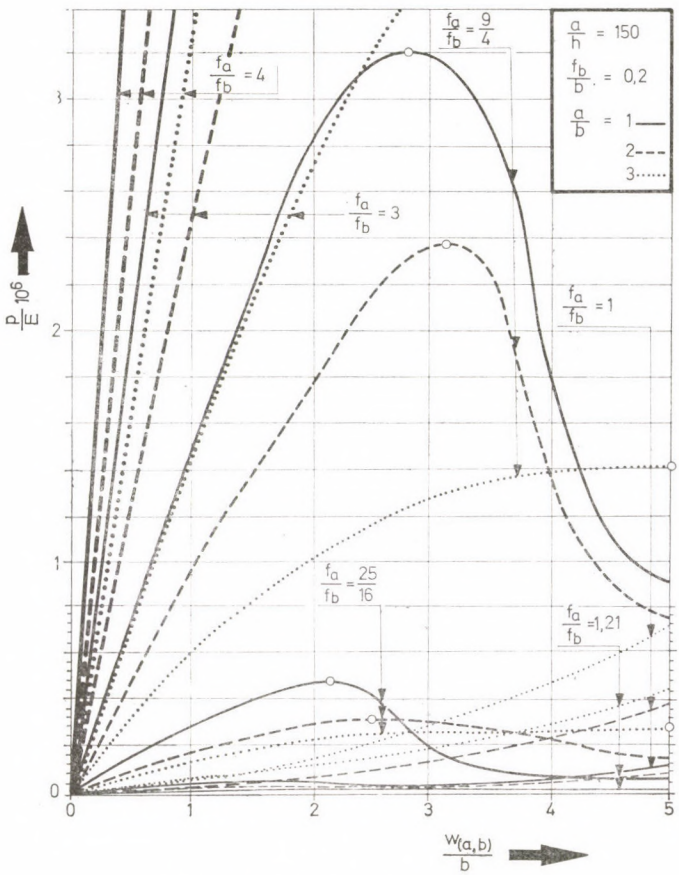

Bild 9. Nichtlineares Tragverhalten

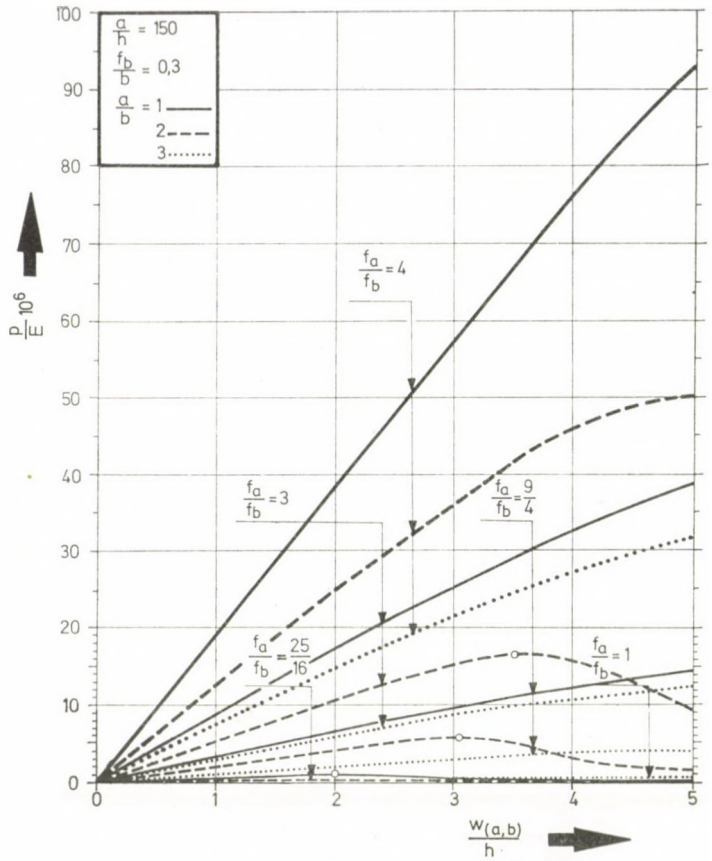

Bild 10. Nichtlineares Tragverhalten

ausschließlich im Fall von bei den Platten üblichen Verhältnisse a/h ($a/h = 15 \div 20$) angewandt werden können.

Zwischen den erwähnten typischen Fällen (schalenartiges bzw. plattenartiges Verhalten) gibt es auch Übergangsstadien: die zu diesen gehörenden Schaubilder haben *Inflexionspunkte* aber keine stationäre Werte (bzw. keine waagerechte Tangente).

Die verschiedene Art des plattenartigen und des schalenartigen Tragverhaltens wird auch durch die abweichenden Wirkungen veranschaulicht, die das Seitenverhältnis a/b ausübt. Mit abnehmender Abmessung b nimmt die Tragfähigkeit der plattenartig wirkenden HP-Schalen immer mehr zu, hingegen nimmt die Tragfähigkeit der schalenartig wirkenden HP-Schalen immer mehr ab.

Sowohl die Art der Kurven als auch das Maß der Tragfähigkeit verweisen auf ***das Fehlen der horizontalen*** (seitlichen) ***Biegesteifigkeit und der Drillsteifigkeit der Randbogen.***

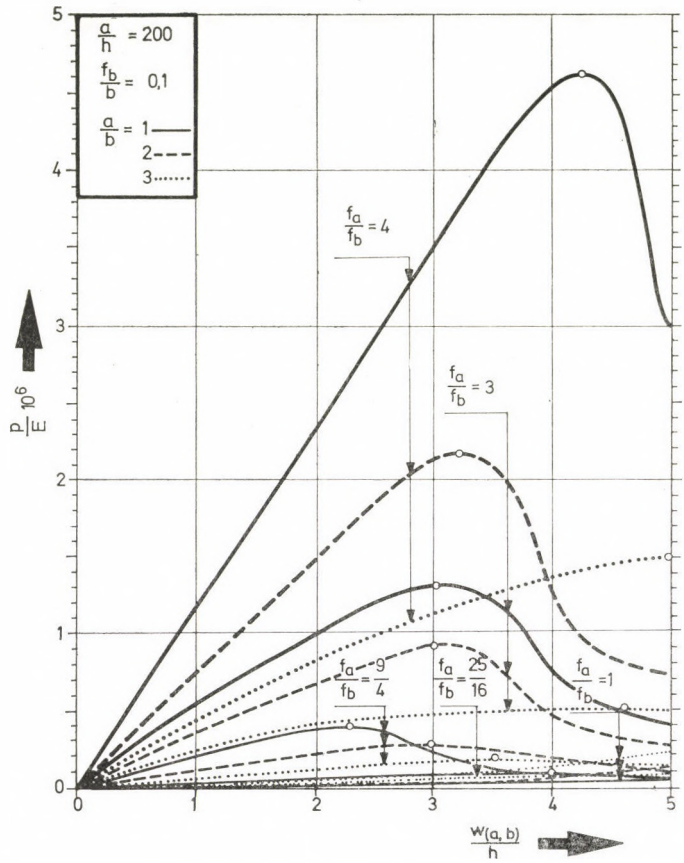

Bild 11. Nichtlineares Tragverhalten

In Verbindung mit der praktischen Anwendbarkeit der Tafeln und Diagrammen wird darauf verwiesen, daß wenn sich der folgende Zusammenhang bei konstanten Parametern α und γ

$$\beta_1 \varrho_1 = \beta_2 \varrho_2 , \tag{3.33}$$

erfüllt, dann ist diese Formel anzuwenden

$$\frac{p_2}{p_1} = \left(\frac{\beta_1}{\beta_2}\right)^4 . \tag{3.34}$$

Ein Vergleich der Ergebnisse der theoretischen Untersuchungen über die Eigenheiten der *antimetrischen Beulung* ([6]: p_{kr}^{lin}, $w_0 = 0$) sowie des soeben behandelten *Durchschlagen* ($\overline{p}_{kr}$) führt zu folgenden Schlußfolgerungen:

1. Die Schalen, die ihre Lasten auch nach der Theorie I. Ordnung [5] zum überwiegenden Teil durch Biegeschnittkräfte tragen ($f_a/f_b = 1 \div (1{,}5 \div 2)$), darf man nicht nach der linearen Stabilitätstheorie untersuchen.

Die »halbnormale« Schale ($f_a/f_b = 1$) und die Schale, deren Pfeilhöhenverhältnisse von dem f_a/f_b Wert von 1 bloß geringfügig abweichen, weisen keine *Verzweigungserscheinung* auf. Die zu diesen Parametern gehörenden HP-Schalen haben eine *monoton zunehmende* Tragfähigkeitsart. Beim Verhältnis $f_a/f_b = 1$ besitzen diese Kurven auch keinen Inflexionspunkt.

2. Es stellte sich heraus, daß sich die meisten behandelten HP-Schalen nach dem Bild 2.c verhalten.

2.1 Bei kleinen Werten von f_a/f_b und f_b/b, sowie bei großen Seitenverhältnissen a/b ist *die kritische Durchschlagslast* ($\bar{p}_{kr}$) *geringer* als die lineare kritische Last (p_{kr}^{lin}, $w_0 = 0$).

2.2 Im größten Teil des untersuchten Parametersbereiches — hauptsächlich bei den Parametern $f_a/f_b = (1{,}5 \div 2) \div 4$, $f_a/b = 0{,}2 \div 0{,}3$, $a/b = 1 \div$

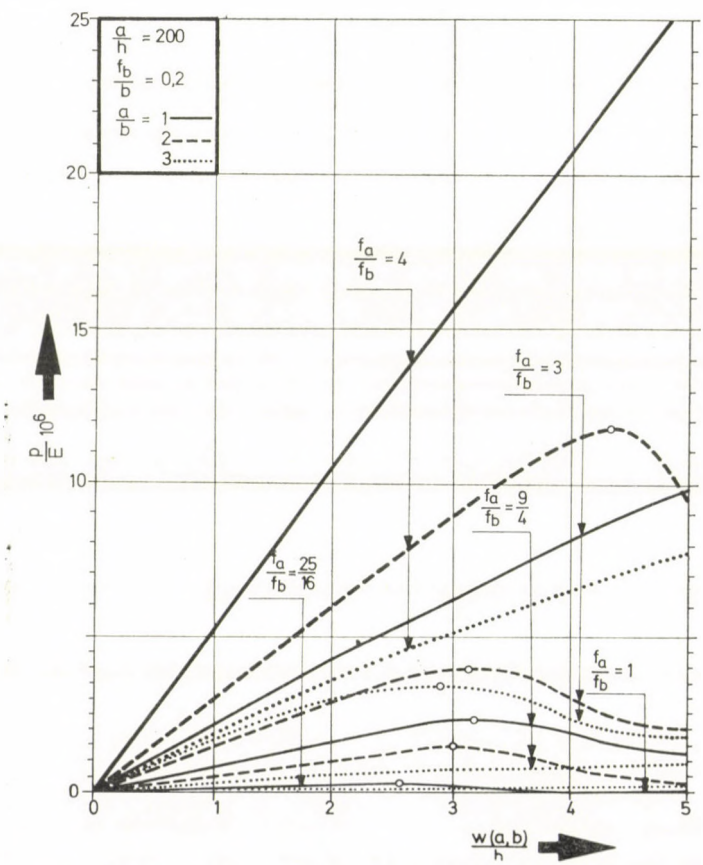

Bild 12. Nichtlineares Tragverhalten

÷ 2 (3) sind *die kritischen Durchschlagslasten* $\overline{p}_{kr}$ größer bzw. viel größer als die kritischen Lasten p_{kr}^{lin} (Bild 17), die zur aus dem unverformten Grundzustand auftretenden Verzweigung gehören.

Für diese Schalen ist die Verzweigung maßgebend.

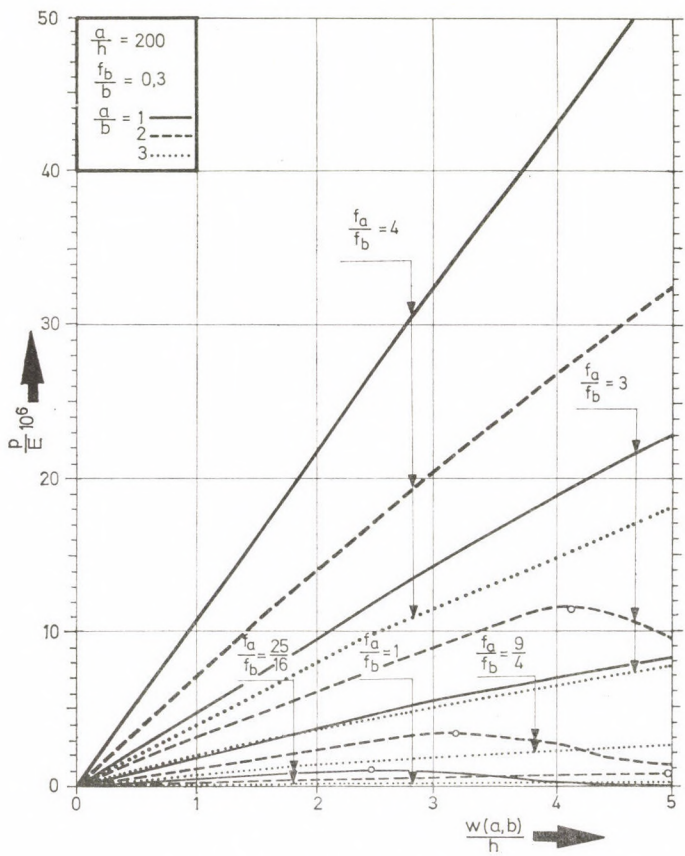

Bild 13. Nichtlineares Tragverhalten

Tafel I/1

$\frac{P}{E} \cdot 10^6$ ( ) $E \cdot 10^{-6} = \overline{P}_{kr}$

$\frac{f_b}{b}$	$\frac{a}{h}$	$\frac{a}{b}$	$\frac{w}{h} =$ / $\frac{f_a}{f_b}$	1	2	3	4	5
0,1	100	1	1	0,018	0,067	0,170	0,348	0,622
			1,21	0,020	(0,022) 0,021	0,036	0,091	0,204
			25/16	0,145	(0,175) 0,172	0,102	0,022	0,024
			9/4	0,813	(1,258)	0,504	0,165	0,029
			3	2,116	3,922	(4,172) 1,618	0,566	0,400
			4	4,797	9,019	(9,240) 6,680	2,822	1,051
		2	1	0,095	0,271	0,598	1,138	1,944
			1,21	0,081	0,180	0,381	0,774	1,447
			25/26	0,133	0,174	0,201	0,306	0,550
			3	1,355	2,175	(2,430) 2,404	1,959	1,197
			9/4	0,516	0,714	(0,725) 0,665	0,477	0,258
			4	3,123	5,516	(6,872)	4,523	2,598
		3	1	0,343	0,790	1,441	2,388	3,714
			1,21	0,333	0,719	1,270	2,094	3,307
			25/26	0,346	0,650	1,021	1,565	2,394
			9/4	0,539	0,844	1,033	(1,239)	1,228
			3	0,965	1,506	1,720 (1,750)	1,720	1,622
			4	1,940	3,197	3,847 (4,080)	3,983	3,722

Tafel I/2

				$\frac{p}{E} \cdot 10^6$								( ) $E \cdot 10^{-6} = \overline{P}_{kr}$	
$\frac{f_b}{b}$	$\frac{a}{h}$	$\frac{a}{b}$	$\frac{w}{h} =$ / $\frac{f_a}{f_b}$	1		2		3		4		5	
0,2	100	1	1	0,018		0,067		0,170		0,348			0,622
			1,21	0,076	(0,080)	0,076		0,038		0,019			0,011
			25/16	0,653		1,012	(1,120)	0,431		0,140			0,026
			9/4	3,320		6,192	(6,280)	3,411		1,456			0,443
			3	8,576		16,350		(21,184)		12,048			6,528
			4	19,47		37,70		55,62		73,98		(75,20)	47,55
		2	1	0,095		0,271		0,598		1,138			1,944
			1,21	0,099		0,149		0,235		0,442			0,852
			25/16	0,418		0,560	(0,580)	0,502		0,348			0,205
			9/4	2,150		3,653		(4,317)		3,283			1,914
			3	5,584		10,288		(14,176)		7,504			4,298
			4	12,56		23,79		33,38	(34,56)	19,91			11,73
		3	1	0,343		0,790		1,441		2,388			3,714
			1,21	0,330		0,656		1,084		1,720			2,673
			25/16	0,480		0,767		0,971		1,192			1,536
			9/4	1,433		2,280		2,681	(2,880)	2,750			2,583
			3	3,334		5,776		7,328		8,032		(8,202)	7,984
			4	7,434		13,54		18,32		21,67			23,29

Tafel I/3

$\frac{p}{E} \cdot 10^6$ ( ) $E \cdot 10^{-6} = \overline{P}_{kr}$

$\frac{f_b}{b}$	$\frac{a}{h}$	$\frac{a}{b}$	$\frac{w}{h} =$ / $\frac{f_a}{f_b}$	1	2	3	4	5
0,3	100	1	1	0,018	0,067	0,170	0,348	0,622
			1,21	0,186	(0,250) 0,234	0,141	0,039	0,023
			25/16	1,501	2,443	(2,510) 0,992	0,317	0,120
			9/4	7,530	14,31	(16,27) 16,11	9,054	4,553
			3	19,47	37,70	54,63	70, 09	83,52
			4	44,14	86,40	126,7	165,1	201,2
		2	1	0,095	0,271	0,598	1,138	1,944
			1,21	0,153	0,191	0,200	0,265	0,455
			25/16	0,953	1,455	(1,560) 1,519	1,206	0,725
			9/4	4,909	8,975	12,05	(12,320) 6,642	3,797
			3	12,57	23,78	33,99	(35,20) 19,91	11,73
			4	28,23	54,25	78,12	(81,30) 75,87	48,92
		3	1	0,343	0,790	1,441	2,388	3,714
			1,21	0,348	0,635	0,967	1,445	2,163
			25/16	0,751	1,160	1,330	1,373	(1,401)
			9/4	3,046	5,138	6,440	7,079	(7,168)
			3	7,43	13,54	18,33	21,67	23,29
			4	16,58	31,34	44,36	55,63	64,54

Tafel I/4

$\frac{p}{E} \cdot 10^6$ ( ) $E \cdot 10^{-6} = \overline{P}_{kr}$

$\frac{f_b}{b}$	$\frac{a}{h}$	$\frac{a}{b}$	$\frac{f_a}{f_b}$ \ $\frac{w}{h}=$	1	2	3	4	5
0,1	150	1	1	0,004	0,013	0,034	0,069	0,123
			1,21	0,007	(0,008)	0,004	0,005	0,017
			25/16	0,070	(0,105) 0,100	0,051	0,017	0,010
			9/4	0,367	0,664	(0,685) 0,263	0,088	0,045
			3	0,948	1,782	(1,930) 1,320	0,656	0,208
			4	2,150	4,119	5,851	(5,905) 3,984	2,388
		2	1	0,019	0,053	0,118	0,225	0,384
			1,21	0,017	0,031	0,057	0,111	0,204
			25/16	0,048	(0,063)	0,052	0,043	0,030
			9/4	0,244	0,377	0,427	(0,435) 0,415	0,356
			3	0,617	1,089	(1,357)	0,893	0,513
			4	1,398	2,603	3,692	(3,700) 1,986	1,082
		3	1	0,068	0,156	0,285	0,472	0,734
			1,21	0,064	0,132	0,225	0,362	0,560
			25/16	0,077	0,131	0,182	0,252	0,360
			9/4	0,177	0,274	0,315	(0,325) 0,320	0,314
			3	0,383	0,631	0,760	(0,802) 0,787	0,735
			4	0,832	1,461	1,891	2,123	(2,162)

Tafel I/5

$\frac{P}{E} \cdot 10^6$ ( ) $E \cdot 10^{-6} = \bar{P}_{kr}$

$\frac{f_b}{b}$	$\frac{a}{h}$	$\frac{a}{b}$	$\frac{f_a}{f_b}$ \ $\frac{w}{h}$ =	1	2	3	4	5
0,2	150	1	1	0,004	0,013	0,034	0,069	0,123
			1,21	0,037	(0,049) 0,046	0,028	0,008	0,005
			25/16	0,297	0,480	(0,490) 0,196	0,063	0,024
			9/4	1,487	2,826	(3,206) 3,182	1,797	0,899
			3	3,846	7,447	10,79	13,84	16,50
			4	8,719	17,06	25,03	32,60	39,74
		2	1	0,019	0,054	0,118	0,225	0,384
			1,21	0,030	0,038	0,040	0,052	0,090
			25/16	0,188	0,288	(0,308) 0,300	0,238	0,143
			9/4	0,970	1,773	2,375	(2,383) 1,322	0,750
			3	2,482	4,698	6,713	(6,953) 3,933	2,317
			4	5,576	10,72	15,23	(16,06) 14,99	9,66
		3	1	0,068	0,156	0,285	0,472	0,734
			1,21	0,069	0,125	0,191	0,285	0,427
			25/16	0,148	0,229	0,263	0,271	(0,277)
			9/4	0,602	1,015	1,272	1,398	(1,416)
			3	1,468	2,675	3,619	4,281	4,601
			4	3,275	6,191	8,762	10,99	12,75

Tafel I/6

$\frac{P}{E} \cdot 10^6$ ( ) $E \cdot 10^{-6} = \bar{P}_{kr}$

$\frac{f_b}{b}$	$\frac{a}{h}$	$\frac{a}{b}$	$\frac{w}{h} =$ / $\frac{f_a}{f_b}$	1	2	3	4	5
0,3	150	1	1	0,004	0,013	0,034	0,069	0,123
			1,21	0,089	(0,140) 0,132	0,061	0,021	0,007
			25/16	0,672	(1,255)	0,704	0,304	0,035
			9/4	3,380	6,538	9,467	12,14	14,46
			3	8,712	17,01	24,84	32,13	38,80
			4	19,73	38,90	57,51	75,54	92,98
		2	1	0,019	0,053	0,118	0,225	0,384
			1,21	0,059	(0,075)	0,065	0,048	0,041
			25/16	0,440	0,738	0,911	(0,977)	0,951
			9/4	2,182	4,119	5,884 (6,050)	3,283	1,912
			3	5,576	10,72	15,43 (16,34)	14,99	9,66
			4	12,57	24,45	35,63	46,08	49,93
		3	1	0,068	0,156	0,285	0,472	0,734
			1,21	0,082	0,136	0,182	0,242	0,335
			25/16	0,282	0,452	0,532	(0,540)	0,500
			9/4	1,292	2,337	3,132	3,664	3,893
			3	3,275	6,191	8,762	10,99	12,75
			4	7,707	14,72	21,07	26,78	31,85

Tafel I/7

$\frac{P}{E} \cdot 10^6$ ( ) $E \cdot 10^{-6} = \overline{P}_{kr}$

$\frac{f_b}{b}$	$\frac{a}{h}$	$\frac{a}{b}$	$\frac{w}{h} =$ / $\frac{f_a}{f_b}$	1	2	3	4	5
0,1	200	1	1	0,001	0,004	0,011	0,022	0,039
			1,21	0,0048	(0,0050) 0,0048	0,0024	0,0012	0,0007
			25/16	0,0408	0,0633	(0,070) 0,0269	0,0088	0,0016
			9/4	0,208	0,387	(0,393) 0,213	0,091	0,028
			3	0,536	1,022	(1,324)	0,753	0,408
			4	1,217	2,356	3,476	4,624	(4,700) 2,972
		2	1	0,006	0,017	0,037	0,071	0,122
			1,21	0,006	0,009	0,015	0,028	0,053
			25/16	0,026	0,035	(0,036) 0,031	0,022	0,013
			9/4	0,134	0,228	(0,270)	0,205	0,120
			3	0,349	0,643	(0,886)	0,469	0,268
			4	0,785	1,487	2,124	(2,100) 1,246	0,733
		3	1	0,021	0,049	0,090	0,149	0,232
			1,21	0,020	0,041	0,067	0,108	0,167
			25/16	0,030	0,048	0,061	0,075	0,096
			9/4	0,090	0,143	0,168	(0,180) 0,172	0,161
			3	0,209	0,361	0,458	0,502	(0,513) 0,499
			4	0,465	0,846	1,145	1,354	1,456

Tafel I/8

$\frac{p}{E} \cdot 10^6$ ( ) $E \cdot 10^{-6} = \bar{P}_{kr}$

$\frac{f_b}{b}$	$\frac{a}{h}$	$\frac{a}{b}$	$\frac{w}{h} =$ / $\frac{f_a}{f_b}$	1	2	3	4	5
0,2	200	1	1	0,001	0,004	0,012	0,025	0,047
			1,21	0,022	0,033	(0,035)	0,030	0,021
			25/16	0,168	0,312 (0,330)	0,148	0,057	0,034
			9/4	0,842	1,620	2,329 (2,400)	1,997	1,269
			3	2,175	4,247	6,210	8,061	9,783
			4	5,460	10,74	15,84	20,75	25,49
		2	1	0,006	0,017	0,039	0,077	0,135
			1,21	0,015	(0,019)	0,017	0,014	0,015
			25/16	0,109	0,178	0,214	(0,221)	0,205
			9/4	0,546	1,024	(1,461)	0,766	0,440
			3	1,394	2,669	3,830 (4,002)	3,107	1,960
			4	3,140	6,088	8,842	11,39 (11,90)	9,59
		3	1	0,021	0,050	0,091	0,153	0,241
			1,21	0,024	0,041	0,058	0,080	0,115
			25/16	0,073	0,115	0,133 (0,140)	0,134	0,124
			9/4	0,327	0,577	0,757	0,874	0,935
			3	1,709	2,876 (3,480)	3,259	2,289	1,799
			4	1,826	3,507	5,051	6,477	7,834

Tafel I/9

$\frac{p}{E} \cdot 10^6$ ( ) $E \cdot 10^{-6} = \overline{P}_{kr}$

$\frac{f_b}{b}$	$\frac{a}{h}$	$\frac{a}{b}$	$\frac{f_a}{f_b}$ \ $\frac{w}{h}$ =	1	2	3	4	5
0,3	200	1	1	0,001	0,004	0,012	0,025	0,047
			1,21	0,052	(0,080)	0,032	0,011	0,002
			25/16	0,380	0,719 (0,790)	0,659	0,354	0,150
			9/4	1,910	3,730	5,433	7,037	8,343
			3	4,925	9,693	14,300	18,750	23,030
			4	11,13	22,03	32,69	43,11	53,28
		2	1	0,006	0,017	0,039	0,077	0,135
			1,21	0,033	(0,046)	0,045	0,034	0,020
			25/16	0,254	0,446	0,582	0,668	(0,708)
			9/4	1,226	2,341	3,354 (3,450)	2,494	1,549
			3	3,140	6,088	8,842	11,39 (11,63)	9,592
			4	7,087	13,88	20,37	26,55	32,40
		3	1	0,021	0,050	0,091	0,153	0,241
			1,21	0,033	0,052	0,063	0,073	0,089
			25/16	0,152	0,253	0,312	(0,335)	0,329
			9/4	0,740	1,361	1,871	2,276	2,583
			3	1,826	3,507	5,051	6,477	7,834
			4	4,368	8,444	12,23	15,74	18,98

4. Verzweigung aus dem verformten Grundzustand

Sowohl theoretisch als auch praktisch ist die folgende Frage gerechtfertigt: bei welcher Belastung aus der symmetrischen Deformation der HP-Schale, die nach der (nichtlinearen) Theorie der großen Verformungen verfolgt wird, eine »benachbarte« antimetrische Ausbeulung abzuzweigen vermag. Es wird die Last $p_{kr,v}^{\text{lin}}$ bestimmt, die das Bild 2.c darstellt.

Die Verzweigung selbst kann nach der linearen Theorie verfolgt werden, d. h., es ist eine lineare Eigenwertaufgabe mit den vorangegangenen nichtlinearen symmetrischen Verformungen zu kombinieren.

4.1 Grundannahmen

Bei Untersuchung der Möglichkeit der *antimetrischen* Ausbeulung, die aus dem *symmetrisch* verformten Grundzustand ($w_0 \neq 0$) abzweigt, werden die inneren Kräfte der (nichtlinearen) Theorie der großen Verformungen (s. Abschnitt 3.) berechnet.

Im Verlauf dieser wird die in der Fachliteratur allgemein angenommene folgende Näherung benutzt: *die geometrischen Angaben der Schale werden durch die Durchbiegungsform nach der nichtlinearen Theorie (w_0) verändert.*

Die lineare kritische Last (s. [6]: $w_0 = 0$) *dieser Schale von veränderter Form* wird als die approximative lineare kritische Last der Verzweigungserscheinung, die aus dem verformten Grundzustand ($w_0 \neq 0$) erfolgt, betrachtet.

Diese Auflösungsmethode steht mit den Verfahren von BUSHNELL [1], DULÁCSKA [2] und WEDELLSBORG [14] in Einklang.

Der sehr beträchtliche Rechenaufwand für die Bestimmung der oberen kritischen Lasten (s. Bild 2: $p_{kr}^{\text{obere}}(w_a)$) wurde von den erwähnten Verfassern, wie folgt, verringert.

Zuerst veränderten sie die geometrische Form der Schalen *durch die Vorbeulamplitude (Anfangsausmittigkeit)* w_a. Sodann bei Bestimmung der Eigenwertaufgabe in Bezug auf die Schale von veränderter Form betrachteten sie die dazugehörigen Eigenwerte als obere kritische Lasten.

Ihre Resultate ließen erkennen, daß die Abnahme dieser kritischen Lasten $p_{kr,v}^{\text{lin}}$ gegenüber den linearen kritischen Lasten p_{kr}^{lin} ($w_0 = 0$) zum größten Teil durch Vorbeulen verursacht wurde.

An Hand des Vergleiches der exakten und der näherungsweisen Werte hat sich herausgestellt, daß *die geometrische Nichtlinearität bloß einen kleineren Teil der Abnahme der kritischen Last verursacht.*

Im Falle der soeben erörterten Erscheinung kennzeichnet die geometrische Nichtlinearität lediglich den Grundzustand und deshalb, wenn diese mit einer hinreichenden Näherung berücksichtigt wird, erhält man — auf Grund des obigen Gedankenganges — die kritischen Lasten $p_{kr,v}^{\text{lin}}$ mit einer für die Praxis geeigneten Genauigkeit.

4.2 Grundgleichungen

Die zweite Variation der potentiellen Energie der Schale von Verformungen w_0 kann als die Summe der zweiten Variation der potentiellen Energie der Mittelflächen- und der Biegeschnittkräfte (U_m und U_b) sowie der äußeren Kräfte (V_0) wie folgt geschrieben werden:

$$\delta^2 U_{m0} = \frac{1}{Eh}\int_0^{2a}\int_0^{2b} \left[\bar{F}^{\prime\prime 2} - 2\mu\,\bar{F}^{\cdot\cdot}\,\bar{F}^{\prime\prime} + \bar{F}^{\cdot\cdot 2} + 2(1+\mu)\bar{F}^{\cdot\prime 2} + \right.$$
$$\left. + Eh(F_0^{\prime\prime}\,\bar{w}^{\cdot 2} - 2F_0^{\cdot\prime}\,\bar{w}^{\cdot}\bar{w}^{\prime} + F_0^{\cdot\cdot}\,w^{\prime 2})\right] dx\,dy\,, \tag{4.1}$$

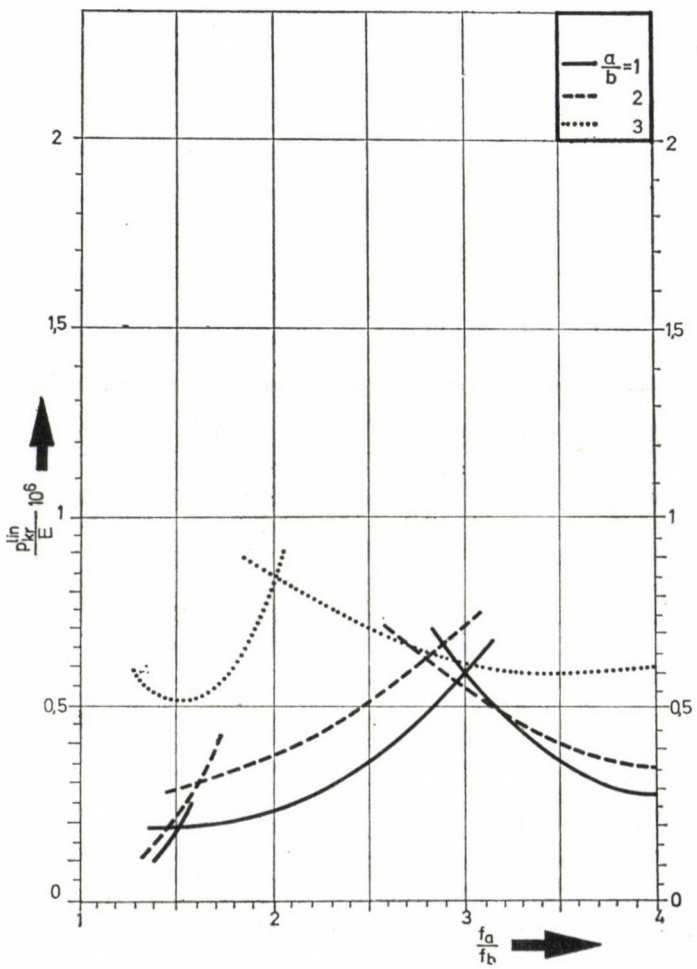

Bild 14. Lineare kritische Last der HP-Schale ($a/h = 150$, $f_b/b = 0{,}1$)

$$\delta^2 U_{b0} = B \int_0^{2a} \int_0^{2b} \left[\overline{w}^{\text{II}2} + 2\mu \overline{w}^{\cdot\cdot} \overline{w}^{\text{II}} + \overline{w}^{\cdot\cdot 2} + 2(1-\mu)\, \overline{w}^{\cdot\text{I}2} \right] dx\, dy\,, \tag{4.2}$$

$$\delta^2 V_0 = 0\,, \tag{4.3}$$

$$\delta^2 U_0 = \int_0^{2a} \int_0^{2b} u_0\, dx\, dy = \delta^2 U_{m0} + \delta^2 U_{b0}\,, \tag{4.4}$$

$$\delta^2 \Pi_0 = \int_0^{2a} \int_0^{2b} \pi_0\, dx\, dy = \delta^2 U_0 + \delta^2 V_0\,. \tag{4.5}$$

Hier ist u_0, bzw. π_0 der spezifische Wert der zweiten Variation der inneren, bzw. der vollständigen potentiellen Energie.

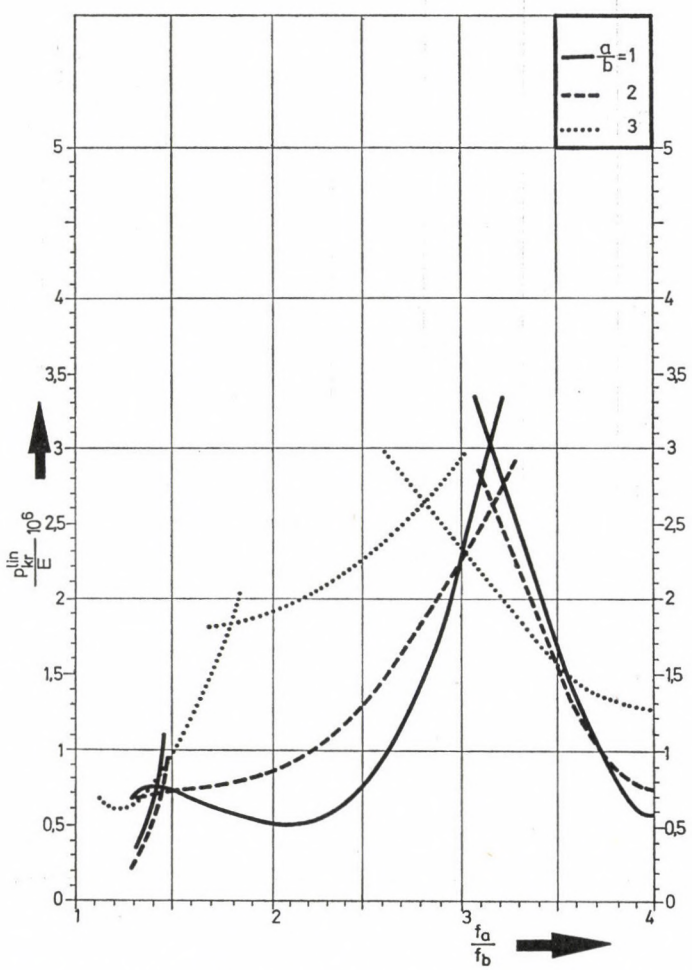

Bild 15. Lineare kritische Last der HP-Schale ($a/h = 150, f_b/b = 0{,}2$)

In diesen Gleichungen hängt die Funktion $\overline{F}$ von $\overline{w}$ ab: $\overline{F} = \overline{F}(\overline{w})$. In den Ausdrücken der Verzerrungen treten auch die Glieder $w_0^{\prime}\overline{w}^{\prime}$, $w_0^{\cdot}\overline{w}^{\cdot}$, $w_0^{\prime}\overline{w}^{\cdot} + w_0^{\cdot}\overline{w}^{\prime}$ auf.

Ist bei einer störenden Verformung $\overline{w}$ der (symmetrischen) Gleichgewichtslage jede erste Variation der kleinen Störungsenergie $\delta^2\Pi_0$ von zweiter Ordnung gleich Null, so liegt ein indifferentes Gleichgewicht vor. Für eine solche *spezielle* zweite Variation des elastischen Potentials Π_0, dessen *jede* erste Variation gleich Null ist, lautet das Indifferenzkriterium:

$$\delta(\delta^2 \Pi_0) = 0 \,. \tag{4.6}$$

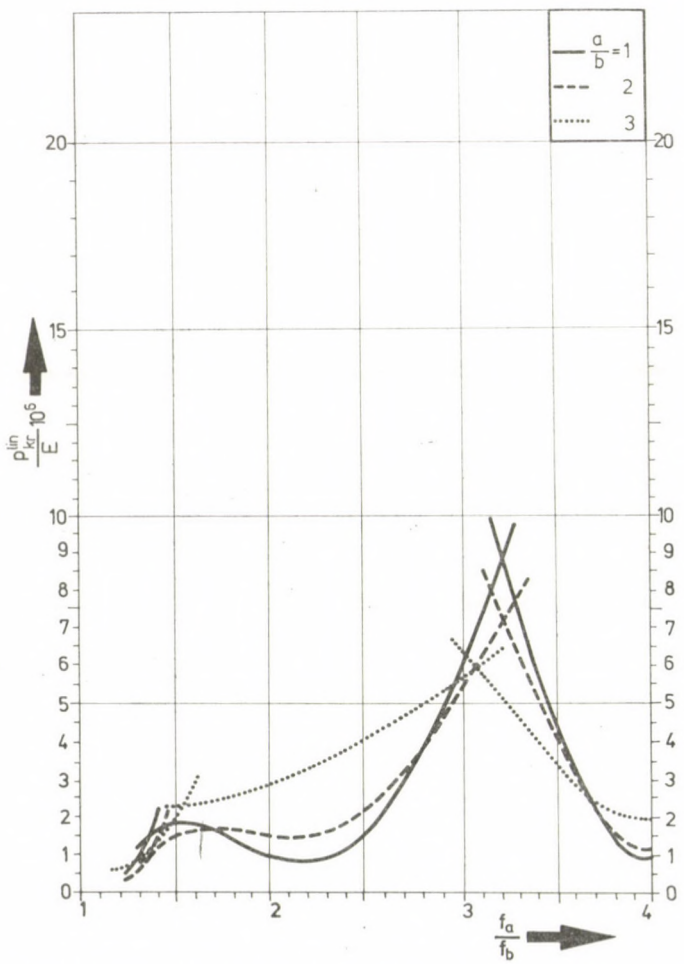

Bild 16. Lineare kritische Last der HP-Schale ($a/h = 150$, $f_b/b = 0{,}3$)

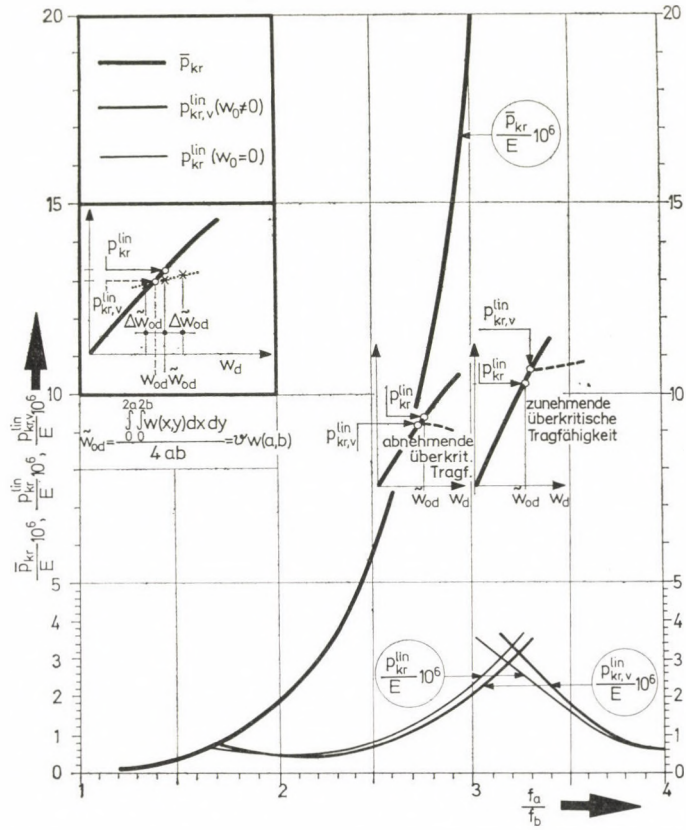

Bild 17a. Vergleich der verschiedenen kritischen Lasten ($a/h = 150$, $f_b/b = 0{,}2$, $a/b = 1$)

Zur Bestimmung der Last $p^{lin}_{kr,v}$ muß man die Variationsaufgabe (4.6) lösen. Es wird gefragt, für welche Funktion $\bar{w} = \bar{w}(x, y)$ das Integral $\delta^2 \Pi_0$ einen stationären Wert aufnimmt.

Die Extremale $\bar{w}$, die für das Funktional einen stationären Wert liefert, erhält man durch die Lösung der Euler-Langrangeschen Differentialgleichung

$$\frac{\partial \pi_0}{\partial \bar{w}} - \left(\frac{\partial \pi_0}{\partial \bar{w}'}\right)' - \left(\frac{\partial \pi_0}{\partial \dot{\bar{w}}}\right)^{\cdot} + \left(\frac{\partial \pi_0}{\partial \bar{w}''}\right)'' + \left(\frac{\partial \pi_0}{\partial \dot{\bar{w}}'}\right)^{\cdot\prime} + \left(\frac{\partial \pi_0}{\partial \bar{w}^{\cdot\cdot}}\right)^{\cdot\cdot} = 0 \ . \quad (4.7)$$

Nach Durchführung der durch die Gl. (4.7) vorgeschriebenen Operationen, ergibt sich die *Gleichgewichtsgleichung* der aus dem verformten Grundzustand ($w_0 \neq 0$) erfolgenden Verzweigungserscheinung der flachen Schalen [3], [15] zu:

$$B \triangle \triangle \bar{w} - L_p(\bar{F}, w_0 + z) - L_p(F_0, \bar{w}) = 0 \ . \quad (4.8)$$

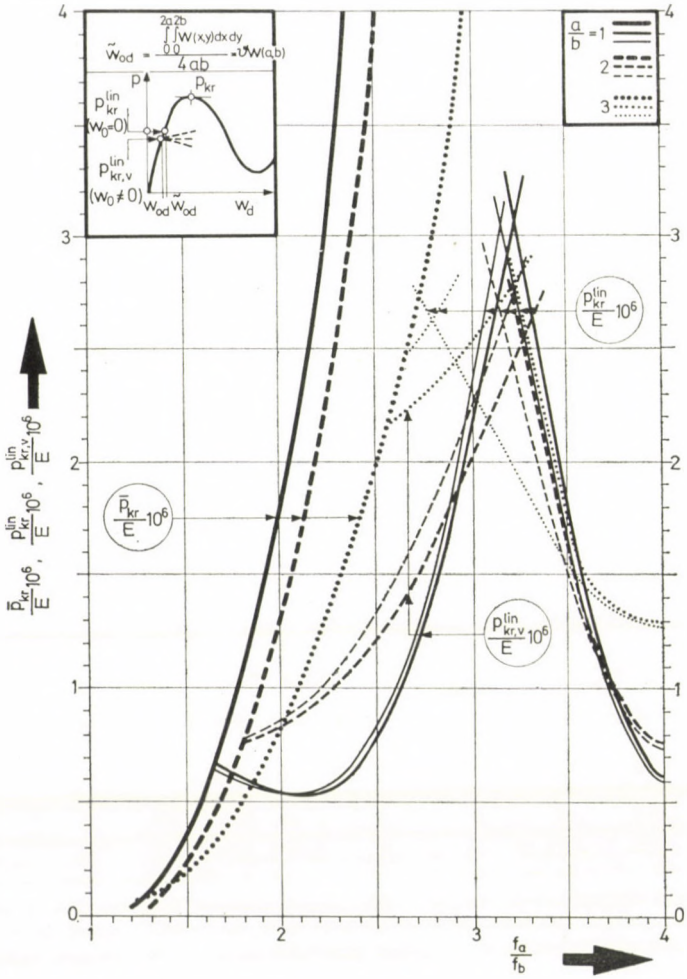

Bild 17. Vergleich der verschiedenen kritischen Lasten ($a/h = 150$, $f_b/b = 0{,}2$, $a/b = 1, 2, 3$)

Wird nun die zweite Variation der potentiellen Energie der Mittelflächenkräfte in die nachfolgende Form umgestaltet, dann erhält man:

$$\delta^2 U_{m0} = \int_0^{2a}\int_0^{2b} \Big\{ 2\left[\bar{F}^{\cdot\cdot}(\bar{v}^{\cdot} - \bar{w}\bar{z}^{\cdot\cdot} + \bar{w}_0^{\cdot}\bar{w}^{\cdot}) - \bar{F}^{\cdot\cdot}(\bar{u}^{\cdot} + \bar{v}^{\cdot} + w_0^{\cdot}\bar{w}^{\cdot} + w_0^{\cdot}\bar{w}^{\cdot}) + \right.$$
$$+ \bar{F}^{\cdot\cdot}(\bar{u}^{\cdot} - \bar{w}\bar{z}^{\cdot\cdot} + w_0^{\cdot}\bar{w}^{\cdot})\Big] - \frac{1}{Eh}\left[\bar{F}^{\cdot\cdot 2} - 2\mu\,\bar{F}^{\cdot\cdot}\bar{F}^{\cdot\cdot} + \bar{F}^{\cdot\cdot 2} + \right. \tag{4.9}$$
$$\left.\left. + 2(1+\mu)\,\bar{F}^{\cdot 2}\right] + \left[F_0^{\cdot\cdot}\bar{w}^{\cdot 2} - 2F_0^{\cdot\cdot}\bar{w}^{\cdot}\bar{w}^{\cdot} + F_0^{\cdot\cdot}\bar{w}^{\cdot 2}\right]\right\} dx\,dy.$$

Mit Hilfe dieser Gleichung soll — an Hand des Prinzips vom stationären Wert der Ergänzungsenergie — die erste Variation des Funktionals $\delta^2 \Pi_0$ nach

$\bar{F}$ gebildet werden. Bei Durchführung der durch die Euler-Lagrangesche Dgl.

$$\left(\frac{\partial u_0}{\partial \bar{F}^{\prime\prime}}\right)^{\prime\prime} + \left(\frac{\partial u_0}{\partial \bar{F}^{\cdot\prime}}\right)^{\cdot\prime} + \left(\frac{\partial u_0}{\partial \bar{F}^{\cdot\cdot}}\right)^{\cdot\cdot} = 0 \tag{4.10}$$

vorgeschriebenen Operationen ergibt sich die Gleichung:

$$\triangle\triangle\bar{F} + D(1-\mu^2)[L_p(\bar{w}, z) + L_p(\bar{w}, w_0)] = 0 \ . \tag{4.11}$$

Das ist die *Verträglichkeitsgleichung* der untersuchten Erscheinung [3], [15].

4.3 Durchbiegungsformen und Spannungsfunktionen

Die Durchbiegungsfunktion w_0 des Grundzustandes und die (antimetrische) Beulfunktion $\bar{w} \equiv \delta w_0$ muß den folgenden geometrischen (»künstlichen«) und statischen (»natürlichen«) Randbedingungen der Aufgabe Genüge tun:

$$w = w_0 + \bar{w} \ , \tag{4.12}$$

$$w\Big|_{\substack{x=0\\x=2a}} = 0 \ , \quad w\Big|_{\substack{y=0\\y=2b}} = 0 \ , \quad w^{\prime\prime}\Big|_{\substack{x=0\\x=2a}} = 0, \quad w^{\cdot\cdot}\Big|_{\substack{y=0\\y=2b}} = 0 \ . \tag{4.13a—d}$$

Die Schale ist an ihren Rändern *normalkraftfrei* abgestützt, folglich gelten:

$$F = F_0 + \bar{F} \ , \tag{4.14}$$

$$F^{\prime\prime}\Big|_{\substack{y=0\\y=2b}} = 0 \ , \quad F^{\cdot\cdot}\Big|_{\substack{x=0\\x=2a}} = 0 \ . \tag{4.15a—d}$$

Die folgenden trigonometrischen Reihen, die sich aus den linearen unabhängigen Gliedern zusammensetzen, befriedigen sämtliche geometrische und statische Randbedingungen des Problems:

$$w_0 = \sum\sum w_{rs} \sin\frac{r\pi}{2a}x \sin\frac{s\pi}{2b}y \ , \tag{4.16a—b}$$

$$F_0 = \sum\sum F_{rs} \sin\frac{r\pi}{2a}x \sin\frac{s\pi}{2b}y \ ,$$

$$r = 1, 3, 5, \ \ldots, R$$

$$s = 1, 3, 5, \ \ldots, S$$

$$\overline{w} = \sum\sum \overline{w}_{ij} \sin\frac{i\pi}{2a} x \sin\frac{j\pi}{2b} y\,, \qquad (4.17\text{a}-\text{b})$$

$$\overline{F} = \sum\sum \overline{F}_{ij} \sin\frac{i\pi}{2a} x \sin\frac{j\pi}{2b} y\,.$$

$$i = 1, 2, 3, \ldots, I$$

$$j = 1, 2, 3, \ldots, J$$

Bei Lösung der Aufgabe nach dem Galerkinschen Verfahren sind diese Funktionen als Durchbiegungs- und Spannungsfunktionen des Grund- bzw. Nachbarzustandes zu betrachten.

An Hand des im Abschn. 4.1 beschriebenen Gedankenganges wird statt der soeben erörterten exakten Methode ein *Näherungsverfahren* angewandt.

Demgemäß werden die approximativen linearen kritischen Lasten $p_{kr,v}^{\text{lin}}$ ($w_0 \neq 0$) durch die Tragfähigkeitskurven der Bilder 3—13 und die nach [6] berechneten linearen kritischen Lasten p_{kr}^{lin} ($w_0 = 0$) bezogen auf die HP-Schale mit *veränderten Parametern* bestimmt.

4.4 Näherungsverfahren

Betrachten wir jetzt den Zustand der HP-Schale, wenn ihr Mittelpunkt ($x = a$, $y = b$) unter Einwirkung der Last p_{kr}^{lin} ($w_0 = 0$) eine Durchbiegung der Größe w (a, b) erleidet hat (vgl. mit den Bildern 3—13). In diesem Zustand weist die *Schale mit veränderten geometrischen Verhältnissen* näherungsweise die folgenden Parameter auf:

$$\alpha^* = \frac{f_a^*}{f_b^*} = \frac{f_a - \tilde{w}_{0d}}{f_b + \tilde{w}_{0d}} = \frac{\alpha - \dfrac{\tilde{w}_{0d}}{h} \cdot \dfrac{\gamma}{\beta\varrho}}{1 + \dfrac{\tilde{w}_{0d}}{h} \cdot \dfrac{\gamma}{\beta\varrho}}\,,$$

$$\beta^* = \beta = \frac{a}{h}\,, \qquad (4.18\text{a}-\text{d})$$

$$\gamma^* = \gamma = \frac{a}{b}\,,$$

$$\varrho^* = \frac{f_b^*}{b} = \frac{f_b + \tilde{w}_{0d}}{b} = \varrho + \frac{\tilde{w}_{0d}}{h} \cdot \frac{\gamma}{\beta}\,,$$

wo $\tilde{w}_{0d}$ die durchschnittliche Durchbiegung der Fläche bedeutet (s. ausführlicher in den Bildern 17 a—b).

Die Girlandenkurven $p^{\text{lin}}_{kr,v}$, die durch unser Näherungsverfahren bestimmt worden sind, sind in den Bildern 17 a—b dargestellt. Die linearen kritischen Lasten die den Parametern (4.18 a—d) entsprechen, sind nach den Girlandenkurven der Bilder 14—16 berechnet worden.

Auf Grund der Form der Girlandenkurven der Bilder 14—16 läßt sich leicht feststellen, daß die kritischen Lasten $p^{\text{lin}}_{kr,v}$ $(w_0 \neq 0)$ sowohl *größer* als auch *kleiner* als die kritischen Lasten p^{lin}_{kr} $(w_0 = 0)$ sein können.

Im Parameterbereich $\alpha \approx 2 \div 3$ führt die Abnahme der Größen α auf α^* zur *Abnahme* der linearen kritischen Lasten. Demgegenüber verursacht im Parameterbereich $\alpha \approx 3 \div 4$ die Abnahme der Parameter α (α^*) eine Tragfähigkeits*steigerung*. Infolgedessen sollen die Größen $p^{\text{lin}}_{kr,v}$ als Resultat der (fallweise vermindernden, bzw. steigernden) Wirkung der Parameteränderung

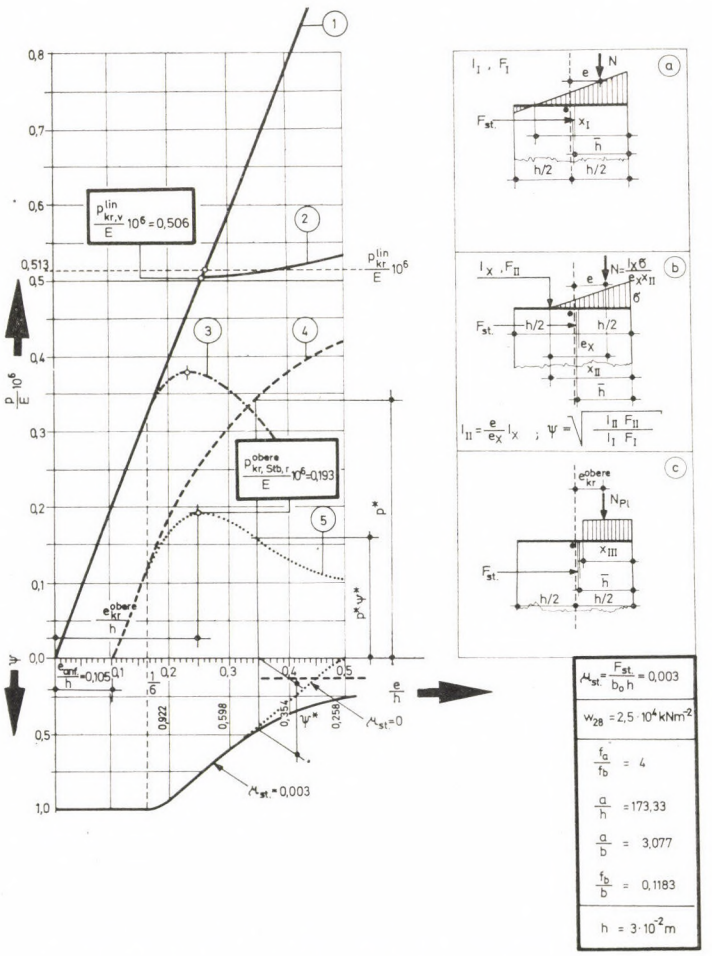

Bild 18. Prüfung der Stabilität einer erbauten Schale

$\triangle\alpha = \alpha^* - \alpha$ sowie der gleichzeitigen (immer steigernden) Wirkung der Parameteränderung $\Delta\varrho = \varrho^* - \varrho$ ermittelt werden.

Die Werte $p^{\text{inl}}_{kr,v}$ wurden graphisch erhalten: vor allem wurden in den Punkten $\tilde{w}_{0d} \pm \triangle\tilde{w}_{0d}$ (die sich in der kleinen Umgebung des Punktes $\tilde{w}_{0d}$ befinden, s. Bild 17a) die linearen kritischen Lasten $p^{\text{lin}}_{kr}(\alpha^*, \varrho^*)$ bestimmt und dann wurde die so erhaltene Kurve mit der entsprechenden »nichtlinearen« Tragfähigkeitskurve geschnitten. Der Schnittpunkt liefert die lineare kritische Last $p^{\text{lin}}_{kr,v}$.

Das Bild 17b. zeigt, daß die *größte Wirkung* der durch die Belastung hervorgerufenen Durchbiegungen (w_0), (bei den untersuchten geometrisch Verhältnissen) in den Bereich $f_a/f_b = 2{,}5 \div 3{,}5$ entfällt. Die Girlandenkurven wurden bis zur Kurve der kritischen Durchschlagslasten $\bar{p}_{kr}$ aufgetragen.

Die größten prozentuellen Abweichungen der kritischen Lasten $p^{\text{lin}}_{kr,v}$ ($w_0 \neq 0$) von den kritischen Lasten p^{lin}_{kr} ($w_0 = 0$) sind wie folgt: im Falle $a/b = 1$ $\triangle\sim +10\% \div -8\%$, bei $a/b = 2$ $\triangle\sim +13\% \div -9\%$, bei $a/b = 3$ $\triangle\sim +39\% \div -11\%$. Trotz der Änderungen liegen die *Maximalwerte* der linearen kritischen Lasten weiterhin in der Nähe des Verhältnisses $f_a/f_b \sim 3$.

Die Tragfähigkeit der in der Praxis häufig angewandten HP-Schalen (die »normale« Schale mit dem Pfeilhöhenverhältnis $f_a/f_a = 4$ und die Schale mit einem solchen von $f_a/f_b = 9/4$), wird von den Durchbiegungen des Grundzustandes nur wenig beeinflußt. Diese Wirkung ist für die Schalen am *gefährlichsten*, deren Pfeilhöhenverhältnisse in der Nähe des Wertes $f_a/f_b \sim 3$ liegen.

Auf Grund unserer Berechnungen kann auch festgestellt werden, daß die Tragfähigkeit im größten Maß gleichfalls im erwähnten Parameterbereich $f_a/f_b \sim 2{,}5 \div 3{,}5$ durch die *Anfangsausmittigkeit* (Vorbeulen) verringert wird. Diese Methode gibt gleichzeitig auch den Charakter der *überkritischen Tragfähigkeit an.*

Die überkritische Tragfähigkeit weist fallweise einen*abnehmenden* Bild. 18. ($f_a/f_b \sim 2 \div 3$), bzw. *zunehmenden* ($f_a/f_b \sim 3 \div 4$) Charakter auf. Es ist auch nachgewiesen worden (Bild 17a—b), daß die kritischen Durchschlagslasten $\bar{p}_{kr}$ etwa im Bereich $f_a/f_b \sim 2{,}5 \div 4$ größer bzw. viel größer sind als die linearen kritischen Lasten ($p^{\text{lin}}_{kr,v}$ bzw. p^{lin}_{kr}).

Es soll noch bemerkt werden, daß die Parameterbereiche, bei denen ein *(antimetrischer)* Gleichgewichtszustand (s. gestrichelte Linie in Bild 2.c), der mit Abzweigung verbunden ist, außer dem *symmetrischen Gleichgewichtszustand* (s. ausgezogene Linie im Bild 2.c) *vor dem Durchschlagen* existiert, hauptsächlich durch folgende Verhältnisse gekennzeichnet werden können: $f_b/f_a = 2 \div 4$, $f_a/b = 0{,}2 \div 0{,}3$, $a/b = 1 \div 2(3)$.

In diesem Abschnitt wurde die Möglichkeit der Abzweigung, die *vor* dem Erreichen der kritischen Durchschlagslast $\bar{p}_{kr}$ auftritt, untersucht.

Nach Erreichen der kritischen *Durchschlagslast* sind zwei Fälle des Tragverhaltens möglich:

a) Der Vorgang ist durchwegs *symmetrisch.*

b) Aus dem labilen Ast zweigt eine *antimetrische* Ausbeulung ab. Dieser Fall wurde nicht behandelt, weil die Schale als bei der Last $\bar{p}_{kr}$ zugrunde gegangen betrachtet werden kann.

5. Praktische Anwendung

HRUBAN schreibt in seinem Aufsatz »Die Biegetheorie der Translationsflächen und ihre Anwendung im Hallenbau« (*Acta Tech.* Hung. 7 (1953), S. 425—464.) über eine erbaute sattelförmige, an ihren Rändern normalkraftfreie HP-Schale. Die Angaben der Schale bezüglich der Bewehrung, der Festigkeit und der geometrischen Verhältnisse, sind in Bild 18 dargestellt (wo W_{28} die Würfelfestigkeit ist). Die maßgebende Belastung (Schalendicke: $3 \cdot 10^{-2}$ m, Isolierschichten, Schneelast) beträgt:

$$p_M = 2{,}25 \text{ kNm}^{-2} .$$

Vor allem haben wir die nichtlineare Tragfähigkeitskurve $p - w(a, b)$ nach dem Abschnitt 3 bestimmt. Danach wurde diese Kurve so umgeformt, daß die Ordinaten p als eine Funktion von $\tilde{w}_{0d} = \vartheta w(a, b)$ (statt $w(a, b)$) aufgetragen wurden.

Dann wurde die Kurve $p - e/h$ aufgetragen (s. Kurve ① in Bild 18), wo »e« die Ausmittigkeit von der Mittelfläche bedeutet. Im Hinblick darauf, daß die Ordinaten p in dem untersuchten Ausmittigkeitsbereich um vieles kleiner sind als die kritische Durchschlagslast $\bar{p}_{kr}$, ist diese Anfangsstrecke des Diagramms fast eine Gerade.

Der folgende Schritt war die Berechnung der linearen kritischen Last: $p_{kr}^{\text{lin}} = 0{,}513 \times E^{-6}$ (nach [6]; Verzweigung: $w_0 = 0$). Danach wurde die Durchbiegung der Mittelfläche ($w_0 \neq 0$) nach Abschnitt 4.4 berücksichtigt: $p_{kr,v}^{\text{lin}} = 0{,}509\ E \times 10^{-6}$. Die Abnahme der Tragfähigkeit ist gering. Die Tragfähigkeitskurve weist im überkritischen Bereich einen mäßigen Anstieg auf. Die Beulung tritt überwiegend dehnungslos ein. Hieraus folgt, daß der Kurvenast ② der entsprechenden überkritischen Kurve von ebenen Platten ähnlich ist.

Für die Standsicherheit der *homogenen, isotropen* Schale aus *idealem elastischem Werkstoff gilt*:

$$k_{si} = \frac{p_{kr,v}^{\text{lin}}}{p_M} = \frac{0{,}506 \times E \times 10^{-6}}{2{,}25} = 0{,}225 E \times 10^{-6} ,$$

Der Würfelfestigkeit $W_{28} = 2{,}5 \times 10^4$ kNm^{-2} entspricht der *Anfangselastizitätsmodul*

$$E_{b0} = 5{,}5 \times 10^7 \cdot \frac{K_{28}}{K_{28} + 20000} = 3{,}05 \times 10^7 \text{ kNm}^{-2} .$$

Nach dem Ablauf des *Kriechvorganges* gilt für den *Formänderungsmodul* E_{bd} der Wert

$$E_{bd} = 1{,}33 \times 10^7 \text{ kNm}^{-2} .$$

Nach Einsetzen dieser Größe in den Ausdruck für k_{si} erhält man

$$k_{si} = 3 .$$

Die tatsächliche Standsicherheit ist aber wesentlich kleiner als 3, weil die folgenden verringernden Auswirkungen unbedingt berücksichtigt werden müssen:

a) *Die Risse* des Stahlbetonquerschnittes beeinflussen wesentlich die »Schalenbeulsteifigkeit« $K = \sqrt{BD}$ (hier bezeichnen B bzw. D die Biege- bzw. die Dehnungssteifigkeit des Schalenquerschnittes).

b) Die ungewollte *Anfangsausmittigkeit* (e_{anf}).

c) Die *plastischen* Formänderungskennwerte des Betons (ξ_{pl}).

Das Ausmaß der Tragfähigkeitsabnahme wird nach dem Verfahren von DULÁCSKA [8] ermittelt.

ad a. *Die Risse*

Die Biegesteifigkeit B und die Dehnungssteifigkeit D von Stahlbetonkonstruktionen hängen von der Bewehrung und von der Ausmittigkeit der Druckkraft ab, weil die zugbeanspruchte Betonzone mit zunehmender Ausmittigkeit Risse erleidet und ihre Steifigkeit abnimmt.

Die Steifigkeiten gehen mit den dem Stadium II von Stahlbetonkonstruktionen entsprechenden Werten ($B_{II} = EI_{II}$, $D_{II} = EF_{II}$), d. h. mit den Kennwerten für den in der Zugzone eingerissenen, *linear elastischen* Betonquerschnitt in die Berechnung ein. Diese Steifigkeiten hängen von der Ausmittigkeit »e« der inneren Druckkraft ab (s. Bild 18 a—b).

Die Berechnungen nach der Stahlbetontheorie ermöglichen es, die Werte von I_{II}, I_I und F_{II}, F_I sowie den Wert des Quotienten

$$\psi = \sqrt{\frac{I_{II} F_{II}}{I_I F_I}}$$

zu bestimmen [8].

Im Bild ψ ist auch die Funktion ψ für den unbewehrten Querschnitt ($\mu_{st} = 0$ durch eine punktierte Linie) angezeigt.

In Kenntnis des Diagramms ψ erhält man die Kurve ③ durch Multiplizieren der Ordinaten $p/E\ 10^6$ der Kurve ①.

ad b. *Die Anfangsausmittigkeit (Vorbeule)*

Die maßgebende ungewollte Anfangsausmittigkeit läßt sich nach [8], wie folgt, ansetzen:

$$e_{\text{anf.}} = \frac{R_d}{3500},$$

$$R_d = \sqrt{|R_x|\,|R_y|},$$

$$R_x = 16{,}90\ m, \quad |R_y| = 7{,}14\ \text{m}, \quad R_d = 10{,}98\ \text{m},$$

$$e_{\text{anf.}} = \underline{3{,}14 \times 10^{-3}}\ \text{m},$$

wo R_d den durchschnittlichen Krümmungshalbmesser bedeutet.

Im Hinblick darauf, daß das Diagramm $p-e$ (bzw. $p-w$) der Schale mit der Anfangsausmittigkeit $e_{\text{anf.}}$ unbekannt ist, bedarf es also Näherungsverfahrens zum Konstruieren des Kraft-Verformungs-Diagramms $p(w)$ (bzw. $p[e]$) der mit Vorbeulen behafteten Schalen. Di-Näherung bedient sich der Methode, den Zusammenhang

$$p = p_{kr}^{\text{lin}} \cdot \left(1 - \frac{e_{\text{anf.}}}{e}\right)$$

für den exzentrisch gedrückten geraden Stab durch verhältnisgleiche Reduzierung seiner Ordinaten so zu verzerren, daß sich seine Kurve nicht an die waagerechte Gerade p_{kr}^{lin}, sondern an die Kurve ①—② der Beulverformung der geometrisch vollkommenen Schale anschmiegt.

In diesem Fall ist dies eine gute Näherung, weil der Kurvenzweig ② (im untersuchten kleinen Bereich) nur in geringem Maß ansteigt.

Die auf diese Art erhaltene Kurve ④ läuft unter der (unbekannten) wirklichen Kurve, da ja die Schale über eine zunehmende überkritische Tragfähigkeit verfügt.

Naturgemäß soll auch die Kurve ④ durch die reduzierenden Koeffizienten ψ verzerrt werden (s. $p^* \to \psi^* \cdot p^*$).

Die so bestimmte Kurve ⑤ bildet die Tragfähigkeitskurve $p - e/h$ der *eingerissenen* (r) Stahlbetonschale (Stb.) aus idealem *elastischen* Werkstoff. Der Scheitelpunkt liefert die obere kritische Last:

$$p_{kr,\,\text{Stb.},\,r}^{\text{obere}} = 0{,}193\ E \times 10^{-6}.$$

ad c. *Die Auswirkung der Plastizität*

Kommt es beim Ausbeulen einer Schale zu plastischen Verformungen, so sinkt ihre kritische Last unter den nach der elastischen Theorie bestimmten Wert. Die plastische Reduk-

tion wird von [8] durch den Multiplikationsfaktor

$$\xi_{pl} = \sqrt{\frac{1}{1 + \left(\frac{p^{\text{obere}}_{kr,\text{Stb.},r}}{p_{pl}}\right)^2}}$$

berücksichtigt. Hierbei p_{pl} bedeutet die Last die *ohne Beulung* bei der Ausmittigkeit e^{obere}_{kr} (s. Kurve ⑤) in dem Querschnitt einen plastischen Festigkeitsbruch hervorruft (s. die plastische Grenzkraft in Bild 18 c).

In unserem Fall: $N_{pl} = 176$ kNm^{-1}, $p_{pl} = 35$ kNm^{-2}. Für eine Dauerlast gilt der Formänderungsmodul

$$E = E_{bd} = 1{,}33 \times 10^7 \text{ kNm}^{-2},$$

also

$$p^{\text{obere I}}_{kr,\text{Stb.},r} = 0{,}193 \times 1{,}33 \cdot 10^7 \cdot 10^{-6} = 2{,}57 \text{ kNm}^{-2}.$$

Die Schneelast wirkt nicht dauernd, sondern nur kurzzeitig, verursacht also nur ein geringfügiges Kriechen. Demnach rechnen wir im Falle der *totalen* Last ($p_M = 2{,}25$ kNm^{-2}) mit dem Formänderungsmodul:

$$\tilde{E}_b = 1{,}64 \times 10^7 \text{ kNm}^{-2}.$$

Die entsprechende obere kritische Last ist:

$$p^{\text{obere II}}_{kr,\text{Stb.},r} = 0{,}193 \times 1{,}64 \times 10^7 \times 10^{-6} = 3{,}17 \text{ kNm}^{-2}.$$

Ein Vergleich der oberen kritischen Lasten mit der plastischen Bruchlast p_{pl} zeigt, daß die Schale bei etwa $7{,}3 \div 8{,}8\%$ der plastischen Bruchlast beult.

Die Reduktionsfaktoren sind in den behandelten beiden Fällen fast gleich:

$$\xi^{\text{I}}_{pl} = 0{,}997, \text{ bzw. } \xi^{\text{II}}_{pl} = 0{,}996.$$

Im Endergebnis ergibt sich bei einer Dauerlast die obere *plastische* kritische Last der *eingerissenen*, ausmittig gedrückten Stahlbetonschale zu

$$p^{\text{obere I}}_{kr,\text{Stb.},pl} = p^{\text{obere}}_{kr,\text{Stb.},r} \times \xi^{\text{I}}_{pl} = 2{,}56 \text{ kNm}^{-2}.$$

Für die totale Last gilt:

$$p^{\text{obere II}}_{kr,\text{Stb.},r} = p^{\text{obere II}}_{kr,\text{Stb.},r} \times \xi^{\text{II}}_{pl} = 3{,}15 \text{ kNm}^{-2}.$$

Die *Sicherheitskoeffizienten* ($p_M = p_{da} + p_{ev} = 1{,}25 + 1{,}0 = 2{,}25$ kNm^{-2}) sind:

$$k^{\text{I}}_{si} = \frac{p^{\text{obere I}}_{kr,\text{Stb.},pl}}{p_{da}} = 2{,}05,$$

$$k^{\text{II}}_{si} = \frac{p^{\text{obere II}}_{kr,\text{Stb.},pl}}{p_M} = 1{,}40.$$

So haben die Risse (ψ) die Vorbeulen ($e_{\text{anf.}}$) sowie in geringem Maße die Plastizität (ξ_{pl}) die kritische Last $p^{\text{lin}}_{kr,v}$ in großem Maße herabgesetzt. Die Konstruktion ist zum Tragen der Belastung geeignet.

Es soll noch bemerkt werden, daß die Kurve ⑤ mit zunehmender Ausmittigkeit »e« einen steigenden Charakter aufweist, weil die Kurve ④ monoton zunimmt und die Kurve ψ einem Grenzwert (reine Biegung) zustrebt.

6. Zusammenfassung

In dieser Abhandlung sind die Bestimmung der Besonderheiten der Gleichgewichtszustände von flachen, sattelförmigen, an ihren Rändern normalkraftfreien HP-Schalen, unter gleichmäßig verteilter Belastung, nach der

»nichtlinearen« Theorie der beschränkten großen Verformungen behandelt worden.

Auf Grund der Gleichgewichts- und Verträglichkeitsgleichungen der flachen Schalen, die die *geometrische Nichtlinearität* berücksichtigen, sind die Tragfähigkeitskurven nach dem Galerkinschen Verfahren ermittelt worden.

Es wurde festgestellt, daß das *Durchschlagen* bei einem bestimmten Wert der Lastintensität auftreten kann, wenn die geometrischen Proportionen der HP-Schale gewissen geometrischen Bedingungen entsprechen.

Die »halbnormale« HP-Schale ($f_a/f_b = 1$) und die Schalen, deren Pfeilhöhenverhältnisse von dem Wert $f_a/f_b = 1$ bloß geringfügig abweichen, weisen eine *monoton wachsende* Tragfähigkeit auf. Das Maß der Tragfähigkeit dieser Schale ist jedoch sehr klein, daher ist ihre Anwendung ausschließlich bei ebene Platten kennzeichnenden geometrischen Verhältnissen möglich.

Im größeren Teil des untersuchten Pfeilhöhenverhältnisbereiches sind *die kritischen Durchschlagslasten* $\bar{p}_{kr}$ höher bzw. viel höher als die linearen kritischen Lasten p_{kr}^{lin}, die zur aus dem unverformten Grundzustand ($w_0 = 0$) auftretenden Verzweigungserscheinung gehören.

Die theoretischen Untersuchungen gingen auch der Frage nach, bei welcher Belastung von der *symmetrischen* Verformung der HP-Schale, die nach der Theorie der größen Verformungen verfolgt wird, eine »benachbarte« *antimetrische* Ausbeulung abzuzweigen vermag (Abzweigung).

Wie es sich herausgestellt hat, neigen die meisten behandelten Schalen zum »Überspringen« in eine antimetrische Ausbeulung.

Bild 2.c stellt den Sonderfall dar, in dem sich die Schale symmetrisch zu deformieren beginnt, wobei sich von der Kurve noch vor Erreichen des Scheitelpunktes (d. h. der Durchschlagslast $\bar{p}_{kr}$) in einem Punkt eine antimetrische Beulform abzweigt und die Schale zugrunde geht.

Diese Beulform zweigt jedoch bei einer Lastintensität an der bereits *in anderer Form verformten* Schale ab. An der *unverformten* Schale würde eine Instabilität in dieser Beulform bei einer *größeren* oder *kleineren* Lastintensität auftreten.

An Hand dieser Analyse hat sich herausgestellt, daß die Wirkung der Verformungen des Grundzustandes für die Schalen mit Pfeilhöhenverhältnissen von $f_a/f_b \sim 3$ am gefährlichsten ist. Die Tragfähigkeit der in der Praxis häufig angewandten HP-Schalen (die »normale« Schale mit dem Pfeilhöhenverhältnis $f_a/f_b = 4$ und die Schale mit einem solchen von $f_a/f_b = 9/4$), wird durch die Verformungen des Grundzustandes nur wenig beeinflußt.

Aus unseren Ergebnissen kann man auch darauf schließen, daß wahrscheinlich die Schalen mit den Parametern $f_a/f_b \sim 2{,}5 - 3{,}5$ auf Vorbeulen am empfindlichsten reagieren.

Die theoretischen Resultate kurz zusammengefaßt ist festzustellen, daß die behandelten HP-Schalen die folgenden *vier Typen des Gleichgewichtszustandes* nach der Theorie II. Ordnung haben:

1. Bei den Schalen, die den größten Teil ihrer Lasten durch Biegesteifigkeit tragen, zeigt sich *kein Instabilitätsproblem*. Die monoton wachsenden Schaubilder $p-w$ besitzen keine stationären Punkte. Bei der »halbnormalen« Schale $f_a/f_b = 1$ haben die Kurven auch keine Inflexionspunkte.

2. Bei gewissen geometrischen Verhältnissen verlieren die Schalen ihre Stabilität infolge *Durchschlagens*. Innerhalb von diesem Typ sind zwei Fälle möglich. Der Unterschied zwischen diesen zeigt sich im verschiedenen Verhalten *nach dem Durchschlagen:*

2.1 In diesem Fall verläuft der Durchschlagsvorgang *durchwegs symmetrisch.*

2.2 Hierbei erfolgt nach dem Durchschlagen eine *antimetrische* Verzweigung an dem labilen Ast. Diese Möglichkeit wurde nicht untersucht, weil die Konstruktion bei Erreichen der Last $\bar{p}_{kr}$ als zugrunde gegangen betrachtet werden kann.

3. Für den größten Teil der untersuchten HP-Schalen ist kennzeichnend, daß auch ein *antimetrischer* Gleichgewichtszustand (s. gestrichelte Linie in Bild 2.c), der mit *Verzweigung* verbunden ist, außer dem *symmetrischen* Gleichgewichtszustand (s. ausgezogene Linie in Bild 2.c) vor dem Durchschlagen existiert. Diese Schalen neigen also zum »Überspringen« in eine antimetrische Ausbeulung.

Die *überkritische* Tragfähigkeitsart nach dieser Abzweigung weist fallweise *abnehmenden* bzw. *zunehmenden* Charakter auf.

SCHRIFTTUM

1. Bushnell, D.: Symmetric and Nonsymmetric Buckling of Finitely Deformed Eccentrically Stiffened Shells of Revolution. *AIAA Journ.* **5** (1967), 1455—1462
2. Dulácska, E.: A héjak hullámossága kritikus terhet csökkentő vizsgálata lineáris elmélettel. *Építés- és Építészettudomány* **8** (1976) 3—4, 279—293. (auf ungarisch) (Untersuchung der vermindernden Wirkung der Vorbeulen auf die kritische Last)
3. Dulácska, E.: Vibration and Stability of Anisotropic Shallow Shells. *Acta Techn. Hung.* **65** (1969), 225—260
4. Flügge, W.—Geyling, F. T.: A General Theory of Deformations of Membrane Shells. *International Association for Bridge and Structural Engineering.* **17** (1957), 23—46
5. Jankó, L.: Analyse des Verhältnisses zwischen Membran- und Biegeschnittkräften in sattelförmigen, flachen, normalkraftfrei gelagerten HP-Schalen unter gleichmäßig verteilter Belastung. *Acta Tech. Hung.* 91 (1980), 19—55
6. Jankó, L.: Untersuchung der Stabilität sattelförmiger, flacher, normalkraftfrei gelagerter HP-Schalen unter gleichmäßig verteilter Belastung. *Acta Techn. Hung.* 91 (1980)
7. Kollár, L.: Héjak nyúlásmentes alakváltozásai. *Építés- és Építészettudomány* **3** (1971) 19—38. (auf ungarisch) (Dehnungslose Verformungen der Schalen)
8. Kollár, L.—Dulácska, E.: Schalenbeulung. Werner, Düsseldorf—Akadémiai Kiadó, Budapest 1974
9. Leet, K. M.: Study of Stability in the Hyperbolic Paraboloid. *Journ. Eng. Mech. Divis. Proc. ASCE*, **92** (1966), No 1, 121—142

10. MARGUERRE, K.: Über die Anwendung der energetischen Methode auf Stabilitätsprobleme. *Jahrbuch 1938 der deutschen Luftfahrtforschung*, 433—443
11. PFLÜGER, A.: Stabilitätsprobleme der Elastostatik. 2. Aufl. Springer-Verlag, Berlin—Göttingen—Heidelberg—New York 1964
12. REISSNER, E.: On Some Aspects of the Theory of Thin Elastic Shells. Boston Society of Civil Engineers 1955, 100—133
13. TIMOSHENKO, S. P.—GERE, J. M.: Theory of Elastic Stability. McGraw-Hill Book Company, New York—Toronto—London 1961
14. WEDELLSBORG, B. W.: Critical Buckling Load on Large Spherical Shells. *Journ. Struct. Divis. Proc ASCE*, **88** (1962), St. 1. 111—121
15. WEINITSCHKE, H. J.: On Asymmetric Buckling of Shallow Spherical Shells. *Journal of Mathematics and Physics* **44** (1965), 141—163
16. WEINITSCHKE, H. J.: On the Stability Problem for Shallow Spherical Shells. *Journal of Mathematics and Physics* **38** (1960), 209—301
17. WEINITSCHKE, H. J.: On the Nonlinear Theory of Shallow Spherical Shells. *J. Soc. Indust. Appl. Math.* **6** (1958), 209—232
18. WOLMIR, A. S.: Biegsame Platten und Schalen. VEB Verlag für Bauwesen, Berlin 1962

A Nonlinear Analysis of the Equilibrium Path of Shallow Shaddle-shaped Hypar Shells, Supported by Shear Diaphragms, under Uniform Load, with Special Respect to Bifurcation and Snapping. — This paper is the third and the final part of a series. In the first part the problems of the existence and uniqueness of the membrane solution of the hypar shells and the kinematic uncertainty of the surface are treated. In the second part, the phenomenon of branching out from the basic undeformed state are dealt with. In the present paper the author tries to give a response to the question whether the failure can take place without branching, caused by cracking through (i.e., of what character are the load-strain diagrams of large deformation). It is also investigated, whether the load bearing capacity beyond the branching, from the deformed basic state, is increasing or decreasing.

INDEX

PRINTED IN HUNGARY

Akadémiai Nyomda, Budapest

Acta Techn. Hung. **91** (1980), pp. 239—246

HEINLOO, M.: *Limit Analysis of Concrete Tubes, Reinforced by a Set of Thin Shells*

The paper deals with limit analysis of thick-walled concrete tubes, reinforced by a set of thin cylindrical membrane shells and loaded by internal pressure. The exact solution of the problem is obtained and the influence of the location of the shells to the limit pressure is analysed.

Acta Techn. Hung. **91** (1980), pp. 247—256

CSONKA, P.: *Sectorial Shell without Ties with Unbent Edge Arches and Dividing Ribs*

The stress pattern generated by uniformly distributed vertical load in special shaped sectorial shells is analysed in the framework of the membrane theory. It is proved that the edge members (edge arches in horizontal and dividing ribs in vertical planes) of these shells do not undergo bending and torsional effects, but are only affected by axial (funicular) forces. The lateral tension of the dividing ribs is cancelled by the lateral tensile forces of the edge arches. That is why for this type of shells no ties or struts are to be applied between the abutment points of the ribs.

Acta Techn. Hung. **91** (1980), pp. 257—264

BÉRES, E.: *High Accuracy Interpolation of Stresses*

Dividing a solid into elements by parallel and perpendicular planes, the accuracy of stress distribution may be improved by extending the required fitting of the approximative polynomial, in addition to the element corners, also to neighbouring nodes, meaning 32 fittings in space, 12 in the plane, and 4 along the straight line. The suggested three-variable polynomial of 32 terms will be presented to change in plane and along the straight line into two-variable and single-variable polynomials of 12 and 4 terms, respectively. Distribution is uniform at element interfaces, showing the approximation to be continuous and unambiguous throughout the solid.

Acta Techn. Hung. **91** (1980), pp. 265—302

JANKÓ, L.: *Stability of Shallow Saddle-shaped Hypar Shells, Supported by Shear Diaphragms, under Uniform Load.*

This paper is the second part of a series consisting of three parts, the first of which treated theoretical problems (i.e., existence and uniqueness of the membrane solution, kinematic uncertainty) the response to which assures a suitable fundament for performing the present stability analyses. In the paper, the phenomenon of branching from the undeformed state of the saddle-shaped flat hypar shells without lateral thrust is dealt with. In this connection also the question is analysed if the possibility of the development of a deformation without elongation what influence it has on the process of losing stability.

Acta Techn. Hung. **91** (1980), pp. 303—320

FARKAS, M.—FRITZ, J.—MICHELBERGER, P.: *On the Effect of Stochastic Road Profiles on Vehicles Travelling at Varying Speed*

Vehicles participating in mass transportation are frequently constrained to change their velocities due to traffic and other reasons. It is assumed that the road profile, as a function of the distance from the origin, is a steady state stochastic process and the distance covered by time-dependent variable speed is a process of steady-state increment. Assuming them to be independent processes, it is pointed out that the complex process, i.e., the road profile as a time-dependent function is a steady-state process. The particular case of the bus applied in town traffic is detailed which, between two stops runs with uniform speed, decelerates and accelerates uniformly at the stopping places while it is assumed that the placement of the stations might be simulated by a kind of Poisson's processes.

Acta Techn. Hung. **91** (1980), pp. 321—334

KARSAI, K.: *Heatings and Losses Occurring in the Magnetic Stray Fields of Transformers*

Heatings and losses being produced in the magnetic stray fields of transformers are treated. The places of production of heating and losses: the magnetic core, tank, cover, screws between cover and tank, zone of the bushings and yoke-clamp device are detailed. Methods reducing the detrimental consequences of stray fields are dealt with. Admissible heating values are recommended both to bare and insulated surfaces. Eventually, different methods are evaluated which are suitable to the determination of dangerous heatings having been produced in the stray field.

Acta Techn. Hung. **91** (1980), pp. 335—354

GÁSPÁR, L.: *Making use of the Industrial By-products in the Field of Road Construction in Hungary*

Utilization of the fly ash, blast furnace cinder and waste rock in the way written in the paper is, from the viewpoint of people's economy very significant. With the view of the earliest possible overall introduction of the combined utilization of the industrial by-products, the thermal power plants, ironworks, stone and gravel industry, as well as the highway departments and the construction material industry should develop further quantity of the calcium hydrate, because the lack of this material keeps back the large-scale construction of the base courses. — Surmounting the difficulties of the introduction of the measures proposed would efficiently foster the economy on material and energy which is very much on the carpet at present.

Acta Techn. Hung. **91** (1980), pp. 355—372

HOLNAPY, D.: *Applying Abstract Algebraic Structures to Structural Designing*

Previously, in the process of the computerized designing technique in connection with system construction, the design of objects was defined by a selection of the system components according to a given policy. In this paper, this method of designing based on the selection of the system components will be formulated by using abstract algebraic structures. Although this principle is of general validity, yet the concepts as discussed in the present paper, are restricted to beam structures only.

Acta Techn. Hung. **91** (1980), pp. 373—392

BUKHARI, M. A. T.: *Saturated Phase Enthalpy Relationships for Solid CO^2 in CH_4 Cryogenic Phase Behaviour*

With low temperature processing of CO_2 contaminated natural gas becoming an established practice, the design of cryogenic installations for freezing out solid CO_2 produces, economically, much more refined natural gas than in now offered by more conventional techniques. Although the cryogenic phase behaviour of the CH-—CO_2 system has been extensively investigated, the full potential of low-temperature processing cannot be realized until reliable thermodynamic data has become available. The main purpose of this paper is to present, analytically, some useful data, based on reliable correlations, for use in the design of cryogenic processes involving solid CO_2 in CH_4.

Acta Techn. Hung. **91** (1980), pp. 393—398

CSONKA, P.: *Some Special Cases of Inextensional Deformations of Shallow Shells*

Certain instances for the inextensional deformations of shallow shells are dealt with, where the differential equations and the functions characterizing the deformations are of extraordinarily simple form in spite of the fact that the flexural rigidity of the shell wall is also taken into consideration.

Acta Techn. Hung. **91** (1980), pp. 399—410

SZANISZLÓ, M.: *Adaptive Planning of Electric Power Distribution Networks and of their Complex Control Engineering Subsystems; Interactive Effects*

The paper presents an integrated planning system of distribution network, operation control and control engineering system. A new adaptive method for longterm planning of distribution network and control engineering is described which is adaptable to external and internal changes. Adaptivity is extended to process, model, algorithm, network and control engineering. As a model for planning a distribution network control engineering system — as a practical example — the planning of computerized telecontrol systems of regional dispatching centres is presented. Based on the analysis of interactions an increasing interaction between network and control engineering is experienced. The new control engineering subsystems have a reducing effect on the overall costs, and outage duration, result in increased network utilization and reliability and, finally, accomplish complex system control of distribution networks. The consideration of interactions yield improved system parameters.

Acta Techn. Hung. **91** (1980), pp. 411—418

DULÁCSKA, E.: *Buckling of the Saddle-Shaped Hypar Shell Acting Like an Arch*

The paper presents the determination of the linear critical load of the uniformly loaded saddle-shaped hyperbolic paraboloid shell stiffened along two opposite edges by diaphragms rigid only in their own planes, while rigidly supported in all directions along the other two edges. The buckled shape always consists of a combination of two sine functions which make the displacement vanish along the rigidly supported edges. The numerical values of the coefficient necessary to compute the critical loads are given in a table, facilitating practical computations.

Acta Techn. Hung. **91** (1980), pp. 419—467

JANKÓ, L.: *A Nonlinear Analysis of the Equilibrium Path of Shallow Shaddle-shaped Hypar Shells, Supported by Shear Diaphragms, under Uniform Load, with Special Rospect to Bifɔrcation and Shapping.*

This paper is the third and the final part of a series. In the first part the problems of the exieshtk and uniqueness of the membrane solution of the hypar shells and tencenematic uncertainty of the surface are treated. In the second part, the phenomenon of branching out from the basic underformed state are dealt with. In the present paper the author tries to give a response to the question whether the failure can take place without branching, caused by cracking through (i.e., of what character are the load-strain diagrams of large deformation). It is also investigated, whether the load bearing capacity beyong the branching, from the deformed basic state, is increasing or decreasing.

The *Acta Technica* publish papers on technical subjects in English, French, German and Russian.

The *Acta Technica* appear in parts of varying size, making up one volume.

Manuscripts should be addressed to

Acta Technica
H-1051 Budapest
Münnich Ferenc u. 7.
Hungary

Correspondence with the editors and publishers should be sent to the same addres

Orders may be placed with "Kultura" Foreign Trading Company (H-1389 Budapest 62, P.O.B. 149. Account No. 218-10990) or its representatives abroad.

Les *Acta Technica* paraissent en français, allemand, anglais et russe et publient des travaux du domaine des sciences techniques.

Les *Acta Technica* sont publiés sous forme de fascicules qui seront réunis en volumes.

On est prié d'envoyer les manuscrits destinés à la rédaction à l'adresse suivante:

Acta Technica
H-1051 Budapest
Münnich Ferenc u. 7.
Hongrie

Toute correspondance doit être envoyée à cette même adresse.

On peut s'abonner à l'Entreprise du Commerce Extérieur «Kultura» (H-1389 Budapest 62, P.O.B. 149. Compte courant No. 218-10990) ou chez représentants à l'étranger.

«*Acta Technica*» публикуют трактаты из области технических наук на русском-немецком, английском и французском языках.

«*Acta Technica*» выходят отдельными выпусками разного объема. Несколько вы пусков составляют один том.

Предназначенные для публикации рускописи следует направлять по адресу:

Acta Technica
H-1051 Budapest
Münnich Ferenc u. 7.
Венгрия

По этому же адресу направлять всякую корреспонденцию для редакции и администрации.

Заказы принимает предприятие по внешней торговле «Kultura» (H-1389 Budapest 62, P.O.B. 149. Текущий счет № 218-10990) или его заграничные представительства и уполномоченные.

Reviews of the Hungarian Academy of Sciences are obtainable at the following addresses:

AUSTRALIA
C.B.D LIBRARY AND SUBSCRIPTION SERVICE, Box 4886, G.P.O., *Sydney N.S.W. 2001*
COSMOS BOOKSHOP, 145 Ackland Street, *St. Kilda (Melbourne), Victoria 3182*

AUSTRIA
GLOBUS, Höchstädtplatz 3, *1200 Wien XX*

BELGIUM
OFFICE INTERNATIONAL DE LIBRAIRIE, 30 Avenue Marnix, *1050 Bruxelles*
LIBRAIRIE DU MONDE ENTIER, 162 Rue du Midi, *1000 Bruxelles*

BULGARIA
HEMUS, Bulvar Ruszki 6, *Sofia*

CANADA
PANNONIA BOOKS, P.O. Box 1017, Postal Station "B", *Toronto, Ontario M5T 2T8*

CHINA
CNPICOR, Periodical Department, P.O. Box 50, *Peking*

CZECHOSLOVAKIA
MAD'ARSKÁ KULTURA, Národní třida 22, *115 66 Praha*
PNS DOVOZ TISKU, Vinohradská 46, *Praha 2*
PNS DOVOZ TLAČE, *Bratislava 2*

DENMARK
FJNAR MUNKSGAARD, Norregade 6, *1165 Copenhagen*

FINLAND
AKATEEMINEN KIRJAKAUPPA, P.O. Box 128 *SF-00101 Helsinki 10*

FRANCE
EUROPÉRIODIQUES S.-A., 31 Avenue de Versailles, *78170 La Celle St.-Cloud*
LIBRAIRIE LAVOISIER, 11 rue Lavoisier, *75008 Paris*
OFFICE INTERNATIONAL DE DOCUMENTATION ET LIBRAIRIE, 38 rue Gay Lussac, *75240 Paris Cedex 05*

GERMAN DEMOCRATIC REPUBLIC
HAUS DER UNGARISCHEN KULTUR, Karl-Liebknecht-Strasse 9, *DDR-102 Berlin*
DEUTSCHE POST ZEITUNGSVERTRIEBSAMT, Strasse der Pariser Kommüne 3—4, *DDR-104 Berlin*

GERMAN FEDERAL REPUBLIC
KUNST UND WISSEN ERICH BIEBER, Postfach 46, *7000 Stuttgart 1*

GREAT BRITAIN
BLACKWELL'S PERIODICALS DIVISION, Hythe Bridge Street, *Oxford OX1 2ET*
BUMPUS, HALDANE AND MAXWELL LTD., Cowper Works, *Olney, Bucks MK46 4BN*
COLLET'S HOLDINGS LTD., Denington Estate, *Wellingborough, Northants NN8 2QT*
W.M. DAWSON AND SONS LTD., Cannon House, *Folkestone, Kent CT19 5EE*
H. K. LEWIS AND CO., 136 Gower Street, *London WC1E 6BS*

GREECE
KOSTARAKIS BROTHERS, International Booksellers, 2 Hippokratous Street, *Athens-143*

HOLLAND
MEULENHOFF-BRUNA B.V., Beulingstraat 2, *Amsterdam*
MARTINUS NIJHOFF B.V., Lange Voorhout 9—11, *Den Haag*
SWETS SUBSCRIPTION SERVICE, 347b Heereweg, *Lisse*

INDIA
ALLIED PUBLISHING PRIVATE LTD, 13/14 Asaf Ali Road, *New Delhi 110001*
150 B-6 Mount Road, *Madras 600002*
INTERNATIONAL BOOK HOUSE PVT. LTD., Madame Cama Road, *Bombay 400039*
THE STATE TRADING CORPORATION OF INDIA LTD., Books Import Division, Chandralok, 36 Janpath, *New Delhi 110001*

ITALY
EUGENIO CARLUCCI, P.O. Box 252. *70100 Bari*
INTERSCIENTIA, Via Mazzé 28, *10149 Torino*
LIBRERIA COMMISSIONARIA SANSONI, Via Lamarmora 45, *50121 Firenze*
SANTO VANASIA, Via M. Macchi 58, *20124 Milano*
D. E. A., Via Lima 28, *00198 Roma*

JAPAN
KINOKUNIYA BOOK-STORE CO. LTD., 17-7 Shinjuku-ku 3 chome, Shinjuku-ku, *Tokyo 160-91*
MARUZEN COMPANY LTD., Book Dpartment, P.O. Box 5056 Tokyo International, *Tokyo 100-31*
NAUKA LTD. IMPORT DEPARTMENT, 2-30-11 Minami Ikebukuro, Toshima-ku, *Tokyo 171*

KOREA
CHULPANMUL, *Phenjan*

NORWAY
TANUM-CAMMERMEYER, Karl Johansgatan 41—43, *1000 Oslo*

POLAND
WĘGIERSKI INSTYTUT KULTURY, Marszałkowska 80, *Warszawa*
CKP I W ul. Towarowa 28 *00-958 Warszawa*

ROMANIA
D. E. P., *Bucureşti*
ROMLIBRI, Str. Biserica Amzei 7, *Bucureşti*

SOVIET UNION
SOJUZPETCHATJ — IMPORT, *Moscow*
and the post offices in each town
MEZHDUNARODNAYA KNIGA, *Moscow G-200*

SPAIN
DIAZ DE SANTOS, Lagasca 95, *Madrid 6*

SWEDEN
ALMQVIST AND WIKSELL, Gamla Brogatan 26, *101 20 Stockholm*
GUMPERTS UNIVERSITETSBOKHANDEL AB, Box 346, *401 25 Göteborg 1*

SWITZERLAND
KARGER LIBRI AG, Petersgraben 31, *4011 Basel*

USA
EBSCO SUBSCRIPTION SERVICES, P.O. Box 1943, *Birmingham, Alabama 35201*
F. W. FAXON COMPANY, INC., 15 Southwest Park, *Westwood, Mass. 02090*
THE MOORE-COTTRELL SUBSCRIPTION AGENCIES, *North Cohocton, N. Y. 14868*
READ-MORE PUBLICATIONS, INC., 140 Cedar Street, *New York, N. Y. 10006*
STECHERT-MACMILLAN, INC., 7250 Westfield Avenue, *Pennsauken, N. J. 080110*

VIETNAM
XUNHASABA, 32, Hai 3a Trung, *Hanoi*

YUGOSLAVIA
JUGOSLAVENSKA KNJIGA, Terazije 27, *Beograd*
FORUM, Vojvode Mišiča 1, *21000 Novi Sad*

HU ISSN 0001—7035

Index: 26.025